NORTHERN HYDROLOGY
Selected Perspectives

T.D. Prowse and C.S.L. Ommanney, Editors

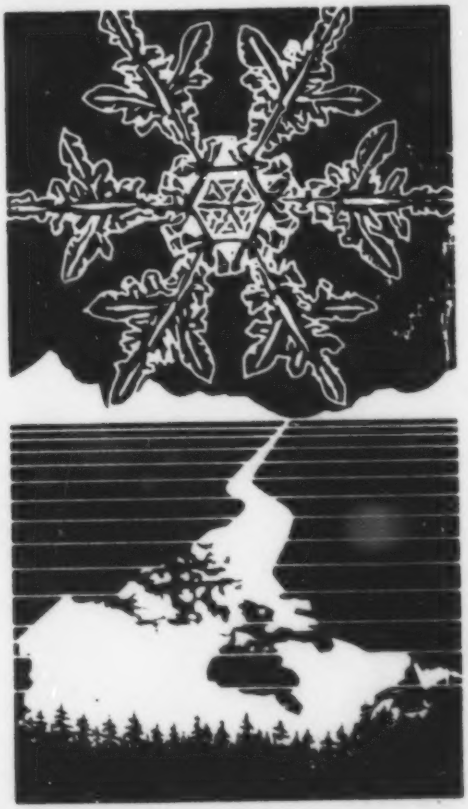

NHRI Symposium No.6

92-04307/

NORTHERN HYDROLOGY: SELECTED PERSPECTIVES

Proceedings of the Northern Hydrology Symposium
10-12 July 1990, Saskatoon, Saskatchewan

Editors

T.D. Prowse and C.S.L. Ommanney

Organized and sponsored by:
National Hydrology Research Institute, Environment Canada

Co-sponsored by:
Water Resources Division, Department of Indian and Northern Affairs Canada
Western Committee of Regional Executives of Environment Canada
Canadian Water Resources Association

National Hydrology Research Institute
Inland Waters Directorate
Conservation and Protection
Environment Canada

11 Innovation Boulevard
Saskatoon, Saskatchewan
Canada S7N 3H5

© Minister of Supply and Services
Canada 1991

NHRI Symposium No. 6

Cat. En 36-512/6E
ISSN 0838 1984
ISBN 0-662-18742-3

FOREWORD

Northern research is an important scientific program of the National Hydrology Research Institute. The vastness of the Canadian North, and the relatively limited research undertaken there, make it a virtual scientific terra incognita. As such, it presents intriguing and challenging opportunities for the researcher. However, the research must be focused to produce information relevant to the major issues facing the region.

In the long run, the pristineness and isolation of the North may be compromised by local industrial development, or by demands for northern water resources from more populated parts of the continent. Water transfers have already been proposed to solve the problem of shortages in some areas. Both global atmospheric and oceanic circulation are transporting industrial contaminants into the North, where sensitive ecosystems are perhaps ill-adapted to assimilate them.

Many northerners still rely on the flora and fauna of their local area for the basics of life - food, shelter and the wherewithall to purchase necessities. Others derive a livelihood from their environment through an involvement in tourism, hunting and fishing, etc. Policies for the sustainable development of these northern environments have to be an essential component of any strategy that supports industrial investment as well as ensuring the continuation of indigenous industries and traditional lifestyles.

Sound management and accurate assessments of the impact of change both demand that the northern hydrological cycle be well understood. The terrain, morphology and climate of the North make direct transfer of hydrological knowledge from other climatic zones unreliable for management and planning purposes. Consequently, northern hydrological systems must be studied by dedicated researchers who have developed the appropriate expertise and who are able to recognize how the unique aspects of the northern environment may impact physical processes.

Northern researchers must share their knowledge and work together to provide the reliable scientific information needed for optimum regional and national management of the available resources. The results of investigations and collaborations should be organized and made available to all. Hence, these proceedings are an example of one way to encourage synergism.

Editors and organizers, Prowse and Ommanney, as well as all the scientists who contributed their data and ideas, are to be congratulated on this Symposium, and the Proceedings, which are important steps in the long process of understanding and documenting the northern hydrological environment. Thanks are due to all of them for their hard work.

The contributions by co-sponsors who supported the Symposium and Proceedings are very much appreciated.

The National Hydrology Research Institute will continue to produce reports, and to be a source of expertise, on Canada's North.

T. Milne Dick

T. Milne Dick, Director

National Hydrology Research Institute
Environment Canada
Saskatoon, Saskatchewan, S7N 3H5

12 August 1991

PREFACE

Water is perhaps the most important renewable resource in the North. It is crucial not only for sustaining native and traditional lifestyles, but also for supporting many economic development activities. Canada's North is richly endowed with majestic rivers, expansive wetlands and a myriad of lakes. Because most north-flowing streams have headwaters in southern Canada, there has been a tendency to first look south to determine the condition of water resources and to access southern research centres to gain an understanding of hydrological processes. Such myopic views, however, can be seriously flawed. In Canada, we must recognize that expertise on cold regions or northern rivers can be gained by looking across the North to our circumpolar neighbours.

The Northern Hydrology Symposium, which was held in Saskatoon in July 1990, is an excellent example of Canadian scientists, researchers and water managers looking beyond their borders to learn from others. The Department of Indian Affairs and Northern Development was pleased to participate in this symposium and proud of its leadership role in fostering exchanges and conducting research programs with Canada's neighbours. We are currently participating in the Canada-USSR Agreement on Cooperation in the Arctic and the North to conduct joint water-related research and working with the other seven circumpolar countries to negotiate an arctic environmental protection strategy.

We were pleased to be able to co-sponsor the symposium and support Environment Canada in the production of this volume. It will extend and broaden the focus of northern hydrological processes and pave the way for fruitful cooperation in northern hydrological research.

David Milburn

D. Milburn, A/Chief

Water Resources Division
Indian and Northern Development
Northern Affairs Program
Environment and Renewable Resources
Natural Resources and Economic Development Branch
Les Terrasses de la Chaudière
Ottawa, Ontario, K1A 0H4

15 July 1990

INTRODUCTION

This book is the second of a three-volume set dedicated to the subject of northern hydrology. The first (Prowse and Ommanney, 1990) was published in June 1990 and released at the Northern Hydrology Symposium, Saskatoon, Canada, 10-12 July 1990. It contains reviews of past, present and required future research in subject areas of special significance to northern latitudes: snow hydrology, permafrost hydrology, ground-water hydrology, hydrology of floating ice, glacier hydrology, regional energy balances, water quality, regional hydrology, water legislation and a general overview of the Canadian situation.

This second volume contains papers from the Northern Hydrology Symposium. Although it was originally planned as a small national meeting, information from the first announcement spread rapidly and abstracts were submitted from several circumpolar nations. Given the apparent international interest, it was decided to solicit a set of international theme papers from key researchers in the circumpolar countries. Authors were requested to review the overall status of northern hydrology in their respective countries focusing primarily on the subjects addressed in the first volume. Although these papers were presented at the Symposium, they will be released as a third volume entitled "Northern Hydrology: International Perspectives" (Prowse and Ommanney, in preparation).

Section 1 of this volume, "General Papers", is comprised of all scientific papers that were presented at the Symposium and received a full-scientific review. Those with a modelling focus are contained in Section 2, "Modelling". The remainder are in Section 3, "Other Contributions", with annotations on the first page of each as to which were presented and/or received full-scientific review. To ensure a high standard for the Symposium proceedings, assistance for the review process was obtained from some key scientific committees of the National Research Council of Canada (NRCC). These included, with their designated representative: the Subcommittee on Glaciers (Dr. P.G. Johnson), the Subcommittee on Hydraulics of Ice Covered Rivers (Drs. K.S. Davar and S. Beltaos), both of the Associate Committee of Hydrology; and the Subcommittee on Permafrost (Dr. M.-K. Woo) and the Subcommittee on Snow and Ice (Dr. D.M. Gray) both of the Associate Committee on Geotechnical Research. Special thanks are due the committee representatives and their anonymous scientific reviewers. Thanks are also due the various other reviewers who assisted in subject areas outside the expertise of the selected NRCC committees.

Hosting of the Symposium was not possible without the financial contributions and support of its four co-sponsors: the National Hydrology Research Institute, the Water Resources Division of the Department of Indian and Northern Affairs Canada, the Western Committee of Regional Executives of Environment Canada (CORE), and the Canadian Water Resources Association. The success of the Symposium was very much a result of the dedication shown by the organising committee headed by Dr.

A.D. Stanley and including M. Conly, B. Doell, L. Fedosoff, J. Gibson, C. Onclin, K. Ulmer, all of NHRI, and the support provided by M. Gillies of the Canadian Water Resources Association.

In attempting to maintain the standard set in the first volume of this Northern Hydrology Series, the editors have relied on the abilities and talents of several people. Firstly, the editors acknowledge the special efforts of Philip K. Gregory (NHRI) in redrafting many of the figures. Second, thanks are due to L. Watson and the NHRI library staff for their countless literature searches and verifications. Lastly, the editors would like to formally recognize the tremendous contribution of K. Ulmer in the overall production of this text.

We hope the publication of these proceedings will further serve to integrate the hydrological sciences and circumpolar countries in the understanding of northern hydrology.

T.D. Prowse, Editor

C.S.L. Ommanney, Editor

National Hydrology Research Institute
Environment Canada
Saskatoon, Saskatchewan, S7N 3H5

24 April 1991

OTHER CITED PUBLICATIONS

Prowse, T.D. and C.S.L. Ommanney (Editors), 1990. Northern Hydrology: Canadian Perspectives, NHRI Science Report No.1, National Hydrology Research Institute, Environment Canada, Saskatoon, Saskatchewan, 308 pp.

Prowse, T.D. and C.S.L. Ommanney (Editors), in preparation. Northern Hydrology: International Perspectives, NHRI Science Report No.3, National Hydrology Research Institute, Environment Canada, Saskatoon, Saskatchewan

TABLE OF CONTENTS

FOREWORD i

PREFACE iii

INTRODUCTION v

SECTION 1: GENERAL PAPERS

Case Study of a Grounded Jam; Restigouche River, New Brunswick
by S. Beltaos and B.C. Burrell 1

Water Balance and Geochemistry Studies in a Tundra Watershed, District of Keewatin, Northwest Territories
by G.G. Bursey, T.W.D. Edwards and S.K. Frape 17

River Icing Mounds: a Winter Water Source on the Eastern North Slope of Alaska
by E.F. Chacho, C.M. Collins, A.J. Delaney and S.A. Arcone 33

Geochemical Evolution of Water in a Continental High Boreal Wetland Basin: Preliminary Results
by D. Craig 47

A Physical Model of Ice Overthrust during the Break-Up of Intact River-Ice Covers
by M.N. Demuth and T.D. Prowse 57

Seasonal Changes in the Hydrochemistry of Land Drainage: Colour Lake Catchment, Axel Heiberg Island, N.W.T.
by M. English, S. Schiff, M. Ecclestone, W.P. Adams, M. Hinton, L. Pezzutto, R. Elgood, C. Allan and D. Pierson 75

Shape, Length and Flow Conditions of Conduits at South Cascade Glacier, Washington State, U.S.A.
by A.G. Fountain 89

CO_2-Rich Ground Waters of the Flat River Valley, N.W.T.
by S.M. Hamilton, F.A. Michel and C.W. Jefferson 105

Regional Snow Ablation in the Alaskan Arctic
by L.D. Hinzman, D.L. Kane and R.E. Gieck 121

Regionalization of Low Flows in Yukon Territory
by J.R. Janowicz 141

Discharge Regimes of a Glacierized Basin, Slims River, Yukon
by P.G. Johnson 151

Pulses in Glacier Discharge: Indicators of the Internal Drainage System of Glaciers
by P.G. Johnson 165

Drainage of an Ice-Dammed Lake, Kaskawulsh Glacier Basin, Yukon
by J.N. Kasper and P.G. Johnson 177

On Areal Distribution of Snowcover in a Mountainous Area
by Å. Killingtveit and K. Sand 189

Hydrogeochemical Aspects of Two Selected Sites in a Fringe Zone of Discontinuous Permafrost
by Y.T.J. Kwong, D. Craig and M. Griffin 205

Ice-Cover Growth and Freeze-Out of Solutes in a Mackenzie Delta Lake
by L.F.W. Lesack, P. Marsh and R.E. Hecky 219

Hydrological Processes in a Small Catchment Containing a Perennial Snowbank, Melville Island, N.W.T.
by A.G. Lewkowicz and K.L. Young 237

On Modelling Surface Meltwater Discharge from Arctic and Alpine Glaciers
by D.S. Munro 253

A High Arctic Occurrence of Seasonal Frost Mounds
by W.H. Pollard 263

Relationships between Snow Chemistry and Blowing Snow: Initial Findings
by J.W. Pomeroy, T.D. Davies and M. Tranter 277

Peatlands of the Lake Melville Coastal Plain, Labrador
by J.S. Price, D.A. Maloney and F.G. Downey 293

Constraints on the Origin of Acidity in Colour Lake, Axel Heiberg Island (79°25'N)
by S. Schiff, M. English, M. Ecclestone, R. Elgood, M. Hinton and L. Pezzutto 303

Longitudinal Dispersion in the Ice-Covered Athabasca River
by G. Van Der Vinne and D. Andres 319

Economic Impact of River Ice Jams in Canada
by G. Van Der Vinne, T.D. Prowse and D. Andres 333

Estimation of Mass-Balance and Run-Off Component of Urumqi Glacier No.1 from Water-Balance Analysis
by Z. Yang 353

SECTION 2: MODELLING

Interactive Modelling of Cold Regions Watersheds with SSARR
by E.A. Cassell and T. Pangburn 363

Estimates of Evaporation in the Yukon and Northwest Territories
by J. Haas 379

A Basin Water-Storage Model to Forecast Columbia River Discharge
by W. Tangborn 393

Preliminary Findings from Experiments on Frazil and Anchor Ice in a Circular Flume
by G. Tsang and B. Trapp 405

On Computer Simulation of Ice Motion in Rivers
by O.G. Vinogradov, A. Springer and P. Wierzba 419

SECTION 3: OTHER CONTRIBUTIONS

Transformation of Heavy Metals under Tidal Flows in the Severnaya Dvina Estuary
by V.F. Brekhovskikh, A.N. Malutin and M.A. Mordasov 427

Northern River: BOD-DO Model
by V.F. Brekhovskikh and G.V. Volpian 437

Water Storage in Alpine Glaciers (Abstract)
by M.M. Brugman 443

Snowmelt Infiltration into Frozen Soil at Sites in the Discontinuous Permafrost Zone Near Mayo, Yukon Territory
by C.R. Burn 445

Use of Periphyton Indices as a Biological Measure of Water Quality in Small Rivers
by E.A. Goncharevich 461

Yukon and Northwest Territories Ground-Water Data Base
by P. Hardisty, V. Schilder, T. Dabrowski and J. Wells 465

Some Aspects of Glacier Hydrology in China
by X. Hu and Z. Yang 483

Modelled Estimates of Changes in the Water Balance of Forested Northern River Basins
by Yu.G. Motovilov and N.A. Nazarov 499

Study of Surface Water Quality in the Northern Region Subject to Pollution
by A.N. Shammasov 515

Response of Riverine and Lacustrine Biocenoses to Human Impact
by N.S. Zolotareva and M.A. Mordasov 521

APPENDIX A: LIST OF PARTICIPANTS 525

SECTION 1

GENERAL PAPERS

CASE STUDY OF A GROUNDED JAM; RESTIGOUCHE RIVER, NEW BRUNSWICK

S. Beltaos[1] and B.C. Burrell[2]

[1]National Water Research Institute
Burlington, Ontario
L7R 4A6 CANADA

[2]New Brunswick Department of the Environment
Fredericton, New Brunswick
E3B 5H1 CANADA

ABSTRACT

The formation, evolution and release of a break-up jam are described and the associated measurements analyzed and interpreted using existing theories and models. The Restigouche River forms the eastern portion of the boundary between New Brunswick and Quebec. Severe ice jams are known to occur and a pertinent study was initiated in 1988, jointly by the National Water Research Institute and the New Brunswick Department of the Environment.

In 1988, the ice began to break up in early April and by the evening of April 5, an ice jam had formed several kilometres upstream of the town of Matapédia. Detailed surveys of the water level profile were carried out near the toe of the jam. Following release of the jam on April 9, the shear wall height, being a measure of jam thickness, was determined at several locations. Using this information and bathymetric data obtained later, it was possible to reconstruct the configuration of the jam and deduce that it was practically grounded at the toe. The small area available for unobstructed flow under the jam would indicate implausibly high velocities if seepage through the jam were to be neglected. The recently developed model, RIVJAM, that takes seepage into account, gave good results when applied to the present measurements. This is the first data set where seepage is important and more data are needed to adequately define related parameters.

INTRODUCTION

The Restigouche is an interprovincial river, draining parts of Quebec and New Brunswick. The headwaters of the main stem of the Restigouche lie in the Chaleur Uplands. The largest tributaries are the Matapédia, Patapedia, Kedgwick and Upsalquitch rivers. The latter rises in the New Brunswick highlands while the former three rise in Les Notre-Dame mountains in Quebec.

The farthest downstream Water Survey of Canada gauge is located near the mouth of Rafting Ground Brook. At this site, the drainage area of the river is 7,740 km^2. The long-term average discharge is 165 $m^3 \cdot s^{-1}$ which, for open water conditions, corresponds to a mean depth and a width of 1.4 m and 140 m respectively. The local water surface slope is 0.8 $m \cdot km^{-1}$. About 10-km downstream is the town of Matapédia, situated on the Quebec side by the confluence of the Matapédia River, and known to have experienced severe ice-jam related problems in the past (Gidas, 1981). Farther downstream, several communities on the New Brunswick side have experienced similar problems, e.g., Flatlands, Tide Head, Atholville and Campbellton (Leger, 1986). Below Matapédia, the Restigouche widens and gradually changes to estuarine character by the time it reaches Chaleur Bay at Dalhousie.

In 1987, a joint research project was initiated by the provincial and federal Environment departments to study ice break-up and jamming processes in the lower Restigouche River. This river was chosen mainly because its hydroclimatic regime differs from that of previously studied rivers in Ontario and New Brunswick. It is only subjected to one break-up event per season (usually in April) and its relatively large slope and width can cause very thick and destructive ice jams. The main objectives of the study are to understand how the break-up event is initiated and ice jams develop, with possible forecasting applications. Figure 1 shows the study reach which, for most of its length, has excellent river access thanks to riverside roads along both banks.

A major ice jam that formed during the 1988 break-up is described herein. Pertinent measurements are interpreted with the aid of a numerical model developed recently at the National Water Research Institute.

THE 1988 ICE BREAK-UP EVENT

Mild weather began near the end of March with 20 mm of rainfall during March 25 to 27. The water level at the gauge site rose from a winter low of 1.3 m on March 25 to 2.1 m on March 30 and held at this stage for the next few days. Another 13 mm of rain fell during April 2 to 4 and caused additional water level rises leading to break-up.

By the late afternoon of April 5, an ice jam had formed near Babcock Brook, incorporating ice from the Upsalquitch River that had run on April 4. The toe (downstream end) of the jam was 300-m upstream of the brook mouth while the head (upstream end) was just downstream of the gauge by Rafting Ground Brook (Figure 1). Downstream of the toe, mostly intact sheet-ice cover prevailed with ice blocks accumulated under it. For a distance of 1.5 km, pressure ridges and mounds were evident, diminishing in frequency and height in the downstream direction (Figure 2). Water levels along this jam were recorded photographically at a few locations and surveyed later during open-water conditions.

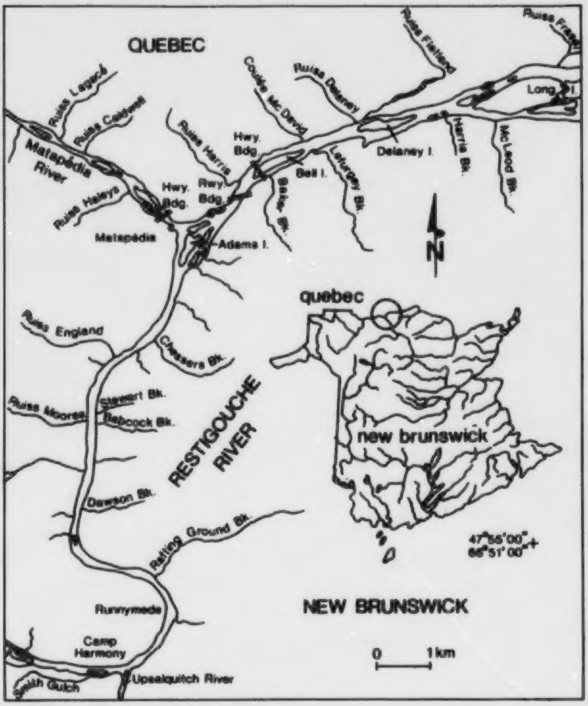
QUEBEC
Ruiss. Fréchet
Ruiss. Flatland
Ruiss. Legacé
Ruiss. Caldwell
Couillée McDavid
Ruiss. Delaney
Ruiss. Harris
Hwy. Bdg.
Long I.
Delaney I.
Harris Bk.
McLeod Bk.
Matapédia River
Ruiss. Haleys
Hwy. Bdg.
Rwy. Bdg.
Bell I.
Baker Bk.
Leturgey Bk.
Matapédia
Adams I.
N
quebec
Ruiss. England
Chasseurs Bk.
Stewart Bk.
Ruiss. Moores
Babcock Bk.
RESTIGOUCHE RIVER
new brunswick
Dawson Bk.
Rafting Ground Bk.
47°55'00"
66°51'00"
Runnymede
NEW BRUNSWICK
Camp Harmony
0
1 km
Upsalquitch River
Smith Gulch

Figure 1. Study reach.

Upon return to the site on the morning of April 6, evidence was found that a surge of water had gone by, causing fresh high-water marks, exceeding the prevailing water levels by 0.6 m. Moreover, the water level was now higher than in the previous evening and low sections of the riverside roads were flooded. Aerial reconnaissance revealed that the jam now extended much farther upstream for a length of 20 km. The river was open upstream of this jam, at least as far as the Patapedia River, i.e., another 35 km. Large shear walls were present throughout this reach indicating previous ice jamming and release. It thus appears certain that an ice run took place in the early morning hours which is consistent with a local observer's report that the ice was running at a speed of about 20 km·h^{-1} a little upstream of the Upsalquitch.

In the afternoon and evening of April 6, the water level profile near the toe of the jam was surveyed with a level and this was repeated on April 7. The respective results are shown in Figure 3 and do not appear to differ significantly, suggesting a steady-state condition. Spot checks on April 8 also indicated little change of water levels. A changing feature during this time was a lead (i.e., an elongated opening in the ice) near the toe of the jam. When first noticed in the morning of April 6, it was no more than a few metres in size. It gradually grew to much greater width and length, so that by April 9 it had joined a larger lead that had been present since April 5, some 500-m downstream of the toe.

At 08:00 on April 9, evidence was found of overnight jamming and recent release below the jam so that the sheet ice cover holding it in place was now only 2-km long. As a result, the water levels at the jam site were visibly lower. The lead near the toe had extended ~70 m into the ice rubble and the water moved in it at a speed of 2 to 3 $m \cdot s^{-1}$. Ice blocks also moved into the lead, a sign of imminent release which occurred at 09:45. During the release of the jam, water surface velocities near the toe area were estimated by timing the movement of ice floes at 3.2 $m \cdot s^{-1}$, close to an estimate obtained from the simple theory of Henderson and Gerard (1981). After the ice run, the height of shear walls left within the previously jammed reach was measured at several locations. Though crude (Calkins, 1983), this is the only possible estimate of the thickness of a break-up jam. Figure 4 shows these data plotted versus river distance. Noteworthy are (a) the nearly constant-thickness reach (22 to 27 km), which could be considered an "equilibrium" reach; and (b) the sharp increase in thickness near the toe, followed by a decrease.

Figure 2. Photos of jam, p.m., April 5.

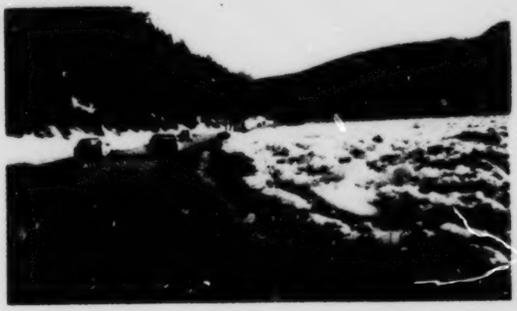

Figure 2a. Looking upstream from near toe; note the high water level threatening the road.

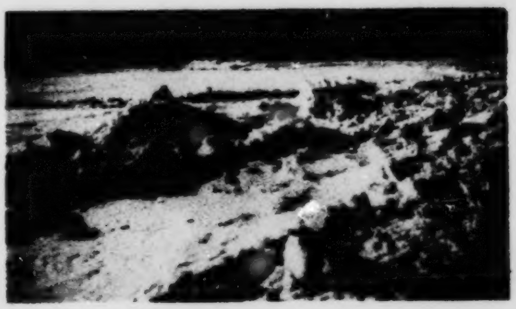

Figure 2b. Looking downstream from near toe; note the pressure ridges and evidence of crushing action between ice slabs.

This is consistent with the plan view of the shear wall, illustrated in Figure 5.

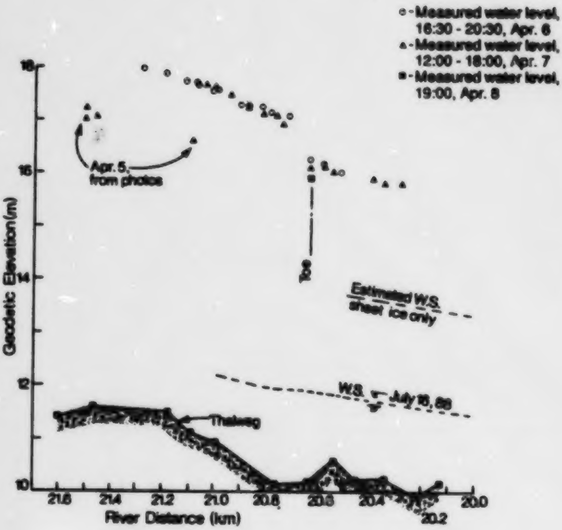

Figure 3. River profile and measured water levels near the toe of the jam. River distance is measured upstream from Old Mission Point, Atholville.

River bathymetry was measured at several cross-sections, spaced closely near the toe area and farther apart elsewhere. These sections are located at 20.535, 20.635, 20.765, 20.995, 21.090, 21.180, 21.460, 21.615, 21.977, 22.420, 23.590, 24.460, 25.740 and 26.410 km, measured along the river, upstream from Old Mission Point in Atholville. The river section at the toe (20.635 km) is shown in Figure 6, along with the April 6 water level and the jam's approximate lower boundary, based on the local shear-wall height. Severe grounding is evident at this site from the considerable reduction of the effective width of the river. More importantly, the area available for unobstructed flow under the jam is only three percent of the total area under the water level (950 m^2).

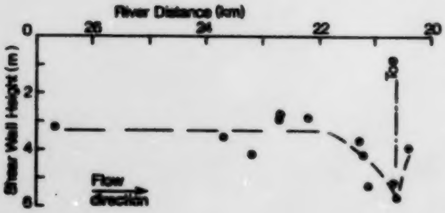

Figure 4. Shear-wall heights measured along the jammed reach.

The available data on water levels, shear-wall heights and river bathymetry provide an opportunity to apply the RIVJAM model, a recently developed algorithm that computes the configuration of break-up jams (Beltaos and Wong, 1990).

Figure 5. Post-release photos.

Figure 5a. Shear wall near Upsalquitch confluence; estimated height above water level ~2 m.

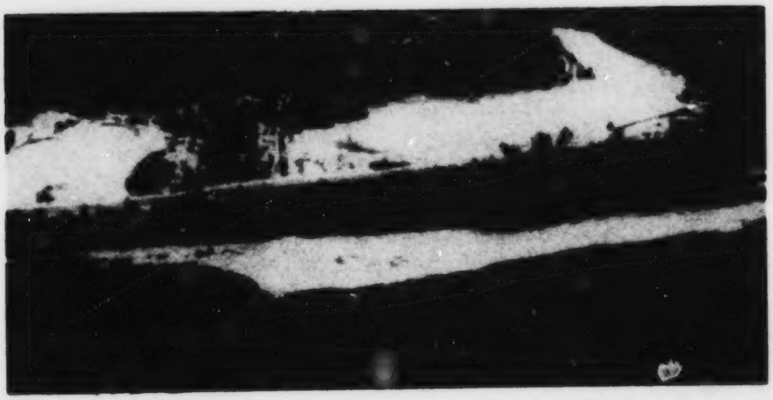

Figure 5b. Aerial view of grounded ice-jam remnants at the (former) toe; note planar geometry indicating rapid increase of jam thickness upstream of the toe and gradual decline downstream.

NUMERICAL SIMULATION

The RIVJAM Model

This is a modified, more robust version of a model developed earlier to investigate the configuration of ice jams near their toe (Beltaos and Wong, 1986). It is based on the flow continuity and momentum equations and the stability conditions of cohesionless, "wide" jams (Pariset *et al.*,1966). The latter is expressed as (Beltaos, 1988):

$$[1] \qquad \frac{dt_s}{dx} = \frac{s_i/(1-s_i)}{(1-p)K_x}\left[S_w\,(1+\beta\,\frac{h}{t_s}) - \frac{\mu(1-s_i)}{s_i}\,\frac{t_s}{B}\right]$$

in which t_s = submerged portion of jam's thickness; x = downstream distance; S_w = water surface slope; h = average depth of flow under the jam; B = channel width at the bottom level of the jam; s_i = specific gravity of ice; p = porosity of the jam; K_x = ratio of longitudinal to vertical stresses within the jam; μ = coefficient related to the internal friction of the jam, as originally defined by Pariset *et al.* (1966); and $\beta = f_i/2f_o$ with f_i = friction factor of the jam's underside and f_o = composite friction factor for the flow under the jam. If a jam is long enough, dt_s/dx will approach zero far upstream of the toe, hence leading to "equilibrium" conditions where jam thickness and flow depth are approximately uniform. Accordingly, if the LHS of Equation 1 is set equal to zero, the equilibrium thickness of the jam can be calculated simply via a relationship that is equivalent to that of Pariset *et al.* (1966).

In the past, it has been generally assumed that the seepage flow through the voids of the jam is negligible so that the entire discharge must flow under the jam. Near the toe of a jam, however, this assumption produces flow velocities far in excess of the "erosion limit" which makes it difficult to predict the local jam profile (e.g., see Flato, 1988). A good example is Figure 6 where, if no seepage is allowed for, the flow velocity would have to be 10 m·s^{-1}! RIVJAM accounts for seepage using the relationship (Wong and Beltaos, 1985).

$$[2] \qquad Q_s = \lambda\,A_j\,\sqrt{S_w}$$

in which Q_s = discharge through the voids of the jam; A_j = wetted area of the jam, and λ = seepage coefficient in m·s^{-1}; the average seepage velocity is equal to $\lambda\,\sqrt{S_w}/p$. As a jam thickens near the toe, both A_j and S_w increase so that an increasing portion of the total discharge (Q_T) flows as seepage. In this manner, the flow velocity underneath the jam does not increase appreciably.

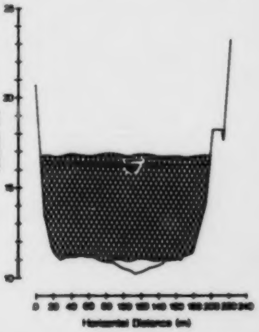

Figure 6. River cross-section at the toe of the jam; note practically grounded condition.

The momentum equation is expressed simply as:

$$[3] \qquad S_w = (\tau_i + \tau_b)/\rho gh = 0.25\, f_o\, \rho u^2$$

in which τ_i, τ_b = flow shear stresses applied on the ice and bed respectively; ρ = density of water; g = gravitational acceleration; and u = average velocity of the flow under the jam.

An additional differential equation is obtained by consideration of the water surface gradient, i.e.,

$$[4] \qquad \frac{dh_o}{dx} = S_o - S_w - \frac{dt_s}{dx}$$

in which h_o = vertical distance of the underside of the jam from a datum line of slope S_o, equal to the average open-water slope in the computation reach. The datum line is located so as to pass through the invert of the cross-section where the computation starts. With Equations 2 and 3, and considering that continuity requires the total flow discharge (seepage through plus flow underneath, the jam) to be constant, it can be shown that S_w, h, and B are fully defined at a given x when h_o and t_s are specified. In essence, therefore, two differential equations (Equations 1 and 4) with two unknowns (h_o and t_s) have to be solved. This is done by a Runge-Kutta numerical technique. Computation may proceed either upstream or downstream starting at a site where the water level and jam thickness are known.

Channel bathymetry is specified by a set of surveyed cross-sections, inputted in the HEC-2 format (U.S. Army Corps of Engineers, 1979). Between successive sections, the bathymetry is interpolated linearly.

Coefficients

Several coefficients must be specified in order to run the model. They relate to ice and water properties; hydraulic resistance and seepage characteristics of the jam; and material properties of the jam, assumed to behave as a floating granular mass.

The coefficient (f_o) which relates the average shear stress [= 0.5 ($\tau_i + \tau_b$)] to the average flow velocity is empirically expressed as:

$$[5] \qquad f_o = c\, t_s^{m_1}\, h^{-m_2}$$

in which various choices of the constants c, m_1, m_2 represent different assumptions concerning resistance. For example, $m_1 = m_2 = 0$ implies that f_o = constant = c; while $m_1 = 0$, $m_2 = 1/3$ implies n_o = constant = $0.10\sqrt{c}$ (n_o = Manning roughness coefficient). Where $m_1 > 0$, an effect of jam thickness on resistance is implied, as has been found empirically (Nezhikhovskiy, 1964; Beltaos, 1988). By examining data on equilibrium jams, Beltaos and Wong (1986) deduced $c \approx 0.5$ and $m_1 = m_2 = 1.2$. The coefficient β (= $f_i/2f_o$) is assumed to be constant along a jam for simplicity, even though this is not necessarily true. Often, β is fixed at 0.50 but could vary between 0.3 and 0.8 (Beltaos, 1983). User-imposed limits can be applied to f_0 in cases where Equation 5 gives implausibly high or low values, e.g., near the toe or head of the jam.

Equation 1 indicates that it is the product of K_x and 1-p that governs the solution rather than the individual values of K_x and p. Since p is not known by measurement, it can be fixed at the commonly quoted value of 0.40 and K_x be allowed to vary so as to reproduce the appropriate value of $K_x(1 - p)$. The only field-based determination of K_x gave $K_x(1 - p) = 6$, so that $K_x = 10$ (Beltaos, 1988). The coefficient μ has an average value of 1.2 to 1.3 but could be as low as 0.8 and as high as 2.0.

The seepage coefficient (λ) is not known under natural conditions. Laboratory experiments with plastic blocks, simulating natural ice floes, and theoretical considerations have indicated that (Wong and Beltaos, 1985):

$$[6] \qquad \lambda/\sqrt{gh_i} = \sqrt{\alpha\, p^3/(1 - p)}$$

in which h_i = thickness of ice blocks in the jam. The coefficient α depends on block orientation. For randomly-oriented blocks, as is expected to be the case for the Restigouche jam, $\alpha = 1.4$. The porosity (p) of the laboratory block accumulations varied between 0.32 and 0.75 and averaged 0.56. Extrapolating these results to the present case ($h_i = 0.60$ m), gives $\lambda = 1.0$ to 1.8 $m \cdot s^{-1}$, respectively for $p = 0.40$ (commonly assumed value for ice jams) to 0.56 (average laboratory value).

Application to Restigouche River Jam

The water levels obtained on April 6 and 7 and the shear-wall heights measured after the release of the jam provide an excellent opportunity to study the characteristics of jams near the grounding condition. However, the flow discharge has to be evaluated first. During the break-up, water-level gauge records are not helpful in this regard because of the backwater effects of ice jams. Using the measured water levels along the jam and the shear-wall heights, together with plausible friction factors, the discharge was estimated as 290 $m^3 \cdot s^{-1}$, applicable to the relatively steady-state period of April 6 to 8. Another approach is to extrapolate pre-break-up (i.e., prior to April 5) discharge estimates obtained on the basis of gauge readings and hydraulic analysis of flow with sheet ice cover. This resulted in 350 $m^3 \cdot s^{-1}$. Though approximate, these estimates, define a range of expected discharge values.

Numerous runs of RIVJAM were made and good performance (Figure 7) was obtained with the following set of parameters: $p = 0.40$; $c = 0.40$; $m_1 = m_2 = 1.0$; $\beta = 0.50$; $K_x = 12.0$; $\mu = 0.80$; $\lambda = 2.5$ $m \cdot s^{-1}$; total flow discharge = 330 $m^3 \cdot s^{-1}$. This set was not defined by rigorous optimization but by varying the parameters within plausible ranges until a "satisfactory" prediction was obtained. The latter was based on three criteria, (a) accurate reproduction of the measured water levels near the toe

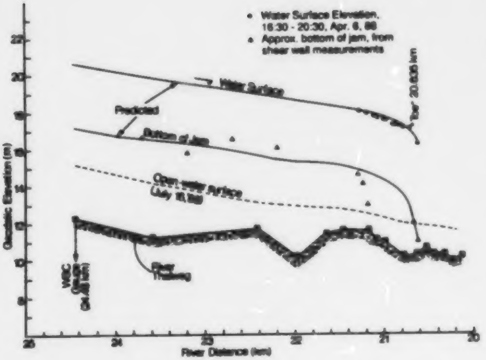

Figure 7. Comparison between RIVJAM predictions and measurements for the April 6 water level survey; note "equilibium" condition predicted to start a few river widths above the toe.

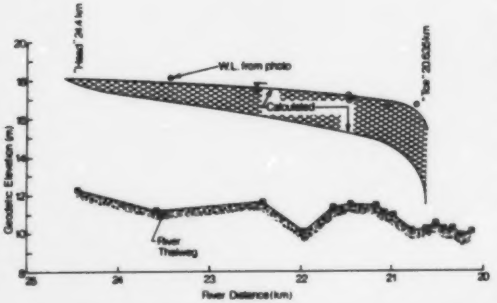

Figure 8. Comparison between RIVJAM predictions and measurements for the short jam on April 5; the water levels are crude (from photos) but head location is predicted to within a river width.

of the jam; (b) approximate reproduction of ice-jam thickness as deduced from shear-wall heights; and (c) prediction of an equilibrium, or constant-thickness, condition starting some distance above the toe which should have been the case, given the considerable length of the jam on April 6. Table 1 shows that the calculated flow velocity is about 0.5 $m \cdot s^{-1}$ in the "equilibrium" reach but attains a maximum value of 0.7 $m \cdot s^{-1}$ just upstream of the toe, before dropping to 0.4 $m \cdot s^{-1}$ at the toe itself. The percentage of flow going through the rubble steadily declines from nearly 100% at the toe to 12 to 15% in the "equilibrium" reach.

An additional application of the model can be made by considering the few approximate water levels for April 5 that were obtained from photographs. The main interest here is to check whether RIVJAM can predict the location of the head of this short, non-equilibrium jam. While the length of a jam is governed by the amount of ice fed into it, the longitudinal variations of thickness and water level are controlled by the processes that RIVJAM simulates. Therefore, predicting the location of the head (zero thickness) while simultaneously reproducing

Table 1. Computed flow characteristics from the April 6 ice jam.

Distance upstream of the toe (m)	Submerged thickness of the ice jam (m)	Water surface slope	Average flow velocity under the jam (m·s^{-1})	Percentage of flow going through the ice rubble (%)
0 (toe)	5.2	0.019	0.42	96
5	5.1	0.018	0.44	93
10	5.0	0.016	0.54	86
20	4.8	0.013	0.63	74
30	4.6	0.0099	0.67	64
50	4.4	0.0068	0.67	51
70	4.2	0.0052	0.65	43
100	4.0	0.0039	0.62	36
150	3.8	0.0028	0.60	29
200	3.7	0.0022	0.58	25
300	3.5	0.0016	0.55	20
500	3.3	0.0012	0.53	17
700	3.2	0.00094	0.49	15
1000	3.1	0.00071	0.49	12
1500	3.3	0.00082	0.51	13
2000	3.2	0.00081	0.47	14
3000	3.3	0.00083	0.53	12
4000	3.4	0.00096	0.51	15
5000	3.3	0.00092	0.50	15

Note: After a distance of about 1,000 m, a condition of approximate equilibrium is attained.

the water-level profile along the jam, is a partial test of the model. Figure 8 indicates that the predicted location is within 200 m (about a river width) of the observed while water levels are simulated correctly. It was necessary, however, to increase c to 0.60 (from 0.40) which is plausible because jams are expected to become smoother with time by thermal erosion. The flow discharge was reduced slightly to 315 m^3·s^{-1} which suggests that the rise in water levels during the night of April 5 to 6 was primarily caused by the lengthening and thickening of the jam.

DISCUSSION

The two applications of RIVJAM to the April 5 and April 6 ice jams have been encouraging because the values of the coefficients used to obtain good predictions are plausible. There is one discrepancy, however, and it results from the model value of 2.5 $m \cdot s^{-1}$ for λ which exceeds what would be expected by extrapolating laboratory data, as discussed earlier. The extrapolation is based on existing theories which require that λ vary in proportion to the square-root of particle (or ice block) size (Equation 6). However, re-analysis of available data on flow through rockfill suggests that λ grows with particle size faster than implied by the square-root relationship (Beltaos, unpublished). This means that λ could well be more than 1.0 to 1.8 $m \cdot s^{-1}$ in nature, though it is not known whether 2.5 $m \cdot s^{-1}$ is reasonable. It is also possible that the unobstructed flow area shown in Figure 6 is enlarged by dislodgement and transport of ice blocks under the jam. In that case, the percentage of discharge flowing through the unobstructed area would increase and hence the calculated value of λ would decrease. Clearly, more studies of very thick or grounded jams are needed. Relatively steep and wide rivers with good water's edge access, such as the Restigouche, are the most suitable.

An important aspect that cannot be quantified at present, pertains to the conditions downstream of the toe. Our measurements of April 6 and 7 indicate water levels that are higher than those estimated for flow under sheet ice cover without any ice-block accumulation underneath (Figure 3). It follows that between the toe of the jam and the end of under-ice accumulation, there should be a transitional reach in which the thickness of the accumulation decreases from a maximum at the toe to zero. In the present case, it is not possible to adequately describe this transition because our surveys did not extend far enough downstream.

The abrupt change in water surface slope at the toe suggests a change in hydraulic conditions, likely related to the open lead mentioned earlier. It is estimated that this lead could carry most of the discharge at the relatively mild slope downstream of the toe ($\approx$0.0015 as opposed to $\approx$0.02). It is not known why these leads form but they are very conmon and seem to be significant with respect to the eventual release of the jam. The fact that the jam remains stable even long after the lead has attained appreciable dimensions is also not well understood but could perhaps be explained by the development of cohesion with time by freeze-bonding (e.g., see Schaefer and Ettema, 1986). Eventually the lead becomes so wide that the local strength of the jam is exceeded and the ice rubble moves into the lead, followed by a general surge of ice and water.

SUMMARY AND CONCLUSIONS

A grounded jam that formed in the Restigouche River during the 1988 break-up has been described along with pertinent measurements and data interpretation. It was found that if seepage flow through the voids of the jam is considered, it is possible to predict the configuration of the jam near the toe. This can be accomplished using a numerical algorithm, such as RIVJAM, that solves the appropriate differential equations. On the other hand, if seepage had been neglected, extremely high flow velocities, far exceeding the jam erosion limit, would have to be postulated.

In general, the various coefficients and parameters used in the model were in agreement with previous findings elsewhere. However, the seepage coefficient was about twice what would have been projected from laboratory experiments. This could be due to a size effect or to ice transport under the jam but more information is needed before any conclusions can be made. Wide and steep rivers like the Restigouche are suitable for this purpose because they are subject to formation of very thick or grounded jams. Downstream of the toe of the jam, an open lead developed and progressively grew in size during the 3½ days that the jam was in place. The final release of the jam was preceded by ice discharges into the lead, much as has been observed elsewhere. More detailed information is needed with regard to the reach downstream of the toe in order to understand the conditions of release.

ACKNOWLEDGMENTS

W. Moody of NWRI conducted the hydraulic surveys following the break-up event, including channel bathymetry, water surface slopes and ice jam elevation surveys from photos. R. Lane of Water Survey of Canada, Fredericton, assisted in establishing data-recording and accessing devices in the gauge shed and in obtaining ice thicknesses during the winter. W. Waite assisted in setting up hydrometeorological instruments in the study area and provided specialized weather forecasts for the lower Restigouche reach. L. Irvine, our local observer, made pre-break-up and break-up observations and provided helpful advice for subsequent hydraulic surveys.

LIST OF SYMBOLS

A_j	wetted area of the jam (m^2)
B	channel width at the level of the bottom surface of the jam (m)
c	coefficient used in Equation 5 ($m^{-m_1 \div m_2}$)
f_i	friction factor of the jam's underside (dimensionless)
f_o	composite friction factor for the flow under the jam (dimensionless)
g	gravitational acceleration ($m \cdot s^2$)
h	average depth of flow under the jam (m)
h_i	thickness of ice blocks in the jam (m)
h_o	vertical distance of the underside of the jam from a datum line (m)
K_x	ratio of longitudinal to vertical stresses within the jam (dimensionless)
m_1, m_2	coefficients used in Equation 5 (dimensionless)
n_o	composite Manning roughness coefficient for the flow under the jam ($m^{-1/3} \cdot s^{-1}$)
p	porosity of the jam (dimensionless)
Q_s	flow discharge through the voids of the jam ($m^3 \cdot s^{-1}$)

Q_T	total flow discharge ($m^3 \cdot s^{-1}$)
s_i	specific gravity of ice (dimensionless)
S_o	slope of data line (dimensionless)
S_w	water surface slope (dimensionless)
t_s	submerged portion of jam thickness (m)
u	average velocity of flow under the jam ($m \cdot s^{-1}$)
x	longitudinal distance measured along the river (m or km)
α	coefficient used in Equation 6 (dimensionless)
β	ratio $f_i/2f_o$ (dimensionless)
λ	seepage coefficient ($m \cdot s^{-1}$)
μ	coefficient related to the internal friction of the jam (dimensionless)
ρ	density of water ($kg \cdot m^3$)
τ_i, τ_b	flow shear stresses, respectively applied on the jam underside and the river bed ($N \cdot m^2$)

REFERENCES

BELTAOS, S., 1983. River ice jams: theory, case studies and applications. Journal of Hydraulic Engineering, American Society of Civil Engineers, 109(10), 1338-1359 and discussion.

BELTAOS, S., 1988. Configuration and properties of a breakup jam. Canadian Journal of Civil Engineering, 15(4), 685-697

BELTAOS, S. and J. WONG, 1986. Downstream transition of river ice jams. Journal of Hydraulic Engineering, Hydraulics Division, American Society of Civil Engineers, 112(2), 91-110

BELTAOS, S. and J. WONG, 1990. Ice jam configuration: second generation model. NWRI Contribution No.90-65, National Water Research Institute, Environment Canada, Burlington, Ontario, submitted to American Society of Civil Engineers' Cold Regions Engineering Conference, February 1991, Hanover, New Hampshire, 12 pp.

CALKINS, D.J., 1983. Ice jams in shallow rivers. Canadian Journal of Civil Engineering, 10(3), 538-548

FLATO, G.M., 1988. Calculation of ice jam profiles. M.Sc. thesis, Department of Civil Engineering, University of Alberta, Edmonton, Alberta, 196 pp.

GIDAS, N.K., 1981. Recherche sur les meilleures solutions contre les inondations de la Matapédia causées pas les débâcles. Comptes rendus, Symposium international sur la glace de l'AIRH, Association internationale de recherches hydrauliques, Vol.1, 27-31 juillet 1981, Québec (Québec), 266-275

HENDERSON, F.M. and R. GERARD, 1981. Flood waves caused by ice jam formation and failure. Proceedings, IAHR International Symposium on Ice, International Association for Hydraulic Research, 27-31 July 1981, Québec, Quebec, Vol.1, 277-287; Discussion, 288-297

LEGER, R.D., 1986. A report on ice jams on the Restigouche River basin. Department Report No.I-8601, New Brunswick Department of Municipal Affairs and Environment, Fredericton, New Brunswick, 27 pp.

NEZHIKHOVSKIY, R.A., 1964. Coefficients of roughness of bottom surface of slush-ice cover. Soviet Hydrology, Selected Papers No.2, American Geophysical Union, Washington, D.C., 127-150

PARISET, E., R. HAUSSER and A. GAGNON, 1966. Formation of ice covers and ice jams in rivers. Journal of the Hydraulics Division, American Society of Civil Engineers, 92(HY6), 1-24

SCHAEFER, J.A. and R. ETTEMA, 1986. Experiments on freeze-bonding between ice blocks in floating ice rubble. Proceedings, 8th International Symposium on Ice, International Association for Hydraulic Research, 18-22 August 1986, Iowa City, Iowa, Vol.I, 401-413

U.S. ARMY CORPS OF ENGINEERS, 1979. HEC-2 water surface profiles: users manual. Hydrologic Engineering Laboratory, U.S. Army Corps of Engineers, Davis, California, July, 39 pp. + appendices

WONG, J.S. and S. BELTAOS, 1985. Preliminary study of grounded ice accumulations. NWRI Contribution No.85-09, Hydraulics Division, National Water Research Institute, Environment Canada, Burlington, Ontario, February, 30 pp.

WATER BALANCE AND GEOCHEMISTRY STUDIES IN A TUNDRA WATERSHED, DISTRICT OF KEEWATIN, NORTHWEST TERRITORIES

G.G. Bursey[1], T.W.D. Edwards[2] and S.K. Frape[2]

[1]Fracflow Consultants Inc.
36 Pearson Street
St. John's, Newfoundland
A1A 3R1 CANADA

[2]Waterloo Centre for Groundwater Research
Department of Earth Sciences
University of Waterloo
Waterloo, Ontario
N2L 3G1 CANADA

ABSTRACT

Results are reported from hydrological field studies in the summers of 1988 and 1989 in a tundra watershed in the eastern Arctic. Investigations of the water cycle in terrain underlain by continuous permafrost are being conducted using isotopic and geochemical data from precipitation, surface water, and active-layer ground water, coupled with hydrogeological and hydrological field observations.

Water-balance calculations based primarily on isotopic data ($^{18}O/^{16}O$ *and* $^{2}H/^{1}H$ *ratios) indicate wide variation in the degree of evaporation from various levels in the drainage system. Evaporation can account for 40% or more of the discharge from shallow tundra ponds, whereas the average annual vapour discharge from the entire watershed is likely about 10%, in spite of the arid low-arctic climate. Evaporative losses are minimized in part by the relative importance of subsurface storage and flow within the active layer.*

Surface and subsurface waters are characterized by extremely low solute concentrations and are undersaturated with respect to most mineral phases, except the amorphous forms of silica and $Fe(OH)_3$*. High iron contents (up to 0.68* $mmol \cdot L^{-1}$*) in some ground-water samples may stem from complexing with dissolved organic carbon. Other processes such as cation exchange and freezing influence the chemistry of ground waters within the active layer.*

INTRODUCTION

The results from water-balance and geochemistry studies in the central District of Keewatin presented here provide insight into the nature of water cycling in perennially-frozen terrain. Understanding the factors controlling water quantity and quality are critical to the sound management of water resources over the vast low-

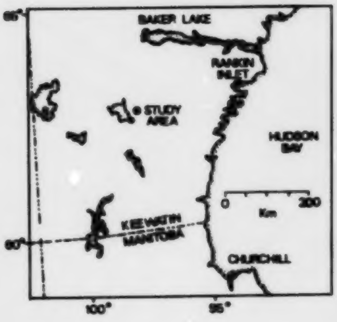
BAKER LAKE
RANKIN INLET
STUDY AREA
HUDSON BAY
0
200
Km
KEEWATIN
MANITOBA
CHURCHILL
60°
100°
95°

Figure 1. Location map of the study area.

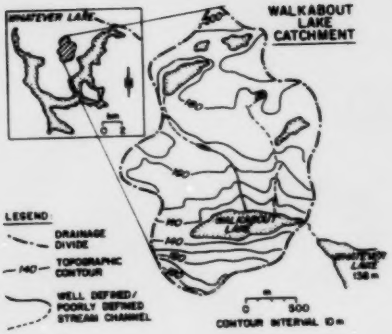
WHATEVER LAKE
WALKABOUT LAKE CATCHMENT
0
2
km
LEGEND
DRAINAGE DIVIDE
140
TOPOGRAPHIC CONTOUR
WELL DEFINED/ POORLY DEFINED STREAM CHANNEL
WALKABOUT LAKE
WHATEVER LAKE 138 m
m
0
500
CONTOUR INTERVAL 10 m

Figure 2. Location map of the Walkabout Lake catchment, with respect to the main Whatever Lake watershed showing drainage area and relief: contour interval is 10 metres.

arctic tundra of central Canada. The present studies seek to answer fundamental questions about the storage and movement of water as it passes through the hydrological system, including consideration of the interactions between ground waters and surface waters, and geochemical controls on its chemistry. Here we summarize the results of detailed field investigations conducted in 1989 that have permitted modification and refinement of preliminary interpretations from field reconnaissance in 1988 (see Bursey *et al.*, 1990). A more exhaustive discussion of these studies appears elsewhere (Bursey, 1990).

Setting

The study area is located in the central District of Keewatin, N.W.T. (62°41'N, 97°03'W; Figure 1), about 170 km north of the tree line, and is referred to as the "Whatever" Lake watershed. Field work was conducted during the periods of July 28 to August 11, 1988 and June 25 to August 8, 1989. The watershed covers approximately 850 km^2 and discharge is directed through Whatever Lake. These investigations were focused on a small headwater catchment, tributary to Whatever Lake (Figure 2), and its informally-named "Walkabout" Lake. This catchment has a surface area of approximately 3.5 km^2 and a maximum relief close to 60 m. Topographic gradients range from 0 to 0.2 and a mean value of about 0.1 is considered to represent the average water-table gradient. Discharge is through Walkabout Lake, which has a surface area of about 0.17 km^2, a maximum depth of 11 m, and an average depth of 4.4 m.

The study area lies within the Low Arctic Ecoclimatic Region (Ecoregions Working Group, 1989): the mean annual precipitation is likely less than 300 mm and the mean annual air temperature is estimated to be -12°C. Mean monthly temperatures above freezing occur in the June through September period. The autumn and winter months are dominated by intense arctic air systems moving east and southeast. A shift in circulation patterns occurs in spring, creating less-stormy summers (July, August) that have more variable winds and low pressure centres (Maxwell, 1986).

Continuous permafrost beneath the watershed may be hundreds of metres thick, based on Brown's (1978) estimate for Baker Lake (175 km NNE), but its extent below lakes is not known. The depth of seasonal thaw (active-layer thickness) depends on such factors as the texture and thickness of the insulating-vegetative cover, the saturation state, and the proximity to water bodies. Thaw depths measured in this study and by others (Shilts and Dean, 1975; Dalton, 1981) ranged between 15 and 200 cm.

The Whatever Lake watershed lies within the Churchill Province of the Canadian Shield. Gneisses of granitic to dioritic composition predominate with less frequent mafic units of volcanic affinity (Eade, 1986). The overburden is glacially-derived and discontinuous, averaging about 3 m thick across the region (Kaszycki and Shilts, 1979). The local till comprises largely quartz and feldspars, with minor micas and amphiboles. The area lies within the dispersal train of hematitic sedimentary and volcanic rocks of the Proterozoic Dubawnt Group.

The active layer has a complicated small-scale stratigraphy due to cryoturbation and redistribution of material caused by liquefaction (e.g., mudboil development). The till is dominantly sandy, with moderate silt and low clay contents. Hydraulic conductivities (K) measured by rising head tests (Hvorslev, 1951) average 2.9×10^{-4} $\mathrm{cm \cdot s^{-1}}$ ($\sigma = 6.8 \times 10^{-4}$, $n = 18$). The hydraulic character of peat (5 to 25-cm thick) was not investigated, but greater K values of 10^{-3} $\mathrm{cm \cdot s^{-1}}$ are expected, considering measurements in peat from similar terrain (Roulet and Woo, 1986).

Analytical Methods

Stable-isotope analyses were performed on untreated water samples in the Environmental Isotope Laboratory, University of Waterloo, using standard techniques (Coleman *et al.*, 1982; Epstein and Mayeda, 1953). The $^{2}H/^{1}H$ and $^{18}O/^{16}O$ ratios are expressed in "δ" notation as permil (‰) deviations from the international standard SMOW (Standard Mean Ocean Water):

$$[1] \qquad \delta = \frac{R_{sample} - R_{standard}}{R_{standard}} \times 1000\ ‰$$

where, $R = {}^{18}O/{}^{16}O$ or $^{2}H/^{1}H$. Analytical uncertainties are ± 0.2‰ for $\delta^{18}O$ and ± 4‰ for $\delta^{2}H$.

In the field, water samples for chemical analysis were filtered through 0.45 µ Millipore filters, acidified (cations only), and 50 mL aliquots titrated for alkalinity as HCO_3^-. A HACH alkalinity kit was used in 1988 for colorimetric titrations of unfiltered waters. Gran titrations (Stumm and Morgan, 1981) were conducted on filtered waters in 1989 to minimize suspected interference from dissolved organic carbon. Major ion and dissolved organic carbon analyses were performed at the Water Quality and the Organic Geochemistry Laboratories respectively, University of Waterloo.

Hydrology

Permafrost has a major influence on ground-water flow at this site. The low permeability of frozen material restricts infiltration and impedes ground-water movement. Depression of the frost-table during the thaw season creates an irregular surface, leading to complex subsurface flow patterns within the overlying active layer that may be unrelated to surface topography (Woo and Steer, 1983). A relief of about 1 m was measured for the frost-table at our site by the middle of the thaw season (late-July to early-August). Summer rainfall is typically insufficient to maintain saturation and the water-table gradually declines over the season with the drainage of melting ground-ice and deepening of the frost-table.

Unusually wet conditions during field work in 1989 emphasized the importance of subsurface storage and flow within the active layer. For example, negligible surface run-off occurred in the Walkabout catchment despite a rainfall that approached the mean annual precipitation for Baker Lake within a span of only five days.

Seasonal sources of moisture can be identified on a plot of $\delta^{18}O$ versus δ^2H (Figure 3). Snow from the winter of 1989 is slightly depleted in both ^{18}O and ^2H compared with snow sampled in 1988, and both fall on the Global Meteoric Water Line (GMWL, Figure 3, line 1; $\delta^2H = 8\ \delta^{18}O + 10$) of Craig (1961). The cluster of rain samples from 1989 plots to the right of the GMWL (except for one sample), as does the single rain sample obtained in 1988. Although direct sampling of fall precipitation (September to October) was not undertaken, its isotopic composition is assumed to be equivalent to that of the active-layer ground ice, which should represent stored fall recharge: this is evident from the different isotopic signature of ground ice relative to summer rainfall (Figure 3).

The bulk isotopic composition of precipitation (δ_p) likely falls within the narrow mixing triangle defined by mean compositions of the seasonal components (Figure 3). δ_p should lie close to a weighted regression line (Figure 3, line 2: $\delta^2H = 7.4\delta^{18}O - 5.7$; $r = 0.998$) through these data, representing a Local Meteoric Water Line (cf. Fritz *et al.*, 1987). The intersection of this line with the Local Evaporation Line (Figure 3, line 3: $\delta^2H = 5.5\delta^{18}O - 49$; $r = 0.977$), defined by regression of surface water compositions, provides the best estimate for δ_p ($\delta^{18}O = -22.7‰$, $\delta^2H = -174‰$).

Water-Balance Calculations

Evaporation is an important component of the water budget that is often difficult to assess, especially in remote locations. Isotope mass-balance analysis takes advantage of the progressive isotopic enrichment of waters affected by evaporation to estimate vapour loss. This technique can be applied at various scales within the drainage system and does not require detailed instrumentation.

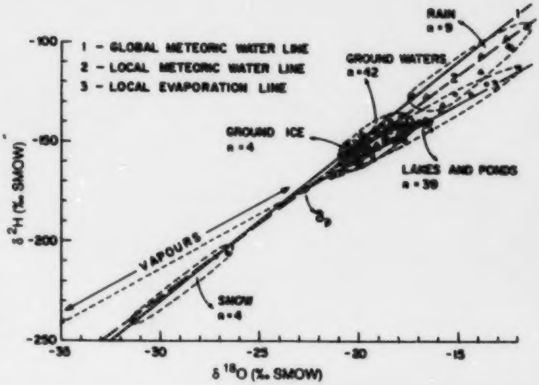

***Figure 3.** $\delta^{18}O$ versus δ^2H diagram showing representative data for sampled waters. Isotopic behaviour is characterized with three lines: 1 = Global Meteoric Water Line; 2 = Local Meteoric Water Line; 3 = Local Evaporation Line. The isotopic composition of mean annual precipitation (δ_p) is estimated by the intercept between lines 2 and 3.*

Water balance for a headwater drainage area is represented by:

[2] $$P = O + E$$

where, P = mean annual precipitation or total input, O = surface plus subsurface outflow, and E = evaporative outflow.

For our purposes, O can be separated into isotopically altered (i.e., evaporatively enriched) and unaltered components, therefore:

[3] $$P = U + A + E$$

where, U = unaltered meteoric water, and A = altered water.

Our use of the term unaltered meteoric water is used with reference to the Local Meteoric Water Line that has been established here. The isotope mass balance expressions are:

[4] $$P\delta_{px} = U\delta_{ux} + A\delta_{ax} + E\delta_{ex}\text{, and}$$

[5] $$P\delta_{py} = U\delta_{uy} + A\delta_{ay} + E\delta_{ey}$$

where δ refers to the oxygen (x) and hydrogen (y) isotope compositions of the respective components. Equations 3, 4, and 5 can be solved with isotopic data to yield estimates of U, A, and E as percentages of P. An analogous approach can be used to estimate evaporation from a lake by accounting for inflow as a mixture of unaltered precipitation falling directly on the lake plus altered and unaltered water from the catchment. This approach assumes that the lakes are well-mixed.

Previous efforts to evaluate water balance in lakes, using either oxygen or hydrogen isotope data (e.g., Welhan, 1974; Zimmermann, 1979), have been hampered by difficulties in estimating the isotopic separation between water and escaping vapour. The present studies benefit by combining oxygen and hydrogen isotope data to constrain possible compositions for δ_e (i.e., the location of δ_e in $\delta^{18}O$ versus δ^2H space). The mean composition of vapour lost from different parts of the watershed should vary along the Local Evaporation Line (or along its extension to the left of the Local Meteoric Water Line: Figure 3, line 3). This vapour will be depleted in ^{18}O and ^2H with respect to the associated vapour source by varying amounts, depending on local temperature, humidity and wind conditions. We estimate the mean isotopic separation between altered water and derived vapour (δ_a-δ_e) to have a maximum value of about 24‰ for $\delta^{18}O$: this estimate is based on an analysis of evaporation pan data obtained in 1989 using the methods of Welhan (1974).

By accounting for the displacement of samples from δ_p ($\delta^{18}O$ = -22.7‰, δ^2H = -174‰) along the Local Evaporation Line, it is possible to quantify vapour losses from water at different levels in the drainage system (that is by solving Equations 3 to 5 above). The small isotopic offset of surface outflow from Whatever Lake ($\delta^{18}O$ = -20‰, δ^2H = -158‰) for example, represents a maximum of 10% vapour loss from the entire watershed; the vapour losses may exceed 40% from small, shallow ponds exhibiting more enriched isotopic compositions (e.g., $\delta^{18}O$ = -12‰, δ^2H = -113‰). Most of the vapour losses from the watershed probably occur from the tributary catchments rather than from the lake's surface, considering the difference in surface areas: Whatever Lake covers 3.2% of the total watershed area. This is also demonstrated for the Walkabout Lake catchment whereby total evaporation is estimated at 10%, while about 1% originates directly from the lake surface: Walkabout Lake covers 4.9% of the total catchment area. Varying losses to evaporation would be expected for other catchments tributary to Whatever Lake, depending on topography, amount of bedrock exposure, depth and area of surface water bodies, and other factors.

Geochemistry

Typical chemical data for lakes and ponds, and ground waters from springs and piezometers are shown in Table 1. The complete data set can be found in Bursey (1990). The mean charge deficit for surface waters is 14% (n = 37) and the average for ground waters is 13% (n = 20). This analytical charge imbalance is usually caused by greater total cation than total anion concentrations.

The chemical quality of waters in this region is influenced by dissolved organic carbon (DOC) and it is significant that samples with high concentrations (0.4 to 1.3 mmol·L^{-1}) are associated with excess cations. This situation is clarified by judging

Table 1. Typical analytical results for surface and subsurface waters in the study area: values of electrical conductivity have been corrected to 25°C.

	Surface Waters			Springs			Piezometers		
	GB31	GB45	GB46	GB57	GB133	GB134	GB65	GB132	GB141
Depth (cm)	--	--	--	--	--	--	50	38	116
pH	7.1	7.3	6.7	6.5	6.2	6.3	6.8	6.2	6.6
Eh (mV)	--	481	458	468	571	512	234	421	265
DO (mg·L^{-1})	--	--	--	9.6	--	--	--	0.7	0.2
Temp (°C)	13.0	16.5	13.5	4.0	14.0	3.5	20.0	11.5	15.0
Cond (25°C)	17	30	17	57	28	58	66	203	262
Ions (mmol·L^{-1} * 100, unless otherwise stated)									
Ca^{2+}	11	6.5	3.1	10	5.2	9.9	9.7	4.6	26
Mg^{2+}	2.9	4.4	2.2	5.5	4	4.2	6.8	3.5	12
Na^+	3.6	3.9	2.5	4.1	3.0	3.8	11	5.6	9.1
K^+	0.9	0.6	0.7	1.4	0.3	0.5	3.5	0.8	3.9
Fe	0.6	0.5	0.6	2.9	0.5	0.6	2.7	68	5.3
Mn^{2+}	--	--	0.0	0.0	--	--	0.2	0.4	1.3
SiO_2	--	--	--	23	19	20	38	45	79
HCO_3^-	23	18	6.1	27	19	24	44	110	86
Cl^-	1.0	2.0	2.0	1.8	0.5	1.4	6.1	3.0	4.5
SO_4^{2-}	0.2	0.4	0.5	0.5	0.8	2.0	0.5	0.8	0.9
Charge Balance (%)	14.8	14.0	24.3	18.3	3.2	9.1	2.4	18.4	4.9
DOC	--	--	51	--	51	--	--	130	84
Saturation Indices									
Calcite	-2.6	-2.7	-4.1	-3.1	-3.7	-3.4	-2.6	-3.3	-2.2
Solomite	-5.7	-5.5	-8.4	-6.7	-7.5	-7.4	-5.3	-6.8	-4.7
Gypsum	-5.0	-4.8	-5.0	-4.5	-4.6	-3.9	-4.6	-4.8	-4.0
$Fe(OH)_3A$	2.6	2.6	2.2	2.7	1.7	1.8	1.7	3.6	1.7
SiO_2A	--	--	--	-0.5	-0.8	-0.5	-0.6	-0.4	-0.2

the relationship between SiO_2 and DOC (Figure 4). SiO_2 and DOC are used respectively to represent the contributions of acid buffering from inorganic and organic carbon sources. The concentrations of dissolved SiO_2 are directly derived from

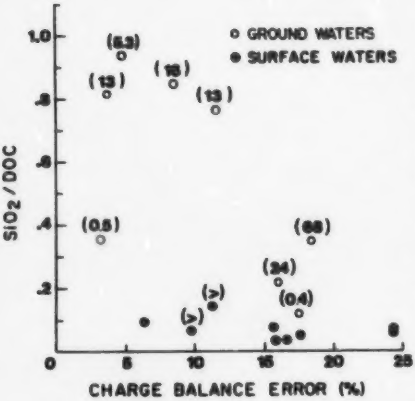

Figure 4. Charge balance errors are plotted against the SiO_2/DOC molar ratio for ground-water and surface-water samples. In brackets, total iron concentrations are given in mmol·L^{-1} X 100, while the ">" indicates surface-water samples with SiO_2 above the detection limit of 0.033 mmol·L^{-1}: SiO_2/DOC ratios for samples with SiO_2 below this limit are calculated for detection limit concentrations.

mineral weathering and are therefore presumed to reflect the amounts of dissolved inorganic carbon (DIC) in these waters. The choice of SiO_2 rather than one of the major ions is based on Antweiler and Drever's (1983) work that shows SiO_2 behaves independently of DOC concentrations, unlike the ions Ca^{2+}, Mg^{2+}, Na^+, K^+, Al, and Fe. The concentrations of DOC are good indicators of the contribution of organic acids to the acid neutralizing capacity of waters, as exemplified by numerous studies (e.g., Litaor and Thurman, 1988).

The trend for ground waters that have total iron concentrations above 0.5 mmol·L^{-1}, shows that decreasing SiO_2/DOC ratios are associated with increasing charge balance errors, and generally more total iron (Figure 4). Complexing of iron by DOC is evident and is the only reasonable explanation for high iron levels in oxidized, intermediate pH waters (e.g., sample GB132, Table 1), as particulate iron oxides or hydroxides were not observed in filtered samples. Sample preservation by acidification will release any complexed iron to solution and because the anion contribution from organic acids is unknown, excess total cation concentrations are calculated.

The reason for the absence of a relation for the surface waters similar to that for the ground waters (Figure 4) is not certain, but it is also not surprising considering that surface and subsurface waters are parts of two contrasting geochemical environments. A major difference is in the partial pressures of CO_2 gases in these waters, which are usually greater in ground waters as a consequence of the respiration and decay of organic matter (see Drever, 1988). The trend for surface waters in Figure 4 does suggest that the DIC is low relative to the DOC, and therefore the latter is probably the more important source for alkalinity.

SiO_2 is a major component of the active-layer ground waters suggesting that silicate minerals are a major source of solutes. The dilute nature of the waters attest to slow rates of weathering however, especially since the active layer remains frozen for about eight months of the year.

The degree of chemical interaction between active layer solids and waters, and the chemical condition of surface waters were evaluated with an equilibrium thermodynamics approach using the PHREEQE (Parkhurst *et al.*, 1980) and WATEQF (Plummer *et al.*, 1976) codes. The PHREEQE code was preferred because of its simplicity and it was used to compute the results presented in Table 1. WATEQF was used to supplement the calculations by PHREEQE because of the more extensive database of the former code.

In these codes, saturation indices (SI) describe the potential for mineral dissolution ($SI < 0$), precipitation ($SI > 0$) and equilibrium with the aqueous phase ($SI = 0$). Waters from the study site are extremely undersaturated with respect to most minerals, except the amorphous forms of $Fe(OH)_3$ and SiO_2 (Table 1). Edmunds and Kinniburgh (1986) commented that calcite is likely absent if $SI_{calcite}$ is less than -0.3. It follows that calcite, dolomite and gypsum are probably not present in the active layer at this site, but mineralogical analyses are necessary to substantiate this: detailed soil properties are being investigated by researchers at the University of Guelph.

Physical observations and stable isotopes in ground ice reveal that unsaturated zones commonly develop on land during the thaw season. This contrasts with the constantly saturated active layer beneath the shores of lakes and prompted a comparison of the geochemistry in both environments. Although some overlap does occur, distinction is made between ground water from each location (Figure 5). The passage of water from the surface to the subsurface is characterized by increasing Na^+ relative to Mg^{2+}/Ca^{2+} along with increasing Cl^-: the choice of $(Mg^{2+}/Ca^{2+})/Na^+$ rather than $(Mg^{2+} + Ca^{2+})/Na^+$ merely improves the resolution of data points. This cation behaviour suggests that exchange is occurring between adsorbed Na^+ on the surfaces of clay minerals and Ca^{2+} and Mg^{2+} in solution. Exchange is most pronounced in the shore areas of Walkabout Lake in view of the grouping of ground-water compositions in Figure 5.

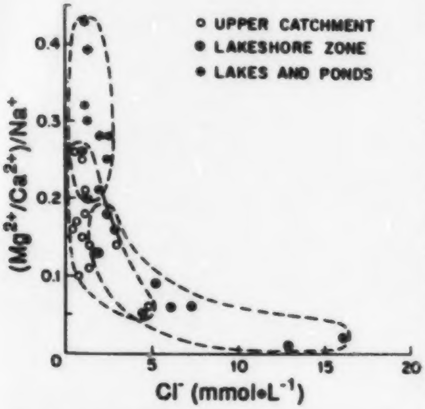

Figure 5. A plot of Cl^- versus $(Mg^{2+}/Ca^{2+})/Na^+$ (molar ratio) for ground waters sampled beneath the shore of Walkabout Lake and for those sampled from further upslope, along with surface waters. The data fields for each group are encircled.

Freezing effects may be responsible for the high ionic contents and slightly depleted isotopic compositions of ground waters beneath the shore of Walkabout Lake. Redistribution and exclusion of ions from ice during freezing and the subsequent concentration of ions in residual water is documented in several studies (Anisimova, 1978; Hallet, 1978; Herut *et al.*, 1990). Isotopic fractionation between water and ice observed in similar till material leaves the ice enriched and the remaining water depleted in ^{18}O and ^{2}H by a few permil during freezing (Michel, 1982). A weak inverse relation is evident in the Cl^- versus $\delta^{18}O$ plot between ground waters sampled close to the lake relative to others sampled further upslope (Figure 6): a similar trend is observed using δ^2H. This process is generally most effective beneath the shore areas, where maximum thaw depths and complete saturation provide the greatest volume of water. The magnitude of these freezing effects depends on the depth of sampling within the active layer.

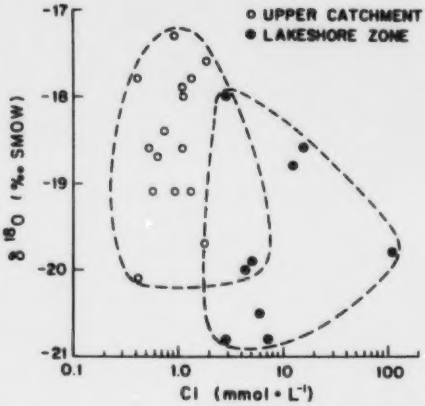

***Figure 6.** Cl^- against $\delta^{18}O$ for ground-water samples from beneath the shore of Walkabout Lake relative to those sampled further upslope. Data fields for each group are encircled.*

DISCUSSION

A tentative separation of the annual hydrograph for inflow to Walkabout Lake is made using meteorological records, direct observations, and stable-isotope data (Figure 7). The annual hydrological cycle is viewed through a narrow window encompassing the June to September thaw season. The hydrograph is strongly divergent in character, dominated initially by surface run-off followed by increasingly important ground-water flow.

The onset of thaw in late-May or early-June generates a strong pulse of surface run-off, enhanced by restricted infiltration of snowmelt into the still-frozen active layer. A maximum estimate for run-off is about 45%, which is largely the proportion of annual precipitation represented by snow. Most spring run-off is abated by late-June.

Depending on the saturation state at freezing the previous fall, some snowmelt will penetrate the frozen ground and remain in temporary storage. Ground-water flow becomes progressively more important as the frost-table declines, releasing stored water and increasing its capacity to accept recharge from summer rain. Peak flow is probably attained by late-August and slowly diminishes through September.

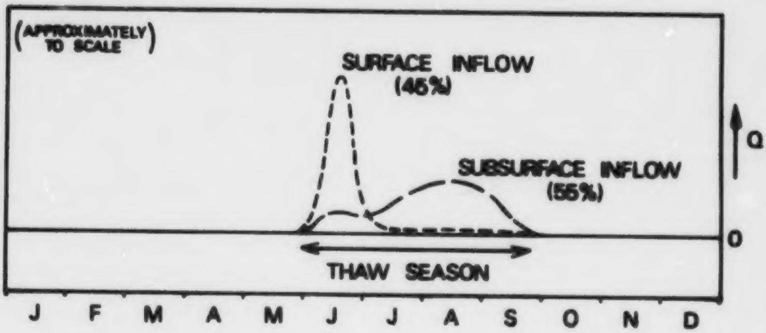

Figure 7. Schematic annual hydrograph describing long-term average inflow to Walkabout Lake; this may not represent conditions for individual years.

Our best estimate indicates that ground-water flow comprises 55% or more of the average annual water balance.

The hydrograph developed for inflow to Walkabout Lake represents a site-specific, time-averaged condition for a small tundra catchment. The shape and separation of this hydrograph may deviate strongly from year-to-year, depending on several factors: variability of snow and rain amounts, thickness of the active layer (i.e., thaw season temperatures), and saturation state of the active layer at freeze-up (i.e., greater snowmelt will be diverted from surface run-off to infiltration if ice content is low). The summer rainfall in 1989 was unusually high, exceeding the mean annual precipitation recorded at Baker Lake. The 1989 hydrograph for Walkabout Lake would have a pulse of subsurface flow equivalent to the total area beneath both curves in the long-term schematic hydrograph in Figure 7. Spatial differences are also anticipated for the hydrological response in other small catchments throughout the Whatever Lake watershed. Hydrographs will show a stronger surface flow component in areas having greater stream density and/or bedrock exposure for example.

Evaporation is expected to be at a minimum in spring although the importance of snow sublimation is not known. Vapour losses increase in July and August when the temperatures are highest and the humidities are lowest. Evaporation declines in September but may remain significant for large lakes with water temperatures still in excess of ambient air temperatures. The overall evaporation from the Whatever Lake watershed amounts to only 10%, despite the arid low-arctic climate. This attests to the importance of ground-water flow in the catchment area and fairly short residence times for water within the lake.

CONCLUSIONS

Investigations in a small-tundra catchment indicates that surface run-off is most important during snowmelt and is largely confined to the first few weeks of the thaw season. Ground-water discharge builds up more gradually, but persists throughout the summer and autumn months as the active layer thickness increases. Subsurface waters are a mixture of ground-ice melt derived from late-season rain of the previous year, rainfall from the current year, and more local recharge from streams and ponds. Evaporation is of variable importance to the water budget at different levels in the drainage system, being most significant for the small tundra ponds as opposed to large lakes. The small tundra ponds can lose almost half of their total outflow to vapour, while larger lakes such as Whatever Lake show evaporative losses of 10% or less.

Three processes have been identified that control the chemical quality of ground waters within the active layer. DOC is a prominent constituent that probably complexes with iron and mobilizes it independently of redox and pH conditions in solution. DOC concentrations are also related to charge balance errors and provide additional acid buffering capacity to sources of inorganic alkalinity. Relations between Ca^{2+}, Mg^{2+}, and Na^{+} are probably governed by cation exchange whereby Ca^{2+} and Mg^{2+} in solution are replaced by Na^{+} on clay mineral surfaces. Freezing is apparently responsible for elevated ion concentrations in ground waters beneath the shore of Walkabout Lake.

ACKNOWLEDGEMENTS

Funding for this project was provided by grants from the National Research Council of Canada and Indian and Northern Affairs Canada (Northern Studies Training Program), and contracts from the Waterloo Centre for Groundwater Research and the National Hydrology Research Institute. The authors greatly appreciate logistical support provided by the Geological Survey of Canada and the personal efforts of W.W. Shilts and A. Rencz.

LIST OF SYMBOLS

A	altered (i.e. evaporated) water (% of P)
E	evaporative outflow (% of P)
K	hydraulic conductivity (cm·s^{-1})
O	surface plus subsurface outflow (% of P)
P	mean annual precipitation (1 or 100%)
R	ratio of $^{18}O/^{16}O$ or $^{2}H/^{1}H$
U	unaltered meteoric water (% of P)
δ	oxygen or hydrogen isotopic composition of the components P, O, E, U, and A (‰)

REFERENCES

ANISIMOVA, N.P., 1978. Cryogenous metamorphization of chemical composition of subsurface water (exemplified in central Yakutia). Permafrost, U.S.S.R. Contribution, 2nd International Conference, U.S. National Academy of Sciences, Washington, D.C., 365-370

ANTWEILER, R.C. and J.I. DREVER, 1983. The weathering of a late Tertiary volcanic ash: importance of organic solutes. Geochimica et Cosmochimica Acta, 47(3), 623-629

BROWN, R.J.E., 1978. Influence of climate and terrain on ground temperatures in the continuous permafrost zone of northern Manitoba and Keewatin District, Canada. Proceedings of the Third International Conference on Permafrost, 10-13 July 1978, Edmonton, Alberta, sponsored by the National Research Council of Canada, Ottawa, Ontario, 16-21

BURSEY, G.G., 1990. Geochemical and isotopic investigations in a watershed of the eastern Arctic, Northwest Territories. M.Sc. thesis, Department of Earth Sciences, University of Waterloo, Waterloo, Ontario, 214 pp.

BURSEY, G.G., T.W.D. EDWARDS and S.K. FRAPE, 1990. Hydrology and geochemistry studies, District of Keewatin, Northwest Territories, Canada. Permafrost - Canada, Proceedings of the 5th Canadian Permafrost Conference, 6-8 June 1990, Québec, Quebec, National Research Council Canada and Centre d'études nordiques, Collection Nordicana, No.54, 159-165

COLEMAN, M.L., T.J. SHEPHERD, J.J. DURHAM, J.E. ROUSE and G.R. MOORE, 1982. Reduction of water with zinc for hydrogen isotope analysis. Analytical Chemistry, 54(6), 993-995

CRAIG, H., 1961. Isotopic variations in meteoric waters. Science, 133(3465), 1702-1703

DALTON, J.A., 1981. Hydrometeorological data from the Saqvaqjuac project, N.W.T., 1977 to 1980. Fisheries and Aquatic Sciences Data Report No.273, Fisheries and Oceans Canada, Winnipeg, Manitoba, 43 pp.

DREVER, J.I., 1988. The geochemistry of natural waters. 2nd edition, Prentice Hall, Engelwood Cliffs, New Jersey, 437 pp.

EADE, K.E., 1986. Precambrian geology of the Tulemalu-Yathkyed Lake area, District of Keewatin. GSC Paper No.84-11, Geological Survey of Canada, Ottawa, Ontario, 31 pp. + map

ECOREGIONS WORKING GROUP, 1989. Low arctic ecoclimatic region. In - Ecoclimatic Regions of Canada, First Approximation, Canadian Committee on Ecological Land Classification, Ecological Land Classification Series No.23, Canadian Wildlife Service, Environment Canada, Ottawa, Ontario, 12

EDMUNDS, W.M. and D.G. KINNIBURGH, 1986. The susceptibility of UK groundwaters to acidic deposition. Journal of the Geological Society, London, 143(4), 707-720

EPSTEIN, S. and T. MAYEDA, 1953. Variations of O^{18} content of waters from natural sources. Geochimica et Cosmochimica Acta, 4(5), 213-224

FRITZ, P., R.J. DRIMMIE, S.K. FRAPE and K. O'SHEA, 1987. The isotopic composition of precipitation and groundwater in Canada. In - Isotope Techniques in Water Resources Development, Proceedings of a Symposium, 30 March - 3 April 1987, Vienna, Proceedings Series, International Atomic Energy Agency, Vienna, Austria, 539-550

HALLET, B., 1978. Solute redistribution in freezing ground. Proceedings of the Third International Conference on Permafrost, 10-13 July 1978, Edmonton, Alberta, Volume 1, sponsored by the National Research Council of Canada, Ottawa, Ontario, 85-91

HERUT, B., A. STARINSKY, A. KATZ and A. BEIN, 1990. The role of seawater freezing in the formation of subsurface brines. Geochimica et Cosmochimica Acta, 54(11), 13-21

HVORSLEV, M.J., 1951. Time lag and soil permeability in groundwater observations. Bulletin No.36, Waterways Experiment Station, U.S. Army Corps of Engineers, Vicksburg, Mississippi, 50 pp.

KASZYCKI, C.A. and W.W. SHILTS, 1979. Average depth of glacial erosion, Canadian Shield. In - Scientific and Technical Notes in Current Research, Part B, Geological Survey of Canada Paper No.79-1B, Ottawa, Ontario, 395-396

LITAOR, M.I. and E.M. THURMAN, 1988. Acid neutralizing processes in an alpine watershed Front Range, Colorado, U.S.A. 1. Buffering capacity of dissolved organic carbon in soil solutions. Applied Geochemistry, 3(6), 645-652

MAXWELL, J.B., 1986. A climate overview of the Canadian inland seas. In - Canadian Inland Seas, I.P. Martini (Editor), Elsevier Oceanography Series No.44, Elsevier, New York, 79-99

MICHEL, F.A., 1982. Isotope investigations of permafrost waters in northern Canada. Ph.D. thesis, Department of Earth Sciences, University of Waterloo, Waterloo, Ontario, 424 pp.

PARKHURST, D.L., D.C. THORSTENSON and L.N. PLUMMER, 1980. PHREEQE - a computer program for geochemical evaluations. Water Resources Investigations No.80-96, U.S. Geological Survey, Reston, Virginia, 210 pp.

PLUMMER, L.N., B.F. JONES and A.H. TRUESDELL, 1976. WATEQF, a FORTRAN IV version of WATEQ, a computer program for calculating chemical equilibrium of natural waters. Water Resources Investigations No.76-13, U.S. Geological Survey, Reston, Virginia, 61 pp.

ROULET, N.T. and M.-K. WOO, 1986. Hydrology of a wetland in the continuous permafrost region. Journal of Hydrology, 89(1-2), 73-91

SHILTS, W.W. and W.E. DEAN, 1975. Permafrost features under arctic lakes, District of Keewatin, Northwest Territories. Canadian Journal of Earth Sciences, 12(4), 649-662

STUMM, W. and J.J. MORGAN, 1981. Aquatic chemistry: an introduction emphasizing chemical equilibria in natural waters. 2nd edition, John Wiley and Sons, New York, N.Y., 780 pp.

WELHAN, J.A., 1974. Feasibility of the oxygen-18 mass balance method in the calculation of the water balance of a small lake. M.Sc. thesis, Department of Earth Sciences, University of Waterloo, Waterloo, Ontario, 71 pp.

WOO, M.-K. and P. STEER, 1983. Slope hydrology as influenced by thawing of the active layer, Resolute, N.W.T. Canadian Journal of Earth Sciences, 20(6), 978-986

ZIMMERMANN, U., 1979. Determination by stable isotopes of underground inflow and outflow and evaporation of young artificial groundwater lakes. In - Isotopes in Lake Studies, Proceedings of an Advisory Group Meeting, 29 August - 2 September 1977, Vienna, Panel Proceedings Series, International Atomic Energy Agency, Vienna, Austria, 87-94

RIVER ICING MOUNDS: A WINTER WATER SOURCE ON THE EASTERN NORTH SLOPE OF ALASKA

E.F. Chacho, Jr.[1], C.M. Collins[1], A.J. Delaney[2] and S.A. Arcone[2]

[1]U.S. Army Cold Regions Research and Engineering Laboratory
Alaska Projects Office, Building 4070
Ft. Wainwright, Alaska 99703-7860
U.S.A.

[2]U.S. Army Cold Regions Research and Engineering Laboratory
72 Lyme Road
Hanover, New Hampshire 03755
U.S.A.

ABSTRACT

The icing mounds on two eastern North Slope rivers, the Sadlerochit and Hulahula, were investigated in April 1989. Approximately 100 mounds were surveyed on each river, representing about half the total number observed. The surveys were conducted using an airborne short-pulse radar system, from which water-bearing mounds could be distinguished from dry mounds and ice thickness, and mound height could be estimated. The distribution of icing mounds was measured on a 50- to 70-km reach of each river, extending from the coast to the Sadlerochit Mountains. The ice thickness of water-bearing mounds was generally greater than 1.5 m, while icing mounds with an ice thickness of less than 1.3 m were generally dry. All mounds exceeding a height of 1.25 m over the surrounding ice surface were found to contain water.

INTRODUCTION

On the eastern North Slope of Alaska measurable flow in most river channels ceases by the end of the winter. The river channels generally consist of either an ice cover frozen solid to the stream bed or large aufeis formations. River icing mounds are features common to both ice cover conditions and are potential sources of available water during the winter (Figure 1).

The term "icing mound" refers to a category of seasonal frost mound that is composed entirely of ice (Pollard, 1988), although a thin layer of sediment may be found at one or more layers within the ice formation (Nekrasov, 1969). Essentially, the formation of icing mounds is limited to river ice covers or aufeis areas. The term icing mound was first used by Muller (1945), although Leffingwell (1919) first reported the occurrence of icing mounds in northern Alaska. Further classification was proposed by van Everdingen (1978), who describes a mound formed by hydraulic lifting of an ice cover as an icing blister, which may occur by either hydrostatic pressure or pressure of crystallization of injected water; and refers to a mound formed by the accumulation of successive overflow events as an icing mound. The National Research Council of Canada, (Canada, 1988), using the same classification system, distinguish the mound types by the presence of a layer of clear ice in the icing blister. The distinction is a result of the formation process of the mound, which may be difficult to determine solely by external appearance and, as stated by Pollard (1988), may require an examination of the internal structure of the mound. For further discussion of icing mounds see the recent review by Pollard (1988).

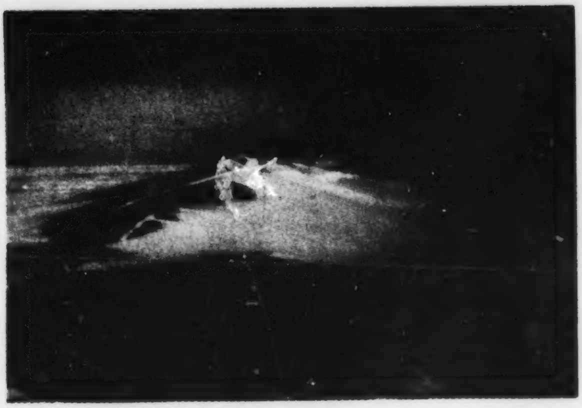

Figure 1. River icing mound located in the Arctic National Wildlife Refuge.

The results presented here are based primarily on airborne radar surveys and visual observations of the fully-developed icing mounds near the end of the winter. Therefore, in this paper the term icing mound is applied generically with no distinction implied as to the mound-formation process.

Investigation of the icing mounds is one portion of an ongoing study of winter water supply in the Arctic and Subarctic. The mounds are appealing as a potential water source for several reasons: a) their relative abundance, as they are present on nearly all major rivers on the eastern North Slope (Arcone *et al.*, 1989a, 1989b; Elliot, 1989); b) their ease of identification, as their high relief on the flat river surface ensures visibility from a relatively great distance; and c) the finding that a high proportion of the mounds are water-bearing. In this paper we present the results of an airborne survey conducted on two large river systems to determine the distribution of the icing mounds and to investigate factors that may be used to predict whether an icing mound is water-bearing or dry. Complementary to the regional study reported here, a detailed investigation of an individual icing mound was also conducted and has been reported elsewhere by Arcone *et al.* (1990).

SITE DESCRIPTION

The study was done in April 1989 in the Arctic National Wildlife Refuge on the Arctic Coastal Plain on the eastern North Slope of Alaska (Figure 2). Winter water-detection surveys had been conducted in the area during the previous winter, indicating the presence of water within numerous icing mounds observed on all the major rivers (Arcone *et al.*, 1989a, 1989b; Elliot, 1989). Based on the 1988 surveys, two rivers, the Sadlerochit and Hulahula, were selected for further study of the water-bearing aspects of the icing mounds. The surveys ran from the coast to the foothills and a short distance into the Sadlerochit Mountains, covering approximately 50 to 70 km of river length on each river. The two surveyed rivers lie in adjacent drainages and exhibit similar characteristics. Both rivers occupy single incised channels in the mountains and foothills and become heavily braided as they enter and cross the Coastal Plain. Both basins contain at least one year-round flowing spring (Childers *et al.*, 1977). More detailed descriptions of the area can be found in U.S. Department of the Interior (1987).

METHODS

Instrumentation

Airborne surveys of the mounds were conducted using a high-frequency short-pulse radar system, SIR Model 4000, manufactured by GSSI (Geophysical Survey Systems, Inc., Hudson, NH). A Model 3102 GSSI antenna, operating near 500 MHz, was externally mounted to a Bell 206L Jet Ranger helicopter. Data were recorded on a GSSI DT6000 tape recorder. The control unit, tape recorder and operator occupied the rear seat of the helicopter during the survey flights. Data interpretation was based on the simple echo delay formula:

$$d = ct/2n \qquad [1]$$

where d is the depth of a reflector (cm), t is the echo time delay (ns), c is the speed of electromagnetic waves in a vacuum ($30\ \text{cm}\cdot\text{ns}^{-1}$) and n is the index of refraction of the material through which the waves have propagated. The factor of 1/2 accounts for the round-trip of the echo. The values used in this study were $n = 1.79$ for ice, in computing the ice thickness, and $n = 1.0$ for air, in computing the mound height. The radar system and data interpretation are described in greater detail by Arcone and Delaney (1987) and Arcone *et al.* (1989a).

Data Collection

The rivers were surveyed by flying along their courses. In the case of the Hulahula River, the survey proceeded upstream from near the coast into the foothills of the Romanzof Mountains, while the Sadlerochit River was surveyed from the Sadlerochit Mountains downstream. One day was spent on each river. The aircraft

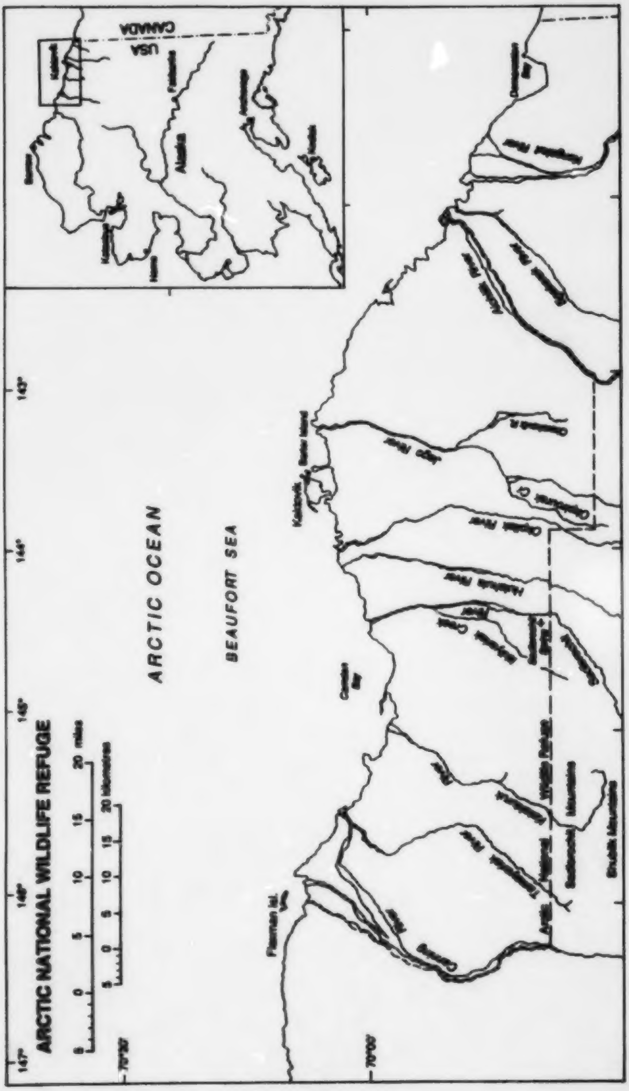
ARCTIC NATIONAL WILDLIFE REFUGE
ARCTIC OCEAN
BEAUFORT SEA
CANADA
USA
Alaska
143°
144°
145°
146°
147°
70°30'
70°00'
0 5 10 15 20 miles
5 0 5 10 15 20 kilometres

Figure 2. General location map of the study area in the Arctic National Wildlife Refuge.

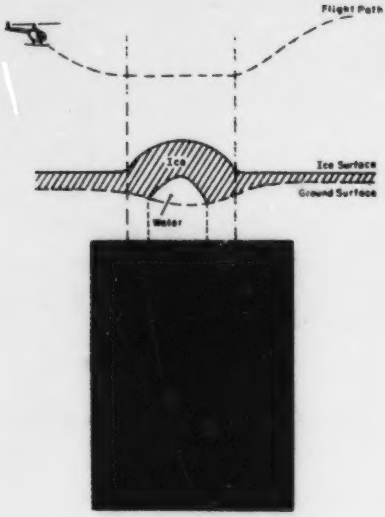

Figure 3. Schematic of the radar survey flight path and typical radar return over an icing mound, where MD indicates the portion of the radar return between the event markers locating the boundaries of the mound and WD indicates the portion of the radar return where water was present beneath the ice cover. Mound height is represented by $h=(h_1+h_2)/2$, with h_1, h_2 measured at each event marker locating the boundaries of the mound and ice thickness is represented by T, measured from the top of the mound to the dark return of the ice/water interface.

followed the channel of the river at sufficient height and speed to safely observe the ice surface. When a mound was approached, the aircraft dropped to a height of approximately 5 m above the ice surface and attempted to maintain a level flight path over the length of the mound with the antenna situated above the mound crest, presumably where the ice thickness was maximum (Figure 3). The capability to maintain a level flight path depended on local wind and terrain conditions. An event marker was used to locate the boundaries of the mound on the radar trace.

An attempt was made to survey every mound on each river and was successfully done throughout the non-braided reaches. However, in some portions of the braided reaches, mound density was so high that this was not practical. In those areas a sample of mounds, assumed to be representative of the mound field, was surveyed and the total number of mounds estimated (Table 1).

Ground position was maintained by continuously plotting the flight path on USGS 1:63,360 quadrangle sheets. Periodic checks were made against the altitude and LORAN instrumentation aboard the aircraft; however, position must be considered approximate. The location of individual mounds, mound fields and footage of the radar tape were noted directly on the maps.

Data Reduction

During the flight, the radar data were recorded on cassette tape and later transferred to chart paper from which measurements could be made (Figure 3). To estimate the height of a mound, the travel times measured at both event marks on

Table 1. Summary of surveyed icing mounds and mound estimates.

Site	Surveyed				Estimated			
	Distance (km)	# Mounds	# with water	% with water	# Mounds	# with water	% with water	Mounds /km
HULAHULA RIVER								
Braided	30	81	67	83	153	129	84	5.3
Non-braided	22	11	9	82	11	9	82	0.4
Total	52	92	76	83	164	138	84	--
SADLEROCHIT RIVER								
Braided	38	72	62	86	179	163	91	4.8
Non-braided	34	35	18	51	35	18	51	0.9
Total	72	107	80	75	214	181	85	--

the radar trace were averaged to compensate for deviations from a level flight path, and height was computed using the echo-delay formula. Ice thickness was computed by measuring the distance on the radar trace from the peak of the ice-surface return between the event markers to the return from either the water surface or the ground surface. The presence of water within the mound was noted by the stronger return relative to that from the ice or ground surface (Figure 3).

RESULTS

Mound Distribution

The distribution of the mounds on the Hulahula and Sadlerochit Rivers is displayed as a function of stream length in two ways. In the upper portions of Figures 4 and 5, the cumulative total number of mounds is shown relative to the stream profile and pertinent geomorphological parameters. Observations of icing conditions made during the aerial surveys are also included. In the lower portions of the figures the incremental distributions of mounds, both with and without water, are shown. The data shown in Figures 4 and 5 represent the estimated total number of mounds observed during the aerial surveys. In the areas of high mound density where only a sample of the mounds were surveyed, the proportion of mounds containing water in the surveyed sample was extrapolated to the estimated total count for the specific area. The data from the actual surveys and the estimated mound counts are included in Table 1.

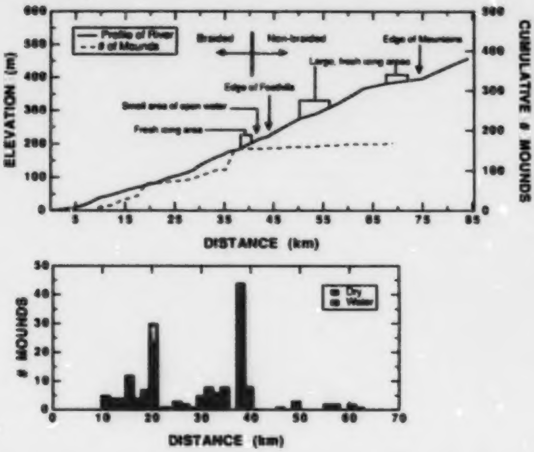

Figure 4. Hulahula River profile including significant geomorphological parameters and number of icing mounds represented by the cumulative total and distribution of water-bearing and dry mounds vs. stream length, April 1989.

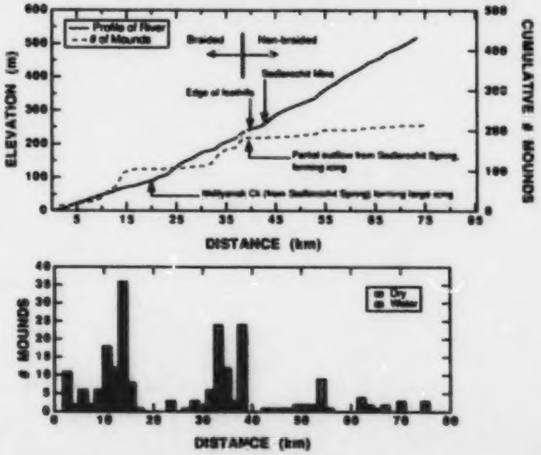

Figure 5. Sadlerochit River profile including significant geomorphological parameters and number of icing mounds represented by the cumulative total and distribution of water-bearing and dry mounds vs. stream length, April 1989.

Due to local weather conditions the aerial survey on the Hulahula River was started about 9.6-km upstream of the coast. A total of 92 mounds were surveyed. The majority of those (81) were located in the braided reach of the river, which included a number of mound fields where the total number of mounds was estimated. Using the estimates, 164 mounds were observed, of which 93% were located in the braided reach of the river. As shown in Table 1, the proportion of mounds containing water was nearly the same in the braided and non-braided reaches, with 84% of the total count containing water.

On the Sadlerochit River, 107 mounds were surveyed, with the majority of the mounds also located in the braided reach of the river. Using the estimates for the mound fields, 214 mounds were counted, with 84% located in the braided reach. The proportion of mounds containing water was slightly higher in the braided reach (91%) than on the Hulahula River, but lower (51%) in the non-braided reach. However, for the entire surveyed reach of the river the overall proportion of mounds containing water (85%) is nearly identical to that of the Hulahula River (Table 1).

The density of mounds in the braided reaches of the rivers was relatively high: 4.8 mounds/km on the Sadlerochit River and 5.3 mounds/km on the Hulahula River (Table 1). The mounds in the braided reaches of both rivers were bimodally distributed, with a distinct skew to the downstream side of the distribution at each mode (Figures 4 and 5). On both rivers the upstream distribution peak occurs just downstream of the edge of the foothills and the second peak occurs at approximately half the distance to the coast. The peaks in the distribution of the mounds appear to be associated with fresh aufeis formations. This was the case on both rivers near the edge of the foothills and also for the downstream peak on the Sadlerochit River. A fresh aufeis formation was not noted in the vicinity of the downstream mound distribution on the Hulahula River; however, that may be due to neglect in recording data at the beginning of the survey. A discussion of the mound-formation process is beyond the scope of this paper, but the apparent supply of water at the location of the aufeis seems to have contributed to a higher density of mound formation in these areas. There does not appear to be any pattern to the distribution of dry mounds within the braided reach.

In the non-braided reaches of both rivers there does not appear to be any pattern to the overall distribution of mounds, with formation and growth probably a function of local conditions. On the Sadlerochit River, mound density was relatively low or nonexistent, except at 53 km where a higher concentration of mounds was observed, of which the majority were dry. Overall, about half the mounds on the non-braided portion of the Sadlerochit River were dry and, with the exception of the group at 53 km, there was no apparent pattern to the distribution of dry mounds. On the Hulahula River only 11 mounds were observed on the non-braided reach, all of which contained water except for the two mounds at 56 km that were both dry. The density of mounds throughout the non-braided reaches was relatively low, 0.9 mounds/km on the Sadlerochit River and 0.4 mounds/km on the Hulahula River (Table 1).

Ice Thickness

As discussed above, ice thickness was a parameter measured on the radar printout. Ice thickness was obtainable on all mounds that contained water. On a few of the dry mound traces the ice/ground interface was not distinct enough to permit measurement of the ice thickness. Ice thickness is plotted as a function of elevation for the Hulahula and Sadlerochit Rivers in Figures 6 and 7. Elevation was selected as the independent variable to determine if there was an orographic effect on ice thickness. Regression analysis (results not included in this paper), as well as inspection of the data shown in Figures 6 and 7, indicate no such effect.

The braided reaches of each river are also indicated in Figures 6 and 7. Inspection of the data indicates no apparent change in ice thickness between the braided and non-braided reaches of the rivers.

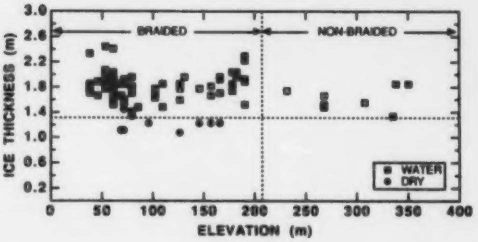

Figure 6. Ice thickness of water-bearing and dry mounds vs. stream elevation on the Hulahula River, April 1989.

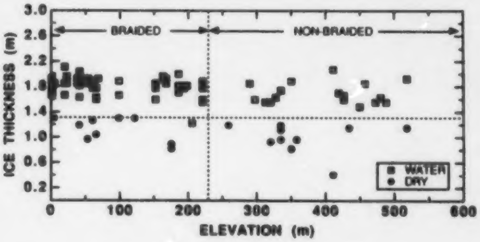

Figure 7. Ice thickness of water-bearing and dry mounds vs. stream elevation on the Sadlerochit River, April 1989.

At an ice thickness of 1.3 to 1.5 m there is a distinct division that groups the mounds into those containing water and those which are dry. (Dry mounds are simply the mounds that have frozen solid.) All dry mounds on the two rivers had ice thicknesses of less than 1.5 m and, with the exception of two mounds on the Hulahula River, all were less than 1.3 m. With the exception of one mound on the Sadlerochit River, all mounds containing water on the two rivers had ice thicknesses greater than 1.3 m, with the majority greater than 1.5 m. This indicates that weather conditions were such that any body of water less than 1.3-m deep froze solid during the 1988-89 winter. Analysis of the minimum ice thickness of the mounds is not as straightforward as that of lakes in the region, since there is still some question as to when the mound formation takes place and the source of water contained within the mounds.

Maximum ice thickness was about 2.5 m, which was reached by only a few mounds on the Hulahula River; otherwise, all ice thicknesses were under 2.1 m. These data are comparable to reported maximum ice thicknesses for lakes on the Arctic Coastal Plain (for example, Bilello and Bates, 1969) and are consistent with the blister-type mound formation process. Mounds formed by repeated point source overflow events may have ice thicknesses that exceed these values and may approach the maximum ice thickness of greater than 5 m reported for aufeis on the eastern Arctic Coastal Plain (Sloan *et al.*, 1976). Few mounds were ground surveyed during this study, but observations made during the aerial surveys of the shape of the mounds and the presence of a characteristic longitudinal crack indicated all mounds to be in the blister-type category.

Ice thickness appears to be a useful parameter to distinguish water-containing mounds from dry or solidly-frozen mounds. However, without the use of airborne radar, the measurement of ice thickness cannot be efficiently conducted for large areas, such as entire river systems, or by lightly-equipped field parties desiring to locate a water source.

Mound Height

As discussed above, mound height can be estimated from the radar printouts based on the assumption of a level flight path and the use of event markers to indicate the mound boundaries. At the beginning of the aerial surveys, measurement of mound height from the radar trace had not been considered; as a result, imprecise use of the event marker at the mound boundaries prohibited the measurement of height on the Hulahula River survey. At the time of the survey on the Sadlerochit River, field techniques had been modified with the intent of measuring mound heights on the radar trace.

The snowpack was sufficient that extensive drifting occurred around the mounds. In many cases the exposed ice of the mound crest was visible, as was an obvious mounding beneath the snow. However, the actual height of the mounds was obscured due to the surrounding drifts. The presence of snow drifts did not, however, affect the radar survey, permitting the mound height above the surrounding ice cover to be measured on the radar traces.

The data were sufficient to measure the height of 103 of the 107 mounds surveyed on the Sadlerochit River. Ice thickness as a function of mound height is shown in Figure 8 for both the water-bearing mounds and the dry mounds. The dry-mound data are bracketed by ice thicknesses of 1.3 m and mound heights of 1.25 m. Any mound with a height greater than 1.25-m contained water. Of the mounds less than 1.25-m high, 53% contained water. No surveyed mound less than 0.45-m high contained water. Separating the mound-height data for the braided and non-braided reaches did not add any information and has not been displayed in this paper.

Recall that mound height is defined as the maximum height of the mound above the surrounding ice surface. Some mounds of very small height may not have been spotted during the aerial survey or may have been snow-covered and obscured from view; therefore, the data for small mounds may not be fully representative of the actual count in the field.

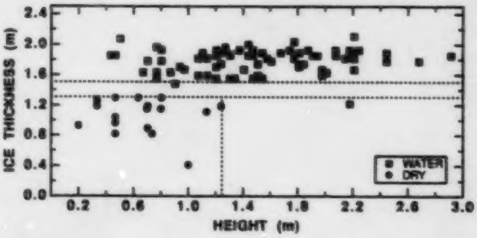

Figure 8. Ice thickness of water-bearing and dry mounds vs. mound height on the Sadlerochit River, April 1989.

SUMMARY AND CONCLUSIONS

Based on the April data, about 85% of the icing mounds present on the surveyed rivers were water-bearing near the end of the winter. On the Hulahula River 93% of the total number of mounds observed were located in the braided reach. The percentage of the mounds that were water-bearing was the same in the braided and non-braided reaches of the river. On the Sadlerochit River, 84% of the total number of mounds observed were located in the braided reach with a density (mounds/km) slightly lower than on the Hulahula River. However, on the Sadlerochit River a higher percentage of the mounds were water-bearing. The Sadlerochit River had a higher concentration of mounds in the non-braided reach than did the Hulahula River, but only about half were water-bearing (Table 1).

In general, the concentration of mounds per river length was much higher in the braided reaches than in the non-braided reaches. However, if the width of the floodplain is considered, the mound concentration per unit area may be similar in the braided reach and non-braided reaches. The chance of locating a water-bearing mound in the braided reaches of these two river systems was about the same to nearly twice as great as in the non-braided reaches.

Mounds with an ice thickness in excess of 1.5 m were water-bearing while nearly all mounds with ice thickness less than 1.3 m were dry. On the Sadlerochit River, where mound height was measured, all mounds greater than 1.25 m in height were water-bearing. The division of water-bearing from dry mounds by ice thickness results from frost penetration in the water body, which may be complicated by the formation process and source of water. Mound height above the surrounding ice surface results from the interaction of hydrostatic pressure in the water cavity and the overlying ice cover. If the water pressure results strictly from crystallization pressure, the mound-formation and growth processes are controlled by heat loss and creep of the ice, which will vary with weather conditions and ice thickness but should be relatively predictable over the course of the winter. If the water pressure results from water injection beneath the ice cover, regardless of what the source may be, the growth of the mound may occur in spurts followed by periods of slower growth due to heat loss, as described previously. The formation process and the timing of mound growth are important factors in determining the availability and the quantity of water that may be accessible throughout the winter. Our present studies are addressing these factors.

NOTE: Since the initial submission of this paper we have become aware of the publication of a report by Elliott and Lyons (1990) that also addresses the distribution of icing mounds in the Arctic National Wildlife Refuge. Interested readers may want to investigate this report.

LIST OF SYMBOLS

d	depth of a reflector (cm)
t	echo time delay (ns)
c	speed of electromagnetic waves in a vacuum (30 $\mathrm{cm \cdot ns^{-1}}$)
h	average mound height (cm)
h_1,h_2	mound height, measured on the radar trace at each event marker locating the boundaries of the mound and computed as d, in echo-delay formula (cm)
n	index of refraction of the material through which waves have propagated
T	ice thickness, computed as d, in echo-delay formula (cm)
MD	indicates the portion of the radar return between the event markers locating the boundaries of the mound
WD	indicates the portion of the radar return where water was present beneath the ice cover

REFERENCES

ARCONE, S.A., E.F. CHACHO, C.M. COLLINS and A.J. DELANEY, 1990. Surface radar investigations of an icing mound on the Sagavanirktok River, Alaska. In - Ice Technology for Polar Operations, T.K.S. Murthy, J.G. Paren, W.M. Sackinger and P. Wadhams (editors), Proceedings, 2nd International Conference on Ice Technology, 18-20 September 1990, Cambridge, U.K., Computational Mechanics Publications, Boston, Massachusetts, 353-363

ARCONE, S.A. and A.J. DELANEY, 1987. Airborne river-ice thickness profiling with helicopter-borne UHF short-pulse radar. Journal of Glaciology, 33(115), 330-340

ARCONE, S.A., A.J. DELANEY and D.J. CALKINS, 1989a. Water detection in the coastal plains of the Arctic National Wildlife Refuge using helicopter-borne short-pulse radar. CRREL Report No.89-7, Cold Regions Research and Engineering Laboratory, U.S. Army Corps of Engineers, Hanover, New Hampshire, 25 pp.

ARCONE, S.A., A.J. DELANEY and D.J. CALKINS, 1989b. Correspondence: River-ice mounds on Alaska's North Slope. Journal of Glaciology, 35(120), 288-289

BILELLO, M.A. and R.E. BATES, 1969. Ice thickness observations, North American Arctic and Subarctic, 1964-65, 1965-66. CRREL Special Report No.43, Part IV, Cold Regions Research and Engineering Laboratory, U.S. Army Corps of Engineers, Hanover, New Hampshire, 130 pp.

CANADA, NATIONAL RESEARCH COUNCIL OF CANADA, 1988. Glossary of permafrost and related ground-ice terms. Technical Memorandum No.142, Permafrost Subcommittee, Associate Committee on Geotechnical Research, National Research Council of Canada (NRCC 27952), Ottawa, Ontario, 156 pp.

CHILDERS, J.M., C.E. SLOAN, J.P. MECKEL and J.W. NAUMAN, 1977. Hydrologic reconnaissance of the eastern North Slope, Alaska, 1975. U.S.G.S. Open File report No.77-492, U.S. Geological Survey, Anchorage, Alaska, 65 pp.

ELLIOT, G.V., 1989. Winter water availability on the 1002 area of the Arctic National Wildlife Refuge. Alaska Fisheries Technical Report No.3, U.S. Fish and Wildlife Service, Anchorage, Alaska, 30 pp.

ELLIOT, G.V. and S.M. LYONS, 1990. Quantification and distribution of winter water within river systems of the 1002 area, Arctic National Wildlife Refuge. Alaska Fisheries Technical Report No.6, U.S. Fish and Wildlife Service, Anchorage, Alaska, 18 pp.

LEFFINGWELL, E. de K., 1919. The Canning River region, northern Alaska. U.S. Geological Survey Professional Paper No.109, Washington, D.C., 251 pp.

MULLER, S.W., 1945. Permafrost or permanently frozen ground and related engineering problems. Strategic Engineering Study No.62, Military Intelligence Division, U.S. Army Office of the Chief of Engineers, Washington, D.C., 231 pp.

NEKRASOV, I.A., 1969. On ground interbeddings in ice hummocks of naleds. In - Naledi Sibiri, V.R. Alekjseyev (Editor), Nauka, Moscow, 1969, 192-196, CRREL Draft Translation No.399, Cold Regions Research and Engineering Laboratory, U.S. Army Corps of Engineers, Hanover, New Hampshire, April 1973, 130-133

POLLARD, W.H., 1988. Seasonal frost mounds. In - Advances in Periglacial Geomorphology, M.J. Clark (Editor), Wiley-Interscience Publications, John Wiley & Sons, Chichester, 201-229

SLOAN, C.E., C. ZENONE and L.R. MAYO, 1976. Icings along the Trans-Alaska pipe-line route. U.S. Geological Survey Professional Paper No.979, Washington, D.C., 31 pp.

U.S. DEPARTMENT OF THE INTERIOR, 1987. Arctic National Wildlife Refuge, coastal plain resource assessment. Report and Recommendation to the Congress of the United States and Final Legislative Environmental Impact Statement, U.S. Fish and Wildlife Service, Department of the Interior, Anchorage, Alaska, April, 208 pp.

van EVERDINGEN, R.O., 1978. Frost mounds at Bear Rock, near Fort Norman, Northwest Territories, 1975-1976. Canadian Journal of Earth Sciences, 15(2), 263-276

GEOCHEMICAL EVOLUTION OF WATER IN A CONTINENTAL HIGH BOREAL WETLAND BASIN: PRELIMINARY RESULTS*

D. Craig

Northern Environment Project
National Hydrology Research Institute
11 Innovation Boulevard
Saskatoon, Saskatchewan
S7N 3H5 CANADA

ABSTRACT

A study on the geochemical evolution of water in the Manners Creek watershed near Fort Simpson, N.W.T., has been underway since June 1989. The watershed is felt to be typical of the wetland basins that cover large segments of that region. Preliminary investigations of water chemistry, sediment stratigraphy and mineralogy have been carried out. The chemistry of shallow ground water, as well as water in the active layer, in the wetland, and in the stream draining the wetland has been examined. The water in the basin can be classified as a Ca^{2+} *-* HCO_3^- *water and it is felt that the primary reactions determining water chemistry within the basin are the dissolution of calcite and dolomite. Shallow ground waters in the lower river valley of the basin have elevated levels of dissolved sulphate due to the dissolution of gypsum. The presence of gypsum is limited to the deeper sediments in the basin. During the spring melt period of 1990 significant concentrations of calcium, magnesium, and alkalinity were observed in the basin run-off. Vertical transport (upward) processes in the unsaturated zone, probably driven by evapotranspiration, may be important in moving carbonates to the surficial layer of sphagnum, where they are readily available for dissolution during the spring snowmelt period. Shallow active-layer flow was probably the predominant process generating run-off during the spring 1990 run-off period.*

INTRODUCTION

The objective of this paper is to examine the role that water-flow paths play in determining the chemical characteristics of stream water. Water following different flow paths (i.e., surface run-off, interflow, active-layer flow, or ground-water flow) within a basin can have different geochemical signatures. These geochemical signatures are determined by the chemistry of the precipitation falling on the basin, any water-mineral and -biochemical reactions occurring within the terrestrial or aquatic portion of the basin, and the initial chemistry of any water in storage within the flow system. It follows that examination of the temporal variations in the

*National Hydrology Research Institute Contribution Series Number CS-90007.

chemistry of waters draining the wetland can provide information on the significance of the various flow paths at different times of the year. This emphasis on geochemical methods in the study is designed to provide flow information in an environment that is not conducive to other methods of hydrological investigation, that is, the large wetlands in Canada's North. As a first step in this process it is necessary to determine the major water/mineral interactions and to examine general water chemistry within the basin.

Watershed hydrology in northern basins underlain by permafrost is controlled by two major factors (Roulet, 1987). Firstly, the permafrost acts as an underlying confining layer, restricting major hydrological processes to the active layer. Secondly, the over-winter accumulation of snow, followed by a quick release of the stored water during the spring melt produces the peak of spring run-off characteristic of northern basins. The hydrographs of wetlands in areas of permafrost are unique in that they have extended periods of recession following peak flow (Brown *et al.*, 1968; Roulet, 1987; Roulet and Woo, 1986) relative to other non-wetland basins in similar environments.

Study Area

The Manners Creek watershed (61°40'N; 121°00'W) near Fort Simpson, N.W.T., is located in the region of discontinuous permafrost and is thought to be typical of the wetlands that cover wide areas of that region (Figure 1). It was selected on the basis of accessibility, logistics, and its location in the discontinuous-permafrost zone.

The Manners Creek basin covers an approximate area of 400 to 500 km^2 with a maximum relief of 80 m. The basin itself is dominated by two main topographical zones. Zone one, the headwater zone of the basin, is located on an extensive plateau, and is composed of areas of standing water with low, discontinuous sand ridges projecting above the water-table. The wetland areas comprise extensive organic fens dominated by sedge grasses with minor dwarf birch and tamarack. The topography is flat to gently sloping and the drainage is unorganized (Hawes, 1975). The sand ridges are vegetated mainly by sphagnum and black spruce. Zone two occurs lower in the basin where steeper slopes have allowed a relatively well-defined channel system to develop. Vegetation distribution in this zone is influenced strongly by aspect and drainage conditions. Sphagnum and spruce are abundant on north-facing slopes where subsurface drainage is impeded by the presence of permafrost. Aspen woodlands are found on south-facing slopes which are better drained due to the absence of shallow permafrost.

The general stratigraphy of the unconsolidated sediments in the terrestrial portion of the catchment can be summarized as follows. Organic muskeg of varying thickness (0.5 to 3 m) is developed over a layer of sand or silty sand (0.5 to 4 m in thickness) that blankets the area. This in turn overlies a clay-clay silt unit of at least 15-m thickness in the upper portion of the basin. On some of the better-drained slopes of the lower basin (Zone 2) the layer of organic muskeg is not present. No bedrock outcrops have been observed in the basin.

Due to the large size of the Manners Creek basin, a smaller tributary that reflects the overall topographical configuration and conditions of the entire basin was selected for detailed evaluation (Figure 2). This sub-basin is referred to as the Manners Creek Unnamed Tributary (MCUT) sub-basin.

Field Methods and Installations

Sediment samples were collected from along the "A" transect (Figure 2) in the study tributary and at the site where the pipeline crosses Manners Creek in the upper basin (Figure 1). A total of nine profiles of the unconsolidated sediments were collected from soil pits or by hand auger from the surface to depths of 0.8 to 3.4 m. The profiles were subsampled using intervals of 10 or 20 cm, depending on the visible stratigraphy and uniformity, resulting in 89 subsamples. These subsamples were stored in clean plastic bags. On return to the laboratory the subsamples were air dried and split by mechanical sieving into greater than and less than 20 mesh size fractions. A portion of the less than 20 mesh size fraction was pulverized and the bulk mineralogy determined using a Scintag XDS-2000 powder diffractometer. The morphology and composition of individual selected grains were examined using a Jeol 840-A scanning electron microscope (SEM) equipped with a

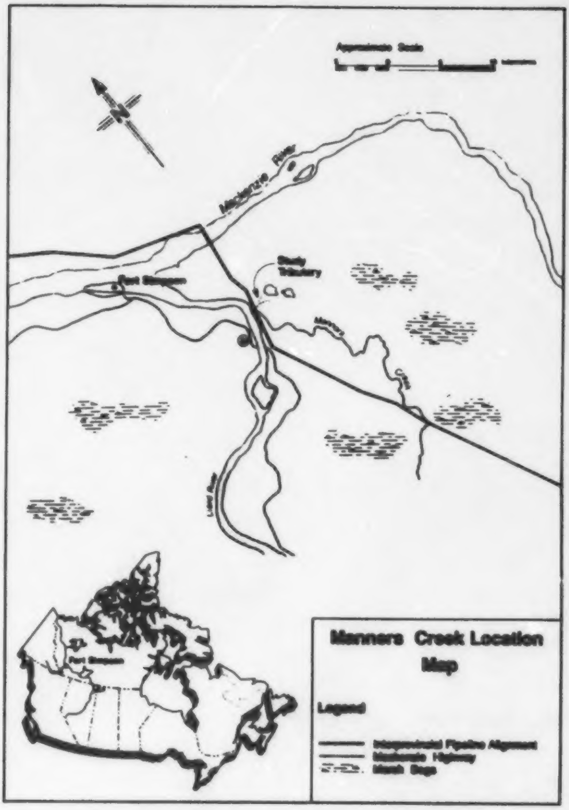
Approximate Scale
N
Mackenzie River
Fort Simpson
Study Tributary
Manners Creek
Liard River
Manners Creek Location Map
Legend
Interprovincial Pipeline Alignment
Mackenzie Highway
Marsh Bogs

Figure 1. General location of Manners Creek and the detailed study sub-basin.

Kevex energy dispersive X-ray (EDX) analyser.

Test wells constructed out of 5-cm diameter PVC (polyvinyl chloride) pipe were installed along the "A" transect in the MCUT sub-basin (Figure 2) using 5-cm hand augers. This work was carried out during late-September (1989) in order to have the benefit of maximum development of the active layer. On the north-facing slope, test wells were drilled to refusal at the top of the permafrost and the entire thickness of the active layer screened. Water samples were collected from both surface waters and the test wells. Sampling locations are shown in Figure 3. One litre samples were returned to the field laboratory, analyzed for pH and conductivity, filtered (0.45 µm), preserved and shipped to the National Hydrology Research Institute in Saskatoon for analyses in accordance with methods outlined by Canada, Environment Canada (1979). Water samples were collected for chemical analysis during June and September, 1989, and during the spring-melt period (April through June), 1990. During the latter period the frequency of sample collection was much higher, ranging from daily during the period of peak run-off to a maximum interval of weekly.

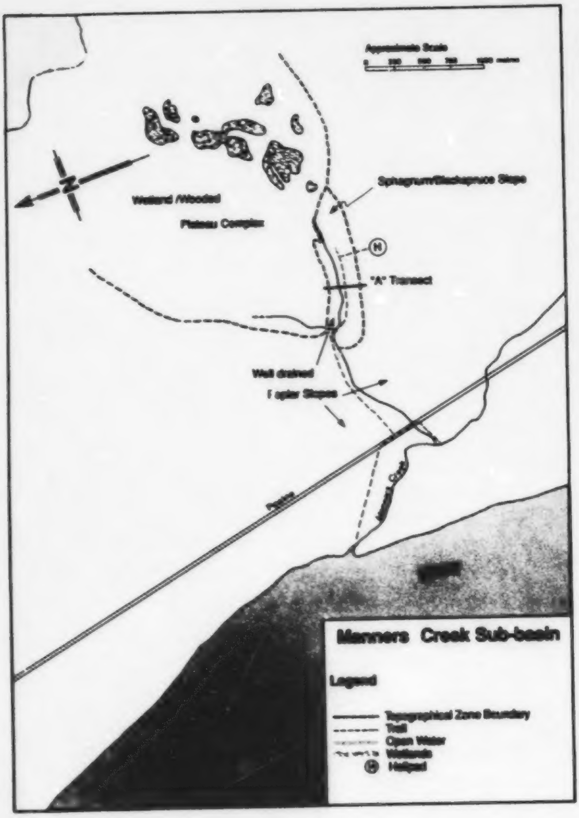
Approximate Scale
0 250 500 750 1000 metres
N
Wetland /Wooded
Plateau Complex
Sphagnum/Blackspruce Slope
H
"A" Transect
Well drained
Aspen Slopes
Manners Creek
Manners Creek Sub-basin
Legend
Topographical Zone Boundary
Trail
Open Water
Wetlands
Helipad

Figure 2. Detailed study sub-basin tributary. Note the upper sub-basin flat lying wetland/wooded plateau complex and the lower well-drained valley slopes.

RESULTS AND DISCUSSION

Basin Mineralogy

The surficial layer of muskeg is composed primarily of organic matter. Significant secondary calcite is present in this layer, probably as a result of upward percolation of water and subsequent evapotranspiration resulting in precipitation of the calcite.

The mineralogy of the sand layer is dominated by quartz, with minor calcite, dolomite, feldspar, hornblende, muscovite, chlorite, illite and goethite. The individual sand grains in this unit are coated with fine-grained chlorite, carbonate and goethite. The mineral species in this layer having major significance to water chemistry are calcite, dolomite and goethite.

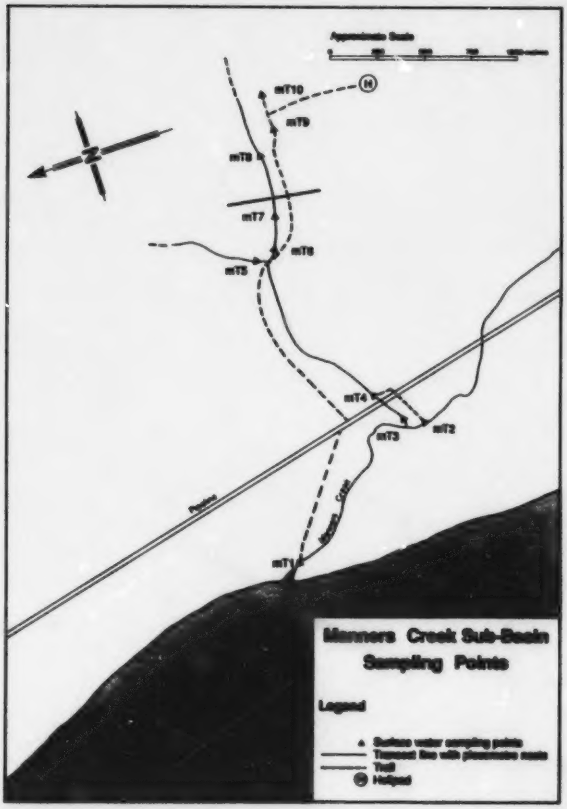
Approximate Scale
N
mT10
H
mT9
mT8
mT7
mT6
mT5
mT4
mT3
mT2
mT1
Pipeline
Manners Creek
Manners Creek Sub-Basin
Sampling Points
Legend
Surface water sampling points
Transect line with piezometer nests
Trail
Helipad

Figure 3. Sampling points for water chemistry within the MCUT sub-basin. Ground-water samples were collected along the "A" transect.

The lower clay or clay-silt layer is composed of quartz, calcite, dolomite, chlorite, illite, and gypsum. In this unit calcite, dolomite, and gypsum have major significance with regard to water chemistry.

In general, the active layer is somewhat leached with respect to calcite and dolomite. The vertical distribution of total carbonate in several test profiles is shown in Figure 4. The distribution of carbonates in the active layer and in the shallow soils that are not underlain by permafrost is different. This difference is a result of different hydrological pathways in the different soil systems and reflects the net movement of water through that soil layer. In the active layer the water is prevented from going deeper into the sediment profile by the confining, basal permafrost. The active-layer water-table is maintained at a depth (0 to 1.5 m) such that the effects of soil suction and evapotranspiration from the near surface zone will cause a net upward movement towards the evaporation front. Carbonates are leached from the active layer and the dissolved constituents are advected upwards to the evaporation front where calcite is precipitated. Visual and SEM examinations show secondary calcite that has precipitated around rootlets and other particles in the organic layer of the upper soils (i.e., at less than 20-cm depth). Downslope, lateral flow can probably occur in conjunction with the above process. The relative importance of the two flow paths out of the active layer will depend on climatic and hydrological conditions at a specific location and time. The above process probably gives rise to the observed carbonate distribution in the active layer. This distribution shows a pronounced near-surface peak in carbonate content. Below this the active layer is partially leached with respect to carbonate and deeper in the soil profile the carbonate content appears to approach background levels. In the deeper parts of the active layer, carbonate dissolution will be limited by time in the unfrozen state. In adjacent soils that are not underlain by permafrost, the observed distribution of soil carbonate is strikingly different. In this regime there is no surficial peak, but rather the surface layers are leached of carbonate, reflecting the net downward flux of water. While some evapotranspiration of water will occur from such soils the water-table must be isolated from such effects, that is, no hydraulic connection exists in the unsaturated zone between the soil/atmosphere interface and the water-table to produce the wicking effect observed in the active-layer system. In this area test wells were installed to a 3.4-m depth, but the water-table was not encountered.

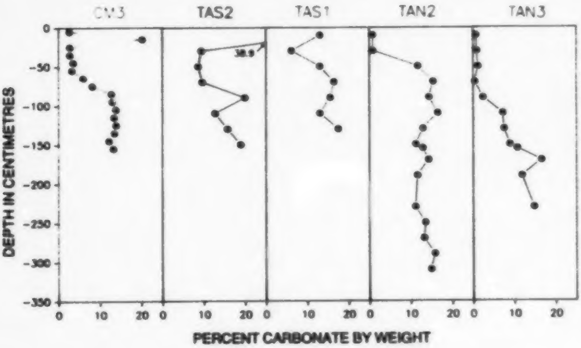

Figure 4. The vertical distribution of total carbonates within the terrestrial sediments of the Manners Creek basin. Note the surface peak in cores CM3, TAS2, TAS1 which are from the active layer overlying permafrost and the lack of a surface peak in TAN2 and TAN3 in which no permafrost was encountered.

Water Chemistry

In order to understand which components of flow were dominant within the basin during the spring-melt period, the various components were sampled with respect to their major ion chemistry. These components include channel icings, snow, ground water and seeps (confined to the active layer), and stream water. Preliminary results are shown in Table 1. Surface-water chemistries discussed in this paper are taken from station mT4 (see Figure 3).

The water can be classed as a Ca^{2+}-HCO_3^- water (Table 1) and the water chemistry within the Manners Creek basin is dominated by the dissolution of carbonates. An analysis of water chemistry in relation to solid-mineral phases using WATEQ (Truesdell and Jones, 1974) indicates that all waters sampled within the basin are in equilibrium with calcite ($CaCO_3$) and slightly supersaturated with respect to dolomite $CaMg(CO_3)_2$. This seems to correspond to the water flowing through the sand layer as part of the active layer. Water that flows deeper in the system, i.e., in contact with the clay or silt layer, has the characteristic signature of high sulphates caused by the dissolution of gypsum ($CaSO_4$*$2H_2O$)

Table 1. Major ion chemistry of various run-off-generating components within the MCUT sub-basin.

SPRING FRESHET COMPONENT CHEMISTRY												
Sample	Date	pH	Ca $meq \cdot L^{-1}$	Mg $meq \cdot L^{-1}$	K $meq \cdot L^{-1}$	Na $meq \cdot L^{-1}$	Cl $meq \cdot L^{-1}$	NO_3 $meq \cdot L^{-1}$	SO_4 $meq \cdot L^{-1}$	ALK $meq \cdot L^{-1}$	(1) $Log(^{IAP}/KEQ)_{Calcite}$	(2) % CBE
N=10 Channel Icings	March 90	8.80(3) 0.46(4)	0.767 0.268	0.973 0.573	0.017 0.010	0.108 0.070	0.013 0.008	0.002 0.003	0.035 0.015	1.692 0.885	0.12	3.41%
N=3 Snow	Mar-Apr 90	6.00 0.05	0.013 0.003	0.005 0.000	0.003 0.004	0.002 0.002	0.004 0.003	0.003 0.001	0.003 0.001	0.014 0.002	-6.40	0.46%
N=6 Ground Water and Seeps	89 - 90	7.97 0.33	7.014 2.846	4.065 2.585	0.072 0.019	0.326 0.075	0.044 0.011	0.000 0.000	2.973 5.582	7.826 1.364	0.76	2.84%
N=1 Stream Water	15 June 89	8.33	3.947	2.353	0.037	0.208	0.024	0.000	0.377	5.795	0.89	2.74%
N=1 Stream Water	19 April 90	7.84	2.001	0.979	0.058	0.118	0.026	0.000	0.143	2.778	-0.19	3.43%

(1) Log $(^{IAP}/KEQ)_{Calcite}$ = calcite saturation index.
(2) CBE% = charge balance error.
(3) Mean.
(4) Standard deviation.

that occurs in minor amounts in this unit. However, with respect to the overall basin water chemistry, sulphate is a minor component, indicating that deeper ground-water flow is minimal in this basin.

Significant dilution effects were observed during the peak spring run-off period (Figure 5) as would be expected in this type of aquatic system. However, even during the periods of greatest dilution (e.g., April 19, 1990), the stream water was close to saturation with respect to calcite (Table 1). This is a result of the distribution of the carbonate minerals in the soils of the active layer. The surficial layer of secondary calcite in the top 20 cm of the organic layer is readily available for dissolution by the infiltrating snowmelt waters. During the spring run-off, 1990, a large proportion of the water in the snowpack apparently either sublimated, evaporated, or infiltrated directly into the shallow active layer, resulting in the overland-flow component (and thus the dilution) being greatly reduced.

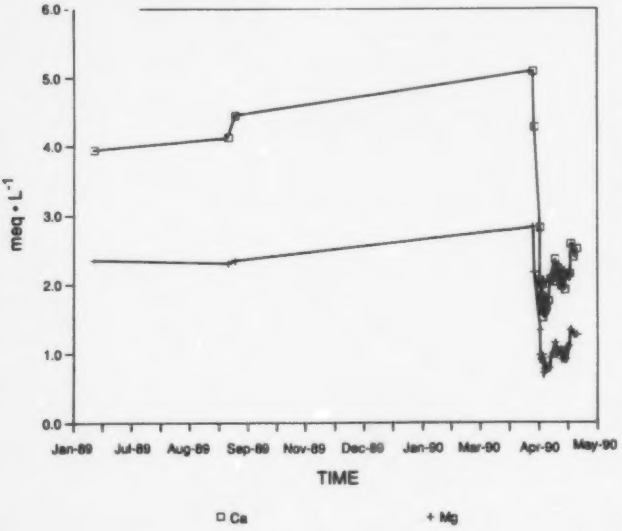

Figure 5. Concentration of calcium and magnesium during period 6-89 through 5-90. Note the dilution during the spring-melt period, however, even during this period surface waters were close to saturation with respect to the carbonate minerals.

CONCLUSIONS

Mineralogical and water-chemistry data confirm the ubiquitous distribution of calcite within the basin and its predominance in determining water chemistry. During the spring-melt period of 1990 substantial alkalinity as well as significant concentrations of calcium and magnesium were observed in the basin run-off. Vertical transport (up-ward) processes in the unsaturated zone, probably driven by evapotranspiration, may be important in moving carbonates to the surficial layer of sphagnum, where they are readily available for weathering during the spring snow-melt period. Shallow active-layer flow was likely the predominant process generating run-off during the spring 1990 run-off period.

REFERENCES

BROWN, J., S.L. DINGMAN and R.I. LEWELLEN, 1968. Hydrology of a drainage basin on the Alaskan Coastal Plain. CRREL Research Report No.240, Cold Regions Research and Engineering Laboratory, U.S. Army Corps of Engineers, Hanover, New Hampshire, 18 pp.

CANADA, ENVIRONMENT CANADA, 1979. Analytical methods manual. Water Quality Branch, Inland Waters Directorate, Environment Canada, Ottawa, Ontario, 620 pp.

HAWES, R.J. (Compiler), 1975. Surficial geology and geomorphology, Fort Simpson, District of Mackenzie. GSC Map No.3-1978, 1:125,000, Geological Survey of Canada, Ottawa, Ontario

ROULET, N.T., 1987. The influence of wetlands on the hydrology of permafrost drainage basins. Proceedings, Symposium '87 Wetlands/Peatlands, C.D.A. Rubec and R.P. Overend, 23-27 August 1987, Edmonton, Alberta, Wetlands/Peatlands '87 Coordinator, Ottawa, Ontario, 333-339

ROULET, N.T. and M.-K. WOO, 1986. Hydrology of a wetland in the continuous permafrost region. Journal of Hydrology, 89(1-2), 73-91

TRUESDELL, A.H. and B.F. JONES, 1974. WATEQ, a computer program for calculating chemical equilibrium of natural waters. Journal of Research of the U.S. Geological Survey, 2(2), 233-248

A PHYSICAL MODEL OF ICE OVERTHRUST DURING THE BREAK-UP OF INTACT RIVER-ICE COVERS*

M.N. Demuth and T.D. Prowse

National Hydrology Research Institute
11 Innovation Boulevard
Saskatoon, Saskatchewan
S7N 3H5 CANADA

ABSTRACT

The passage of water surges resulting from ice-jam releases or spring run-off events can lead to the fracture of intact ice covers, ice runs and further jamming downstream. The nature of the fracturing and clearance processes plays an important role in the probability and severity of ice jamming. To date, considerable effort has been concentrated on the treatment of ice-accumulation dynamics and jam stability, however characterization of the processes by which the initial cover fractures has received limited attention. This paper discusses and illustrates the mechanism of overthrusting flexural failure, a fragmentation process commonly observed during river-ice break-up. The role of natural flaws and cover variability in the initiation of this fragmentation process is also addressed.

INTRODUCTION

River-ice breakup is comprised of numerous ice-failure processes operating at a variety of spatial scales. As proposed by Prowse and Demuth (1989), failure processes can be classified as either *pre-frontal* or *frontal* and further subdivided according to traditional ice-failure nomenclature such as bending, buckling and compression. Pre-frontal failure processes refer to those that occur prior to arrival of the main break-up front. Large-scale horizontal failures or transverse cracks that are believed to result from planform shear-stress variations (Beltaos, 1984) are a case in point. Frontal failures are those associated directly with the passage of the main break-up front. In the analysis of frontal-failure processes most attention has focused on the potential for large-scale horizontal flexural failure that could result from large changes in the hydraulic gradient associated with the downstream passage of a spring flood wave (e.g., Billfalk, 1982; Beltaos, 1990). In a further attempt to model break-up behaviour, Ferrick and Mulherin (1989) have proposed that the main phase of break-up can be divided into processes operating to produce the large-scale bank-to-bank failure and those responsible for the smaller-scale fragmentation of the ice along a brash-ice front.

---

*National Hydrology Research Institute Contribution Series Number CS-90026.

In all the above analyses of pre-frontal or frontal break-up processes, however, either at the large- or small-scale, vertical and horizontal homogeneity in structural and mechanical properties of the ice cover have been assumed. Given the significant spatial differences in ice formation, growth and decay processes, this is unlikely to be the case. Moreover, information exists from analogous studies of sea-ice offshore structure interactions that ice strength, thickness, effective strain modulus, deformation rate and, perhaps most importantly, the variability of these in the vicinity of interaction, control the failure process (e.g., Sanderson, 1988). Similarly, it has been concluded from studies of ice rafting and pressure-ridge formation that variability in cover thickness (i.e., presence of thin ice zones) can significantly reduce the forces necessary to induce such formations (e.g., Parmerter, 1974; Kovacs and Sodhi, 1980; Mellor, 1986). Given the above, it is logical to assume that cover variability could play a significant role in affecting ice-failure processes and the related forces required for the initiation and progression of river-ice break-up. For example, one frontal ice-failure process (fragmentation), that is commonly observed at a range of spatial scales, involves the overthrusting of up-stream ice onto the downstream cover and ultimately, a flexural failure (Figure 1).

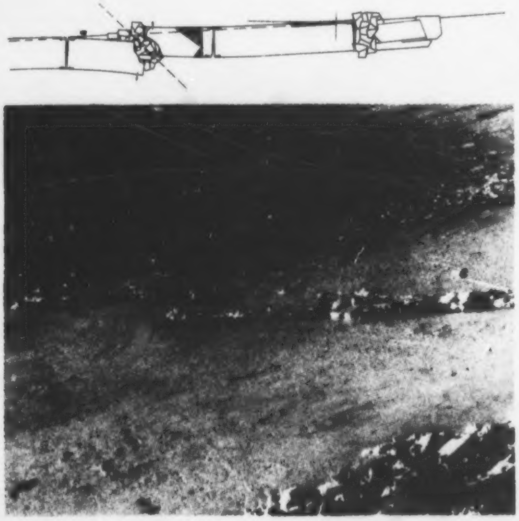

Figure 1. General cross-sectional configuration and example of the ice overthrust flexural failure process during break-up, Mackenzie River, N.W.T., Canada. Ice thickness is ≈ 1 m.

This paper discusses the range of cover characteristics and processes that could lead to irregularities or *flaws* in a river-ice sheet that would in turn promote overthrust flexural failure along brash-ice fronts. Also discussed are the levels of downstream forcing required to initiate such failure. Notably, it will be shown that overthrust flexural-failure processes induced by cover variability require significantly lower downstream forcing than those required to fail a homogeneous cover in elastic buckling; the latter mode often considered as a benchmark case for assessing break-up ice failure.

THEORETICAL BACKGROUND

The initiation and progression of river-ice break-up is governed by the state of balance between processes contributing to downstream forcing and ice resistance. For the purpose of examining ice overthrust flexural failure, the following sections describe the hydro-mechanical components of downstream forcing and the nature of ice resistance and its role in generating ice overthrust.

Downstream Forces

Downstream forces exerted on an ice cover can be divided into two major categories: i) body force derived from the downstream component of the ice-cover weight (F_w); ii) hydrodynamic forces derived from leading-edge form drag (F_t) and friction drag (F_d), imparted to the ice cover by under-ice fluid flow. These components are illustrated in Figure 2 and described by the following (Michel, 1978):

$$[1] \qquad F_w' = \rho_i \; t \, L \, S_f \, g$$

$$[2] \qquad F_t' = \frac{\left[1 - \dfrac{d}{D}\right]^2 U^2 D \rho_w}{2}$$

$$[3] \qquad F_d' = \frac{\rho_w \; d \, S_f \, n_i^{3/2} \, L \, g}{2 n_c^{3/2}}$$

where ρ_i and ρ_w are the density of ice and water, t is the ice thickness, L is the length of the converging ice cover, S_f is the energy slope, g is the acceleration due to gravity, d and D are the under-ice and upstream waterway depths, U is the mean under-ice velocity and n_i and n_c represent Manning's roughness coefficient for ice and the composite section (prime denotes per unit width).

Ice Resistance

The resistance of an ice cover is determined not only by its internal strength but also by its boundary states (thickness, lateral and streamwise horizontal extent and support conditions) which influence the characteristics of deformation and failure. Although it is recognized that the transmittance of downstream forces to the channel boundary can significantly influence the force-resistance balance (e.g., Ferrick and Mulherin, 1989), it will be assumed that the geographical location of this ice-failure process is sufficiently removed from the channel boundary that its influence need not be considered. Moreover, in some cases, significant boundary decoupling and meso-scale fracturing can occur prior to the arrival of the brash-ice front thereby significantly reducing channel boundary effects (e.g., Henderson and Gerard, 1981; Prowse and Demuth, 1989). Indeed the pre-frontal failures identified in Prowse and Demuth (1989) are identified in this paper as one element which characterizes ice-cover variability.

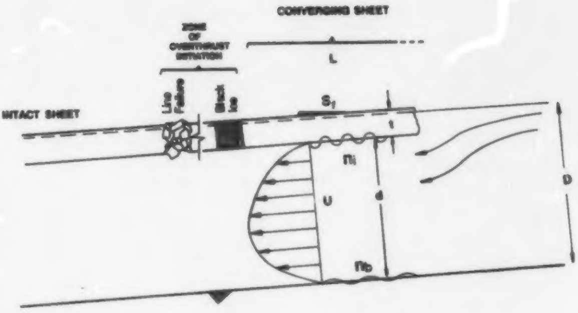

Figure 2. Schematic of impending convergence illustrating the elements of hydro-mechanical forcing.

Characterizing resistance is a difficult task given the dearth of concomitant observations of ice failure and magnitude of downstream forcing. Observations indicate that the variability of ice-cover composition and mechanical properties also plays an important role in characterizing resistance. The body of river-ice strength data, detailing the pre-break-up deterioration and its large-scale spatial variability, are limited primarily to those of Ashton (1985), Bulatov (1970), Kozitsky and Bybin (1967) and more recently of Prowse *et al.* (1988, 1990a, 1990b). There is, however, considerable evidence that the effects of variability are linked to the observed scale-effect pertaining to the measure of ice strength. In a review addressing the perception of scale-effect, Timco (1989) reviews the concepts of non-simultaneous failure and various scaling laws accounting for the size and distribution of flaws in ice. Given particular attention in his review is the question of what constitutes a controlling flaw with respect to the evolution of failure. The following section identifies flaws (variability) that can permit the evolution of overthrust.

Ice-cover Flaws and Variability

Flaws and variability in the context of the present discussion are limited to large-scale phenomena including: i) structural discontinuities in reaches comprised of a variety of structural ice forms, thicknesses and horizontal extent, and ii) cracks or *line failures* resulting from thermal strain or previous ice failure. Microscale flaws and fracture phenomena associated with crack initiation and propagation are not discussed, but are recognized as also being important. Thermal processes can accentuate or minimize the susceptibility to failure of most flaws. The effect of these flaws can be significant in that they may modify ice-cover confinement, providing conditions which promote certain types of ice interaction and deformation leading to ice overthrust.

Structural Variability. Thermal and hydraulic freeze-up conditions strongly control the growth and distribution of ice types in a river system (Figure 3). Typical ice types include: i) superimposed ice (snow ice and surface ice); ii) secondary ice (columnar ice and congealed frazil slush); and, iii) agglomerate ice. Besides differing in mechanical properties (e.g., Michel, 1978), their characteristic decay by radiation is also markedly different. For example, a cover having a granular white-ice surface is effectively insulated from short-wave radiation whereas zones consisting entirely of columnar ice can undergo significant structural decay and may result in an area possessing little compressive or tensile strength. Such structural variability could, for example, promote localized compressive failure and allow the upstream sheet to converge on the intact cover. Similarly, variable cover formation processes can also result in extreme variations in ice thickness. Given the spatial variability resulting from formation and growth processes, zones of especially thin ice can be produced during the pre-break-up period through the combined effects of hydraulic erosion and surface ablation. Localized eccentric bending failure and subsequent convergence could result from this type of structural variability (e.g., Sanderson, 1988). Agglomerate ice or rubble fields, produced during failure events at freeze-up or in advance of the main break-up, will provide another form of structural discontinuity which may lead to a variety of ice-ice interactions.

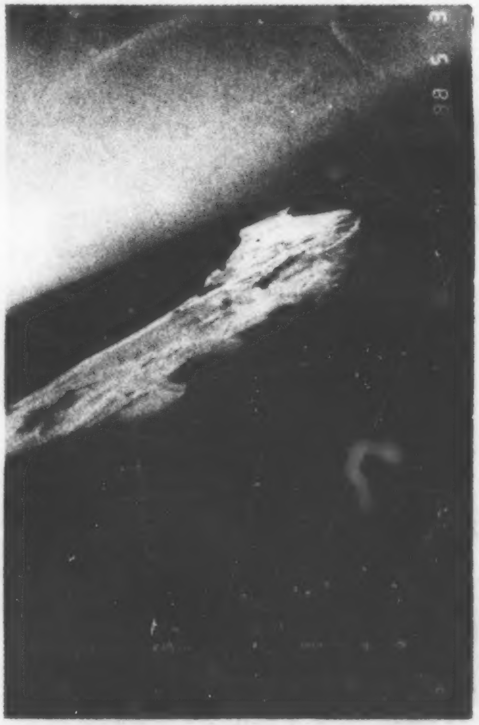

Figure 3. Mackenzie River just prior to break-up showing typical variability in ice-cover types.

Thermal Cracks. The degree to which thermal cracks influence resistance depends strongly on thermal conditions subsequent to their formation. In floating ice, thermal cracks may heal

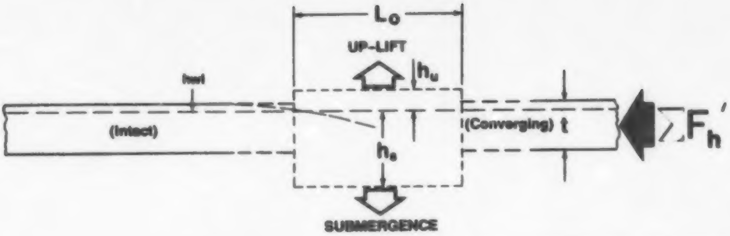

Figure 4. Elements of ice overthrust.

should infiltrating water refreeze. However the quality of the freeze-bond may be affected by the ice structure and freeze geometry produced (e.g., Metge, 1976). The flaw may re-manifest under certain thermal conditions such as radiation melt. Observations by the authors (unpublished) indicate that refrozen thermal cracks in undeteriorated columnar ice samples subject to flexural loading, have not influenced the flexural strength until warming and localized radiation melt re-established the zone of discontinuity. Dry thermal cracks, not extending through the entire ice thickness, are also commonly observed.

ANALYSIS OF OVERTHRUST - FLEXURAL FAILURE

Overthrust Initiation

Figure 4 illustrates the process of ice overthrust flexural failure. The forcing level necessary to promote overthrust is characterized primarily by: i) that required to overcome the weight and buoyancy of the ice zone acted upon by overthrust (R_{gb}') and ii) once overthrust is established, that required for vertical- and axial-end load induced flexural failure (R_b'). Field observations suggest the tendency is for upstream ice to overthrust the intact cover rather than to underthrust it. The incoming ice cover being generally less constrained than the intact cover, may offer some explanation for this tendency. In addition, zones of intact ice exhibiting radiation-induced surface granulation or candling (Prowse *et al.*, 1990a) may allow the converging cover to plough into and over the intact cover. The subsequent analysis, however, is applicable for either an overthrusting or underthrusting interaction.

Uplift and Submergence

To evolve overthrust, potential energy must be supplied to uplift a portion of the converging sheet against gravity, and to submerge a portion of the intact sheet. The work done (W') is equated to the potential energy gained (E_p') as an ice sheet of thickness (t) overthrusts a distance (dL_0) (primes denotes per unit width):

[4] $dW' = dE_p' = R_{gb}'\, dL_0$

The total potential energy of the overthrust zone is:

[5] $E_p' = E_{pu}' + E_{ps}'$

where the potential energy of the uplifted portion (E_{pu}') is given by:

[6] $$E_{pu}' = \frac{M_u'\, g\, h_u}{2}$$

and of the submerged portion (E_{ps}'):

[7] $$E_{ps}' = \frac{M_s'\, g_{eff}\, h_s}{2}$$

where M_u' and M_s' are the mass per unit width of the uplifted and submerged portion of the overthrust zone and h_u and h_s represent the height and depth from the hydrostatic water level, attained by the same respective portions. The effective value of g for submerged ice (g_{eff}) (Mellor, 1986) is given by:

[8] $g_{eff} = |(1 - \rho_w / \rho_i)|\, g$

The mass per unit width of the overthrust zone is:

[9] $M' = M_u' + M_s' = \rho_u\, h_u\, L_0 + \rho_s\, h_s\, L_0$

where ρ_u and ρ_s represent the densities of the uplifted and submerged ice, where:

[10] $\rho_u = \rho_s = (1 - n)\rho_i$

where n is the porosity of the overthrust zone. Combining Equations 6-10 results in:

[11] $$E_p' = \frac{(1 - n)\, \rho_i\, g\, L_0}{2} \left[h_u^2 + h_s^2 \left(\frac{\rho_w}{\rho_i} - 1 \right) \right]$$

Ice mass dM' is contributed during an incremental overthrust (dL_0) such that:

[12] $$\frac{dM'}{dL_0} = 2t\, \rho_i$$

Now from Equation 4:

[13] $$R_{gb}' = \frac{dE_p'}{dh} \cdot \frac{dh}{dL_0}$$

or:

[14] $$R_{gb}' = \frac{dE_p'}{dh} \cdot \frac{dM'}{dL_0} \cdot \frac{dh}{dM'}$$

If geometric similarity holds during the overthrust process (isostatic equilibrium of the overthrust zone is not assumed) then:

$$[15] \qquad \frac{h_u}{h_s} = C$$

Thus from Equation 11:

$$[16] \qquad \frac{dE_p'}{dh} = h_u(1 - n)\,\rho_i\, g\, L_0 \left[1 + \frac{1}{C^2}\left(\frac{\rho_w}{\rho_i} - 1\right)\right]$$

and:

$$[17] \qquad \frac{dM'}{dh} = (1 - n)\,\rho_i\, L_0 \left[1 + \frac{1}{C}\right]$$

Substituting Equations 12 and 15 to 17 results in the following expression for the resistance of the overthrust zone to uplift and submergence:

$$[18] \qquad R_{gb}' = \frac{2\,\rho_i\, g\, t\, h_u \left[C + \frac{1}{C}\left(\frac{\rho_w}{\rho_i} - 1\right)\right]}{C + 1}$$

The action of overthrust effectively doubles the ice thickness in the overthrust zone, thus:

$$[19] \qquad h_u + h_s = 2t$$

Figure 5 illustrates the level of forcing required to create a zone of overthrust by uplift and submergence for given ice thicknesses and ratio C, with $\rho_w = 1{,}000\ \text{kg}\cdot\text{m}^{-3}$, $\rho_i = 900\ \text{kg}\cdot\text{m}^{-3}$. Observations of overthrust in rivers indicate C varies considerably. If conditions are indeed isostatic, $C << 1$. However, the lateral boundary conditions confining the deformation of the intact cover are normally higher than those for the converging cover and thus C may approach unity.

Flexural Failure

Flexural stresses, generated by the action of overthrust, can be described by considering the elastic deformation of an elastically-founded semi-infinite beam, subject to vertical- and axial-end loads (Figure 6). The differential equation governing the vertical deflection of such a beam is:

$$[20] \qquad EI\,\frac{d^4z}{dx^4} + N\,\frac{d^2z}{dx^2} + kz = 0$$

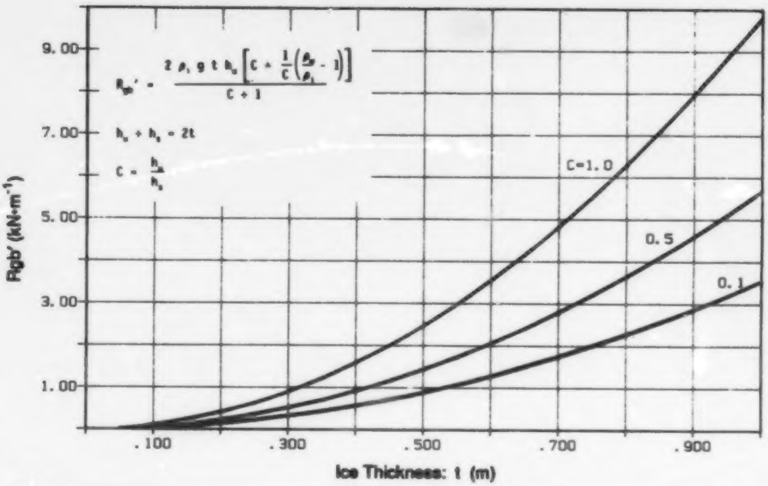

Figure 5. Resistance to uplift and submergence.

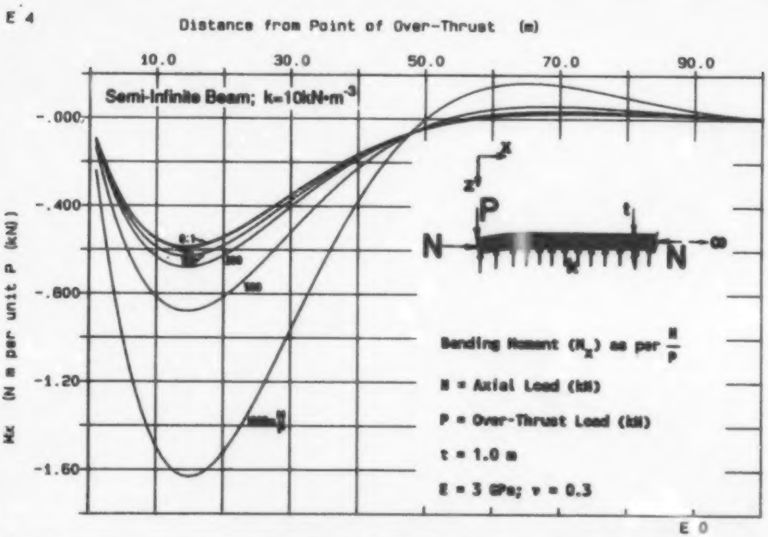

Figure 6. Bending moment distribution of an elastically-founded beam subject to vertical- and axial-end loads.

where E is the effective strain modulus for ice, I is the section modulus of the beam which is analogous to the plate rigidity $t^3/12(1-v^2)$ where t is the ice thickness, N is the axial (compressive) load, k is the foundation stiffness ($k = \rho_w g = 10\ \mathrm{kN \cdot m^{-3}}$), v is the poisson ratio and z represents the vertical deflection at position x along the beam length. Mellor (1986) used a similar analysis to describe the same phenomenon in sea ice. The beam analysis however did not include a term accounting for significant axial end loads. Figure 6 nevertheless, shows that axial-end loads need to be very high to significantly augment the bending moment experienced by the downstream cover. The solution of Equation 20 for this particular case of a homogenous beam (Hetenyi, 1946) is given by:

$$[21a] \qquad z = \frac{2P\lambda^2}{\alpha\, k(3\beta^2 - \alpha^2)}\, e^{-\beta x}\, [2\alpha\beta \cos \alpha x + (\beta^2 - \alpha^2) \sin \alpha x]$$

where P is the vertical overthrust load and α and β are described by:

$$[21b] \qquad \alpha = \left[\lambda^2 + \frac{N}{4EI}\right]^{1/2} \qquad\qquad [21d] \qquad \lambda = \left[\frac{k}{4EI}\right]^{1/4}$$

$$[21c] \qquad \beta = \left[\lambda^2 - \frac{N}{4EI}\right]^{1/2}$$

Elastic buckling stability dictates that $N < 2[kEI]^{1/2}$. This upper limit for N is reasonable since, for all but the thinnest ice covers, downstream forces will rarely reach the levels required for elastic buckling. For example, for $t = 1.0$ m, $E = 3$ GPa, $v = 0.3$ and $k = 10\ \mathrm{kN \cdot m^{-3}}$ would result in $N' = 3.3\ \mathrm{MN \cdot m^{-1}}$.

The distribution of bending moment (M_x) along the beam is:

$$[22] \qquad M_x = \frac{d^2z}{dx^2} = \frac{-2P\lambda^2}{\alpha\,(3\beta^2 - \alpha^2)}\, e^{-\beta x} \sin \alpha x$$

The maximum bending moment position can be determined where $\partial M_x/\partial x = 0$. This occurs at $x \rightarrow \infty$ or $x = i\pi/4\lambda$; $i = 1,3,5\ldots$ (Figure 6)[1]. Thus failure should take place at:

$$[23] \qquad x_f = \frac{\pi}{4}\left[\frac{Et^3}{3k(1-v^2)}\right]^{1/4}$$

---

[1] Mellor (1986) reports the location of maximum bending moment to be $x = i\pi/2\lambda$ (p.270). In a subsequent computation the radian measure adopted by π was not incorporated. These two apparent oversights combined resulted in higher values for the vertical overthrust failure load than those reported here.

Now, it is assumed that the axial load N is negligible once overthrust has been established. Thus, from simple bending theory, the maximum bending moment value at failure is:

$$[24] \qquad M_{xf} = \frac{S_{tf}\, t^2}{6\,(1-v^2)}$$

where S_{tf} is the tensile strength. Combining Equations 22, 23 and 24 gives the overthrust load at failure (P_f'):

$$[25] \qquad P_f' = -\frac{S_{tf}\, e^{\pi/4}}{6 \sin(\pi/4)} \left[\frac{3kt^5}{E(1-v^2)^3}\right]^{1/4}$$

Substituting t = 1.0 m, E = 3 GPa, v = 0.3 and taking pre-break-up values for S_{tf} in the range cf 0.1 to 0.4 MPa (Prowse *et al.*, 1990b; Mellor, 1986)[2], P_f' ranges from approximately 3.1 kN·m^{-1} to 12.5 kN·m^{-1}.

The action of overthrust occurs at some interface angle (ϕ) such that:

$$[26] \qquad P = n \cos\phi - \mu_k\, n \sin\phi$$

$$[27] \qquad N = \mu_k\, n \cos\phi + n \sin\phi$$

where n is the load orthogonal to the overthrust plane, μ_k is the coefficient of kinetic friction and $\mu_k n$ represents the friction force tangential to the overthrust plane. For small overthrust slopes ($\sin\phi \approx 0$; $\cos\phi \approx 1$) the horizontal force per unit width (R_b') necessary to impart an overthrust force leading to flexural failure can be estimated from:

$$[28] \qquad R_b' = \mu_k\, |P_f'|$$

Taking $\mu_k = 0.3$ (Mellor, 1986), and for the above ranges in tensile strength, Figure 7 illustrates the resistance to flexural failure during overthrust for varying ice-cover thickness.

If overthrust slopes are substantial, the resulting axial loads may contribute to the distribution and magnitude of bending moment. Large axial loads would effectively reduce the flexural stiffness of the cover (Sirosh *et al.*, 1989). Little is known about the actual overthrust geometry other than it may be highly random. Analysis of cover slope once overthrust has occurred, suggests ϕ is indeed small and axial loads are thus influenced primarily by μ_k. There are a number of factors, which can affect the transfer of frictional forces during overthrust, whose relative importance are unknown. One example is ice roughness and its modification by water flooding onto

---

[2] Considerable variability has been observed in the majority of data available describing the effective strain modulus and the tensile and flexural strength of ice. See Mellor (1986) for an extensive review.

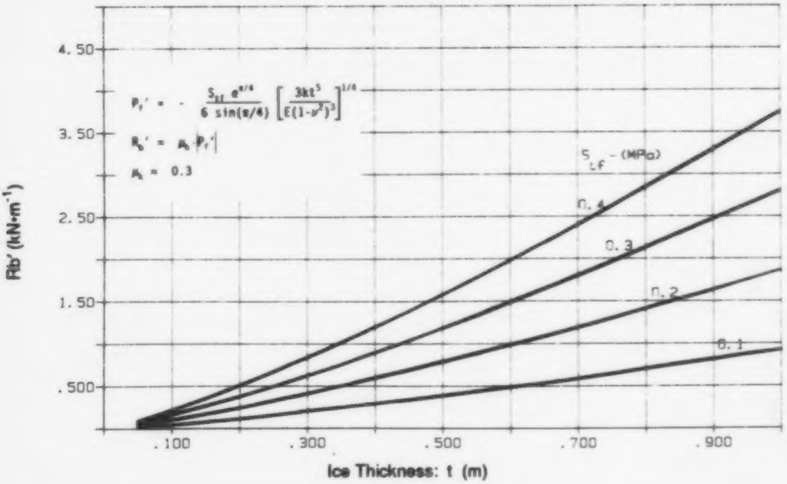

Figure 7. Resistance to flexural failure.

the ice sheet from turbulent wash or infiltration during the deflection of the intact cover. This would tend to reduce the frictional resistance of the overthrust interface.

ANALYSIS OF HYDRO-MECHANICAL FORCING

In the previous section the resistance of the converging and intact covers to uplift, submergence and flexural failure was examined. Neglecting friction, failure could occur if:

[29] $\sum F_h' \geq R_{gb}', R_b'$

where, the sum of the hydro-mechanical forcing elements ($\Sigma F_h'$) is given by:

[30] $\sum F_h' = F_t' + F_d' + F_w'$

These elements are now examined in terms of a convergence (Figure 2). Convergence occurs when the ice sheet upstream of a flaw or zone of variability has the potential to overthrust the intact cover. Using Equations 1 to 3 with typical ice-cover and waterway parameters, estimates of F_t', F_d' and F_w' are made for covers of varying characteristics (Table 1). The effect of channel roughness, converging sheet size, energy slope, mean under-ice water velocity and upstream flow depth (diagonal italicized values, Table 1) can be compared to a reference case (first line

Table 1. Hydro-mechanical forcing magnitudes and ice-cover and waterway parameters.

t	D	d	U	S_f	L	n_i	n_b	n_c	F_t'	F_d'	F_w'
m	m	m	$m \cdot s^{-1}$	$m \cdot m^{-1}$	m	dimensionless			$kN \cdot m^{-1}$		
1.0	5.0	4.08	3.0	0.001	100	0.028	0.028	0.028	0.76	2.00	0.90
1.0	5.0	4.08	3.0	0.001	100	0.028	***0.140***	0.095	0.76	0.32	0.90
1.0	5.0	4.08	3.0	0.001	100	0.028	***0.006***	0.019	0.76	3.58	0.90
1.0	5.0	4.08	3.0	0.001	100	***0.040***	0.006	0.026	0.76	3.77	0.90
1.0	5.0	4.08	3.0	0.001	***1000***	0.028	0.006	0.019	0.76	35.80	9.03
1.0	5.0	4.08	3.0	***0.005***	100	0.028	0.006	0.019	0.76	17.90	4.51
1.0	5.0	4.08	***1.0***	0.001	100	0.028	0.006	0.019	0.09	3.58	0.90
1.0	5.0	4.08	***5.0***	0.001	100	0.028	0.006	0.019	2.12	3.58	0.90
1.0	***3.0***	2.08	3.0	0.001	100	0.028	0.006	0.019	1.27	1.83	0.90

Table 1). Typical downstream forces, associated with hydrodynamic thrust, friction drag and cover weight, could result in failure provided zones of overthrust initiation are present. Notably, these forces are some three orders of magnitude lower than those required for elastic buckling of a homogenous floating ice-cover (e.g., Mellor, 1986; Kerr, 1978).

In general, F_d and F_w are the greatest contributors to downstream forcing. F_t may not be present at all depending on upstream ice conditions. However, provided a leading edge exists, it may become significant as the under-ice water velocity increases and when ice thickness relative to the waterway depth is large. The changes in F_d associated with ice and bed roughness modification suggest adequate knowledge of n_i and n_b are necessary when estimating downstream forces. This is particularly important when attempting to characterize break-up of relatively thin covers where energy slope changes may be of little consequence (Billfalk, 1982). The reference case uses a typical $n_i = 0.028$ with $n_b = n_i$. Modification of bed roughness ($n_b = n_i/2$ and $n_b = n_i/5$) illustrates its importance in the overall process of closed-conduit water shear. Of greatest consequence to both F_d and F_w, however, are the length of the upstream cover and the energy slope. An order of magnitude change in L results in comparable increases in F_d and F_w. A five-fold increase in S_f, typical of surges produced by a rapid ice-jam release, has a pronounced effect on both F_d and F_w.

CONCLUSION

A simple physical model of ice overthrust flexural failure has been presented and describes a commonly observed frontal-scale fragmentation process. The presented case study illustrates that, where flaws and variability of suitable geometry exist, downstream forces are of sufficient magnitude, under typical break-up conditions, to promote an ice overthrust flexural-failure process. There is evidence to suggest that typical river-ice covers exhibit considerable variability and possess flaws likely to permit ice overthrust. In particular, it was shown that the per unit width forcing required to produce overthrust-induced flexural failures is approximately three orders of magnitude lower than that required for elastic-buckling failures in homogeneous covers; the later often considered as a benchmark case for assessing break-up ice failure.

Weaknesses in the present analysis stem from limited knowledge of the overthrust interface geometry and the relative magnitudes of uplift and submergence. A more rigorous solution of overthrust, describing the flexural action of the over-riding, submerged and elastically-founded intact cover could provide insight into the fragmentation of relatively competent, uniform covers where flaws consist primarily of wet cracks produced, initially, by thermal strain or pre-frontal failures. Although the present analysis examines ice-overthrust at a relatively small scale, consideration should also be given to larger-scale ice overthrust processes which could occur at near bank-to-bank scale. Here, consideration of stress distribution and the shedding of stress to the banks must be incorporated.

Overthrust flexural failure is only one of many modes of ice interaction and failure observed during break-up. Adequate modelling and measurement of forcing inputs are necessary for realistic modelling of the break-up process given the known dependence of strength and deformation mode on load duration and magnitude. The probability of an overthrust event or other ice-failure process occurring will depend largely upon the distribution and variability of ice structure, ice strength and flaws. Thus a probabilistic approach could be taken with respect to the distribution of ice resistance when attempting to describe ice break-up. Such an approach may involve the modelling or observation of the areal distribution of strength (thickness, structure and internal strength) which is then categorized into a number of levels. A hypothesized model of ice interaction and break-up could then use this categorization of resistance to determine the most probable mode of interaction or failure and the required forces.

LIST OF SYMBOLS

C	ratio h_u:h_s
d	under-ice waterway depth (L)
D	upstream waterway depth (L)
E	effective strain modulus ($F \cdot L^{-2}$)
E_p	total potential energy of overthrust ($F \cdot L$)
E_{pu}	potential energy of uplifted portion of overthrust ($F \cdot L$)
E_{ps}	potential energy of submerged portion of overthrust ($F \cdot L$)
ΣF_h	sum of the downstream force components (F)
F_w	downstream component of ice-cover weight (F)

F_t	downstream leading-edge thrust force (F)
F_d	downstream under-ice drag force (F)
g	acceleration due to gravity ($M \cdot T^{-2}$)
g_{eff}	submerged equivalent of g ($M \cdot T^{-2}$)
hwl	hydrostatic water line
h_s	depth of submergence below hydrostatic water level (L)
h_u	height of uplift above hydrostatic water level (L)
I	beam section modulus (L^3)
k	foundation stiffness (water:$\rho_w g$) ($M \cdot L^{-2} \cdot T^{-2}$)
L	length of converging sheet (L)
L_0	length of overthrust zone (L)
dL_0	incremental overthrust length (L)
M_s	mass of submerged portion of overthrust (M)
M_u	mass of uplifted portion of overthrust (M)
M_x	bending moment about x axis (F·L)
n_b	Manning's roughness coefficient: bed
n_c	Manning's roughness coefficient: composite section
n_i	Manning's roughness coefficient: ice
N	axial compressive load (F)
n	orthogonal overthrust-interface load (F)
n	porosity of overthrust zone
P	vertical overthrust load (F)
R_b	resistance: flexural failure (F)
R_{gb}	resistance: uplift and submergence (F)
S_{tf}	tensile strength ($F \cdot L^{-2}$)
S_f	energy slope ($L \cdot L^{-1}$)
t	ice thickness (L)
U	mean under-ice water velocity ($L \cdot T^{-1}$)
W	work (F·L)
x	longitudinal (stream-wise) ice-sheet co-ordinate
z	vertical displacement ice-sheet co-ordinate
α	constant Equation 21
β	constant Equation 21
ϕ	overthrust interface angle (degree)
λ	constant Equation 21
ν	poisson ratio
μ_k	coefficient of kinetic friction
ρ	density ($M \cdot L^{-3}$)
'	superscript denoting *per unit width*
f	subscript denoting *failure*
i	subscript denoting *ice*
s	subscript denoting *submerged ice*
u	subscript denoting *uplifted ice*
w	subscript denoting *water*

REFERENCES

ASHTON, G.D., 1985. Deterioration of floating ice covers. Journal of Energy Resources Technology, 107(2), 177-182

BELTAOS, S., 1984. A conceptual model of river ice breakup. Canadian Journal of Civil Engineering, 11(3), 516-529

BELTAOS, S., 1990. Fracture and breakup of river ice cover. Canadian Journal of Civil Engineering, 17(2), 173-183

BILLFALK, L., 1982. Break-up of solid ice covers due to rapid water level variations. CRREL Report No.82-3, Cold Regions Research and Engineering Laboratory, U.S. Army Corps of Engineers, Hanover, New Hampshire, 17 pp.

BULATOV, S.N., 1970. Raschet prochnosti tayushchego ledyanogo prokrova i nachala vetrovogo drefya l'da (Calculating the strength of thawing ice cover and the beginning of wind-activated ice drift). Trudy Vypysk No.74, Gidrometeorologicheskiîe Nauchno-Issledovatel'skiîi Tsentr, Leningrad, 118 pp., CRREL Translation No.IR-799, Cold Regions Research and Engineering Laboratory, U.S. Army Corps of Engineers, Hanover, New Hampshire, 121 pp.

FERRICK, M.G. and N.D. MULHERIN, 1989. Framework for the control of dynamic ice breakup by river regulation. CRREL Report No.89-12, Cold Regions Research and Engineering Laboratory, U.S. Army Corps of Engineers, Hanover, New Hampshire, 14 pp.

HENDERSON, F.M. and R. GERARD, 1981. Flood waves caused by ice jam formation and failure. Proceedings, IAHR International Symposium on Ice, International Association for Hydraulic Research, Vol.1, 27-31 July 1981, Québec, Quebec, 277-287

HETÉNYI, M., 1946. Beams on elastic foundations: theory with applications in the fields of civil and mechanical engineering. University of Michigan Press, Ann Arbor, Michigan, 255 pp.

KERR, A.D., 1978. On the determination of horizontal forces a floating ice plate exerts on a structure. Journal of Glaciology, 20(82), 123-134

KOVACS, A. and D.S. SODHI, 1980. Shore ice pile-up and ride-up: field observations, models, theoretical analysis. Proceedings, International Workshop on the Seasonal Sea Ice Zone, 26 February - 1 March 1979, Monterey, California, Cold Regions Science and Technology, Vol.2, 209-288

KOZITSKY, I.E. and E.A. BYBIN, 1967. Eksperimental'nye issledovaniia prochnosti ledianogo pokrova na razlichnykh stadiiakh ego razrusheniia (Testing ice strength at various levels of deterioration). Trudy No.148, Gosudarstvennyi Gidrologicheskii Institut, Leningrad, (in Russian) 45-63

MELLOR, M., 1986. Mechanical behavior of sea ice. In - Geophysics of Sea Ice, N. Untersteiner (Editor), NATO Advanced Study Institute on Air-Sea Interaction, Proceedings, 28 September - 10 October 1981, NATO ASI Series, Series B: Physics, Vol.146, Plenum Press, New York, 165-281

METGE, M., 1976. Thermal cracks in lake ice. Ph.D. thesis, Queen's University, Kingston, Ontario, 499 pp.

MICHEL, B., 1978. Ice mechanics. Les Presses de l'Université Laval, Québec, Quebec, 499 pp.

PARMERTER, R.R., 1974. Dimensionless strength parameters for floating ice sheets. Proceedings, 2nd International Conference on Port and Ocean Engineering under Arctic Conditions, University of Iceland, Reykjavík, Iceland, 490-501

PROWSE, T.D. and M.N. DEMUTH, 1989. Failure modes observed during river ice breakup. Proceedings, 46th Annual Eastern Snow Conference, 7-9 June 1989, Québec, Quebec, 237-241

PROWSE, T.D., M.N. DEMUTH and C.R. ONCLIN, 1988. Using the borehole jack to determine changes in river ice strength. Proceedings, 5th Workshop on Hydraulics of River Ice/Ice Jams, 21-24 June 1988, Winnipeg, Manitoba, 283-303

PROWSE, T.D., M.N. DEMUTH and H.A.M. CHEW, 1990a. Changes in the flexural strength of ice under radiation decay. 8th International Northern Research Basins Symposium and Workshop, 26-30 March 1990, Abisko, Sweden, Water Resources Engineering, Luleå University of Technology, 29 pp. Nordic Hydrology, 21(4-5), 341-354

PROWSE, T.D., M.N. DEMUTH and H.A.M. CHEW, 1990b. The deterioration of freshwater ice due to radiation decay. Journal of Hydraulic Research, 28(6), 685-697

SANDERSON, T.J.O., 1988. Ice mechanics: risks to offshore structures. Graham and Trotman, Boston, Massachuestts, 253 pp.

SIROSH, S.N., A. GHALI and A.G. RAZAQPUR, 1989. A general finite element for beams or beam-columns with or without an elastic foundation. International Journal for Numerical Methods in Engineering, 28(5), 1061-1076

TIMCO, G.W., 1989. Scale effects in ice. Proceedings of Workshop on Ice Properties, 21-22 June 1988, St. John's, Newfoundland, Associate Committee on Geotechnical Research Technical Memorandum No.144, National Research Council of Canada (NRCC 30358), Ottawa, Ontario, June, 183-199

SEASONAL CHANGES IN THE HYDROCHEMISTRY OF LAND DRAINAGE: COLOUR LAKE CATCHMENT, AXEL HEIBERG ISLAND, N.W.T.

M. English[1], S. Schiff[2], M. Ecclestone[3], W.P. Adams[3], M. Hinton[2], L. Pezzutto[1], R. Elgood[1], C. Allan[3] and D. Pierson[3]

[1]Department of Geography
Wilfrid Laurier University
Waterloo, Ontario
N2L 3C5 CANADA

[2]Waterloo Centre for Groundwater Research
University of Waterloo
Waterloo, Ontario
N2L 3G1 CANADA

[3]Department of Geography
Trent University
Peterborough, Ontario
K9J 7B8 CANADA

ABSTRACT

This study examines the quality and quantity of land drainage into Colour Lake on Axel Heiberg Island, Northwest Territories, during the two periods of the year when drainage pathways to the lake are significantly different: spring melt and fall. During spring the active layer is very shallow and the total load of Ca^{2+}, SO_4^{2-} *and* Mg^{2+} *transported from land to the lake is 18.3, 47.6 and 4.1* $kg \cdot d^{-1}$ *respectively. During late fall when the active layer is most pronounced the total transport of* Ca^{2+}, SO_4^{2-} *and* Mg^{2+} *from land to lake increases significantly from the spring values to 66.3, 270 and 30* $kg \cdot d^{-1}$ *respectively. Long-term climate warming in the High Arctic may result in drainage chemistry entering Colour Lake which for a greater percentage of the thaw-year resembles current fall drainage chemistry.*

INTRODUCTION

The purpose of the research is to understand the natural hydrological and chemical interactions between the terrestrial and aquatic (stream and lake) portions of a high-arctic catchment during the time of the year when the transfer of water from the terrestrial catchment to the lake is most pronounced: late May to late August. This paper addresses the two periods when hydrological pathways are the most dissimilar: spring melt and the late fall.

During spring melt, run-off from the terrestrial catchment to the lake is largely restricted to drainage along well-defined surface streams and overland flow.

Widespread, saturated, concrete frost (originally defined by Trimble *et al.*, 1958) in the upper layer of the mineral soil is largely responsible for this. During the late fall, active-layer formation (as defined by Brown, 1971) has reached its maximum annual depth; consequently drainage into the lake originates from potentially different sources than spring melt water and the water, regardless of source, is following different pathways to the lake.

This research continues to be carried out in the Colour Lake catchment, Axel Heiberg Island, N.W.T. The study site is located at 79°25'N, 90°45'W near the headwaters of the Expedition River (Figure 1). Research on physical and biological processes (e.g., limnology, climatology, permafrost, soils, etc.) has been conducted at this well-defined catchment sporadically since 1959 (Adams, 1987). The most intensive research conducted on the basin prior to this work was directed at understanding the physical limnology of Colour Lake (Caflisch, 1972). Caflisch (1972) suggests that Colour Lake is approximately 9,000 years old and was formed by glacial erosion or by the melting of dead ice. The geology of the Colour Lake catchment has been described by Fricker (1963). Basically the catchment consists of some till deposits, sedimentary rock and anhydrite diapir formations.

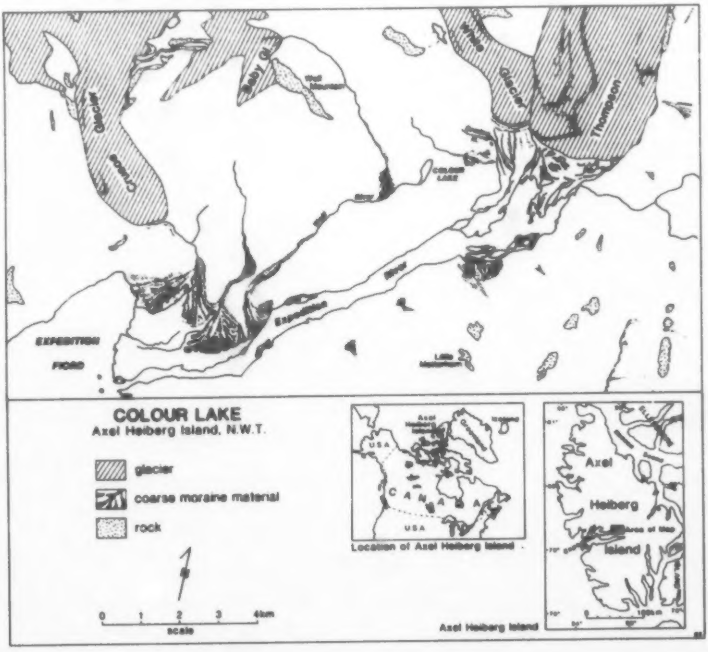
Crusoe Glacier
Baby Gl.
White Glacier
Thompson
COLOUR LAKE
Expedition River
EXPEDITION FIORD
COLOUR LAKE
Axel Heiberg Island, N.W.T.
glacier
coarse moraine material
rock
0 1 2 3 4km
scale
Axel
USA
C A N A D A
USA
Location of Axel Heiberg Island
Axel
Heiberg
Island
Area of Map
Axel Heiberg Island

Figure 1. Location of Colour Lake catchment, Axel Heiberg Island, Northwest Territories.

The climate of this region is described by Ohmura (1972). Of note are: 1) the long periods of cloudless days in May and June when basin albedo is highest; and, 2) the frequent cyclonic activity through the region in July and August which reduces solar radiation input to the basin at a time when the basin albedo is lowest. These conditions are not favourable to significant active-layer development. Although complete climatic records from Expedition Fiord are best described as sporadic in nature, the spring melt usually is initiated in mid- to late-May and freeze-up begins between late-August to mid-September.

Hydrologically the catchment is divided into the lake and six sub-basins (Figure 2); the ratio of land area (72 ha.) to lake area (10 ha.) is 7.2:1. Various basin dimensions are listed in Table 1. Of the six surface streams identified in Figure 2, only the streams draining the West Inflow and the East Inflow sub-basins flow continuously during spring, summer and fall. The other streams flow for varying periods of time during the spring melt. The outflow of the lake is best described as marshy and of low gradient. As the banks of the lake's outflow stream are very poorly defined, the width of the outflow increases as the flow increases. The depth of the water, even at high-flow periods, seldom exceeds 0.20 m.

METHODOLOGY

The spring-melt and fall periods compared in this paper are from different years. This is principally due to the fact that it was logistically impossible to sample the spring-melt and fall period during the same year. The spring melt reported here was sampled in 1985 (May 20 to June 17) and most of the fall data reported were collected in 1988 (August 14 to 31). Some subsurface seepage chemistry data retrieved from piezometers during late August 1989 are included. Though it is

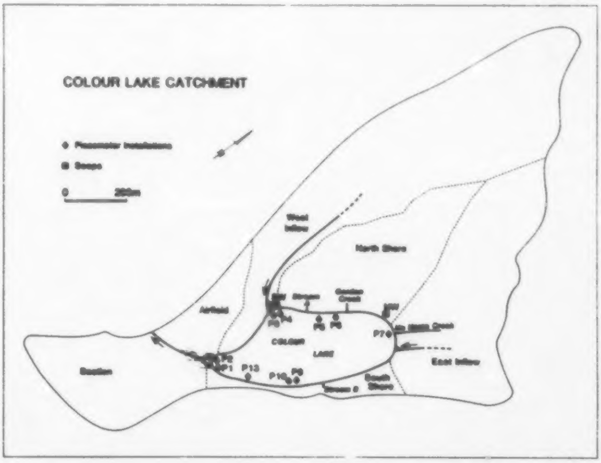

Figure 2. Sub-basins and instrumentation of Colour Lake catchment.

recognized that climatic differences from year-to-year occur, the purpose of this paper is to compare the hydrology and chemistry of waters draining the terrestrial basin during periods of significant overland flow and minimal infiltration (typical of spring melt) and periods when active-layer formation is pronounced (typical of late fall). In this sense, comparison of the 1985 spring melt and the 1988 late-fall periods is justified.

To determine the volume of water discharging from Colour Lake and the surface stream volume flowing into the lake, stream cross-sectional area was measured, and velocity was determined by dye injection. Dispersion of the dye was not a problem as the dye maintained its integrity along the 1.0-m pathway used for recording the velocity. The frequency of measurement and sampling for water chemistry varied, but generally speaking the streams and lake discharge were gauged and sampled more than once a day for both the spring period in 1985 and the fall period in 1988.

Table 1. Colour Lake catchment, sub-basin and lake areas (m^2). Refer to Figure 2 for locations of sub-basins.

Colour Lake	102,070
North Shore	140,598
West Inflow	319,471
East Inflow	201,940
Airfield	52,983
Bastion	108,510
South Shore	33,909

During the 1985 spring melt, a Belfort water-level recorder was installed in the lake such that continuous monitoring of lake-stage change was achieved. Changes in lake level during the fall of 1988 were taken from a protected staff gauge.

Daily precipitation was sampled using a standard Atmospheric Environment Service (Environment Canada) precipitation gauge located within the catchment (Figure 2). Black ice, white ice and snow-depth measurements were recorded each day during the spring of 1985; the results are reported by Allan *et al.*, 1987.

Depth to the permafrost table was monitored during both time periods by measuring the depth to the permafrost table in excavated soil pits and the depth of penetration of a steel probe driven into the active layer. The details of the survey are reported for the 1985 spring-melt period in Allan *et al.* (1987); basically transects were run from the lake shore to more elevated portions of the catchment. Measurements were taken each few metres. A small number of soil pits were excavated so the depth to permafrost recorded by the steel probe could be checked. In all cases the measurements were accurate to within 0.05 m. These excavated active-layer pits were used to extract frozen soil from the upper portion of the permafrost table for isotopic analysis.

Chemical analyses of all anions and cations in water samples were carried out by the National Water Research Institute of Environment Canada, the Ontario Ministry of the Environment and the Water Quality Laboratory Waterloo Centre for Groundwater Research at the University of Waterloo. Conductivity and pH determinations were done at the Colour Lake base camp. Stable-isotope analyses were performed at the Isotope Laboratory of the Earth Sciences Department at the University of Waterloo.

Mini-seepage piezometers were installed by hand at various points in the shallow littoral areas of Colour Lake (Figure 2) to provide samples for water analyses and to monitor hydraulic properties of the upper phreatic zone. The piezometers were installed to the permafrost table which, in the shallow littoral zone of the lake, ranged between 0.20 and 0.34 m below the lake sediments. *In situ* measurements were undertaken, one time at each piezometer, to calculate the hydraulic conductivity of the phreatic zone; samples for water chemistry were taken after the piezometers had been purged several times.

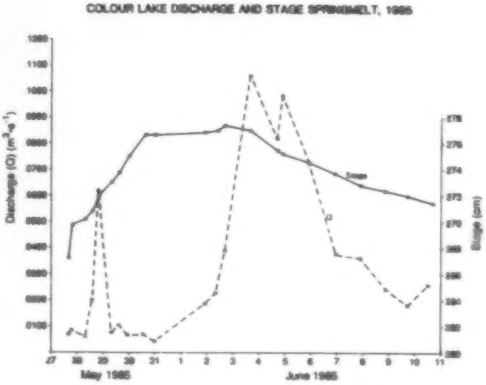

Figure 3. Relationship between lake stage and discharge from Colour Lake, May to June, 1985.

SPRING MELT 1985

The most significant hydrological aspect of spring-melt run-off within the Colour Lake catchment is the large volume of surface run-off from the land to the lake by well-defined surface streams and overland flow. During the early spring run-off a significant portion of the meltwater of terrestrial origin was diverted to the discharging stream of Colour Lake via a moat which formed around the perimeter of the lake ice cover. Figure 3 illustrates the relationship between lake stage and discharge from the lake. There is no apparent relationship between lake stage and discharge up to June 4, 1985; thereafter linear regression analysis indicates a very significant relationship (r=0.93, 99% Confidence Interval). The lack of a relationship prior to June 4 is thus attributable to minimal mixing of this inflowing terrestrial meltwater with the lake proper.

The relative contributions of water draining directly to the lake by well-defined surface streams during the spring melt of 1985 are shown in Table 2. To determine the volume of ungauged, terrestrial-source, snowmelt water directly entering the lake by overland flow and/or seepage during the spring, the total calculated surface-stream inflow to the lake from the terrestrial basin, the total lake snowcover and white-ice loss for the period, the change in lake volume and the total lake discharge are considered in the following manner:

$$[1] \qquad SO \quad (LQ \quad [TS \cdot IPI]) \pm \Delta LV$$

where:
SO = seepage and/or overland flow draining into the lake (m^3)
LQ = total discharge from the lake (m^3)
TS = total surface stream inflow to the lake (m^3)
IPI = white ice and/or direct precipitation input to lake (m^3)
ΔLV = change in lake volume (m^3)

Evaporation has been left out of this equation as the potential error in this term, using empirical equations employing our meteorological data, would be large. As the temperatures are low and the land:lake ratio is 7.2:1, evaporation would not likely represent a large number relative to the inflows to the lake and the discharging stream of the lake.

Substituting the appropriate numbers into Equation 1, the volume of ungauged overland flow/seepage entering Colour Lake during the spring melt of 1985 is calculated as 38,127 m^3, or 63% of the total spring run-off from the land to the lake.

Table 2. Spring-melt water balance[1] and total transfer of Ca^{2+}, SO_4^{2-}, and Mg^{2+} from the terrestrial portion of Colour Lake catchment to the lake during the spring-melt period of 1985. Water is reported in m^3, ions are reported in kg and mg m^{-2}.

	Water	Ca^{2+}	SO_4^{2-}	Mg^{2+}
Total surface stream inflow (TS^2)	22,100	170(236)	350(486)	44(61)
East Inflow	6,573	99(493)	226(1,120)	17(85)
West Inflow	15,323	63(197)	101(317)	26(81)
Overland Flow	38,127	362(503)	1,029(1,430)	76(105)
Total transport to the lake from land	60,227	532(739)	1,379(1,916)	120(166)
Ice and direct precipitation to the lake (IPI^2)	5,573	119*	231*	24*
Change in lake water level (ΔLV^2)	+4,000	--	--	--
Total lake discharge (LQ^2)	61,800	1,014	4,220	519

[1] *Evaporation is ignored in this water balance, please see text.*
[2] *See Equation 1.*

**These values include a significant amount of white ice (relative to direct precipitation on the lake during the spring-melt period) and as such the masses reported for Ca^{2+}, SO_4^{2-} and Mg^{2+} also include a significant amount of lake water; the exact proportions are not known.*

FALL 1988

During the monitoring period in the fall of 1988, the active layer had most probably reached the maximum seasonal thickness as surface stream run-off ceased in early September and temperatures began to drop. As such, infiltration of precipitation falling onto the ground during the two-week sampling period would be essentially 100%. Overland flow was not observed in the basin at this time. Surface stream discharge was only observed in the principal surface streams draining the West Inflow and East Inflow sub-basins. Flow in the East Inflow stream ceased on August 24 and discharge from the West Inflow stream ended on August 27. Surface flow in these streams was not observed again during the remainder of the fall field season. While surface flow had ceased, the lake discharge did not drop significantly while observations were maintained up to and including September 3.

To determine the volume of indirect seepage to Colour Lake during the fall period in 1988 the components of the water balance listed in Table 3 are substituted into Equation 1. This calculation tells us that 8970 m^3 of water was flowing into Colour Lake by direct ground-water seepage during this period of the fall of 1988. This seepage value equals approximately 80% of the total calculated inflow from the terrestrial portion of the catchment. During this period approximately 20% of the terrestrial run-off enters the lake from surface streams.

Table 3. Late fall (15-27 August 1988) water balance[1] and total transfer of Ca^{2+}, SO_4^{2-} and Mg^{2+} from the terrestrial portion of Colour Lake catchment to the lake. Water is reported in m^3, ions are reported in kg and $mg \cdot m^{-2}$.

	Water	Ca^{2+}	SO_4^{2-}	Mg^{2+}
Total surface stream inflow (TS^2)	2,259	94(180)	310(594)	51(98)
East Inflow	752	31(153)	90(456)	26(129)
West Inflow	1,507	63(197)	220(688)	25(78)
Groundwater input into the lake	8,969	768(1,068)	3,200(4,448)	339(129)
Total transport to the lake from land	11,228	862(1,248)	3,310(4,758)	390(227)
Direct precipitation to lake (IPI^2)	170	0.020*	0.100*	0.001*
Change in lake water level (ΔLV^2)	-418	--	--	--
Total lake discharge (LQ^2)	11,816	420	1,559	100

[1] Evaporation is ignored in this water balance, please see text.
[2] See Equation 1.

**As precipitation to the lake during this time period is very small the mass load of Ca^{2+}, SO_4^{2-} and Mg^{2+} is reported to three significant digits.*

DIFFERENCES BETWEEN SPRING AND FALL HYDROLOGICAL FLOW PATHWAYS

The primary difference between the spring-melt run-off of 1985 and the drainage calculated for the fall period of 1988 is that most, if not all, drainage reaching the lake during the spring melt was surface run-off. Active-layer formation for the period when most of the spring melt run-off occurred, June 1 to 6, was minimal. On May 29, active-layer depth averaged 0.13 m (range 0.00 to 0.48 m, n = 47). During the fall period, most of the waters draining the terrestrial portion of the catchment entered the lake by subsurface seepage. Active-layer depth in the late fall (August 23, 1988) averaged 0.63 m (range 0.53 to 0.81 m, n = 16).

TERRESTRIAL DRAINAGE CHEMISTRY

Spring Melt 1985

Table 4 illustrates the total transport of Ca^{2+}, SO_4^{2-}, and Mg^{2+} from the terrestrial portion of the Colour Lake catchment during the spring-melt period of 1985. The total input from surface streams is included as is the individual transport from the two principal contributing streams draining the West Inflow and East Inflow sub-basins. These two surface streams are hydrologically important as their total flow during the spring-melt period equals 99% of the total, terrestrial surface, stream drainage. The ungauged water reaching the lake from the terrestrial portion of the catchment (calculated using Equation 1) is reported as 'overland flow/seepage'. Enrichment of snowpack water in Ca^{2+}, SO_4^{2-} and Mg^{2+} in spring 'overland flow/ seepage' and surface-stream water is indicated in Table 4. For comparison the Ca^{2+}, SO_4^{2-}, and Mg^{2+} concentrations in phreatic-zone water sampled in the fall of 1989 are included. Chemically, 'overland flow/seepage' water is more or less the same as surface-stream water, which indicates that the contact time of snowmelt water with the regolith is very similar in both cases. During spring the ratio of measured surface-stream volume to calculated 'overland flow/seepage' volume is 0.58:1; the similar ratio of Ca^{2+} mass transport during the same time period is 0.47:1, that of SO_4^{2-} is 0.34:1 and Mg^{2+} is 0.58:1.

Fall 1988

Table 4 shows the Ca^{2+}, SO_4^{2-} and Mg^{2+} concentrations in fall precipitation, stream inflows and ground water. Ground water is shown both as 'seep' and as 'phreatic' water; the former has some contact with surface soils as it exits from the subsurface onto the ground above the lake level, the phreatic water has been extracted from depth using a mini piezometer. Of particular interest is the very significant chemical enrichment of both the East and West Inflow streams from the spring values. Of note is the chemical enrichment of precipitation as it percolates through the ground; more pronounced than that noted (Table 4) during the spring.

Table 4. Concentrations of Ca^{2+}, SO_4^{2-} and Mg^{2+} in precipitation, surface water and ground water during the spring melt of 1985 and the fall of 1988. All values in $mg{\cdot}L^{-1}$.

A. SPRING

	Precipitation	East Inflow	West Inflow	Overland Flow Shallow Seepage
Ca_{2+}	1.50 r: 0.54-2.22 n: 28	12.90 r: 11.58-16.47 n: 10	4.50 r: 2.05-12.49 n: 28	9.50 r: 4.43-13.17 n: 13
SO_4^{2-}	2.30 r: 1.02-3.27 n: 27	28.20 r: 25.20-49.30 n: 10	7.50 r: 2.52-16.00 n: 24	27.00 r: 4.46-46.80 n: 15
Mg^{2+}	0.07 r: 0.02-0.16 n: 28	3.80 r: 1.53-3.09 n: 10	1.90 r: 0.33-6.83 n: 28	2.00 r: 0.82-4.56 n: 15

B. FALL

	Precipitation[1]	East Inflow[2]	West Inflow[2]	Ground-water Seepage[3]	Phreatic Water[4]
Ca^{2+}	0.13	40.90	41.90	66.10 r: 50.20-81.90 n: 2	127.00
SO_4^{2-}	0.59	120.00	146.00	230.00 r: 138.00-322.00 n: 2	608.00
Mg^{2+}	0.03	6.90	17.10	28.60 r: 12.3-44.9 n: 2	79.00

[1] *There was only one minor measureable precipitation event, on August 25.*

[2] *For the fall sampling, we report only one data point for the East and West Inflows. The sample variation is expected to be small as the active layer is at its maximum thickness and precipitation during the fall period is negligible.*

[3] *Ground-water seepage is defined as water seeping out of the ground surface above the lake level.*

[4] *Phreatic water is sampled in the shallow littoral zone of the lake and hence is representative of ionic concentrations of ground water prior to entering the lake proper. The values reported here for the three ions are the minimum values derived from three functioning mini piezometers. Therefore the calculations based upon ground-water seepage concentrations are conservative estimates with respect to the data available.*

Table 3 illustrates the total transport of Ca^{2+}, SO_4^{2-} and Mg^{2+} from the terrestrial catchment to the lake during the later fall season of 1988 (August 15 to 27). During this period of time ground-water seepage into the lake represents a very significant fraction of the total water transport to the lake. The ratio of surface stream to subsurface seepage is 0.25:1; similarly constructed ratios for Ca^{2+} transport are 0.12:1, SO_4^{2-}: 0.09:1 and Mg^{2+}: 0.15:1. Relative to the flow volumes, the subsurface seepage is notably enriched in the three ions. The similar relationship reported above for the spring-melt period indicates a similar result, that is the Ca^{2+}, SO_4^{2-}, and Mg^{2+} exported in 'overland flow/seepage' are enriched in mass relative to the transport in surface streams.

COMPARISON OF TERRESTRIAL ION TRANSPORT BETWEEN SPRING AND FALL

Comparison of ion transport from the terrestrial portion of the basin to the lake between spring and fall is difficult as the fall period represents a much shorter period of time than the spring period. To account for this the data are normalized for daily transport (Table 5).

The ratio of total water drainage per day from the terrestrial basin in spring (762 m^3) to fall (173 m^3) is 4.38:1. The similar normalized ratio for total Ca^{2+} mass transport for the two seasons, spring and fall, is 0.28:1, that of total SO_4^{2-} mass is 0.17:1 and total Mg^{2+} mass is 0.14:1. The significant enrichment, between spring and fall noted when comparing the water-transport ratio to the three ion-transport ratios is illustrated in Table 5. The total Ca^{2+}, SO_4^{2-}, and Mg^{2+} transport per day from the terrestrial portion of the catchment for the spring and fall periods is listed in Table 6. This transport of terrestrial-source ions during the fall period represents an increase over spring transport of 360%, 570% and 730% for Ca^{2+}, SO_4^{2-}, and Mg^{2+}, respectively.

It is noteworthy that while the total surface-stream transport of ions increases from spring to fall and is most pronounced for SO_4^{2-} and Mg^{2+} (Table 6), the surface streams of the East Inflow and West Inflow sub-basins exhibit somewhat opposite patterns of transport for Ca^{2+} and SO_4^{2-}. In the West Inflow, surface-water transport of all ions increases notably from spring to fall, while in the East Inflow only Mg^{2+} transport increases from spring to fall while both Ca^{2+} and SO_4^{2-} transport decrease.

Table 5. Export of water, Ca^{2+}, SO_4^{2-} and Mg^{2+} from the terrestrial portion of the Colour Lake catchment to the lake normalized for daily contribution for the spring and fall periods.

	Water	Ca^{2+}	SO_4^{2-}	Mg^{2+}
TOTAL SPRING TRANSPORT				
m^3	762	--	--	--
$kg \cdot d^{-1}$	--	18.3	47.6	4.1
$mg \cdot m^{-2} \cdot d^{-1}$	--	25.5	66.1	5.7
Total kg	--	532.0	1,379.0	120.0
TOTAL FALL TRANSPORT				
m^3	174	--	--	--
$kg \cdot d^{-1}$	--	66.3	270.0	30.0
$mg \cdot m^{-2} \cdot d^{-1}$	--	95.8	387.7	43.7
Total kg	--	862.0	3,510.0	76.0

The most notable increase in ionic transport from spring to fall is the comparison between overland flow/seepage in the spring

Table 6. Total export per day from the surface streams, the streams draining the West and East Inflow sub-basins and calculated ungauged inflow (overland flow/ground-water seepage), normalized for daily input for the spring and fall periods of study.

kg·d^{-1}	Ca^{2+}		SO_4^{2-}		Mg^{2+}	
	Spring	Fall	Spring	Fall	Spring	Fall
Total Surface Stream Export	5.9	7.2	12.1	23.8	1.5	3.9
West Inflow Stream Export	2.2	4.8	3.5	16.9	0.9	1.9
East Inflow Stream Export	3.4	2.4	7.8	6.9	0.6	2.0
Overland Flow and/or Ground-Water Seepage Export	12.5	59.0	35.5	246.2	2.6	26.1

mg·m^{-2}·d^{-1}	Ca^{2+}		SO_4^{2-}		Mg^{2+}	
	Spring	Fall	Spring	Fall	Spring	Fall
Total Surface Stream Export	12.6	13.8	25.9	45.7	3.3	7.5
West Inflow Stream Export	6.8	15.2	10.9	52.9	2.8	6.0
East Inflow Stream Export	17.0	11.7	38.6	35.1	2.9	9.9
Overland Flow and/or Ground-water Seepage Export	17.3	82.0	49.3	342.0	5.7	36.2

with seepage in the fall (Table 6). As discussed above, the spring stream water and overland flow/seepage chemistry (Table 4) are similar. As such, a better comparison between spring and fall transport of ions from the terrestrial catchment would be the combined stream and 'overland flow/seepage' transport for the spring and the subsurface transport for the fall, representing the two major flowpaths of water reaching the lake.

The significant enrichment in ionic mass transport from spring to fall is attributed to the different flowpaths which water takes at these different times of the year. Specific reasons for the increased mass transport during fall are unknown; some isotopic evidence centres on the source as fall precipitation and perhaps some melting of the permafrost table. As precipitation percolates into the unsaturated active layer it has greater time to reach chemical equilibrium with the regolith. As such the ground-water seepage water will be enriched relative to surface-drainage water especially in the spring when the active layer is so shallow and the chemical interaction between run-off and the regolith is minimized. An additional source of chemically-enriched water may come from the thawing permafrost table. Plausible means of identifying the source of the ground water entering Colour Lake involve examining the $\partial^{18}O$ in the potential components contributing to the ground water, including the precipitation and the permafrost. The reader is referred to Drever (1988) for theory supporting the use of stable isotopes in hydrology.

The single permafrost ∂^{18}O value we have is -24‰. The snowmelt run-off ∂^{18}O values average -28‰ and the ground-water seepage values average -23.7‰, equalling the permafrost value (the error associated with ^{18}O analysis is ±0.2‰). Average fall precipitation values are -22.8‰; however, the range of values varies considerably: -27‰ to -18.5‰. Snowmelt water ∂^{18}O at -28‰ does not appear to be a significant contributor to ground-water flow in the fall. Though freeze-thaw of precipitation may enrich the isotope ratio by 2 - 3‰ (Michel and Fritz, 1982), the difference between an altered snowmelt isotopic signature and the ground water is too large. The volume of snow water required to contribute significantly to the ground water does not exist as almost 90% of the estimated water equivalence of the terrestrial snowpack can be accounted for in the spring drainage of water from the land to the lake.

Isotopically the ground water resembles permafrost, however the range of fall precipitation ∂^{18}O values does not exclude the possibility of rainfall contribution. In fact if the basin run-off for the 13-day study period is applied through the summer and early fall (defined here as June 18 to August 14), and this run-off is directly equated to precipitation falling at that time, then the total summer and fall precipitation would equal 6.2 cm.

Ohmura (1972) reports the calculated water balance for the Colour Lake area from mid-June to August 23, 1969 yields total run-off of 5.2 cm. This figure is in close agreement with the calculated value of 6.2 cm noted above for essentially the same time period in 1988. In terms of water mass therefore, the late summer and autumn precipitation could account for the ground-water flow and hence the higher chemical concentrations of ground water would not necessarily be a result of thawing of permafrost but rather the precipitation equilibrating with the regolith.

The ∂^{18}O signature of summer precipitation while unmeasured is in good probability at the heavier side of the known range of fall precipitation, i.e., -18.5‰. Summer precipitation recorded at most latitudes is isotopically heavier than winter precipitation (Drever, 1988). It is thought that the fall drainage into Colour Lake while certainly containing some summer precipitation is not dominated by it. The mean fall value of ground water (-23.7‰) closely resembles the average value for fall precipitation (-22.8‰) however the small volume of precipitation, just less than 2 mm, during the fall 1988 monitoring period could only account for approximately 13% of the total run-off. If it is assumed that summer precipitation accounts for the remaining 87% of the total run-off then isotopic mixing of the fall (∂^{18}O:-22.8‰) and summer (∂^{18}O:-18.5‰) precipitation would produce ground water with a ∂^{18}O of -19.1‰; 4.6‰ heavier than the measured value. It is possible that precipitation prior to the initiation of fieldwork in August of 1988 contributed to run-off during this time. It is also possible that old water contained within the active layer and permafrost table contributes to the late-fall terrestrial drainage.

CONCLUSIONS

This research has identified and quantified very significant differences in the chemistry of terrestrial drainage to Colour Lake between the spring and fall period. During spring melt much of the snowmelt is directed along the surface either along well-defined stream beds or by overland flow and shallow seepage. Chemical enrichment of snowmelt water does occur during this period but potentially significant quantities of the exported water and accompanying ions may never mix with the lake, but rather are diverted along the surface of the ice cover to the lake via a moat. The degree of this mixing will vary from year-to-year. The work of Heron (1985) documents the processes involved in high-arctic ice decay including the formation and importance of the moat.

Terrestrial run-off during the fall is largely ground-water seepage at or below the water level of the lake. The change in ion transport from the land to the lake from the spring to the fall is quantified. The concentrations of dissolved ions in stream flow increase very significantly from spring to fall, indications of a change in the flow pathways and source of water reaching the stream. During the fall the ice cover on the lake has significantly decayed or is completely gone. The potential for mixing of the highly-concentrated fall terrestrial seepage into the lake is very high.

Long-term implications of potential climate warming include a significant increase in the duration and quantity of subsurface seepage entering the lake. Weathering reactions would speed up as a result of increased soil temperatures, biological productivity and decomposition. Frozen regolith previously isolated from chemical weathering in the permafrost zone could now be exposed to weathering. Hence the solute load entering Colour Lake could well increase significantly.

ACKNOWLEDGEMENTS

Funding for this project was provided initially by NSERC through an operating grant awarded to W.P. Adams of Trent University and later through an NSERC operating grant awarded to M. English. The Polar Continental Shelf Project of Energy Mines and Resources Canada generously provided 'air time' and ground support through a grant to W.P. Adams (grant number 123-83). The Northern Scientific Training Grant program of the Department of Indian and Northern Affairs enabled students to participate in this research. Laboratory analyses of water samples was in part provided by Dr. D.S. Jeffries of the National Water Research Institute (anions) and Dr. P.J. Dillon of the Dorset Research Centre of the Ontario Ministry of the Environment (cations). Research grants to M. English from Wilfrid Laurier University and to S.L. Schiff from the Waterloo Centre for Groundwater Research paid for the stable isotope analysis. Pam Schaus of the Department of Geography at Wilfrid Laurier University drafted the figures.

REFERENCES

ADAMS, P. (Editor), 1987. Field Research on Axel Heiberg Island, N.W.T., Canada: Bibliographies and Data Reports with Appendices of Data from the McGill Subarctic Research Station, Schefferville, P.Q. McGill Subarctic Research Paper No.41, Axel Heiberg Island Research Report, Miscellaneous Papers No.2, Occasional Paper No.12, Department of Geography, Trent University, Peterborough, Ontario, Centre for Northern Studies and Research, McGill University, Montréal, Quebec, 207 pp.

ALLAN, C., S. SCHIFF, D. PIERSON, M. ENGLISH, M. ECCLESTONE and W.P. ADAMS, 1987. Colour Lake, Axel Heiberg Island, N.W.T., a naturally acid, High Arctic, lake - data report. In - Field Research on Axel Heiberg Island, N.W.T., Canada: Bibliographies and Data Reports with Appendices of Data from the McGill Subarctic Research Station, Schefferville, P.Q., P. Adams (Editor), McGill Subarctic Research Paper No.41, Axel Heiberg Island Research Report, Miscellaneous Papers No.2, Occasional Paper No.12, Department of Geography, Trent University, Peterborough, Ontario, Centre for Northern Studies and Research, McGill University, Montréal, Quebec, 67-189

BROWN, R.J.E., 1971. Characteristics of the active layer in the permafrost region of Canada. Proceedings, Seminar on the Permafrost Active Layer, 4-5 May 1971, Vancouver, B.C., Technical Memorandum No.103, Associate Committee on Geotechnical Research, National Research Council of Canada, Ottawa, Ontario, 1-7

CAFLISCH, T., 1972. Limnological investigations of Colour and Phantom Lakes. Miscellaneous Papers by Fritz Müller and Members of the Expedition, Axel Heiberg Island Research Reports, McGill University, Montréal, International Geographical Union, Field Tour Ea 2: Arctic Archipelago I, 22nd International Geographical Congress, August, 49-56

DREVER, J.I., 1988. The geochemistry of natural waters. 2nd edition, Prentice Hall, Engelwood Cliffs, New Jersey, 437 pp.

FRICKER, P.E., 1963. Geology of the Expedition Fiord area, western central Axel Heiberg Island, Canadian Arctic Archipelago. Jacobsen-McGill Arctic Research Expedition 1959-62, Geology No.1, Axel Heiberg Island Research Reports, McGill University, Montréal, Quebec, December, 156 pp.

HERON, R., 1985. Decay of a high arctic lake ice cover. Ph.D. thesis, Department of Geography, McMaster University, Hamilton, Ontario, 189 pp.

MICHEL, F.A. and P. FRITZ, 1982. Significance of isotope variations in permafrost waters at Illisarvik, N.W.T. In - The Roger J.E. Brown Memorial Volume, Proceedings of the Fourth Canadian Permafrost Conference, H.M. French (Editor), 2-6 March 1981, Associate Committee on Geotechnical Research, National Research Council of Canada, Ottawa, Ontario, 173-181

OHMURA, A., 1972. Some climatological notes on the Expedition Area. Miscellaneous Papers by Fritz Müller and Members of the Expedition, Axel Heiberg Island Research Reports, McGill University, Montréal, International Geographical Union, Field Tour Ea 2: Arctic Archipelago I, 22nd International Geographical Congress, August, 5-13

TRIMBLE, G.R., R.S. SARTZ and R.S. PIERCE, 1958. How type and soil frost affects infiltration. Journal of Soil and Water Conservation, Vol.13, 81-82

SHAPE, LENGTH AND FLOW CONDITIONS OF CONDUITS AT SOUTH CASCADE GLACIER, WASHINGTON STATE, U.S.A.

A.G. Fountain

U.S. Geological Survey
PO Box 25046 MS-412
Denver, Colorado 80225
U.S.A.

ABSTRACT

The hydraulic properties of the subglacial drainage system of South Cascade Glacier are inferred by examining the time of travel of artificial tracers injected into the glacier and water discharge in streams draining the glacier. Results from the injection of tracers, corroborated by water-budget calculations, indicate that South Cascade Glacier is divided into two main basins. Each basin is drained by a single stream. Mean velocity and dispersion of tracers also are significantly different in each basin. It is hypothesized that one stream drains from an isolated conduit and daily meltwater in the ablation zone reaches the conduit directly through englacial channels. The other stream drains a distributed subglacial network of interconnected paths such as linked cavities or permeable debris.

The cross-sectional geometry and sinuosity of the isolated conduit is inferred by analyzing the dispersion and travel time of tracers. The dispersion is assumed to result from the velocity shear in the conduit. The flow depth is calculated from the travel time of the initial tracer concentration and peak concentration. The width of the conduit, determined from the measured value of the discharge and calculations of flow depth and velocity, is very broad relative to the depth. The subglacial channels are quite sinuous. The estimated flow velocity is much faster than the apparent velocity and indicates that water moves slowly through the body of the glacier relative to its speed in a subglacial conduit. Comparing the slope of the logarithm of travel time versus the logarithm of water discharge for measured values to the slope of theoretical values based on Manning's equation, it is inferred that the conduit was probably pressurized in mid-summer, during maximum ice melt, and later changed to partially-full conduit flow.

INTRODUCTION

Water from glaciers is important to the water resources of high alpine areas and high latitude regions. Glaciers also store and catastrophically release water, resulting in floods (Paterson, 1981). To better predict run-off from glaciers for both resource evaluation and hazard assessment, the processes of water flow through the glacier must be better understood.

The characteristics of water movement at and near the glacier's surface are reasonably well known. In the ablation zone, water percolates vertically through the snow as unsaturated flow until it reaches the impermeable ice underneath, where it flows horizontally in a saturated layer (Colbeck, 1974). Once the ablation zone is free from snow, the water flows in the near-surface zone of permeable weathered ice (Larson, 1977) or in surface streams. In the accumulation zone, the water percolates through the snow to the underlying firn where a fairly thick saturated layer forms (Oerter and Moser, 1982; Fountain, 1989). The water drains away from the near-surface region and into the body of the glacier via crevasses or moulins that intersect the surface (Fountain, 1989). The processes that govern the rapid movement of large volumes of water through the body of the glacier are still conjectural.

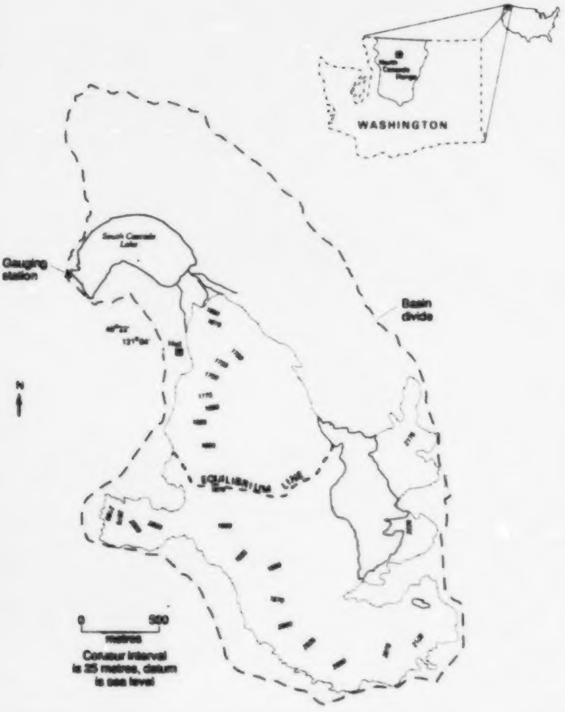

Figure 1. South Cascade Glacier, September 1985.

Water is thought to move through the glacier and at the glacier bed in conduits (Röthlisberger, 1972), and at the glacier bed as sheet flow (Weertman, 1972), in interconnected cavities (Kamb, 1987), or through the subglacial debris layer much like a confined aquifer (Clarke, 1987). To determine which of these processes might be important for subglacial flow through a temperate valley glacier, a field study was started in 1986 at South Cascade Glacier in Washington State, U.S.A. (Figure 1). This paper briefly describes one aspect of this study, the results and analysis of tracers injected into the glacier. The subglacial water flux cannot be directly measured, therefore its hydraulics are inferred from indirect observations. Tracers were injected into the glacier to estimate the geometry of the flow system from the tracer travel time and dispersion.

FIELD METHODS

The tracers used in this study were Rhodamine WT and Tinopal CBS-X. Rhodamine is a fluorescent dye often used in tracer studies in general (Smart and Laidlaw, 1977; Fischer *et al.*, 1979) and in glacier studies (Krimmel *et al.*, 1973; Seaberg *et al.*, 1988; Brugman, 1986). Tinopal is an optical brightener and has been used previously as a tracer (Gaspar, 1987; Brugman, 1986). These two tracers were selected because their excitation spectra are sufficiently different that they may be used simultaneously without mutual interference.

In this study, tracers were usually poured into crevasses in the belief that crevasses are the principal feature responsible for draining water from the surface of the glacier (Fountain, 1989). However, tracers were only poured into those crevasses in which water was heard flowing to avoid crevasses that might be sealed. Tracer concentrations in Streams 1 to 3 (Figure 2) were measured by siphoning the water through tubes to a central location where a switching device routed the water to two fluorometers connected in series. Each

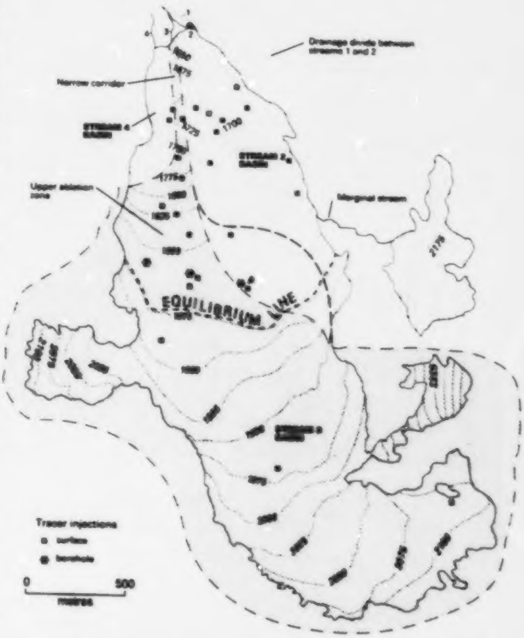
1
3
2
Drainage divide between streams 1 and 2
Narrow corridor
1975
STREAM 4 BASIN
1725
1700
STREAM 2 BASIN
1775
Upper ablation zone
Marginal stream
2175
EQUILIBRIUM LINE
Tracer injections
surface
borehole
0
500
metres

Figure 2. Glacier drainage basins. The location of tracer injections are denoted by solid squares and stars. "A" indicates the location of a paired injection at the surface and in a borehole. The different streams, 1 to 4, are indicated by numbers at the top of the diagram. The long-dashed line is the postulated position of a subglacial water divide.

fluorometer was dedicated to one tracer and the output from both instruments was recorded on a solid-state data logger. The logger also controlled the switching device. This measuring system is explained in more detail by Fountain (1991).

In addition to the tracer measurements, stream discharge and conductivity were recorded and surface melt was intermittently measured.

DRAINAGE BASINS

During the two field seasons a consistent pattern emerged between the location of tracer injection and the stream in which it was detected. This pattern indicated that three drainage basins existed on the glacier (Figure 2). Most of the ablation zone drained to Stream 2; all of the accumulation zone, a part of the ablation zone, and a narrow drainage strip in the lower ablation zone drained to Stream 3; and a small part of the ablation zone on the west side drained to Stream 4. No tracer appeared in Stream 1 indicating that this stream drained the nonglacierized valley walls on the east side.

To delineate more precisely the boundaries of the two main basins a seasonal water balance was calculated for Stream 2 and Stream 3 based on their basin area, measurements of meltwater and rain input, and stream discharge. The boundary between the two basins was moved until the relative error in the balance of each basin was equal. The adjusted boundary was not allowed to contradict the results of surface injections of the tracers. The details of this procedure will be more completely developed in a future paper. For both years that the balance was calculated, 1986 and 1987, the results were similar; Stream 2 drained 30% of the glacier surface and Stream 3 drained 69%.

The basin boundaries define the surface-drainage pattern; however, the subglacial-flow pattern may be different. Two simultaneous injections, one into a surface crevasse and the other into a nearby borehole, were made on the upper ablation zone (Figure 2, point marked A) near the boundary between stream basins 2 and 3. The surface injection was detected in Stream 2 whereas the borehole injection was detected in Stream 3. This indicates an overlap of surface and subsurface paths and implies that the surface and subsurface flow paths may not be always vertically connected.

EVIDENCE FOR DIFFERENT FLOW PROCESSES

The daily variations in water discharge and electrical conductivity, an indicator of solute concentration, show similar behaviour in both streams in terms of relatively-smooth diurnal variations and exhibiting the typical inverse relation between solute concentration and water discharge. As the season progressed, the variations became more peaked in Stream 3 as a consequence of the thinning snowpack and upglacier retreat of the snowline, which allows meltwater to run off more rapidly. However, the daily variation between water discharge and solute load is quite different. In Stream 2, the variations in solute load and water discharge are in phase, whereas in Stream 3, the load is roughly constant and shows no correlation with discharge. Solute load, rather than concentration, is a better indicator of subglacial processes because it is unaffected by meltwater dilution, which dominates the variation in solute concentration.

Considering that the bedrock slope and rock type are about the same under both basins, the difference in load variation is caused by the residence time of subglacial water. In the Stream 2 basin, the residence time is sufficiently long to acquire significant solute mass and in the Stream 3 basin the residence time, in the ablation zone, is comparatively short such that solute acquisition is insignificant. Therefore, the subglacial-flow velocities are faster in the Stream 3 basin that in the Stream 2 basin and are caused by a difference in hydraulic conditions. To explain the constant load in Stream 3, a solute source must be located in a region unaffected by diurnal variations in meltwater input, such as the subglacial region under the accumulation zone.

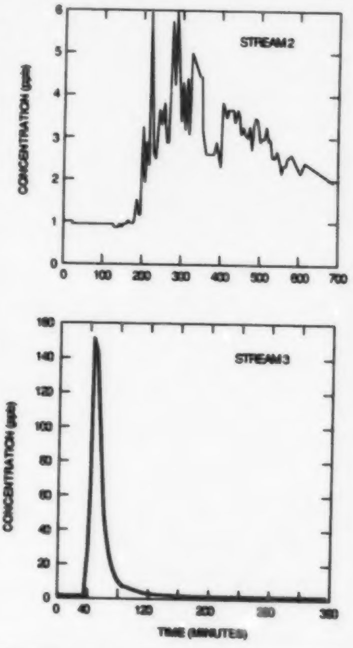

Figure 3. Typical tracer-concentration versus time curves for tracers injected in the Stream 2 and Stream 3 basins. The Stream 2 concentration was from a tracer injected immediately upglacier from the 1,725 m contour and 1,750 m contours in the narrow strip of drainage (Figure 2).

Further evidence for different flow processes is derived from tracer injections. Typical concentration-time curves for each basin are shown in Figure 3. There is some dependence of the arrival time of peak concentration with time of day and, hence, water discharge, but there is otherwise little correspondence between the shape of the concentration curve and changes in discharge. Tracers injected into the Stream 2 basin characteristically have a much larger dispersion and longer travel time than tracers injected into the Stream 3 basin. Occasionally, a concentration-time curve from a tracer injected into the Stream 3 basin will exhibit a longer recession limb with the smooth form of an exponential decay, but will not contain individual concentration spikes characteristic of tracers detected in Stream 2. Average velocity, calculated from the travel time of peak tracer concentration and assuming a straight-line distance from injection location to exit from the glacier for the Stream 2 basin is 0.056 $m \cdot s^{-1}$ and for the

Stream 3 basin is 0.12 $m \cdot s^{-1}$. These velocities are within the range of velocities found by Krimmel *et al.* (1973).

The small dispersion observed in tracers injected in the Stream 3 basin indicates a channelized-flow system, such as conduits. The existence of a narrow strip of surface drainage, which was revealed by tracer injections, indicates such a conduit and probably results from the longitudinal alignment of surface crevasses parallel to a subsurface conduit. Tracers injected into the upper ablation zone flow through a conduit system, probably englacial, that connects with the conduit in the narrow drainage strip. The flow velocity is fairly large in conduits and consequently the residence time of water in contact with the bed is short, limiting the acquisition of solutes.

The large dispersion of the tracers detected in Stream 2 indicates a distributed-flow system. The concentration spikes, typical of these concentration-time curves (Figure 3), indicate multiple flow paths, like those for braided streams or a network of interconnected cavities. The flow velocity through such a system is relatively slow and the residence time of water is correspondingly longer, which results in a greater solute acquisition.

SUBGLACIAL CONDUIT GEOMETRY OF STREAM 3

Where Stream 3 flows from the terminus of the glacier, a subglacial conduit is observed to extend up-glacier. In 1987, the conduit was about 0.4-m high and 2-m wide, with an ice roof and bedrock bottom and was incised into subglacial debris consisting of coarse sand. For the short distance that it could be observed, the conduit was very sinuous forming a hairpin turn of about 3 m in radius. The limited distance viewed does not provide much information about the extension of the conduit further upglacier, and the conduit appearance at the terminus is probably a result of local conditions. The conduit geometry results from the conduit position on the bed, thickness of the glacier, and variation in water discharge. A conduit existing at the base of a glacier has two different boundaries: the conduit bottom is rock and the roof and walls are ice. Ice melt results from heat generated in the viscous dissipation of energy in the flowing water when the water is in contact with the ice. The movement of bed material in a stream channel is dependent on the shear stress of the flowing water exceeding a critical shear stress sufficient to move particles (Wiberg and Smith, 1987). Particle movement is required to erode bedrock or to scour granular beds. Because ice melt occurs for any flow condition whereas bed erosion occurs after a minimum condition, the conduits should generally be incised up into the ice rather than eroded into the bed. Certainly, a variety of conditions can occur to promote bed erosion. The following discussion of conduits will assume that the channel is incised into the ice roof with a flat bottom. The water flow through the conduit should vary diurnally because the meltwater input varies diurnally. Where the water is in contact with the ice, the ice will melt and the conduit enlarge. The rate of conduit enlargement from the viscous dissipation of heat of the flowing water compared to the rate of ice closure is about 44 times faster, for ice thicknesses typical of the lower ablation zone (roughly 70 m) and for a conduit 1 m in diameter.

The diurnal discharge of water cannot maintain a filled conduit. Although the roof of the conduit is not always in contact with the water, the walls are in contact and the conduit widens. At some point, equilibrium is reached with the mean diurnal discharge and the geometry of the cross section is like a half-ellipse with its long axis parallel to the bed.

The vertical profile of water velocity in a conduit, with a large width-to-depth ratio, is assumed to be the same as that for an infinitely-wide conduit. According to Shimizu (personal communication), the bed shear stress accounts for more than 90% of the total shear stress in channels with a width-to-depth ratio of 10:1, indicating that the effect of the walls is small. The form of vertical velocity profiles in subglacial conduits is unknown, but a logarithmic-parabolic profile is used as a first approximation (Rattray and Mitsuda, 1974).

$$[1] \qquad \begin{aligned} u &= \frac{u_*}{k} \ln \frac{\varepsilon}{\varepsilon_\circ} && \varepsilon \leq 0.2 \\ u &= \frac{u_*}{k} \left\{ \ln \frac{0.2}{\varepsilon_\circ} + 6.24(\varepsilon - 0.5\varepsilon^2 - 0.18) \right\} && \varepsilon \geq 0.2 \end{aligned}$$

where u is the velocity; u_* is the shear velocity (and equal to $gHS^{1/2}$) where, g is gravity, H is flow depth, and S is the channel slope; k is Von Kármán's constant (0.4). ε is the nondimensional depth (depth within the flow divided by total flow depth), and $\varepsilon_\circ$ is the nondimensional roughness scale (height of the roughness on the stream bed divided by the total flow depth divided by 30). The roughness height in this equation is the actual vertical dimension of the roughness on the stream bed. The factor (30) is based on the assumption of hydrodynamically rough flow (Nikuradse, 1933 summarized by Robertson and Crowe, 1985). The maximum flow velocity (u_{max}) is at the flow surface for partially-full conduit flow; and midway between the conduit roof and floor for pressurized flow. It can be calculated from Equation 1 as:

$$[2] \qquad u_{max} = \frac{u_*}{k}(0.388 - \ln \varepsilon_\circ)$$

and the vertically-averaged flow velocity from:

$$[3] \qquad \bar{u} = \frac{u_*}{k}(0.743 + \ln \varepsilon_\circ)$$

The longitudinal dispersion of a tracer in a stream is probably caused by horizontal velocity changes in the vertical dimension. If it is assumed that the first arrival, or minimum travel time (T_{min}), of the tracer, corresponds to the maximum flow speed, and the time of peak arrival (T_{peak}), corresponds to the vertically-averaged flow speed, the flow depth can be calculated from the travel times and estimate of the roughness. The flow distance can be expressed as the product of the travel time and flow velocity. The flow distance is the same for all parts of the tracer curve; therefore, substituting Equations 2 and 3 yields:

$$[4] \qquad \frac{T_{min}\, u_*}{k}\left(0.388 + \ln \varepsilon_\circ\right) = \frac{T_{peak}\, u_*}{k}\left(-0.743 + \ln \varepsilon_\circ\right)$$

Solving this equality for the flow depth (H) which is imbedded in the term for shear velocity u_*, results in:

$$[5] \qquad H = z_\circ \exp\left(\frac{0.388\, T_{min} + 0.743\, T_{peak}}{T_{min} - T_{peak}}\right)$$

where $z_\circ$ is the roughness scale.

The length of the flow path is calculated by an iterative procedure. First, the flow depth is calculated from Equation 5 and mean velocity is initially calculated from Equation 3. A first estimate of the channel slope in Equation 3 is acquired from the change in bed elevation between the location of injection (known from radar measurements of the ice thickness (Hodge, 1979)) and point of detection divided by the straight line distance between them. A revised estimate of the path length is calculated by multiplying the travel time of the peak concentration by the mean flow velocity ($T_{peak}\bar{u}$). The conduit slope is then recalculated and used to update the new shear velocity (u_*) and consequently a new mean velocity (Equation 3). The procedure iterates until the difference between the new and previous value of path length is small, in this application, 1%. The sinuosity is simply derived from the path length divided by the straight-line distance between the point of injection to the measuring location. The conduit width is estimated from the calculated values of flow depth and velocity, and the measured value of discharge.

However, the conduit roughness is not known and due to the time interval of tracer sampling, the exact arrival times of the first and peak tracer concentrations are not known. Practical limits can be placed on the magnitude of the roughness and the arrival times are known to within a few minutes. With a number of tracer injections, the flow parameters can be fairly well constrained because roughness, conduit width and sinuosity would not be expected to vary over a short period of a few days, and the flow depth is deeper for greater water discharge.

This analysis was applied to 10 of the 15 surface injections in the Stream 3 basin because this subset also had coincident discharge measurements that are required for the conduit-width estimate. The results are summarized in Table 1.

Table 1. Summary of the inferred flow parameters of the subglacial conduit assuming a bed roughness of 0.02 m and partially-full conditions. Distance is that of a straight line drawn between the point of injection and the point of measurement. Q is the water discharge, sinuosity (λ) is the length of the flow path divided by the distance, and $\bar{u}$ is the mean flow velocity as estimated by Equation 3.

Injection Date	Time PDT[1]	Distance m	Flow $m^3 \cdot s^{-1}$	Flow Depth m	Conduit Width m	λ	$\bar{u}$ $m \cdot s^{-1}$
July 20	10:46	485	0.72	0.09	8.5	3.7	0.9
23	11:35	485	0.50	0.08	7.5	3.6	0.8
23	12:40	785	0.59	0.08	7.7	4.2	1.1
August 18	15:52	785	0.80	0.11	6.1	3.8	1.2
20	11:15	1160	0.43	0.07	8.7	5.9	0.7
20	16:05	485	0.61	0.09	8.9	4.6	0.8
September 19	13:10	485	0.18	0.04	9.2	3.3	0.5
19	16:10	485	0.24	0.05	8.3	3.3	0.6
20	12:40	835	0.29	0.06	7.4	4.6	0.7
20	16:15	660	0.41	0.07	7.8	3.8	0.8

[1] *Pacific daylight time.*

The calculated values of sinuosity are much larger than values for subaerial fluvial systems, which do not often exceed 2 (Schumm, 1977). The large values of sinuosity indicate that the average flow speed from glacier surface to exit from the glacier is much slower than the calculated speed in the conduit. To achieve a slower flow speed in a conduit, the flow depth must be decreased (Equation 1), and to maintain continuity with the measured discharge, the flow width is increased. If the sinuosity is set equal to 2, and the flow depth decreased so the flow speed matches the measured speed, then the flow width increases by a factor of about 10, resulting in conduits roughly 40 to 60 metres in width. These widths are unlikely because a continuous ice roof would probably not be sustained but rather islands of ice in contact with the substrate would exist and create a braided flow system that would result in multiple tracer peaks. Also, of the 8 boreholes drilled in the narrow strip of drainage only one is thought to connect to a conduit about 21-m away. If conduits of such large width existed more boreholes would have connected to the conduit.

The analysis assumes that the tracer is injected directly into the subglacial conduit rather than routed though the vertical extent of the glacier. If the tracer encounters many englacial cavities or a particularly tortuous path from the surface to the bed, the apparent flow velocity would be much slower than the calculated flow velocity. Although the actual value of the sinuosity and perhaps conduit width are questionable, the qualitative conclusion is unchanged; the conduit is wide compared to its depth and the flow path is quite sinuous. Also the routing of water through the englacial passages cannot be ignored when discussing flow speeds through a glacier.

Sensitivity of the calculation to the estimate of roughness was examined by first multiplying the roughness by 2. In response, the flow depth doubled, as one would expect from Equation 5, the conduit width decreased by half, the sinuosity increased by about 20%, and the mean flow velocity increased by about 20%. When the roughness was divided by 2, the response was about the same, but reversed. The magnitude of conduit sinuosity and width are not very sensitive to changes in the estimate of roughness. There are practical limits to the estimate of the roughness. The maximum roughness is not more than 10 cm, approximately the mean diameter of the largest cobbles found in the proglacial outwash.

SUBGLACIAL FLOW CONDITIONS OF STREAM 3

Theoretical Considerations

The hydraulic condition of conduit flow, i.e., partially-full conduit or pressurized, can be determined by examining the relation between time of travel of injected tracers and water discharge. The time of travel (T) of a tracer can be expressed as:

$$[6] \qquad T = \frac{L}{\bar{u}}$$

L is the path length and ū is the mean water flow velocity. The mean flow velocity is equal to the water discharge (Q) divided by the cross-sectional area of the flow (A). Making this substitution and taking the derivative of the logarithm of travel time with respect to the logarithm of discharge yields:

$$[7] \qquad \frac{d\ \log(T)}{d\ \log(Q)} = \frac{d\ [\log(A) + \log(L) - \log(Q)]}{d\ \log(Q)}$$

For repeated tracer injections at the same location the path length L is assumed constant and the equation reduces to:

$$[8] \qquad \frac{d\ \log(T)}{d\ \log(Q)} = \frac{d\ \log(A)}{d\ \log(Q)} - 1$$

If the water is flowing in a pressurized conduit, the cross-sectional flow area does not change and the derivative is equal to -1. Therefore when the logarithm of travel time is plotted as function of the logarithm of the discharge, the slope for pressurized flow will be -1.

For partially-full conduit conditions the slope will be larger (less negative) and is related to the geometry of the conduit cross section. Assuming that the relation between cross-sectional area and discharge is adequately described by Manning's equation (Robertson and Crowe, 1985), the water discharge can be described in terms of the geometric parameters of the flow, including a Manning roughness, and the water slope.

$$[9] \qquad Q = \frac{AR^{2/3}S^{1/2}}{n}$$

where S is water surface slope (approximated by the bed gradient), R is the hydraulic radius and n is the Manning's roughness coefficient. Equation 9 is rearranged to solve for the area, and after taking the logarithm of both sides of the equation results in:

$$[10] \qquad \log(A) = \log\left(\frac{n}{S^{1/2}}\right) + \log(Q) - \frac{2}{3}\log(R)$$

Substituting Equation 9 into 7 yields:

$$[11] \qquad \frac{d\ \log(T)}{d\ \log(Q)} = \frac{d}{d\ \log(Q)}\left[\log\left(\frac{n}{S^{1/2}}\right) - \frac{2}{3}\log(R)\right]$$

If the roughness and water-surface slope are constant (the surface slope closely approximates the bed slope), then Equation 11 reduces to:

$$[12] \qquad \frac{d\ \log(T)}{d\ \log(Q)} = -\frac{2}{3}\frac{d\ \log(R)}{d\ \log(Q)}$$

indicating that the slope of log T versus log Q is a function of the changing hydraulic radius, hence the flow geometry.

To theoretically assess the slope of log T versus log Q for various cross-sectional shapes, the travel time (T) was calculated from a given discharge and roughness by Manning's Equation 9 using a constant distance for the flow path. The results (Figure 4) show that the slopes for a partially-filled conduit vary from -0.40 for a rectangle for a width-to-height ratio of 50:1 to a slope of -0.02 for a ratio of 1:50. The slope for a circular cross section closely approximates a square (1:1) and a half-circle closely approximates a rectangle with a ratio of 3:1. The exception to this trend occurs for circular-type geometries when the water almost fills the conduit. In this region the length of the wetted perimeter increases faster than the cross-sectional area of the flow and increases the slope to 0.02.

From these simple relations it might seem that one may distinguish between partially-filled and pressurized conduits, and with careful field procedures, the geometry of the flow cross section. However, a conduit may be pressurized for some distance but partially-filled for the remainder. The effect of this situation was calculated by assuming a conduit of circular cross section with two sections of different radii. The smaller conduit is pressurized and the larger conduit is partially full. The slope is then calculated by averaging the slope of the pressurized and partially-filled portions, each weighted by their fraction of total length. Although this conceptualization is not a truly accurate description of changing hydraulic conditions the approximation is probably good. For conduits of different cross-sectional shapes, the slope will change in a manner similar to the example for circular cross sections although the actual magnitude of the slope will be different. Table 2 shows the change in slope for different fractions of partially-full conduit flow.

Application to the Conduit in the Stream 3 Basin

This method requires a data set composed of multiple injections at approximately the same location over a relatively-short time period of a few days on the same glacier. The time constraint is necessary because the geometry of the flow system changes over time. Multiple injections were made at South Cascade Glacier during the 1987 field season, but not at the frequency at a single location necessary for this analysis. This difficulty was avoided by scaling the time of travel by the ratio of a constant distance to the actual distance. The results are tabulated in Table 3. Stream 2 is not included because it is unlikely that the flow from injection site to glacier exit is conduit flow as previously discussed.

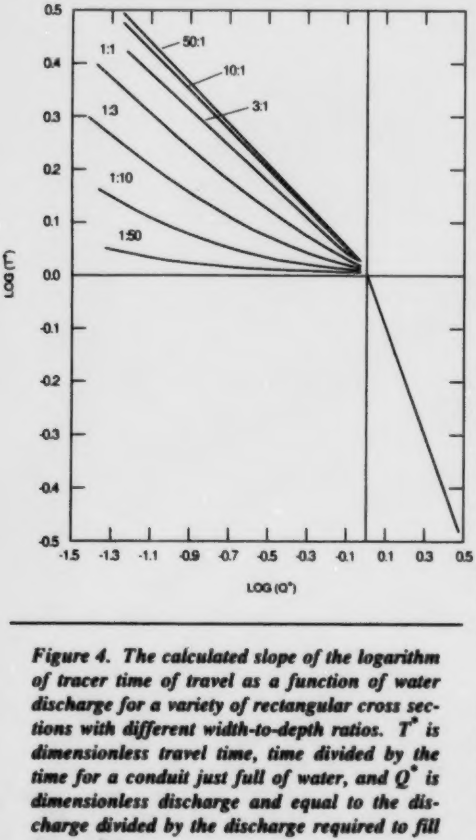

Figure 4. The calculated slope of the logarithm of tracer time of travel as a function of water discharge for a variety of rectangular cross sections with different width-to-depth ratios. T^* is dimensionless travel time, time divided by the time for a conduit just full of water, and Q^* is dimensionless discharge and equal to the discharge divided by the discharge required to fill the conduit.

Interpretation of the results without regard to the flow processes between the ice surface and subglacial conduit may lead to erroneous conclusions. Unfortunately, the influence of intermediate flow processes cannot be ascertained from the methods presented. However, there are two limiting cases: 1) the surface water reaches the conduit directly, unaffected by intermediate processes; and the temporal changes in the relation between the travel time and discharge are solely caused by changes in the flow condition of the subglacial conduit; 2) the intermediate routing of water greatly affects the flow of surface water to the subglacial conduit and is primarily responsible for the temporal changes in the relation between travel time and water discharge.

If meltwater directly reaches the subglacial conduit, the positive slope in July may be the result of water backing up in the englacial passages. Although a positive slope is expected for flow near the crown of a circular-shaped cross section, as previously

Table 2. The dependence of the slope of log(T)/log(Q) for different fractions of a circular conduit flowing partially full.

Fraction of Conduit Flowing Partially Full	Slope
0	-1.00
0.1	-0.92
0.3	-0.77
0.5	-0.63
0.7	-0.48
0.9	-0.33
1.0	-0.33

explained, the magnitude of the slope in the table is too large. The crevasse may be connected to the conduit by a passage that fills with water when the conduit is pressurized. The tracer must move through this column of water to reach the conduit. As the pressure increases in the conduit, the water level rises in the connecting passage and the tracer injected at the surface requires a longer time to reach the conduit. If this increase in time exceeds the decrease in time flowing in the channel, the net travel time will increase, and result in a positive slope. The flow rate through the passage depends on the flux of water into the passage and cross-sectional area of the passage. In August and September, the slope is negative, but between -1 and -0.4, suggesting that the water is flowing part way in a pressurized conduit and part way in a partially-full conduit. The discharge for the two periods in July and August are similar, although there is a significant difference in slope. If the subglacial conduit enlarged during the intervening time between injection periods, the water would be flowing in a partially-full condition. In September, the slope is less negative, indicating that more of the conduit path is flowing partially full. The discharge during this period is smaller than in the previous two periods, which explains why more is partially-full.

The influence of intermediate flow processes is not clear. One reason is the variety of these processes that include englacial and subglacial flow. In routing of water through the vertical extent of the glacier the water may flow in crevasses (Fountain, 1989), narrow passages through the ice, and small tortuous veins (Raymond and Harrison, 1975) that connect to the subglacial conduit. These paths may reach the glacier bed some distance away from the conduit and the water may drain from the passage, flowing along the glacier bed, to the conduit. Although it is unlikely that these processes will change the sign of the slope, they may change its magnitude, particularly if the hydraulic resistance of these features changes over time. If the intermediate flow passages sufficiently delay the transit time of the water, the values of the slope would be more negative than for true values of the tracer reaching the conduit directly. Also, if these passages enlarge with time, their delaying effects would diminish and result in less negative values.

Table 3. Summary of slope of log(T) versus log(Q) and discharge for Stream 3 at South Cascade Glacier during 1987.

Period	Slope	Q
July 19-23	1.45	0.653
August 19-20	-0.70	0.663
September 19-20	-0.54	0.280

Most likely, the conduit is flowing partially full for most of each day in August and

September. The ice depth is fairly uniform over the conduit and the water flux is almost constant along its length in the narrow corridor. The area of surface input in the narrow corridor is small relative to the source areas upglacier. Therefore, ice closure from the overburden pressure and enlargement from the flux of water are relatively constant along the length of much of the conduit and consequently the flow conditions should be constant. For this situation, a negative slope probably indicates open-channel flow. The relatively large negative values are the result of the intermediate flow processes that transport the water from the surface of the glacier to the conduit.

CONCLUSIONS

In the Stream 2 basin, water is routed from the surface to the glacier bed, where it flows in a distributed network of channels or connected cavities. In the Stream 3 basin, most of the water from the ablation zone is routed through conduits, probably englacial, to a subglacial conduit in the lower ablation zone.

The cross-sectional shape of the conduit was initially assumed to be very wide and low in height. The resulting analysis is consistent with this initial hypothesis. The conduit was probably water filled in July during the period of tracer injections. If the hydraulic gradient approximates the bed slope, then the water depth is twice that presented for July in Table 1 and the channel width is half that presented. By August, the water flows at atmospheric pressure. The channel width in September did not significantly change from that in August. Although the water discharge is much smaller in September than in the previous two months, the closure rate of the ice is sufficiently slow that the conduit can maintain its width for a long period of time.

The sinuosity of the channel is large and does not seem to significantly change with time. However, the calculated sinuosities are unreasonably large and indicate that the actual flow speed from surface to exit from the glacier is much slower than the speed through a conduit. The processes that route water from the surface to the subglacial conduit are unknown, however, they probably significantly affect the overall rate at which water drains from the glacier. This topic needs more study.

More theoretical work is required to better use the data gained from field work in order to quantify the shape of subglacial conduits in contact with the bed. That different subglacial flow processes exist in the same basin or differ between basins indicates that models of glacier movement will have spatially-varying subglacial boundary conditions. To make better use of the techniques presented here, more accurate measurements of water discharge and dense time series of tracer-concentration measurements are required. The findings and techniques presented in this paper should motivate more theoretical and field studies of conduit shape and the movement of tracers.

LIST OF SYMBOLS

A	cross-sectional area of flow (m^2)
g	acceleration due to gravity ($m \cdot s^{-2}$)
H	flow depth (m)
k	Von Kármán's constant (dimensionless)
L	path length of flow (m)
n	Manning's roughness ($m^{-1/2} \cdot s^{-1}$)
Q	flow discharge ($m^3 \cdot s^{-1}$)
Q^*	dimensionless discharge
R	hydraulic radius (m)
S	water-surface slope ($m \cdot m^{-1}$)
T	travel time (s)
T_{min}	minimum travel time (s)
T_{peak}	time of peak arrival (s)
T^*	dimensionless travel time
u	flow velocity ($m \cdot s^{-1}$)
u_*	friction velocity ($m \cdot s^{-1}$)
$\bar{u}$	mean flow velocity ($m \cdot s^{-1}$)
u_{max}	maximum flow velocity ($m \cdot s^{-1}$)
z_o	roughness scale (m)
ε	nondimensional flow depth
ε_o	nondimensional roughness height
λ	sinuousity

REFERENCES

BRUGMAN, M.M., 1986. Water flow at the base of a surging glacier. Ph.D. thesis, California Institute of Technology, Pasadena, California, 267 pp.

CLARKE, G.K.C., 1987. Subglacial till: a physical framework for its properties and processes. Journal of Geophysical Research, 92(B9), 9023-9036

COLBECK, S.C., 1974. Water flow through snow overlying an impermeable boundary. Water Resources Research, 10(1), 119-123

FISCHER, H.B., E.J. LIST, R.C.Y. KOH, J. IMBERGER and N.H. BROOKS, 1979. Mixing in inland and coastal waters. Academic Press Inc., Toronto, Ontario, 483 pp.

FOUNTAIN, A.G., 1989. The storage of water in, and hydraulic characteristics of, the firn of South Cascade Glacier, Washington State, U.S.A. Proceedings of the Symposium on Snow and Glacier Research relating to Human Living Conditions, 4-9 September 1988, Lom, Norway, Annals of Glaciology, Vol.13, 69-75

FOUNTAIN, A.G., 1991. Automatic system for measuring and recording fluorometric data from multiple sources. Water Supply Paper No.2340, U.S. Geological Survey, Washington, D.C., (in press)

GASPAR, E., 1987. Modern trends in tracer hydrology. Volume 1. CRC Press Inc., Boca Raton, Florida, 145 pp.

HODGE, S.M., 1979. Direct measurement of basal water pressures: progress and problems. Journal of Glaciology, 23(89), 309-319

KAMB, B., 1987. Glacier surge mechanism based on linked cavity configuration of the basal water conduit system. Journal of Geophysical Research, 92(B9), 9083-9100

KRIMMEL, R.M., W.V. TANGBORN and M.F. MEIER, 1973. Water flow through a temperate glacier. Proceedings of the Banff Symposia, the Role of Snow and Ice in Hydrology, Vol.2, September 1972, IAHS Publication No.107, International Association of Hydrologic Sciences, I.U.G.G., UNESCO-WMO-IAHS, 401-416

LARSON, G.J., 1977. Internal drainage of stagnant ice: Burroughs Glacier, southeast Alaska. Institute of Polar Studies Report No.65, Ohio State University, Columbus, Ohio, 33 pp.

OERTER, H. and H. MOSER, 1982. Water storage and drainage within the firn of a temperate glacier (Vernagtferner, Oeztal Alps, Austria). In - Hydrological Aspects of Alpine and High Mountain Areas, J.W. Glen (Editor), Proceedings of the Exeter Symposium, 19-30 July 1982, IAHS Publication No.138, International Association of Hydrological Sciences, 71-81

PATERSON, W.S.B., 1981. The physics of glaciers. 2nd Edition, Pergamon Press, New York, N.Y., 380 pp.

RATTRAY, M., Jr and E. MITSUDA, 1974. Theoretical analysis of conditions in a salt wedge. Estuarine and Coastal Marine Science, 2(4), 375-394

RAYMOND, C.F. and W.D. HARRISON, 1975. Some observations on the behavior of the liquid and gas phases in temperate glacier ice. Journal of Glaciology, 14(71), 213-233

ROBERSTON, J.A. and C.T. CROWE, 1985. Engineering fluid mechanics. 3rd edition, Houghton-Mifflin, Boston, Massachusetts, 712 pp.

RÖTHLISBERGER, H., 1972. Water pressure in intra- and subglacial channels. Journal of Glaciology, 11(62), 177-203

SEABERG, S.Z., J.Z. SEABERG, R.LeB. HOOKE and D.W. WIBERG, 1988. Character of the englacial and subglacial drainage system in the lower part of the ablation area of Storglaciären, Sweden, as revealed by dye-trace studies. Journal of Glaciology, 34(117), 217-22

SCHUMM, S.A., 1977. The fluvial system. Wiley-Interscience, John Wiley & Sons, New York, N.Y., 338 pp.

SMART, P.L. and I.M.S. LAIDLAW, 1977. An evaluation of some fluorescent dyes for water tracing. Water Resources Research, 13(1), 15-33

WEERTMAN, H., 1972. General theory of water flow at the base of a glacier or ice sheet. Reviews of Geophysics and Space Physics, 10(1), 287-333

WIBERG, P.L. and J.D. SMITH, 1987. Calculations of the critical shear stress for motion of uniform and heterogeneous sediments. Water Resources Research, 23(8), 1471-1480

CO_2-RICH GROUND WATERS OF THE FLAT RIVER VALLEY, N.W.T.*

S.M. Hamilton[1], F.A. Michel[1] and C.W. Jefferson[2]

[1]Department of Earth Sciences
Carleton University
Ottawa, Ontario
K1S 5B6 CANADA

[2]Geological Survey of Canada
601 Booth Street
Ottawa, Ontario
K1A 0E4 CANADA

ABSTRACT

A series of CO_2-rich (>1 atm. pCO_2) travertine-depositing cold springs were identified along the western margin of the Flat River valley during a hydrogeological investigation of springs in a portion of the Ragged Ranges adjacent to Nahanni National Park Reserve, N.W.T.

The chemical composition of the springs is dominated by Ca^{2+}, Mg^{2+} and HCO_3^- with large quantities of gaseous CO_2 bubbling in all vents. pH values range between 5.9 and 6.3, while water temperatures vary between 1.6 and 8.9°C. $\delta^{13}C$ values for dissolved inorganic carbonate (-0.4 to +3.9‰) and calculated values for $\delta^{13}C_{CO_2}$ (-4.9 to -1.2) indicate that the CO_2 may be derived from metamorphic reactions at depth with a possible input of mantle CO_2. Oxygen and hydrogen stable-isotope data for the spring waters suggest a meteoric origin, while the presence of tritium implies a relatively short subsurface residence time.

A model is presented where a CO_2-rich fluid, generated through metamorphic decarbonation reactions at depth, and with a possible mantle-derived component, rises along a structural lineament and mixes with shallow circulating ground water prior to discharge within the valley.

INTRODUCTION

A hydrogeological investigation of springs was conducted in 1986 and 1987 as part of a non-renewable resource assessment by the Geological Survey of Canada of proposed extensions to Nahanni National Park Reserve (Hamilton *et al.*, 1988). During the investigations, three geochemically-distinct water types (Hamilton, 1990) were sampled in the Flat River valley (Figure 1). The first water type discharges as

---

*Geological Survey of Canada Contribution Series Number 30790.

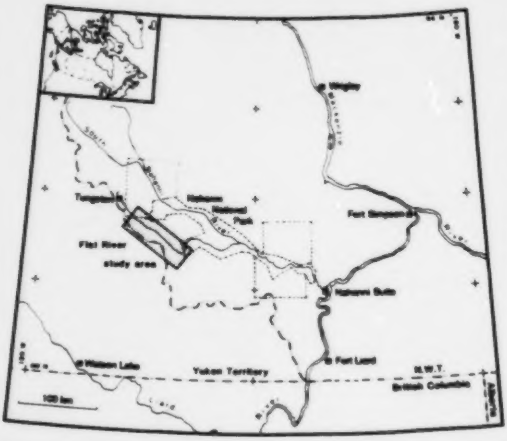

Figure 1. Location map showing the Flat River valley study area.

hot springs (42 to 64°C) which are spatially and geochemically associated with quartz monzonite plutons in the area. The second group are travertine-precipitating thermal springs located in the lower southeast section of the Flat River valley. The third group of waters, which are the focus of this paper, discharge as high-pCO_2, travertine-precipitating cold springs within the central portion of the Flat River valley.

Various aspects of the thermal springs have been examined previously by Atchison (1964), Gabrielse *et al.* (1973), Crandall and Sadlier-Brown (1978), Hall *et al.* (1988) and Bowman (1990). Crandall and Sadlier-Brown (1978) reported several large travertine and iron-hydroxide precipitating cold springs, which constitute Group 3, and geochemically analyzed the waters of one of these springs.

CO_2-rich springs, such as those in Group 3, are known elsewhere in Canada and the world. In Canada, they are presently known to occur in three other areas (Barnes *et al.*, 1978, 1984): southern British Columbia, north-central British Columbia at Mt. Edziza, and in the St. Lawrence valley.

DATA COLLECTION AND ANALYSIS

Field work was conducted during the months of July and August of 1986 and two springs were resampled in August 1987 (Table 1). Spring waters were sampled for major ion and trace-element chemistry. A one-litre bottle for cations and trace elements was acidified with approximately 10 mL of dilute HCl in 1986, and with 5 mL of 1 molar HNO_3 in 1987 to keep cations and metals in solution. A 500-mL bottle for anions was also collected at each vent. Samples were strained through glass wool but not filtered. At each vent, pH, electrical conductivity and temperature were measured. Estimates of flow rate and various other field observations were also made at the site. Field measurements and spring locations are given in Table 1 and Figure 2, respectively.

***Table 1.** Field measurements and analytical results for springs in Group 3 (springs 017 and 055 to 058) and for spring 059. Major ions are reported in ppm and trace elements are reported as shown below. $HCO_3^-{}_{(calc)}$ is HCO_3^- which has been corrected by charge-balance techniques as explained in the text. pCO_2 is reported in log(bars). $\delta^{18}O$ and δ^2H are reported in ‰ SMOW and $\delta^{13}C$ is reported in ‰ PDB. $\delta^{13}C_{(gas)}$ was obtained from $^{13}C_{(DIC)}$ using equilibrium calculations. Tritium is reported in tritium units (T.U.). See text for methods and laboratories. Sample 057 (in brackets) was taken from a small lake, into which 056 flows, rather than an actual vent and thus the chemistry of the water is slightly altered. Bracketed temperature values for samples 86-057 and 87-058 are higher than expected due to solar warming.*

	86-017	87-017	86-055	86-056	(86-057)	86-058	87-058	(86-059)
Temp. °C	5.5	5.5	1.6	7.7	(14.2)	8.9	(11)	5.5
pH	6.3	6.1	5.9	6.1	6.8	6.2	6.2	7.2
Ca	685	635	345	579	456	530	484	128
Mg	57	55	42	111	95	55	51	20
Na	46	46	10	85	56	29	25	7
HCO_3	718	925	447	807	633	686	488	286
$HCO_{3\ (calc)}$	2428	2273	1100	2236	1722	1918	1759	483
SO_4	55	49	126	283	243	38	27	13
Cl	3	3	5	22	20	4	3	0
Fe (ppb)	20766	58	15850	33	161	28	<5	480
Mn (ppb)	1503	1498	587	34	521	158	275	157
pCO_2	0.18	0.05	0.08	0.19	- 0.59	- 0.03	0.03	-1.61
$\delta^{13}C_{(DIC)}$	- 0.5	- 0.4	0.9	2.5	3.9	0.4	--	--
$\delta^{13}C_{(CO2)}$	- 4.9	- 4.1	- 1.9	- 1.2	- 2.8	- 3.7	--	--
$\delta^{18}O_{(H2O)}$	- 23.3	-23.2	- 22.9	-21.6	-20.8	-22.5	--	-22.3
$\delta_2H_{(H2O)}$	- 184	--	-183	--	--	-179	--	--
^3H	87	--	--	12	--	55	--	--

Major ions, including Ca^{2+}, Mg^{2+}, Na^+, Cl^-, SO_4^{2-} and HCO_3^-, were analyzed (Table 1) by the Geological Survey of Canada (Hall *et al.*, 1988; Hamilton *et al.*, 1988). Ca^{2+}, Mg^{2+} and Na^+ were analyzed using atomic-absorbtion techniques (AA) in 1986 and Inductively Coupled Plasma Mass Spectrometry (ICPMS) in 1987 with detection limits of 0.2 and 1 ppm respectively. Cl^- and SO_4^{2-} were analyzed by DIONEX ion chromatography with detection limits of 0.05 and 0.2 ppm respectively. HCO_3^- was determined in the laboratory by titration with a detection limit of 0.2 ppm. Erroneously low values for HCO_3^- were obtained from the supersaturated

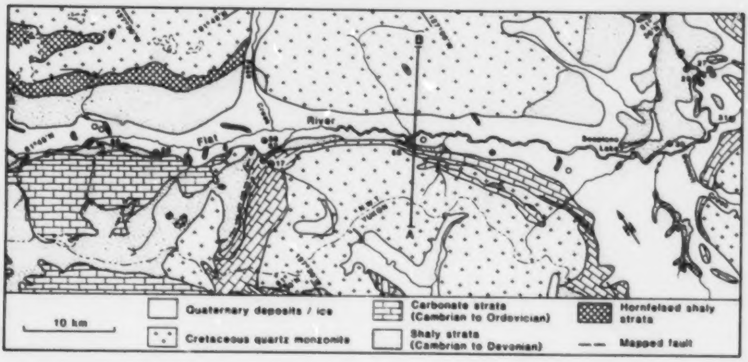
B
River
Flat
Creek
Seaforth Lake
A
10 km
Quaternary deposits / ice
Cretaceous quartz monzonite
Carbonate strata (Cambrian to Ordovician)
Shaly strata (Cambrian to Devonian)
Hornfelsed shaly strata
Mapped fault

Figure 2. Simplified geology (after Gabrielse et al., 1973) and spring locations of the Flat River valley. The black dots represent known springs, labels indicate those which were sampled. Open circles represent possible springs interpreted from air photographs. Line A-B is the location of the cross section shown in Figure 7.

Group 3 waters due to precipitation of calcite. It was necessary, therefore, to correct these by charge-balance techniques. Total cation concentrations in equivalence were compared with those of the anions SO_4^{2-} and Cl^-, and the anion deficiency was assumed to be entirely due to HCO_3^-. Comparison of the measured and calculated HCO_3^- values (Table 1) indicates a loss of between 60 and 75% of the original bicarbonate.

In 1986, gas samples were collected using plastic bottles of the same variety as those used for sampling water. They appeared to allow diffusion of CO_2 through the container walls and, therefore, were unsuitable. Samples taken in 1987 were collected in glass bottles but were unfortunately damaged during transport. Only one was analyzed and even that may be in error. This sample, from spring 058, reportedly contained 56% CO_2.

Samples for oxygen-18, deuterium, and tritium isotope analysis were collected in 250- and 125-mL bottles. Samples for isotopic analysis of SO_4^{2-} and dissolved inorganic carbon (DIC) in water were collected in 8-litre plastic bottles. The species were precipitated in the field by adding NaOH to raise the pH above 11, then adding $BaCl_2$. After the precipitate had settled, it was decanted, transferred into a smaller container, and packed for transport back to the laboratory.

$\delta^{18}O$ and the 1987 $\delta^{13}C$ analyses were conducted at the Stable Isotope Laboratory, Ottawa-Carleton Geoscience Centre, and were reported with an average uncertainty for both isotopes of ±0.2‰. ^{2}H and 1986 ^{13}C analyses were conducted at the Environmental Isotope Laboratory, Department of Earth Sciences, University of Waterloo and were reported with average uncertainties of ±2.0 and 0.2 respectively. Analyses for all the stable isotopes were obtained using mass spectrometry. Tritium was analyzed at the University of Waterloo using direct-counting liquid scintillation with an average uncertainty of ±8 T.U.

PHYSICAL AND GEOLOGICAL SETTING

The Group 3 springs are located in a section of the Flat River valley beginning 25-km downstream from the town of Tungsten and continuing approximately to the park boundary, a total distance of 80 km (Figure 1). The northwest-southeast trending portion of the valley is remarkably linear, U-shaped, and varies in width from 4 to 8 km. The Flat River flows along the southwest side of the valley and is partially incised into the thick glacial sediments at its base. The springs of interest vent in a narrow space between the river and the southwest valley wall. Associated travertine terraces are extensive in this area but are also found in at least one tributary valley.

The rock units in the study area, shown in Figure 2, include strata of the Ordovician to Devonian Selwyn Basin and adjacent Mackenzie Platform which are exposed in the Mackenzie Mountain fold and thrust belt. Cambro-Ordovician limestone of the Rabbitkettle Formation forms the southwestern margin of the Flat River valley along nearly the entire length of the area. On the northeastern side of the valley the Rabbitkettle Formation is exposed only in the northwest, toward Tungsten. Middle Ordovician carbonates of the Sunblood Formation flank the Flat River on the southeast, where it turns 90° toward the northeast. The exact contact between the Sunblood carbonate and the overlying Road River shale is obscured in most places by Quaternary deposits. Calcareous shales of the Road River Group and siliceous, baritic shales interpreted as Earn Group constitute scattered outcrops on the floor of the valley. The Road River Group crops out along most of the north-eastern slopes. The shales also overlie Rabbitkettle carbonates on the western side of the valley.

The youngest rock unit in the area is Cretaceous quartz monzonite. Plutons are exposed on both sides of the river and in the valley floor. Heat flow due to radioactive decay in these plutons is suspected to be very high, although quantitative data are not available. High convective heat flow is empirically shown by the abundance of hot springs (Group 1) which are spatially and geochemically associated with the plutons (Hamilton, 1990).

DESCRIPTION OF SPRINGS

Following is a brief description of the physical characteristics of each of the five springs that were sampled in Group 3 (017, 055, 056, 057, 058). Three more springs of similar appearance have been identified by aerial reconnaissance but were not sampled due to logistical constraints.

Spring 017 is located in the valley of a tributary to the Flat River, southwest of the linear belt defined by the other Group 3 springs (see Figure 2). This is the smallest of the Group 3 springs. The flat, terraced deposit is 50-m long and 10 to 20-m across. It has one active vent which flows at about 15 $L \cdot s^{-1}$ but the extent of the deposits suggests other vents have been active in the past. The deposit consists of orange to red iron-hydroxide-rich travertine in flat terraces. The vent, 2-m across, contains an accumulation of ferruginous-calcareous mud through which the spring water flows and gas continuously bubbles. Gas also exsolves from the spring waters, nucleating on solid objects within the vent.

Spring 055 is located 50-m above the river just below a locally-prominent bedrock lineament which trends parallel to the valley. The deposit consists of patches of barren or sparsely-vegetated red, carbonate-ochre precipitate covering an area of about 50 m by 100 m. Two main vents were noted, both with significant gas being discharged but only a small flow of water. The flow rate was estimated at 5 to 10 $L \cdot s^{-1}$ in 1986 and there was no detectable surface flow in 1987. Air-photo interpretation and iron-oxide deposits visible from the air suggest that additional smaller springs are located within several kilometres along the same lineament, at approximately the same altitude.

Springs 056 and 057 were noted as a cold spring on the Flat River geology map (Gabrielse *et al.*, 1973) and the location was also mentioned but not sampled by Crandall and Sadlier-Brown (1978). The deposit is large, measuring approximately 125 m by 150 m and forms a terrace 40-m high. It impounds a small lake 165 by 275 m in size. Vegetation surrounds the lake but the area of apparent perennial seepage is not vegetated. Sample 057 is of the lake water and sample 056 is of a small spring which flows directly into the lake. Gas continuously discharges as streams of bubbles over at least half the surface extent of the lake, suggesting that additional springs may be situated beneath the lake. Water discharges from 056 at about 0.5 $L \cdot s^{-1}$ and gas discharges continuously from the red mud at the vent bottom.

Spring 058, known as "Flat Fruit Mineral Springs", was previously sampled by Crandall and Sadlier-Brown (1978). It consists of a sparsely-wooded terrace 190 m by 350 m in size with two active discharge areas. The size of the terrace is limited by a small creek which cuts down along its north side. Samples of water and gas were taken at the back of the terrace. In this area, water discharge is small and appears to all evaporate as it seeps over the deposits, whereas gas discharge is extremely large (tens of litres per second). Numerous pools are found in this discharge area, about 1/4 of which are active. Many unusual travertine structures are present such as hollow tufa mounds, pisolites, riffles and terraces. Similar structures were described by Atchison (1964) at Caesar Lake spring. The second discharge area is on the front (northeast) edge of the terrace along its steep 40-m high slope. Zones of active seepage were observed from the air.

Spring 059 is located 3 km northwest of 058 and is in approximately the same position relative to the river and valley slope as 058. The deposit is large (150 by 250 m), partly vegetated and has a large flow (30 to 50 L·s^{-1}). It does not have the same chemical characteristics as the Group 3 springs but the size of the deposits and proximity to 058 suggests that it may have been formed from similar waters in the past. Further investigation is needed to determine if the stable isotope and chemical composition of the deposits are similar to those of deposits formed by Group 3 waters.

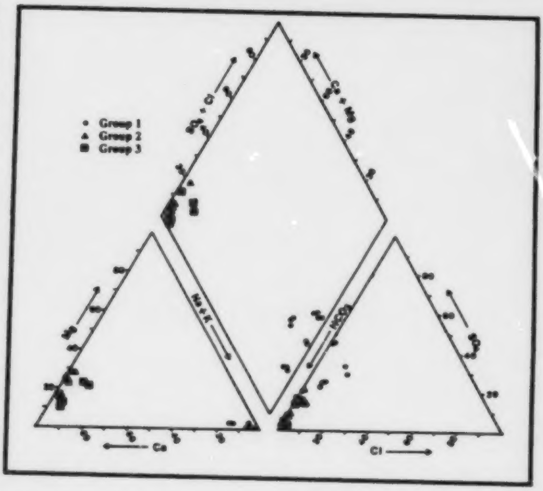

Figure 3. Piper diagram showing major ion chemistry for springs of the three dominant groups in the Flat River valley.

The springs of Group 3 all have similar characteristics. The associated travertine deposits are large, water temperatures are low and a large quantity of gas (mostly CO_2) is being emitted at each of the vents. The waters are dominated by Ca^{2+} and HCO_3^- (Figure 3), both of which have extremely high concentrations. Several other elements, such as Mg^{2+} and, locally, Fe and Mn, are also present in high concentrations. The pH of the water is invariably low (<6.3) but rises sharply with increasing distance from the vent due to exsolution of CO_2. pCO_2 values calculated for waters at each of the vents (Figure 4) are very high (>1 bar).

Figure 5 illustrates the range of $\delta^{13}C$ concentrations obtained for the three main spring groups in the study area. The values for $\delta^{13}C_{(gas)}$ were estimated from the $\delta^{13}C_{(DIC)}$ data using the following mass-balance equation (Clark, 1980):

$$[1] \quad \delta^{13}C_{(DIC)}\, M_{(DIC)} = M_{H_2CO_3}\,(\delta^{13}C_{CO_2} + \varepsilon_{H_2CO_3/CO_2}) + M_{HCO_3}\,(\delta^{13}C_{CO_2} + \varepsilon_{HCO_3/CO_2}) + M_{CO_3}\,(\delta^{13}C_{CO_2} + \varepsilon_{CO_3/CO_2})$$

where: M = molality, ε = enrichment factor = 1000 ln α, (α = fractionation factor).

Values for the enrichment factors were obtained from Mook *et al.* (1974) and Deines *et al.* (1974). The concentrations of H_2CO_3 and CO_3^{2-} were calculated based on the known HCO_3^- concentrations and pH values as was pCO_2 which was necessary to the calculation.

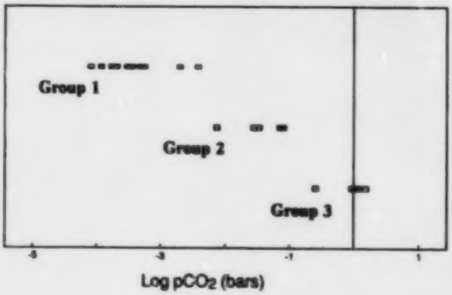

Figure 4. Log pCO_2 (calculated) for springs of the three dominant groups in the Flat River valley.

The above equation assumes isotopic equilibrium between carbon in DIC and the gas phase. Batard *et al.* (1982) found this to occur in mineral springs with relatively low pCO_2 in France. However, they also reported significant disequilibrium occurring between these two phases in high pCO_2 spring waters. In these cases, measured values show larger fractionations between $\delta^{13}C_{CO_2}$ and $\delta^{13}C_{DIC}$ than would be expected from equilibrium calculations. Thus, the actual isotopic composition of the gas may be somewhat lower than shown on Figure 5.

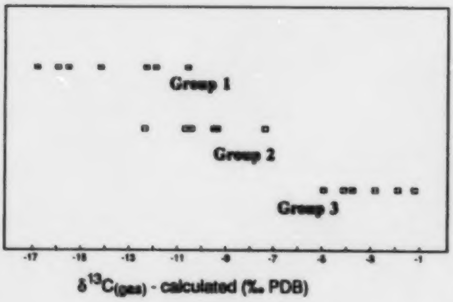

Figure 5. Calculated $\delta^{13}C_{(gas)}$ for springs of the three dominant groups in the Flat River valley. The above values were obtained from $\delta^{13}C_{(DIC)}$ using equilibrium calculations as explained in text.

^{18}O and ^2H data for all springs which were sampled in the Nahanni area are plotted on Figure 6. ^{18}O and ^2H data for precipitation in the area are unavailable and therefore an approximation of the Local Meteoric Water Line (LMWL) was made by plotting a regression through the spring data. Its similar slope and relative position (see Fritz *et al.*, 1987) with respect to the Global Meteoric Water Line (GMWL) suggests at least a close approximation to the true LMWL. Three springs from Group 3 were analyzed for both ^{18}O and ^2H (Table 1). These plot very close to the LMWL indicating a probable meteoric origin for the water. This is supported by the presence of tritium in the three spring waters which were analyzed for tritium (Table 1).

DISCUSSION OF RESULTS

All of the unusual chemical characteristics of these springs result directly or indirectly from the presence of excess CO_2. The dissolution of limestone is aided by CO_2 according to the following reactions:

[2] $$H_2O + CO_{2(g)} \rightleftharpoons H_2CO_{3(aq)}$$

[3] $$H_2CO_{3(aq)} + CaCO_3 \rightleftharpoons Ca^{2+} + 2HCO_3^-$$

The exsolution of CO_2 as waters discharge at the surface causes these reactions to proceed to the left and consequently $CaCO_3$ is precipitated. This process is well known and occurs commonly in waters throughout the Nahanni area. However, the presence of such large quantities of CO_2 in ground water is not common and there are a number of possibilities as to its source.

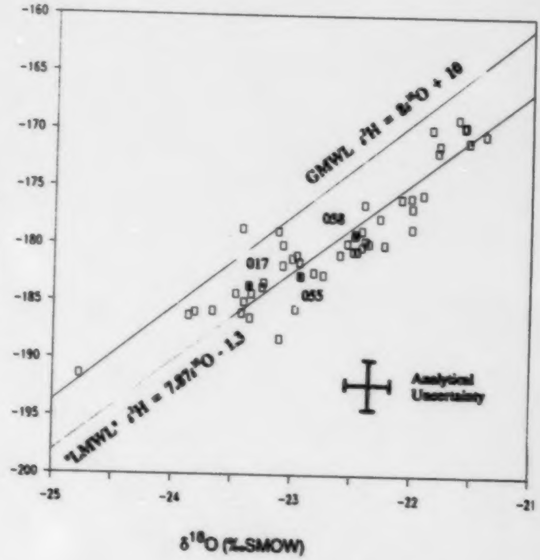

Figure 6. $\delta^{18}O$ and δ^2H plot of spring waters in the Nahanni region. The global meteoric water line is from Craig (1961) and the Local Meteoric Water Line (LMWL) is a regression line (R=0.99) for all sampled springs in the Nahanni region as explained in text. Filled-in squares represent group 3 waters of the Flat River valley.

Atmospheric and plant CO_2 are the most common sources of CO_2 in ground water, but the high partial pressures (between 1 and 3 orders of magnitude higher than CO_2 in the soil zone) and large volume of gas in the Group 3 springs precludes either of these as primary sources. Potential sources which are capable of producing these high pCO_2 conditions are mantle gases and gases given off during the metamorphic decomposition of carbonates. This interpretation is supported by the calculated $\delta^{13}C_{(gas)}$ values for Group 3 which range between -4.9 and -1.2‰. Most authors (e.g., Irwin and Barnes, 1980; Mattey, 1987; Blavoux *et al.*, 1982) consider the range of mantle-derived CO_2 to be -8 to -4‰ and that values above this indicate a metamorphic source. Gerlach and Taylor (1990) measured $\delta^{13}C$ of mantle CO_2 discharging from Kilauea Volcano. Their data are well constrained and values range between -4.1 and -3.4‰. Decarbonation reactions during metamorphism of impure carbonates produce CO_2 of predictable $\delta^{13}C$ composition depending on the temperature of reaction (see Bottinga, 1968) and on the initial $\delta^{13}C$ composition of the rocks (see Valley, 1986). With a temperature of reaction for calc-silicates of between 180 and 300°C (Muffler and White, 1968, 1969) and with an initial $\delta^{13}C$ composition of the rocks of between 2.7 and 0.7‰ (Rabbitkettle limestone and Road River calcareous shale), the range of expected $\delta^{13}C_{CO_2}$ is 2.6 to -3.6‰. This range takes into account the fractionation of ^{13}C as a result of metamorphism and the gradual depletion of the initial carbonate throughout metamorphism. The $\delta^{13}C$ composition of the gas would likely be toward the higher end of this range since most of the decarbonation occurs during the initial stages of metamorphism. Therefore, assuming equilibrium between DIC and CO_2 at the surface, the gas in these springs falls in the upper range of mantle CO_2 and the lower range of metamorphic CO_2.

Discharges of metamorphic and mantle CO_2 are known worldwide. Blavoux *et al.* (1982) described springs in France which appear to have a mantle source of CO_2, with $\delta^{13}C_{(gas)}$ values ranging between -8 and -3.7‰. These are located along major faults or fractures within the Central Massif and within or near Tertiary volcanic centres. Contact metamorphism of marine carbonates and associated CO_2 discharges also occur in areas of recent volcanic activity in central and southern France (Blavoux *et al*, 1982).

Figure 7 depicts a possible model for the production, transport and venting of the CO_2-rich fluids. The Cretaceous quartz monzonite plutons are assumed to have high heat flow because of the numerous hot springs spatially and geochemically associated with them, although quantitative data are not yet available. CO_2 may be produced at depth by metamorphic decarbonation of carbonates or calcareous shales in close proximity to these plutons. Latent heat of crystallization of these plutons would long have ceased to be a factor in metamorphism, however, radioactive decay could result in metamorphism of carbonates at relatively shallow depths and would explain the apparent high heat flow. Assuming moderately-high conductive heat-flow rates of 200 $mW \cdot m^{-2}$, and a temperature of reaction between 180 and 300°C, the depth range for the production of CO_2 would be approximately 3 to 5 km.

The next important requirement of the model is that some pathway exists for the CO_2 to reach the surface. The most likely way to have so many similar discharges forming a linear pattern is to have a large fault acting as a conduit. Barnes *et al.* (1984) noted such localization of CO_2 discharges along major faults in California, including segments of the San Andreas fault. CO_2 discharging along faults is often found to be mantle-derived and a component of mantle CO_2 in the gases being discharged in the Flat River valley is not unlikely based on carbon isotopes. This would only be possible if the fault were a very deep structure which would provide a

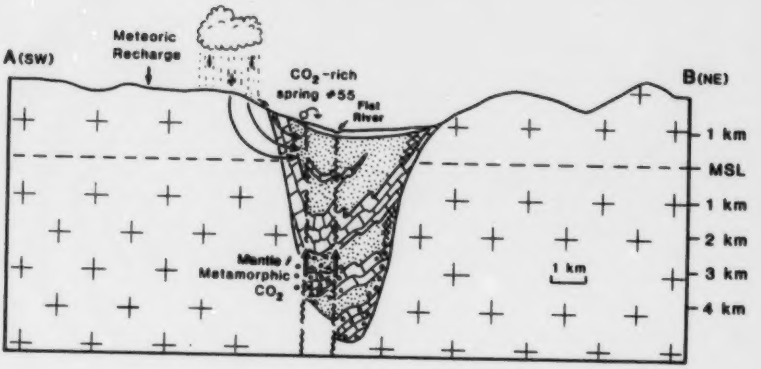

Figure 7. Schematic cross section of the Flat River valley showing the possible model for the origin of CO_2-rich fluids. Surface geology is from Gabrielse et al. (1973). Thickness of units and structural style are modelled after data from Blusson (1967) projected about 30 km along the Flat River valley from the northwest. Location of section is shown on Figure 2. CO_2 is produced in the shallow crust by metamorphism of carbonates in contact with Cretaceous plutons with possible input from mantle CO_2. The CO_2 travels upward along an inferred fault and mixes with shallow meteoric water. The waters dissolve large quantities of carbonates which are re-precipitated on surface upon discharge.

pathway for the upward migration of mantle CO_2. There is presently no fault mapped in the Flat River valley, nevertheless, major gouge zones were encountered during field work in 1990. It could have been missed during the reconnaissance-scale mapping of the mid 1960's, due to the thick glacial deposits and forest cover on the valley floor. The fault suggested here corresponds to a lineament visible on the LANDSAT images. The springs are also visible on LANDSAT images and occur along the lineament. Although widespread discontinuous permafrost is present in the area, the effect on a fault-controlled discharge path would be minimal (Michel, 1986).

Figure 7 depicts the upward migration of CO_2 along the inferred fault into the zone of active meteoric water. Oxygen, deuterium and tritium isotope data indicate that water discharging from the springs is of meteoric origin and has been recently recharged (< 35 years). In addition, there is no evidence that high-temperature water-rock exchange reactions have occurred (Figure 6). If these had occurred there would have been a detectable shift (from the LMWL) of the $\delta^{18}O$ composition of the water due to exchange with the isotopically-heavier oxygen in the wall rock. These results suggest that a CO_2-rich "deep" fluid, metamorphically derived with a possible mantle component, is travelling upward from depth and mixing with large quantities of shallow meteoric water. The isotopic composition of the water component of the deep fluids would be masked by its small volume relative to that of the meteoric water. The CO_2-rich meteoric water would dissolve large quantities of carbonate which would then re-precipitate upon discharge at the surface as the CO_2 exsolves from the water.

Irwin and Barnes (1980) discussed the close coincidence between regional seismic activity and areas of CO_2 discharge. CO_2 discharges are known to coincide with on-land segments of linear seismicity, i.e., active faults. Examples of this include branches of the San Andreas fault in California. As CO_2 discharges represent a long-term event relative to the historic record of seismicity, Irwin and Barnes (1980) suggest that the presence of CO_2 discharges may be useful in detecting areas of potential seismic activity. Earthquake data for the area (R. Wetmiller, personal communication) show a line of weak seismicity, parallel to, but west of the valley. The development of the large carbonate terraces must be post-glacial and the radiocarbon dating of wood in travertine at spring 017 suggests a possible increase in CO_2 activity between 1100 and 1700 years B.P. Further work is required to determine whether all the terraces are of a similar age.

CONCLUSIONS

The Flat River valley, N.W.T., is host to a linear group of travertine-precipitating springs, the waters of which have very high pCO_2. The high pCO_2 results in high Ca^{2+} and HCO_3^- concentrations due to dissolution of carbonate minerals in the subsurface. High tritium values in the water and $\delta^{18}O$ and δ^2H values similar to all other springs in the area and unaltered by water-rock reactions, indicate water of shallow meteoric origin, recently recharged. However, ^{13}C concentrations in DIC and the large volumes of CO_2 gas being discharged at these springs indicate a large external input of CO_2, derived either from metamorphic decomposition of carbonate rocks at depth or the mantle or a combination of both. We favour the metamorphic hypothesis because the calculated $\delta^{13}C$ composition of the gas falls mostly above that expected for mantle CO_2 and because of the evidence of high heat flow associated with the plutons. The temperatures required to initiate calcium-bearing silicate reactions and their resulting CO_2 production could be a result of radioactive decay within the plutons.

The model proposed to explain this phenomenon is as follows. CO_2 is produced at a relatively-shallow depth (<5 km) by metamorphism of carbonate rocks which are adjacent to Cretaceous quartz-monzonite plutons. Fluids, with a high proportion of CO_2, travel upward from depth along an inferred fault, possibly mixing with mantle CO_2. The deep fluids eventually mix with shallow meteoric waters, resulting in the dissolution of large quantities of carbonate minerals. Carbonate is re-precipitated as travertine on the surface upon discharge of the waters. The upward transport of the CO_2 and the linear discharge pattern of the springs strongly suggest a fault conduit. It is likely, therefore, that a large, unmapped and relatively open fault exists within this portion of the Flat River valley. Further study into the chemical and isotopic composition of the gases emitted and travertine precipitated at the Group 3 springs will allow testing of this hypothesis.

CO_2 springs are found almost exclusively in seismically-active areas around the globe and are known to delineate active faults (Barnes *et al.*, 1984). There is a potential for seismicity in the Flat River valley, although earthquake activity since 1961 has been relatively minor.

ACKNOWLEDGEMENTS

This project is part of a resource assessment of proposed extension areas to the Nahanni National Park Reserve. The assessment was jointly funded by the Departments of Energy, Mines and Resources, Indian and Northern Affairs (DINAC) and the Environment. Logistical support, including helicopter time, was provided by the Polar Continental Shelf Project to C.W. Jefferson. Additional support for isotope analyses and other expenses came through F.A. Michel from NSERC grant A2646. Travelling and living expenses for the first author were supported by a Northern Studies Training Grant from DINAC.

Canada Tungsten Mining Corporation personnel, in particular Jim Wilson and Stan Bartlett, extended hospitality, support and generous exchange of information during the two field seasons. Thanks are due to staff at the analytical chemistry laboratories of the Geological Survey of Canada, especially G. Lachance, G.E.M. Hall, P. Belanger, J. Vaive, and W. Nelson for their care and help in designing methods and standards. Dr. I. Clark of the University of Ottawa shared his expertise in the field of carbonate systems and his discussions are much appreciated. The critical reviews of B.E. Taylor and two anonymous reviewers improved this paper.

REFERENCES

ATCHISON, M.E., 1964. A study of springs and spring deposits in the Flat River map area, District of Mackenzie, N.W.T. B.Sc. thesis, Department of Geological Sciences, University of British Columbia, Vancouver, British Columbia, 53 pp.

BARNES, I., W.P. IRWIN and D.E. WHITE, 1978. Global distribution of carbon dioxide discharges and major zones of seismicity. Water Resources Investigations Open File Report No.78-39, U.S. Geological Survey, Washington, D.C., 12 pp.

BARNES, I., W.P. IRWIN and D.E. WHITE, 1984. Global distribution of carbon dioxide discharges and major zones of seismicity. Miscellaneous Investigation Series Map I-1528, scale 1:40,000,000, U.S. Geological Survey, Washington, D.C., map

BATARD, F., J.C. BAUBRON, B. BOSCH, A. MARCÉ and J.J. RISLER, 1982. Isotopic identification of gases of a deep origin in French thermomineral waters. Journal of Hydrology, 56(1-2), 1-21

BLAVOUX, B., J. DAZY and J. SARROT-REYNAULD, 1982. Information about the origin of thermomineral waters and gas by means of environmental isotopes in eastern Azerbaijan, Iran, and southeast France. Journal of Hydrology, 56(1-2), 23-38

BLUSSON, S.L., 1967. Nahanni, District of Mackenzie and Yukon Territory. GSC Map No.8-1967, Geological Survey of Canada, Ottawa, Ontario, map

BOTTINGA, Y., 1968. Calculation of fractionation factors for carbon and oxygen isotopic exchange in the system calcite - carbon dioxide - water. The Journal of Physical Chemistry, 72(3), 800-808

BOWMAN, V.J., 1990. Stable isotope geochemistry of travertine depositing springs and their deposits in the South Nahanni River region, District of Mackenzie, N.W.T. B.Sc. thesis, Department of Geography, Carleton University, Ottawa, Ontario, 40 pp.

CLARK, I.D., 1980. Isotope hydrology and geothermometry of the Mount Meager geothermal area. M.Sc. thesis, Department of Earth Sciences, University of Waterloo, Waterloo, Ontario, 131 pp.

CRAIG, H., 1961. Isotopic variations in meteoric waters. Science, 133(3465), 1702-1703

CRANDALL, J.T. and T.L. SADLIER-BROWN, 1978. Data on geothermal areas - Cordilleran Yukon, Northwest Territories, and adjacent British Columbia, Canada. Contract No.ISQ5-0136, Open File Report No.78-1, Earth Physics Branch, Energy, Mines and Resources Canada, Ottawa, Ontario, 80 pp. + maps

DEINES, P., D. LANGMUIR and R.S. HARMON, 1974. Stable carbon isotope ratios and the existence of a gas phase in the evolution of carbonate ground waters. Geochimica et Cosmochimica Acta, 38(7), 1147-1164

FRITZ, P., R.J. DRIMMIE, S.K. FRAPE and K. O'SHEA, 1987. The isotopic composition of precipitation and groundwater in Canada. In - Isotope Techniques in Water Resources Development, Proceedings of a Symposium, 30 March - 3 April 1987, Vienna, Proceedings Series, International Atomic Energy Agency, Vienna, Austria, 539-550

GABRIELSE, H., S.L. BLUSSON and J.A. RODDICK, 1973. Geology of Flat River, Glacier Lake and Wrigley Lake map-areas, District of Mackenzie and Yukon Territory. GSC Memoir No.366, Geological Survey of Canada, Ottawa, Ontario, Part 1 - 153 pp.; Part 2 - 268 pp. + maps

GERLACHE, T.M. and B.E. TAYLOR, 1990. Carbon isotope constraints on degassing of carbon dioxide from Kilauea Volcano. Geochimica et Cosmochimica Acta, Vol.54(7), 2051-2058

HALL, G.E.M., C.W. JEFFERSON and F.A. MICHEL, 1988. Determination of W and Mo in natural spring waters by ICP-AES (Inductively Coupled Plasma Atomic Emission Spectrometry) and ICP-MS (Inductively Coupled Plasma Mass Spectrometry): application to South Nahanni River area, N.W.T., Canada. Journal of Geochemical Exploration, 30(1), 63-84

HAMILTON, S.M., 1990. The application of spring water geochemistry and hydrogeology to a non-renewable resource assessment of the South Nahanni River area, N.W.T. M.Sc. thesis, Department of Geology, Carleton University, Ottawa, Ontario, 169 pp.

HAMILTON, S.M., F.A. MICHEL and C.W. JEFFERSON, 1988. Groundwater geochemistry, South Nahanni resource assessment area, District of Mackenzie. In - Current Research Part E, Cordillera and Pacific Margin, Geological Survey of Canada Paper No.88-1E, Ottawa, Ontario, 127-136

IRWIN, W.P. and I. BARNES, 1980. Tectonic relations of carbon dioxide discharges and earthquakes. Journal of Geophysical Research, 85(B6), 3115-3121

MATTEY, D.P., 1987. Carbon isotopes in the mantle. Terra Cognita: the Journal of the European Union of Geosciences, 7(1), 31-37

MICHEL, F.A., 1986. Hydrogeology of the central Mackenzie valley. Journal of Hydrology, 85(3-4), 379-405

MOOK, W.G., J.C. BOMMERSON and W.H. STAVERMAN, 1974. Carbon isotope fractionation between dissolved bicarbonate and gaseous carbon dioxide. Earth and Planetary Science Letters, 22(2), 169-176

MUFFLER, L.J.P. and D.E. WHITE, 1968. Origin of CO_2 in the Salton Sea geothermal system, southeastern California, U.S.A. Proceedings of Symposium II, Genesis of Mineral and Thermal Waters, Section 17, G. Kačura (Editor), 23rd International Geological Congress, 1968, Prague, Czechoslovakia, 185-194

MUFFLER, L.J.P. and D.E. WHITE, 1969. Active metamorphism of upper Cenozoic sediments in the Salton Sea geothermal field and the Salton Trough, southeastern California. Geological Society of America Bulletin, 80(2), 157-181

VALLEY, J.W., 1986. Stable isotope geochemistry of metamorphic rocks. In - Stable Isotopes in High Temperature Geological Processes, J.W. Valley, H.P. Taylor, Jr and J.R. O'Neil (Editors), Reviews in Mineralogy Vol.16, Mineralogical Society of America, 445-489

REGIONAL SNOW ABLATION IN THE ALASKAN ARCTIC

L.D. Hinzman, D.L. Kane and R.E. Gieck

Water Research Center
Institute of Northern Engineering
University of Alaska
Fairbanks, Alaska 99775-1760
U.S.A.

ABSTRACT

The rates of snowpack ablation were monitored at three sites in northern Alaska for four years in a transect from the Brooks Range north to the Arctic Coastal Plain. These data were analyzed along with meteorological data collected at each site. The initiation of ablation was site specific being largely controlled by the complementary addition of energy from radiation and sensible-heat flux. Although the research sites were only 115 km apart, the rates and mechanisms of snowmelt varied greatly. Snowmelt begins at the mid-elevations in the foothills and progresses northwards toward the coast and southwards up into the mountains. In the more southerly sites, snowpack ablation progressed much faster when compared to the northerly site. The southerly sites are much more influenced by sensible heat advected from areas south of the Brooks Range. A comparison of the measured energy balances reflected the increasing importance of net radiation in the more northerly site. Many possible reasons exist to explain regional differences in certain climatic parameters such as long-wave or short-wave radiation. The purpose of this paper is not to fully explain the climatic variability but rather, from a limited data base, to explore trends and examine differences.

INTRODUCTION

Spring snowmelt on the North Slope of Alaska is the dominant hydrological event of the year (Kane *et al.*, 1991) and also the period when the surface energy balance undergoes its most dramatic changes (Hinzman, 1990). The mechanism and timing of snowpack ablation has implications in the prediction of snowmelt run-off, initiation of waterfowl migration, and the diversity of plant communities. The pattern of snowmelt across the North Slope is especially important in dictating the position of migratory waterfowl in their spring journey to the nesting grounds of northern Alaska. Snowmelt is the primary source of moisture for the arctic wetlands in spring and early summer and, due to its great areal extent, it impacts the global energy and water balances. Regional differences in the energy budget impact these topics and dozens of other physical, biological, and anthropogenic aspects of the northern biome. Energy-balance studies on a regional scale in the North are necessary to delineate these differences, especially with indications of climatic warming being potentially greater in high latitudes (Rouse, 1990).

Determination of the areal extent of snowpack and the rates of snowpack ablation are frequent applications of remote-sensing techniques (Holmgren *et al.*, 1973; Robinson, 1984). Attempts to analyze the ablation process in the Arctic utilizing satellite imagery have led to incorrect conclusions because the basic physical processes were not included in the analysis (Robinson, 1986). The Arctic Slope has been selected for this type of analysis due to the large tracts of flat, treeless and relatively-uniform landforms (Hall *et al.*, 1986). Difficulties in these analyses arise due to the variability in snowpack structure and temperature. It is hoped that the observations presented in this paper will improve models of snowpack ablation, especially those which utilize remotely-sensed data.

SITE DESCRIPTIONS AND INSTRUMENTATION

Three research sites were established in a north-south transect across the Alaskan North Slope (Figure 1). All sites were located within 4 km of the Dalton Highway and were therefore accessible by truck or snow machine throughout the year. Each of these sites is completely underlain by permafrost although the maximum depth of the permafrost and the maximum depth of the active layer varies among the locations.

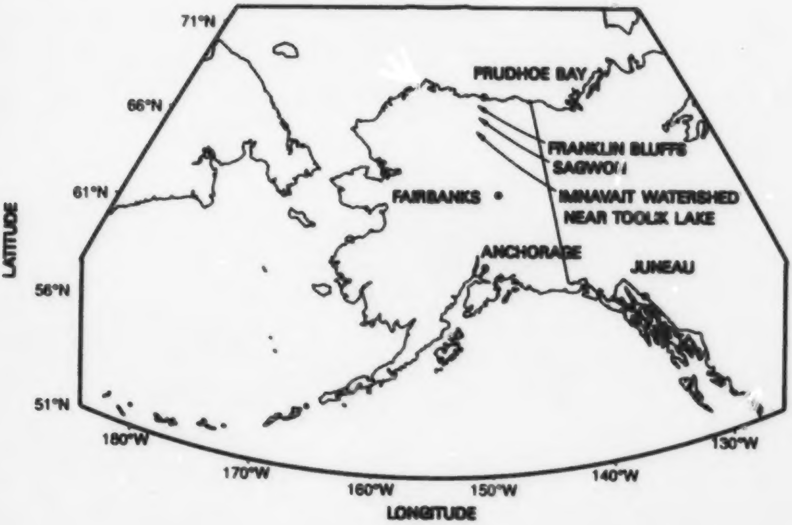
71°N
66°N
61°N
56°N
51°N
LATITUDE
PRUDHOE BAY
FRANKLIN BLUFFS
SAGWON
IMNAVAIT WATERSHED
NEAR TOOLIK LAKE
FAIRBANKS
ANCHORAGE
JUNEAU
180°W
170°W
160°W
150°W
140°W
130°W
LONGITUDE

Figure 1. Map showing the relative location of the study sites.

The first site established was located in the foothills on the north side of the Brooks Range in a small watershed at the headwaters of Imnavait Creek (68°37'N, 149°17'W). The Imnavait Creek watershed lies at an average elevation of 910 m and is approximately 165-km south of the Beaufort Sea at Prudhoe Bay. This site is only 15-km north of an abrupt transition from gradually rolling piedmont hills to the rugged mountains of the Brooks Range and 40-km north of the continental divide. Soils in this area are organic and quite wet and generally classified as Histic Pergelic Cryaquepts (Rieger *et al.*, 1979). The dominant vegetation type in the foothills is tussock sedge tundra (Walker *et al.*, 1989). Instruments were installed at mid-slope on a 10% west-facing slope. Data have been collected for six years (1985 to 1990) at this site. The hydrology, meteorology and ecology of this watershed have been studied extensively (Everett and Ostendorf, 1988; Kane and Hinzman, 1988; Kane *et al.*, 1989; Walker *et al.*, 1989).

Another site was established near the Sagwon Bluffs (69°25'N, 148°45'W) approximately 100-km south of Prudhoe Bay. This site was selected because it was a transitional zone between the coastal plain and the foothills. The elevation was 370 m and the vegetation was also characteristically tussock tundra. The soils were loamy and poorly drained with a peaty surface layer (Everett, 1980). Instruments were installed near the top of a 10% north-facing slope. Data have been collected for four years (1987 to 1990) at this site, although failure of the net radiometer during the spring-melt in 1988 prevented calculation of the surface energy balance.

The site near Franklin Bluffs (69°50'N, 148°45'W) was established on the coastal plain 50-km south of Prudhoe Bay. This site was located in the Sagavanirktok River floodplain at an elevation of 80 m in an area of relatively little surface relief. Vegetation on this very wet tundra consisted of a continuous cover of grasses and sedges rooted in mosses and lichens (Komárková and Webber, 1980). The soils were poorly drained and generally did not thaw to depths of more than 50 cm. Organic materials of variable thickness overlie silt-loam textured mineral soils (Everett, 1980). Data have been collected for four years (1987 to 1990) at this site.

A meteorological station was installed at each site with instrumentation sufficient to permit detailed analysis of the surface energy balance. Meteorological parameters included air temperature, relative humidity, precipitation, wind velocity, wind run, wind direction, soil heat flux, soil and snow temperatures and the radiation components. Radiation measurements included incoming short-wave, reflected short-wave, atmospheric long-wave, emitted long-wave, net radiation absorbed, total incoming radiation, and total emitted radiation. Emitted long-wave radiation was not measured at the Sagwon site. Soil and snow temperatures were measured hourly and averaged daily. All other instruments were sampled every minute and averaged hourly. These measurements were recorded on Campbell Scientific 21X data loggers. All values of radiation reported in this paper were measured with a horizontal sensor 1.5 m above the soil or snow surface. No correction for slope was considered. All radiation sensors were calibrated annually in our laboratory and returned to the Eppley Laboratory in 1989 for recalibration.

Incoming and reflected solar radiation are measured using the Weathertronics albedometer and Eppley double-dome spectral pyranometers. The spectral range of these sensors was 0.3 to 3 µm, which excludes long-wave terrestrial radiation. The accuracy of each sensor was reported as ±1%. The cosine response was less than 1% when the sun angle was within 0 to 70° of perpendicular of the sensor plane. Long-wave radiation was measured with Eppley precision infrared pyrgeometers. The spectral range of these sensors was between 4 and 50 µm and the cosine response was better than 5% from normalization. The net absorbed radiation (0.3 to 60 µm) was measured using Swissteco net radiometers. These sensors measured the total radiation absorbed. The accuracy of the Swissteco radiometers was not reported and is difficult to judge. At the Imnavait watershed site, we also measured net radiation with a second sensor, a Weathertronics pyrradiometer. This sensor measures the total-incoming and total-emitted radiation, the difference being the net-absorbed radiation. The accuracy of the pyrradiometer was reported within 2%. Output of this sensor compared well with the Swissteco instrument most of the time, but often measured a somewhat lower peak radiation absorbed at midday.

At Imnavait watershed, we initially used a Weathertronics humidity/temperature probe housed in a self-aspirating radiation shield to measure air temperature and relative humidity. The accuracy of the temperature sensor was ±0.10°C in the range measured. The relative-humidity probe was accurate to ±2% between 0 and 80%, and ±3% between 80 and 100% relative humidity. We presently use the Campbell Scientific model 207 temperature and relative-humidity probes at each site to determine the temperature and humidity gradients. Campbell Scientific reports worst-case accuracy of ±0.4°C between -33°C and +48°C for the temperature sensor, and 3% error between 12 and 100% relative humidity. These probes were housed in a self-aspirating radiation shield.

Mean wind speed, mean wind-vector direction, and standard deviation of direction were recorded hourly. Wind velocity and wind run were measured using a Weathertronics anemometer at Imnavait watershed. The threshold of wind measurement was 0.22 $m \cdot s^{-1}$. The accuracy was ±0.07 $m \cdot s^{-1}$. Also at Imnavait watershed and at the other sites, Campbell Scientific anemometers were employed to obtain wind-velocity gradients above the ground. The threshold of wind measurement of the Campbell Scientific anemometers was reported as 0.5 $m \cdot s^{-1}$ and the accuracy was ±1.5%. One 10-m tower was installed at Imnavait watershed to measure wind speed, wind direction and air temperature; wind speed was also measured at 1 m and 3 m at all sites. Wind direction was measured using Campbell Scientific wind-direction sensors. Direction can be measured within 5°.

Wind run and precipitation are totalized continuously. All other meteorological parameters are measured every minute. Those measurements are recorded and totalized or averaged hourly by the Campbell Scientific 21X data loggers. Except for air temperature, relative humidity and wind sensors, all meteorological instruments are positioned 1.5 m above the snow or soil surface. The radiation sensors at Imnavait watershed were lowered or raised as the snow depth changed.

In addition to the above measurements, the snowpack water equivalent was measured periodically during the winter and during snowmelt with an Adirondack snow sampler. The values of snowpack water equivalents for Sagwon and Franklin Bluffs represent the average of 20 measurements; Imnavait Creek is the average of 40 measurements. Wyoming precipitation gauges located at the Imnavait Creek and Sagwon sites measured daily accumulation of snow and rain. A Wyoming precipitation gauge located near Prudhoe Bay was also used to establish regional trends. The Wyoming precipitation gauge appears to provide the best available method for measuring precipitation in windy areas such as the North Slope when compared to other gauges (Benson, 1982; Clagett, 1988).

METHODS

The energy balance approach is a very effective method to demonstrate the importance of each component of energy transfer in the snowmelt process (Price and Dunne, 1976; Male and Gray, 1981). This concept is easily understood, however it is not always easy to accurately determine the magnitude of each of the components. The energy-budget equation for a control volume of snowpack is:

$$Q_m = Q_{sw} - Q_{sr} + Q_{lw} - Q_{le} - Q_h + Q_e + Q_a + Q_c - Q_{cc} \tag{1}$$

where:

Q_m = energy utilized in the snowmelt process ($W{\cdot}m^{-2}$)
Q_{sw} = energy input to the surface from short-wave radiation ($W{\cdot}m^{-2}$)
Q_{sr} = energy lost from the surface as reflected short-wave radiation ($W{\cdot}m^{-2}$)
Q_{lw} = energy input to the surface from atmospheric long-wave radiation ($W{\cdot}m^{-2}$)
Q_{le} = energy lost from the surface as emitted long-wave radiation ($W{\cdot}m^{-2}$)
Q_h = energy flux by convection between surface and air ($W{\cdot}m^{-2}$)
Q_e = energy transfer in evaporation, sublimation or condensation ($W{\cdot}m^{-2}$)
Q_a = energy advected in moving water (i.e., rainfall) ($W{\cdot}m^{-2}$)
Q_c = energy flux via conduction between the soil surface and subsurface ($W{\cdot}m^{-2}$)
Q_{cc} = energy deficit or cold content of the snowpack ($W{\cdot}m^{-2}$)

The radiation components were measured individually and the sum of incoming and outgoing components were compared to values determined from the net radiometers. The arithmetic sum of incoming short-wave and incoming long-wave minus reflected short-wave and emitted long-wave equals the net radiation (Q_{net}) and is a dominant component of the summer energy balance. Energy transferred by rain or running water and that used for biological activity is not included in the analysis. Precipitation in the form of rain never occurred during snowmelt so it was not necessary to consider this component. Convection of sensible heat is the energy transferred between the air and the snow surface. Unlike radiation, this energy flux is not normally measured directly. It is usually calculated as a function of the temperature gradient, wind speed and surface conditions:

$$Q_h = C_p \rho_a D_{h(n,s,u)} (T_a - T_{ss}) \qquad [2]$$

where:

C_p = specific heat of air ($J \cdot kg^{-1} \cdot {}^{\circ}C^{-1}$)
ρ_a = density of air ($kg \cdot m^{3}$)
T_a = temperature of air (°C)
T_{ss} = temperature of the surface (°C)
D_{hn} = neutral convective transfer coefficient ($m \cdot s^{-1}$) = $k^2 u_z / (\ln (z/z_o))^2$
D_{hs} = stable convective transfer coefficient ($m \cdot s^{-1}$) = $D_{hn} / (1 + (\sigma \, Ri))$
D_{hu} = unstable convective transfer coefficient ($m \cdot s^{-1}$) = $D_{hn} \, (1 - (\sigma \, Ri))$
Ri = Richardson number = $(g \, z \, [T_a - T_{ss}]) / (u_z^2 \, (T_a + 273.15))$
u_z = wind speed at height z ($m \cdot s^{-1}$)
z = height of the wind speed measurement (m)
z_o = roughness length (m) = $\exp[((u_{z2} \ln z_1) - (u_{z1} \ln z_2)) / (u_{z2} - u_{z1})]$
σ = empirical constant = 10
g = gravitational constant ($m \cdot s^{-2}$)
k = von Kármán's constant = 0.41

The convective heat transfer term (Q_h) is calculated from field measurements however, the heat-exchange coefficient ($D_{h(n,s,u)}$) was derived by assuming the momentum-exchange coefficient (D_m) between the atmosphere and ground to be equal to the heat-exchange coefficient (D_h) (Szeicz *et al.*, 1969) following the formulation of Moore (1983). This relationship is only valid for neutral (isothermal) conditions, which are common during the snowmelt period. A correction must be applied to account for the stability of the air just above the ground surface. This is possible using either the Monin-Obuchov factor or, as in this paper, the Richardson number (Price and Dunne, 1976).

Effective surface temperatures for the Q_h calculation (Equation 2) were obtained by back calculation using the Stefan-Boltzman law and the emitted terrestrial long-wave radiation. Difficulties in this approach are discussed by Rouse (1984a). Daily heat-exchange coefficients were adjusted to compensate for air stability based on the air-temperature profile between the surface and 10 metres using D_{hn} for neutral, D_{hs} for stable and D_{hu} for unstable conditions. The average surface-roughness length (z_o) was determined from wind-speed profiles between 1.5 and 10 metres. The roughness length over snow was estimated at 0.0013 m by averaging calculations made from several hundred wind-profile measurements during near neutral conditions., This value falls well within the reported values (Szeicz *et al.*, 1969) and yields reasonable results. Energy advected with precipitation (Q_a) was assumed to be negligible because of minimal precipitation during ablation.

Conductive heat transfer is the energy passed particle-to-particle within the soil matrix. Conduction (Q_c) can be calculated from Fourier's Law:

$$[3] \qquad Q_c = -K \frac{dT}{dx}$$

where:

K = thermal conductivity ($W \cdot m^{-1} \cdot {}^{\circ}C^{-1}$)
$\frac{dT}{dx}$ = thermal gradient (${}^{\circ}C \cdot m^{-1}$)

After snowmelt was complete, the active layer was still frozen below the surficial mosses. Although these mosses are quite desiccated (Kane and Hinzman, 1988), some errors result from latent-heat transfers in thawing of ice in the top 10 cm. The energy utilized for evaporation was calculated in a similar manner to the sensible-heat transfer except the vapour-pressure gradient was used instead of the temperature gradient and the latent heat of vapourization was used instead of the specific heat:

$$[4] \qquad Q_e = L_v \, \rho_a \, D_{h(n,s,u)} \, (0.622/P) \, (e_a - e_{ss})$$

where:

L_v = latent heat of vapourization ($J \cdot kg^{-1}$)
P = air pressure (mb)
e_a = vapour pressure of the air (mb)
e_{ss} = vapour pressure of the surface (mb)

Although the volumes of water transferred by evaporation and condensation are minimal, the associated energy is quite high. Evaporation can be relatively high during the day and condensation can be significant at night, but on a daily basis, they often tend to offset total gains and losses. The cold content, or energy deficit of the snowpack is that amount of energy required to warm the snowpack to isothermal conditions at the phase-change temperature before snowmelt may begin. This value was of primary importance before snowmelt began and when the snowpack cooled significantly at night. This parameter was determined from snowpack temperatures and properties. It was assumed that no energy was stored in the snowpack; i.e., the residual energy was utilized to melt snow.

DISCUSSION

The following discussion represents the integration of observations over many years and relies heavily upon measurements collected between 1985 and 1990. Due to space constraints, only graphical representations of the data from 1987 are

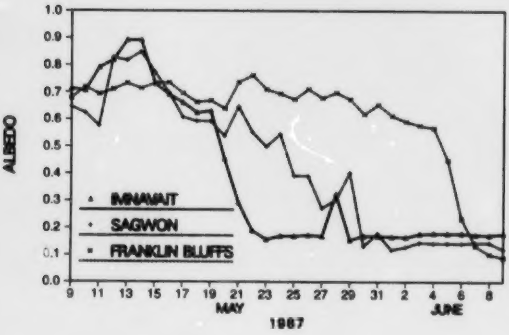

Figure 2. Average daily daytime albedo during snowpack ablation at Imnavait Creek, Sagwon and Franklin Bluffs in 1987.

presented. This particular year was selected for several reasons. The total snowpack water content and distribution were indicative of average conditions. Snowmelt began in early-May, but then ceased in mid-May due to a dramatic change in meteorological conditions. This variability of the energy-transfer processes in 1987 actually makes the interdependence and effect of each mechanism more obvious.

Snowmelt on the North Slope of Alaska is a very brief event, but very important hydrologically and through its impact on the balance. Prior to ablation, the snow surface has an albedo of about 80% ± 10% (Figure 2). Snowmelt occurs at a time when incident solar radiation at the ground surface is approaching its annual maximum; the overall drop in albedo results in a four- to five-fold increase in absorbed radiation at the surface. The tundra of the North Slope is covered with dry, wind-packed snow for eight to nine months each year (Benson, 1969) which usually ablates in one to three weeks in late-May or June. Precipitation in the Alaskan Arctic comes from cyclonic disturbances moving eastward from the Bering Sea or the Siberian Arctic Coast (Conover, 1960). The improved measurement technique of the Wyoming snow gauge indicates that there may be a trend of increasing precipitation as one proceeds from south to north toward the coast (Table 1). The opposite was thought to be true (Holmgren *et al.*, 1973), but conclusive data are not yet available. In part due to the low total precipitation on the North Slope, these observations are subject to great variability.

Rates of redistribution and sublimation of snow are greater in windier areas and are also affected by temperature and grain size (McKay and Gray, 1981). The spring snowpack on the coastal plain is usually less than that in the foothills in a

Table 1. Winter precipitation (mm) as recorded by the Wyoming Snow Gauge, October through May.

Site	Average Winter Precipitation	Number of Years	Standard Deviation
Imnavait Creek	88	9	19
Sagwon	89	9	50
Prudhoe Bay	132	10	40

Table 2. Snowpack water equivalent (mm) on the ground just prior to spring snowmelt, measured from snow surveys.

Site	1987	1988	1989	1990	Average	Standard Deviation
Imnavait Creek	108	78	155	106	112	32
Sagwon	60	53	150	61	81	46
Franklin Bluffs	75	54	218	47	98	81

given year (Table 2) probably due to greater winter losses of snow on the coastal plain. The Sagwon site is also quite windswept and the snowpack there is reduced by increased rates of redistribution and sublimation. Wind speeds are usually higher on the coastal plain than in the foothills, and the coastal plain also experiences fewer periods of calm weather throughout the winter. Comparisons of the May 1987 wind patterns are displayed in Figure 3. The greater topographical variation in the foothills compared to the coastal plain also serves to trap more snow in the valley bottoms and on the leeward side of ridges (Liston, 1986). Vast quantities of snow are trapped near the bluffs of the major rivers on the coastal plain (Benson, 1982). These observations are based on a very limited data base and may be insufficient to draw conclusions about regional trends.

The data requirements for a complete energy budget are extensive and the instrumentation is expensive, but the primary problem with this method is that the

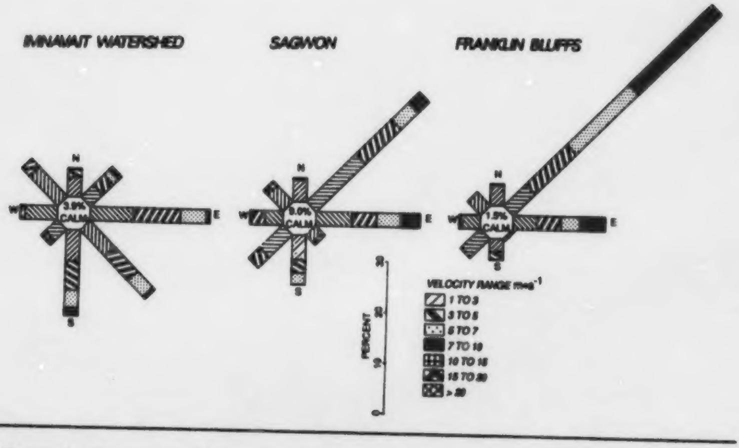

Figure 3. Comparison of wind roses at Imnavait Creek, Sagwon and Franklin Bluffs in May, 1987.

error in measurement of each component is collected in the residual term, in this case the estimate of snowmelt. Another dilemma is that there can be a small amount of energy storage in the unfrozen water in the ripe snowpack, which in this formulation will be considered snowmelt. Not all of the energy which is transported with snowmelt water into the soil matrix will be accounted for in the heat-conduction term of the soil. Riming, or condensation, is a common process in the Arctic and a significant energy-transfer mechanism. Riming appears in the energy balance as a positive value due to the release of latent heat. Many aspects of the energy balance of the Arctic were discussed by Weller and Holmgren (1974). Rouse (1990) presents a thorough review of regional differences in the energy balance in arctic regions and in comparison to subarctic and temperate regions.

The snowmelt process has been studied intensively at the Imnavait Creek site (Liston, 1986; Hinzman and Kane, 1991; Kane *et al.*, 1991) and a comparison of this process at other sites will facilitate an understanding of regional similarities and differences. Previous studies at Imnavait watershed have demonstrated that initiation of the snowmelt process is dependent upon net radiation and sensible heat transferred from south of the Brooks Range (Kane *et al.*, 1991). At Imnavait Creek, the spring-melt event is quite brief, usually lasting about 10 days (Figure 4). The total time required for ablation is dependent upon the total water equivalent in the snowpack and the number of days of warm weather. The maximum snowpack water equivalent in Imnavait watershed has ranged between 7.8 and 15.5 cm and the timing of melt has occurred between May 8 and June 6 during the period of the study (Figure 4).

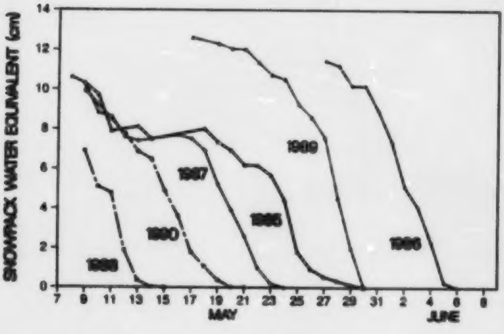

Figure 4. Spring snowpack ablation at Imnavait Creek from 1985 through 1990.

In contrast, at the Franklin Bluffs site, snowmelt usually occurred several weeks later and the time required for ablation was longer even though the total water equivalent of the snowpack was less (Figure 5); except in 1990, when the snowpack at Franklin Bluffs was less than half of that at Imnavait watershed. The snowmelt event at Sagwon usually began after Imnavait watershed, but the time required for total ablation was sometimes greater and sometimes less than that of Franklin Bluffs. Snowmelt normally began first in the southern foothills near Imnavait watershed and progressed northwards toward the coast and southwards up into the mountains. This pattern has also been observed through analysis of satellite imagery (Holmgren *et al.*, 1973; Kane *et al.*, 1975). Snow near the road (≈100 m) also melted sooner than the snow farther removed from the road. This is due to the lower albedo associated with snow which is frequently covered with dust from the road. The downwind side of the road (generally southwest on coastal plain and northwest in southern foothills) normally melted back farther than the upwind side on a given day early in the melt. Imnavait watershed and Franklin Bluffs were quite distant from the road and upwind from the predominant winter winds, but the Sagwon site may have been influenced by the effects of road dust. This phenomena has been observed since the construction of the Dalton Highway (Benson *et al.*, 1975; Walker and Everett, 1987).

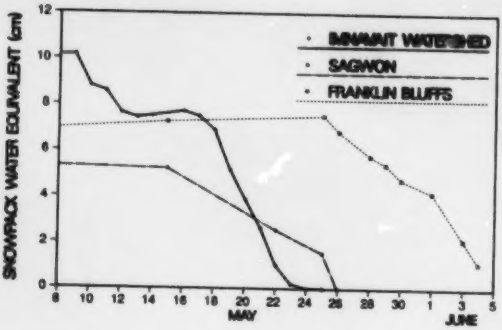

Figure 5. Snowpack ablation at Imnavait Creek, Sagwon and Franklin Bluffs, Spring 1987.

In an analysis of spring ablation of the arctic snowpack based upon satellite imagery, Robinson (1986) concluded that initiation of the springmelt was dependent upon a short-wave radiation threshold. The incoming short-wave at these three sites varied somewhat during the snowmelt period, but the differences were not enough to produce the observed melt sequence. The daily peak incoming short-wave radiation ranged between 400 and 750 $W \cdot m^{-2}$. The reflected radiation clearly identifies the timing of complete ablation. The reflected radiation drops from a daily peak of 300 to 500 $W \cdot m^{-2}$ to a daily peak of about 100 $W \cdot m^{-2}$ and correlates directly with measurements of snowpack water equivalent (Figures 4 and 5). The reflected short-wave radiation appears clearly on certain satellite imagery as an indicator of the progress of ablation, however it is a consequence of ablation, not the sole cause of ablation. The short-wave radiation is strongly affected by atmospheric conditions (Fouquart *et al.*, 1990), being greatly reduced on cloudy days, and by sun angle, being greatest near solstice and solar noon. Reflected short-wave is naturally most dependent upon incoming short-wave, and secondly upon the albedo. The albedo, ratio of reflected short-wave radiation to incoming short-wave radiation, clearly indicates the progression of the snowpack ablation at each site. The average daytime albedo, collected between 06:00 and 18:00 AST (Alaska-Hawaii Standard Time), are displayed in Figure 2. The albedo varies as a function of surface condition and sun angle, but responds primarily to the presence of snowcover. The snow does not melt in the winter and therefore the albedo remains near 0.8 from October to May, dropping to 0.2 after snowmelt. The peaks in albedo occurring at Imnavait Watershed and Sagwon in late-May were caused by a light snowfall which melted quickly (Figure 2). This snowfall was too light to be reflected in snowpack measurements (Figure 5). Our measurements of albedo agree well with the measurements over tundra made by Rouse (1984a) showing similar diurnal variation.

Another possible energy-transfer mechanism which may explain the difference in snowpack ablation is the quantity of atmospheric long-wave radiation. Long-wave radiation is emitted from the snow or soil surface as a function of surface condition and temperature and from the atmosphere as a function of cloud cover and temperature. It is difficult to separate reflected and emitted long-wave radiation, so these are commonly considered collectively. The differences in atmospheric long-wave radiation among the three sites was more pronounced than the differences in incoming short-wave radiation. This may be due to more cold air advection off the Arctic Ocean near the coast as compared to the more inland sites. There are other factors which affect atmospheric emission such as cloud properties (Fouquart *et al.*, 1990); however, we do not have measurements of these variables. Low clouds such as thin stratus and fog are common on the coastal plain while low and middle clouds such as cumulus and alto-cumulus are common in the foothills. The emitted long-wave radiation is a function of the surface temperature and whether the surface is snow-free or snow-covered.

Net radiation is the sum of the incoming short-wave and atmospheric long-wave radiation minus the reflected short-wave and emitted long-wave radiation. Net radiometers, which directly measure this component, were installed at each site. The major determinant of the net-radiation magnitude is the presence of snowcover, due to its high short-wave radiation reflectivity and lower temperature yielding a lower emittance of long-wave radiation. The presence of clouds also impacts net radiation. When the sun angle is high, clouds always decrease the amount of incoming short-wave radiation, and in the Arctic, clouds also tend to increase the amount of atmospheric long-wave radiation. The net result is that, at night, the presence of clouds tend to favor warmer conditions and accelerate snowmelt. During the day, clouds will decrease the amount of incoming short-wave radiation and yield cooler conditions, slowing melt. Cloudy conditions at night are more common on the coastal plain when compared to night-time conditions in the foothills, increasing the importance of net radiation on the coastal plain.

The air temperatures at the three sites were substantially different day-by-day and as melt progressed. At Imnavait watershed, there was much greater diurnal variation and peak temperatures were much higher during and after snowmelt. The air temperatures at Franklin Bluffs normally did not rise more than a few degrees above freezing during the snowmelt period (Figure 6). This reflects the greater importance of sensible-heat transfer at Imnavait watershed and the reduced importance of this mechanism at Franklin Bluffs.

The differences in the snowmelt mechanisms become most apparent through analysis of the surface energy balance. The absolute magnitudes of the energy transfers occurring daily in 1989 are displayed in Figures 7, 8 and 9. The relative magnitudes for each component of the energy balance for the entire melt period for 1987, 1988, 1989 and 1990 are displayed in Table 3. The absolute magnitudes of each component cannot be readily compared because the time required for complete ablation varied between years and sites. The total energy exchange is listed as a percentage of the total sources and sinks. The negative numbers represent the sinks.

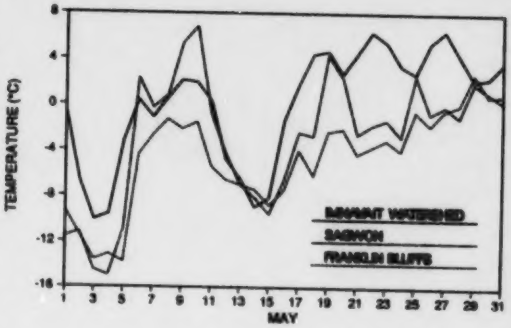

Figure 6. Average daily mean air temperature during snowpack ablation at Imnavait Creek, Sagwon and Franklin Bluffs, May 1987.

Figures 7, 8 and 9 are much better at displaying day-by-day differences in the importance of each particular component. Calculations were based upon hourly data, but the results are summarized as the total daily fluxes. In particular, notice the behavior of the sensible-heat component. Early in the snowmelt period, sensible heat is a major source of energy at Imnavait watershed when the major air flow is from the south (Figure 7). However, the sensible heat often

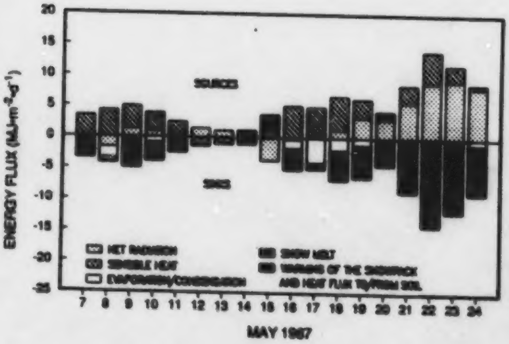

Figure 7. Surface energy balance, Imnavait Creek, Spring 1987.

becomes a sink, or a loss term in the energy-balance equation on certain days when the air flow is from the more northerly directions off the Arctic Ocean. When airflow is from the south, air temperatures are much warmer and the sensible-heat flux will complement the radiative-heat flux tending to accelerate the melt process. Rouse (1984b) observed a similar process for off-shore and onshore winds at Churchill on Hudson Bay. The sensible heat is much less important in the total energy balance at the Franklin Bluffs site (Figure 9). Strong northerly winds from the Arctic Ocean are more common during snowmelt at the Franklin Bluffs site (Figure 3) than in the foothills and substantially influence the snowmelt process.

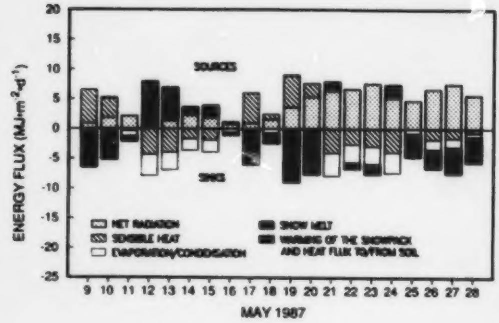

Figure 8. Surface energy balance, Sagwon, Spring, 1987.

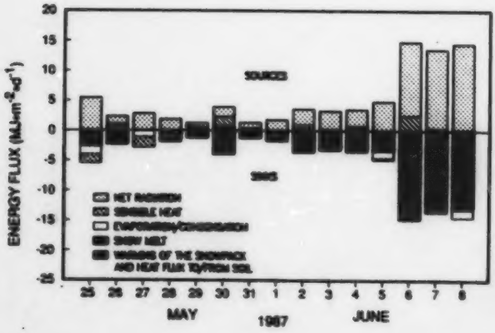

Figure 9. Surface energy balance, Franklin Bluffs, Spring 1987.

The net radiation is much more important and more likely to be the dominant energy source on the coastal plain. Weller and Holmgren (1974) also determined net radiation was the dominant term in the energy balance on the coastal plain at Barrow. Table 3 underscores the relative importance of each component and clearly demonstrates the regional differences in snowmelt mechanisms.

Table 3. Comparison of the relative magnitudes (percentage) of components of the surface energy balance at Imnavait Creek, Sagwon and Franklin Bluffs in 1987, 1988, 1989 and 1990.

Location	Year	Net Radiation (%)		Sensible Heat (%)		Evaporation Condensation (%)		Heat Flux Into Soil (%)		Snow Melt (%)		Snow Melt Period
		+	-	+	-	+	-	+	-	+	-	
Imnavait Creek	1987	47.9	6.4	47.5	0.8	0.1	16.1	4.5	41.5	0.0	35.2	May 8-25
Imnavait Creek	1988	65.0	7.9	31.4	9.0	0.1	21.0	3.4	23.7	0.0	38.4	May 10-14
Imnavait Creek	1989	59.1	4.4	39.9	0.0	0.0	14.3	1.0	25.0	0.0	56.4	May 18-30
Imnavait Creek	1990	65.3	3.5	34.4	0.0	0.0	15.4	0.3	44.3	0.0	36.8	May 7-20
Sagwon	1987	63.3	0.0	19.4	25.6	0.2	27.0	17.0	30.2	0.0	17.1	May 9-28
Sagwon	1988	*	*	*	*	*	*	*	*	*	*	May 20-June 7
Sagwon	1989	76.9	0.0	18.5	4.4	2.3	8.9	2.2	30.1	0.0	56.6	May 20-June 1
Sagwon	1990	36.9	0.0	61.3	0.4	0.8	22.9	1.0	15.5	0.0	61.2	May 5-15
Franklin Bluffs	1987	88.8	0.0	9.7	4.6	0.8	10.1	0.8	52.7	0.0	32.6	May 25-June 8
Franklin Bluffs	1988	71.5	0.0	21.3	4.6	1.6	16.4	5.6	43.6	0.0	35.4	May 22-June 3
Franklin Bluffs	1989	76.8	0.0	15.2	0.8	7.7	1.3	0.2	26.0	0.0	71.9	May 27-June 11
Franklin Bluffs	1990	82.9	0.0	14.3	0.2	1.9	5.6	1.0	35.0	0.0	59.2	May 9-14

**Instrument failure prevented analysis.*

CONCLUSIONS

This analysis represents six years of data from Imnavait watershed and four years data from Sagwon and Franklin Bluffs, and all conclusions are based essentially upon comparisons among these three sites. This is a very limited data base, making it difficult to draw firm conclusions on regional processes. There is considerable variation in the ablation of the snowpack on the Alaskan North Slope, both spatially and temporally. Much of the spatial variation can be explained by redistribution of snow by the wind. Temporal variation results from differences in the surface energy balance. Year-to-year variations in the surface energy balance can increase the snow-free period by almost one month at Imnavait Creek, but along the Arctic Coast, the snowfree period only varied by about two weeks. Within a given year, snowmelt initiation usually occurs first in the foothills and then progresses both north onto the coastal plain and south into the Brooks Range. Sensible heat transfer is a very important process in snowmelt near the Brooks Range and becomes less important as one progresses northward. Radiation is the dominant energy process of snowmelt on the coastal plain. Snowcover has a dominant effect on the surface energy balance and hydrology of arctic watersheds. Therefore it is very important that we understand quantitatively the processes associated with the accumulation, redistribution and ablation of the snowcover.

ACKNOWLEDGMENTS

This research was supported by the U.S. Department of Energy's Office of Health and Environmental Research, Ecological Research Division. Elizabeth K. Lilly assisted in data collection and reduction and preparation of figures.

LIST OF SYMBOLS

C_{pa}	the specific heat of air ($J \cdot kg^{-1} \cdot {}^\circ C^{-1}$)
D_{hn}	neutral heat exchange coefficient ($m \cdot s^{-1}$)
D_{hs}	stable heat exchange coefficient ($m \cdot s^{-1}$)
D_{hu}	unstable heat exchange coefficient ($m \cdot s^{-1}$)
$\frac{dT}{dx}$	thermal gradient ($C \cdot m^{-1}$)
e_a	vapour pressure of the air (mb)
e_{ss}	vapour pressure of the surface (mb)
g	gravitational constant ($m \cdot s^{-2}$)
k	von Kármán's constant (0.41)
K_s	thermal conductivity of soil ($W \cdot m^{-1} \cdot {}^\circ C^{-1}$)
L_v	latent heat of vaporization ($J \cdot kg^{-1}$)
P	air pressure (mb)
Q_a	energy advected in moving water (i.e., rainfall) ($W \cdot m^{-2}$)
Q_c	energy flux via conduction between the soil surface and subsurface ($W \cdot m^{-2}$)
Q_{cc}	energy deficit or cold content of the snowpack ($W \cdot m^{-2}$)
Q_e	energy transfer in evaporation, sublimation or condensation ($W \cdot m^{-2}$)
Q_h	energy flux by convection between surface and air ($W \cdot m^{-2}$)
Q_{le}	energy lost from the surface as emitted long-wave radiation ($W \cdot m^{-2}$)
Q_{lw}	energy input to the surface from atmospheric long-wave radiation ($W \cdot m^{-2}$)
Q_m	energy utilized in the snowmelt process ($W \cdot m^{-2}$)
Q_{net}	energy transferred by net radiation ($W \cdot m^{-2}$)
Q_{sr}	energy lost from the surface as reflected short-wave radiation ($W \cdot m^{-2}$)
Q_{sw}	energy input to the surface from short-wave radiation ($W \cdot m^{-2}$)
Ri	Richardson number
T_a	air temperature (°C)
T_{ss}	surface temperature (°C)
u_z	wind speed at height z ($m \cdot s^{-1}$)
z	height of the wind speed measurement (m)
z_0	roughness length (m)
ρ_a	the density of air ($kg \cdot m^{-3}$)
σ	empirical constant = 10

REFERENCES

BENSON, C.S., 1969. The seasonal snow cover of arctic Alaska. Research Paper No.51, Arctic Institute of North America, Montréal, Quebec, February, 86 pp.

BENSON, C.S., 1982. Reassessment of winter precipitation on Alaska's Arctic Slope and measurements on the flux of wind blown snow. Report No.R-288, Geophysical Institute, University of Alaska, Fairbanks, Alaska, September, 26 pp.

BENSON, C.S., B. HOLMGREN, R. TIMMER, G. WELLER and S. PARRISH, 1975. Observations on the seasonal snow cover and radiation climate at Prudhoe Bay, Alaska during 1972. In - Ecological Investigations of the Tundra Biome in the Prudhoe Bay Region, Alaska, J. Brown (Editor), Special Report No.2, Biological Papers of the University of Alaska, Fairbanks, Alaska, October, 13-50

CLAGETT, G.P., 1988. The Wyoming windshield - an evaluation after 12 years of use in Alaska. Proceedings, 56th Annual Western Snow Conference, 19-21 April 1988, Kalispell, Montana, 113-123

CONOVER, J.H., 1960. Macro- and microclimatology of the Arctic Slope of Alaska. Technical Report No.EP-139, Quartermaster Research and Engineering Center, Environmental Protection Research Division, U.S. Army, Natick, Massachusetts, 65 pp.

EVERETT, K.R., 1980. Soils and mapping. In - Environmental Engineering and Ecological Baseline Investigations along the Yukon River-Prudhoe Bay Haul Road, J. Brown and R.L. Berg (Editors), CRREL Report No.80-19, Cold Regions Research and Engineering Laboratory, U.S. Army Corps of Engineers, Hanover, New Hampshire, 48-52

EVERETT, K.R. and B. OSTENDORF, 1988. Hydrology and geochemistry of a small drainage basin in upland tundra, northern Alaska. Proceedings, 5th International Conference on Permafrost, K. Senneset (Editor), 2-5 August 1988, Trondheim, Norway, Tapir Publishers, Vol.1, 574-579

FOUQUART, Y., J.C. BURIEZ, M. HERMAN and R.S. KANDEL, 1990. The influence of clouds on radiation: a climate-modeling perspective. Reviews of Geophysics, 28(2), 145-166

HALL, D.K., A.T.C. CHANG and J.L. FOSTER, 1986. Seasonal and interannual observations and modeling of the snowpack on the Arctic Coastal Plain of Alaska using satellite data. Proceedings of the Symposium: Cold Regions Hydrology, D.L. Kane (Editor), 22-25 July 1986, Fairbanks, Alaska, American Water Resources Association Technical Publication Series No.TPS-86-1, Bethesda, Maryland, 521-529

HINZMAN, L.D., 1990. The interdependence of the thermal and hydrologic processes of an arctic watershed and their response to climatic change. Ph.D. thesis, School of Engineering, University of Alaska, Fairbanks, Alaska, May, 403 pp.

HINZMAN, L.D. and D.L. KANE, 1991. Snow hydrology of a headwater arctic basin. 2. Conceptual analysis and computer modeling. Water Resources Research, 27(6), 1111-1121

HOLMGREN, B., C.S. BENSON and G. WELLER, 1973. A study of the breakup on the Arctic Slope of Alaska by ground, air and satellite observations. In - Climate of the Arctic,

G. Weller and S. Bowling (Editors), Proceedings, 24th Alaskan Science Conference, 15-17 August 1973, Geophysical Institute, University of Alaska, Fairbanks, Alaska, 358-366

KANE, D.L., R.F. CARLSON and R.D. SEIFERT, 1975. Alaskan arctic coast ice and snow dynamics as viewed by the NOAA satellites. Proceedings, 3rd International Symposium on Ice Problems, 18-21 August 1975, Hanover, New Hampshire, G.E. Frankenstein (Editor), International Association of Hydraulic Research, November, 567-577

KANE, D.L. and L.D. HINZMAN, 1988. Permafrost hydrology of a small arctic watershed. Proceedings, 5th International Conference on Permafrost, K. Senneset (Editor), 2-5 August 1988, Trondheim, Norway, Tapir Publishers, Vol.1, 590-595

KANE, D.L., L.D. HINZMAN, C.S. BENSON and K.R. EVERETT, 1989. Hydrology of Imnavait Creek, an arctic watershed. Holarctic Ecology, 12(3), 262-269

KANE, D.L., L.D. HINZMAN, C.S. BENSON and G.E. LISTON, 1991. Snow hydrology of a headwater arctic basin. 1. Physical measurements and process studies. Water Resources Research, 27(6), 1099-1109

KOMÁRKOVÁ, V. and P.J. WEBBER, 1980. Vegetation. In - Environmental Engineering and Ecological Baseline Investigations along the Yukon River-Prudhoe Bay Haul Road, J. Brown and R.L. Berg (Editors), CRREL Report No.80-19, Cold Regions Research and Engineering Laboratory, U.S. Army Corps of Engineers, Hanover, New Hampshire, 37-42

LISTON, G.E., 1986. Seasonal snow cover of the foothills region of Alaska's Arctic Slope: a survey of properties and processes. M.Sc. thesis, University of Alaska, Fairbanks, Alaska, 123 pp.

MALE, D.H. and D.M. GRAY, 1981. Snowcover ablation and runoff. In - Handbook of Snow: Principles, Processes, Management & Use, D.M. Gray, and D.H. Male (Editors), Pergamon Press Canada Ltd., Toronto, Ontario, 360-436

McKAY, G.A. and D.M. GRAY, 1981. The distribution of snowcover. In - Handbook of Snow: Principles, Processes, Management & Use, D.M. Gray, and D.H. Male (Editors), Pergamon Press Canada Ltd., Toronto, Ontario, 153-190

MOORE, R.D., 1983. On the use of bulk aerodynamic formulae over melting snow. Nordic Hydrology, 14(4), 193-206

PRICE, A.G. and T. DUNNE, 1976. Energy balance computations of snowmelt in a Subarctic area. Water Resources Research, 12(4), 686-694

RIEGER, S., D.B. SCHOEPHORSTER and C.E. FURBUSH, 1979. Exploratory soil survey of Alaska. Soil Conservation Service, U.S. Department of Agriculture, Washington, D.C., February, 213 pp.

ROBINSON, D.A., 1984. Spring snow dissipation in Alaska. Proceedings, The Potential Effects of Carbon Dioxide-Induced Climatic Changes in Alaska, J. McBeath (Editor), 7-8 April 1982, Fairbanks, Miscellaneous Publication No.83-1, School of Agriculture and Land Resources Management, University of Alaska, Fairbanks, March, 124-128

ROBINSON, D.A., 1986. Initiation of spring snowmelt over arctic lands. Proceedings of the Symposium: Cold Regions Hydrology, D.L. Kane (Editor), 22-25 July 1986, Fairbanks, Alaska, American Water Resources Association Technical Publication Series No.TPS-86-1, Bethesda, Maryland, 547-554

ROUSE, W.R., 1984a. Microclimate at arctic tree line. 1. Radiation balance of tundra and forest. Water Resources Research, 20(1), 57-66

ROUSE, W.R., 1984b. Microclimate at arctic tree line. 3. the effects of regional advection on the surface energy balance of upland tundra. Water Resources Research, 20(1), 74-78

ROUSE, W.R., 1990. The regional energy balance. In - Northern Hydrology: Canadian Perspectives, T.D. Prowse and C.S.L. Ommanney (Editors), NHRI Science Report No.1, National Hydrology Research Institute, Environment Canada, Saskatoon, Saskatchewan, 187-206

SZEICZ, G., G. ENDRÖDI and S. TAJCHMAN, 1969. Aerodynamic and surface factors in evaporation. Water Resources Research, 5(2), 380-394

WALKER, D.A. and K.R. EVERETT, 1987. Road dust and its environmental impact on Alaskan taiga and tundra. Arctic and Alpine Research, 19(4), 479-489

WALKER, M.D., D.A. WALKER and K.R. EVERETT, 1989. Wetland soils and vegetation, Arctic Foothills, Alaska. Biological Report No.BR-89(7), U.S. Fish and Wildlife Service, Washington, D.C., 89 pp.

WELLER, G. and B. HOLMGREN, 1974. The microclimates of the arctic tundra. Journal of Applied Meteorology, 13(8), 854-862

REGIONALIZATION OF LOW FLOWS IN YUKON TERRITORY

J.R. Janowicz

Water Resources Division
Indian and Northern Affairs Canada
200 Range Road
Whitehorse, Yukon Territory
Y1A 3V1 CANADA

ABSTRACT

There is an increasing demand for low-flow information for water-management purposes in northern regions. The emphasis to date has been on the estimation of peak flows; however, it is now apparent that low flows are often the limiting factor in many water-use applications. A method for estimating 7-day low flows for ungauged streams throughout Yukon Territory was developed. The Territory was separated into four regions of homogeneous low-flow response based on the analysis of various low-flow parameters and air temperature. Low flows generally decrease with increasing latitude and distance from the moderating effects of the Pacific Ocean. This trend is largely controlled by the distribution of permafrost which influences ground-water contributions to winter streamflow. Mean annual air temperature distribution, through its use in defining the hydrological regions, was found to be a good indicator of the relative influence of the underlying permafrost on hydrological response. Isotherms of mean annual air temperature were used in a supportive role to define low-flow regions. Functional relationships were developed between 7-day low discharge at selected return periods and physical basin and climatic parameters.

INTRODUCTION

The demand for low-flow information for water-management purposes in northern regions is increasing. In the past considerable attention was paid to high flows, but with increasing development in northern regions, it is becoming apparent that low flows are often the limiting factor in the design and operation of many projects. Low-flow information is required for both water-quantity and quality purposes. Water-quantity applications include domestic water use, industrial water supply and hydro-electricity generation. Potentially significant water-quality concerns are associated with the dilution and transport of industrial and municipal waste and suspended sediment under low-flow conditions.

Indian and Northern Affairs Canada has the responsibility of managing the water resources of the Yukon and Northwest Territories. To provide a management tool the Yukon Region of the Department undertook to develop a methodology for estimating the low-flow characteristics of ungauged streams throughout the Yukon

Territory. The study consisted of three components which included a single station drought flow-frequency analysis using historical streamflow data, the division of Yukon Territory into homogeneous low-flow regions, and the development of functional relationships between the low-flow characteristics and physical basin and climatic parameters.

SETTING

Yukon Territory is situated in northwestern Canada between the Northwest Territories and Alaska. The Territory has a drainage area of 540,000 km^2 which ranges from its southern border at 60°N latitude to the Beaufort Sea at approximately 70°N. With the exception of the arctic coastal plain and the Liard Plateau in southeastly Yukon, most of the Territory is within the largely mountainous Cordilleran region. The Yukon Cordilleran consists of an interior zone of rolling uplands, plateaus and low-lying mountain ranges. This region is bounded on the east by the Mackenzie Mountains and on the west by the rugged coast and Saint Elias Mountains, which include the 5,956-m Mount Logan, the highest peak in Canada. Vegetation consists of boreal forest and tundra. South of the Ogilvie Mountains spruce, pine and poplar are found at lower elevations and alpine fir at higher elevations. Treeline lies between the elevations of 1,050 m in the west and 1,500 m in the south and east. North of the Ogilvie Mountains the vegetation consists largely of tundra, and mixed tundra and forest with black and white spruce the predominant tree species (Oswald and Senyk, 1977). The arctic treeline occurs at approximately 68°N.

The Yukon climate is classified as subarctic and arctic continental which is characterized by a large annual variation in temperature, low relative humidity and relatively low precipitation. Mean annual temperatures range from near zero in the south to -10°C in the north (Wahl *et al.*, 1987). July is the warmest month with monthly means ranging from 16°C in the south to 0°C in the north. January is the coldest month with mean temperatures ranging from -15 to -35°C. Extreme minimum low temperatures are in the order of -50°C. Precipitation within the basin is generally low, though portions of the Saint Elias and Coast Mountains receive annual precipitation amounts of 1,000 to 3,500 mm. Precipitation throughout the remainder of the basin ranges from 300 to 700 mm in the south, to less than 200 mm in the north.

The greater part of the Territory is within the zone of discontinuous permafrost with scattered permafrost occuring in the southern portion of this zone. The region north of the Arctic Circle lies within the zone of continuous permafrost. The effect of permafrost on the hydrological response of the Territory is significant. This impact is complete within the zone of continuous permafrost, while varying considerably within the zone of discontinuous permafrost, increasing from south to north. The effect of permafrost is greater on low flows than peak flows.

Streamflow in Yukon Territory is characterized by peak flows in the spring or summer due to snowmelt or glacial inputs, possible secondary peaks due to summer rainfall, followed by a gradual decrease in flow to a minimum in March or April. Ground-water contributions generally maintain streamflow in all but the smallest streams throughout most of the Territory. The arctic region north of the British Mountains is an exception due to the dominant nature of the underlying permafrost. Most streams within this region normally experience zero winter flows. Unit low flows generally decrease with latitude, ranging from 4.23 $L \cdot s^{-1} \cdot km^{-2}$ to 0.

DEVELOPMENT OF REGIONAL RELATIONSHIPS

Regionalization Procedure

Multivariate statistical analyses were used to define the hydrological regions. Cluster analysis was initially used to define rudimentary statistical regions using a program from the Biomedical Computer Program (BMDP) series (Dixon and Brown, 1981). Input parameters included annual 7-day low flow, monthly minimum winter flow, monthly minimum summer flow and mean annual flow. These parameters were standardized by dividing by drainage area. Three clear groups and a fourth transitional group were evident. Multiple discriminant analyses were used to refine the groups.

As expected the derived regions are characterized by progressively diminishing low flows from south to north. Since these zones are presumably largely controlled by the relative effect of the underlying permafrost, mean annual air temperature information was used to refine regional boundary locations. Four statistically defined regions with relatively high degrees of accuracy were defined (Figure 1).The Southern zone is bounded in the north by the -2°C isotherm (Wahl *et al.*, 1987). This region corresponds fairly closely with the scattered permafrost subzone of the discontinuous permafrost zone with an approximate latitude of 62°N. Low flows within the Southern region range from 1.02 to 4.23 with a mean of 2.1 $L \cdot s^{-1} \cdot km^{-2}$. Because of its relative southerly location and frequent Pacific influence all streams experience winter flows.

The northern boundary of the Interior low-flow zone closely follows the -6°C isotherm in the eastern part of the Territory and the -5°C isotherm in the west. Within the zone of discontinuous permafrost, the northern boundary coincides with the Ogilvie Mountains at 64°N but drops down to 62°N in the extreme western part of the Territory. Flows range from 0.040 to 2.24 with a mean of 1.28 $L \cdot s^{-1} \cdot km^{-2}$. Small gauged streams, with drainage areas in the order of 500 km^2 or less, occasionally experience zero winter flows. A drainage area of 1,800 km^2 has been found to be the lower limit in size for generating flow at the 50-year return period. Similarly, 5,000 km^2 has been found to be the lower limit for the 100-year event or greater.

The Northern low-flow zone is bounded in the north by the continuous permafrost zone boundary which roughly coincides with the -8°C isotherm. Flows within the

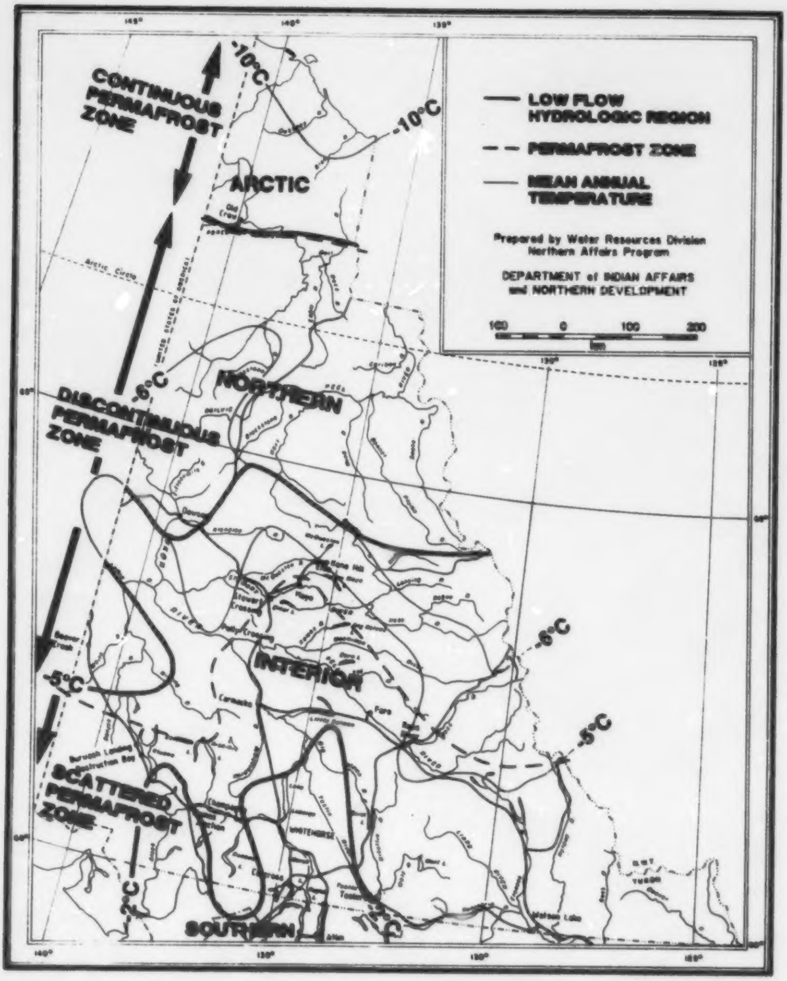
CONTINUOUS PERMAFROST ZONE
-10°C
-10°C
ARCTIC
NORTHERN
DISCONTINUOUS PERMAFROST ZONE
-5°C
INTERIOR
-6°C
-5°C
-5°C
SCATTERED PERMAFROST ZONE
-2°C
-2°C
SOUTHERN
WHITEHORSE
Watson Lake
Arctic Circle
— LOW FLOW HYDROLOGIC REGION
– – PERMAFROST ZONE
— MEAN ANNUAL TEMPERATURE
Prepared by Water Resources Division Northern Affairs Program
DEPARTMENT of INDIAN AFFAIRS and NORTHERN DEVELOPMENT
100 0 100 200
km

Figure 1. Low-flow hydrological regions.

Northern low-flow region range from 0 to 1.14 with a mean of 0.40 $L{\cdot}s^{-1}{\cdot}km^{-2}$. Small gauged streams within the Northern low-flow zone frequently experience zero flows while intermediate size streams, with drainage in the order of 2,000 km^2, occasionally experience zero winter flows. A drainage area of 1,000 km^2 has been found to be the lower limit in size for generating flow at the 50-year return period or greater.

The Arctic low-flow zone is bounded in the north by the Beaufort Sea. Because of the relatively small area of this region, the largest streams may be classed as intermediate in size. Most streams within the Arctic low-flow zone would normally experience zero winter flows. An exception is the Old Crow River which is located on the southern boundary of the region and has significant storage within the Old Crow Flats. The drought flow-frequency analysis indicates that zero flows occur at the 16-year return period. Because of the unique nature of this basin, it was not included in the analysis. The frequency analysis should be referred to directly to obtain discharge values for return periods less than 16 years.

Single-Station Analysis

Single-station drought flow-frequency analyses were carried out using 7-day mean discharge for the October 1 to September 30 run-off year for Water Survey of Canada hydrometric stations in Yukon and selected stations in northern British Columbia. The analysis included hydrometric stations with a range in drainage area from 14 to 264,000 km^2. The mean station record lengths were 29, 20 and 15 years in the Southern, Interior and combined Northern and Arctic regions respectively. With the objective of maximizing the data set, a minimum record length of 8 years was used in the analysis. Other than scanning for anomalous input data and analytical values, quality control measures carried out by Water Survey of Canada were relied upon for screening purposes. Stations with significant artificial control due to storage release for hydro-electric operation during winter low-flow months were eliminated initially leaving 76 stations in the available data set. The analysis was carried out using a low-flow frequency-analysis package developed by Environment Canada (Pilon and Jackson, 1988). The program was developed to use the Gumbel III theoretical probability distribution. Occasionally results cannot be provided using the Gumbel III distribution. When this occurs, the three-parameter lognormal distribution is used. It was not possible to carry out the analysis on data sets with greater than 50% zero flows. Except in the Arctic hydrological region where most streams normally experience zero flows, this was a rare occurrence. Where this did occur, such station data were evaluated subjectively.

Multiple-Regression Analyses

Stepwise multiple-regression analyses were carried out with data from the Southern, Interior and Northern low-flow regions using 7-day low flow as the dependent variable. The three regions were represented by 26, 40 and 7 station records respectively. With the exception of the Old Crow River winter low flows throughout the Arctic low-flow region are normally non-existent due to the dominant influence of the underlying permafrost on streamflow. Independent variables included drainage area, a storage index factor, main channel slope, mean annual basin air temperature, and mean basin latitude. Drainage area was the most significant variable in all cases. Though other parameters were entered in the analysis, they were not generally statistically significant. The exception was the Northern region analysis which also accepted main channel slope in addition to drainage area.

It is believed that air temperature was not found to be significant since isotherms of mean annual temperature were already used in defining the low-flow regions. As such the intra-region variability of air temperature was too great to allow its selection as a statistically significant variable.

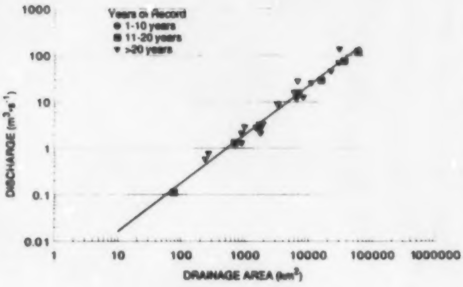

Figure 2. Mean 7-day low flow, Southern region.

The analysis of mean 7-day low flow produced relatively good results yielding values for the coefficient of determination (r^2) of 0.97, and 0.91 for the Southern, Interior low-flow regions, respectively. A value of 0.64 was obtained for the Northern region when using drainage area alone as an independent variable. Plots of mean 7-day low flow against drainage area are presented in Figures 2 to 5. The relationships between mean 7-day low flow and drainage area for the Northern region is provided for comparative purposes. The corresponding relationships for selected return periods for Southern and Interior regions are presented in Table 1.

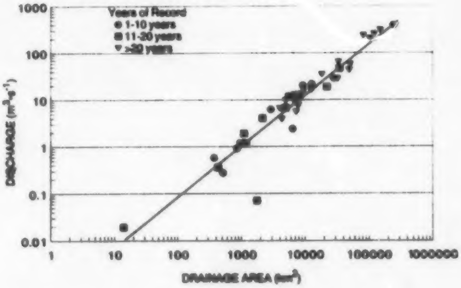

Figure 3. Mean 7-day low flow, Interior region.

These relationships provide a means of obtaining design drought flow estimates with a reasonable degree of confidence for ungauged basins throughout much of the Yukon Territory.

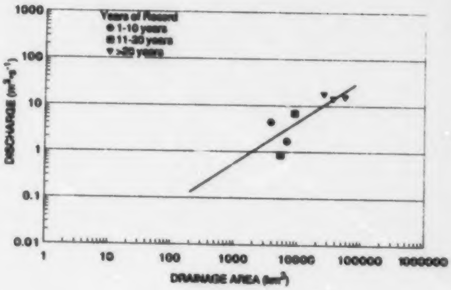

Figure 4. Mean 7-day low flow, Northern region.

Watershed storage was generally found to have some effect on moderating low flows with a significant impact on flows in the Southern region. Surface storage within a watershed is provided by lakes and wetlands. These features moderate low flows by contributing to winter streamflow. The relative degree of contribution depends on the amount of storage and its location within the basin. A storage index factor after Poulin (1971) was used in the study to account for storage contributions to winter flows. This index is defined as the relative amount of watershed drainage area in percent which is controlled by upstream lake or wetlands storage.

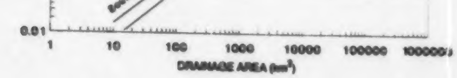

Figure 5. Mean 7-day low flow.

The storage index factor for gauged Yukon watersheds ranges from 0 to 100%, with mean values of 53, 27, 13 and 0% for the Southern, Interior, Northern and Arctic low-flow regions, respectively.

After drainage area, the storage index factor was the second most significant independent variable. Entry of this parameter by the stepwise analyses improved the Southern region results slightly. The

Table 1. Summary of 7-day low-flow equations: $Q=a(AREA)^b$.

7-Day Low Flow	Zone	Regression Constant	Regression Coefficient	Coefficient of Determination
$Q(m^3 \cdot s^{-1})$		a (x 10^{-3})	b	r^2
Mean 7-Day Low Flow	1	1.45	1.041	0.97
	2	0.60	1.081	0.91
2 Year	1	1.44	1.042	0.97
	2	0.49	1.097	0.91
5 Year	1	1.04	1.057	0.97
	2	0.23	1.154	0.90
10 Year	1	0.81	1.075	0.97
	2	0.13	1.201	0.88
50 Year	1	0.44	1.120	0.95
	2*	0.34	1.088	0.87
100 Year	1	0.32	1.149	0.94
	2**	0.27	1.105	0.87
200 Year	1	0.22	1.180	0.91
	2**	0.27	1.098	0.86
500 Year	1	0.12	1.233	0.83
	2**	0.28	1.086	0.82

1 = Southern: not valid for drainage areas greater than 60,000 km².
*2 = Interior: *zero discharge for drainage areas less than 1,800 km².*
***zero discharge for drainage areas less than 5,000 km².*

improvement was not significant however, and the storage parameter was omitted to optimize the utility of developed relationships. This parameter was not as significant as initially envisaged, probably due to the decrease in the number of lakes with increasing latitude. The significant effect of the Old Crow Flats on the response of the Old Crow River is evident; however, since no other storage exists in the Arctic region, this response is unique, and is therefore considered separately. A significant improvement within the Northern region was realized with the entry of main channel slope increasing the coefficient of determination from 0.64 to 0.80 for mean 7-day low flow. Multiple variable relationships for the Northern low-flow region are summarized in Table 2.

DISCUSSION

Simple- and multiple-linear regression relationships were developed for estimating 7-day low flows throughout Yukon Territory. The developed relationships are based on a single-station drought frequency analysis which was carried out with data

Table 2. 7-day low-flow equations for northern region.
$LnQ=a+b_1 ln(AREA^*)+b_2(SLOPE)$

7-Day Low Flow	Regression Constant	Regression Coefficient		Coefficient of Determination
Q ($m^3 \cdot s^{-1}$)	a (x 10^{-3})	b_1	b_2	r^2
Mean 7-Day Low Flow	-15.26	1.640	0.413	0.80
2 Year	-15.71	1.677	0.439	0.81
5 Year	-17.63	1.837	0.498	0.79
10 Year	-18.50	1.911	0.511	0.78
50 Year	-18.97	1.953	0.460	0.69
100 Year	-18.22	1.891	0.372	0.60

**Exercise caution when applied to drainage basins less than 1,000 km^2 and greater than 60,000 km^2.*

from 76 hydrometric stations with at least 8 years of record. The Gumbel III theoretical probability distribution was used throughout.

Four homogeneous low-flow regions were delineated based on the relative effect of the underlying permafrost of winter ground-water contributions to streamflow. The distribution of mean annual air temperature was found to be a good indicator of the relative impact of permafrost on streamflow and, as such, isotherms of mean annual air temperature were used in a supportive role to refine the geographic boundaries of the low-flow regions.

Relationships between 7-day low flow at selected return periods and drainage area were developed for the Southern, Interior and Northern low-flow regions. Zero winter flows normally occur throughout the Arctic low-flow region. Significant improvements were obtained with the entry of main channel slope to the Northern regional relationships. The analyses were generally good as indicated by the relatively high coefficients of determination. The developed relationships provide a simple method of estimating 7-day low flows with a reasonable degree of accuracy throughout Yukon Territory.

ACKNOWLEDGEMENTS

This study could not have been completed without the dedicated support of Laura Spicer who largely carried out the multivariate statistical analysis. Several individuals provided valuable assistance in this project. The data compilation and

single-station analyses were carried out by Tessa Gahan. Glenn Ford produced the plots and drafting services were provided by Bob Lewis.

REFERENCES

DIXON, W.J. and M.B. BROWN, 1981. BMDP statistical software. Department of Biomathematics, University of California Press, Berekely, California, 725 pp.

OSWALD, E.T. and J.P. SENYK, 1977. Ecoregions of Yukon Territory. Canadian Forestry Service, Victoria, British Columbia, 115 pp.

PILON, P.J. and R.J. JACKSON, 1988. Lowflow frequency analysis package. Water Resources Branch, Inland Waters Directorate, Environment Canada, Ottawa, Ontario, 29 pp

POULIN, R.Y., 1971. Flood frequency analysis for Newfoundland streams. Water Planning and Operations Branch, Environment Canada, Ottawa, Ontario, 20 pp.

WAHL, H.E., D.B. FRASER, R.C. HARVEY and J.B. MAXWELL, 1987. Climate of Yukon. Climatological Studies No.40, Atmospheric Environment Service, Environment Canada, Downsview, Ontario, 323 pp.

DISCHARGE REGIMES OF A GLACIERIZED BASIN, SLIMS RIVER, YUKON

P.G. Johnson

Department of Geography
University of Ottawa
Ottawa, Ontario
KIN 6N5 CANADA

ABSTRACT

The discharge and suspended-sediment regimes of the Slims River for 1983 and 1988 contrast a glacier-melt dominated regime with a storm-run-off dominated regime. The Kaskawulsh Glacier basin is 65% glacierized and normally provides 80% of the flow of the river. The glacier-melt dominated regime peaks in August with discharges in the 250 $m^3 \cdot s^{-1}$ *to 350* $m^3 \cdot s^{-1}$ *(previously reported) range. Suspended-sediment concentrations are high and variable early in the season as the glacier-drainage system is being established and are lower and diurnal later in the season when the drainage system is established. The lower basin is 9% glacierized but instantaneous run-off from large storms can produce flood flows for the river. In 1988, a wet early July, superimposed on the snowmelt, saturated the basin and high precipitation on July 14 and 15 resulted in a peak Slims River discharge of 580* $m^3 \cdot s^{-1}$*. Suspended-sediment concentrations were lower during the run-off-dominated period, but total loads were very high, with the primary sediment source from the lower basin not from the glacierized component.*

INTRODUCTION

The physiography of the southwest Yukon has a dramatic range from the icefields of the St. Elias Mountains to the broad valleys of the boreal forest zone. As a consequence, there are hydrological regimes which are dominated by snowmelt and regimes which have elements of snowmelt and glacier-ice melt. Research on the hydrology of the glacierized basins of the region has been limited. The network of stations of the Inland Waters Directorate provides data on a number of rivers, but the length of record is limited (the White and Alsek Rivers since 1974, locations A and B Figure 1). Kluane River at the outlet to Kluane Lake (record since 1953, location C Figure 1) provides some indication of the regime of the Slims River which is the primary supply to Kluane Lake and is the main discharge from the Kaskawulsh Glacier. The White River basin is 34% glacierized (approx. 2,129 km^2 of 6,220 km^2) without any storage equivalent to Kluane Lake. It provides a good indicator of the annual regime of a glacierized basin in the region.

Some hydrological studies have been directed to specific research problems such as glacier ice-dammed lake drainage (e.g., Clarke, 1980) and sedimentation in ice-dammed lakes (e.g., Liverman, 1987). Faber (1972) and Bigras (1982) looked at the hydrological characteristics of the Rusty Glacier and the Grizzly Creek Glacier respectively. There have also been a number of hydrological studies along the Alaska Highway usually in the context of project proposals related to that route. In 1978, for example, the Pacific and Yukon Region of the Inland Waters Directorate published 'Water investigations along the Alaska Highway Pipeline route' (Canada, Environment Canada, 1978). The data from this study were based on reconnaissance methods employed over a period of 18 months and were only intended to develop baseline estimates.

The Slims River (Figure 2) has been the subject of a number of geomorphological and hydrological studies due to its proximity to the Kluane Lake Research Station of the Arctic Institute of North America. The valley is geomorphologically interesting because, at one post-Pleistocene period of a higher Kluane Lake level, drainage was south down the Slims River to the Kaskawulsh and Ålsek River systems. It is also unique in that the terminus of the Kaskawulsh Glacier, its main water source, lies at a drainage divide and changes in the subglacial drainage system occasionally divert most of the discharge from the Slims River to the Kaskawulsh River. Some hydrological monitoring has been done, but usually in the context of other projects (Chauduri, 1963; Barnett, 1974; Bryan, 1972; and, Nickling, 1974). Fahnestock

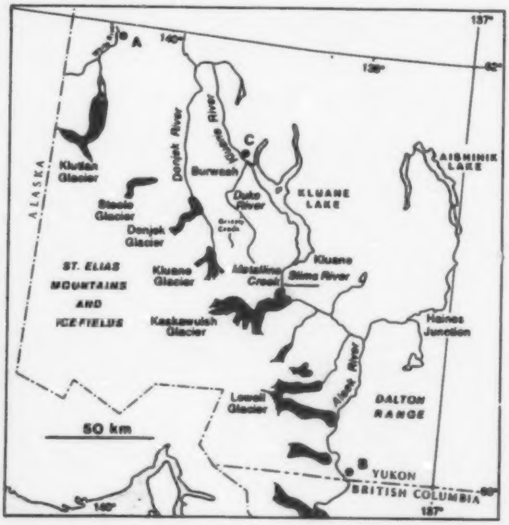
137°
A
140°
138°
62°
Donjek River
Kluane River
C
Burwash
Kluane Glacier
ALASKA
Klutlan Glacier
Steele Glacier
Donjek Glacier
Duke River
Grizzly Creek
KLUANE LAKE
AISHIHIK LAKE
ST. ELIAS MOUNTAINS AND ICEFIELDS
Kluane Glacier
Kaskawulsh Glacier
Kluane
Slims River
Haines Junction
Alsek River
Lowell Glacier
DALTON RANGE
50 km
B
YUKON
BRITISH COLUMBIA
60°
140°
137°

Figure 1. Location map.

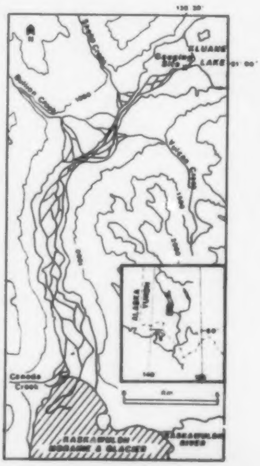
138°30'
KLUANE
LAKE
Bullion Creek
Vulcan Creek
Canada Creek
KASKAWULSH MORAINE & GLACIER
KASKAWULSH RIVER
ALASKA
YUKON
140

Figure 2. General map of the Slims Rivers.

(1969) provided a summary of discharge measurements to that date in which he showed a measured maximum discharge of 320 $m^3 \cdot s^{-1}$. He suggested, but provided no justification for, an extreme maximum discharge of approximately 566 $m^3 \cdot s^{-1}$. Barnett (1974) reported a maximum discharge of only 200 $m^3 \cdot s^{-1}$ in 1970 and the discharges measured by Fahnestock (1969) reached a maximum of only 280 $m^3 \cdot s^{-1}$ in 1965.

The Glaciology Division report (Canada, Fisheries and Environment Canada, 1977) estimated that up to 80% of the normal flow of the Slims River was derived from the Kaskawulsh Glacier, although it is obvious that this percentage varies with dominance of snowmelt and ice melt at different times of the year.

The suspended sediment load of the river has similarly received little attention. Bryan (1972) concluded that the glacier was the major source of the suspended sediment and that it was contributed directly from the glacier and not remobilized sediment from the valley floor. Nickling (1974) however concluded that the variability of the suspended-sediment load was the result of remobilization of the valley-floor sediments.

OBJECTIVES

The objectives of the paper are to present the results of hydrological studies of the Slims River carried out in 1983 and 1988, to place the data from these studies in the context of existing knowledge of glacierized basin hydrology and to assess the implications of the contrasting regimes from the two field seasons.

GLACIERIZED BASIN HYDROLOGY

Extensive research on glacier hydrology and the hydrology of glacierized basins has been conducted in most glacierized regions of the world. Recent summaries have been provided by Glen (1982), Young (1985, 1990) and Gurnell and Clark (1987). Case studies, such as those of the Norwegian Hydro-Electricity Board (e.g., Kjeldsen, 1987), have concentrated on issues pertinent to economic activity or have had a more academic focus, for example Hooke (1989) has summarized the existing knowledge of the nature of the internal drainage systems of glaciers. Hooke proposes that the internal drainage system is composed of a combination of linked cavities and conduits which respond to water and ice overburden pressures. These control the opening and closing of the system and any major changes in the subglacial network. It is these changes, particularly during the early melt season, which produce variability in the discharge at the glacier terminus.

Annual regimes in glacierized basins are controlled by winter precipitation, the summer energy balance, and the summer liquid-precipitation regimes. In years of low snowfall accumulation the deficit in water is contributed by ice melt and in years of high snowfall accumulation ice melt is retarded to lower the discharge variability.

The summer regimes of the glacierized basins are therefore less variable than those of nival basins (Fountain and Tangborn, 1985).

SLIMS RIVER

The Slims River was gauged and sampled at the Alaska Highway bridge near Kluane Lake. The bridge provides a stable platform for measurements and is the only location, apart from at the glacier terminus, where the river is constrained in a single channel. At the highway bridge the drainage basin is approximately 2,456 km^2, of which 2,020 km^2 is the Kaskawulsh Glacier basin (Canada, Fisheries and Environment Canada, 1977). Of the total area, approximately 55% is glacierized and this is distributed as 65% of the Kaskawulsh Glacier basin (1,313 km^2) and 9% of the lower basin (39 km^2). The Glaciology Division report (Canada, Fisheries and Environment Canada, 1977) estimated that 80% of the normal flow of the Slims River is Kaskawulsh Glacier discharge. The glacier is one of the largest valley glaciers on the east side of the St. Elias Mountains. The terminus lies at the hydrological divide between the Alsek River system, with direct egress to the Pacific Ocean, and the Yukon River system, with a long course to the Bering Strait. There is a periodic change of Kaskawulsh Glacier discharge from the Slims River to the Kaskawulsh River which produces a dramatic regime change. In years of flow to the Slims River the regime is that of a glacierized basin, but in years of flow to the Kaskawulsh River the regime is closer to that of a nival basin. This can be illustrated by reference to the Kluane River hydrograph (Figure 3) because the Slims River is the major water source for Kluane Lake and, therefore, for the Kluane River. Six representative years (Figure 3) show three glacierized-basin regimes (1957, 1971, 1980) with a peak flow in August and three years of nival-basin regime (1953, 1967, 1970) with a peak flow in June/July. For comparison, the hydrograph of the White River, a highly glacierized basin (Figure 4), has a July/August peak. Despite the variations in summer flow caused by the switching of drainage, it is interesting to note that the monthly coefficients of variation (Fountain and Tangborn, 1985) are similar for the summer months. The marked contrast in the coefficients of variation for the winter months is probably due to the storage component of Kluane Lake (Table 1).

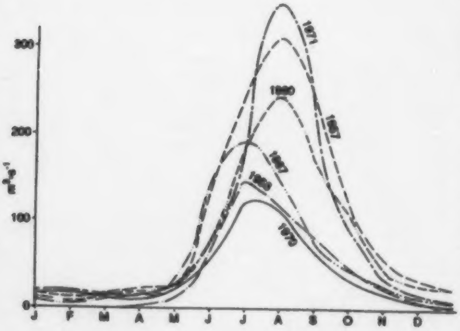

Figure 3. The Kluane River annual hydrograph. Representative years of Slims River and Kaskawulsh River dominance of the Kaskawulsh Glacier drainage are contrasted (Canada, Environment Canada, 1990).

Table 1. Monthly coefficients of variation (CV), and maximum, minimum, means and standard deviations of discharge (10^6 $m^3 \cdot s^{-1}$) for Kluane River (34 years of record) and White River (12 years of record).

	Kluane River					*White River*				
	Max	Min	Mean	σ	CV	Max	Min	Mean	σ	CV
Jan	7.96	0.64	3.46	1.54	0.45	4.55	3.32	3.70	0.37	0.10
Feb	6.33	0.15	2.93	1.29	0.44	4.31	2.83	3.29	0.96	0.14
Mar	5.88	0.17	3.32	1.47	0.44	4.96	2.87	3.75	0.58	0.16
Apr	5.95	0.31	3.77	1.45	0.39	6.32	2.59	4.22	0.98	0.23
May	9.56	1.87	5.87	1.71	0.29	19.23	8.95	15.27	2.99	0.20
June	37.07	8.79	20.17	6.48	0.32	96.16	36.55	59.36	15.74	0.27
July	69.10	32.68	50.89	9.20	0.18	173.83	73.92	114.64	25.95	0.23
Aug	93.20	30.00	65.09	14.92	0.23	129.63	66.42	96.69	24.21	0.25
Sept	60.65	16.12	43.55	11.96	0.27	43.54	14.49	27.22	85.95	0.32
Oct	32.14	8.97	21.59	5.91	0.27	13.45	6.08	10.20	1.76	0.17
Nov	14.67	3.24	9.38	2.73	0.29	6.43	3.34	5.11	1.08	0.21
Dec	9.12	1.40	4.69	1.93	0.41	4.93	2.81	4.04	0.60	0.15

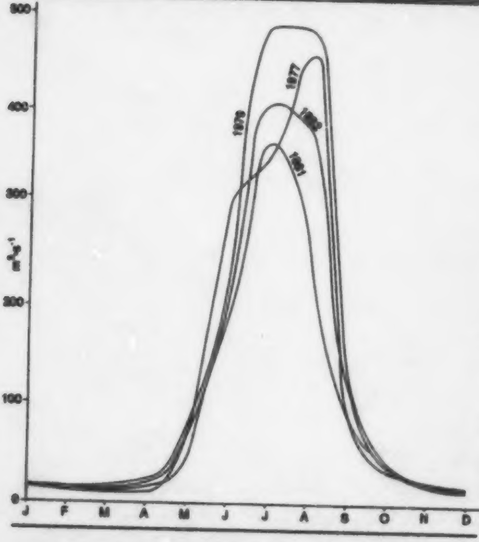

Figure 4. The White River hydrograph. A glacierized basin with no major lacustrine storage component (Canada, Environment Canada, 1990).

Stage and discharge measurements were obtained for the Slims River for June, July and August 1983 and July and August 1988 (Figure 5). Stage records were a continuous trace on an Ott type X recorder. Velocity measurements were obtained by a combination of depth-integrated recordings, 0.6-depth recordings and adjusted surface-velocity measurements. The cross profiles were monitored using a Raytheon sonar system.

Climate data are taken from the Atmospheric Environment Service's monthly records for Burwash Airport (Canada, Environment Canada, 1983, 1988) and Haines Junction (1983). The

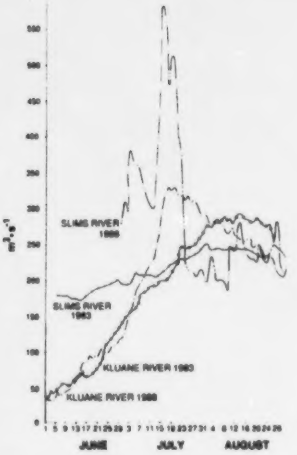

Figure 5. The Slims River discharge curves for 1983 and 1988.

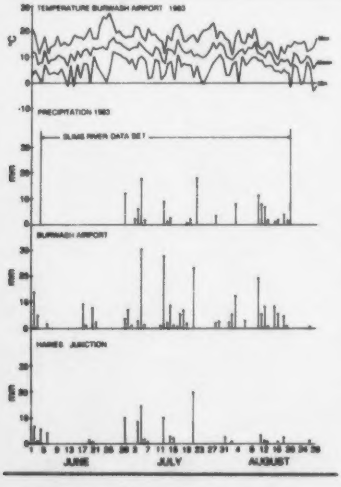

Figure 6. 1983 climate data from Burwash Airport[1], the Slims River and Haines Junction[1]. ([1]Atmospheric Environment Service, Environment Canada)

June and July data for 1988 at Haines Junction were not recorded. In addition, in 1983 climatic data were recorded at the mouth of the Slims River using a Meteorological Research Incorporated mechanical weather station. Trends for the Slims River are most similar to the Burwash Airport data and the contrasts between 1983 and 1988 can be illustrated by the use of these data sets (Figures 6 and 7).

The main source of error lies in the construction of the stage discharge curve which, because of turbulence beneath the highway bridge, did not produce a strong trend.

1983 AND 1988 DISCHARGE REGIMES

In 1983, a cool early-June was followed by a very warm late-June, a variable July and early-August, and a cool late-August (Figure 6). This compares with 1988 when a warm early-June led into variable conditions through the rest of the season (Figure 7). The precipitation regimes for the two years have the greatest contrast (Figures 6 and 7). In 1983, following a dry June, there were a number of precipitation events but no continuous wet period. In 1988, after a dry early-June, there was a continuous wet period in late-June and early-July. In the 19-day period from June 29 to July 17, 1988, there were only 3 days when no precipitation was recorded at Burwash Airport. In the lower basin this would also have been rain-on-snow in middle altitude ranges.

The hydrographs for 1983 and 1988 (Figure 5) illustrate the differences between the normal glacierized-basin hydrograph of 1983, characterized by increasing glacier melt through the summer to peak discharge in August, and the storm-run-off hydrograph of 1988, where saturation of the lower basin in early-July resulted in instantaneous run-off of

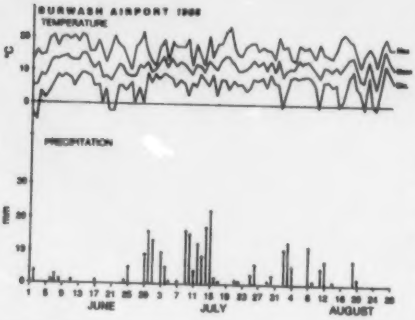

Figure 7. 1988 climate data from Burwash Airport (Atmospheric Environment Service, Environment Canada).

the mid-July rainfall. This run-off produced a flood discharge of 580 $m^3 \cdot s^{-1}$ on July 16. After the flood peak the discharge dropped to very low levels in late-July before recovering with the glacier melt to the glacierized-basin peak-discharge levels of about 250 $m^3 \cdot s^{-1}$. One of the late-season peaks in the 1988 record may be the drainage of an ice-dammed lake along the north margin of the Kaskawulsh Glacier.

The diurnal characteristics of the hydrograph of the ice-melt season are different from those of the flood-run-off season. The 1983 regime had a strong diurnal character reflecting the daily energy flux and the resulting variations in snow- and ice-melt in the glacierized basin. The 1988 regime during the storm-run-off period lost the strong diurnal character but this was re-established after about July 24 when the glacier melt became the dominant flow component.

From the 1983 regime four components of the hydrograph can be identified which can be interpreted as an indication of the development of the glacier drainage system (Figure 8).

1. Snowmelt discharge from the non-glacierized components of the basin and the glacier (Figure 8a). This dominates into early June with a strong diurnal regime peaking at the gauging site at 05:00 to 06:00 P.D.T.[1] The diurnal range was 10 to 15 $m^3 \cdot s^{-1}$ on daily discharge of 180 to 190 $m^3 \cdot s^{-1}$.
2. Development of the subglacial drainage system. Pulses in discharge and suspended sediment are frequent in the early ice-melt period (Johnson, 1990). This was the response to the very warm conditions in late-June and a strong diurnal character is maintained (Figure 8b).
3. The main ice-melt season which occurred from mid-July, when the glacier drainage conduits should be well established, to late-August. There is a continuously rising hydrograph with a less pronounced diurnal character as water is contributed from more and more remote areas of the basin, increasing travel times to the gauging site (Figure 8c).
4. The response to rainfall in this season was limited compared to 1988 due to the temporal separation of the storms and, therefore, the maintenance of infiltration capacity in the basin (Figure 8d).

---

[1] Pacific daylight time.

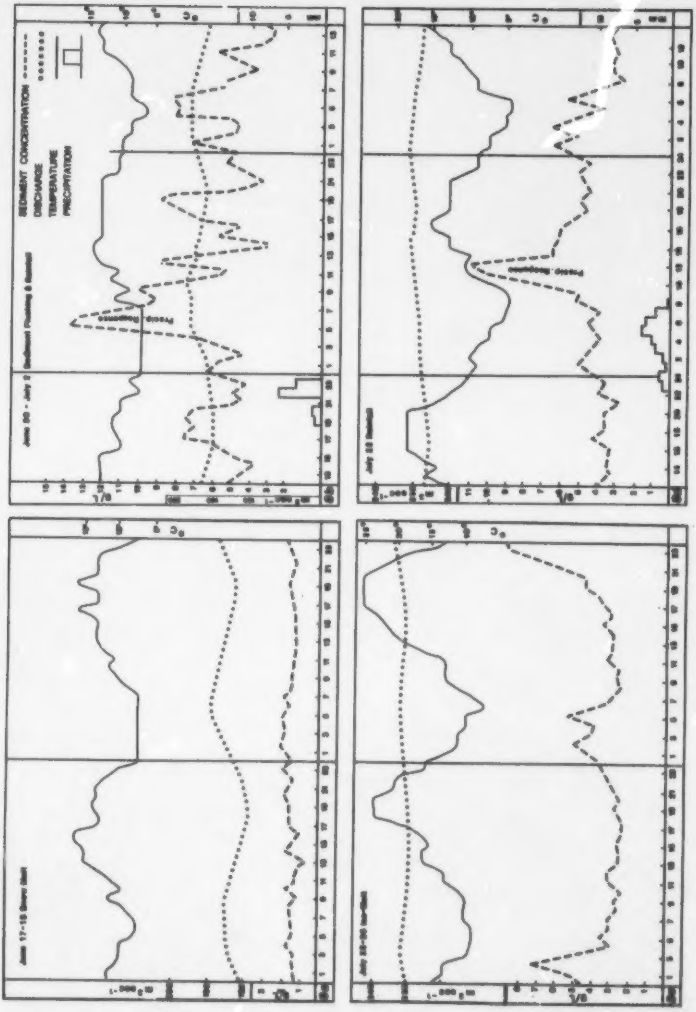

Figure 8. Components of the 1983 Slims River hydrograph illustrating:
a. snowmelt;
b. glacier conduit opening;
c. main ice-melt season; and,
d. effect of precipitation in the basin.

SEDIMENT REGIMES

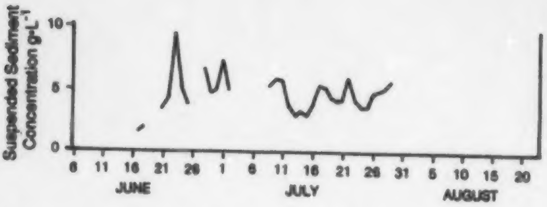

Figure 9. Daily suspended-sediment concentration averages for 1983 on the Slims River.

In 1983 the suspended-sediment concentrations were measured using an automatic water sampler. The sampler was programmed to take one sample each hour, but was plagued by a number of battery problems and was eventually detached from the platform at the end of July. Average daily concentrations, calculated for any day when the sampler successfully obtained 22 or more samples (Figure 9), show a highly variable pattern in late-June and early-July, peaking at 10 g·L^{-1}. In mid- to late-July the variability and the concentrations declined during the rising discharge. This conforms to the glacier discharge patterns with the greatest variability and the highest concentrations occurring during the opening of the subglacial drainage system. The latter part of the melt season, when the subglacial drainage system has been well established, has lower variability and low concentrations.

The location of the sampling site, 20 km from the glacier terminus, has raised the question as to whether the concentrations of sediment, and more specifically the variability of sediment concentrations, could be produced during the migration of channels in the Slims River between the glacier and the sampling site. Bryan (1972) hypothesized that most of the sediment has its source in the glacier system but Nickling (1974) considered that the variations were produced below the glacier. Observations, but no measurements, at the geysers at the glacier terminus indicate that the glacier discharge has a high suspended-sediment load. High loads are maintained along the length of the Slims River, but the extent to which deposition and remobilization of sediment occurs is unknown. Hourly peaks in suspended-sediment concentrations are up to 17 g·L^{-1}. If the magnitude of these peaks above the daily average concentrations of 5 to 10 g·L^{-1} is converted into total load, and into volume of bank collapse required to produce the peaks, then a bank failure of 1 m^2 cross section and 50 m length spread over one minute of discharge would produce them. Bank failures observed during migration were much smaller than this figure. There is also the problem that the data are from only one sample each hour and the nature of short time-frame variability is unknown. On the basis of the magnitude of the peaks and the variability, which have been measured at the terminus of glaciers in the St. Elias by the author, it is postulated that the suspended-sediment concentrations are controlled directly by the glacier. There was no relationship between discharge and concentration in 1983. A plot of the daily average concentrations against discharge has a wide scatter of points (Figure 10). Diurnal discharge-

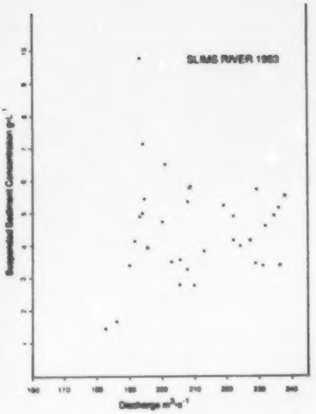

Figure 10. The scatter of discharge and suspended sediment concentration data for 1983.

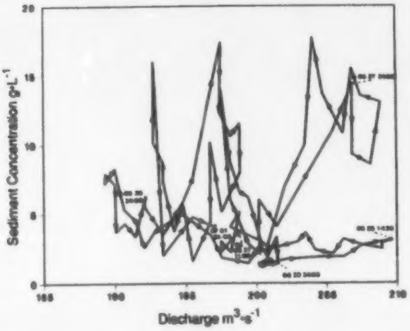

Figure 11. An example of the hourly discharge suspended-sediment concentration relationship for 1983.

discharge-concentration relationships also show no consistent pattern with no trend to positive or negative hysteresis (Figure 11). This is characteristic of the patterns which the author has measured at a number of small glaciers in the St. Elias. It is postulated that this further supports the glacier domination of the regime.

The size of the suspended sediment varies relatively little during the summer. Figure 12 is a composite of plots from a Coulter Counter of 36 samples, dividing each sample into 12 size classes. Mineralogically the sediments are also very homogeneous. The only significant changes are the disappearance of albite late in the season and the appearance of dolomite in mid-July. This may signal the progression of glacier drainage into the higher reaches of

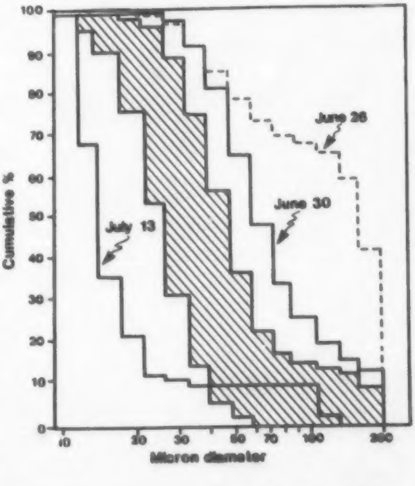

Figure 12. Grain size range of the 1983 suspended-sediment samples.

the basin. If the sediment concentrations were the result of remobilization of sediment deposited over a number of seasons, uniformity of mineral composition might be expected. The results, however, are not conclusive.

In summary, for 1983 there was no relationship between discharge and concentration of suspended sediment. Daily average concentration against discharge has a wide scatter of points (Figure 10). Diurnal discharge-concentration relationships show no hysteresis (Figure 11). These characteristics are similar to the glacier terminus conditions measured elsewhere in the St. Elias.

In 1988 the suspended-sediment sampling used a manual system. Samples were taken in mid-stream on a schedule of four samples per day every second day. This schedule was disrupted by flood conditions and by a blockage of the Alaska Highway by a debris flow. Estimates were made from 30 days of data of daily average concentrations. There is a marked trend in the discharge-suspended sediment relationship (Figure 13) for the discharges greater than 280 $m^3 \cdot s^{-1}$. For discharges below 280 $m^3 \cdot s^{-1}$ there is no strong relationship. The former occurred during the storm-run-off dominated conditions in the early part of the summer and the latter during the glacier-melt dominated regime of the later summer. The low sediment concentrations in 1988 reflect the very high discharges during the storm run-off and only a late season glacier-melt dominance.

The 1983 hourly data demonstrate a number of trends. 1) In the snowmelt season (Figure 8a) the suspended-sediment concentrations are consistently low. 2) In the early glacier-melt season, with the development of the glacier drainage network (Johnson, 1990), concentrations are variable and can be very high (Figure 8b). 3) Rainfall in the basin, and specifically on the glacier, may flush some sediment from the system. On July 22, 1983, a pulse in sediment concentration is lagged by 6 hours from the precipitation, which is a shorter lag time than that of the peak melt discharge. This may be caused by the rapid run-off of rain from the bare ice near the glacier terminus. A response in run-off from the lower basin is unlikely, due to potentially high infiltration rates and a low-magnitude precipitation event when compared with 1988 levels. 4) In the ice-melt season (Figure 8d), with the subglacial drainage system established, suspended-sediment concentrations drop from the early summer peaks and a diurnal pattern is established which is directly related to the diurnal discharge regime.

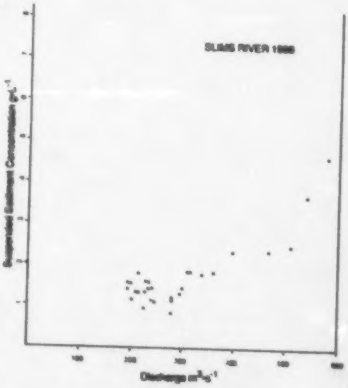

Figure 13. Daily discharge suspended-sediment concentration relationship for 1988 on the Slims River.

CONCLUSIONS

This study of two contrasting seasons on the Slims River indicates the importance of both the glacier-dominated regime and the possible overriding effect of extreme summer precipitation in the basin. It is apparent that the 'normal' glacier-dominated regime, although it can be very variable, may not be the cause of peak-flood flows for the basin. Two aspects must be considered, the potential magnitudes of the late-summer glacier-melt flows and the potential magnitudes and frequencies of rainfall-run-off flows. The variability of climate can be judged from the trends for Haines Junction (Figure 14) (Wahl *et al.*, 1987). Annual precipitation has a coefficient of variation of 0.25 with a range from 140 mm to 430 mm.

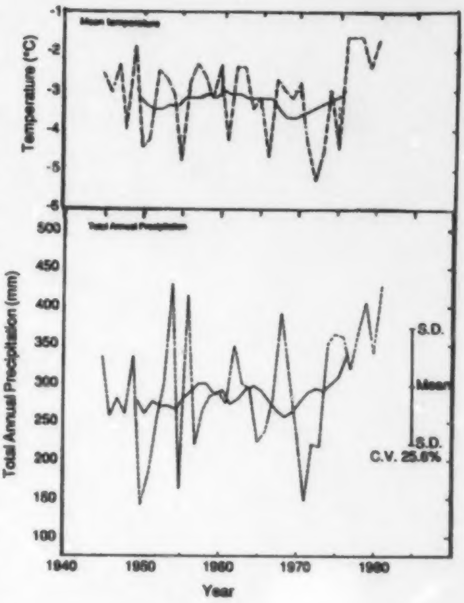

Figure 14. Climate variability at Haines Junction (after Wahl et al., 1987).

Glacier-discharge and basin-run-off dominated regimes of the Slims River produce distinct suspended-sediment regimes. The glacier-discharge regime of 1983 has low concentrations during snowmelt in June, high and variable concentrations in late-June and early-July as the drainage system of the glacier evolves, and lower and less variable concentrations in late-July and August when the glacier drainage system has been established and water contact with available sediment sources has been reduced. With the basin-run-off dominated regime of 1988 the suspended-sediment regime is more closely correlated to discharge.

In mountain areas with some glacierized component, both the glacier-dominated river regimes and the potential storm-run-off regimes must be analysed to determine the characteristics of the river.

ACKNOWLEDGEMENTS

The author is indebted to the Natural Sciences and Engineering Research Council for northern research funding, to the Arctic Institute of North America for the

logistical support of the Kluane Lake Research Station and to Mr. R. Schwartzburg, Mr. G. Kruszynski, Ms. K. Fabbri and M. G. Binda for field and analysis assistance. Equipment was provided at different times by the National Hydrology Research Institute, the National Water Research Institute, the Department of Indian and Northern Affairs and the Yukon Territorial Government.

REFERENCES

BARNETT, A.P., 1974. Hydrological studies of the Slims River, Yukon, June-August 1970. In - Icefield Ranges Research Project, Scientific Results Vol.4, V.C. Bushnell and M.G. Marcus (Editors), American Geographical Society, New York and Arctic Institute of North America, Montréal, Quebec, 143-150

BIGRAS, S.C., 1982. Hydrological investigation of glacial runoff components and their separation through hydrochemical analysis. M.A. thesis, Department of Geography, University of Ottawa, Ottawa, Ontario, January, 173 pp.

BRYAN, M.L., 1972. Variations in quality and quantity of Slims River water, Yukon Territory. Canadian Journal of Earth Sciences, 9(11), 1469-1478

CANADA, ENVIRONMENT CANADA, 1978. Water investigations along the Alaska Highway pipeline route in the Yukon Territory: main report. Inland Waters Directorate, Pacific and Yukon Region, Environment Canada, Vancouver, British Columbia, December, 90 pp.

CANADA, ENVIRONMENT CANADA, 1983. Monthly record - Meteorological observations in Canada. Atmospheric Environment Service, Environment Canada, Downsview, Ontario, microfiches

CANADA, ENVIRONMENT CANADA, 1988. Monthly record - Meteorological observations in Canada. Atmospheric Environment Service, Environment Canada, Downsview, Ontario, microfiches

CANADA, ENVIRONMENT CANADA, 1990. Historical streamflow summary: Yukon and Northwest Territories to 1988; supplement. Water Survey of Canada, Water Resources Branch, Inland Waters Directorate, Environment Canada, Ottawa, Ontario, 19 pp.

CANADA, FISHERIES AND ENVIRONMENT CANADA, 1977. Report on the influence of glaciers on the hydrology of streams affecting the proposed Alcan pipeline route. Report prepared by the Glaciology Division and submitted to the Inland Waters Directorate, Pacific Region, Fisheries and Environment Canada, Vancouver, British Columbia, June, Part 1 - 38 pp. + appendices + map; bibliography - 54 pp.

CHAUDURI, S.L., 1963. Slims River sedimentation, southwest Yukon Territory. Final Report, Project 71, Arctic Institute of North America, Montréal, Quebec, 11 pp.

CLARKE, G.K.C., 1980. An estimate of the magnitude of outburst floods from Lake Donjek, Yukon Territory, Canada. A report prepared for the Department of Indian and Northern Affairs through a contract from the Department of Supply and Services by the Department of Geophysics and Astronomy, University of British Columbia, Vancouver, British Columbia, 20 March, 90 pp.

FABER, Th., 1972. Hydrological study of the Rusty Glacier. In - Icefield Ranges Research Project, Scientific Results Vol.3, V.C. Bushnell and R.H. Ragle (Editors). American Geographical Society, New York and Arctic Institute of North America, Montréal, Quebec, 83-92

FAHNESTOCK, R.K., 1969. Morphology of the Sims River. In - Icefield Ranges Research Project, Scientific Results Vol.1, V.C. Bushnell and R.H. Ragle (Editors). American Geographical Society, New York and Arctic Institute of North America, Montréal, Quebec, 161-172

FOUNTAIN, A.G. and W. TANGBORN, 1985. The effects of glaciers on streamflow variations. Water Resources Research, 21(4), 579-586

GLEN, J.W. (Editor), 1982. Hydrological aspects of alpine and high mountain areas. Proceedings of the Exeter Symposium, 19-30 July 1982, IAHS Publication No.138, International Association of Hydrological Sciences, 350 pp.

GURNELL, A.M. and M.J. CLARK (Editors), 1987. Glacio-fluvial sediment transfer: an alpine perspective. Wiley-Interscience Publication, John Wiley & Sons, Chichester, England, 524 pp.

HOOKE, R.LeB., 1989. Englacial and subglacial hydrology: a qualitative review. Arctic and Alpine Research, 21(3), 221-233

JOHNSON, P.G., 1991. Pulses in glacier discharge: indicators of the internal drainage system of glaciers. Northern Hydrology: Selected Perspectives, T.D. Prowse and C.S.L. Ommanney (Editors), Proceedings of the Northern Hydrology Symposium, NHRI Symposium No.6, National Hydrology Research Institute, Environment Canada, Saskatoon, Saskatchewan, 165-176

KJELDSEN, O. (Editor), 1987. Glasiologiske undersokelser i Norge 1984. V-Publikasjon Nr.7, Vassdragsdirektoratet, Norges Vassdrags- og Energiverk, Oslo, 70 pp.

LIVERMAN, D.G.E., 1987. Sedimentation in ice-dammed Hazard Lake, Yukon. Canadian Journal of Earth Sciences, 24(9), 1797-1806

NICKLING, W.G., 1974. Hydrological investigation of the Slims River, Yukon Territory. Unpublished Ph.D. Seminar Paper, Department of Geography, Ottawa University, Ottawa, Ontario, 26 pp.

WAHL, H.E., D.B. FRASER, R.C. HARVEY and J.B. MAXWELL, 1987. Climate of Yukon. Climatological Studies No.40, Atmospheric Environment Service, Environment Canada, Downsview, Ontario, 323 pp.

YOUNG, G.J. (Editor), 1985. Techniques for prediction of runoff from glacierized areas. IAHS Publication No.149, International Association of Hydrological Sciences, 149 pp.

YOUNG, G.J., 1990. Glacier hydrology. In - Northern Hydrology: Canadian Perspectives, T.D. Prowse and C.S.L. Ommanney (Editors), NHRI Science Report No.1, National Hydrology Research Institute, Environment Canada, Saskatoon, Saskatchewan, 135-162

PULSES IN GLACIER DISCHARGE: INDICATORS OF THE INTERNAL DRAINAGE SYSTEM OF GLACIERS

P.G. Johnson

Department of Geography
University of Ottawa
Ottawa, Ontario
K1N 6N5 CANADA

ABSTRACT

Pulses in discharge measured at the termini of a number of glaciers in the southwest Yukon are similar to "extraordinary" events reported by Hooke (1989) and Röthlisberger and Lang (1987). The pulses are frequent occurrences and can be classified into four hydrograph patterns which can be interpreted as indicators of changes in the internal drainage system of the glaciers. The pulses are concentrated in the spring and early summer when linked conduit and channel drainage networks respond to the increased pressure from the springmelt.

INTRODUCTION

Flash floods are regular occurrences in glacierized basins. Although many of these floods are caused by glacier-dammed lake drainage others are caused by glaciological and climatological conditions. Röthlisberger and Lang (1987), in their overview of the hydro-climatic conditions of glaciers, refer to floods and the problems associated with their prediction. The Norwegian Hydro-Electricity Board, in reports on their glaciology program, note the frequent occurrence of flash floods at glacier termini (e.g., Kjeldsen, 1980). At Nigardsvatn, in the twelve-year period 1968 to 1979, 62 flash floods were recorded, a frequency of 5.16 per year. At Engabrevatn 56 flash floods were recorded in the twelve-year period 1969 to 1980, a frequency of 4.66 per year. Röthlisberger and Lang (1987, p.228) use the Aletschgletscher discharge record as an example of steadily increasing discharge through the melt season; in this record there are a number of flash floods caused by ice damming of the streams. The author has reported flash floods at Peyto Glacier, Alberta (Johnson and Power, 1985) which were caused by a combination of a storm event on a conduit system already at capacity and landslides induced by storm precipitation. The characteristics of these flash floods are different from those produced by ice-dammed lake drainage, but it is apparent that they are frequent occurrences in glacierized basins throughout the world.

Hooke *et al.* (1984) describe three "exceptional water discharge events" at Bondhusbreen, Norway, in 1979, but state that no similar events had been detected since then. It is not clear how these events compare with the flash floods reported elsewhere but the hydrographs are similar to events appearing on the Aletschgletscher record presented by Röthlisberger and Lang (1987, p.228, Figure 10.9). In much of the analysis of discharge records any pulses in the discharge may be masked by the integration on a daily basis of the records. During the course of research programs in the St. Elias Mountains of the southwest Yukon between 1970 and 1988, the discharge regimes of glaciers in the Duke River basin and the Kaskawulsh Glacier basin (Figure 1) have been monitored. The discharge regimes at all of the field locations have exhibited pulses in flow similar to those reported by Hooke *et al.* (1984). These can be attributed to glaciological and climatological causes. A number of the pulses have been of sufficient magnitude to be classified as flash floods.

The purposes of this paper are to discuss the characteristics of drainage pulses from Grizzly Creek Glacier and three unnamed glaciers in the Kaskawulsh Glacier drainage basin (Figure 1), to analyse the probable causes of these events, and to describe the magnitudes and frequencies of the events at different glaciers.

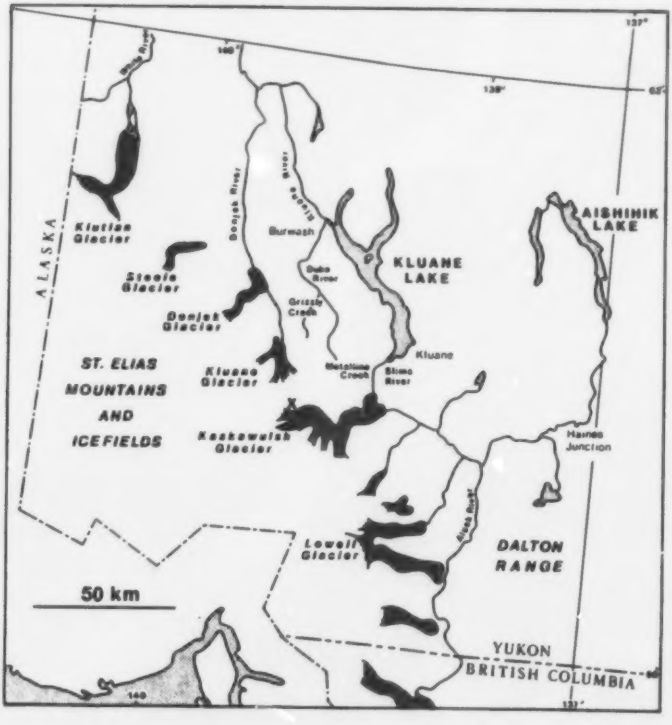
137°
140°
138°
62°
White River
Donjek River
Kluane River
Burwash
KLUANE LAKE
AISHIHIK LAKE
ALASKA
Klutlan Glacier
Steele Glacier
Duke River
Grizzly Creek
Donjek Glacier
Kluane
ST. ELIAS MOUNTAINS AND ICEFIELDS
Kluane Glacier
Metaline Creek
Slims River
Kaskawulsh Glacier
Haines Junction
Alsek River
Lowell Glacier
DALTON RANGE
50 km
YUKON
BRITISH COLUMBIA
140
60°
137°

Figure 1. Location map.

DATA COLLECTION

Stage records were obtained using Ott type X mechanical stage recorders and time-lapse photography. Ott current meters were used for all discharge measurements. Resurveys of the stream channels were made concurrently with the discharge measurements because of the mobile bed conditions in gravels and sands at each site. Sites with mobile bed conditions were necessitated by the absence of bedrock channels and the impracticability of establishing weirs due to environmental controls of the Canadian Parks Service, logistical costs and the high probability of stream migration bypassing sites. Discharge measurements were made at regular intervals throughout the field seasons and an assumption of progressive change in bedform was applied to calculate daily discharges from stage records. It was found that this only introduced large errors with very high magnitude flash floods when rapid aggradation or degradation of channels occurred or channels migrated. Channel migration has forced a number of relocations of equipment, causing problems of continuity of record. High-magnitude floods have resulted in destruction of equipment on four occasions. Time-lapse photography has been used to replace stage recorders on highly variable streams but the loss of the overnight record makes it impossible to produce a statistical assessment of the flow variability.

All of the discharge pulses discussed in this paper were of less than 60 minutes duration, with the majority less than 30 minutes, and the peak discharges are frequently maintained for less than 5 minutes.

PULSE FORM

The pulses can be divided into four types from the form of the traces on the hydrographs (Figure 2). Type a) has a sharp drop in discharge, sometimes to zero flow, followed immediately by a pulse and a return to pre-pulse flow levels. Type b) has a sharp rise in discharge which is then maintained. Type c) is a pulse from baseflow conditions without any preceding drop in the discharge. Type d) is a drop in discharge with a slow recovery. The hydrograph form can provide information on the nature of the internal drainage system of the glaciers and the proglacial zone.

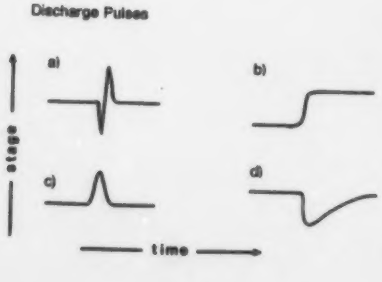

Figure 2. Pulse forms identified from the hydrograph records.

GLACIOLOGICAL CONDITIONS

Active Glacier Ice

During the ablation season englacial and subglacial channels migrate as a result of the structural changes caused by ice deformation and channel changes due to frictional melt of the ice and pressure conditions within the conduits (Röthlisberger, 1972; Shreve, 1972; Hooke *et al.*, 1988; Hooke, 1989). Temporary ponding and release of water during channel migration or closing and opening of linked conduits produces fluctuations in discharge at the glacier terminus. The magnitude of the discharge variation depends on the location of the drainage channel change within the glacier, the volume of the flow and the physical characteristics of the outburst location. The pulses in the Yukon locations have been the result of one, or a combination, of three conditions.

First, consider the diversion of marginal drainage streams into subglacial courses. In the early ablation season the drainage from the Grizzly Creek Glacier and its basin occurs along the ice margin. With the progression of the melt and the opening of subglacial conduits the marginal drainage is diverted into a subglacial course. This may be indicative of pressure changes in the spring causing changes in the linked conduit/channel drainage system as proposed by Hooke (1989). The subsequent build-up of hydrostatic pressure under the glacier results in an outburst flood at the glacier terminus. A type "a" pulse with an instantaneous fall in discharge is followed by a flood wave 30 to 45 minutes later. This flood has deposited up to approximately 1,000 m^3 of sand and gravel at the glacier terminus and caused incision of a new stream channel up to 1.5 m into the braided-stream deposits on the distal side of the Neoglacial maximum moraine 1 km downvalley. Estimates of the discharge from the hydrograph records indicate a fall to less than 1 $m^3 \cdot s^{-1}$ during stream migration with a pulse in excess of 10 $m^3 \cdot s^{-1}$ instantaneous discharge during outburst. The magnitude of the pulse could not be determined accurately because of the degradation of the channel which occurred during the flood.

Second, consider the occurrence of pulses of drainage from surging glaciers. Kamb (1987) has proposed that a linked-cavity configuration of the basal-water conduit system may be responsible for surges. Changes in this system can lead to irregular discharge of water. One of the glaciers in the Kaskawulsh Basin (location "X", see Figure 1) was surging in 1986 to 1987. The glacier surface was broken by a close network of crevasses and the terminus was vertical, unstable, and advancing into the proglacial sediments. There is also photographic evidence for a previous surge of the glacier (National Air Photo Library A-13132-200, 1951). The discharge regime tends to a diurnal pattern during the early melt season but becomes highly irregular from late-June through August. Pulses due to changes in the location of the discharge channel at the glacier terminus have been observed. For example, in 1987 a channel closure and new outlet formation was observed in a period of 15 minutes during routine servicing of the meteorological station at the glacier terminus. All of the discharge fluctuations produced rapid migration of the braided-stream system in the proglacial area. During surge, the structure of a glacier is heavily disrupted and channels frequently close, new channels open, and reservoirs of water are released accounting for the irregular discharge regimes.

Third, the progression of the ablation season in relation to the glacier dynamics and structures can produce irregular regimes. In 1987, a large surface lake formed on the Kaskawulsh Glacier at the confluence of its north and central arms. The lake formed as a result of very high ablation rates in June prior to the opening of the subglacial- and englacial-drainage conduits. On June 20 the lake was approximately 2 km by 1 km. By the end of the month it had drained completely through subsurface channels. There was no monitoring system in place which could indicate the effects of this lake drainage on the Kaskawulsh Glacier discharge.

Proglacial Stagnant Ice

Most Neoglacial deposits in the St. Elias Mountains are cored by stagnant glacier ice (Johnson, 1971, 1974, 1980). Glacier ice cores have been observed in moraines, outwash areas, and rock glaciers. In addition there are examples of the classical situation of extensive stagnant ice tongues. Glacier discharge streams have to flow through these stagnant glacier-ice environments to the lower ice-free zones of the basins. The stream courses are subject to channel migration, channel collapse, ponding, and outburst floods. The only proglacial environments where stagnant glacier ice does not occur are in some basins with small surging glaciers which have eroded the proglacial deposits during repeated advances. In this section, examples of the discharge regimes in Grizzly Creek and the Kaskawulsh basin are used to illustrate the hydrological effects.

The proximal outwash areas and the Neoglacial moraines in Grizzly Creek have an extensive, and probably continuous, ice core (Johnson, 1980). In 1974 and 1975 the discharge stream had a surface course through a meltwater-eroded gap in the Neoglacial maximum moraine. In 1976, ice in the stream channel diverted drainage into a small depression on the east side of the stream where a pond formed. This pond drained periodically through the ice core of the moraine and by some overflow into the old surface channel. The filling and draining cycles had a periodicity of 48 to 72 hours. During these cycles the pond enlarged by melt of the ice core and erosion of the glacial and fluvioglacial deposits to 75 m by 25 m with a maximum depth of 4 m. The resurgence of drainage from the pond occurred along a 20-m section of the terminus of a rock glacier, which had been partially eroded by the advance of the glacier to its maximum Neoglacial position. The regime of Grizzly Creek during this period was dominated by 48 to 72 hours of reduced flow during pond filling, a short pulse as the pond drained, and a period of normal flow levels until the channel under the moraine was blocked and the pond started to refill. Observation of the site in 1989 showed that the pond had been infilled and a braided stream now carries drainage to the old subaerial course through the Neoglacial moraine.

A sub-basin of the Kaskawulsh Glacier system was studied from 1986 to 1988. The deposits of the pro-glacier component of the basin are glacier-ice cored. This ice core is undergoing rapid melt due to exposure by hydrological processes. The discharge from one of the glaciers in the sub-basin enters a subsurface course at a large moulin at the terminus of the active glacier. During the ablation season the stream course migrates as frictional heat (Röthlisberger and Lang, 1987) enlarges the channels producing collapse and stream damming. In early-June 1986 the discharge portal was at an ice cave on the north side of the valley. By late-June this channel closed down and a new channel opened by an outburst flood on the south side of the valley. In mid-July 100 m of this channel collapsed forcing a new outburst close to the glacier terminus. At the end of July this course was abandoned and another outburst occurred 50-m downvalley in a section of old braided fluvioglacial deposits over the ice core.

DEBRIS FLOWS IN THE PROGLACIAL ZONE

Debris flows and landslides are common in proglacial zones particularly during spring-melt and when there is interaction of high precipitation with steep ice-cored moraines. Debris flows infill drainage channels and cause flash floods as the dam is overtopped and eroded (e.g., Johnson and Power, 1985). In the Kaskawulsh Glacier sub-basin the discharge from one of the glaciers flows through a rock gorge which has been infilled a number of times by rock and snow avalanches off the valley walls. Two substantial snow plugs were present through 1986 to 1988 but the stream had established a course through the snow after initial damming. The north-facing valley wall is composed of a thin veneer of glacial and talus deposits over a wedge of stagnant glacier ice and throughout the summer seasons there are debris flows off this slope into the stream channel. Many of the smaller flows only produce a high sediment-load pulse in the stream, but larger flows dam the stream and produce flash floods as the dam is overtopped.

PULSE MAGNITUDE AND FREQUENCY

Data from Grizzly Creek between 1974 and 1978 and from the Kaskawulsh Glacier sub-basin for 1986 and 1987 were analysed for pulse magnitude and frequency. The records consist of stage and discharge data and time-lapse photography records. Although the stage records have many breaks due to the migration of the channels and damage caused by flash floods, a number of segments of the records provide continuous data from which magnitudes and frequencies can be calculated. The time-lapse photography, which was used extensively in 1987, confirms the frequent occurrence of pulses in discharge, but the absence of the overnight record makes statistical analysis impossible.

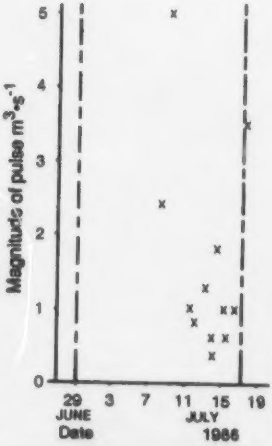

Figure 3. The magnitudes and dates of occurrence of pulses in surging-glacier discharge.

The discharge record from the small surging glacier in the Kaskawulsh sub-basin between June 29 and July 17, 1986 the only period of a long continuous record, exhibited 12 pulses of types "a" and "c" (Figure 3) and 10 of type "d". The average increase

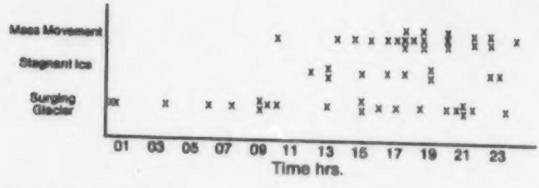

Figure 4. The timing of the pulses during the day from three sites.

of discharge in the 12 pulses was 1.6 $m^3 \cdot s^{-1}$ with a range from 0.4 $m^3 \cdot s^{-1}$ to 5 $m^3 \cdot s^{-1}$. The discharge started to rise on July 6 and the pulses commenced on July 8 (Figure 4). Higher-magnitude pulses occurring after July 17 made it impossible to re-establish a permanent gauge. Pulses are identifiable from the time-lapse photographic record from 1987 throughout the mid-June to mid-August period. They occur throughout the day (Figure 4) which suggests that they are independent of any diurnal regime. In the period from July 6 to July 17 the frequency of pulses was 1.8 per day. The discharge stream through extensive proglacial stagnant ice at the terminus of the downwasting glacier experienced 14 pulses between June 28 and August 4, 1986, a frequency of 0.37 per day. Nine of these events were measured (Figure 5) with an average discharge rise of 1.5 $m^3 \cdot s^{-1}$ and a range of 0.5 $m^3 \cdot s^{-1}$ to 5 $m^3 \cdot s^{-1}$. These were pulses without changes in the stream course. The larger events which were not measured involved major changes in the course of the stream. The largest event, tunnel collapse followed by an outburst flood, can be inferred, from the form of the channel, to have had a discharge considerably in excess of the measured pulses. All of the pulses through the stagnant-ice zone occurred between 12:00 hrs and 23:00 hrs (Figure 4) on the rising limb or at the peak of the hydrograph. Stream migration and channel blockage occurs during the higher-flow conditions and this can be seen in the increase of the magnitude of the pulses through July as the glacier discharge rises. At the glacier, where the stream channel was exposed to debris flows and landslides, 26 pulses were recorded between June 9 and August 14, 1987 (Figure 6), a frequency of 0.36 per day. The average increase in the discharge was 1.2 $m^3 \cdot s^{-1}$ with a range of 0.25 $m^3 \cdot s^{-1}$ to 4.5 $m^3 \cdot s^{-1}$. These pulses were also concentrated in the 12:00 to 24:00 time period (Figure 4) when melt of snow and ice on the valley wall was most active. No pattern of magnitude with respect

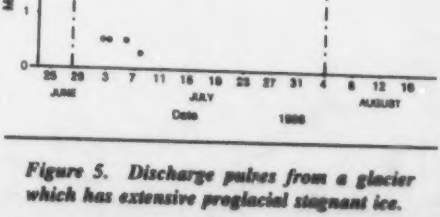

Figure 5. Discharge pulses from a glacier which has extensive proglacial stagnant ice.

to the time of season emerged, reflecting the variability of the magnitude of debris flows through the season.

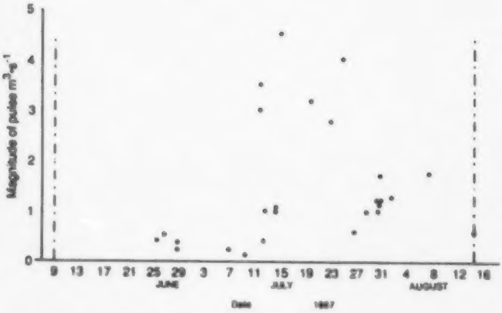

Figure 6. Discharge pulses from a glacier stream affected by debris flows during the melt season.

The outburst floods at the Grizzly Creek Glacier between 1974 and 1979 were annual events. The timing of the change in the drainage system being a function of the progression of the melt season and the amount of winter snow accumulation. The magnitude of the outburst floods was also variable with the maximum event being in excess of 10 $m^3 \cdot s^{-1}$ (estimated from stage record where channel degradation occurred during the flood). This maximum flood deposited 1,000 m^3 of gravel over a snow patch at the glacier terminus.

DISCUSSION

Hooke (1989) has discussed the possibility of the existence of both linked-cavity flow and channel flow in the subglacial environment. He proposes that:

> "accumulating evidence thus favors a model for subglacial drainage in which a tortuous linked-cavity system is transected by a few broad low conduits that drain more directly to the glacier terminus" (p.228).

He also states that for the winter season:

> "it is not known whether the tunnel system collapses entirely, but this is certainly a possibility ... if such remnant conduits do not exist, or if they do not enlarge rapidly enough, the water pressure will rise to the level where Kamb's stability limit for the linked-cavity system is exceeded. New channels may then form ..." (p.228).

Iken and Bindschadler (1986) had concluded that the subglacial system was composed of a combined cavity network and meandering conduits and that the interconnections were not perfect. The system they proposed would be strongly diurnal in character. Blockages and releases would be superimposed on this diurnal pattern.

This suggests that the discharge from the glacier is most subject to variations in the early melt season. Changes in the drainage network are most likely to occur at this time. The changes in pressure and the changes in channels should produce fluctuations in the discharge at the glacier terminus. The fluctuations measured at glaciers in Yukon are indicative of the evolution of the drainage network. The characteristics of the drainage change will dictate the form of the hydrograph response. The four patterns may be used to interpret the evolution of a glacier drainage system. A schematic model of the system is presented in Figure 7. The representation of the conduits is not intended to suggest that they have a straight course. Iken and Bindshadler (1986) proposed a meandering course for the conduits.

Short time-frame pulses in the discharge from glaciers and glacierized basins in the southwest Yukon are frequent. They occur in a number of glaciological and geomorphological situations which affect the frequencies and timing of the pulses. In all situations, although the probability of occurrence may be assessed, prediction of an event is difficult. With fast glacier flow the drainage conduits through the glacier may be interrupted frequently and reservoirs of water may drain irregularly as water pressure and the internal structure of the glacier changes. Pulses in discharge may be caused by the re-orientation of the drainage system or by the release of stored water. The change which occurs and its location in the glacier will dictate the nature of the hydrograph. The release of a pocket of stored water would produce a type "c" pulse. The opening of a previously-

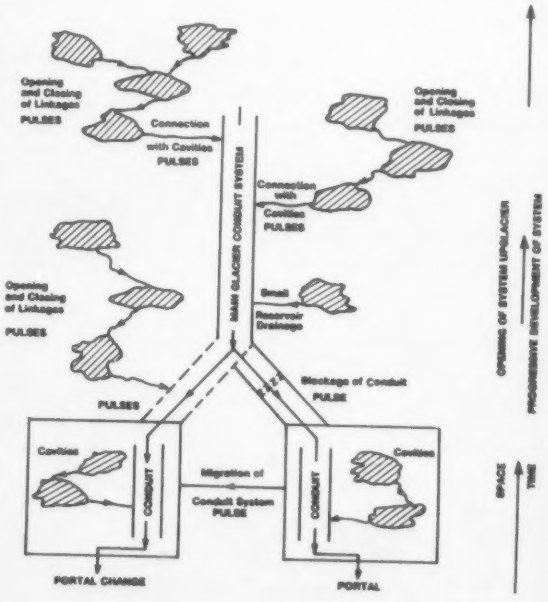
Opening
and Closing
of Linkages
PULSES
Connection
with Cavities
PULSES
MAIN GLACIER CONDUIT SYSTEM
Opening
and Closing
of Linkages
PULSES
Connection
with
Cavities
PULSES
Opening
and Closing
of Linkages
PULSES
Small
Reservoir
Drainage
Blockage of Conduit
PULSE
PULSES
Cavities
CONDUIT
Migration of
Conduit System
PULSE
CONDUIT
Cavities
PORTAL CHANGE
PORTAL
OPENING OF SYSTEM UPGLACIER
PROGRESSIVE DEVELOPMENT OF SYSTEM
SPACE
TIME

Figure 7. Model for the englacial/subglecial drainage system and the causes of the drainage pulses.

closed section of the glacier system would produce a type "b" pulse. The closing of the drainage system and a catastrophic re-opening would produce a type "a" pulse. The timing of the release of water is controlled by volume of discharge, in relation to the conduit dimensions (Hooke, 1989), and by the glaciological conditions and therefore pulses may occur at any time of the day.

With flow through stagnant ice at the glacier terminus, the channels are subject to blockage or total collapse particularly as thermal erosion increases during rising discharge periods. These changes can result in a complete re-orientation of the channel system, usually a type "a" pulse, or fluctuations within the existing channel system, where the pulse takes a number of different forms. In all situations measured, these pulses occur on the rising limb or at the peak of the hydrograph.

The exposure of the terminus area of the glacier to mass movements produces irregular blockage and flash floods. The various causes of mass movements; high storm-water input, high energy input to ice cores, snow avalanches, rockfalls; indicate that these pulses can occur at any time of the year. At the Yukon field sites these events have occurred during periods of high insolation and no storm-water input events have been experienced. Storm input was the cause of floods observed at Peyto Glacier, Alberta, in 1983 and these occurred between 01:00 and 08:00. In general, therefore, mass-movement induced pulses can occur at any time of the season and at any point on the hydrograph.

The pulses discussed in this paper are short-duration and usually low-magnitude events, particularly in comparison with the drainage of glacier ice-dammed lakes. They are, however, common occurrences and can achieve magnitudes which produce significant geomorphological changes such as a total change in the drainage system of the proglacial area.

In conclusion, type "a" pulses are caused by closure or re-orientation of the conduit system followed by outburst, type "b" are caused by the onset of drainage of a reservoir within the glacier, type "c" are caused by the release of a small reservoir with a rapid return to the pre-release levels and type "d" may be caused by the gradual reopening of channels or conduits after closure.

ACKNOWLEDGEMENTS

The author acknowledges the financial support of the Natural Sciences and Engineering Research Council and the logistical support of the Arctic Institute of North America at the Kluane Lake Research Station. Many graduate and undergraduate students were involved with different aspects of this work and their contributions are gratefully acknowledged, in particular Ms. J. Kasper for logistics organization from 1986 to 1988 as well as scientific contributions.

REFERENCES

HOOKE, R.LeB., 1989. Englacial and subglacial hydrology: a qualitative review. Arctic and Alpine Research, 21(3), 221-233

HOOKE, R.LeB., B. WOLD and J.O. HAGEN, 1984. Subglacial hydrology and sediment transport at Bondhusbreen, southwest Norway. Geological Society of America Bulletin, 96(3), 388-397

HOOKE, R.LeB., S.B. MILLER and J. KOHLER, 1988. Character of the englacial and subglacial drainage system in the upper part of the ablation area of Storglaciären, Sweden. Journal of Glaciology, 34(117), 228-231

IKEN, A. and R.A. BINDSCHADLER, 1986. Combined measurements of subglacial water pressure and surface velocity at Findelengletscher, Switzerland: conclusions about drainage system and sliding mechanism. Journal of Glaciology, 32(110), 101-119

JOHNSON, P.G., 1971. Ice-cored moraine formation and degradation, Donjek Glacier, Yukon Territory, Canada. Geografiska Annaler, 53A(3-4), 198-202

JOHNSON, P.G., 1974. Mass movement of ablation complexes and their relationship to rock glaciers. Geografiska Annaler, 56A(1-2), 93-101

JOHNSON, P.G., 1980. Grizzly Creek Glacier ice-cored moraine system. Quaestiones Geographicae, Vol.6, 69-78

JOHNSON, P.G. and J.M. POWER, 1985. Flood and landslide events, Peyto Glacier terminus, Alberta, Canada, 11-14 July 1983. Journal of Glaciology, 31(108), 86-91

KAMB, B., 1987. Glacier surge mechanism based on linked-cavity configuration of the basal water conduit system. Journal of Geophysical Research, 92(B9), 9083-9100

KJELDSEN, O. (Editor), 1980. Materialtransportundersøkelser i Norske bre-elver, 1979 (Sediment transport studies at Norwegian glaciers, 1979). Rapport Nr.1-80, Hydrologisk Avdeling, Vassdragsdirektoratet, Norges Vassdrags- og Elektrisitetsvesen, Oslo, December, (in Norwegian with English summary) 43 pp.

RÖTHLISBERGER, H., 1972. Water pressure in intra- and subglacial channels. Journal of Glaciology, 11(62), 177-203

RÖTHLISBERGER, H. and H. LANG, 1987. Glacial hydrology. In - Glacio-Fluvial Sediment Transfer: an Alpine Perspective, A.M. Gurnell and M.J. Clark (Editors), Wiley-Interscience Publication, John Wiley & Sons, Chichester, U.K., 207-284

SHREVE, R.L., 1972. Movement of water in glaciers. Journal of Glaciology, 11(62), 205-214

DRAINAGE OF AN ICE-DAMMED LAKE, KASKAWULSH GLACIER BASIN, YUKON

J.N. Kasper[1] and P.G. Johnson[2]

[1]Département de géographie
Université Laval
Cité universitaire
Sainte-Foy, Québec
G1K 7P4 CANADA

[2]Department of Geography
University of Ottawa
Ottawa, Ontario
K1N 6N5 CANADA

ABSTRACT

Glacier ice-dammed lakes have been reported from all glacierized regions. The hazards posed by the catastrophic drainage of these lakes, particularly those located close to the glacier terminus, have been extensively studied. Many lakes in upper basin areas are not considered hazards but can be significant hydrologically and geomorphologically. A lake along the margin of the Kaskawulsh Glacier, 35 km from the terminus, drains annually. Ice margin flotation and conduit expansion due to frictional heat are prerequisites for lake drainage. Inititation of the drainage, however, requires connection to the main conduit system of the Kaskawulsh Glacier. Water balance figures indicate a substantial and continuous leakage from the lake. Discharge through a 35-km long conduit to the glacier terminus extends the period of drainage to 7 to 10 days compared to the 1 to 2 days for most terminus location lakes.

INTRODUCTION

Glacier ice-dammed lakes are important components of the hydrological systems of most of the world's glacierized regions. Records from exploration and scientific research in the Karakoram, Himalayan, Andean, Alpine and North American Cordilleran mountain chains (e.g., Collins, 1986; Fushimi *et al.*, 1982; Hewitt, 1982; Lliboutry *et al.*, 1977; Post and Mayo, 1971) as well as from Scandinavia (e.g., Theakstone, 1978) and Iceland (e.g., Thorarinson, 1957) testify to lake occurrence and the occasional catastrophic nature of their drainage. Rapid drainage of lakes produces major changes in the hydrological and geomorphological systems and has the potential for damaging or destroying components of economic systems in the basins. Some ice-dammed lakes are semi-permanent, some fill and drain with irregular periodicities as a result of changes in glacier dynamics, and others drain annually with some regularity in the timing of drainage during the year.

Table 1. Summary of Lakes, by volume, St. Elias Mountains.

Lake Volume 10^6 m^3	>100	10-100	1-10	<1
White River	2	2	9	25
Donjek River	1	1	(2 + est. 85)	
Kaskawulsh Basin	0	2	31	

In the Canadian Cordillera contemporary research on ice-dammed lakes and their drainage characteristics can be traced back to the study of Clague and Mathews (1973) who developed an empirical formula for discharge during catastrophic drainage. Subsequent work has included contributions to the understanding of drainage mechanism; ice barrier flotation and thermal enlargement of subglacial channels; and the development of sophisticated physically-based discharge models (Clarke and Mathews, 1981; Clarke, 1982, 1986).

The St. Elias Mountains of the southwest Yukon have a large number of ice-dammed lakes and lake sites according to Fisheries and Environment Canada, Canada (1977). This report summarized data for the White River and Donjek River basins and the Kaskawulsh Glacier basin. Table 1 is an abstract of these data. Clarke and a number of research associates have studied the larger St. Elias sites; Hazard Lake at the Steele Glacier (Clarke, 1980, 1982; Liverman, 1987), Donjek Lake at the terminus of the Donjek Glacier (Clarke, 1980; Clarke and Mathews, 1981) and Alsek Lake at the Lowell Glacier terminus (Schmok and Clarke, 1989).

OBJECTIVE

The majority of studies in Canada and the rest of the world are of ice-dammed lakes close to glacier termini. This paper discusses the characteristics of a lake 35 km up-valley from a glacier terminus. The lake is dammed by an active and thick section of the glacier (Kasper, 1989). This location changes the characteristics of the drainage and its impact on the hydrological regime at the glacier terminus. It is important to contrast this type of lake with near-terminus lakes if the potential effects of climatic change are to be understood.

KASKAWULSH GLACIER LAKE

The lake basin is along the north margin of the Kaskawulsh Glacier at 60°46'N, 139°07'W (Figure 1), and is 35 km from the glacier terminus. The basin is 48 km^2, of which 34% (16.3 km^2) is glacierized, and has an elevation range from 1600 to 3100 m a.s.l. The lake is dammed by the Kaskawulsh Glacier and fills to a maximum depth of 110 m at its east end, with a volume of 15.5 x 10^6 m^3 at current lake-full condition. It is fed by three small glaciers in the basin, snowmelt and summer precipitation from the non-glacierized part of the basin, and meltwater from the Kaskawulsh Glacier. One of the glaciers was surging in 1986 and 1987 (SG; Figure 1) and two were not very active (NSG and 3rd; Figure 1). The inputs, output

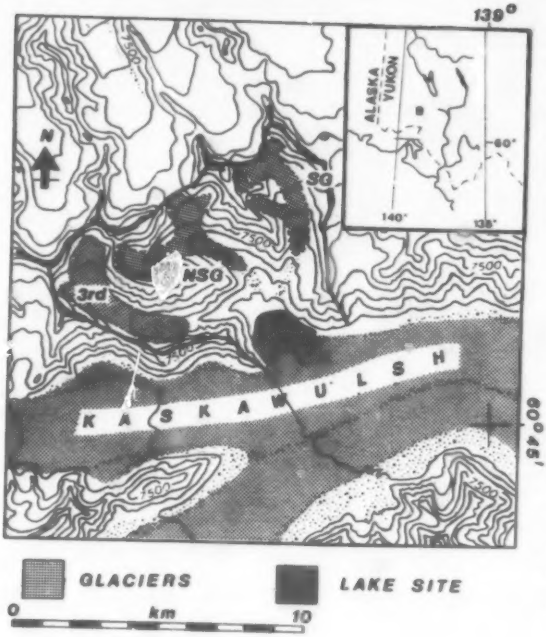

Figure 1. Location map of the ice-dammed lake site. The three contributing glaciers to the basin are labelled SG, NSG and 3rd. The lines at location X are the radio-echo sounding profiles conducted to determine the form of the ice barrier.

and storage were measured or estimated to determine the water balance of the lake. Most of the data presented in this paper are from the 1987 season.

Precipitation and temperature regimes for the summer of 1987 are presented in Figure 2. The only extended period of precipitation was from August 14 to 18. This was snowfall through most of the basin and was after the lake drained. It was not a component of the water balance of the lake. The precipitation in the rest of the season was very low, and its contribution to the water balance was negligible. The input from melt on the glacierized and non-glacierized components of the basin was measured on the three streams originating from the glaciers, at points close to the lake. Discharge was calculated from float-recorder and time-lapse photographic records of stage and manual velocity measurements at 3 to 4 day intervals. The stream courses were unconsolidated gravels and, to account for aggradation and degradation of the channel, profiles were surveyed at each velocity measurement and changes applied to the stage records. The discharge regimes (Figure 3) had provided a total input into the lake basin at drainage initiation of 35.1 x 10^6 m^3. The relative contributions of glacierized and non-glacierized components of the basin were calculated from measurements of glacier melt derived from a standard glacier ablation-stake network on the NSG glacier (Figure 1), and indicated that the two contributions were approximately the same. Input from the Kaskawulsh Glacier was observed at a number of supraglacial, englacial, subglacial and marginal streams. This diversity of input was impossible to monitor and it was

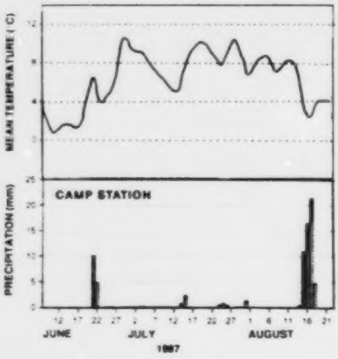

Figure 2. Precipitation and temperature records for the basin in 1987. The location of this meteorological station was in the centre of the basin close to the lake shore.

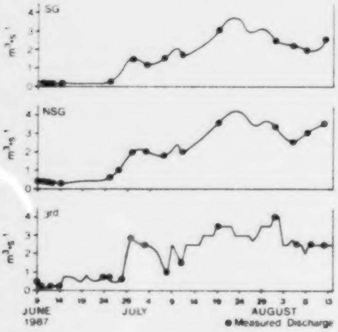

Figure 3. The discharge regimes of the three main streams feeding the lake.

originally proposed to calculate this component from the water-balance equation:

$$[1] \qquad V_L \quad I_b \quad E \quad I_k$$

V_L is the lake volume.
I_b is the basin input.
E is the evaporation loss from the lake.
I_k is the Kaskawulsh Glacier input.

The basin input was, however, over 200% of the lake storage. This precluded any measure of the Kaskawulsh Glacier contribution. During the 1987 field season, ablation of the Kaskawulsh Glacier was greater than 2 m of ice in the vicinity of the lake. Most of the water generated rapidly entered englacial courses through moulins or crevasses. It is postulated that most of this was oriented away from the lake site because low flow volumes were observed in accessible streams and strong inflow currents or large sediment plumes were not observed along the damming ice front. Calculations were made, therefore, without including a Kaskawulsh Glacier input. The discrepancy between measured basin input and storage is, therefore, the minimum loss from the basin. Estimates of evaporation from the lake, from the climatic records, would not provide any further insights into the Kaskawulsh Glacier input or lake dynamics. Thus for an indication of the lake dynamics:

$$[2] \qquad I_b \quad V_L \quad Q$$

Q is the minimum flow loss from the basin (Figure 4).

It is hypothesized that this loss was subglacial. The bedrock of the areas is composed of metamorphosed sedimentary rocks and it is considered that ground-water flow could not account for the large volume of water lost from the basin. There was no observed surface loss along the glacier margins and current profiles along the ice-face detected no flow towards the ice except at the deepest part of the lake. Subglacial loss is also supported by the low sediment accumulations in the lake basin, investigated after drainage, despite the very high inputs as underflows from each of the basin streams. This would imply that it is the heavy sediment-laden bottom water which is the component lost from the lake.

The filling rate of the lake and the total storage was measured from a record of the lake level along a measured profile and a topographical survey of the lake basin after drainage. The error estimate on the lake volume calculations is ±5%. The error estimate on the stream input, based on three discharge measurements per day every 3 to 4 days, was ±5% for the 3rd stream (float stage recorder) and ±10% for the NSG and SG streams (monitored by time-lapse photography).

During June 1987 the basin input was approximately the same as the lake storage (Figure 4). In late-June and early-July the input increased substantially, peaking at 7 x 10^5 $m^3 \cdot d^{-1}$ and although the filling rate initially increased, it peaked at 3 x 10^5 $m^3 \cdot d^{-1}$ and then started to drop. This initial rise in input was the result of the warmer weather in late-June (Figure 2). A cool period in early-July resulted in a fall in both input and filling rates, but the input rate was still in excess of the filling rate by a factor of 4. The warm weather in the second week in July produced a rapid rise in input rate but the filling rate responded slowly. Peaks occurred in the input rate at 9 x 10^5 $m^3 \cdot d^{-1}$ and 10 x 10^5 $m^3 \cdot d^{-1}$ while the peaks in the filling rate were only 3 x 10^5 $m^3 \cdot d^{-1}$.

The possible controls on the leakage are the bottom topography at the ice dam and the response of the ice margin to the increase in water volume. The ice dam is formed by the Kaskawulsh Glacier where it extends into a deglaciated tributary. Radio-echo sounding profiles were conducted by F. Jones in August 1987. The profile locations on the Kaskawulsh Glacier ("X" see Figure 1) were designed to indicate the form of the glacier bed at the margin. They indicate a minimum of 100 m of ice thickening to over 300 m within 500 m of the valley side (Figure 5).

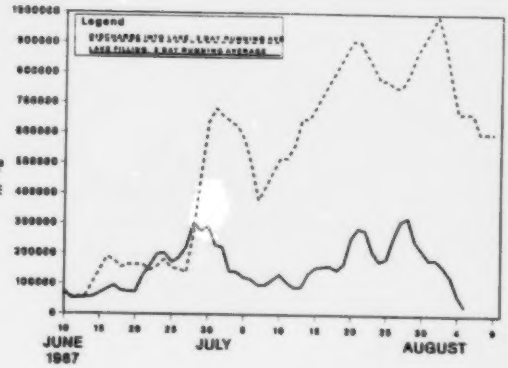

Figure 4. Basin-input rate and lake-storage rate for the summer of 1987.

The total thickness of the Kaskawulsh Glacier in mid-stream has been measured by seismic methods (Dewart, 1968). This showed in excess of 800 m of ice in the North Arm stream of the Kaskawulsh Glacier and in excess of 1000 m in the Central Arm. The ice at the dam is therefore very thin compared to the main stream of the glacier.

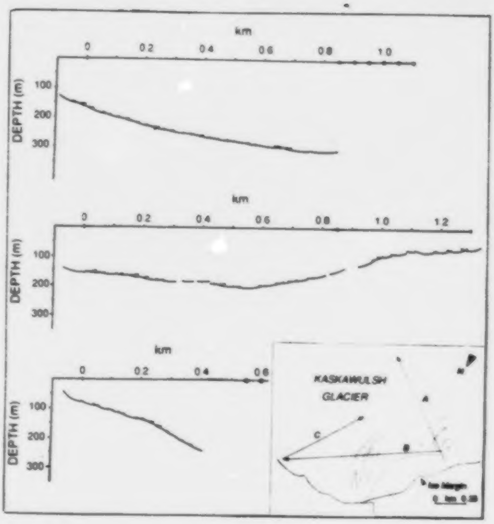

Figure 5. Radio-echo sounding profiles of the Kaskawulsh Glacier margin.

Vertical movement of the ice margin was measured at a series of 10 stakes drilled 2 to 3 m into the ice in a line from the margin towards the centre of the Kaskawulsh Glacier. The positions of Stakes 2, 8 and 10, referred to in this paper, are indicated in Figure 6. The stakes were redrilled when necessary throughout the season. It is projected that any errors due to melt of the stakes into the ice were negligible and as melt-in would be in opposition to vertical movement caused by floating of the ice margin it would not affect interpretation of trends. The stakes were surveyed by triangulation from bench marks which had to be established on unconsolidated moraine. There was no evidence of movement during the study but a wolverine disturbed one site in mid-season. Stakes 1 to 8 were established on the main part of the glacier. Stakes 9 and 10 were located on an area

Figure 6. Photograph of the ice margin, after lake drainage in 1986, showing the arcuate crevasse system at the deepest part of the lake. The locations of the stakes presented in Figure 7 are shown by the stake numbers.

defined by a massive arcuate crevasse system (Figure 6). The movement of Stakes 2, 8 and 10 (Figures 6 and 7) illustrates the ice movement during the filling of the lake. The zone demarcated by the crevasse system, Stake 10, effectively floated freely with the filling of the lake from the start of measurements on June 11. As the lake level rose, the winter lake-ice cover along the glacier margin fractured. The glacier rose faster than the lake level because the remnants of lake ice attached to the glacier rose higher and higher above water level. The rise was greatest near Stake 10 (Figure 6) which was the deepest part of the lake. The elevation difference between Stakes 8 and 10, apparent in Figure 6, reduced rapidly throughout the filling of the lake. Stake 8, located on the main part of the glacier immediately adjacent to the crevasses had an initial rise, perhaps due to being frozen to the crevassed section. It then settled, and it was not until the middle of July that it started to respond to the lake filling. Stake 2, located towards the centre of the Kaskawulsh Glacier, had much less movement and may lie near the hinge line of the floating ice. Although the trends of movement of Stakes 2 and 8 are similar they do not follow exactly the same pattern, particularly in late-July, and this suggests that they are not measurement error. The movement of Stake 2 could be explained by the dynamics of the Kaskawulsh Glacier whereas we postulate that the magnitude and the rate of rise of Stakes 8 and 10 can only be explained by floating of the ice margin by the lake.

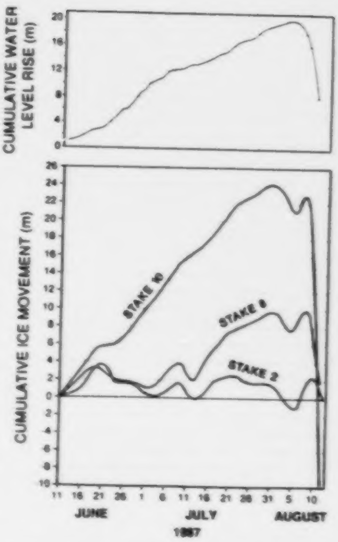

Figure 7. The vertical movement of Stakes 2, 8 and 10 and the water-level rise of the lake.

Comparison of the lake filling rate (Figure 4) with ice-margin flotation indicates that the mid-July movement of Stake 8 was a response to the increased filling rate. This also corresponds to the increased leakage rate (Figure 8). The leakage rate can be explained by the combined flotation of the crevassed zone and main ice margin, together with the development of subglacial conduits. A bedrock channel closed by ice would account for an early start of leakage. Increases later in the season may be due to frictional-heat melt of the overlying ice. It is apparent that the increase of leakage rate, the floating of the ice margin, or the two in combination, are not sufficient to initiate drainage of the lake. Lake-full condition was achieved at the beginning of August in 1986, 1987 and 1988 but drainage was only initiated in mid-September, early-August and late-August, respectively. In the period between lake-full and drainage initiation, the leakage rate must increase to the input rate.

Storage in the lake at the initiation of drainage is approximately 15.5 x 10^6 m^3. In 1987 from initiation to lake-empty, a further 2.4 x 10^6 m^3 was contributed to the lake by the three streams for a total of 17.9 x 10^6 m^3. Any Kaskawulsh Glacier input would increase this total. The 1987 drainage curve (Figure 9) has the usual exponential form. The eight days between the first observation of the lake-level fall and lake-empty contrasts with the two to four days observed for terminus lakes and proposed by Clarke (1980) for the drainage of the Donjek Lake. In 1986, a short period of lake-level fall was observed in early August but this stopped after two days and the level rose again. This may have been indicative of conditions for drainage almost being achieved.

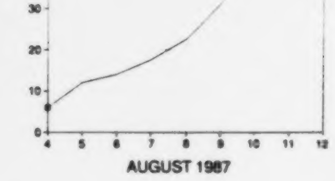

Figure 9. The 1987 drainage curve of the Kaskawulsh lake.

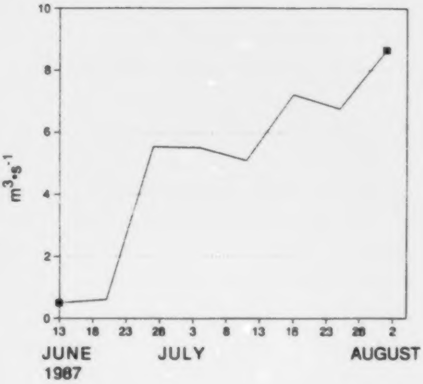

Figure 8. The pattern of leakage from the lake in the summer of 1987.

DRAINAGE MECHANISMS

The control on drainage initiation after the lake-volume and ice-flotation conditions are met can only be hypothesized. The development of a glacier system as a combined conduit/linked-cavity model (Johnson, 1990) may provide the controls. The drainage system of the glacier will develop upvalley as the ablation season progresses.

Cavities may be linked and connected to the conduit system as this development takes place. The conduit system may migrate during one ablation season or change from one season to the next. The location of the Kaskawulsh lake 35 km from the glacier terminus means that drainage of the lake requires connection to the conduit system, in comparison with a terminus lake where the hydraulics of the lake itself can control the drainage.

The critical control on drainage initiation is connection to, or development of, a main conduit system. Water may be lost into the englacial or subglacial drainage network but cannot generate channels for complete drainage. Variations in the rate of development and the location of the conduit system from year-to-year, which affect the lake conduit connection, would explain the variation in drainage dates.

During drainage the floating ice margin collapsed. Stake 10 (Figure 7) dropped more than 34 m and the area disintegrated into large icebergs. This collapse was to below the level of the ice at the start of the measurements. Stakes 2 and 8 settled to their level at the start of the season.

DISCUSSION

The drainage of ice-dammed lakes located a long distance from the glacier terminus is more difficult to predict than the drainage of terminus lakes. The mechanisms of drainage are the same, ice-margin flotation and thermal erosion of channels, but onset of drainage requires the development of a connection to existing englacial or subglacial conduit systems. The lake-full stage, sufficient for drainage initiation, is only the first prerequisite for the system.

The drainage hydrograph is stretched temporally for upper basin lakes. The 24-to 48-hour drainage times predicted for terminus lakes increases three- to four-fold to 7 to 10 days. This lake on the Kaskawulsh Glacier system drained in seven days from the initial detection of water-level drop, but increasing levels of subglacial flow were occurring earlier to accommodate the large input from the basin. The form of the hydrograph is identical to others with the exponential rising limb and sudden cessation of flow. The temporal stretching of the hydrograph is due to the length of subglacial conduit flow to the glacier terminus.

There is a problem with this lake of constant leakage from the basin, apparently subglacially, throughout the filling sequence. The water-balance equation indicates that large volumes of water are involved, so why does this not initiate drainage by frictional-heat melt of channels? It is necessary for the ice margin to disconnect from the bedrock to initiate drainage and the lake must attain a volume, dictated by the nature of the ice dam, to float the ice. Continuous drainage from the lake occurs but as long as input exceeds this continuous output, the lake will continue to fill. The pattern of leakage increase through the season indicates that the channel or channels are enlarging. It is possible that this drainage is along a bedrock channel across the threshold of this basin, which may have a limited flow capacity even with thermal erosion along the roof of the channel. The subglacial leakage would appear to have a very high sediment load. There is low sediment accumulation in the basin in relation to the very high input as underflows from the streams. The high suspended-sediment concentrations may affect the thermal capacity of the stream.

Lacustrine sediments and deltaic deposits at levels above the current lake-full level indicate a larger lake has existed in the past. Thick laminated sediment sections indicate high sedimentation rates compared to the current lake basin and indicate a semi-permanent lake without the subglacial leakage experienced at present. The lake has formed at progressively lower levels in the basin as the damming Kaskawulsh Glacier has downwasted and the ice dam has occurred progressively closer to the mouth of the basin. There has been a progression from a semi-permanent lake to an annually-draining lake, and it can be postulated that with continued downwasting of the retaining glacier and changes in the ice-dam position the lake may cease to fill at all.

The impact of small-lake drainage from the upper basin on the hydrological regime at the glacier terminus is small. The discharge of 15×10^6 m^3 over 7 to 10 days is a relatively small contribution to the Slims River, which in August usually peaks at approximately 300 m^3·s^{-1} in a glacier-melt dominated season. The timing of the lake drainage and the characteristics of each seasonal hydrograph on the Slims River will alter the potential impact, and would have to be assessed on a year-by-year basis.

Although considerable progress has been made on the understanding and modelling of ice-dammed lakes, the emphasis has been placed on near-terminus lakes. The drainage of lakes from the upper regions of glacierized basins presents a more difficult predictive situation because the onset of drainage requires establishing a connection to the existing englacial or subglacial conduit system of the damming glacier.

ACKNOWLEDGEMENTS

The authors wish to acknowledge the financial assistance of the Northern Science Training Grants Program through the Northern and Native Studies Group of the University of Ottawa and the Natural Sciences and Engineering Research Council Operating Grants Program. Logistics support, without which the project would have been impossible, was provided by the Kluane Lake Research Station of the Arctic Institute of North America. A number of students were also instrumental in the field program and eased the task of data collection.

REFERENCES

CANADA, FISHERIES AND ENVIRONMENT CANADA, 1977. Report on the influence of glaciers on the hydrology of streams affecting the proposed Alcan pipeline route. Report prepared by the Glaciology Division and submitted to the Inland Waters Directorate, Pacific Region, Fisheries and Environment Canada, Vancouver, British Columbia, June, Part 1 - 38 pp. + appendices + map; bibliography - 54 pp.

CLAGUE, J.J. and W.H. MATHEWS, 1973. The magnitude of jökulhlaups. Journal of Glaciology, 12(66), 501-504

CLARKE, G.K.C., 1980. An estimate of the magnitude of outburst floods from Lake Donjek, Yukon Territory, Canada. A report prepared for the Department of Indian and Northern Affairs through a contract from the Department of Supply and Services by the Department of Geophysics and Astronomy, University of British Columbia, Vancouver, British Columbia, 20 March, 90 pp.

CLARKE, G.K.C., 1982. Glacier outburst floods from "Hazard Lake", Yukon Territory, and the problem of flood magnitude prediction. Journal of Glaciology, 28(98), 3-21

CLARKE, G.K.C., 1986. Professor Mathews, outburst floods, and other glaciological disasters. In - W.H. Mathews Symposium: a Celebration, 10 October 1984, Vancouver, B.C., Canadian Journal of Earth Sciences, 23(6), 859-868

CLARKE, G.K.C. and W.H. MATHEWS, 1981. Estimates of the magnitude of outburst floods from Lake Donjek, Yukon Territory, Canada. Canadian Journal of Earth Sciences, 18(9), 1452-1463

COLLINS, D.N., 1986. Characteristics of meltwaters draining from the portal of an alpine glacier during the emptying of a marginal ice-dammed lake. Working Paper Series No.4, Alpine Glacier Project, Department of Geography, University of Manchester, Manchester, England, March, 28 pp.

DEWART, G., 1968. Seismic investigation of ice properties and bedrock topography at the confluence of two glaciers, Kaskawulsh Glacier, Yukon Territory, Canada. Institute of Polar Studies Report No.27, Ohio State University, Columbus, Ohio, 207 pp.

FUSHIMI, H., K. SHANKAR, K. IKEGAMI and K. HIGUCHI, 1982. Nepal case study: catastrophic floods. In - Techniques for Prediction of Runoff from Glacierized Areas, G.J. Young (Editor), IAHS Publication No.149, International Association of Hydrological Sciences, 125-130

HEWITT, K., 1982. Natural dams and outburst floods of the Karakorum Himalaya. In - Hydrological Aspects of Alpine and High Mountain Areas, J.W. Glen (Editor), Proceedings of the Exeter Symposium, 19-30 July 1982, IAHS Publication No.138, International Association of Hydrological Sciences, 259-269

JOHNSON, P.G., 1991. Pulses in glacier discharge: indicators of the internal drainage system of glaciers. Northern Hydrology: Selected Perspectives, T.D. Prowse and C.S.L. Ommanney (Editors), Proceedings of the Northern Hydrology Symposium, NHRI Symposium No.6, National Hydrology Research Institute, Environment Canada, Saskatoon, Saskatchewan, 165-175

KASPER, J.N., 1989. An ice-dammed lake in the St. Elias Range, southwestern Yukon Territory: water balance, physical limnology, ice dynamics and sedimentary processes. M.A. thesis, Department of Geography, Ottawa University, Ottawa, Ontario, 197 pp.

LIVERMAN, D.G.E., 1987. Sedimentation in ice-dammed Hazard Lake, Yukon. Canadian Journal of Earth Sciences, 24(9), 1797-1806

LLIBOUTRY, L., B. MORALES ARNAO, A. PAUTRE and B. SCHNEIDER, 1977. Glaciological problems set by the control of dangerous lakes in the Cordillera Blanc, Peru. Journal of Glaciology, 18(79), 239-290

POST, A. and L.R. MAYO, 1971. Glacier dammed lakes and outburst floods in Alaska. Hydrological Investigations Atlas HA-455, U.S. Geological Survey, Department of the Interior, Washington, D.C., 10 pp. + 3 maps

SCHMOK, J.P. and G.K.C. CLARKE, 1989. Lacustrine sedimentary record of ice-dammed Neoglacial Lake Alsek. Canadian Journal of Earth Sciences, 26(10), 2092-2105

THEAKSTONE, W.H., 1978. The 1977 drainage of the Austre Okstindbreen ice-dammed lake, its cause and consequences. Norsk Geografisk Tidsskrift, 32(4), 159-171

THORARINSON, S., 1957. The jökulhlaup from the Katla area in 1955 compared with other jökulhlaups in Iceland. Jökull, No.7, 21-25

ON AREAL DISTRIBUTION OF SNOWCOVER IN A MOUNTAINOUS AREA

Å. Killingtveit[1] and K. Sand[2]

[1]Norwegian Institute of Technology
Trondheim, N-7034
NORWAY

[2]Norwegian Hydrotechnical Laboratory
Trondheim, N-7034
NORWAY

ABSTRACT

Due to strong wind drift the snowcover in mountainous areas tends to become quite unevenly distributed. The uneven distribution has important implications both for the planning and operation of snow-survey networks and for run-off forecasting by hydrological models. To describe the variability of snowcover a number of statistical parameters are used: areal average, standard deviation, coefficient of variation, spatial-correlation function and areal-distribution function. It is important to realize the variability at the different geographical scales: macroscale, mesoscale and microscale. It is also very important to distinguish between forested and unforested areas. In Norway the statistical parameters for snowcover have been investigated and used in a number of catchments during the last 10 to 15 years. Guidelines for design and operation of snow surveys are based on the areal-variability and spatial-correlation structure of snowcover in different types of terrain. The areal-distribution function for snowcover is also used directly in the most common precipitation run-off model, the HBV-model. This model is today in operational use in a number of catchments, mostly by hydropower utilities. This paper describes briefly the use of statistical snowcover parameters for run-off forecasting and snow-survey planning. The main part of the paper summarizes the results from an extensive data-collection program in a 2.655 km² catchment, the Orkla River basin. Characteristic data are given for snow variability in different types of terrain, both above and below the timberline. The results are given both as statistical parameters and empirical distribution functions, for use in hydrological models.

INTRODUCTION

The areal distribution of snowcover became an important object of study in Norway 10 to 15 years ago. The main reason for the renewed interest in snow-distribution data was the need for such data in hydrological models. Hydrological models for run-off forecasting were first used operationally in the Sira Kvina catchment in 1976 (Aam *et al.*, 1977), and have since been used in numerous catchments, mainly for hydropower-systems optimization and flood forecasting.

During the calibration and use of hydrological models in mountainous areas it was soon realized that the classical snow-distribution models were not adequate (Killingtveit, 1978). The small-scale variability of snowcover is of great importance for the snow-melt calculation, and some preliminary tests with what was later termed a "distributed snow model" gave substantial improvements in model performance (Killingtveit and Aam, 1978).

It was also realized that more detailed knowledge of snow distribution on small scales would be useful for the planning and implementation of snow-survey networks. Even though snow surveys have been in operation in some catchments in Norway since around 1920, the older surveys mostly were designed to map regional patterns and not small-scale variability in the snowcover. This work was pioneered by studies in the Nea catchment (Tveit, 1980).

The need for more detailed knowledge of snowcover variability at different scales initiated a large measurement program in the Orkla basin in the years 1981 and 1982 (Sand and Killingtveit, 1983). The results from these measurements were later used both for snow-survey network design and in operational run-off forecasting models for six sub-catchments in the basin. The results were also an important input to the work being done on guidelines for planning and operation of snow measurements for hydropower optimization (Andersen *et al.*, 1982).

AREAL DISTRIBUTION OF SNOWCOVER

Scales of Variability

The areal (or spatial) distribution of snowcover in a catchment is determined by complex interactions between meteorological and physiographic factors integrated over time. The snowcover shows variability over scales ranging from a few centimetres up to hundreds of kilometres. Terms borrowed from meteorology have been used to characterize the variability within three main scales (Gottschalk and Jutman, 1979; Andersen *et al.*, 1982):

- macroscale or regional scale (> a few km);
- mesoscale or local scale (50 m → a few km); and,
- microscale (1 m → 50 m).

These ranges should be considered as orders of magnitude rather than exact ranges.

The macroscale or regional variability in snow is mainly determined by large-scale meteorological and topographical features. The snow variability within a regional scale can be determined by locating a number of snow stations within an area and measuring average snow depth at each station. This is the most common way to arrange snow measurements in Norway and also in the other Scandinavian countries. A plot showing regional variability of snowcover in the Orkla basin is shown in Figure 1.

The mesoscale or local variability in snowcover is mainly determined by local topographical features and their interaction with climate. Wind drift of snow is the most important process in this scale, causing scour of snow at exposed, and deposition at, sheltered places. The process is very complex, but some attempts have been made to relate the final snow distribution to climatic and physiographic parameters (Tveit, 1980). An example of snowcover variability at a local scale is shown in Figure 2 which shows the depth of snow along a snow course in Orkla, station 14 Grønlitjern. This snow course is located 800 m a.s.l., well above the timberline in an open area which is highly exposed to wind. The observed snow distribution can be related to local variation in topography, with two ridges where the snow is blown away and two ravines with large snow deposits.

The microscale variability in snowcover is mainly determined by small-scale variability in surface roughness, and can be considered as "stochastic variations" within the local variation.

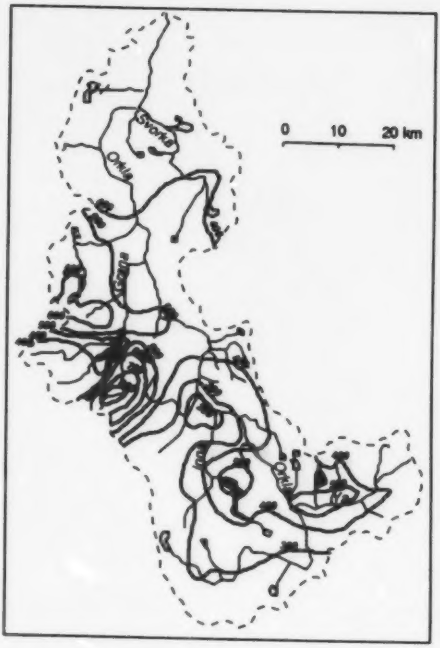

Figure 1. Areal snow distribution (mm of water) 1981, Orkla River basin.

An example showing snowcover variability at the microscale is given in Figure 3. This example is also from a snow survey in Orkla, station Sørøyåsen. Also this station is located 800 m a.s.l., but in a sparsely forested area much less exposed to wind than the previous example.

Snowpack Parameters

Three different parameters were used to characterize the snowpack:
- a) snow depth (h) measured in cm;
- b) snow density (d) measured in g·cm^{-3}; and,

c) snow water equivalent (w = h·d) expressed in mm of water.

Statistical Parameters for the Areal Average and Variability of Snowcover

The areal average and variability of snowcover can be characterized by the following statistical parameters:

- mean (m_x);
- standard deviation (s_x); and,
- coefficient of variation (C_v).

C_v is considered to be the best parameter to compare relative variability from regions with different areal average snowcover. In the rest of this paper C_v will be used to denote the areal variability numerically.

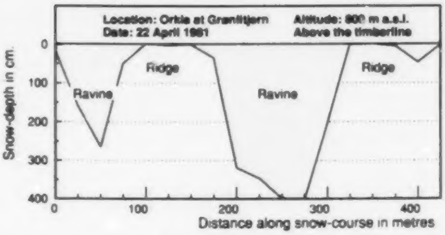

Figure 2. Snow variability at a local scale.

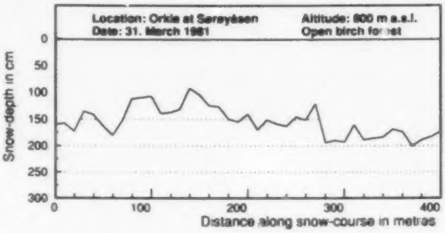

Figure 3. Snow variability at the microscale.

Areal Snow-Distribution Curve

The areal snow distribution can also be described by statistical distribution functions. The Normal, Log-normal and Gumbel distribution functions are well suited (Gottschalk and Jutman, 1979). In the study of the Orkla data we have also applied the Pearson type III function with good results. Figure 4 (upper bar-chart) shows the observed distribution of snow for a group of stations in the Orkla basin. The Log-normal 3 distribution (LN-3) proved to fit best to this data set, and the computed frequency distribution, F(x), is also plotted on the figure. The lower part of the figure shows the cumulative-distribution function, both for observed data and for the fitted LN-3 distribution. The figure shows that the snow distribution is described very closely with a theoretical distribution function.

On the lower part of the figure we also have plotted the cumulative distribution like a "duration curve", 1 - F(x). This type of curve is termed the areal snow-distribution curve.

Spatial Correlation of Snowcover

The snow depths at equidistant points, for example along a snow course, can be considered as a "spatial time series" and analyzed by methods from time-series analysis. An important parameter is the space-correlation function (r_x):

$$[1] \qquad r_x\ (k\ \Delta l) \qquad \frac{\overset{N\ k}{\underset{i}{}}\ (X_i \quad X)\ (X_{i\cdot k} \quad X)}{\overset{N\ k}{\underset{i}{}}\ (X_i \quad X)^2}$$

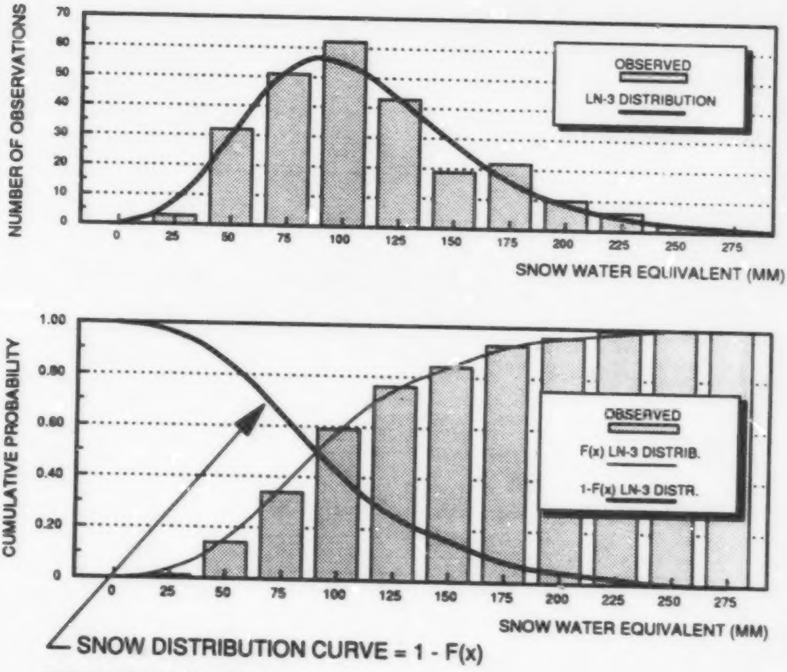

Combined distribution for 250 sampling points in the 800 m interval. Coefficient of variation is 0.38 and coefficient of skewness 0.71

Figure 4. Snow distribution curves.

The space-correlation function is used for analyzing the randomness in snow measurements, and in determining the optimal sampling distance along snow courses. Earlier studies of the space-correlation structure of snowpack in different types of terrain (Gottschalk and Jutman, 1979) were used in the design of the measurement program in Orkla to determine:

- length of snow courses;
- number of sampling points along each snow course; and,
- distance between sampling points.

The relative variability in snow depth and snow density was also taken into account to determine the optimal combination of depth and density measurements along each course. The space-correlation structure and coefficient of variation in each type of terrain were the two most important parameters used in the optimal network design.

FIELD STUDY

During the winters of 1981 and 1982 an extensive field program was carried out to study the areal distribution of the snowcover in the Orkla basin. The main objectives of the investigations were to design a snow-survey network for operational run-off forecasting in the river system and to produce reliable areal snow-distribution curves for six sub-basins in the catchment.

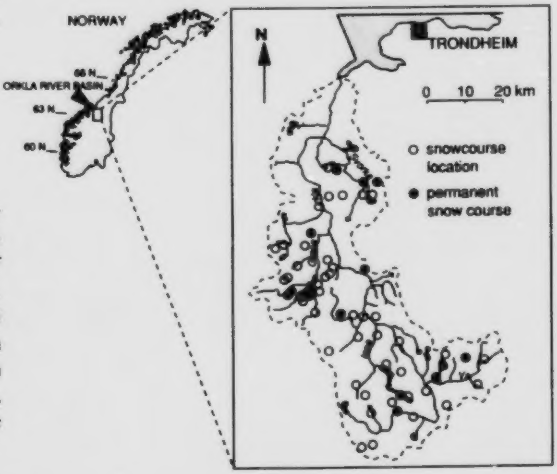

Figure 5. Location and snow courses of the Orkla River basin.

Description of Basin Area

The Orkla River basin is located in the Trøndelag region of Norway (see Figure 5). The total area is 2,655 km^2 and the elevation ranges from 129 m a.s.l. to 1,641 m a.s.l., with a mean altitude of 815 m a.s.l.

The climate ranges from a coastal type in the northern and lower parts of the basin to a continental type in the southern and eastern parts. Precipitation ranges from 400 to 1,200 mm·yr^{-1}. Approximately 50% of the annual precipitation normally is retained in the seasonal snowcover.

The river system is developed for hydropower production which yields an annual production of 1.1 TWh·yr^{-1}.

Snow-Survey Network

The snow-survey network was designed in order to provide information about areal snowcover distribution at micro-, meso- and macroscales.

The snow-depth measurements were taken along straight-line snow courses. The distance between measurement points was 10, 25 or 50 metres, depending on local conditions and space correlation for the snowpack. To cover mesoscale variability the snow courses crossed local topographic features such as ridges and valleys. This required a length of snow course ranging from 250 to 1,250 m, depending on local topography. Variations in the macroscale range were covered by distributing the snow courses evenly over the basin area while simultaneously aiming for an optimal coverage of basin elevation range, different types of terrain and large-scale topographical formations. In order to simplify the analysis, the snow courses were categorized with respect to elevation zone (400, 600, 800, 1,000 and 1,200 m a.s.l.) and terrain type (forested, sparsely-forested and open). Snow-course locations are shown in Figure 5.

Snow-Depth Measurements

A total of 55 snow courses were established (Table 1). Snow-depth measurements were made manually with a graduated measurement rod at equidistant points along the snow courses. A total of 1,546 and 1,637 point measurements of snow depth were made in 1981 and 1982, respectively.

Snow-Density Measurements

Snow density was measured by coring snow segments of the entire snow depth using a Songa tube. The tube is 1-m long, and has a circular orifice with a diameter of 11.0 cm. Three snow-density samples were normally obtained along each snow course.

ANALYSIS

The statistical parameters used in the analysis of the areal snow distribution are areal snow-distribution curves, coefficient of variation and the arithmetic mean value. Regional snow distribution may be displayed on a map with isolines through points

Table 1. Mean snow depth and coefficient of variation at snow courses surveyed 1981 and 1982.

Locality	1981		1982	
	Mean Snow Depth (mm)	C_v	Mean Snow Depth (mm)	C_v
1 Innistuvollen	379	0.35	157	0.56
2 Svartsetra	459	0.23	159	0.53
3 Svartvassåsen	364	0.41	163	0.51
4 Frilsjøen	369	0.36	125	0.64
5 Mjuken	478	0.19	218	0.36
6 Tysksetra	207	0.58	108	0.58
7 Innset	316	0.28	179	0.41
8 Farligheita bru	142	0.80	69	0.98
9 Skogheim	227	0.37	138	0.34
10 Hårstad	251	0.46	121	0.56
11 Brattsetseter	416	0.20	238	0.30
12 Kubbfjellet	435	0.35	176	0.92
13 Haukåsen	403	0.22	96	0.72
14 Grønlitjønna Sør	505	1.24	220	1.68
15 Grønlitjønna Øst	644	0.70	302	0.91
16 Furusjøen	465	0.28	188	0.57
17 Storhauktjønna	574	0.46	245	0.70
18 Svartbekkøyan	491	0.21	155	0.42
19 Sørøyåsen Nord	456	0.29	297	0.47
20 Sørøyåsen Vest	536	0.27	387	0.58
21 Telmyran	507	0.21	329	0.41
22 Godtjønnfjell	348	0.78	195	0.78
23 Rissetra	670	0.44	426	0.58
24 Refshussetra	392	0.41	248	0.55
25 Stavåhøgda Øst-Vest	458	0.62	266	0.93
26 Stavåhøgda Nord	638	0.61	376	1.00
27 Brattskarven	625	0.54	387	0.71
28 Pikfjellet Vest	360	1.36	366	1.41
29 Pikfjellet Nord	566	0.74	403	1.09
30 Leverdalen	878	0.48	645	0.68
31 Leverkinna	343	1.20	259	1.51
32 Uvseter	531	0.37	258	0.47
33 Nonshaugen	421	0.42	262	0.71
34 Såtållia	231	0.71	254	0.64
35 Såtålsjøen	274	1.17	292	1.39
36 Storvangen	546	0.20	377	0.34
37 Breivadseter	370	0.31	161	0.54
38 Dølvad seter	391	0.17	327	0.27
39 Sløbekksetra	286	0.45	241	0.60
40 Dølvadfjell	369	0.81	307	1.00
41 Taraldstjønn	454	0.90	379	0.91
42 Fossetra	591	0.51	468	0.59
43 Øvre Dølvad	360	0.43	249	0.33
44 Vesle Orkelsjø .	337	0.49	246	0.49
45 Vesle Orkelhø	361	0.83	228	1.02
46 Bjørksetra	277	1.23	233	1.29
47 Grytdalseter	376	0.59	246	0.69
48 Eventjønnbekken	308	1.14	424	0.95
49 Tjuvholtjern	466	1.05	377	1.24
50 Hestfjellet	475	0.67	426	0.72
51 Langvatnet	397	0.92	368	2.02
52 Slettestjørn	294	0.37	181	0.43
53 Storinnsjøvangen	340	0.46	263	0.61
54 Rauåsen	464	0.40	--	--
310 Leverkinna ekstra	--	--	412	0.93

of equal snow depth. From the snow survey in 1981 such a map is shown in Figure 1. The isolines are based on arithmetic mean values of water equivalent at each snow course. The method gives rather limited information about the areal snow distribution and does not contain any information about the variability in the meso- and microscales. The areal snow-distribution curves for 1981 and 1982 are shown in Figure 6. From a statistical point of view, these curves contain much more information about the variability of the snowcover. In addition to macroscale variability, both meso- and microscale variabilities are integrated in the areal snow-distribution curves.

RESULTS

Macroscale Variability

The coefficients of variation associated with the snow-distribution curves shown in Figure 6 were 0.67 and 0.95 for 1981 and 1982, respectively.

Snowcover gradients north-south and west-east were examined and displayed by plots of mean water equivalent as a function of X- and Y-coordinates. However, no macroscale gradients were found. The isolines in Figure 1 show that there is a considerable regional variability, but a large-scale pattern is not obvious.

Figure 7 shows the areal snow-distribution curves for the 400-m, 800-m and 1,200-m levels. This figure indicates a fairly even snow distribution at lower levels, while the distribution becomes more and more uneven with increasing elevation. The relationship between snow-cover variability and elevation is also reflected in

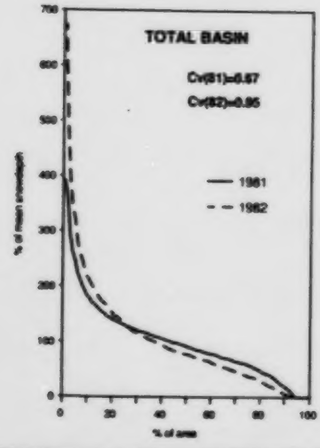

Figure 6. Areal snow-distribution curves 1981 and 1982.

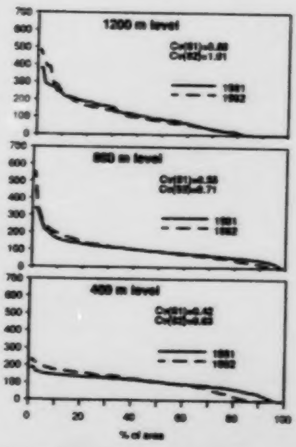

Figure 7. Snow distribution at 400-, 800- and 1200-m levels.

Figure 8, where the coefficient of variation is plotted against elevation. This figure shows a C_v increasing with increasing elevation up to the 1,000-m level, then slightly decreasing above this level.

Mean areal water equivalent is shown in Figure 9 at different levels. It is an interesting observation that in 1982 there was a significant correlation between water equivalent and elevation, while there was no such correlation in 1981. It is also worthwhile to notice the relationship between mean water equivalent and coefficient of variation seen from Figure 8 and Figure 9. In 1981 there was more snow than in 1982, this caused a lower variability in 1981 than in 1982.

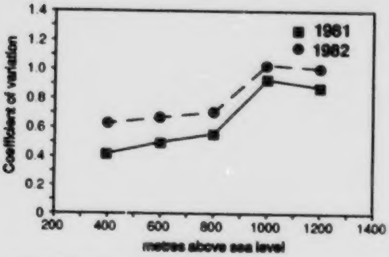

Figure 8. Coefficient of variation.

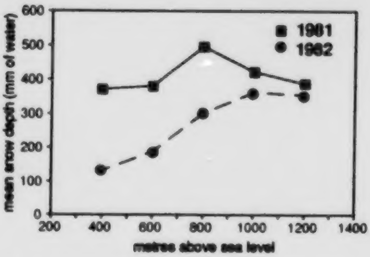

Figure 9. Mean areal snow depth.

Mesoscale Variability

Within each elevation zone the effect of different types of terrain can be identified. Figure 10 shows the snowcover distribution in forested, sparsely-forested, and open terrain at the 800-m level. It is shown that distribution is much more uneven in open terrain than in forested and sparsely-forested terrain. The coefficients of variation (Figure 11) show that variability of the snowcover in forested areas remains almost constant in different levels, while there are significant relationships between variability and elevation both in sparsely-forested and open terrain.

Mean areal snow depths are plotted in Figure 12. Both years there was less snow in forested terrain than in sparsely-forested and open terrain at the 400 and 600-m level. At the 800-m level this trend is not present. Beyond this level we have measurements only in open terrain.

Microscale Variability

The microscale variability is integrated in the macro- and mesoscale variability. In this study the microscale variability was not separated and statistically analyzed.

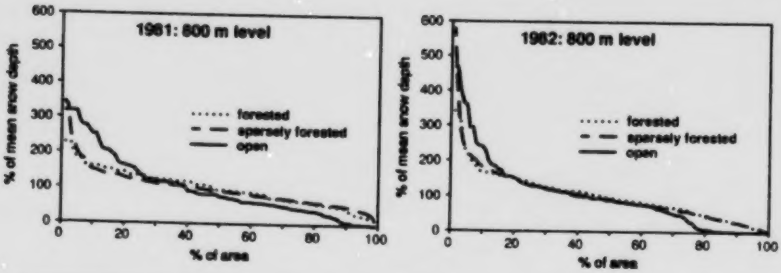

Figure 10. Snow-distribution curves in forested, sparsely-forested and open terrain.

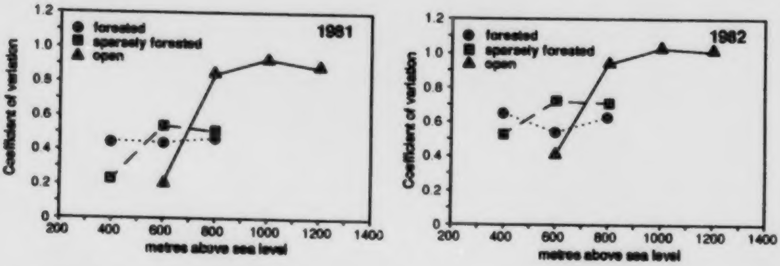

Figure 11. Coefficient of variation in different types of terrain in different elevation zones.

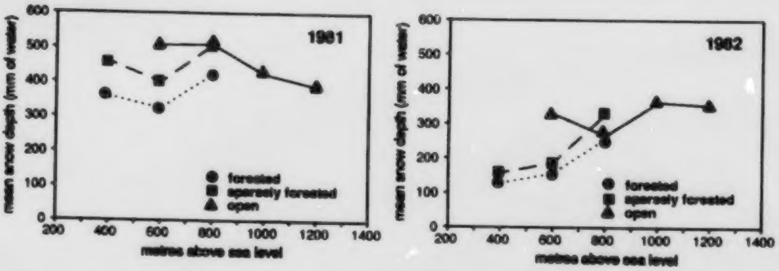

Figure 12. Mean areal snow depth in different types of terrain in different elevation zones.

Table 1 shows calculated mean values and coefficients of variation for each individual snow course. The coefficient of variation ranges from 0.17 to 1.36 in 1981 and from 0.27 to 2.02 in 1982. However, due to the surveying strategy most of these snow courses contain both micro- and mesoscale variability.

Variation from One Year to Another

This study was carried out over two years of very different snow accumulation. Mean snow depth in 1981 was 430 mm water equivalent, but only 278 mm in 1982. The difference in mean snow depth caused an overall higher snowcover variability in 1982 than in 1981, coefficients of variation were 0.95 and 0.67, respectively. This difference is significant both in the macro-, meso- and microscales. The higher variability in 1982 is also reflected by the snow-distribution curves, as the 1982 curves consequently have a steeper slope than the 1981 curves.

With more years of data we might have been able to identify the relationship between mean areal snow depth and the snow-distribution curves. The present data indicate, however, that this variation from one year to another is small.

OPERATIONAL SNOW-SURVEY NETWORK IN ORKLA

One of the main purposes of the measurement program was to design a snow-survey network for operational use. By analyzing the data obtained from more than 50 stations in 1981 and 1982, it was possible to reduce the number of stations to 13 without appreciable loss in accuracy for the computed average snow storage. The thirteen stations (or snow courses) chosen, were: 1, 2, 3, 5, 11, 18, 19, 20, 32, 36, 38, 43 and 50 (see Figure 5 and Table 1). The operational measurements have since been performed each year with measurements being taken February 1 and April 1 each winter.

The procedure developed in Orkla was later adopted in the guidelines for planning and operation of snow measurements for hydropower utilities in Norway (Andersen *et al.*, 1982). Some of the main recommendations for the planning of new snow measurements in these guidelines are:

"1) All new snow measurements should preferably be organized as snow courses with equidistant depth measurements along marked routes in the terrain.

2) As step one in planning, a preliminary measurement program should be carried out over 2 to 3 years. Based on these measurements the areal snow-distribution curve can be determined with good accuracy.

3) Thereafter the measurement can be reduced substantially for operational use. The number and location of permanent snow stations should be based on analysis from the preliminary measurement program, and on water-balance studies for the forecasting period."

A DISTRIBUTED SNOW MODEL

The HBV-model (Bergström, 1976) is the most commonly used model for run-off forecasting in the Nordic countries (Sweden, Norway, Finland and Iceland). The snow routine in the original model was lumped with a simple degree-day model for snow-melt calculation (Bergström 1975). In Norway the "distributed snow routine" was introduced in 1978 (Killingtveit, 1978) and later tested in several basins. In the Orkla River the HBV-model was first used in 1978, with the original lumped snow routine (Aam *et al.*, 1978). Later the distributed snow routine was tested in a sub-catchment, the Næverdal catchment (Killingtveit and Aam, 1978). The snow-distribution curves from the Nea catchment about 100-km northeast of Orkla were used in the model (Tveit, 1980). The results were very promising; on average the distributed model gave 45% better fit than the lumped model. In another test the distributed model was used in the Aursunden catchment 50-km northeast of Orkla. Here the distributed model improved model fit by 40%. This type of snow routine is now used in all HBV-models in operational use in Norway.

The main structure in the distributed snow routine is shown in Figure 13. The catchment is first divided into a number of (max. 10) elevation zones. The snow

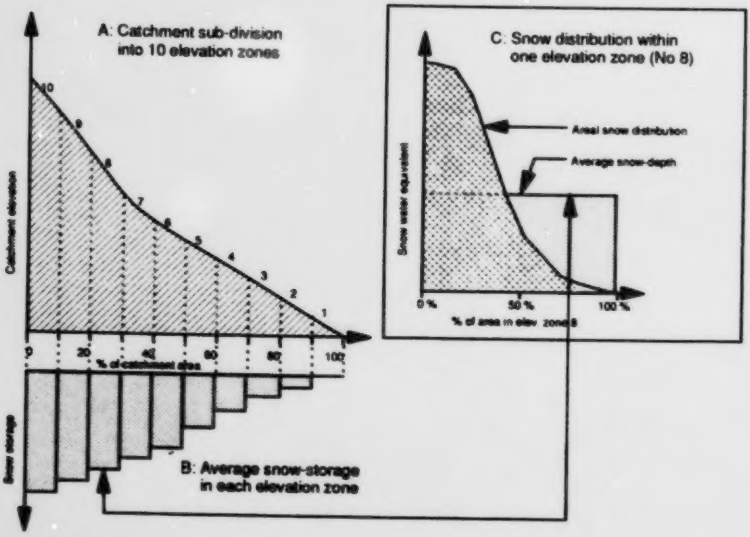
A: Catchment sub-division into 10 elevation zones
Catchment elevation
10
9
8
7
6
5
4
3
2
1
0
20
40
60
80
100
% of catchment area
Snow storage
B: Average snow-storage in each elevation zone
C: Snow distribution within one elevation zone (No 8)
Areal snow distribution
Average snow-depth
Snow water equivalent
0 %
50 %
100 %
% of area in elev. zone 8

Figure 13. Distributed snow routine in the HBV-model.

accumulation and melt within each elevation zone is computed by a simple degree-day model. The snow storage is statistically distributed according to the measured or assumed areal snow-distribution curve within each zone. It is especially important to consider the difference in snow distribution above and below the timber line.

In Orkla a total of six HBV-models now have been fitted to different sub-catchments. Each model has an individual areal snow-distribution curve based on the measurements from 1981 and 1982.

ACKNOWLEDGEMENTS

The project reported was funded by the Water System Management Association and the Orkla River Hydropower Authority. The latter also carried out the major part of the field work. We also want to acknowledge Dr. John Tveit, Norwegian Institute of Technology, who submitted the idea used for snow surveying and also the idea of the snowcover-distribution curve as a statistical description of snowcover variability.

LIST OF SYMBOLS

C_v	coefficient of variation
d	snow density ($g \cdot cm^{-3}$)
$F(x)$	cumulative probability distribution function
h	snow depth (cm)
i	sampling interval (m)
k	lag
m_x	average
N	number of observations
r_x	space correlation function
s_x	standard deviation
w	snow water equivalent (mm)
X	observed value of a stochastic variable
X_i	observed value of X at observation point i

REFERENCES

AAM, S., A. GJELDSVIK and Å. KILLINGTVEIT, 1978. Næverdal-feltet: Tilpassing av HBV- og SNSF-modellene (The Næverdal catchment: fitting the HBV and the SNSF models). Prosjekt Hydrologiske Prognosmodeller, EFI Technical Report No.Tr-2308, B 1-78-11, Division of Hydraulic Engineering, Norwegian Institute of Technology, Trondheim, Norway, (in Norwegian) 67 pp.

AAM, S., M. FJELD, M. FOSSDAL, Å. KILLINGTVEIT and B. WINGÅRD, 1977. Hydrologisk modell for drift av kraftverk (Hydrological models for hydro power operation). Elektrisitetsforsyningens Forskningsinstitutt, Norges Vassdrags- og Elektrisitetsvesen, Institutt for Vassbygging and SINTEF, EFI Technical Report No.TR-2130, Trondheim, Norway, (in Norwegian) 151 pp.

ANDERSEN, T., L. GOTTSCHALK, J. HARESTAD, Å. KILLINGTVEIT, J. TVEIT and S. AAM, 1982. Snømålinger for kraftverksdrift (Snow surveys for hydropower production). Report to the Norwegian Council for Hydropower Hydrology, Project A-113, Trondheim, Norway, 25 January, (in Norwegian) 126 pp.

BERGSTRÖM, S., 1975. The development of a snow routine for the HBV-2 model. Nordic Hydrology, 6(2), 73-92

BERGSTRÖM, S., 1976. Development and application of a conceptual runoff model for Scandinavian catchments. Bulletin Series A No.52, Department of Water Resources Engineering, Lund Institute of Technology, Lund University, Sweden, 134 pp.

GOTTSCHALK, L. and T. JUTMAN, 1979. Statistical analysis of snow survey data. Sveriges Meteorologiska och Hydrologiska Institut (SMHI) Rapporter, Hydrology and Oceanography No.RHO-20, Norrköping, Sweden, 41 pp.

KILLINGTVEIT, Å., 1978. A new approach to snow accumulation modelling? Nordic Hydrological Conference and 2nd Nordic IHP Meeting, 31 July - 3 August 1978, Helsinki, Finland, Ia-1 - Ia-12

KILLINGTVEIT, Å. and S. AAM, 1978. En fordelt modell for snøakkumulering og- avsmelting (A distributed model for snow accumulation and ablation). Prosjekt Hydrologiske Prognosmodeller, EFI Technical Report No.Tr-2312, B 1-78-14, Division of Hydraulic Engineering, Norwegian Institute of Technology, Trondheim, Norway, August, (in Norwegian) 35 pp.

SAND, K. and Å. KILLINGTVEIT, 1983. Snøforhold i Orkla-feltet studie av snøfordeling og forslag til snømåleopplegg (Snow cover in Orkla River basin: a study of areal snow cover distribution and design of snow survey network). Norges Hydrodynamiske Laboratorier, SINTEF Report No.STF 60-83016, Norwegian Institute of Technology, Trondheim, Norway, (in Norwegian) 76 pp.

TVEIT, J., 1980. Representativitet av snømålesystem ut frå topografiske og morfometriske parametrar (A system for representative snow measurements based on topographical and morphometric parameters). Division of Hydraulic Engineering, Norwegian Institute of Technology, Trondheim, Norway, September, (in Norwegian) 243 pp.

HYDROGEOCHEMICAL ASPECTS OF TWO SELECTED SITES IN A FRINGE ZONE OF DISCONTINUOUS PERMAFROST*

Y.T.J. Kwong, D. Craig and M. Griffin

National Hydrology Research Institute
11 Innovation Boulevard
Saskatoon, Saskatchewan
S7N 3H5 CANADA

ABSTRACT

Two sites, of about 1 km² each, located in the fringe zone of discontinuous permafrost in northern Alberta, have been instrumented and sampled to study ground-water chemistry in the discontinuous-permafrost zone. The two sites have similar sediment mineralogy but differ in topography, elevation and the occurrence of permafrost. Isotopic analyses of surface and ground waters suggest a common meteoric water source and insignificant, local evaporation effects for both sites. The water chemistry, however, appears to be highly dependent on the thermal regime under which the water-mineral interactions occur. A progression of calcium-bicarbonate dominated waters to sodium-sulphate type waters is found between the sites in conjunction with differences in the temperature regime. Furthermore, organic-acid aided mineral weathering associated with climatic warming may affect water quality and further study on this topic is recommended.

INTRODUCTION

Chemical reaction rates and equilibrium constants are temperature dependant. It follows therefore that significant long-term changes in thermal regime associated with climatic change or climatic variation may affect geochemical reaction rates and processes in environments subjected to such changes. A natural laboratory for the study of any such changes would likely be found in the southern fringe of the discontinuous permafrost zone where any persistent climatic change (or variation) would slowly affect the distribution of frozen ground. Two sites located in the fringe zone of discontinuous permafrost in northern Alberta have been instrumented and sampled for detailed study. The sites, designated as the Mount Watt site and the Meander River site, lie in the vicinity of the MacKenzie Highway north of High Level, Alberta (Figure 1). A recent survey of the distribution of permafrost along the Highway indicates that the fringe zone of discontinuous permafrost has retreated about 125 km northward in the past 25 years, concurrent with rapid economic development in the area and a local warming trend as revealed by an analysis of weather records (Kwong, 1990). The general regional hydrogeology of the Mount

---

*National Hydrology Research Institute Contribution Series Number CS-90009.

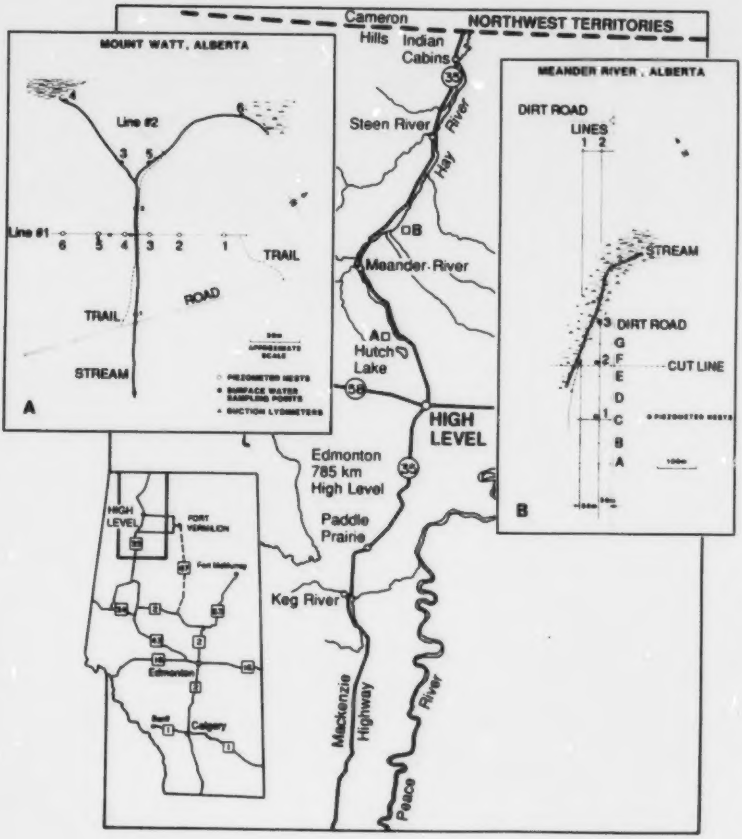
NORTHWEST TERRITORIES
Cameron Hills
Indian Cabins
35
Steen River
Hay River
B
Meander River
A
Hutch Lake
58
HIGH LEVEL
Edmonton 785 km High Level
Paddle Prairie
Keg River
Mackenzie Highway
Peace River
MOUNT WATT, ALBERTA
Line #2
Line #1
TRAIL
ROAD
STREAM
A
MEANDER RIVER, ALBERTA
DIRT ROAD
LINES
1 2
STREAM
DIRT ROAD
G
F
E
D
C
B
A
CUT LINE
B
HIGH LEVEL
FORT VERMILION
Edmonton
Calgary
Banff

Figure 1. Site location map with insets showing detailed sampling locations.

Watt area and that of the region further north in the vicinity of the MacKenzie Highway have been described by Tokarsky (1972) and Ozoray (1980), respectively. The present paper presents chemical and isotopic data from the two study sites which are situated in the same climatic zone and are underlain by glacial deposits of similar mineralogy, but which differ in topography, elevation and, more importantly, the occurrence of permafrost. The presence or absence of permafrost at these two sites can be used as a gross indicator of relative temperature in the soils. As an indicator of prevalent thermal regimes it has the advantage of integrating soil temperatures over several years. By comparing the shallow ground-water geochemistry of the two sites, parameters controlling the evolution of water chemistry associated with a warming temperature regime are suggested.

SITE DESCRIPTION AND SAMPLING

Both study sites occupy an area of about 1 km^2. The Mount Watt site is located about 30 km by road northwest of High Level. It comprises a small basin in an incised valley draining an area of spruce forest at an elevation of about 800 m a.s.l. The basin contains a north- and a south-facing slope meeting at an intermittent stream. The sediments found in this basin are mainly clays with minor silts and some pebbles. A brief description of representative cores is given in Appendix I. This massive glacial drift overlies marine shales of the Lower and Upper Cretaceous Shaftsbury Formation (Green *et al.*, 1970). However, it is felt that the influence of the bedrock on the shallow ground-water geochemistry in this basin is minimal. The vegetative cover, consisting of sphagnum moss with sparse Labrador tea, is generally less than or equal to 10 cm thick. The basin is subjected to seasonal frost with ice sheets and wedges persisting in the vicinity of the stream until early June. No permafrost was found in the basin, based on sediment coring and geophysical surveys. A series of six piezometer nests have been installed along a transect perpendicular to the stream (Figure 1, inset A). These 5.0-cm diameter, PVC (polyvinyl chloride) piezometers were installed using a 5.0-cm diameter hand auger. No foreign material, which might have affected water chemistry, was used to pack the well annulus, instead tightness of fit was relied on to prevent vertical leakage. The depths of the piezometers vary from 0.5 to 4.0 m. Three nests of suction lysimeters were also installed using the same method between the stream and location 5 on the north-facing slope. The lysimeters are completed to depths of 20, 40 and 60 cm and are composed of PVC pipes of 5.0-cm diameter, terminated with a porous ceramic cup.

The Meander River site is situated about 50-km north of High Level. It consists of a low-relief basin at an elevation of about 400 m a.s.l. The basin is rimmed by aspen-covered gravel ridges which grade into a black-spruce peat bog with a central stream. The vegetative cover, consisting mainly of sphagnum moss, Labrador tea and minor amounts of feather moss and grass, reaches a thickness of 15 cm near the swamp and thins out towards the gravel ridges. Adjacent to the swamp, fresh to partially-decomposed organic matter up to 12-cm thick invariably separates the surface vegetation cover and the underlying silty-clay deposit. Bedrock in this area is the silty-marine shale of the Lower Cretaceous Loon River Formation. Due to the thickness of unconsolidated glacial deposits and the hydrology of this basin, it is not anticipated that the bedrock will have any effect on the shallow ground-water geochemistry. Patchy permafrost is found in and below the peat in the bog area. Its distribution has been roughly delineated by geophysical surveys using a Geonics EM31 ground-conductivity meter (Figure 2). Ground truthing at selected locations by hand augering shows that the depth to permafrost varies between 30 and 90 cm, but the permafrost thickness has not been determined. Three piezometers nests have been installed to depths of 0.5 to 4.0 m using the same methods as at the Mount Watt site. The locations of the piezometer nests are shown in Figure 1 (inset B). None of these piezometers intersects permafrost.

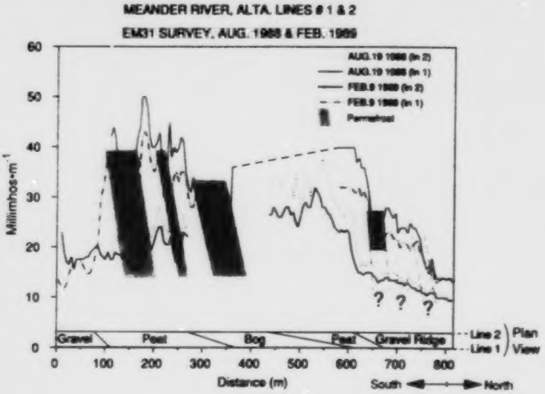

Figure 2. Delineation of permafrost by ground-conductivity measurements.

From the spring of 1988 to the fall of 1989, a total of 94 surface- and ground-water samples were collected for the determination of water chemistry at the two sites and their vicinities. These also include several samples of melted snow from both sites and melted ice pellets from patchy permafrost occurrences in the vicinity of Meander River. Where possible, the pH of the samples was measured in the field. Samples were transported to the National Hydrology Research Institute (NHRI) laboratory in Saskatoon within a one-week period for analyses in accordance with methods outlined by Environment Canada (1979). Samples for water chemistry were then filtered (0.45 μm), and preserved. All water samples were analyzed for major cations and anions within two weeks of collection. In the fall of 1988, 56 samples for oxygen- and hydrogen-isotope analyses were collected using 125 mL high-density linear polyethylene bottles filled in such a manner as to preclude any air space within the bottle. The samples were shipped to and analyzed by the Environmental Isotope Laboratory, University of Waterloo according to established procedures (Coleman *et al.*, 1982; Epstein and Mayeda, 1953). Stable-isotope data were reported in terms of permil deviations from the international standard SMOW (Standard Mean Ocean Water). At both study sites, sediment samples were collected from the surface to the depth of the deepest well at each piezometer nest for detailed chemical and physical characterization.

RESULTS

Isotopic Analyses

Stable isotopes. Figure 3 depicts the stable oxygen- and hydrogen-isotopic composition of 56 surface- and ground-water samples from the study sites and their vicinities. The Mount Watt ground waters define a local meteoric water line systematically offset from the global meteoric water line of Craig (1961) by a δD value of about -5‰. The Mount Watt stream samples and most of the Meander River ground waters also lie along the local meteoric water line, indicating the relative insignificance of evaporation effects occurring at the two study sites. The only exception is shown by ground waters of well MR-3 which is adjacent to the open bog. There is a pronounced shift in isotopic composition between waters collected from the depths of 1.6 and 1.0 m with isotopically heavier, and presumably more, evaporated water on top. The only stream sample from the site bears even a stronger evaporation signature. This variation in isotopic composition suggests that evaporation affects shallow ground waters only in the close vicinity of the open bog. Also plotted on Figure 3 are isotopic compositions of water samples collected from the various tributaries of the Hay River and melted ice samples from scattered permafrost occurrences in the vicinity of the MacKenzie Highway in the Hay River basin. The Hay River data suggest a much stronger evaporation signature on a regional scale than that locally observed at the two study sites. The permafrost data suggest a slightly different trend, but more data are required to define a new local meteoric water line with different evaporation signatures.

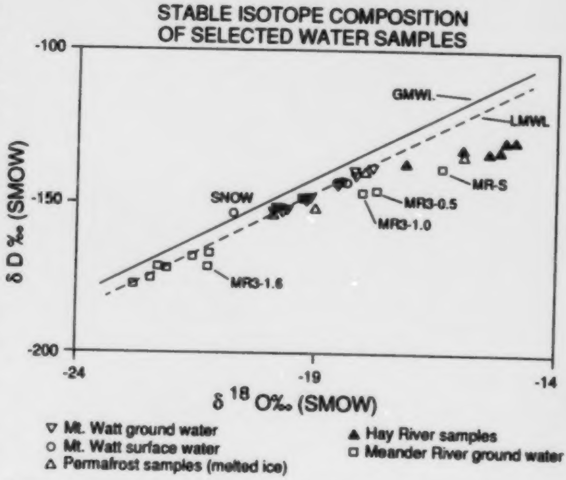

Figure 3. Stable isotope composition of water samples from the study sites and their vicinities.

Radioisotope. Table 1 shows the tritium content of 15 selected water samples collected from the vicinity of the study sites. Whereas all samples from the Mount Watt site are modern waters, a relatively deep (4 m) ground-water sample from the Meander River site is older than 35 years in age. This probably reflects the influence of patchy permafrost on the ground-water flow system. The frozen ground will act as a aquiclude or confining layer and may isolate deeper water from the surface-flow system and/or the regional ground-water flow system. However, further piezometer installation and sampling would be required to substantiate this hypothesis.

Water Chemistry

At both sites, the total dissolved solids (TDS) in the ground water generally increase with depth. However, the Meander River site has a maximum measured TDS of around 800 $mg \cdot L^{-1}$ in contrast to that at Mount Watt with 1,300 $mg \cdot L^{-1}$. Table 2 shows the detailed water chemistry of the two study sites and Figure 4 depicts the major cation and anion composition of ground waters (with ionic-charge balance errors of less than 10%) from the sites. Most ground and surface waters at the Meander River site are slightly basic with Ca^{2+} and Mg^{2+} as the dominant cations and HCO_3^- as the dominant anion. In the vicinity of frozen material and with increasing depth, however, Cl^- may be relatively enhanced. The majority of the ground waters of the Mount Watt site, particularly those collected from the south-facing slope, are slightly basic and can be classified as sodium-bicarbonate-sulphate type waters. Ground waters from the north-facing slope, on the other hand, show no dominant cations and are of the bicarbonate type with respect to anion composition. They are intermediate in composition between the ground waters at Meander River and the south-facing slope at Mount Watt. In fact, with minor exceptions, the ground-water chemistry appears to plot along a transition zone from calcium-bicarbonate dominated waters to sodium-bicarbonate-sulphate type waters (Figure 4). This chemical transition is coincidental with an apparent relative increase in soil temperatures as deduced from aspect and the presence or absence of permafrost. The Mount Watt stream waters, on the other extreme, are dominantly sodium-sulphate type waters with slightly acidic pHs. These waters, as well as a few very shallow ground waters at both sites, exhibit a large imbalance in negative charges. The good charge balance observed in the low TDS snow and other stream-water analyses suggests that analytical error is probably not the cause. Although nitrate has been detected in the near surface samples, its concentration (not shown in Table 2) is too insignificant to account for this error. As will be explained in the next section, it is suspected that the presence of organic acids plays a significant role in balancing ionic charges in these waters.

Table 1. Tritium content of selected water samples.

Sample No.	Field No.	Tritium (±8 T.U.)
A. Surface-water samples from the Hay River Basin		
1	HR-1	27
2	HR-2	45
3	HR-3	36
4	HR-4	34
5	HR-5	28
6	HR-6	58
B. Ground-water samples from the study sites		
7	WM3-1.6	72
8	WM3-4.0	46
9	WM4-1.0	90
10	WM4-1.6	87
11	WM4-4.0	74
12	MR1-4.0	<6
13	MR2-0.5	39
14	MR3-0.5	53
15	MR3-1.0	32

DISCUSSION

Given the differences in physical setting of the two sites (an incised-valley basin without permafrost at high elevation at Mount Watt versus a low-relief spruce bog with scattered permafrost at Meander River), the apparent continuum in water chemistry as observed in Figure 4 is rather intriguing. There are generally three major factors which affect the aqueous chemistry of any watershed: 1) composition of original precipitation; 2) chemical changes, especially water-mineral interactions, or biological processes occurring along the water pathway; and, 3) concentration

Table 2. Mean water chemistry of the two sites (all values except pH are in mg·L^{-1}).

A. Ground-water samples												
Well ID/ Field #	**No. of samples***	**Na**	**K**	**Ca**	**Mg**	**Fe**	**Si**	**pH**	**Cl**	**SO$_4$**	**Alkalinity**	**IBE(%)**
WM1-0.5	2	4.34	0.90	1.00	0.49	0.96	6.30	(ND)	1.0	6.7	(ND)	(NC)
WM1-1.6	3	42.6	1.35	20.4	12.5	4.00	15.3	(ND)	6.7	199	(ND)	(NC)
WM1-2.5	4	233	1.02	79.8	58.0	0.05	5.28	7.1(2)	20.6	[illegible]	85.7	-2.73
WM2-0.5	1	(ND)	(ND)	(ND)	(ND)	(ND)	(ND)	(ND)	2.0	13.4	(ND)	(NC)
WM2-1.1	1	16.0	0.88	2.30	1.03	4.67	10.3	(ND)	1.3	18.8	16.0	18.4
WM2-1.6	2	28.7	0.96	8.12	10.4	0.22	6.55	8.0(1)	1.0(3)	25.0(3)	95.9	1.44
WM2-4.0	4	115	3.14	37.6	27.5	0.13	6.95	7.3(2)	9.1	156	271	1.98
WM3-0.5	3	108	1.51	17.7	15.4	0.53	7.23	(ND)	8.7	167	(ND)	(NC)
WM3-1.0	3	118	1.28	25.9	20.8	0.39	3.50	7.9(2)	9.3	132	248(2)	-1.87
WM3-1.6	4	168	2.28	38.2	31.1	0.56	4.18	7.6(3)	14.6	239	328(3)	0.29
WM3-4.0	4	367	3.95	39.7	30.5	0.06	4.13	7.4(3)	77.7	417	483(3)	-1.05
WM4-0.5	1	14.6	1.28	9.30	5.37	1.12	15.7	(ND)	0.31	26.4	(ND)	(NC)
WM4-1.0	3	64.4	2.93	29.40	20.6	1.25	4.83	7.1	0.46	73.2	216	1.95
WM4-1.6	2	76.6	3.52	37.15	27.5	0.10	5.00	6.8	0.52	100	281	1.47
WM4-4.0	3	173	3.70	23.40	18.0	0.15	4.93	6.9	4.7	107	379	1.09
WM5-0.5	0	(NS)	(NS)	(NS)	(NS)	(NS)	(NS)	(NS)	(NS)	(NS)	(NS)	(NC)
WM5-1.0	1	16.2	2.94	8.20	6.00	10.6	33.4	(ND)	0.59	8.1	35.0	27.9
WM5-1.6	4	19.6	1.51	10.0	7.55	0.31	8.28	6.9(1)	0.27	12.9	80.5(2)	3.56
WM5-4.0	4	19.8	1.55	9.93	7.26	0.19	7.15	7.1(2)	0.26	14.6	78.2(2)	3.23
WM6-4.0	1	3.82	0.66	4.05	2.41	0.42	9.80	(ND)	0.25	3.2	(ND)	(NC)
MR1-0.5	1	1.29	1.42	34.4	7.40	0.13	1.70	(ND)	0.96	9.4	37	25.05
MR1-1.1	2	3.02	1.08	59.2	13.1	0.10	2.55	8.2(1)	0.79	12.4	163	8.50
MR1-1.6	3	2.50	1.30	68.4	16.3	0.01	3.43	7.9(1)	0.86	16.7	205(2)	3.98
MR1-4.0	3	4.10	1.15	72.9	17.0	0.00	4.73	7.9(2)	1.3	15.4	231	2.65
MR2-0.5	4	19.1	0.70	93.1	21.6	0.06	2.90	7.8(3)	5.6	5.1	351(2)	2.82
MR2-1.0	4	17.2	0.71	98.2	22.0	0.09	2.96	7.8(3)	9.6	4.5	356(3)	0.08
MR2-1.5	2	46.0	1.49	149	26.3	0.02	3.75	(ND)	42.1(3)	1.3(3)	415(1)	9.32
MR3-0.5	3	20.0	1.00	66.7	17.8	0.51	7.40	7.5	25.2	47.6	210(1)	1.06
MR3-1.0	3	33.4	1.35	86.4	20.7	2.08	7.60	7.3	29.7	39.2	267(1)	4.08
[illegible]-1.6	1	166	2.50	99.3	22.9	0.19	4.00	(ND)	166	6.3	(ND)	(NC)

**Unless otherwise stated in brackets; NS = no samples collected; ND = not determined; NC = not calculated.*

Table 2. Continued.

B. Lysimeter, surface-water and snow samples												
Well ID/ Field #	No. of samples*	Na	K	Ca	Mg	Fe	Si	pH	Cl	SO_4	Alkalinity	IBE(%)
MW-HL	1	21.5	2.50	21.7	8.50	0.56	3.10	(ND)	3.6	112	15.0	1.17
MW-ML	1	47.7	1.76	16.2	12.1	1.45	6.50	(ND)	0.66	62.6	(ND)	(NC)
MW-ST1	2	6.18	0.48	1.53	0.84	1.93	5.65	5.8(1)	0.77	5.4	5.0(1)	36.0
MW-ST2	2	5.39	0.43	1.26	0.70	1.80	5.40	5.8(1)	0.64	4.7	2.5(1)	44.5
MW-ST3	2	5.15	0.42	1.20	0.61	1.93	5.20	5.5(1)	0.62	3.3	1.5(1)	56.2
MW-ST4	2	6.45	0.68	1.81	1.07	1.34	5.70	5.9(1)	0.88	9.9	3.0(1)	28.5
MW-S1	1	0.67	0.44	2.22	1.10	3.32	10.0	5.5	0.76	4.6	2.0	39.5
MW-SNOW	1	0.32	0.15	0.17	0.05	0.00	0.00	(ND)	0.43	0.56	0.50	-5.34
MW-SNO1	1	0.14	0.89	0.24	0.11	0.00	0.00	(ND)	0.16	0.62	(ND)	(NC)
MW-SNO2	1	0.06	0.17	0.19	0.06	0.00	0.00	(ND)	0.13	0.54	(ND)	(NC)
MR-S	1	4.90	1.68	82.9	19.0	0.23	7.60	7.6	35.0	92.0	192	-6.10
MR-S1	1	61.3	4.72	123	31.8	1.05	12.9	(ND)	59.8	4.9	475	1.30
MR-S13	1	37.3	0.59	66.9	19.8	0.37	11.0	7.7	27.3	49.0	210	5.01
MR-SNO1	1	0.05	0.06	0.09	0.03	0.00	0.00	(ND)	0.08	0.26	(ND)	(NC)
MR-SNO2	1	0.05	0.06	0.19	0.03	0.00	0.00	(ND)	0.08	0.31	(ND)	(NC)

** Unless otherwise stated in brackets; NS = no samples collected; ND = not determined; NC = not calculated.*

effect resulting from evaporation. The isotopic data presented above indicate a common meteoric water source and that evaporation effects on the ground waters at both sites are minimal on a local scale. The chemistry of the precipitation may be assumed to be relatively stable over the long term and, because of its dilute nature, to have little effect on the observed aquatic chemistry in these basins. Therefore, it is the nature and extent of chemical reactions occurring at the sites that control the variation in water chemistry.

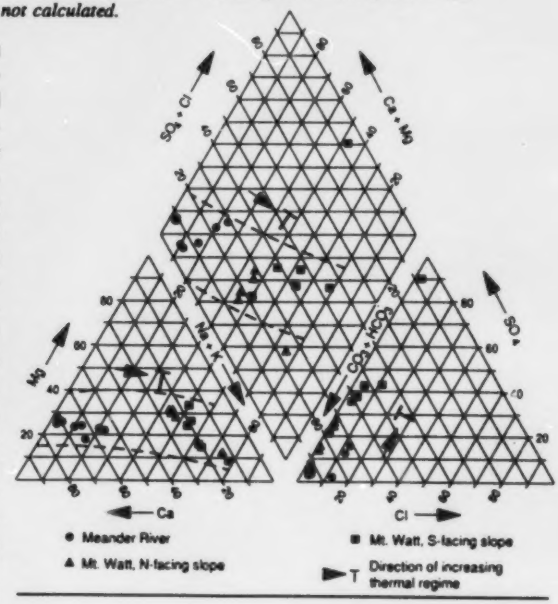

Figure 4. Shallow ground-water chemistry of the two study sites and its apparent evolution in response to increasing thermal regimes.

To interpret the hydrogeochemistry of the two sites and to determine whether the apparent trend in water chemistry observed in Figure 4 is coincidental or real, additional information on the mineralogical composition of the sediments at the sites is required. Analyses of bulk sediment samples (Appendix I) by powder X-ray diffractometry show that sediments at the two study sites are very similar in mineralogical composition. Both are dominated by quartz with subordinate amounts of feldspars, chlorite, and mica. Generally, the Meander River sediments contain more feldspars and less secondary clay minerals than those of Mount Watt. Moreover, on visual examination, the Mount Watt sediments show scattered clots of limonite stain and those of Meander River appear to be darker in colour, presumably due to the presence of organic carbon. In short, sediments from the Mount Watt site show signs of incipient chemical weathering whereas those of Meander River appear to be devoid of alteration.

The high pH values and high alkalinity content of both surface and ground waters from Meander River and most ground waters from Mount Watt indicate the dominance of carbonate equilibria on the local water chemistry. However, with only two minor exceptions, no significant amounts of carbonate minerals (i.e., greater than about 2% as a detection limit of the method used) have been detected in the sediments by X-ray analyses (Appendix I). This apparent contradiction can readily be explained by the fact that very little carbonate is actually required to effect the carbonate equilibria in natural systems (0.01% in an open system as calculated by Freeze and Cherry, 1979). This is especially true at low temperatures because of the inverse relationship of carbonate solubility with temperature.

Taking into account the physical settings of the two sites and their respective hydrogeochemistry, a plausible explanation for the evolution of a calcium-bicarbonate type water to a sodium-bicarbonate-sulphate type water is as follows. At the Meander River site, in the presence of scattered permafrost, water-mineral interactions have been restricted to occur at temperatures not much higher than a few degrees above 0°C even in the summer; and carbonate equilibria dominate. At the Mount Watt site, in the absence of permafrost, weathering of other minerals becomes appreciable depending on the ambient temperature. The net result of weathering is the introduction of other ions like sodium and sulphate into the aqueous system which eventually overshadows the carbonate equilibria. The difference in groundwater chemistry of samples collected from the two slopes reflects a disparity in the extent of weathering. The south-facing slope, characterized by a higher annual thermal regime, allows increased rates of water-mineral interactions and thus gives rise to more chemically-evolved waters than the north-facing slope. The detailed composition of a water sample is, of course, also affected by the heterogeneity of the sediment, water-retention time and the nature of the water pathway.

The stream-water chemistry at Mount Watt is distinctly different from the rest of the data set in that, though low in total dissolved solids, it is of the sodium-sulphate type, is characterized by a acidic pH, and has an average charge imbalance of about 40% excess cations. The slight brownish colour of the water suggest that the low pH is caused by the presence of organic acids. The fact that the anionic component of the organic acids is not totally accounted for in the determination of the carbonate alkalinity may explain the net positive charge imbalance. The relative enrichment of the samples in dissolved iron and silica is also consistent with enhanced iron-silicate weathering due to the presence of organic acids (Schnitzer, 1986). The structural stability of Fe-rich minerals is apparently weakened by the complexing of iron by humic substances. The importance of organic acids or humic material in mineral weathering has been well documented (Antweiler and Drever, 1983; Baker, 1986; Tan, 1986). As most of the scattered permafrost occurrences in the region are found in low areas with an appreciable insulating organic mat (Brown, 1964), the effect of a long-term increase in ambient temperature (reflected by permafrost degradation) on the stability of the organic matter and its subsequent effect on water quality is an issue that deserves further research. The release of organic acids due to accelerated organic decomposition at higher temperatures would complicate the mineral-weathering processes associated with the disappearance of permafrost. The present study suggests that, in terms of general water quality, an increase in total dissolved solids is likely to accompany any long-term warming trends that result in an increase in soil temperatures. Further changes will likely vary with the evolution of the local hydrological regime. A more detailed assessment of any long-term effects on water quality associated with permafrost degradation will thus have to await further investigation.

SUMMARY AND CONCLUSION

Isotopic and hydrochemical data from two selected sites in the fringe zone of permafrost in northern Alberta have been presented and assessed as an attempt to understand the possible evolution of water chemistry associated with a warming climate. Whereas the two sites share a common meteoric source of water and exhibit little local evaporation effect, local aquatic chemistry is strongly affected by the prevalent thermal regime under which water-mineral interaction occurs. Slight differences in the local thermal conditions are reflected in the aspect of sampling locations and the occurrence or absence of permafrost. Carbonate equilibria appears to dominate low-temperature hydrogeochemistry but weathering of other minerals becomes prominent in warmer conditions leading, in this case, to the transition of calcium-bicarbonate dominated waters to sodium-bicarbonate-sulphate type waters. Moreover, it is suggested that the release of organic acids by decaying organic matter may complicate mineral weathering associated with permafrost degradation. More research in this area is recommended.

REFERENCES

ANTWEILER, R.C. and J.I. DREVER, 1983. The weathering of a late Tertiary volcanic ash: importance of organic solutes. Geochimica et Cosmochimica Acta, 47(3), 623-629

BAKER, W.E., 1986. Humic substances and their role in the solubilization and transport of metals. In - Mineral Exploration: Biological Systems and Organic Matter, D. Carlisle, W.L.

Berry, I.R. Kaplan and J.R. Watterson (Editors). Prentice-Hall. Engelwood Cliffs. New Jersey. 377-407

BROWN, R.J.E., 1964. Permafrost investigations on the Mackenzie Highway in Alberta and Mackenzie District. Technical Paper No.175. Division of Building Research. National Research Council of Canada. Ottawa. Ontario. 25 pp.

CANADA. ENVIRONMENT CANADA. 1979. Analytical methods manual. Water Quality Branch. Inland Waters Directorate. Environment Canada. Ottawa. Ontario. 620 pp.

COLEMAN, M.L., T.J. SHEPHERD, J.J. DURHAM, J.E. ROUSE and G.R. MOORE. 1982. Reduction of water with zinc for hydrogen isotope analysis. Analytical Chemistry. 54(6). 993-995

CRAIG, H., 1961. Isotopic variations in meteoric waters. Science. 133(3465). 1702-1703

EPSTEIN, S. and T. MAYEDA. 1953. Variations of O^{18} content of waters from natural sources. Geochimica et Cosmochimica Acta. 4(5). 213-224

FREEZE, R.A. and J.A. CHERRY. 1979. Groundwater. Prentice-Hall. Englewood Cliffs. New Jersey. 604 pp.

GREEN, R., M.A. CARRIGY and G.B. MELLON. 1970. Bedrock geology of northern Alberta. Map. 1:500,000 scale with explanatory notes. Alberta Research Council. Edmonton. Alberta

KWONG, Y.T.J., 1990. Degradation of permafrost along the Mackenzie Highway: causes and effects. Abstracts with Programs. 22(7). Annual Meeting. Geological Society of America. October 29 to November 1. 1990. Dallas. Texas. A19

OZORAY, G., 1980. Hydrogeology of the Steen River - Whitesand River area. Alberta. Earth Sciences Report No.80-2. Alberta Research Council. Edmonton. Alberta. 13 pp. + maps

SCHNITZER, M., 1986. Reactions of humic substances with metals and minerals. In - Mineral Exploration: Biological Systems and Organic Matter. D. Carlisle. W.L. Berry. I.R. Kaplan and J.R. Watterson (Editors). Prentice-Hall. Englewood Cliffs. New Jersey. 408-427

TAN, K.H., 1986. Degradation of soil minerals by organic acids. In - Interactions of Soil Minerals with Natural Organics and Microbes. P.M. Huang and M. Schnitzer (Editors). Special Publication No.17. Soil Science Society of America. 1-27

TOKARSKY, O., 1972. Hydrogeology of the Mount Watt area. Alberta. Report No.72-3. Alberta Research Council. Edmonton. Alberta. 10 pp.

APPENDIX I: BRIEF DESCRIPTION OF SELECTED CORES. (MINERALOGICAL COMPOSITION OF BULK SAMPLES ARE IN BRACKETS.)

MOUNT WATT, HOLE #2 (on south-facing slope)

0.0-0.1 m	Forest litter
0.1-0.4	Beige silty clay with little forest litter (quartz >> plagioclase > minor K-feldspar, chlorite and mica)
0.4-0.9	Dark grey clay with brownish silty lenses (quartz >> mica >= chlorite >= plagioclase > minor K-feldspar ± smectite)
0.9-1.1	Dark grey clay with 5% yellowish pebbles (quartz >> mica >= chlorite >= plagioclase > minor K-feldspar ± smectite)
1.1-1.5	Greyish clay with little pebbles
1.5-1.6	Greyish clay with 3% yellowish brown pebbles (quartz >> mica = K-feldspar >= plagioclase >= chlorite > trace goethite ± smectite)
1.6-3.1	Greyish clay with brownish silty streaks (quartz >> chlorite = mica > plagioclase > minor K-feldspar)
3.1-4.0	Greyish clay with rare beige silty streaks (quartz >> chlorite = mica > = plagioclase > minor K-feldspar) (minor siderite was also detected at 3.9-4.0 m)

MOUNT WATT, HOLE #5 (on north-facing slope)

0.0-0.1 m	Black forest litter
0.1-0.5	Beige clay with minor forest litter (quartz >> plagioclase = chlorite = mica > minor K-feldspar)
0.5-0.8	Greyish clay (quartz >> chlorite >= plagioclase > mica > minor K-feldspar ± smectite)
0.8-1.9	Saturated grey plastic clay (quartz >> chlorite >= mica >= plagioclase >= K-feldspar ± trace smectite)
1.9-2.4	Greyish plastic clay with limonitic clots (quartz >> chlorite = mica = plagioclase > minor K-feldspar)
2.4-2.7	Grey plastic clay with rusty streaks, slightly silty (quartz >> chlorite = mica > plagioclase > minor K-feldspar)
2.7-3.1	Grey plastic clay (quartz >> chlorite = mica > plagioclase > minor K-feldspar)
3.1-4.0	Dark grey clay with minor beige silty streaks and clots (quartz >> chlorite = mica = plagioclase > minor siderite, K-feldspar)

Note: Mica in the mineralogical description includes undifferentiated micaceous clay minerals.

MEANDER RIVER, HOLE #2

0.0-0.1 m	Peat moss with pieces of fresh wood
0.1-0.4	Peat moss
0.4-0.7	Dark grey clayey silt with peat moss (quartz >> plagioclase >> minor K-feldspar, mica ± smectite > trace chlorite, amphibole)

0.7-1.1	Greyish clayey silt with minor organic matter (quartz >> plagioclase, mica ± smectite > minor K-feldspar, chlorite)
1.1-1.5	Greyish silty clay (quartz >> plagioclase >> minor K-feldspar, chlorite, mica ± smectite)
1.5-1.6	Light grey silty clay (quartz >> K-feldspar = mica > chlorite > plagioclase > trace dolomite)

Note: Mica in the mineralogical description includes undifferentiated micaceous clay minerals.

ICE-COVER GROWTH AND FREEZE-OUT OF SOLUTES IN A MACKENZIE DELTA LAKE*

L.F.W. Lesack[1,2], P. Marsh[1] and R.E. Hecky[3]

[1]National Hydrology Research Institute
11 Innovation Boulevard
Saskatoon, Saskatchewan
S7N 3H5 CANADA

[2]Present address:
Department of Geography
Simon Fraser University
Burnaby, British Columbia
V5A 1S6 CANADA

[3]Freshwater Institute
501 University Crescent
Winnipeg, Manitoba
R3T 2N6 CANADA

ABSTRACT

The Mackenzie Delta contains about 25,000 lakes and is part of a north-flowing arctic river system where flood water arrives at the delta from the southern portion of the basin before substantial melting of the ice cover on the delta lakes. As a result, flooding with river water often occurs over the top of the ice on these lakes. The lakes are typically shallow (mean depth less than 2 m), but despite cold arctic temperatures, ice covers reach a maximum thickness of only 0.6 to 1.2 m. A layer of water commonly remains unfrozen beneath the ice cover, and solute exclusion during growth of the ice and solute-remobilization processes can increase solute concentrations within the unfrozen water several fold. At NRC Lake, water-chemistry measurements show that a combination of these processes increased the concentration of the unfrozen lake water by a factor of 4.3 from freeze-up to the time of maximum ice thickness. Profiles of temperature and water density, derived from chemistry measurements, taken during the flooding period indicate that little apparent mixing occurs between the flood water and the denser layer of unfrozen lake water. Despite density differences between the layers of water, which are large relative to differences commonly found in holomictic lakes, the lake is sufficiently shallow that the work required to mix the water column to uniform density (stability) is low, and should be readily accomplished by exposure to significant wind. Hence, the presence of a floating ice cover to shield the lake from wind during the flooding period is critical to whether the flood will flush and initialize the lake with river water, or will simply remove the ice and leave the solutes from the previous year in the lake.

*National Hydrology Research Institute Contribution Series Number CS-90017.

Virtually all lakes which remain flooded for longer than NRC Lake (about 2/3 of the lakes in the central delta) are flooded sufficiently long that complete mixing of the water column should occur. Many of the remaining lakes probably do not mix with the flood water and flush on every occasion they are flooded. However, ice-growth calculations and projected variations in lake geometry indicate that lakes comparable in area to NRC Lake, with a maximum depth of 2.6 to 3.5 m, could have a low, water-column stability. As a result, mixing could occur beneath the ice cover from the shear forces associated with the inflowing and outflowing water movement, and heat contributed by the imported flood water.

INTRODUCTION

Among lakes associated with floodplains and deltas of major world rivers, annual flooding by the river is commonly perceived to play an important role in replenishing nutrients and flushing the lacustrine ecosystems (Junk *et al.*, 1989). The Mackenzie Delta is a lake-rich environment (contains ca. 25,000 lakes), and is part of a north-flowing arctic river system where flood water arrives at the delta from the southern portion of the basin before significant melting of the ice cover on the delta lakes. As a result, flooding often occurs over top of the ice cover on these lakes. Upon submergence, the ice pans quickly fracture along the margins or release from the lake beds, often to form relatively-intact floating ice covers on the surface of the lakes. Despite cold arctic temperatures, delta lakes more than about one metre deep do not often freeze to the bottom. In these lakes a layer of water remains unfrozen beneath the ice cover. Solute exclusion (freeze-out) during ice growth (cf. Welch and Legault, 1986; Schindler *et al.*, 1974; Goldman *et al.*, 1967) provides a mechanism that can potentially increase solute concentrations, and the relative density of the unfrozen water, several fold greater than the density of the lake water prior to freeze-up. The flood water provides a major component of the heat required to melt and remove the ice from these lakes. Moreover, the duration of the flood in many of the lakes is relatively brief (1/3 of the lakes are flooded for less than 14 days each year; Marsh and Hey, 1989). Hence, a major question is whether the flood water can efficiently mix with the denser water in a given lake and effectively flush the lacustrine ecosystem (cf. study of meltwater mixing by Bergmann and Welch, 1985). Such mixing is restricted because the lake surface is shielded from wind by the floating ice cover for a large portion of the flooding period. Without mixing, the flood water only melts the ice and drains from the lake while leaving most of the solutes from the previous year in the lake.

"NRC Lake" is representative of small, shallow lakes in the Mackenzie Delta that, on average, remain flooded for only a brief period each year. Temperature profiles of the water column, measurements of water chemistry, and derived estimates of water density obtained during the 1989 period of flooding, provide evidence that the layers of water remain unmixed through the period that the ice cover is present on the lake. Subsequent evaluations demonstrate whether the lake is likely to be mixed by wind upon removal of the ice cover, and from an understanding of the processes controlling water density during the flood period, we discuss whether incomplete flushing is likely to occur in a broader range of lakes in the Mackenzie Delta.

STUDY AREA DESCRIPTION AND HYDROLOGICAL REGIME

Field work was carried out at NRC Lake (unofficial name), which is located in the eastern portion of the Mackenzie Delta at 68°19'N and 133°50'W, approximately 5-km southwest of Inuvik. The mean annual temperature at Inuvik is -9.8°C, and the mean monthly temperatures are -29.6°C and 13.6°C in January and July, respectively. Annual precipitation is only 266 mm, of which approximately 57% occurs as snow. Although the mean maximum snowcover depth reported by the Atmospheric Environment Service (AES) at Inuvik is 0.5 m (Canada, Fisheries and Environment, 1978), the snowcover on lakes in the Mackenzie Delta is highly variable (McCourt, 1985).

The NRC Lake basin is about 38.1 ha and is covered by a white spruce forest, with tree heights of approximately 15 m, and a dense underbrush of willows and alders. A relatively dense growth of aquatic macrophytes develops within the lake, after the decline of spring water levels, usually dominated by *Potamogeton sp.* and occasional stands of *Equisetum sp.* along the shoreline. NRC Lake is perched above the surrounding Mackenzie River channel system (late-summer elevation of approximately 1.5 m a.s.l.) with a late-summer lake level of approximately 3.8 m a.s.l. This is near the median value for lakes in this part of the Delta (Marsh and Hey, 1989). At this elevation the lake is 6.73 ha with a mean depth of 0.97 m and a maximum depth of 1.8 m. Marsh and Hey (1989) classified NRC Lake as a high-closure lake, representive of 33% of the delta lakes in the Inuvik area.

The hydrological regime of NRC Lake is dominated by an annual, brief (average of 14 days) flooding of the lake by the Mackenzie River. Flooding commences (on average) on May 26, with the mean peak water level of 5.6 m a.s.l. occuring on June 3. After this date, the lake level falls rapidly in response to falling Mackenzie River levels, with water levels dropping on average 1.04 m (or 58% of the flood peak) over a 4-day period following the peak. By the end of June, discharge from the lake falls to near zero. Since flooding by the Mackenzie River does not occur during the summer, the only water input to the lake is rainfall directly on the lake. Since ground-water flow from the lake is restricted by permafrost beneath the land portion of the basin (Johnston and Brown, 1964; 1966) and the unfrozen, low-permeability sediments beneath the lake, the loss of water from the lake during the summer is dominated by evaporation. Since evaporation from the lake is greater than precipitation (Marsh and Bigras, 1988), the NRC Lake level slowly declines until freeze-up in early-October.

METHODS

Lake Bathymetry and Depths of Snow and Ice Cover

The volume and area of NRC Lake as a function of depth was determined from bathymetric surveys performed while the water level was at the average late-summer level of 3.8 m a.s.l. (surface area and mean depth given above). Twenty centimetre contour lines were interpolated from the survey data, then the area within each contour was obtained by planimetry. The volume below and area within each contour were respectively fit as 6° and 5° polynomials to obtain volume and area as continuous functions of depth or water level. Over the range of depths under consideration, the polynomial estimates, in the worst case, only deviated from the value obtained by actual planimetry of the depth contour by less than 2% (usually the difference was less than 1%).

Snow depth and density of the ice cover on NRC Lake were measured with an ESC-30 snow sampler along two transects across the lake in the middle of May, while ice thickness was measured at a number of holes drilled through the ice. At this time both the white- and black-ice component of the ice cover were measured. However, since the lake snowcover is normally thin, the lake ice is composed primarily of black ice.

Collection and Analysis of Water Samples

Water samples were collected with a Van Dorn sampler and were usually shipped within a day to the analytical laboratory at the Freshwater Institute in Winnipeg for subsequent analysis. Sample filtrations, sub-sampling, measurement of pH, and acid titrations were performed promptly upon arrival in Winnipeg (usually within 2 to 3 days of collection), and thereafter samples were kept refrigerated until analyzed. pH and acid titrations were performed on aliquots of unfiltered water, while measurements for major solutes were performed on aliquots of water filtered through rinsed Whatman GF/C glass-fibre filters and a plastic filtration apparatus. Cations (Na^+, K^+, Ca^{2+}, Mg^{2+}) were measured by atomic-absorption spectrophotometry, and anions (Cl^-, SO_4^{2-}) by Dionex ion chromatography. Dissolved inorganic carbon was determined from Gran's plot analysis (Gran, 1950, 1952) of acid-titration curves and for subsequent data analyses was assumed to be in the form of HCO_3^-. Given that the pH range of the samples was 8.4 to 9.1, there was probably significant amounts of CO_3^{2-} in some of the samples. Further details of analytical methods and sample treatment protocols are given in Stainton *et al.* (1977) and in Anema *et al.* (1990).

Estimation of Water Density

Temperature and conductivity profiles were measured with a Yellow Springs Instruments Model 33 SCT meter, with a conductivity-cell constant of 1.0.

Temperatures were derived from a thermistor-bead probe, readable to 0.1°C, and calibrated against a certified thermometer.

The relative densities of the mixture of lake water and river water were estimated analogously to the approach of Millero *et al.* (1976) as:

$$[1] \qquad \rho \quad \rho_o \quad - \quad (M \quad \rho_o \quad \phi_v)\ N/1000$$

where ρ is the density of the solution, ρ_o the density of pure water, M is the mean equivalent weight of salts in the solution, N is the equivalent molarity or normality of the solution, and ϕ_v is the apparent equivalent volume of the mixture of salts. Apparent volumes for the salt mixtures were derived from estimates of partial molal volumes of the individual electrolytes tabulated at 0° and 25°C as in Millero (1972). Apparent volumes at different ambient temperatures were obtained by interpolation. At the range of solute concentrations under consideration, the adjustment in relative density by accounting for the apparent volume of water displaced by the salts in solution is about 15%. The density of pure water (ρ_0) as a function of temperature was obtained from the tabulations in Hutchinson (1957).

By the time that flood water from the river reaches NRC Lake, the concentrations of suspended solids are not high enough to appreciably affect the relative differences in density between the flood water and the lake water. We expect, however, that suspended solids could significantly affect the density of flood water in lower-elevation lakes which are closer to the river channel.

RESULTS AND DISCUSSION

Water-Column Structure During the Flood

To evaluate whether the flood water mixes with the unfrozen lake water while the floating ice cover is present, temperature profiles were measured and water samples were collected at NRC Lake during the 1989 period of flooding. Vertical profiles of temperature and water density (Figure 1), derived from the chemistry of the water samples, indicate that a two-layer structure was maintained in the water column, with little apparent mixing of the lower layer of lake water into the upper layer of flood water, throughout the period that the ice was present. The first set of composite profiles, taken on May 28 (from 10 ice holes distributed over orthogonal transects across the lake), show that the coldest water was just beneath the ice cover (near 0.3°C) and along the lake bottom (0.9°C), with the warmest water (2.3°C) in a thin layer, just above the layer of bottom water, at a depth of about 2m. Spatially, these warmest temperatures were recorded at ice-hole sites closest to the inflow channel and indicate that the imported flood water builds up in a layer on top of the more dense bottom water and is the main source of heat to the lake at this point in time. By May 31, the date of peak water level (6.1 m a.s.l.), the average temperature of the flood water had increased to more than 3°C with the warmest water still just above the layer of bottom water. On June 2 the water levels were significantly declining, and the only source of heat to the lake was now solar radiation rather than imported flood water, as during the rising water period. By June 4, the water level had declined about 1.4 m from the peak, little ice remained on the lake and the water column had still not mixed.

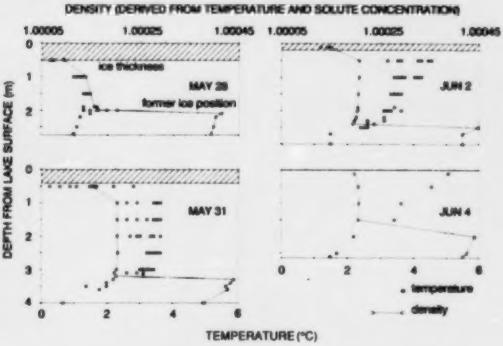

Figure 1. Water-column profiles of temperature and density measured during the 1989 period of flooding. Water temperatures are shown as composite plots of measurements taken from 10 ice holes distributed over perpendicular transects across the lake; except for June 4, where only one profile was taken. Water densities are derived from the average of the temperature profiles and the chemistry of water samples obtained from the layers of flood water and lake water. The dotted line (former ice position) shows the position of the bottom of the ice layer, and also corresponds to the top of the unfrozen layer of lake water, before the lake was flooded.

Although significant erosion of the density gradient between the two layers of water appears to have occurred over the period of observation, mostly as a result of heat input, the density difference between the two layers remained substantial until the ice cover was gone and the lake could potentially be mixed by the wind. Moreover, solute concentrations in the layer of flood water within NRC Lake were actually a little higher than concentrations in the adjacent river channel during the period of flooding (Table 1). Presumably, the additional solutes were acquired in transit from the river channel as some combination of leachate from flooded forest vegetation and water flushed from adjacent lakes. Hence, the density differences between the flood-water layer and the layer of unfrozen lake water could be even greater in lower elevation lakes which are closer to the river channel.

Resistance to Mixing

To determine if complete mixing of the water column is likely to occur before most of the flood water has drained from the lake, we used Schmidt's concept of water-column stability (Hutchinson, 1957) to evaluate the resistence to potential mixing. The stability (S) of a lake is the minimum work required to mix the lake to uniform density without adding or losing heat or solutes and was calculated as (Idso, 1973):

$$S = g / A_0 \int_{z_0}^{z_m} (\rho_z - \rho_u)(z - z_{pu}) A_z \, dz \qquad [2]$$

where g is the acceleration of gravity, A_0 and A_z respectively are the surface area of the lake and the area at depth z, ρ_u is the mean density of the lake (the density that would be obtained after mixing the lake to uniformity), ρ_z is the density at a given depth, and z is depth, where the subscripts pu, 0 and m refer to the depth at which the mean density occurs within the stratified water column, the lake surface and maximum depth, respectively. In the limnological literature g is usually omitted from the stability equation. However, with inclusion of g the results are obtained as ergs·cm^{-2} which can be compared with wind-power integrated over given periods of interest (MacIntyre and Melack, 1982; Stauffer, 1980). From Equation 2, it is apparent that stability is a function of the product between the density distribution and the distance that water of a given density must be moved to achieve uniform density. Therefore, stability is also related to the depth of the lake.

Table 1. Comparison of solute concentrations in the layer of flood water in NRC Lake versus water in the adjacent river channel during the 1989 period of flooding.

Solute	River Channel 26 May 89	River Channel 04 June 89	Flood Water 31 May 89
	mg·L^{-1}		
Na^+	4.50	5.00	10.7
K^+	1.02	1.11	1.46
Ca^{2+}	28.1	29.5	40.4
Mg^{2+}	6.20	6.40	10.3
Cl^-	4.30	5.20	13.8
SO_4^{2-}	20.3	21.5	34.8
HCO_3^-	95.8	94.1	127
Σ solutes	160	163	238

The range of stabilities calculated for NRC Lake is compared with values typically encountered in holomictic and meromictic lakes in Table 2. Despite density differences between the water layers equivalent to a temperature difference of between 4°C and 16°C for pure water, which is large compared to density differences typically encountered in holomictic lakes, the stability values remain low because the lake is shallow. Relatively strong stabilities have been reported for lakes which are comparably shallow (e.g., Cole *et al.*, 1967), however, the salinity gradients were considerably higher. Although wind records are available from the AES weather station at Inuvik, considerable effort would be required to determine precisely the probability and expected duration of time that NRC Lake would remain unmixed after removal of the ice cover. Wind power for a given lake is related to a variety of boundary-layer characteristics interacting between the wind and lake surface which must either be measured at the lake or modelled (cf. Stauffer, 1980). However, the low end of the range of stabilities reported for meromictic lakes (e.g., Devils Bathtub Lake; Table 2) provides a crude measure of the minimum stability that should be required to maintain a stratified water column in a small lake located in topography with reduced wind exposure.

Table 2. Comparison of water column stabilities (S) calculated for NRC Lake with the range of values typically encountered in holomictic and meromictic lakes.

	Range of Values (ergs·cm^{-2})	Typical Value (ergs·cm^{-2})
NRC Lake	300 - 700	--
Holomictic Lakes[1]	<5000 - 7 x 10^6	10^5
Meromictic Lakes[2]	5500 - 58 x 10^6	10^6

[1] Upper value: Pyramid Lake, Nevada (Hutchinson, 1957).
[2] Lower value: Devils Bathtub Lake, New York (Brunskill et al., 1968); Upper value: Big Soda Lake, Nevada (Hutchinson, 1957).

The stability value for NRC Lake on June 4 is about 280 ergs·cm^{-2}. The stability value estimated for an equivalent water-column depth, before the bottom layer had been subjected to shear forces from the inflowing and then outflowing flood water and before energy had been added from solar radiation and heat transfer from the flood water (initial stability), was about 450 ergs·cm^{-2}. Although the evidence is somewhat subjective, since estimates of wind power are not available, even this larger stability value is quite low compared to lakes which remain stratified for significant duration, so the water column could be quickly mixed by one afternoon of relatively moderate winds. Moreover, NRC Lake has been well mixed by mid-June in past years when temperature and conductivity measurements were made, and two adjacent lakes ("Skidoo Lake" and "South Lake"), which flooded and were exposed to the wind earlier than NRC, were well mixed by the time that the first temperature profiles were measured on NRC Lake in 1989 (May 26). The ability of the ice cover to shield the lake from the wind appears to be critical to whether the waters are going to mix or remain stratified during the period of flooding. For wind velocities less than 4 m·s^{-1} blowing over open water (reference height of 10 m above the water), water surfaces are aerodynamically smooth and drag coefficients are not statistically different from those expected above a smooth glass plate (Stauffer, 1980; Wu, 1969). Transition to aerodynamically-rough flow occurs at velocities > 4 m·s^{-1}, which corresponds roughly to the initiation of appreciable vertical mixing in lakes with near-neutral stability (B.C. Kenney, National Hydrology Research Institute, pers. comm.). Since there is a 35% probability of the hourly wind speed being greater than 4 m·s^{-1} at Inuvik during June (Burns, 1973), it seems quite likely that the lake would mix within a few days of the removal of the ice cover. However, since NRC Lake is flooded only briefly, a couple of days of calm weather following the removal of the ice cover may be all that is required to enable the flood water to drain from the lake without mixing with the bottom water.

Although the magnitude of the stability values seems to leave little doubt that normal winds are capable of mixing the water column, there are a number of factors that make the precision of this calculation quite uncertain. The stability values are quite sensitive to the depth of the lake, relative to the amount of change in depth that occurs at this time of the year. On June 4 the maximum depth of NRC Lake was 2.6 m. This represents the depth of the lake on the day when the ice cover was essentially removed, and was thus the first day on which the lake could potentially be mixed by the wind. To roughly estimate how much the stability of the water column had eroded during the period of flooding, which was independent of the rapidly changing depth of the water column during this period, the calculation of initial stability (see above) was based on the date during the rising-water period (May 28) when the lake depth was equivalent to the depth on June 4.

Factors Controlling Water-Volume Reduction and Water Density

The difference between the initial water column stability and the post ice-cover stability is about 200 ergs·cm^{-2}. Hence, if the difference in density between the two layers is reduced sufficiently, such as by reduction of ice growth or change in lake volume geometry, to yield an initial water-column stability of about 200 ergs·cm^{-2}, it is likely that the stability could be eroded to zero during the period of flooding, and the two layers of water could mix before the ice cover has been removed from the lake. However, to generalize the results from NRC Lake to a broader range of lakes in the Mackenzie Delta, it is necessary to determine if the processes controlling the increase in water density as a function of ice-cover growth are predictable.

Change in Solute Mass over Winter

To determine the change in water density expected as the volume of unfrozen water remaining in the lake decreases with increasing ice depth over the winter, it is necessary to determine the efficiency with which solutes are excluded from the growing ice. Also, whether there are other gains or losses of solutes to the water column over the winter. Solute concentrations were measured in NRC Lake during September 1986, prior to freeze-up, and in late-April 1987, at the time of maximum ice thickness (Table 3). Since the volume of unfrozen water in the lake is known for both sampling dates, the change in the mass of each solute in the lake between the sampling dates can be calculated.

There appears to be little net change in the mass of Cl^-, Na^+, and Mg^{2+} in the lake, however, SO_4^{2-} almost completely disappears from the water column while there are large gains of K^+, Ca^{2+}, and HCO_3^- during the winter. There are a number of well-known processes likely to be operating beneath the ice which can both remobilize and remove solutes with respect to the water column. These include decomposition of aquatic macrophytes, redox reactions at the sediment-water interface, and incorporation of solutes into the growing ice cover. An obvious potential source of solutes (especially K^+) and a certain producer of HCO_3^- as a result of respiration is decomposition of macrophyte biomass. In combination with the build up of HCO_3^- is the re-entry of substantial Ca^{2+} into solution during the course of the winter. A major source of the Ca^{2+} was probably $CaCO_3$, which was frequently observed to precipitate during summer periods of high macrophyte growth and subsequent depletion of HCO_3^- (R. Hecky, unpublished data). The equilibrium concentrations for a pure solution of Ca^{2+} and HCO_3^-, which is open to the

Table 3. Comparison of solute concentrations ($mg \cdot L^{-1}$) and estimated solute masses ($g \cdot m^{-2}$) in NRC Lake prior to freeze-up (September 1986) and at the time of maximum ice thickness (April 1987). Using the values for water and ice volumes, masses were normalized per unit surface area of the lake at the time of freeze-up (62,900 m^2). The potential magnitude of solutes incorporated into lake ice was estimated from the mean concentrations of melted ice reported by Welch and Legault (1986) for lakes at Saqvaqjuac.

Solute	SEP 86	APR 87		Net Change	APR/SEP ratio
	Unfrozen Water	Unfrozen Water	Ice Cover		
Water Volume (m^3)	54,200	15,800	--	--	--
Ice Volume (m^3)	--	--	38,400	--	--
pH	9.1	8.4	--	--	--
$mg \cdot L^{-1}$					
Na^+	12.7	40.1	0.05	--	--
K^+	0.77	4.97	0.02	--	--
Ca^{2+}	20.6	109	0.47	--	--
Mg^{2+}	15.2	47.5	0.15	--	--
Cl^-	15.0	55.0	0.21	--	--
SO_4^{2-}	31.0	1.0	0.12	--	--
HCO_3^-	97.6	576	--	--	--
Σ solutes	193	833	--	--	--
$g \cdot m^{-2}$					
Na^+	10.8	10.1	0.03	-0.90	0.92
K^+	0.66	1.25	0.01	0.57	1.88
Ca^{2+}	17.8	27.4	0.29	9.36	1.54
Mg^{2+}	13.1	12.0	0.09	-1.25	0.91
Cl^-	12.9	13.8	0.13	0.77	1.07
SO_4^{2-}	26.7	0.25	0.07	-26.6	0.01
HCO_3^-	84.2	145	--	60.7	1.72

atmosphere, respectively are 16 $mg \cdot L^{-1}$ and 61 $mg \cdot L^{-1}$ with a pH of 8.4 (Garrels and Christ, 1965). Although estimation of the precise equilibrium concentrations is more complex for a multicomponent solution; the concentrations measured prior to freeze-up (Table 3) clearly indicate that the solution was near or in excess of the saturation equilibrium.

The efficiency with which solutes are excluded from the growing lake ice cannot be directly estimated for NRC Lake since it cannot be assumed there are no other gains or losses of solutes from the lake water during the period of ice growth. Assuming that the mass of solutes incorporated per unit volume of lake ice at NRC Lake is the same as that measured in lakes at Saqvaqjuac by Welch and Legault (1986), the potential mass of solutes that could be incorporated into the ice at NRC Lake would be negligible (maximum of 2% loss of mass) relative to the apparent changes in solute mass that occurred in the unfrozen water over the winter. However, Welch and Legault's data are based on measuring the solute content of ice cores obtained from their lakes. Since the concentration of major solutes in NRC Lake is higher than in the Saqvaqjuac lakes, and the degree of water-volume reduction resulting from ice growth in the Saqvaqjuac lakes is not as large as in NRC Lake, the mass of solutes incorporated per unit ice volume in NRC Lake may be greater than in the Saqvaqjuac lakes. By extrapolating Welch and Legault's measurements of solute mass per unit ice volume, the loss of solutes from the unfrozen water layer in NRC Lake, attributable to ice-cover incorporation, could be underestimated.

The net result is that while the volume of unfrozen water in NRC Lake was reduced by a factor of 3.4 from September 1986 to April 1987 (defined as the water-volume reduction factor equivalent to the initial lake volume/final volume of unfrozen lake water), the total solute concentration (by weight) of the unfrozen water in the lake increased by a factor of 4.3 (equivalent to the final concentration of unfrozen lake water/the initial concentration of the water) because there was a net gain of solutes beyond that which could be accounted for by the volume reduction of the unfrozen lake water.

Expected Ice Thickness

Reduction in the volume of water that remains unfrozen during the winter in Mackenzie Delta lakes is directly determined by growth of ice. To determine the range of ice thickness that might be expected in Mackenzie Delta lakes, and the factors to which ice-growth may be sensitive, a simple ice-growth model based on a modified Stefan's equation (Woo and Heron, 1989) was used to calcultate the rate of ice growth (dh_i/dt):

$$[3] \qquad dh_i/dt = \frac{(T_w - T_s)}{(\rho_i\ L_f)} \quad [h_i/k_i + h_s/k_s]^{-1}$$

where T_w is the freezing point of water (0°C), T_s is the surface temperature of the snow, ρ_i is the ice density (910 $kg{\cdot}m^{-3}$), L_f is the latent heat of fusion (335,000 $J{\cdot}kg^{-1}$), k_i is the thermal conductivity of ice (2 $W{\cdot}m^{-1}{\cdot}°C^{-1}$), k_s is the thermal conductivity of snow as a function of snow density (Woo and Heron, 1989), h_s is the snow thickness, and h_i is the ice thickness.

Test calculations demonstrate that the model accurately predicts both the rate of ice growth over the winter and the maximum ice thickness. For example, Figure 2 shows simulated ice thickness and measured ice thickness for both Shell Lake (near Inuvik) for 1982/83 (Sherstone, 1984) and NRC Lake for 1986/87. The mean winter temperatures for these two years was -22.0°C and -18.9°C, while the 30-year mean is -19.3°C. The input data used for these simulations included the depth of snow on the lake ice on day i (h_{si}), calculated as:

$$[4] \qquad h_{si} = \Sigma P_{si} \, D_M / P_T$$

where ΣP_{si} is the cumulative AES daily snowfall up to day i, P_T is the total AES winter snowfall, and D_M is the snow depth on the lake at the end of winter. The density of this snow was assumed to follow the seasonal pattern described by Williams (1957), with densities varying from 221 $kg \cdot m^{-3}$ at the beginning of winter to 259 $kg \cdot m^{-3}$ at the end of winter. The snow surface temperature (T_s in Equation 3) was estimated from the AES mean daily air temperature multiplied by a coefficient of 0.67, which was determined empirically from the Shell Lake data and was then also used for NRC Lake.

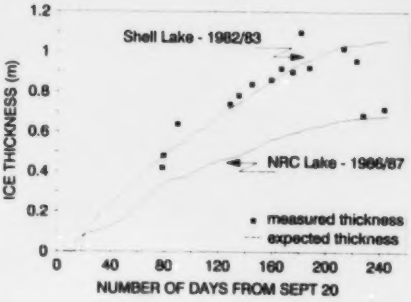

Figure 2. Comparison of ice thickness measurements on NRC Lake (1986/87) and Shell Lake (1982/83), and the thickness expected during the course of the winter as predicted by the ice-growth model.

Table 4. Effect of variation in snow depth on the maximum ice thickness predicted by the ice-growth model.

Maximum Snow Depth (m)	Maximum Ice Thickness (m)
0.25	1.16
0.30	0.97
0.40	0.90
0.50	0.78
0.60	0.69

The sensitivity of the maximum ice thickness to both air temperature and snow depth was tested by varying both variables over the ranges expected due to natural variability and potential climate change. Using the 1986/87 air temperatures and the range of snow depths typically found on delta lakes (0.25 to 0.6 m) gives maximum ice thicknesses of between 1.2 and 0.7 m (Table 4). This range of values is similar to, but slightly higher than, those previously reported for delta lakes (Sherstone, 1984; McCourt, 1985). Variations in air temperature produce, approximately, a 0.035-m change in ice thickness per 1°C change in air temperature. Using the 1986/87 case for NRC Lake as an example, a +6°C change in mean winter temperature would result in a maximum ice thickness of 0.48 m, whereas a -6°C difference in temperature would result in an ice thickness of 0.90 m (cf. measured ice thickness in NRC Lake of 0.7 m during 1986/87).

These calculations demonstrate that despite the cold arctic temperatures, growth of the relatively-shallow ice cover typically observed on NRC Lake can be accounted for, without incorporating a bed heat-flux term, by heat loss to the atmosphere via conduction. The most important contributing factors appear to be the depth of the snowcover, and sufficient shelter from the wind to allow the snowcover to remain in place over the course of the winter. This implies that lakes of large area should grow thicker ice covers than small lakes.

Implications for Mackenzie Delta Lakes

Combining the above information about the importance of the floating ice cover in preventing the water column from mixing, the processes controlling water density, the expected range of ice thicknesses, and the frequency and duration of flooding in the delta lakes (from Marsh and Hey, 1989), it is possible to generalize from NRC Lake to a broader range of lakes. Marsh and Hey concluded that about 2/3 of the lakes in the central Delta flood each year for 14 to 150 days, while the remaining 1/3 flood every 1 to 4 years of 14 days or less. During the 1989 period of observation, 11 days were required to remove the ice cover and expose NRC Lake to the wind. Since the frequency with which NRC Lake is flooded is transitional between these two classes, it is expected that about 2/3 of the lakes should be exposed to the wind for sufficient time to mix and flush. We do not expect the remaining 1/3 to completely flush whenever they are flooded.

Among the 1/3 lakes with short exposure to the wind, it is possible that in those where ice growth is less, or which are deeper or larger than NRC Lake, the density increase of the unfrozen lake water, from solute exclusion during ice-growth and solute-remobilization processes, might be insufficient to maintain a stratified water column throughout the flood period. Mixing could occur while the ice cover is present if the initial difference in density between the two layers had a water-column stability of about 200 ergs·cm^{-2}. For this to occur, it is estimated that the increase in relative water density, caused by some combination of water-volume reduction and solute accumulation beneath the ice cover, would need to be restricted to a factor of about two (compared to 4.3 measured in NRC Lake). In the case of NRC Lake, the depth of the ice cover would need to be reduced to 35 cm to accomplish this. Given the variability in the ice depths observed at NRC Lake (range of 0.61 to 0.82 m during 1983-87) and those obtained by simulating different air temperatures and snow depths with the ice-growth model, this is implausible.

Predicting an alternate lake geometry, where the growth of 70 cm of ice would not concentrate the solutes sufficiently to prevent the two layers of water from mixing, is more difficult. The density of the water that remains unfrozen by the end of the winter is not a direct function of the reduction in lake water volume, but is also influenced by an apparent net gain of solutes derived from the balance of remobilization and loss processes. If the area of the lake is re-scaled without changing the maximum depth and the net gains and losses of solutes over the winter are assumed to be equivalent per unit surface area as in NRC Lake, the lake cannot be made sufficiently large to limit the relative density increase of the bottom water to a factor of two, with the ice thickness remaining at 70 cm. As the area approaches a large size, the lake takes on the shape of a wafer and the change in volume becomes a direct function of depth. The increase in the relative density of bottom water approaches, roughly, a factor of three.

If the depth of the lake is proportionally increased while the area of the lake is held constant, the net gain of solutes beneath the ice cover becomes uncertain. An implication of making the lake deeper is that it probably would have less potential for macrophyte growth, and hence the potential gains and losses of solutes as a result of macrophyte decomposition could be significantly less per unit area of the lake. Basing the relative increase in water density directly on the reduction of water volume as a result of 70 cm of ice growth, the lake would need to be 2.6-m deep to reduce the increase in solute concentration of the bottom water to a factor of two (Figure 3). If the gains and losses of solutes beneath the ice are assumed to be equivalent to the rates per unit surface area in NRC Lake, the lake would need to be 3.5-m deep (corresponding to a reduction in water volume by a factor of 1.6).

If both the depth and area of the lake are changed at the same time, the uncertainty associated with the effectiveness of wind exposure on snow depth and consequent ice growth is probably a more important process than lake geometry *per se*, because the assumption of 70 cm of ice growth becomes unrealistic. Increasing the area of the lake would probably increase the depth of ice growth (cf. depth of ice for Shell Lake; Figure 2). As discussed earlier, ice growth is quite sensitive to the depth of the snowcover on the ice surface. Larger lakes are subject to greater wind-transport effects, which tend to move the snow from the centre of the lake to the edges. Lower snow depths in the middle of the lake provide less insulation and the

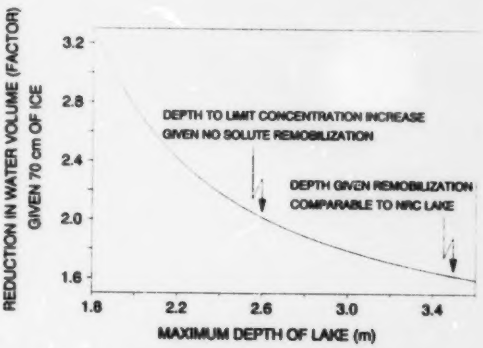

Figure 3. Reduction in the volume of unfrozen water over the winter, given 70 cm of ice, for a hypothetical lake comparable in area to NRC Lake versus the maximum depth of the lake. Also shown are the maximum depths that would be required to limit the increase in solute concentration to a factor of two: first, assuming no solute remobilization during the winter, and second, assuming remobilization rates comparable to NRC Lake.

potential for increased ice growth. The model shows that ice growth can easily range from 70 to 120 cm, depending on the effectiveness of the snowcover-insulation properties (depth and density). Hence, effectiveness of wind exposure is probably a critical limitation to predicting how increasing the surface area of the lake would effect the propensity of the water column to mix during spring flooding.

CONCLUSIONS

Differences in density between the invading flood water and the water in NRC Lake are sufficient to maintain a two-layer water-column structure during the period that floating ice cover was present. Despite the relatively large density differences, compared to density differences commonly encountered in holomictic lakes, the lake is sufficiently shallow that stability values are low and should be readily mixed by exposure to significant wind. Moreover, assuming similar rates of ice growth and solute accumulation beneath the ice, we are unable to envision how alteration of the area or depth of the lake could lead to sufficiently strong stability that the lake could not be readily mixed by normal winds. Hence, the presence of a floating ice cover to shield the lake from wind during the period of flooding appears to be critical to whether the flood will flush and initialize the lake with river water, or will simply remove the ice and leave the solutes from the previous year in the lake. We infer that virtually all lakes which remain flooded for significantly longer duration than NRC Lake (about 2/3 of the lakes in the central portion of the delta) should mix with the flood water and flush.

Of the remaining 1/3 of the lakes, which flood for a duration comparable to NRC Lake or shorter (flooding does not necessarily occur every year in these lakes), it seems probable that many do not mix with the flood water and flush on every occasion that they are flooded. It seems possible, however, that certain types of lake geometries could lead to sufficiently-low water-column stabilities. As a result, mixing could occur beneath the ice cover from the shear forces associated with the inflowing and then outflowing flood water. In addition, erosion of the stability could occur during the period of flooding from addition of solar radiation and heat from the imported flood water. To obtain sufficiently-low stabilities, it is estimated that the relative increase in water density, caused by some combination of water-volume reduction and solute accumulation beneath the ice cover, would need to be restricted to a factor of about two (compared to 4.3 measured in NRC Lake). It is implausible that the ice cover could be sufficiently thin in any delta lake with geometry comparable to NRC Lake to accomplish this. Moreover, a lake of comparable depth cannot be increased in area sufficiently to accomplish this. However, lakes comparable in area to NRC Lake, with a maximum depth of 2.6 to 3.5 m, could maintain sufficiently-low water-column stability that mixing could occur beneath the ice cover during the period of flooding.

ACKNOWLEDGEMENTS

We appreciate the assistance provided by Mary Ferguson and Cory Anema, and the laboratory measurements performed by the analytical unit of the Freshwater Institute. We acknowledge generous logistical support from the Polar Continental Shelf Project, Department of Energy, Mines, and Resources, and the Inuvik Scientific Resource Centre, Department of Indian and Northern Affairs. Financial support was received from the Northern Oil and Gas Action Program (NOGAP) through the Department of Fisheries and Oceans. Our analysis benefitted from the comments of B.C. Kenney, S. MacIntyre, and two anonymous reviewers.

LIST OF SYMBOLS

A_0	surface area of the lake (cm^2)
A_z	the area at depth z (cm^2)
D_M	snow depth on the lake at the end of winter (m)
g	acceleration of gravity ($cm \cdot s^{-2}$)
h_i	ice thickness (m)
h_s	snow thickness (m)
h_{si}	depth of snow on lake ice (m)
k_i	thermal conductivity of ice (2 $W \cdot m^{-1} \cdot {}^{\circ}C^{-1}$)
k_s	thermal conductivity of snow ($W \cdot m^{-1} \cdot {}^{\circ}C^{-1}$)
L_f	latent heat of fusion of ice (335,000 $J \cdot kg^{-1}$)
M	mean equivalent weight of salts in the solution ($g \cdot equivalent^{-1}$)
N	equivalent molarity or normality of the solution ($equivalents \cdot L^{-1}$)
P_{si}	AES daily snowfall up to day i (m)
P_T	total AES winter snowfall (m)
S	stability of the lake ($ergs \cdot cm^{-2}$)
t	time (s)
T_w	freezing point of water (0°C)
T_s	surface temperature of the snow (°C)
z	depth, with subscripts pu, 0, and m respectively denoting the depth at which the mean density occurs within the stratified water column, the surface, and the maximum depth (cm)
ρ	density of the solution ($g \cdot cm^{-3}$)
ρ_i	ice density (910 $kg \cdot m^{-3}$)
ρ_o	density of pure water ($g \cdot cm^{-3}$)
ρ_u	mean density of the lake ($g \cdot cm^{-3}$)
ρ_z	density at a given depth ($g \cdot cm^{-3}$)
ϕ_v	apparent equivalent volume of the mixture of salts ($mL \cdot equivalent^{-1}$)

REFERENCES

ANEMA, C., R.E. HECKY, E.J. FEE, D. NERNBERG and S.J. GUILDFORD, 1990. Water chemistry of some lakes and channels in the Mackenzie Delta and on the Tuktoyaktuk

Peninsula, N.W.T., 1985. Canadian Data Report of Fisheries and Aquatic Sciences No.726, Fisheries and Oceans Canada, 80 pp.

BERGMANN, M.A. and H.E. WELCH, 1985. Spring meltwater mixing in small arctic lakes. Canadian Journal of Fisheries and Aquatic Sciences, 42(11), 1789-1798

BRUNSKILL, G.J., S.D. LUDLAM and W.H. DIMENT, 1968. A comparative study of meromixis. Verhandlungen, Internationale Vereinigung für Theoretische und Angewandte Limnologie, 17(1), 137-139

BURNS, B.M., 1973. The climate of the Mackenzie Valley-Beaufort Sea: Vol.I. Climatological Studies No.24, Atmospheric Environment Service, Environment Canada, Downsview, Ontario, 227 pp.

CANADA, FISHERIES AND ENVIRONMENT, 1978. Hydrological atlas of Canada. Ministry of Supply and Services, Ottawa, Ontario, 78 pp.

COLE, G.A., M.C. WHITESIDE and R.J. BROWN, 1967. Unusual monomixis in two saline Arizona ponds. Limnology and Oceanography, 12(4), 584-591

GARRELS, R.M. and C.L. CHRIST, 1965. Solutions, minerals, and equilibria. Harper's Geoscience Series, Harper and Row, New York, N.Y., 450 pp.

GOLDMAN, C.R., D.T. MASON and J.E. HOBBIE, 1967. Two antarctic desert lakes. Limnology and Oceanography, 12(2), 295-310

GRAN, G., 1950. Determination of the equilivalent point in potentionmetric titrations. Acta Chemica Scandinavica, 4(1), 559-577

GRAN, G., 1952. Determination of the equilivalent point in potentionmetric titrations: Part 2. The Analyst, Vol.77, 661-671

HUTCHINSON, G.E., 1957. A treatise on limnology. Vol.1: Geography, physics, and chemistry. John Wiley and Sons, New York, N.Y., 1015 pp.

IDSO, S.B., 1973. On the concept of lake stability. Limnology and Oceanography, 18(4), 681-683

JOHNSTON, G.H. and R.J.E. BROWN, 1964. Some observations on permafrost distribution at a lake in the Mackenzie Delta, N.W.T., Canada. Arctic, 17(3), 162-175

JOHNSTON, G.H. and R.J.E. BROWN, 1966. Occurrence of permafrost at an arctic lake. Nature, 211(5052), 952-953

JUNK, W.J., P.B. BAYLEY and R.E. SPARKS, 1989. The flood pulse concept in river-floodplain systems. In - Proceedings of the International Large River Symposium (LARS), D.P. Dodge (Editor), Canadian Special Publication of Fisheries and Aquatic Sciences No.106, Fisheries and Oceans Canada, 110-127

MacINTYRE, S. and J.M. MELACK, 1982. Meromixis in an equatorial African soda lake. Limnology and Oceanography, 27(4), 595-609

MARSH, P. and S.C. BIGRAS. 1988. Evaporation from Mackenzie Delta lakes, N.W.T., Canada. Arctic and Alpine Research, 20(2), 220-229

MARSH, P. and M. HEY. 1989. The flooding hydrology of Mackenzie Delta lakes near Inuvik, N.W.T., Canada. Arctic, 42(1), 41-49

McCOURT MANAGEMENT LIMITED. 1985. Studies on muskrat ecology in the Mackenzie Delta, 1983-1984. Report by McCourt Management Limited for Environmental and Socio-Economic Services, B.C. Hydro, Vancouver, B.C., 65 pp.

MILLERO, F.J., 1972. The partial molal volumes of electrolytes in aqueous solutions. In - Water and Aqueous Solutions: Structure, Thermodynamics, and Transport Processes, R.A. Horne (Editor), Wiley-Interscience, John Wiley and Sons Inc., Toronto, Ontario, 519-564

MILLERO, F.J., D. LAWSON and A. GONZALEZ. 1976. The density of artificial river and estuarine waters. Journal of Geophysical Research, 81(6), 1177-1179

SCHINDLER, D.W., H.E. WELCH, J. KALFF, G.J. BRUNSKILL and N. KRITSCH. 1974. Physical and chemical limnology of Char Lake, Cornwallis Island (75°N lat.). Journal of the Fisheries Research Board of Canada, 31(5), 585-607

SHERSTONE, D.A., 1984. Ice thickness in the Mackenzie Delta, winter 1982-83: data obtained from hot-wire gauge systems. Report No.84-1, Inuvik Scientific Resource Centre, Department of Indian and Northern Affairs, Inuvik, N.W.T., February, 16 pp.

STAINTON, M.P., M.J. CAPEL and F.A.J. ARMSTRONG. 1977. The chemical analysis of freshwater. Canadian Fisheries and Marine Service Miscellaneous Special Publication No.25, Fisheries and Oceans Canada, 180 pp.

STAUFFER, R.E., 1980. Windpower time series above a temperate lake. Limnology and Oceanography, 25(3), 513-528

WELCH, H.E. and J.A. LEGAULT, 1986. Precipitation chemistry and chemical limnology of fertilized and natural lakes at Saqvaqjuac, N.W.T. Canadian Journal of Fisheries and Aquatic Sciences, 43(6), 1104-1134

WILLIAMS, G.P., 1957. An analysis of snow cover characteristics at Aklavik and Resolute, Northwest Territories. Research Paper No.40, Division of Building Research, National Research Council of Canada, Ottawa, Ontario, September, 12 pp.

WOO, M.-K. and R. HERON, 1989. Freeze-up and break-up of ice cover on small arctic lakes. In - Northern Lakes and Rivers, W.C. Mackay (Editor), Occasional Publication No.22, Boreal Institute for Northern Studies, University of Alberta, Edmonton, Alberta, 56-62

WU, J., 1969. Wind stress and surface roughness at air-sea interface. Journal of Geophysical Research, 74(2), 444-455

HYDROLOGICAL PROCESSES IN A SMALL CATCHMENT CONTAINING A PERENNIAL SNOWBANK, MELVILLE ISLAND, N.W.T.

A.G. Lewkowicz[1] and K.L. Young[2]

[1]Department of Geography
Erindale College
University of Toronto
Mississauga, Ontario
L5L 1C6 CANADA

[2]Department of Geography
McMaster University
Hamilton, Ontario
L8S 4K4 CANADA

ABSTRACT

The hydrological processes operating in a catchment containing a perennial snowbank and underlain by permafrost were examined in the summer of 1986. The major source in the basin water balance was snowbank melt and the major sink, surface run-off. Both of these exceeded 500 mm, making the flux of water through the basin more than double that of typical basins within the central Canadian Archipelago. This extreme effect resulted from a perennial snow cover of 32% of the basin area, but modelling suggests that covers as low as 5% will significantly enhance mean annual run-off.

The discharge record exhibited the characteristics of a proglacial rather than an arctic-nival regime since a diurnal cycle existed throughout the summer, snowbank melt succeeded basin-wide snowmelt, peak discharge occurred in mid-summer, and daily discharge peaks at the end of the season regularly exceeded those at the beginning. Run-off hydrographs changed in shape and timing over the summer, becoming more sharply peaked with steeper recessions and exhibiting shorter lag times as the snowbank thinned. Run-off coefficients during precipitation events were similar to the percentage of the basin kept near saturation by continuous outflow from the snowbank, indicating the applicability of the partial-area theory of run-off generation to this type of catchment.

INTRODUCTION

Research into catchment hydrology in the permafrost regions of North America has focused on large rivers and on basins with streams exhibiting nival regimes. There has been less investigation of glacierized basins or those possessing perennial snow. The results of a study undertaken in the Eidsbotn Fiord area of Ellesmere Island (Marsh and Woo, 1981), however, suggest that basins containing significant amounts of late-lying and perennial snow may exhibit the characteristics of proglacial rather than nival run-off regimes (see Church, 1974). The mid-summer recession of typical nival streams is absent and hydrographs after this time continue to show strong diurnal fluctuations as snowmelt augments precipitation and water released by active-layer thaw.

This paper adds to the literature concerning the effects of perennial snow on streamflow in a permafrost area. It examines the summer hydrology of a small high-arctic catchment (0.08 km^2) that contains a perennial snowbank. Results of work on the energy balance and hydrology of the snowbank have been published elsewhere (Lewkowicz and Young, 1990; Young and Lewkowicz, 1990). The objectives of this paper are to describe (a) the water balance of the basin, (b) the streamflow regime, and (c) the characteristics of the discharge hydrographs.

STUDY AREA

Fieldwork was carried out at the study catchment located 3 km northwest of Ross Point, Melville Island, N.W.T. (74°57'N, 107°19'W) between June 18 and August 12, 1986. The catchment extends from an elevation of about 1 m at its outlet, to an altitude of 45 m on the plateau upslope of the perennial snowbank (Figure 1). The south-facing snowbank traverses the basin at a distance of 800 m from the coast and is nearly 1000-m long, 150-m wide and up to 10-m deep at the end of winter. About 20% of the snowbank lies within the catchment (see Figure 1). Permafrost is thick and continuous within the area and the active layer is usually <0.5 m in depth.

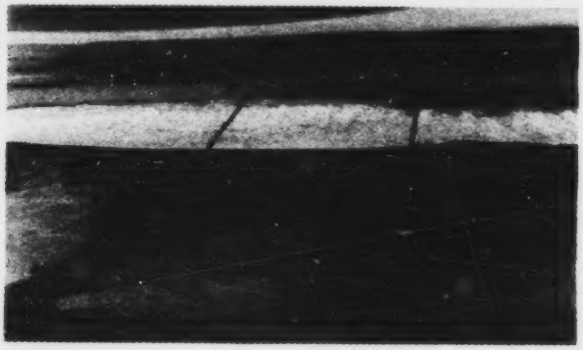

Figure 1. Oblique aerial photograph of the study catchment taken July 7, 1986. Note the contrast between the light-toned, unsaturated raised-beach deposits in the foreground and the dark, saturated colluvium downslope of the snowbank. The watershed boundary is shown as a solid line; lysimeter locations and the stilling-well are marked by circles and a square respectively.

The basin is underlain by Griper Bay Sandstone of Devonian age (Tozer and Thorsteinsson,

1964) but no bedrock exposures are present and the entire site is below the marine limit (Barnett *et al.*, 1977). Surficial deposits include coarse raised beach deposits near the present coast and fine-grained colluvium in the vicinity of the snowbank. In summer, the catchment can be divided into four main hydrological units (Figure 2): (1) snowbank, (2) unsaturated colluvium, (3) saturated colluvium, and (4) unsaturated raised-beach sands and gravels. The areal extent of these units changes through the summer as the snowbank ablates and its margins retreat inwards (Figure 3).

Climatic data for Melville Island are limited to a 16-year record from Rea Point on the east coast. Air temperatures are very low in winter and mean values exceed 0°C for only 3 months during the summer (Table 1). Winter precipitation amounts are small, even allowing for significant underestimation by the weather station (e.g., Woo *et al.*, 1983a). The deep accumulation at the perennial snowbank site is caused by prevailing winter winds from the north and northwest (Canada, Environment Canada, 1982c).

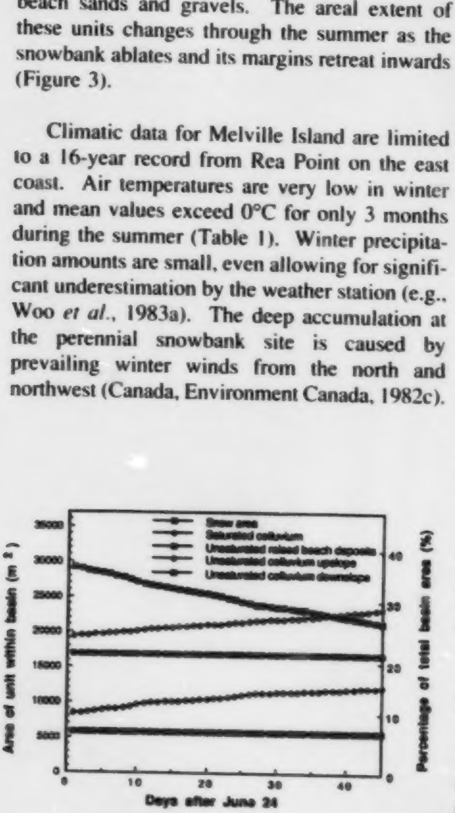

Figure 3. Change in the areal extent of hydrological units during 1986. Note: total basin area is 79,700 m².

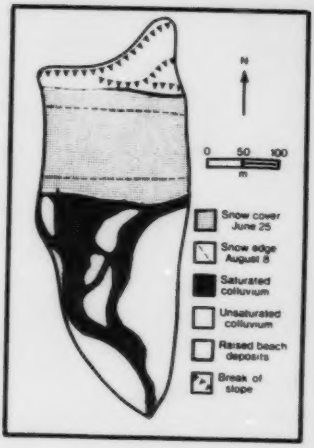

Figure 2. Map of the study catchment illustrating hydrological units.

The mean July temperature at the Ross Point basin in 1986 was 2.3°C and precipitation totalled 27 mm. When compared to the long-term values for Rea Point, these data suggest that the summer of 1986 was colder and wetter than average.

THEORY AND METHODS

After the snow has ripened, the water balance of a basin containing a perennial snowbank can be stated as:

[1] $P+M+V+E+R+\Delta BI+\Delta S=0$

where: P = precipitation, M = snow ablation, V = snow surface

Table 1. Climate of Rea Point and Ross Point, Melville Island.

	J	F	M	A	M	J	J	A	S	O	N	D	Y
Mean Air Temperature (°C)													
Rea Point[a]	-33.0	-34.6	-32.1	-24.0	-10.8	0.3	4.0	1.5	-5.3	-16.7	-25.9	-30.2	-17.2
Ross Point[b]							2.3						
Mean Monthly Precipitation (mm)													
Rea Point[a]	1.4	0.3	1.4	0.9	3.0	3.2	9.2	15.2	6.3	7.6	2.1	1.6	52.2
Ross Point[b]							26.9						

[a] 1969 to 1985, derived from Canada (Environment Canada 1982a; 1982b) for 1969 to 1980 and AES station records for 1981 to 1985.
[b] 1986 from site records.

vapour exchange (negative for evaporation or upward sublimation; positive for condensation or downward sublimation), E = evapotranspiration from the ground surface, R = surface run-off, ΔBI = increase in basal ice storage; and, ΔS = change in storage within the active layer. The experimental design sought to measure or estimate all the variables in Equation 1 except change in active-layer storage (ΔS) which was left as a residual.

Precipitation was measured using a Weathermeasure tipping-bucket rain-gauge to a precision of 0.25 mm. The gauge was located at the foot of the snowbank 100 m west of the edge of the basin.

Snow ablation was obtained from a daily theodolite survey of a snow course consisting of 25 to 30 points located 100 m to the west of the basin, combined with density measurements made using a Mt. Rose snow sampler. Details of the equipment and procedures used are given in Lewkowicz and Young (1990).

Vapour exchange at the snow surface was derived from measurements of the latent heat flux made at three meteorological towers spaced up the snowbank (see Young and Lewkowicz, 1990).

Evapotranspiration was measured from July 3 onwards with four pairs of small lysimeters (98 mm in diameter, 138 mm in depth) located adjacent to the basin (see Figure 1). The lysimeters were filled with undisturbed soil cores, including live plants where the terrain was vegetated. Each pair of lysimeters was treated as being representative of one of the four ground surfaces in the basin (see Figure 3). Lysimeters were weighed daily using a triple-beam balance to a precision of 0.1 g and are believed accurate to ±5% (see Marsh *et al.*, 1981). After weighing, those lysimeters representing saturated terrain received an amount of water equal to that lost over the previous 24 h. Those representing unsaturated areas were left to dry out. Between June 25 and July 2, evapotranspiration was estimated using daily surface-energy data from the snowbank. An empirical logarithmic relationship between the

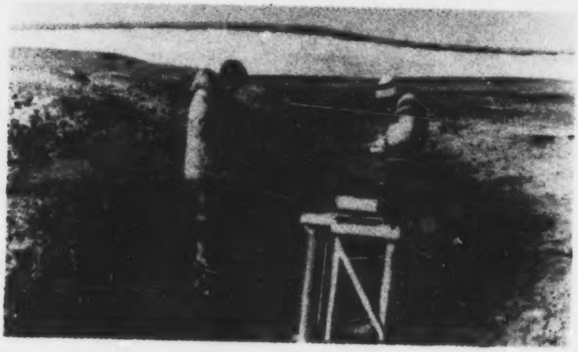

Figure 4. Photograph of the small stream draining the basin at the location of the stilling-well and water-level recorder. Note the Ott pigmy current meter being used to measure stream velocities at 5 cm intervals across the channel.

energy received over the snow and the evapotranspiration loss over the catchment for the remainder of the summer (rain days excepted) yielded an r^2 value of 0.46 (n=21) and an estimated cumulative loss of 8 mm over the 8-day period.

Surface run-off was monitored at the outlet of the basin in an unmodified sandy channel (Figure 4). A Leupold-Stevens Type-F water-level recorder mounted on a stilling well provided a continuous stage record. The velocity-area technique was used to measure discharge and a stage-discharge curve was created. In addition, outflow at the base of the snowbank was measured periodically during the season using portable flumes at a 20-m wide experimental snow plot located 50-m west of the drainage basin (see Young and Lewkowicz, 1988).

Excavation of the snowbank at the end of summer showed that at least 0.5 m of basal ice had developed in the middle of the snowbank and 0.7 m in its lower section over a period of 45 days. Less basal ice appears to have grown in the upslope area of the snowbank, probably due to drainage down the steeper slope (see Wakahama *et al.*, 1976). These observations indicate that a significant amount of water was stored as basal ice and they can be compared with model predictions (using somewhat warmer ground temperatures and a more conductive substrate) of 0.42 m of basal ice growth over 45 days (Marsh and Woo, 1984b). As an approximation, basal-ice growth in the perennial snowbank can be assumed to be between 1 to 2 times the rates predicted in Marsh and Woo (1984b). The volume of water stored in basal-ice growth at the study catchment was calculated from this range of rates, assuming a density for the snow grains and irreducible water of 550 $kg{\cdot}m^{-3}$, a basal ice density of 880 $kg{\cdot}m^{-3}$ (Marsh and Woo, 1984a) and that growth took place over all the snowbank area except where the ice was exposed at the surface and ablation was occurring. Field observations showed that the area of the snowbank where basal ice was exposed increased through the summer from 4,500 m^2 on June 25 to 9,000 m^2 on August 8. Although water was lost from basal ice storage in these areas, this flux was included within M in Equation 1 and was not calculated separately.

RESULTS

Water Balance

The water balance of the basin over the summer is shown in Table 2. Comparative data (e.g., Table 1 in Church (1974) and Table 1 in Woo (1988)) suggest that the total water flux through the study basin is more than twice that of catchments in the central Canadian Archipelago containing mainly seasonal snow. It is similar to basins in the eastern Arctic which are highly glacierized or subject to heavy orographic precipitation.

Table 2. Drainage basin water balance, June 25 to August 8, 1986.

Precipitation[a] (mm)	31(+10 trace events)
Snow Ablation[a] (mm)	535
Snow Surface Vapour Exchange[b] (mm)	-6
Evapotranspiration[c] (mm)	-43
Surface Run-off[a] (mm)	-548
Growth of Basal-Ice Storage[d] (mm)	-66 to -133
Residual[e]	97 to 164

[a] *Measured;*

[b] *Calculated from energy-balance measurements (Young and Lewkowicz, 1990);*

[c] *Measured, except estimated for June 25 to July 2 (see text);*

[d] *Range of estimates produced using predictions of Marsh and Woo (1984b); and,*

[e] *Incorporates change in storage within the active layer and errors in assessment of other variables.*

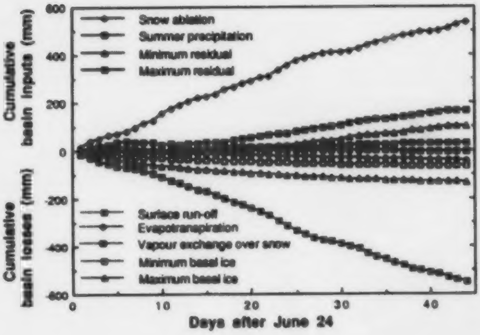

Figure 5. Cumulative daily water balance for the drainage basin. Data derived as shown in Table 2.

The most important elements of the water balance are snowmelt and surface run-off both of which exceed 500 mm. These are minimum values for the melt season since basin-wide snowmelt took place before monitoring began. Vapour exchange over the snow and evapotranspiration from the ground were relatively unimportant, while basal-ice growth appears to have been of greater significance.

The residual in the water balance, which includes change in active-layer storage and measurement errors, represents between 15 and 22% of the total inputs of water to the basin and is strongly influenced by the assumptions made about the rate of production of basal ice. Cumulative evaluation of the water balance on a daily basis (Figure 5) shows that assuming the minimum growth of basal ice, the residual starts to become strongly positive about 20 days after the start of the record (i.e., July 15). It is possible that some of the change in the residual is due to uni-directional error in the measurement of one or more variables. Snow-ablation and energy-balance measurements over the snow are in good agreement (Lewkowicz and Young, 1990), so the most likely source of error is overestimation of surface run-off, possibly resulting from changes in the cross-section at the gauging point due to the transport and deposition of sand on the bed. However, some portion of the residual may also be due to water released from storage within the active layer. The thaw front in vegetated terrain downslope from the snowbank reached a depth of 0.4 m by mid-July and may have been encountering ice lenses near the base of the active layer. Annual storage changes of up to 66 mm have been reported from Cornwallis Island (Woo *et al.*, 1983b) and, assuming the minimum growth of basal ice, the cumulative residual is of a similar order of magnitude.

Streamflow Regime

Surface run-off was continuous throughout the measurement period (Figure 6). The magnitude of stream discharge and its diurnal variation are mainly linked to energy received by the snowbank surface and hence to meltwater generation. Summer precipitation generated detectable run-off on five occasions (see below) but each event was of minor significance in comparison to the snowmelt which accompanied it.

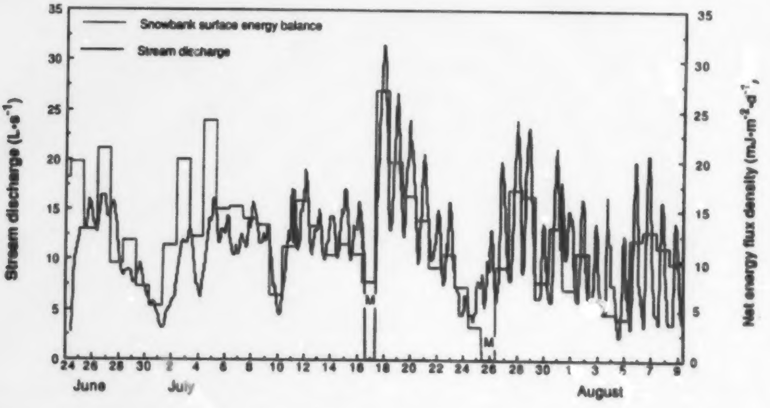

Figure 6. Stream discharges and daily energy-flux density over the snowbank (09:00-09:00 h, calculation/measurement period) in 1986. Note: M shows missing data due to instrument malfunction.

The streamflow record has four characteristics which make it similar to a proglacial rather than an arctic-nival regime (Church, 1974). First, discharge was continuous throughout the summer which is not usual for nival basins of this small size. Second, basin-wide snowmelt took place prior to the perennial snowbank becoming isothermal in a manner analogous to basin snowmelt preceeding glacier melt. Third, the peak instantaneous discharge occurred in mid-summer on July 17 when high radiation inputs to the snowbank were combined with large transfers of sensible and latent heat. In contrast, small nival rivers generally experience peak flow near the beginning of melt since the snow area rapidly declines during the melt season. Finally, peak daily discharges at the beginning of August regularly exceeded those in late-June and early-July in a manner similar to a glacierized basin (e.g., Church, 1974).

Discharge Hydrographs

Shape and Timing

In the first 36 h of the record, stream discharges increased rapidly without an equivalent change in energy transfers to the snow surface (see Figure 6). This increase is primarily attributed to a change in the area of the snowbank contributing meltwater. Temperature measurements show that snow near the upslope and downslope margins of the snowbank was isothermal to a depth of about 2 m on June 20 while the central part was isothermal to a depth of <1.5 m. Qualitative observations indicate that discharges increased from June 22 onwards as deeper snow became isothermal and consequently the area of isothermal snow contiguous with the downslope edge increased in size. Some of this run-off may also have been caused by finger flow within colder snow (e.g., Marsh and Woo, 1984a). Substantial drainage of isothermal snow near the upslope margin of the snowbank, however, was probably restricted by the cold central core where snow >3 m deep remained sub-zero (e.g., -14°C at a depth of 4.5 m on June 24) until June 25. A dye experiment carried out on the afternoon of June 24 lends support to this hypothesis. Rhodamine dye poured onto the snow surface of the lower part of the snowbank emerged at the downslope edge after 5 to 12 h. Dye injected onto the central and upslope parts, however, did not emerge until 35 h later on the morning of June 26. It appears, therefore that warming of the central part of the snowbank to 0°C on June 25 allowed the gradual drainage of the upslope part of the snowbank and resulted in the rise of the stream hydrograph.

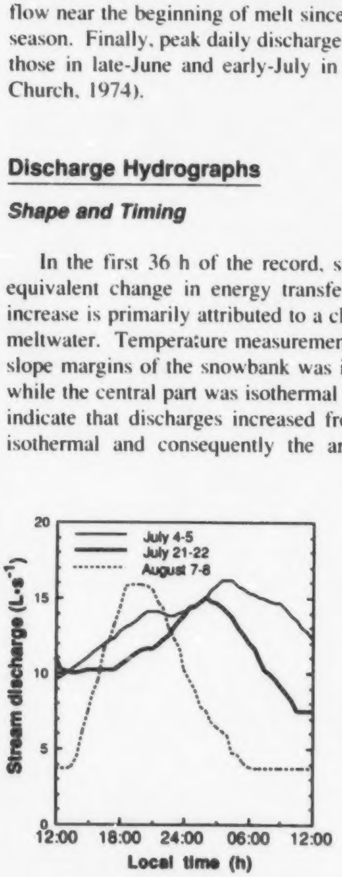

Figure 7. Comparison of three stream-flow hydrographs with similar peak discharges.

From June 26 onwards, the snowbank was isothermal and diurnal cycles of discharge prevailed. There is a clear relationship between the magnitude of the energy received at the snow surface and the amount of surface run-off (e.g., July 18 to 24, Figure 6). Daily discharge peaks were initially broad or plateau-like, and recessions were relatively slow. On some days, diurnal cycles were replaced by gradual rises or falls in discharge in reponse to changes in weather conditions (e.g., June 30 to July 2). As the season progressed and the snowbank declined in thickness, rising and falling limbs steepened and hydrographs of similar size became more sharply peaked (Figure 7). In contrast, outflow hydrographs collected at the experimental snow plot retained plateau-like characteristics throughout the summer (Figure 8). The plateau is attributed to the greater depths of snow at the experimental plot and the spatial heterogeneity of depths, while much of the eastern part of the snowbank draining to the gauging site was thinner and more uniform in thickness. At the beginning of August, a large part of this section appeared as an expanse of ablating basal ice. The more peaked appearance of the stream hydrographs, suggests that melt waves produced simultaneously at the snow surface arrived close together at the basin outlet.

A further indication of the effect of gradual snow ablation on hydrograph shape is obtained by comparing peak-to-trough discharge ratios (Figure 9). These increased exponentially from average values of 1.2 at the beginning of the season to >4 at the end. This change was caused by a combination of steeper recessions and peaks which occurred progressively earlier in the day, allowing more time for recession to occur before the next day's rise (see Figure 7).

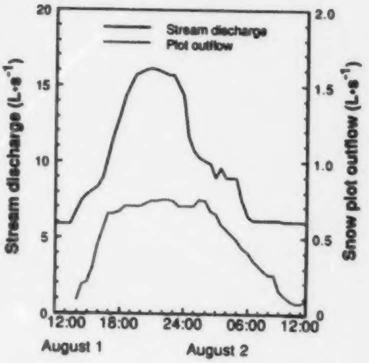

Figure 8. Comparison of stream discharge and outflow from the snowbank collected at the experimental snow plot, August 1 to 2, 1986. Note: Outflow was measured directly at the plot located 50-m west of edge of catchment (see Young and Lewkowicz, 1988).

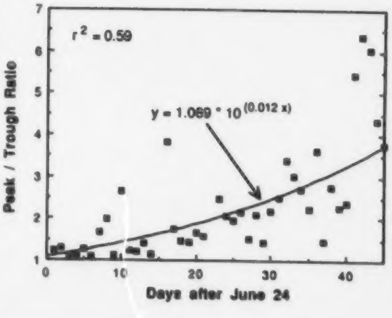

Figure 9. Daily ratio of peak-to-trough stream discharges, with best-fit exponential line.

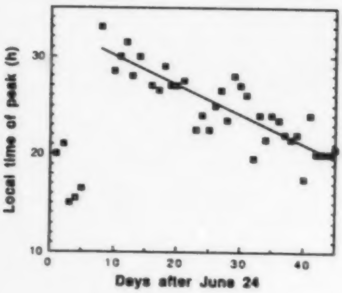

Figure 10. Time of peak stream discharge. Best-fit line applies only to dates after July 1 (Y = 30.85 - 0.29X; n = 37, r^2 = 0.74). Note: Hours >24 represent peaks which occurred in the early morning (i.e., 30 is 06:00 h); on days of steady discharge decline or rise, no peak developed.

Stream hydrographs can be divided into two groups in terms of their timing. Until July 1, peak flow took place prior to 21:00 h. After this date, peaks occurred in the early morning hours and arrived progressively sooner as the season advanced (Figure 10). A dye experiment conducted on June 29 at moderate flow showed that the transit time between the downslope snow edge and the stilling well was <0.5 h. Since peak energy input onto the snow surface generally occurred around 13:00 h (solar noon), the vast majority of the lag-to-peak run-off is due to vertical and horizontal flow within the snow.

One explanation for the relatively short lag times at the beginning of the season is that the effective permeability (McGurk and Kattelman, 1986) of the snowbank was high due to the continued existence of numerous ice layers within the snow. These could have concentrated and diverted flow (e.g., Marsh and Woo, 1985) leading to lower residence times within the snowbank. Alternatively, a large ice lens of low permeability located within the pack may have diverted most of the meltwater laterally. Once this ice layer increased in permeability the effective thickness of the pack would have increased rapidly, accounting for the sudden change in lag times.

From July 2 onwards, lag times appear to have been dominated by thinning of the snowbank, leading to an average decrease in the lag-to-peak of 17 min·d^{-1}. Since there was no corresponding change in the time-of-rise, the rising limbs of the snowmelt hydrographs became progressively steeper. A gradual decrease in the peak-to-peak lag has also been described for slope run-off from a seasonal snowbank (Lewkowicz and French, 1982). It would not normally be observed for streamflow since this usually integrates the discharges from a number of sources with different individual lags.

An estimate of the velocity of vertical flow in the snow on the rising limb of the hydrograph over the season can be derived by comparing the change in lag time after July 1 (11 h) with the decrease in snow thickness (3 m). Assuming no change in the snow permeability after this date, the mean vertical velocity was 0.08 mm·s^{-1}. This is two orders of magnitude less than downslope velocities of 1.5 to 2.6 mm·s^{-1} measured by dye tracing from the upslope to the downslope edge of the snowbank. Both sets of values are of the same orders of magnitude as results from a late-lying snowbank in central Banks Island (vertical velocity, 0.19 mm·s^{-1}, downslope velocity, 6.0 mm·s^{-1} (Lewkowicz, 1981)).

Effect of Rain

Most summer rainfall events were of low intensity and relatively short duration. In catchments without antecedent saturated areas, these storms would not have produced observable changes in stream discharge since rainfall intensities did not exceed infiltration capacities. However, five storms did produce rises in stream discharge that could be separated from "baseflow" produced by ablation of the snowbank (Figure 11). Run-off coefficients for these events ranged from 10 to 28% (Table 3).

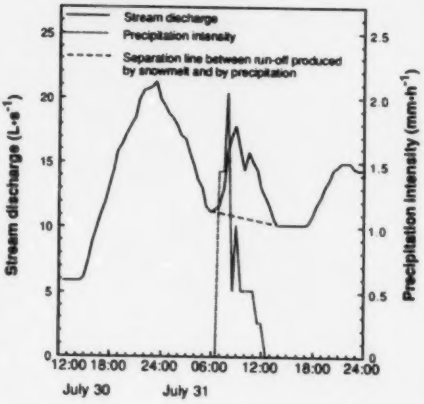

Figure 11. Response of stream discharge to summer rainfall, July 30 to 31, 1986. Note: The basin lag time is 1.0 to 1.5 h.

The maximum values of the run-off coefficients closely approximate the area of the catchment kept at or near saturation by continuous outflow from the snowbank. The lowest coefficient was produced during a snowfall and some of the snow was temporarily stored on the ground surface. In all the storm events, precipitation which fell on the snowbank itself apparently did not generate run-off immediately since it had to move vertically and horizontally through the snow in the same way as a normal melt-wave. The general accordance between the run-off coefficient and the percent saturated area suggests that the unsaturated parts of the catchment (see Figure 2) also did not generate run-off during these low-intensity events. It appears, therefore, that this catchment behaves in accordance with the theory of partial-area run-off generation. Source areas are contiguous with the stream channel and are kept saturated by surface and sub-surface flow from the melting snowbank upslope.

Table 3. Run-off response to summer precipitation events.

Date	Type	Duration (h)	Precipitation Amount (mm)	Run-off Amount (mm)	Run-off Coefficient (%)	Saturated Area (%)
7/7	Rain	3	1.8	0.4	20	26
10/7	Rain + Snow	17	8.4	2.3	28	26
25/7	Snow	3	2.0	0.2	10	27
31/7	Rain	6	4.6	1.1	25	28
3/8	Rain + Snow	3	3.6	0.7	19	29

DISCUSSION

It is interesting to consider the effect of basin size on the results. At Ross Point, the snowbank occupied 37% (29,200 m^2) of the basin at the start of monitoring and 27% (21,200 m^2) at the end. A simple empirical model based on the performance of this catchment can be devised in which the areas covered by perennial snow and those which are saturated remain constant while the basin area and the unsaturated zones are allowed to vary in size. Catchment totals of snow ablation, snow-surface vapour exchange and the growth of basal ice are directly proportional to the ratio of perennial snow to basin area while summer precipitation is held constant. Evapotranspiration is calculated from the proportions of the catchment that are saturated, unsaturated and under snow. The residual is calculated as a proportion of the surface run-off since it probably relates to errors in this variable. Surface run-off due to summer precipitation is derived using run-off coefficients based on the saturated proportion of the catchment. Run-off due to snow ablation is then calculated from the sum of the other variables.

The modelled effect of basin size on summer run-off is shown in Figure 12. The importance of perennial snow of fixed extent declines rapidly as the basin size increases. However, a snowbank with a mean summer area of 0.025 km^2 still produces >50 mm of surface run-off even in a basin of 0.6 km^2, an amount that should cause a measurable increase in the annual basin discharge. Although there is some enhancement of discharge in basins larger than this, it appears that a minimum summer perennial snowcover of about 5% is required before the annual basin run-off is greatly affected.

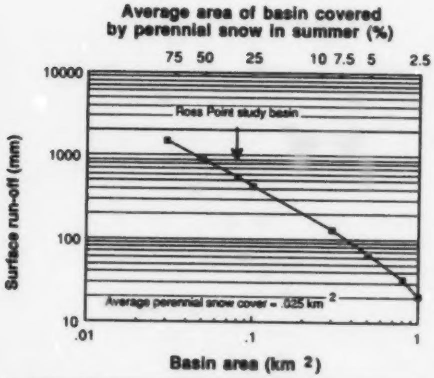

Figure 12. Modelled effect of basin area on summer surface run-off for catchments with an average perennial snowcover of 0.025 km^2.

CONCLUSIONS

First, the water balance of the basin studied was dominated by inputs of snowbank melt and by losses of surface run-off. Summer precipitation, evapotranspiration and the growth of basal ice were of lesser importance. The total flux of water through the catchment exceeded 550 mm, more than double the amount recorded within typical catchments of the central Canadian Archipelago that contain only seasonal snow.

Second, analysis of the streamflow record supports the observations of Marsh and Woo (1981) that a basin with a large percentage cover of late-lying or perennial snow develops a discharge regime with proglacial characteristics. In contrast to an arctic-nival regime, streamflow in the Ross Point catchment was continuous throughout the summer, snowbank melt succeeded basin-wide snowmelt, peak discharge occurred in mid-summer, and daily discharge peaks at the end of summer regularly exceeded those at the beginning of the season.

Third, the shape and timing of discharge hydrographs changed through the season as the snowbank gradually became thinner. Except for the first week when ice layers within the snow may have been diverting drainage, lag times between energy inputs and peak discharges diminished by an average of 17 $\text{min}\cdot\text{d}^{-1}$. In addition, peak discharges became more sharply defined, recession limbs became steeper and the ratio of peak-to-trough discharges increased exponentially. These effects are not normally observed in streamflow resulting from snowmelt because run-off sources are usually scattered spatially and possess heterogeneous orientations and depths.

Fourth, run-off coefficients during light summer precipitation events were <28% and apparently relate to the area of the catchment continuously saturated by outflow from the snowbank. These results indicate the applicability of partial-area theory to run-off generation in this high-arctic catchment.

Finally, the importance of perennial snowbanks is highly dependent on the percentage of the basin covered by these features. These results were obtained in a catchment with a mean perennial snowcover over the summer of 32%. While a decrease in the percentage snowcover causes a reduction in its effect on annual basin run-off, simple modelling suggests that discharges of small- to medium-sized basins should be detectably influenced by perennial snowcovers exceeding 5%.

ACKNOWLEDGEMENTS

This study was supported by the Natural Sciences and Engineering Research Council of Canada and by a Northern Scientific Training Grant, Department of Indian Affairs and Northern Development, Canada. Generous logistical support was provided through G.D. Hobson, Director, Polar Continental Shelf Project, Department of Energy, Mines and Resources, Canada. The authors are grateful for the excellent field assistance of S.I. Hamilton and for the suggestions made by the anonymous referees.

LIST OF SYMBOLS

E	evapotranspiration from the ground surface ($\text{mm}\cdot\text{d}^{-1}$)
M	snow ablation ($\text{mm}\cdot\text{d}^{-1}$)
P	precipitation ($\text{mm}\cdot\text{d}^{-1}$)
R	surface run-off ($\text{mm}\cdot\text{d}^{-1}$)

V	snow surface vapour exchange (negative for evaporation or upward sublimation, positive for condensation or downward sublimation) ($mm \cdot d^{-1}$)
ΔBI	increase in basal ice storage ($mm \cdot d^{-1}$)
ΔS	change in storage within the active layer ($mm \cdot d^{-1}$)

REFERENCES

BARNETT, D.M., S.A. EDLUND and L.A. DREDGE, 1977. Terrain characterization and evaluation: an example from eastern Melville Island. GSC Paper No.76-23, Geological Survey of Canada, Ottawa, Ontario, 18 pp.

CANADA, ENVIRONMENT CANADA, 1982a. Canadian climate normals, 1951-1980. Vol.2 - Temperature. Canadian Climate Program, Atmospheric Environment Service, Environment Canada, Downsview, Ontario, 306 pp.

CANADA, ENVIRONMENT CANADA, 1982b. Canadian climate normals, 1951-1980. Vol.3 - Precipitation. Canadian Climate Program, Atmospheric Environment Service, Environment Canada, Downsview, Ontario, 602 pp.

CANADA, ENVIRONMENT CANADA, 1982c. Canadian climate normals, 1951-1980. Vol.5 - Wind. Canadian Climate Program, Atmospheric Environment Service, Environment Canada, Downsview, Ontario, 283 pp.

CHURCH, M., 1974. Hydrology and permafrost with reference to northern North America. In - Permafrost Hydrology, Proceedings of Workshop Seminar 1974, Canadian National Committee for the International Hydrological Decade, Ottawa, Ontario, 7-20

LEWKOWICZ, A.G., 1981. A study of slopewash processes in the continuous permafrost zone, Banks Island, western Canadian Arctic. Ph.D. thesis, University of Ottawa, Ottawa, Ontario, 300 pp.

LEWKOWICZ, A.G. and H.M. FRENCH, 1982. The hydrology of small runoff plots in an area of continuous permafrost, Banks Island, N.W.T. In - The Roger J.E. Brown Memorial Volume, Proceedings of the Fourth Canadian Permafrost Conference, 2-6 March 1981, Calgary, Alberta, Associate Committee on Geotechnical Research, National Research Council of Canada, 151-162

LEWKOWICZ, A.G. and K.L. YOUNG, 1990. Hydrology of a perennial snowbank in the continuous permafrost zone, Melville Island, Canada. Geografiska Annaler, 72A(1), 13-21

MARSH, P., W.R. ROUSE and M.-K. WOO, 1981. Evaporation at a high arctic site. Journal of Applied Meteorology, 20(6), 713-716

MARSH, P. and M.-K. WOO, 1981. Snowmelt, glacier melt, and high arctic streamflow regimes. Canadian Journal of Earth Sciences, 18(8), 1380-1384

MARSH, P. and M.-K. WOO, 1984a. Wetting front advance and freezing of meltwater within a snow cover. 1. Observations in the Canadian Arctic. Water Resources Research, 20(12), 1853-1864

MARSH, P. and M.-K. WOO, 1984b. Wetting front advance and freezing of meltwater within a snow cover. 2. A simulation model. Water Resources Research, 20(12), 1865-1874

MARSH, P. and M.-K. WOO, 1985. Meltwater movement in natural heterogeneous snow covers. Water Resources Research, 21(11), 1710-1716

McGURK, B.J. and R.C. KATTLEMAN, 1986. Water flow rates, porosity and permeability in snowpacks in the central Sierra Nevada. Proceedings of the Symposium: Cold Regions Hydrology, D.L. Kane (Editor), 22-25 July 1986, Fairbanks, Alaska, American Water Resources Association Technical Publication Series No.TPS-86-1, Bethesda, Maryland, 359-366

TOZER, E.T. and R. THORSTEINSSON, 1964. Western Queen Elizabeth Islands, Arctic Archipelago. GSC Memoir No.332, Geological Survey of Canada, Ottawa, Ontario, 242 pp.

WAKAHAMA, G., D. KUROIWA, T. HASEMI and C.S. BENSON, 1976. Field observations and experimental and theoretical studies on the superimposed ice of McCall Glacier, Alaska. Proceedings, International Symposium on the Thermal Regime of Glaciers and Ice Sheets, Journal of Glaciology, 16(74), 135-149

WOO, M.-K., 1988. Problems of studying water balance in small high arctic basins. Proceedings, Canadian Hydrology Symposium No.17 - 1988, Canadian Research Basins: Successes, Failures and Future, CHS-88-SCH, 9-11 May 1988, Banff, Alberta, Associate Committee on Hydrology, National Research Council of Canada (NRCC No.30416), 245-254

WOO, M.K., R. HERON, P. MARSH and P. STEER, 1983a. Comparison of weather station snowfall with winter snow accumulation in high arctic basins. Atmosphere-Ocean, 21(3), 312-325

WOO, M.-K., P. MARSH and P. STEER, 1983b. Basin water balance in a continuous permafrost environment. Permafrost, Fourth International Conference, Proceedings, 17-22 July 1983, Fairbanks, Alaska, National Academy Press, Washington, D.C., 1407-1411

YOUNG, K.L. and A.G. LEWKOWICZ, 1988. Measurement of outflow from a snowbank with basal ice. Journal of Glaciology, 34(118), 358-362

YOUNG, K.L. and A.G. LEWKOWICZ, 1990. Surface energy balance of a perennial snowbank, Melville Island, Northwest Territories, Canada. Arctic and Alpine Research, 22(3), 290-301

ON MODELLING SURFACE MELTWATER DISCHARGE FROM ARCTIC AND ALPINE GLACIERS

D.S. Munro

Department of Geography
Erindale Campus
University of Toronto
Mississauga, Ontario
L5L 1C6 CANADA

ABSTRACT

An energy-balance model for glacierized basins has been developed in which the microclimate of the glacierized area of the basin interacts with that of the non-glacierized part through horizontal heat exchange. Given the distribution of the winter mass balance, the model proceeds to calculate the summer mass balance and consequent meltwater discharge from the glacier surface. Absorbed global radiation and net long-wave loss are the dominant energy controls upon meltwater production, so reduced run-off is the consequence of an increase in either the altitude or the latitude of the glacier. Because other energy-exchange terms are important as well, changes in the characteristics of the non-glacierized part of the basin, and climatic change, can be shown to affect melt rates.

INTRODUCTION

Recent attempts to relate glacier mass balances to climatic conditions have produced significant correlations with winter precipitation and summer temperature (Young, 1981; Letréguilly and Reynaud, 1989). The statistical approach also appears to be useful in estimating glacier run-off (Collins, 1989). Nevertheless, the explanatory power of the statistical approach is limited because it does not deal with the interplay among surface characteristics, energy exchange and the mass-balance components, such as mass loss due to melting ice and snow.

The limitation is probably more serious for hydrological work than it is for the mass balance, because mass exchange is evaluated for the glacier surface itself, while discharge is measured below the snout of the glacier. The glacier surface can be viewed much like a filter through which the effects of climatological forcing pass, though it is a variable filter because surface characteristics change with time. This introduces a form of variability into the climate-run-off relationship which can be dealt with by adopting a physical modelling approach.

The physical approach is well represented in micrometeorological studies of energy exchange at the glacier surface (Müller and Keeler, 1969; Föhn, 1973; Munro, 1990) which have been used to link energy exchange to local short-term run-off response for both ice and snow (Derikx, 1975; Price, 1977). The results of such point studies cannot readily be extrapolated to the entire surface of a glacier, but the information which they yield about surface processes can be used to model glacier mass balance (Oerlemans and Hoogendoorn, 1989). The hydrological aspect of such work, in the form of glacier surface-meltwater discharge, is pursued here by expanding a modelling approach earlier described by Oerlemans (1986).

MODEL STRUCTURE

Oerlemans (1986) investigated the question of glacier response to climate by constructing a simple two-surface scheme, such that the energy balance at the glacier surface would be sensitive to the conditions of its surroundings. The model is forced by radiative heating, which evokes temperature responses from the surfaces, and their boundary layers. When ice and snow reach the melting point, no further temperature increase is allowed, so the flux density of energy received at the surface (Q_s) is converted to the melt rate (M):

$$[1] \qquad M = Q_s/\rho_w L_f$$

where ρ_w is the density of water, and L_f is the latent heat of fusion.

According to energy-balance theory (Oke, 1987) the solar and atmospheric radiative-flux densities, K↓ and L↓, respectively, are the main heat sources for Q_s, while the surface temperature (T_s) controls variations in radiative and convective loss:

$$[2] \qquad Q_s = K{\downarrow}\,(1 - \alpha) + L{\downarrow} - \varepsilon_s\, \sigma\, T_s^4 - \frac{\rho\ c_p\, k^2\, u\, (T_s - T_a)}{[\ln\,(z/z_0)]^2}$$

where α is the short-wave reflection coefficient, ε_s the surface emissivity (taken to be unity), and σ is the Stefan-Boltzmann constant. The last group of terms in Equation 2 is the bulk formula for sensible-heat transfer in which ρ is the air density, c_p the specific heat of air at constant pressure, k von Kármán's constant, u the wind speed at height, z, above the surface, z_0 is the surface roughness length, and T_a the air temperature. Evaporation has been ignored because it is usually small over glaciers (Paterson, 1981), particularly for the case considered here (Munro, 1990). It is included in Q_s calculations for non-glacierized areas, however, using the equilibrium form of the Penman model (Monteith, 1973).

Equation 2 applies simultaneously to ice, snow, and land beyond the glacier margin, using α and z_0 values appropriate to each surface type (Figure 1). The temperature response over time (t) is then determined for each surface according to the force-restore scheme outlined in Deardorff (1978):

$$[3] \qquad \Delta T_s/\Delta t = 2\, Q_s/C_s d_s - 2\pi\ (T_g - T_s)/\tau_d$$

where T_g is the temperature of a sub-surface layer, C_s the volumetric heat capacity of the substrate, d_s the daily damping depth, and τ_d is the day length. Simple forcing

(Deardorff, 1978) of sub-surface temperature by Q_s is used for T_g, taking the annual damping depth to be 19 times d_s (Oke, 1987).

Although T_s can rise no higher than 0°C on the glacier, it does so in the non-glacierized part of the basin, thus contributing to melt through boundary-layer heating and heat advection across the glacier margin (Oerlemans, 1986):

$$[4] \qquad \Delta T_a/\Delta t = \frac{k^2\, u\, (T_s - T_a)}{h_b\, [\ln\, (z/z_0)]^2} + K_h\, (T_{a,n} - T_{a,g})/A$$

in which h_b is boundary-layer thickness, K_h an advective heat-exchange coefficient (Oerlemans, 1986), and A is the area of either the glacierized or the non-glacierized part of the basin, denoted by their respective subscripts, g and n. Thus, the effect of advection upon Q_s is felt in the air-temperature response, which determines T_a in Equations 2 and 4. Separate boundary layers for ice and snow are not specified (Figure 1) in order to avoid the occurrence of large $\Delta T_a/\Delta t$ when A is close to zero, as will be the case for initial ice exposure at the start of summer, or as can be the case if the snowcover melts entirely. The order of $T_{a,n}$ and $T_{a,g}$ is reversed when Equation 4 is used for the non-glacierized part of the basin.

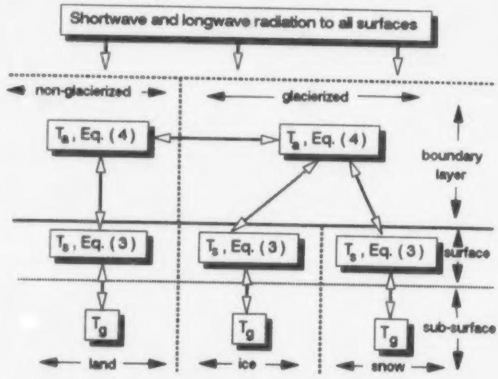

Figure 1. Schematic outline of the model structure, showing direction of major energy flows (open arrows).

The global-radiation scheme described in Munro and Young (1982) is used to simulate K↓, taking the global average value of 0.5 (Sommerville, 1985) to be the basin cloud cover. L↓ is calculated from the Stefan-Boltzmann relationship, treating the atmosphere like a grey-body radiator, with suitable correction for cloud cover (Monteith, 1973; Oke, 1987). Atmospheric emissivity is calculated after Idso and Jackson (1969). A key point is the use of a fixed background temperature for L↓ calculations, which is set close to the mean annual temperature for the basin. This is done to compensate for the fact that, due to changes in the environmental lapse rate, coupling between T_a and atmospheric thermal mass (Paltridge, 1970) must vary with the seasons. Topographic effects upon K↓ and L↓ within the basin are not considered, but the radiation components are sensitive to basin elevation.

The system of equations is evaluated in hourly time steps, starting from initial values of T_a, T_g and T_s. Oerlemans (1986) has shown that the temperature responses will adjust to the energy regime within ten days of simulation. A more conservative adjustment period was used in this case, as model temperatures were initialized at the mean annual temperature appropriate to the location, 60 days prior to the first of the year.

Because the need for climatological data is kept to the minimum, one need only specify latitude, elevation, cloud cover and background temperature to simulate a new energy regime. Surface properties are chosen to be consistent with information gained from field investigations. Hence, given the elevation distribution of winter accumulation on a particular glacier, such as Peyto, it is possible to simulate the annual mass balance and surface-meltwater production.

MASS-BALANCE SIMULATION

Peyto Glacier is located in the eastern ranges of the Canadian Rocky Mountains, on the Alberta side of the continental divide. The glacier has an extensive history of mass balance, climate and hydrological research, both on the glacier itself and in the surrounding basin (Østrem, 1966; Föhn, 1973; Derikx, 1975; Collins and Young, 1981; Young, 1981; Munro and Young, 1982; Munro, 1990). Information from these sources determines the model conditions (Table 1).

Table 1. Model conditions for Peyto Glacier.

A. Climate Conditions		*B. Surface Conditions*	
Mean Annual T_a	-3°C	A, Glacierized	13.4 km^2
Cloud Cover	0.5	A, Non-Glacierized	9.6 km^2
Elevation	2220 m	z_o, Non-Glacierized	100 mm
Latitude	51.7°N	z_o, Glacierized, Ice	2.5 mm
K_h (Equation 4)	10 $m^2 \cdot s^{-1}$	z_o, Glacierized, Snow	5.5 mm
b_w (Water Equivalent)	1.4 $m \cdot yr^{-1}$	α, Non-Glacierized	0.2
u (Equations 2, 4)	5 $m \cdot s^{-1}$	α, Glacierized, Ice	0.25
---	---	α, Glacierized, Snow	0.65

The snow water equivalent in Table 1 is a 13-year mean value of the specific winter mass balance (b_w) taken from Young (1981). Young's data are tabulated according to elevation zones, so they may be used to initialize the snow distribution on the glacier (Figure 2). The annual mass balance for any zone ($b_{a,i}$) is obtained by placing Equation 1 within the mass-balance equation:

$$[5] \qquad b_{a,i} = b_{w,i} - \int_{t_1}^{t_2} M_i \, dt$$

where t_1 and t_2 refer to the start and end of the melt period, during which $T_s = 0°C$, and i refers to a given elevation zone. The integration is approximated as a cumulative sum, and it is assumed that M is the sole agent of mass loss. Thus the simulation begins with a winter mass-balance distribution which is reduced by melting during the ablation season. Eventually the melt period ends, leaving behind a simulated annual mass-balance distribution which compares approximately with Young's (1981) field data (Figure 2).

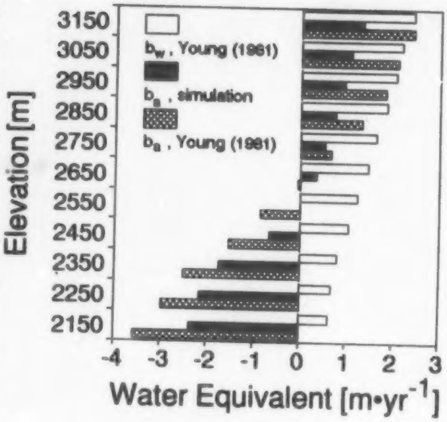

Figure 2. Elevational distributions of winter and annual mass balances.

Even though the altitudinal variation of heat exchange within the basin is not considered, the model is able to simulate the seasonal migration of the snow line because snow thickness increases with each step in elevation. Thus, despite a uniform snowmelt rate over the whole glacier, the tongue is exposed first, followed by ice at higher elevations. The exposed ice continues to melt at a higher rate because it reflects less solar radiation. Also, the area of each elevation zone is known, so it is possible to calculate the whole glacier mass balance and accumulation area ratio for a particular simulation. The conditions displayed in Table 1 yielded $b_a = 0.05$ m, and an accumulation area ratio of 0.52.

The result is consistent with Young (1981) in suggesting that $b_a = 0$ when the accumulation area ratio is close to 0.5. Thus it seems that the model provides a realistic portrayal of snow-line retreat during the melt season. This is crucial to providing a reasonable simulation of glacier-surface discharge.

SURFACE MELTWATER DISCHARGE

Total surface meltwater discharge (M_t) is taken to be the area weighted sum of the melt in each elevation zone:

$$[6] \qquad M_t = A^{-1} \sum_{i=1}^{n} M_i A_i$$

where n is the total number of zones. Equation 6 may also be subdivided, to calculate separate M_t values for the ice and snow areas of the glacier. The passage of the snow line through a zone is smoothed by making the proportion of snowcover in the zone equal to the proportion of snow left in the initial snowpack.

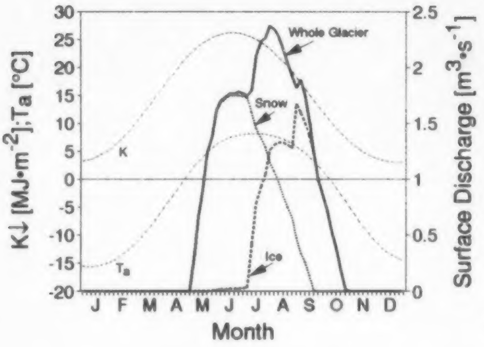

Figure 3. Components of modelled surface-discharge response for Peyto Glacier.

The interesting features of the simulation results are lags in the responses to solar heating (Figure 3). The force-restore method is effective in producing the expected lag of temperature behind solar energy. Surface-meltwater discharge lags still further, occurring nearly six weeks after the time of maximum solar heating. This compares well with the timing suggested in partial discharge measurements from Peyto Creek (Collins and Young, 1981), though the modelled discharge is quite low in comparison to measurements. Although the model does not claim accuracy at this stage of its development, it should be noted that much of the underestimation could arise from the fact that Peyto Creek data apply to the whole basin, and include rainfall inputs, while the simulation applies solely to meltwater production at the glacier surface.

The lag in the timing of maximum surface discharge is a consequence of the migrating snow line. At first, snowmelt accounts for most of the discharge, which rises in direct response to solar heating. As the snow line advances up the glacier, ice melt becomes increasingly important, gradually supplanting snowmelt to become the dominant discharge source toward the end of the ablation season. Ice has more than twice the capacity to absorb K↓ that snow has, so for a while the growth in ice area more than compensates for the late-summer reduction in K↓.

The delay of surface discharge by snow-line retreat is an important aspect of the general problem of discharge delay from glacierized basins. Stenborg (1970) explained the delay in terms of the time required for the internal drainage system of the glacier to develop during the melt season. Work done since then shows that the development of englacial and subglacial drainage is a crucial aspect of glacial hydrology (Hooke, 1989). So too, however, is the transformation of the surface by melting. This point was raised by Collins (1989) who, in assessing statistical relationships between climatic variables and glacier-basin discharge, noted the importance of snow-line migration but was unable to demonstrate it explicitly.

The discharge simulation (Figure 3) shows that attempts to statistically relate discharge to solar radiation and air temperature cannot produce relationships which are both definitive and generally applicable. It is especially pertinent to note that the smooth temporal patterns in K↓ and T_a are not matched by a smooth discharge

Table 2. Peyto Glacier simulation for different climatic types.

	Latitude	Elevation	b_w/b_{wo}	Temperature	b_a
Arctic	75°N	400 m	0.15	-8°C	0.07
Continental	52°N	2,220 m	1.00	-3°C	0.05
Maritime	50°N	1,800 m	2.00	5°C	0.02

pattern. This arises because glacier-surface properties are unevenly distributed in space, so as the surface evolves over time, the effects of spatial variability are transferred to the discharge response. This behaviour would persist if surface characteristics were to be described in finer detail, as the result would be to produce more detailed discharge variations.

The model can demonstrate the effects of changing climate and surface conditions upon the discharge regimes of glaciers. Climatic change is examined by choosing an appropriate latitude, elevation, and accumulation regime for the climate type in question, then finding a background temperature which results in a slightly positive mass balance (Table 2). The impact of altered surface conditions is examined by changing the albedo of the non-glacierized area of the basin.

Peyto Glacier resides within a continental climate regime. Two others of interest are maritime and arctic, plausible climatic conditions which were estimated from information collected at Sentinel Glacier, B.C. (Scnmok, 1988) and Devon Island, N.W.T. (Holmgren, 1971), respectively (Table 2). A winter mass-balance ratio, b_w/b_{wo}, where b_{wo} represents Peyto accumulation, is estimated and applied to Young's (1981) winter mass-balance distribution before the simulation begins. As expected, the drier, colder arctic climate allows net accumulation at a much lower elevation than Peyto. Winter accumulation, appears to be dominant in the switch to maritime conditions, allowing a slightly lower elevation for net accumulation, as noted in Østrem (1966).

The various climates produce marked differences in surface discharge, consistent with the change from low- to high-energy environments. A low-energy climate, like that of the Arctic, produces a short season of low discharge, while the warmth and high precipitation of maritime climatic conditions result in an extended season of high discharge (Figure 4). While differing radiation regimes offer a ready explanation for contrasts between arctic and continental glacier discharge, the same cannot be said for the maritime-continental comparison. Increased maritime discharge is attributed principally to warmer temperatures because solar radiation incomes at 50°N and 52°N are virtually the same (Figure 4).

Discharge responses to changes in the non-glacierized part of the basin are relatively small by comparison to those induced by different climatic regimes, and highly speculative. The speculation is expressed in terms of tree-line movement, where a darker surface is the expected result of tree-line advance, and surface brightening is expected to follow tree-line retreat. The two cases are simulated by changing α for the non-glacierized area to 0.15 and 0.25, repectively. Small, but discernable increases in discharge volume arise from tree-line advance, but the opposite occurs for tree-line retreat (Figure 5).

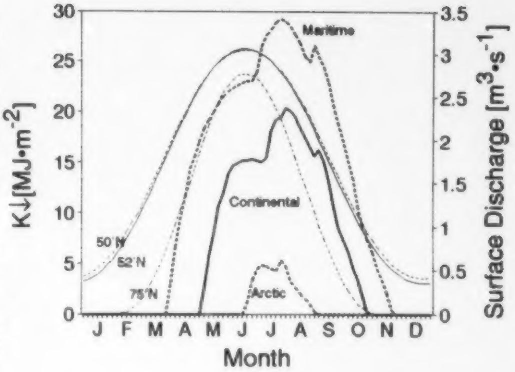

Figure 4. Radiative regimes (light lines) and surface-discharge responses (heavy lines) for three climatic types.

Despite their speculative nature, the tree-line scenarios portrayed here suggest that climatic impacts upon glacier discharge should not be evaluated in isolation from changes which may occur elsewhere in a drainage basin. One could, for instance, imagine afforestation and increased surface melt to be concurrent results of climatic amelioration, where forest expansion reinforces the enhancement of glacier discharge. Some changes, such as clear cutting of forest, could occur independently of climatic change, yet still affect meltwater production.

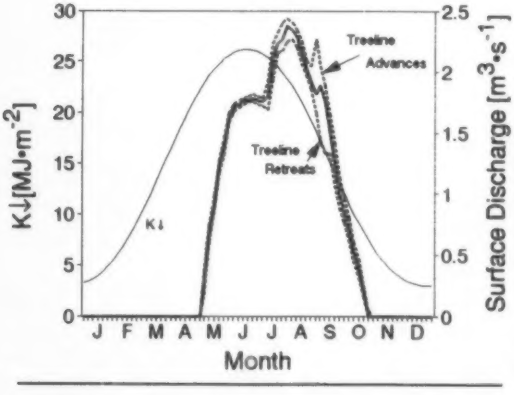

Figure 5. Simulated effects of tree-line migration upon surface discharge.

CONCLUSION

The model is still at an early stage of development, so much remains to be done to mould it into a precise hydrological tool. Some features, like the Oerlemans and Hoogendoorn (1989) model of altitudinal variation within the basin, could readily be added provided the demand for detail is not too great. Topographical mapping approaches (Munro and Young, 1982) provide the greatest challenges for comprehensive energy-balance modelling, not the least of which is to specify the spatial distribution of surface albedo. Here, remote-sensing methods could prove useful, particularly to map the snowcover.

Although doubts may attend the quantitative predictions of the model, the results are exciting from a conceptual standpoint because surface characteristics play an explicit role in the modelling framework. The effect is to produce hydrological-response patterns which can readily be interpreted in terms of changing climatic and surface conditions. Both are important in assessing the present and future contribution of glaciers to hydrological resources.

ACKNOWLEDGEMENTS

The support of the Visiting Fellows Programme, Cooperative Institute for Environmental Studies, University of Colorado is gratefully acknowledged, as is general institutional support from the University of Toronto. Research funding was obtained through the Natural Sciences and Engineering Research Council of Canada. A special note of thanks is expressed to the National Hydrology Research Institute, Environment Canada, Saskatoon for its support of field work related to this study.

REFERENCES

COLLINS, D.N., 1989. Hydrometeorological conditions, mass balance and runoff from alpine glaciers. In - Glacier Fluctuations and Climatic Change, J. Oerlemans (Editor), Kluwer Academic Publishers, Boston, Massachusetts, 235-260

COLLINS, D.N. and G.J. YOUNG, 1981. Meltwater hydrology and hydrochemistry in snow- and ice-covered mountain catchments. Nordic Hydrology, 12(4-5), 319-334

DEARDORFF, J.W., 1978. Efficient prediction of ground surface temperature and moisture, with inclusion of a layer of vegetation. Journal of Geophysical Research, 83(C4), 1889-1903

DERIKX, L., 1975. The heat balance and associated runoff from an experimental site on a glacier tongue. Proceedings of the Moscow Symposium, August 1971, Snow and Ice in Mountainous Areas, IAHS Publication No.104, International Association of Hydrologic Sciences, International Union of Geodesy and Geophysics, 59-69

FÖHN, P.M.B., 1973. Short-term snow melt and ablation derived from heat- and mass-balance measurements. Journal of Glaciology, 12(65), 275-289

HOLMGREN, B., 1971. Climate and energy exchange on a sub-polar ice cap in summer. Arctic Institute of North America Devon Island Expedition, 1961-1963. Part A. Physical climatology. Meddelande No.107, Meteorologiska Institutionen, Uppsala Universitet, 83 pp.

HOOKE, R.LeB., 1989. Englacial and subglacial hydrology: a qualitative review. Arctic and Alpine Research, 21(3), 221-233

IDSO, S.B. and R.D. JACKSON, 1969. Thermal radiation from the atmosphere. Journal of Geophysical Research, 74(23), 5397-5403

LETRÉGUILLY, A. and L. REYNAUD, 1989. Spatial patterns of mass-balance fluctuations of North American glaciers. Journal of Glaciology, 33(120), 163-168

MONTEITH, J.L., 1973. Principles of environmental physics. Arnold, London, U.K., 241 pp.

MÜLLER, F. and C.M. KEELER, 1969. Errors in short-term ablation measurements on melting ice surfaces. Journal of Glaciology, 8(52), 91-105

MUNRO, D.S., 1990. Comparison of melt energy computations and ablatometer measurements on melting ice and snow. Arctic and Alpine Research, 22(2), 153-162

MUNRO, D.S. and G.J. YOUNG, 1982. An operational net shortwave radiation model for glacier basins. Water Resources Research, 18(2), 220-230

OERLEMANS, J., 1986. Glaciers as indicators of a carbon dioxide warming. Nature, 320(6064), 607-609

OERLEMANS, J. and N.C. HOOGENDOORN, 1989. Mass-balance gradients and climatic change. Journal of Glaciology, 35(121), 399-405

OKE, T.R., 1987. Boundary layer climates. 2nd edition, Methuen, New York, 435 pp.

ØSTREM, G., 1966. Mass balance studies on glaciers in western Canada, 1965. Geographical Bulletin, 8(1), 81-107

PALTRIDGE, G.W., 1970. Day-time long-wave radiation from the sky. Quarterly Journal of the Royal Meteorological Society, 96(410), 645-653

PATERSON, W.S.B., 1981. The physics of glaciers. 2nd Edition, Pergamon Press, New York, N.Y., 380 pp.

PRICE, A.G., 1977. Snowmelt runoff processes in a subarctic area. McGill Sub-Arctic Research Paper No.29, Climatological Research Series No.10, Department of Geography, McGill University, Montréal, Quebec, 106 pp.

SCHMOK, J., 1988. 1988 mass-balance determination of Sentinel, Place and Helm Glaciers, British Columbia. NHRI Contract Report No.88002, Contract No.KW504-8-0865/01-SB, Department of Geophysics and Astronomy, University of British Columbia, Vancouver, British Columbia for Surface Water Division, National Hydrology Research Institute, Environment Canada, Saskatoon, Saskatchewan, December, 22 pp.

SOMERVILLE, R.C.J., 1985. Clouds and climate regulation. Nature, 315(6022), 713-714

STENBORG, T., 1970. Delay of run-off from a glacier basin. Geografiska Annaler, 52A(1), 1-30

YOUNG, G.J., 1981. The mass balance of Peyto Glacier, Alberta, Canada, 1965 to 1978. Arctic and Alpine Research, 13(3), 307-318

A HIGH ARCTIC OCCURRENCE OF SEASONAL FROST MOUNDS

W.H. Pollard

Department of Geography
McGill University
805 Sherbrooke Street West
Montréal, Quebec
H3A 2K6 CANADA

ABSTRACT

During 1988 and 1989, nineteen frost blisters and five icing blisters were observed in the Expedition Fiord area, Axel Heiberg Island, N.W.T. Frost mounds form each year in the sandy floodplain sediments immediately downslope from a group of mineralized perennial springs on the north side of Expedition River. Discharge occurs from at least 12 to 15 spring outlets near the base of Gypsum Hill. Discharge rates range from 0.2 to 1.4 L·s^{-1}*. Each winter an icing up to 2.5-m thick is produced. A group of frost blisters, ranging from 0.9 to 3.5-m high and up to 41-m long, develop in association with the icing. Icing blisters up to 2.5-m high also develop near the spring outlets. Frost-blister ice cores 0.4 to 2.0-m thick occur beneath arched bedded fluvial sand. Ice-core petrographic and stratigraphic characteristics are consistent with a ground-water injection origin. In some cases, large open cavities within the ice core indicate drainage of the ground-water reservoir before freezing was complete. Chemical analyses of samples from mound ice cores, the icing and spring discharge indicate that the springs are the main source of water for both icing and frost-mound activity. High concentrations of dissolved salts result in a depression of the freezing temperature of spring discharge thus allowing spring flow to continue after the onset of freeze-back. The study area is located at the head of Expedition Fiord, and although there are no deep temperature measurements for this area, permafrost is thought to be relatively deep. Spring activity at this location has been reported previously but this is the first reference to seasonal frost mounds and icings. Furthermore, this is the most northerly reported occurrence of seasonal frost-mound activity, a phenomenon usually restricted to discontinuous-permafrost or warmer continuous-permafrost environments.*

INTRODUCTION

This paper presents preliminary observations on seasonal frost-mound activity and a ground-water icing associated with perennial springs near the head of Expedition Fiord, Axel Heiberg Island, N.W.T. Perennial spring occurrence at Gypsum Hill was first described by Beschel (1963) and subsequently by Hoen (1964) and Allan *et al.* (1987). However, there are no previous references to frost mounds associated with these springs and only Beschel's brief description of icings. Since perennial springs and seasonal frost mounds are rare in areas characterized by deep permafrost and severe climate conditions typical of this latitude, their presence at Expedition Fiord raises a number of interesting questions about the geological, geocryological and hydrological conditions of this area.

The primary aims of this paper are to describe the morphological and structural characteristics of seasonal frost mounds and ground-water icings and to discuss how the mineralized nature of spring discharge produces hydrological conditions suitable for seasonal frost-mound development despite climatic and permafrost conditions normally considered too severe for their occurrence.

BACKGROUND

The term 'frost mound' is the family name for all mounds produced by the combined action of: (a) the volumetric expansion of water during its phase change to ice, (b) the hydrostatic or hydraulic pressure of ground water, and (c) the force of crystallization during freezing (Muller, 1945; Williams, 1965). On the basis of genetic processes, frost mounds are either perennial (i.e., growth processes occurring for several years, e.g., pingos) or seasonal (i.e., growth limited to a single season).

Seasonal frost mounds are small- to medium-sized features (from <1.0 to 8.0-m high), formed by upheaval of frozen ground and/or ice in response to hydraulic and/or hydrostatic pressures in suprapermafrost ground water trapped within residual zones of the active layer during winter freeze-back (Pollard and French 1984; van Everdingen, 1982). They are characterized by rapid growth and a duration usually lasting between a few months and one-to-two years, but rarely longer. They have been reported most frequently in areas of high relief and discontinuous or thin continuous permafrost. Three types of seasonal frost mounds are recognized: frost blisters, icing blisters and icing mounds. Frost blisters are mounds or upwarps of ground produced by localized high hydraulic or hydrostatic pressure of ground water. Frost blisters typically consist of a surface layer of soil or peat overlying a layer of clear ice vaulted over a water-filled cavity. During late-winter, the water-filled cavity may freeze completely and form a core of solid ice.

Icing mounds and icing blisters occur in association with both ground water and river icings. In contrast to frost blisters, which include a layer of sediment over an ice core, icing mounds and blisters are composed entirely of ice. Icing mounds are localized icings of substantial thickness but more-or-less limited in areal extent (Muller, 1945). Icing blisters are mounds formed by the hydraulic lifting of icing layers by water under high hydraulic potential (van Everdingen, 1978).

There are only a few reported occurrences of seasonal frost mounds in high-arctic locations. Ackerman (1980) described a variety of frost mounds in the Kapp Linné area, west Spitsbergen (78°04'N, 13°38'E), including forms that closely resemble frost blisters. Although the Kapp Linné area has a high-arctic location, the climate displays a strong maritime influence resulting in a mean annual air temperature of -4.6°C and mild winters (mean monthly temperature for January is -11.2°C). Thus conditions suitable for seasonal frost-mound growth (Pollard, 1988) are readily met. A series of icing blisters were reported by Frederking (1979) in the Cape Dorset area, Baffin Island. Isolated occurrences of frost blisters have also been reported in northern Alaska (Lewis, 1962) and the Mackenzie Delta (Mackay, 1979).

STUDY AREA

The frost mounds described in this paper occur near the McGill University Axel Heiberg Research Station at Expedition Fiord, Canadian Arctic Archipelago (Figure 1). The McGill station is located at 79°26'N, 90°46'W, near the head of Expedition Valley and the termini of the White and Thompson Glaciers. The Expedition River is roughly 12.5-km long and has a flood plain 1 to 2-km wide. It is fed primarily by glacial meltwater and snowmelt from the surrounding mountains. There is no year-round weather record for the study area; however, observed summer temperatures (e.g., mean July temperature of +6.1°C) are comparable to temperatures recorded at Eureka (79°59'N, 85°56'W). Eureka has a mean annual air temperature of -19.7°C. The mean monthly temperatures for January and July are -36.1 °C and +5.4°C, respectively (Canada, Environment Canada, 1984).

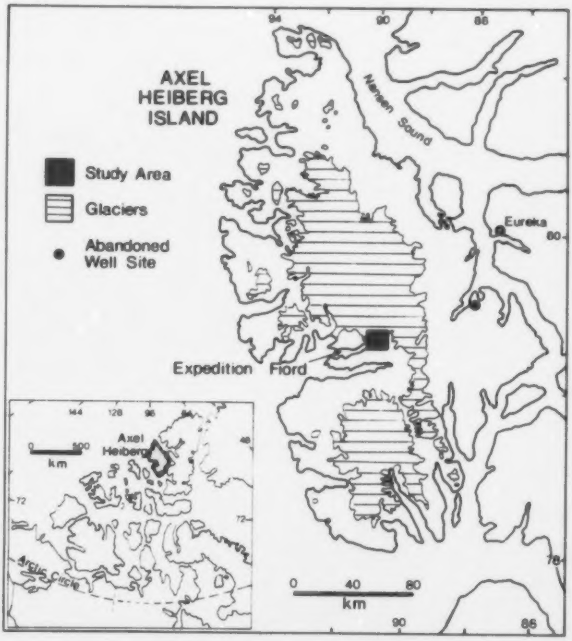
AXEL
HEIBERG
ISLAND
Study Area
Glaciers
Abandoned Well Site
Nansen Sound
Eureka
Expedition Fiord
94
90
86
80
78
0 40 80
km
144
128
96
0 500
km
Axel Heiberg
48
72
72
Arctic Circle

Figure 1. Study area map showing location of the spring and frost-mound activity, Expedition Fiord, Axel Heiberg Island, N.W.T.

A permafrost thickness of >400 m was documented in an exploration well on the east side of Axel Heiberg, roughly 60 km from Expedition Fiord (Taylor and Judge, 1976). It is reasonable to assume that similarly deep continuous permafrost may also exists in the study area. However, the relative proximity of the ocean, present and past glaciation could produce local variation in permafrost depth. Large high-centred ice-wedge polygons occur adjacent to the floodplain of the Expedition River near the study site. During this study, maximum seasonal thaw depths reached 40 cm by early-August.

Axel Heiberg Island lies within the Sverdrup Basin. The geology of the area is complex, consisting of folded and faulted Mesozoic sedimentary rocks intruded by evaporite diapirs. Intrusion of the diapirs is associated with early Tertiary (Innuitian) orogenic activity.

FROST-MOUND ACTIVITY

Setting and Morphology

Field studies were carried out in the Expedition Fiord area during June to July, 1988 and May to August, 1989. During this period, more than 26 seasonal frost mounds were documented in sandy floodplain (outwash) deposits downslope from a group of perennial springs at the base of Gypsum Hill (Figures 2 and 3a). The mounds occur at an elevation of 20 m a.s.l., at or below the break of slope that marks the edge of the Expedition River floodplain and the valley side. At this location, the floodplain is composed of medium to coarse dark-brown (7.5YR3/2) sand with beds of fine gravel. It has a slope of 1.5° toward the southwest (downstream). Gypsum Hill comprises the northwestern part of Expedition diapir and is composed of gypsum and anhydrite. Gypsum Hill forms a steep ridge, up to 278.6 m a.s.l., aligned roughly parallel to the Expedition River. The perennial springs discharge near the base of Gypsum Hill at an elevation of 25 m a.s.l.

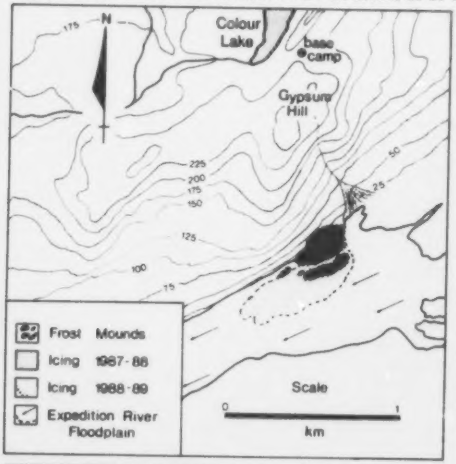

Figure 2. A geomorphological map of the spring, frost-mound and icing area near the head of Expedition Fiord, Axel Heiberg Island.

In 1988, 10 frost blisters, 1 icing blister and 1 icing mound were documented (e.g., Figures 3b and c). The following year, at least 9 new frost blisters, 5 icing blisters and 1 large icing mound

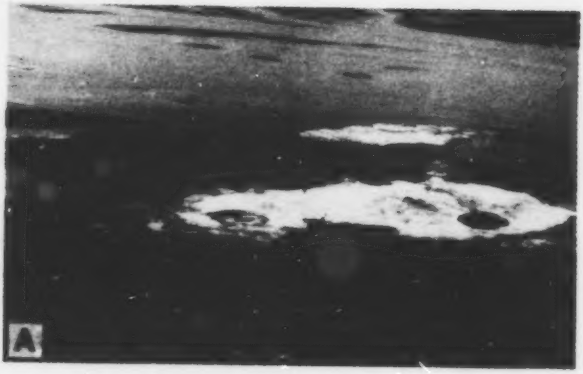

Figure 3a. Frost-blister setting (July, 1988).

Figure 3b. A partially excavated frost blister exposing a massive ice core (July, 1989).

developed in the same location. In 1988, only a small icing remained by late-June and the degradation of frost mounds by thaw and mechanical erosion was well advanced. By comparison, cool wet conditions in 1989 preserved much of the icing and associated frost mounds into late-July, although all had thawed completely by late-August. Early in the season, the icing conformably overlaid most of the frost blisters. The absence of deformation in the icing cover indicates that frost blister formation was initiated prior to icing formation.

Frost blisters at Axel Heiberg range from 0.9 to 3.5-m high and 6.0 to 41.0-m long with an average height of 1.9 m and average length of 18 m. The majority of frost blisters are oval and elongated parallel to the local slope. They have an average length-to-width ratio of 2.03. In places, 2 or 3 mounds coalesce generating irregular or complex forms. In general, frost blisters have simple shapes and display smooth to slightly asymmetrical longitudinal profiles with very steep side slopes (25 to 48°) and flat tops. Dilation cracks dissect mound surfaces but quickly infill with loose sand once thaw begins. Compound and complex forms have undulating longitudinal profiles. By comparison, icing mounds and blisters are generally smaller, they have a narrower size range, smoother profiles and display less morphological diversity.

Internal Structure

In the absence of detailed process observations, stratigraphic and ice-petrographic analyses provide one way of inferring mound origin. The internal structure

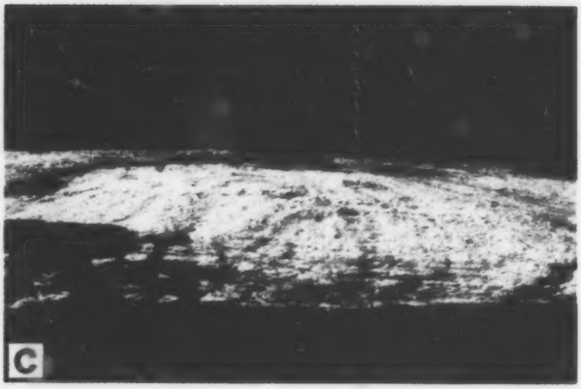

Figure 3c. An icing mound (July, 1988).

Figure 3d. An excavated frost blister with a partially-drained internal cavity (July, 1989).

Figure 3e. An area of perennial spring discharge at the base of Gypsum Hill.

of 7 frost blisters was determined either by manually excavating full cross-sections or by cleaning natural exposures of partially-collapsed mounds (Figure 3d). The typical mound stratigraphy is illustrated in Figure 4. In all cases, these frost blisters had a surface layer of horizontally-bedded, medium to coarse fluvial sand, 25 to 40 cm thick, with thin, fine gravel layers. The bedded sand was arched over a core of pure ice between 40 and 200-cm thick. The ice core was underlain by horizontally-bedded fluvial sand. Both the upper and lower contacts between the ice and sand were abrupt and unconformable, suggesting an intrusive origin for the ice. The base of the core was observed in only 3 mounds, in other cases it lay below the water-table. The massive ice core had a faintly foliated milky-white appearance and was composed of either solid ice or layered ice with an internal cavity up to 60-cm high. High concentrations of small spherical to vertically-elongated tubular gas inclusions caused the milky-white colour and layered appearance. The central cavity represented drainage of a residual reservoir of ground water within the ice core.

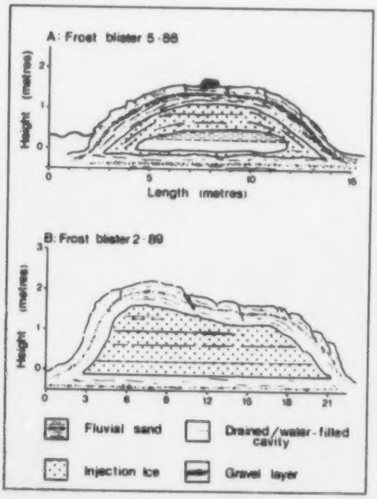
A: Frost blister 5-88
Height (metres)
0
1
2
0
5
10
15
Length (metres)
B: Frost blister 2-89
Height (metres)
0
1
2
3
0
3
6
9
12
15
18
21
Fluvial sand
Drained/water-filled cavity
Injection ice
Gravel layer

Figure 4. A diagrammatic cross-section through two frost blisters at Expedition Fiord, Axel Heiberg Island.

Petrographic analyses were performed on thin sections prepared from oriented block samples taken from the ice core. Two fabric and texture patterns are differentiated. First, a chill zone of small subhedral ice crystals with *c*-axis orientations ranging from random to a loose girdle parallel to the internal layering and perpendicular to the freezing direction. The second pattern was best developed deep within the ice core where textures were characterized by large, vertically-oriented, long columnar anhedral crystals elongated normal to the compositional layering and parallel to their growth direction. Crystal *c*-axes displayed a strong preferred pattern normal to the internal layering and the inferred growth direction. These fabrics are similar to those observed in frost blisters in northern Yukon (Pollard and French, 1984) and are consistent with an injection origin for water forming the ice core.

One aspect of these frost blisters that distinguishes them from other frost blisters described in the literature is their occurrence in sandy sediments in an active river channel and the absence of a peat or vegetative cover. In other studies (Lewis, 1962; Pollard and French, 1983, 1984; van Everdingen, 1978, 1982) it was found that a vegetation and peat mat helped maintain the strength of surficial materials during mound formation and collapse.

Icing blisters in this area consisted of 40 to 130 cm of layered pale-white to clear icing ice arched over an oval to disk-shaped cavity 35 to 97-m high. The cavity was usually partially drained. In 1988, coring of an intact icing blister encountered water under pressure within the cavity. In this case, discharge produced a fountain of water roughly 25-cm high. Artesian flow rapidly diminished and stopped completely after 10 minutes. This suggests either the mound was cut-off hydrologically from the spring system or that the height of the mound was above the piezometric level of the feeder spring.

Petrographic studies reveal that icings are characterized by small, equigranular subhedral crystals with random dimensional and *c*-axis orientations. This reflects the incremental growth of icings by the addition of thin layers of ice. Each layer is the result of moderately-rapid freezing of localized overflow and in some layers the inclusion of snow imparts a distinct texture. Yellowish-white gypsum precipitate covers much of the icing surface and occurs as isolated pockets and layers within the ice. Ice formed by freezing of water within icing blisters is identical to the frost-blister ice core. The chill zone contact between the icing and injection ice is difficult to determine.

By comparison, icing mounds are composed completely of thin horizontal to gently dipping layers of pale-white and clear icing ice. These accumulations are up to 2.5-m thick. Where frost blisters are frozen through it is very difficult to distinguish between icing mounds and icing blisters. However, it can usually be accomplished petrographically.

Frost-Blister Degradation

Once the snow and icing cover melted sufficiently to expose the frost-blister surface, the thaw of dark sandy materials proceeded rapidly. The coarse granular cover material had little cohesive strength and exhibited rapid drainage of meltwater which enhanced thawing. By mid- to late-June, thaw on top of most frost blisters penetrated to the ice core. At this stage, the sand on the steep frost-blister sides began to "slough-off" as blocks, or as loose sediment gradually assuming its natural angle of repose. Continued melt of the ice core maintained instability of the cover sediment. Occasionally, the ice core became exposed accelerating thaw degradation. In some cases, sloughing began after only 10 to 15 cm of thaw. Since many of the mounds occurred on the active floodplain and river bed, fluvial erosion was also responsible for collapse of several mounds. As a result, complete collapse of all frost blisters took place by late-July to early-August.

PERENNIAL SPRINGS AND ICING

The perennial springs are divided into two groups (Figure 2). The first group discharge from at least 12 to 15 outlets located in bedrock and colluvial deposits. This group occurs within a narrow band, 160-m long and 20-m wide, along the lower slopes of Gypsum Hill (Figure 3e). The second group discharge at several points within the main channel and floodplain of the Expedition River. The latter were observed within the icing during May 1989 and are inferred from the presence of small isolated icings and icing mounds up to 100 m into the floodplain cut off by active channel flow. The discharge of gas bubbles in pools and river channels is another indication of their presence. Gas discharge is also associated with the first group of springs. The gas is nonflammable and has a strong sulphurous odour detectable up to 3-km away.

Spring discharge rates range from 0.2 to 1.2 $L \cdot s^{-1}$ and the average discharge rate for 15 springs in group 1 in July 1988 was 0.45 $L \cdot s^{-1}$. Discharge temperatures range from -1.5 to +6.5°C and average 2.4°C. These values are comparable with observations made by Beschel (1963). The springs with the warmest temperatures also had the highest discharge. These springs are clustered into two distinct zones roughly 70-m apart and both temperature and discharge decrease with increasing distance away from these zones. Spring discharge continues year round and produces a large ground-water icing that merges with a river icing associated with run-off from the White and Thompson Glaciers. A yellow mineral precipitate covers the ground-water icing and ground surface around the springs. When fieldwork began on June 28, 1988, the icing was roughly 30,000 m^2 and had been dissected into 3 parts, the largest associated with the main spring group. In 1989, the ground-water icing extended nearly 300 m into the floodplain and more than 700-m downstream, covering approximately 200,000 m^2. The maximum icing thickness was roughly 2.1 m, however, the average was between 1.0 to 1.5 m giving an estimated icing volume of up to 300,000 m^3. Assuming that winter discharge rates are comparable to those observed in summer and comparable rates for springs situated in the bed of the Expedition River, this estimate is surprisingly close to the approximate volume of water (+9%) discharging from the springs between September and June. This evidence, together with observation of spring activity in May when mean daily air temperatures are still below -10°C, support the hypothesis that spring discharge continues through winter.

Hydrochemistry

Water samples for chemical analysis were collected from spring outlets and from river flow upstream from the springs. Water temperature, conductivity and pH were measured in the field at the time of sampling. Chemical analyses of water derived from icing and frost-blister ice were also undertaken. The results of chemical analyses are listed in Table 1. Spring discharge was high in dissolved solids with particularly high concentrations of chloride, sodium and sulphate. The composition of spring water did not vary between 1988 and 1989 or between seasons and is similar to the spring chemistry reported by Beschel (1963, p.185) for samples taken in July of 1961 and 1962. Icing and frost-blister ice contained considerably lower concentrations of dissolved solids than spring water but both had higher concentrations than stream flow from glacier run-off or precipitation. The composition of frost-blister ice is sufficiently similar to that of icings to suggest they share a common source. The relative proportions of the various ions support the interpretation that spring discharge is the water source for both icing and frost-blister formation.

DISCUSSION

The significance of seasonal frost-mound activity at Expedition Fiord is directly related to the extreme northern location of phenomena usually associated with less severe permafrost conditions. The hydrological implications of seasonal frost-mound

Table 1. Hydrochemical data for springs, river flow, precipitation, icings and frost-blister ice from Expedition Fiord, Axel Heiberg Island.

Source	Spring No. 1		Spring No. 2	Icing Ice	Frost Blister Ice	Precipitation	River Flow
Date	7/7/88	11/7/89	11/7/89	8/7/89	13/7/89	13/7/88	15/7/89
Temperature (°C)	5.50	5.80	4.50	--	--	0.50	2.50
pH (units)	6.78	6.50	6.84	6.73	7.50	6.80	6.94
Conductivity	102.00	100.50	103.00	2.18	2.17	7.00	0.19
Ca ($mg \cdot L^{-1}$)	2140.00	2180.00	2115.00	530.00	93.60	1.35	1.50
Mg ($mg \cdot L^{-1}$)	120.00	115.00	115.00	5.00	1.00	0.05	0.15
Na ($mg \cdot L^{-1}$)	26967.04	27962.56	28024.57	801.42	346.46	0.13	1.36
K ($mg \cdot L^{-1}$)	50.44	62.56	48.09	9.78	9.78	0.04	1.06
HCO_3 ($mg \cdot L^{-1}$)	350.80	391.79	362.10	--	--	--	--
SO_4 ($mg \cdot L^{-1}$)	3652.80	3724.80	3763.20	1530.24	532.80	1.82	3.17
Cl	42430.77	44212.38	44079.43	1375.30	265.20	0.37	2.62
F	0.68	0.63	0.48	0.09	0.70	0.06	0.00
Sum	75712.53	78750.22	78507.87	4251.83	1249.54	3.82	9.86

Conductivity in $\mu S \cdot cm^{-1}$.

occurrence in an area of deep continuous permafrost (e.g., their association with perennial springs) are particularly significant. In this case, the warm saline nature of spring discharge suggests a subpermafrost origin and the presence of a through talik. Both are probably related to the geological structure and tectonic evolution of Expedition diapir (e.g., see Hoen, 1964). The chemical and thermal properties of spring discharge alter the permafrost and active-layer regimes sufficiently to create conditions suitable for frost-mound formation. The warm ground-water temperatures maintain discharge year round, keep spring outlets free of ice and enhance active-layer development. Seasonal frost mounds readily occur where the chemically-depressed freezing point of spring discharge combines with the permeable floodplain sediments to produce zones of ground-water transmission into the winter. Preliminary tests indicate the freezing temperature of spring water at Expedition Fiord is approximately -5 to -7°C, and with solute rejection during freezing residual waters may freeze at even lower temperatures.

There is limited information on saturated ground-water flow in the High Arctic. It is generally assumed that thick accumulations of permafrost, common in the arctic islands, provide an effective aquitard preventing ground-water discharge and resulting in the separation of ground water into sub-, intra- and suprapermafrost systems. According to Williams and van Everdingen (1973), the saline springs at Expedition Fiord are typical of the Canadian Arctic Archipelago. Other examples of high-arctic ground-water flow occur in the Nanisivik Mine area, northern Baffin Island and the Polaris Mine area, Little Cornwallis Island (Weyer, 1981).

CONCLUSIONS

These are preliminary observations -- more research is needed to fully understand the nature of the ground-water and frost-mound systems. At this stage two general conclusions can be made, (1) the frost mounds occurring at Expedition Fiord near springs and seeps discharging from the base of Gypsum Hill are seasonal in nature; and, (2) their occurrence under such harsh permafrost and climatic conditions is a direct result of spring thermal and chemical characteristics.

ACKNOWLEDGEMENTS

Funding for this study was provided by a grant from the Natural Sciences and Engineering Research Council of Canada. Logistical support was provided by the Polar Continental Shelf Project, E.M.R. The author also wishes to express sincere appreciation to the Science Institute of the Northwest Territories for permission to undertake this study and McGill University for use of research facilities on Axel Heiberg Island. The field assistance of M. Hinton in 1988 and Y. Moisan in 1989 are gratefully acknowledged. Travel costs for field assistants were covered by funds supplied by the Northern Scientific Training Programme, D.I.N.A. Finally, the author wishes to express appreciation to Dr. Peter Adams for many useful discussions and suggestions prior to undertaking work on Axel Heiberg Island.

REFERENCES

ACKERMAN, J., 1980. Studies on periglacial geomorphology in West Spitsbergen. Meddelanden fra Lunds Universitets Geografiska Institutionen Avhandlingar, Vol.89, 297 pp.

ALLAN, C., S. SCHIFF, D. PIERSON, M. ENGLISH, M. ECCLESTONE and W.P. ADAMS, 1987. Colour Lake, Axel Heiberg Island, N.W.T., a naturally acid, high arctic, lake - data report. In - Field Research on Axel Heiberg Island, N.W.T., Canada: Bibliographies and Data Reports with Appendices of Data from the McGill Subarctic Research Station, Schefferville, P.Q., P. Adams (Editor), McGill Subarctic Research Paper No.41, Axel Heiberg Island Research Report, Miscellaneous Papers No.2, Occasional Paper No.12, Department of Geography, Trent University, Peterborough, Ontario, Centre for Northern Studies and Research, McGill University, Montréal, Quebec, 67-189

BESCHEL, R.E., 1963. Sulphur springs at Gypsum Hill. In - Preliminary Report 1961-1962, by F. Müller et al., Jacobsen-McGill Arctic Research Expedition 1959-1962, Axel Heiberg Island Research Reports, McGill University, Montréal, Quebec, December, 183-187

CANADA, ENVIRONMENT CANADA, 1984. Monthly record - Meteorological observations in Canada. Atmospheric Environment Service, Environment Canada, Downsview, Ontario, microfiches

FREDERKING, R.M.W., 1979. Rupture of an ice mound near Cape Dorset, N.W.T. Canadian Geotechnical Journal, 16(3), 604-609.

HOEN, E.W., 1964. The anhydrite diapirs of central western Axel Heiberg Island. Jacobsen-McGill Arctic Research Expedition 1959-1962, Geology No.2, Axel Heiberg Island Research Reports, McGill University, Montréal, Quebec, March, 102 pp.

LEWIS, C.R., 1962. Icing mound on the Sadlerochit River, Alaska. Arctic, 15(2), 145-150

MACKAY, J.R., 1979. Pingos of the Tuktoyaktuk Peninsula area, Northwest Territories. Géographie Physique et Quaternaire, 33(1), 3-61

MULLER, S.W., 1945. Permafrost or permanently frozen ground and related engineering problems. Strategic Engineering Study No.62, Military Intelligence Division, U.S. Army Office of the Chief of Engineers, Washington, D.C., 231 pp.

POLLARD, W.H., 1988. Seasonal frost mounds. In - Advances in Periglacial Hydrology, M.J. Clark (Editor), Wiley-Interscience Publications, John Wiley & Sons, 201-229

POLLARD, W.H. and H.M. FRENCH, 1983. Seasonal frost mound occurrence, North Fork Pass, Ogilvie Mountains, northern Yukon, Canada. Permafrost, Fourth International Conference, Proceedings, 17-22 July 1983, Fairbanks, Alaska, National Academy Press, Washington, D.C., 1000-1004

POLLARD, W.H. and H.M. FRENCH, 1984. The groundwater hydraulics of seasonal frost mounds, North Fork Pass, Yukon Territory. Canadian Journal of Earth Sciences, 21(10), 1073-1080

TAYLOR, A.E. and A.S. JUDGE, 1976. Canadian geothermal data collection - northern wells 1975. Geothermal Series No.6, Earth Physics Branch, Department of Energy, Mines and Resources, Ottawa, Ontario, 142 pp.

van EVERDINGEN, R.O., 1978. Frost mounds at Bear Rock, near Fort Norman, Northwest Territories, 1975-1976. Canadian Journal of Earth Sciences, 15(2), 263-276

van EVERDINGEN, R.O., 1982. Frost blisters of the Bear Rock Spring area near Fort Norman, N.W.T. Arctic, 35(2), 243-265

WEYER, K.U., 1981. Ground water occurrences near mining developments in the High Arctic. Fourth Canadian Permafrost Conference, 2-6 March 1981, Calgary, Alberta, Abstracts-Programme-résumés, 122

WILLIAMS, J.R., 1965. Ground water in permafrost regions, an annotated bibliography. Water Supply Paper No.1792, U.S. Geological Survey, Washington, D.C., 294 pp.

WILLIAMS, J.R. and R.O. van EVERDINGEN, 1973. Groundwater investigations in permafrost regions of North America: a review. In - Permafrost, 2nd International Conference, North American Contribution, National Academy of Sciences, Washington, D.C., 435-446

RELATIONSHIPS BETWEEN SNOW CHEMISTRY AND BLOWING SNOW: INITIAL FINDINGS*

J.W. Pomeroy[1], T.D. Davies[2] and M. Tranter[3]

[1]National Hydrology Research Institute
Environment Canada
11 Innovation Boulevard
Saskatoon, Saskatchewan
S7N 3H5 CANADA

[2]School of Environmental Sciences
University of East Anglia
Norwich NR4 7TJ
UNITED KINGDOM

[3]Department of Oceanography
The University
Southampton SO9 5NH
UNITED KINGDOM

ABSTRACT

Measurements of acidic blowing and surface snow in the Cairngorm Mountains of northern Britain indicate profound changes in snow chemistry during wind redistribution of snow. Concentrations of contaminants can be up to three times greater in blowing snow than in eroding surface snow and up to two times greater in accumulating than in eroding snow. Contaminant concentrations in blowing snow increase with height, though contribution from falling snow and recently-eroded surface snow can mask this effect. Sublimation of ice to water vapour during wind transport concentrates the remaining contaminants in blowing snow to a degree which explains much of the observed increase in concentrations. Other ion-specific processes may also affect concentrations.

INTRODUCTION

Pollutants accumulate in snowcovers by both wet and dry deposition. Extreme examples of "wet deposition" occur in the Cairngorm Mountains of Scotland where occasional falls of an acidic "black snow" have profound effects on snowcover chemistry. Under these conditions, the pH of snowfall can be approximately 3.0, and the particulate and organic-carbon loading so great that the fallen snow appears black or grey (Davies *et al.*, 1984, 1988). The chemical composition of windswept snowcovers is complex, and varies notably over a range of horizontal and vertical scales. Upon snowmelt, contaminants are rapidly removed from the snowpack in the flow of meltwater. Even single heavily-contaminated snowfalls can directly affect stream chemistry upon the melting of the snowpack (Tranter *et al.*, 1988).

---

*National Hydrology Research Institute Contribution Series Number CS-90010.

Polluted snowfalls may be transported, chemically-altered and mixed with other snows during blowing-snow events. Wind redistribution of snow is frequent in windswept, exposed terrain such as the Scottish Highlands, leading to marked spatial variability in the composition of snowcovers (Tranter *et al.*, 1987). Although the spatial variability has been quantified, the causal processes have, thus far, only been speculated (Davies *et al.*, 1987; Delmas and Jones, 1987; Pomeroy and Male, 1987; Tranter *et al.*, 1987). The physical properties of snow particles are transformed during wind transport as they shatter during impact with the surface, develop electrostatic charges and sublimate (Pomeroy, 1988, 1989; Schmidt, 1972, 1982; Tabler *et al.*, 1990). Wind transport of snow may be an important controlling factor in the evolution of snowcover chemistry in open, northern areas.

Here we present some initial findings on the relationship between blowing snow and snow chemistry, based upon measurements of a) the mass flux of blowing snow, b) the concentrations of some major ions in blowing snow, together with concentrations in surface snow undergoing c) erosion and d) deposition. The findings are used to examine the effect that sublimation of blowing snow may have in concentrating contaminants in snow.

MEASUREMENTS

Field Measurements

The experiment was conducted on the dissected high plateaux of the Cairngorms, in the north of Scotland, Lat. 57°07'N, Long. 3°38'W. The Cairngorms are particularly suited for such a study as they are subject to frequent and severe blowing snow storms (Green, 1981), that often scavenge heavily-polluted air arriving from industrial zones to the south and in eastern Europe.

The blowing-snow measurements were conducted near Cairn Gorm on a level, well-exposed plateau at an elevation of 1135 m. The bedrock is granitic, overlain by thin, gravelly soils. Vegetation is sparse, consisting of a barren alpine/arctic fell-field community (Ratcliffe, 1981). The plateau provides a uniform fetch for 300 m to the southwest, the sector from which the wind most commonly blows. Winds atop Cairn Gorm (1245 m a.s.l.) have reached 88 $m \cdot s^{-1}$. Snowfalls occur in all seasons. Snowcover on the plateau is variable and may be frequently relocated to nearby corries by wind transport. Snow accumulation in the corrie, Ciste Mhearad, at the edge of the plateau can reach 20 metres in depth. During the study period, erosion of the snowcover from the plateau frequently revealed partially ice-covered boulders exposed typically 0.3 m from a clear-ice plain; small snowdrifts occupied the wake of the boulders.

Two meteorological masts (see Figure 1) were employed. The larger held the cup anemometers, blowing-snow particle detectors (Brown and Pomeroy, 1989), thermistors and hygrometers, whilst the smaller held the blowing-snow chemistry samplers and a blowing-snow electrostatic charge gauge (designed by R.A. Schmidt). The snow-chemistry samplers consist of a machined PVC (Polyvinyl Chloride) tube "nozzle" of 40 mm inside diameter with a sewn nylon filter-fabric sack of 0.03 m^3 volume hanging downwind. The filter-fabric sack is of 80 μm diameter mesh and traps blowing snow whilst allowing air to pass through. Hygrometers and thermistors were placed at heights of approximately 0.3 and 0.9 m. Particle detectors and anemometers were spaced at four heights which increased logarithmically from near the snow surface to a maximum near 2.0-m height.

A measurement "run" consisted of attaching the blowing-snow chemistry samplers to mast arms at heights of approximately 0.1, 0.2, 0.5 and 0.9 m, and uncovering the caps until the bags near the surface had filled with snow. With the caps replaced, the samplers were taken to a tent, where the contents were emptied into acid-washed plastic bottles. The bottles were then sealed in clean plastic bags. The samplers were washed with deionised water before each day's use. In the laboratory, no measurable increase in ion concentrations in snow was found for snow placed and handled in samplers which had been cleaned by deionised water in this manner. The quantity of ions collected by the traps does not correspond to the quantity of air moving through them, suggesting the solute collected is that contained in blowing-snow particles, rather than that free in the atmosphere as aerosol.

During each blowing-snow chemistry "run", surface snow was sampled at sites on the plateau within 100 m upwind of and parallel to the mast. Sites of active snow erosion and deposition were selected based upon visual identification. For example,

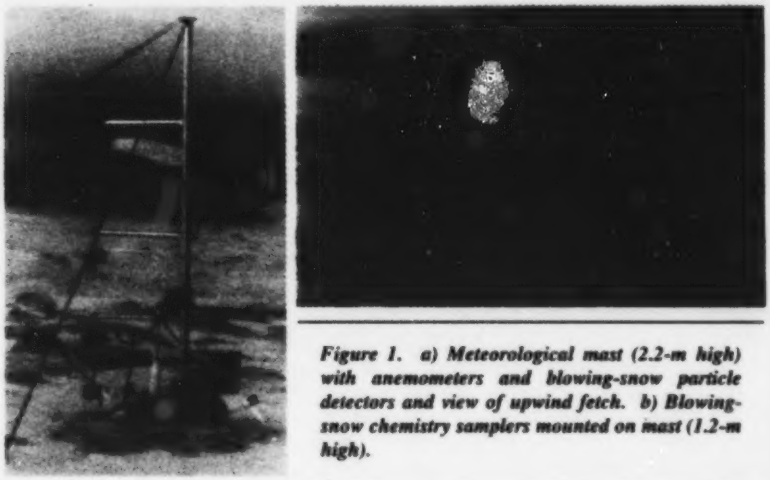

Figure 1. a) Meteorological mast (2.2-m high) with anemometers and blowing-snow particle detectors and view of upwind fetch. b) Blowing-snow chemistry samplers mounted on mast (1.2-m high).

erosion is evident on well-exposed snow surfaces where thin layers of snow are revealed at the edges of or within a snowpatch, whereas deposition appears as a lighter, fresher snow accumulating in a protected site. Acid-washed (3% HNO_3 solution), PTFE (Poly Tetrafluoroethylene) coated plastic hand scoops were used to skim the top 20-mm layer of these surface snows. An acid-washed 500-mL bottle of eroding and one of accumulating snow were filled for each run and then sealed in clean bags.

Laboratory Analysis

All snow samples were kept frozen until analysis. Samples were rapidly melted, filtered through 0.45 μm nucleopore filters (blank-tested), then stored in acid-washed bottles at 4°C. The concentrations of Cl^-, NO_3^- and SO_4^{2-} were determined using a Dionex Model 2000i ion chromatograph with precision of 2% and detection limits of $0.2\ \mu eq \cdot L^{-1}$. Ammonium concentrations were measured using the blue indophenol method (Parsons *et al.*, 1984) with a precision of $0.055\ \mu eq \cdot L^{-1}$. Analysis of the cations, Na^+, K^+ and Mg^{2+} was performed on a Pye Unicam SP9 atomic absorption spectrophotometer. Precision was between 1 and $2\ \mu eq \cdot L^{-1}$, a magnitude greater than the limits of detection.

Sample size collected by the blowing-snow samplers diminished with height above the surface, hence for some runs the volume of samples was too small to analyze the complete set of ions.

DESCRIPTION OF FINDINGS

Blowing-Snow Mass Flux

Suites of meteorological and chemistry measurements were satisfactorily completed for 27 runs, spaced over five days in late-March, 1989. The length of time comprising a run depends on the time required to fill the blowing-snow samplers and varied from 10 to 67 min., with an average of 23 min. The runs are grouped into four sets, based upon the day of measurement. Table 1 summarizes the meteorological and snowcover conditions for the sets of runs. Conditions on a whole were relatively mild and dry for northern British mountains.

Vertical profiles of wind speed measured from heights of 0.2 to 1.8 m matched the logarithmic increase with height quite well, indicating a neutral, fully-developed boundary-layer with most turbulence generated mechanically.

Typical examples of the vertical profiles of blowing-snow mass flux for each of the sets of runs are plotted in Figure 2, along with vertical profiles derived from measurements by Pomeroy (1988; 1989) in fully-developed blowing-snow conditions, over extensive, level, completely snowcovered terrain on the Canadian prairies. The mass fluxes measured on the Cairngorm plateau exhibit a more rapid decline with

Table 1. Summary of meteorological and snowcover conditions measured on the Cairngorm plateau, for sets of runs.

Run Number	Date March 1989	Surface Cover %	Mass Flux in Saltation $kg \cdot m^{-2} \cdot s^{-1}$	Air Temperature °C	Wind Speed/ Direction at 1.8-m $m \cdot s^{-1}$
			Peak	Mean	Peak/Mean
1-7	20-21	90% ice & rock 10% snow	1.48	-5.5	12.1/SW
8-16	22	100% fresh snow	1.91*	-5.5	14.0/SW
17-21	28	30% rock 70% fresh snow	0.25	-2.5	11.0/SW
23-29	29	95% rock & soil 5% snow	0.62	-3.0	23.5/SSE

**During Snowfall*

height than do the fully-developed profiles. An exception is Run 10 which was measured during heavy snowfall over a fresh, nearly complete snowcover. The mass fluxes without snowfall are roughly an order of magnitude less than the fully-developed case and Run 10. A similar phenomenon was noted in blowing-snow measurements on a small alpine plateau by Meister (1989), who found an unusually rapid decline in blowing-snow mass concentration with height, except during snowfall. Meister attributed his modified blowing-snow profiles to a short fetch, insufficient for fully-developed diffusion of snow. The wind profiles measured here display full development of turbulent-transfer mechanisms; this and

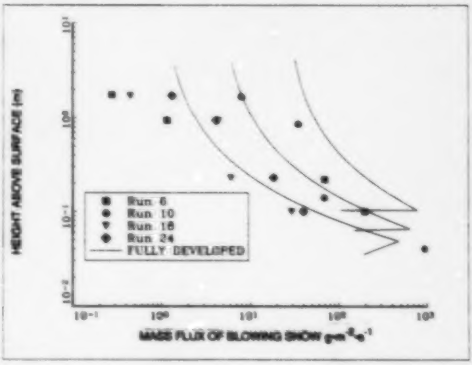

Figure 2. Typical vertical profiles (4) of blowing-snow mass flux measured on the Cairngorm plateau and for comparison three examples of fully developed profiles for u_{10} = 12, 15 and 20 $m \cdot s^{-1}$ (Pomeroy, 1988).

the 300-m fetch are sufficient for full-development of blowing snow near the surface when there is complete snowcover (Takeuchi, 1980; Pomeroy, 1989). Runs 6, 18 and 24, however, represent blowing snow that developed over a complete snowcover several hundred metres upwind, and then travelled over about 300 m of patchy snowcover to the point of measurement. The travel distance is sufficient for blowing-snow particles to have undergone significant sublimation. In these cases the opportunity to replace the depleted atmospheric snow load with eroding surface snow is limited and Runs 1 to 7, 17 to 21 and 23 to 29 represent "well-sublimated" blowing snow. During Runs 8 to 16, there was a greater opportunity to replace sublimated snow with "fresh" falling or surface snow and these conditions represent "poorly-sublimated" blowing snow.

Surface-Snow Chemistry

Mean values of ion concentration in eroding surface snow are listed for the four sets of runs in Table 2. The values are typical for moderately acid precipitation of largely maritime origin over western Europe (Snoeyink and Jenkins, 1980). For Runs 1 to 7, eroding surface snow contained the highest concentrations of sea salt (Na^+, Cl^-, Mg^{2+}) and high NH_4^+ concentrations but relatively low concentrations of H^+, NO_3^- and SO_4^{2-}. This composition indicates relatively unpolluted maritime sources of deposition onto the surface snow. The eroding snow for Runs 8 to 16 is much different, being derived from snow which fell that day, presumably under the influence of a less maritime source. The H^+, NH_4^+ and sea salt ions are in concentrations about one-half to one-third those of the previous day and NO_3^- and SO_4^{2-} are in somewhat higher concentrations. The eroding snow chemistry for Runs 17 to 30 reflects a fresh, more acidic, and less "maritime" snow early on March 28. However, this snow is still several orders of magnitude less acidic than that occasionally recorded for the "black/grey" snowfalls in the Cairngorms (Davies *et al.*, 1984). Concentrations of sea salt ions for Runs 17 to 30 are less than those measured for Runs 1 to 7. The highest concentrations of NO_3^-, SO_4^{2-}, NH_4^+ and K^+ measured in this experiment are found in Runs 17 to 30.

Table 2. Mean ion concentrations ($\mu eq \cdot L^{-1}$) in eroding surface snow for sets of runs.

Run Number	H^+	Cl^-	NO_3^-	SO_4^{2-}	NH_4^+	Na^+	K^+	Mg^{2+}
1-7	10.5	86.1	11.7	13.6	4.5	57.4	2.5	11.8
8-16	7.41	47.5	19.2	17.3	1.25	25.0	2.0	5.17
17-22	38.9	60.0	25.2	18.4	4.4	40.0	2.9	11.8
23-30	33.1	69.9	17.9	23.3	4.7	40.2	1.7	11.3

Effect of Wind Transport on Snow Chemistry

The mean ion concentrations in different snow types, surface snow at sites of erosion and of deposition, and blowing snow at the four measurement heights above the surface, are shown in Figures 3a and 3b. The concentrations are normalized with respect to eroding surface-snow values. Two distinctive blowing-snow conditions are shown: Runs 8 to 16 in Figure 3a developed from snow precipitating and blowing over a complete snowcover, and Runs 23 to 30 in Figure 3b developed from snow blowing out of the snow-filled corrie of Ciste Mhearad, and sublimating whilst travelling over a locally discontinuous snowcover. The initial surface snow for each set of runs differs; that for Runs 8 to 16 represents snow which fell that day near the measurement site, while that for Runs 23 to 30 represents older snow on the edge of Ciste Mhearad. Mean ion concentrations are generally greater in blowing snow than in eroding surface snow, except during Runs 8 to 16 for Cl^-, NO_3^-, SO_4^{2-}, Na^+ and Mg^{2+} at the lowest blowing-snow height and Na^+ and Mg^{2+} at the second lowest height. To evaluate the difference between concentrations in eroding and blowing snow, blowing-snow values from all four heights are

Figure 3. Mean ion concentrations normalized to eroding snow values for various snow classes: eroding snow, blowing snow at four heights and accumulating snow.

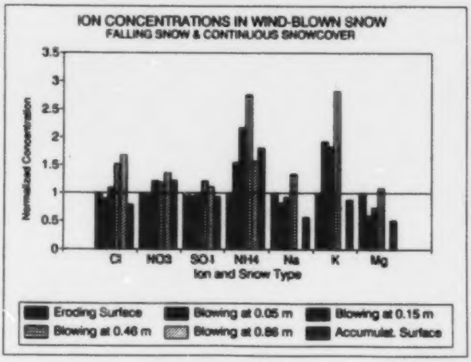

Figure 3a. Runs 8 to 16 during snowfall with continuous snowcover.

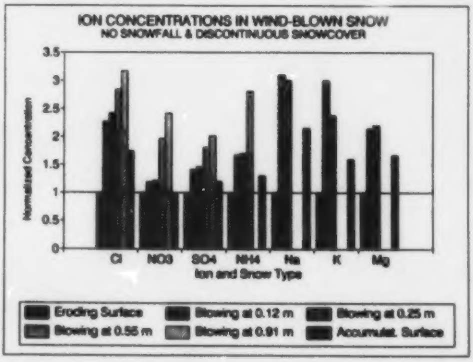

Figure 3b. Runs 23 to 30 no precipitation, snow blowing at least 300 m over a discontinuous snowcover.

combined and compared to eroding-snow values using the Student's "t" test. The probability (0 to 1) that the measured concentrations reflect actual differences between eroding and blowing snow is shown for each ion and set of runs in Table 3. The dissimilarities between the two sets of runs are indicated by the probabilities. For Runs 23 to 30 there is an approximately 0.99 or better chance that the ions in blowing snow are more concentrated than those in eroding snow. However, for Runs 8 to 16, only NH_4^+ and K^+ displayed this probability, the next highest being Cl^- at 0.84.

Table 3. Probability of a difference in ion concentration between eroding surface and blowing snows.

Run Number	Cl^-	NO_3^-	SO_4^{2-}	NH_4^+	Na^+	K^+	Mg^{2+}
8-16	+.836	+.713	--	+.991	-.032	+.997	--
23-30	+.999	+.989	+.999	+.996	+.999	+.999	+.999

"+" denotes concentration in blowing snow greater than that in eroding snow;
"-" denotes concentration in blowing snow less than that in eroding snow.

An analysis of variance F-test compared the ion concentrations in eroding and accumulating surface snow. The probability that measured concentrations of eroding and accumulating snow are different is shown for each ion and set of runs in Table 4. For Runs 8 to 16, only NH_4^+ has a probability greater than 0.8 of being more concentrated in accumulating snows, whilst Mg^+, Na^+ and Cl^- have probabilities greater than 0.7 of being more concentrated in eroding snows. For Runs 23 to 30, accumulating snow has higher concentrations than eroding snow of the following ions, ranked from greatest to least difference based upon the F-statistic,

$$Na^+ > Cl^- > Mg^+ > K^+ > SO_4^{2-} > NH_4^+$$

NO_3^- shows no difference in mean values. The probabilities for these differences are greater than 0.9 for Na^+, Cl^- and Mg^+; greater than 0.8 for K^+ and SO_4^{2-}; and, greater than 0.75 for NH_4^+. For Runs 23 to 30, NO_3^- never shows notably different

Table 4. Probability of a difference in ion concentration between eroding and accumulating surface snows.

Run Number	Cl^-	NO_3^-	SO_4^{2-}	NH_4^+	Na^+	K^+	Mg^{2+}
8-16	-.728	+.661	-.363	+.977	+.758	-.305	-.777
23-30	+.934	+.130	+.807	+.784	+.943	+.856	+.892

"+" denotes concentration in accumulating snow greater than that in eroding snow
"-" denotes concentration in accumulating snow less than that in eroding snow.

concentrations between accumulating and eroding snows. NH_4^+ displays the next least difference. Interestingly, and only during Runs 8 to 16, NO_3^- and NH_4^+ display the accumulating snow concentrations which are most elevated with respect to eroding snow. This behaviour may be associated with vapour transfer of these ions from and to snow particles and is a topic worthy of further investigation.

To examine the increase of blowing-snow ion concentration with height, an analysis of variance was conducted for each ion within each set of runs, with the 4-measurement levels as "treatments". For Runs 8 to 16 the ions generally show an increase in mean concentration with height. Based upon F-statistics from the analysis of variance the differences with height of the ion concentrations may be ranked from greatest to least as:

$$Cl^- > Na^+ > Mg^+ > NO_3^- > NH_4^+ > K^+ > SO_4^{2-}$$

These differences are significant at the 99% level of confidence for Cl^-, at the 90% level of confidence for Na^+, at the 80% level of confidence for Mg^+, NO_3^- and NH_4^+ and at only the 65% level of confidence for K^+. For Runs 23 to 30, only the anions show a significant increase in concentration with height. Noting that the cations are only available at the two lowest heights; Na^+ and K^+ decrease with height, only the decrease in K^+ being significant at the 75% level of confidence. Ion concentrations which increase with height may be ranked with regard to their F-statistic as:

$$SO_4^{2-} > NO_3^- > Cl^- > NH_4^+ > Mg^+$$

The differences are significant at the 99% level of confidence for SO_4^{2-}, NO_3^- and Cl^- and at the 95% level of confidence for NH_4^+.

For conditions of blowing snow when there is potential for sublimation, the measurements indicate that:

i) ion concentrations in blowing snow at heights from 0.1 to 0.9 m are higher than those in eroding and accumulating surface snow - an effect masked somewhat by concurrent snowfall and entrainment of fresh surface snow;
ii) ions become more concentrated in blowing snow with increasing height;
iii) the consistency from ion-to-ion and magnitude of the increase in concentration with height are greater without snowfall and with an incomplete snowcover; and,
iv) ion concentrations are greater in accumulating snow than in eroding snow. This effect is masked somewhat by mixing of snowfall and snow recently eroded from complete snowcovers with wind-blown snow in accumulating snow.

SUBLIMATION OF BLOWING SNOW AS A CONCENTRATING EFFECT

There are several processes besides sublimation of ice which may contribute to the changes in snow chemistry during wind transport, among these are:

i) scavenging of particulates by charged blowing-snow particles;
ii) uptake of nitric acid vapour into the ice lattice of particles exposed by wind erosion;
iii) mixing of snows having different ion concentrations;
iv) enhanced deposition of particulates onto accumulating snow;
v) a change in the volume of aqueous solution on the surface of snow particles due to shattering and metamorphism during transport; and,
vi) selective upward diffusion and transport of small snow particles.

The following analysis, however, is solely concerned with the effect that sublimation of blowing snow has on concentrating chemicals in wind-blown snow particles. This effect is evaluated for Runs 23 to 30 where there was limited opportunity for contribution from surface or falling snow for several hundred metres upwind of the measurement site.

Normalized concentration $C_x(t)$ of an ion (x) in a mass of snow where the mixture changes over time may be expressed as:

$$[1] \quad C_x(t) = \frac{\left[\dfrac{m_x(t)}{m_p(t)}\right]}{\left[\dfrac{m_x(i)}{m_p(i)}\right]}$$

where m_x is the mass of ion, m_p is the snow-particle mass, i represents the initial condition and t is the time elapsed. If m_x is constant over time, the blowing-snow sublimation rate provides an evaluation of Equation 1.

Schmidt (1972) developed a comprehensive expression for the sublimation rate of a blowing-snow particle, based upon a balance of energy and water-vapour transfer equations and the results of Thorpe and Mason's (1966) measurements of sublimation from ice spheres. The calculation is based upon the assumption that sublimating blowing-snow particles rapidly reach the "ice-bulb" temperature. Lee (1975) confirmed most of Schmidt's model, modifying the calculation for turbulence; Tabler (1975) and Pomeroy *et al.* (1990) confirmed the application of the sublimation calculation using field measurements of the mass balance of wind-blown snow and operational procedures for calculating sublimation. The blowing-snow sublimation rate coefficient for some size distribution of blowing-snow particles may be expressed as the proportional mass of a blowing-snow particle possessing mean mass sublimated per unit time, where:

$$\frac{\frac{dm_p}{m_p}}{dt} \quad m_p^{1} \frac{2 \pi \ r_m \sigma \qquad \frac{Q_r}{\lambda_T \ T \ Nu}\left[\frac{L_s \ M}{R \ T} \quad 1\right]}{\frac{L_s}{\lambda_T \ T \ Nu}\left[\frac{L_s \ M}{R \ T} \quad 1\right] \qquad \frac{1}{D \ \rho_s \quad Sh}} \tag*{[2]}$$

and symbols are listed at the end of text. A procedure for determining the environmental variables in Equation 1 described by Pomeroy (1988) is employed here.

This algorithm is used to estimate blowing-snow sublimation by calculating the sublimation that an initial column of fully-developed blowing snow would experience travelling over a fetch of uniform conditions. Particle height does not change over this fetch. The algorithm uses iterations of Equation 2 in that the initial mean particle mass is "sublimated" for 0.5 s, reset for the resulting radius, sublimated, reset and so forth. The normalized ion concentration at any time (t) is found using Equation 1 with m_p = particle mass and $m_x(i) = m_x(t)$. Time (t) is the fetch distance divided by particle speed (assumed equal to wind speed at the chemistry sampling height). The following initial conditions are set without regard to height, based upon observations during Runs 23 to 30: T = -2.6°C, RH = 89%, Q_r = 120 J·m^{-2}·s^{-1}. The wind speed and initial particle mass depend on height and are set to values predicted for the sampling heights. The assumption that these conditions prevail upwind of the measurement site is weak, though roughly similar conditions may have extended for 1,000 m back to the base of Ciste Mhearad. Table 5 shows initial wind speed and mean particle radius and the resultant $C_x(t)$ at times (t) representing fetch distances of 300 m and 1,000 m. Estimates for the two fetches represent an "envelope" of the concentration effects due to sublimation during transport from the possible surface snow sources to the mast.

There are several reasons why the algorithm might underestimate sublimation and hence $C_x(t)$. One is the variation in measured atmospheric parameters over the fetch. For instance, the sublimation response to a step change in relative humidity is skewed in that an increase of 5% RH reduces the estimated ion concentrations by 25% while a decrease of 5% RH raises

Table 5. Normalized concentration of ion, $C_x(t)$, due to sublimation of ice from blowing-snow particles for T = -2.6°C, RH = 89%.

Height m	U_z m·s^{-1}	r_m µm	C_x(t)(300 m)	C_x(t)(1000 m)
0.12	9.8	98	1.15	1.66
0.25	12.6	80	1.17	1.82
0.55	15.7	60	1.25	2.45
0.91	17.6	50	1.33	3.48

concentrations by 41%. A second reason is that the equality between particle speed and ambient wind speeds becomes less valid near the surface where particles may occasionally enter the saltation layer and experience much smaller horizontal velocities and longer travel times (Pomeroy and Gray, 1990).

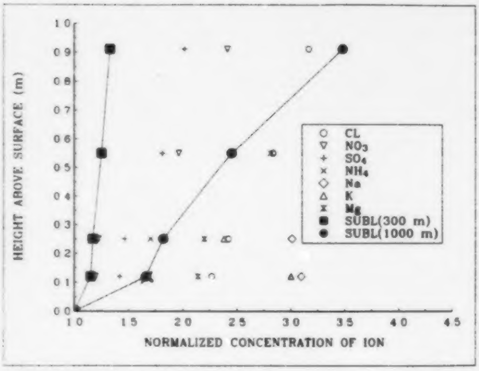

Figure 4. Normalized concentrations of ions in eroding and blowing snow (Runs 23 to 30) plotted with concentrations modelled using a blowing-snow sublimation algorithm for two possible upwind fetches, 300 and 1,000 m.

Noting these reservations, the envelope of normalized concentration due to sublimation and the normalized concentrations of measured ions are plotted against height above the snow surface in Figure 4. The normalized concentrations of NO_3^-, SO_4^{2-} and NH_4^+ all fit within the "sublimation effect envelope" (NH_4^+ at the 0.55 m height may not), however the other ions display values in excess of the envelope, particularly at the lowest height. It should be noted that the ions Cl^-, NO_3^-, SO_4^{2-}, and NH_4^+ are the most concentrated and are measured with the most precision, however the variation amongst ions is large and cannot be entirely discounted. In particular, Cl^-, a "conservative" and precisely measured ion, has relative concentrations double those suggested by comparing its slope to the envelope concentration slope for Subl(1000). It is expected that the increase in ion concentration with height is also due to a number of processes besides sublimation, some of which vary amongst ions. However, concentration due to sublimation is of sufficient order of magnitude to explain a large component of the higher ion concentrations in blowing snow, particularly for those ions which are most confidently measured.

CONCLUSIONS

Measurements of acidic blowing and surface snow in the Cairngorm Mountains of Scotland indicate important changes in snow chemistry during wind transport of snow. Concentrations of major cations and anions can be as much as three times greater in blowing snow than in eroding surface snow and as much as two times greater in accumulating snow than in eroding snow. These changes may be summarized as:

i) ion concentrations in blowing snow are elevated with respect to surface-snow values and increase with increasing height;
ii) the consistency from ion-to-ion and magnitude of the elevated concentrations and their increase with height are greater without snowfall and with an incomplete snowcover, i.e., conditions in which particles have undergone greater wind transport and sublimation;
iii) ion concentrations in accumulating snow are elevated with respect to eroding snow values;
iv) the enhancement of ion concentrations in accumulating snow is greater and more consistent from ion-to-ion where accumulating particles have undergone greater wind transport and sublimation; and,
v) relative concentrations of ions vary inconsistently with each other.

Several processes may contribute to the changes in snow chemistry during redistribution. One process, concentration of contaminants due to sublimation of ice from snow particles, has been examined using a model of sublimation during blowing snow. The effect of sublimation on ion concentration increases with height, air temperature, solar radiation and wind speed and decreases with particle size and atmospheric humidity. A comparison of the sublimation model results to measured concentrations suggests that sublimation explains much of the measured changes in chemistry associated with blowing snow for certain ions. However, the variation amongst ions suggest other processes may also contribute to the changes in snow chemistry. Given the highly redistributed snow found in open, northern areas, further research which assesses sublimation and other blowing-snow processes in a wide range of environments is necessary to adequately model the chemical evolution of these snowcovers.

ACKNOWLEDGEMENTS

The support of the North Atlantic Treaty Organization; the Royal Society, London; the USDA Forest Service, Rocky Mountain Forest and Range Experiment Station, Laramie, Wyoming, U.S.A. and the Division of Hydrology, University of Saskatchewan, Saskatoon, Canada made this experiment possible. The assistance of A. Jones and M. Varly, University of East Anglia, Norwich; Prof. G. Jones, INRS, Quebec; Dr. Z. Zeman, Czechoslovakian Academy of Sciences, Most; and D. Pomeroy in inclement and hazardous field conditions is greatly appreciated.

LIST OF SYMBOLS

$C_x(t)$	Normalized concentration of an ion (x) in a mass of snow at time t. (dimensionless)
D	Diffusivity of water vapour in the atmosphere ($m \cdot s^{-1}$).
i	Initial condition.
L_s	Latent heat of sublimation ($J \cdot kg^{-1}$).

m_p	Mass of snow particle (kg).
m_x	Mass of anion or cation (kg).
M	Molecular weight of water ($kg \cdot kmole^{-1}$).
Nu	The Nusselt number, the ratio of conductive to convective resistance to heat transfer from particle to atmosphere (dimensionless).
Q_r	Radiant energy received by the blowing-snow particle ($J \cdot m^{-2} \cdot s^{-1}$).
r_m	Radius of blowing-snow particle of mean mass (m).
R	Universal gas constant ($J \cdot kmole^{-1} \cdot K^{-1}$).
Sh	The Sherwood number, the ratio of convective to molecular resistance to transfer of water vapour by the atmosphere surrounding the particle (dimensionless).
t	Time over which sublimation occurs (s).
T	Ambient atmospheric temperature (K).
U_z	Mean horizontal wind speed at height z ($m \cdot s^{-1}$).
x	Cation or anion solute in snow.
λ_T	Thermal conductivity of the atmosphere ($J \cdot m^{-1} \cdot s^{-1} \cdot K^{-1}$).
ρ_s	Saturation density of water vapour at T ($kg \cdot m^{-3}$).
σ	Ambient atmospheric undersaturation of water vapour with respect to ice (dimensionless).

REFERENCES

BROWN, T. and J.W. POMEROY, 1989. A blowing snow particle detector. Cold Regions Science and Technology, 16(2), 167-174

DAVIES, T.D., P.W. ABRAHAMS, M. TRANTER, I. BLACKWOOD, P. BRIMBLECOMBE and C.E. VINCENT, 1984. Black acidic snow in the remote Scottish Highlands. Nature, 312(5989), 58-61

DAVIES, T.D., P. BRIMBLECOMBE, M. TRANTER, S. TSIOURIS, C.E. VINCENT, P.W. ABRAHAMS and I. BLACKWOOD, 1987. The removal of soluble ions from melting snowpacks. In - Seasonal Snowcovers: Physics, Chemistry, Hydrology, H.G. Jones and W.J. Orville-Thomas (Editors), NATO ASI Series, Series C: Mathematical and Physical Sciences, Vol.211, Proceedings of the NATO Advanced Studies Institute on Chemical Dynamics of Seasonal Snowcovers, 13-25 July 1986, Les Arcs, France, D. Reidel Publishing Co., Dordrecht, 337-392

DAVIES, T.D., P. BRIMBLECOMBE, I.L. BLACKWOOD, M. TRANTER and P.W. ABRAHAMS, 1988. Chemical composition of snow in the remote Scottish Highlands. In - Acid Deposition at High Elevation Sites, M.H. Unsworth and D. Fowler (Editors), NATO ASI Series, Series C: Mathematical and Physical Sciences, Vol.252, Proceedings of the NATO Advanced Studies Institute on Acid Deposition at High Elevation Sites, 8-13 September 1986, Edinburgh, Scotland, Kluwer Academic Publishers, 517-539

DELMAS, V. and H.G. JONES, 1987. Wind as a factor in the direct measurement of the dry deposition of acid polluants to snowcovers. In - Seasonal Snowcovers: Physics, Chemistry, Hydrology, H.G. Jones and W.J. Orville-Thomas (Editors), NATO ASI Series, Series C: Mathematical and Physical Sciences, Vol.211, Proceedings of the NATO Advanced

Studies Institute on Chemical Dynamics of Seasonal Snowcovers, 13-25 July 1986, Les Arcs, France, D. Reidel Publishing Co., Dordrecht, 321-335

GREEN, F.H.W., 1981. Climate and weather. In - The Cairngorms, their Natural History and Scenery, D. Nethersole-Thompson and A. Watson (Editors), The Melvern Press, Perth, Scotland, 228-236

LEE, L.W., 1975. Sublimation of snow in turbulent atmosphere. Ph.D. thesis, University of Wyoming, Laramie, Wyoming, 173 pp.

MEISTER, R., 1989. Influence of strong winds on snow distribution and avalanche activity. Proceedings of the Symposium on Snow and Glacier Research relating to Human Living Conditions, 4-9 September 1988, Lom, Norway, Annals of Glaciology, Vol.13, 195-201

PARSONS, T.R., Y. MAITA and C.M. LALLI, 1984. Determination of ammonia (alternative method). In - A Manual of Chemical and Biological Methods for Seawater Analysis, Pergamon International Library of Science, Pergamon Press, Oxford, U.K., 14-17

POMEROY, J.W., 1988. Wind transport of snow. Ph.D. thesis, Division of Hydrology, University of Saskatchewan, Saskatoon, Saskatchewan, 226 pp.

POMEROY, J.W., 1989. A process-based model of snow drifting. Proceedings of the Symposium on Snow and Glacier Research Relating to Human Living Conditions, 4-9 September 1988, Lom, Norway, Annals of Glaciology, Vol.13, 237-240

POMEROY, J.W. and D.H. MALE, 1987. Wind transport of seasonal snowcovers. In - Seasonal Snowcovers: Physics, Chemistry, Hydrology, H.G. Jones and W.J. Orville-Thomas (Editors), NATO ASI Series, Series C: Mathematical and Physical Sciences, Vol.211, Proceedings of the NATO Advanced Studies Institute on Chemical Dynamics of Seasonal Snowcovers, 13-25 July 1986, Les Arcs, France, D. Reidel Publishing Co., Dordrecht, 119-140

POMEROY, J.W. and D.M. GRAY, 1990. Saltation of snow. Water Resources Research, 26(7), 1583-1594

POMEROY, J.W., W. NICHOLAICHUK, D.M. GRAY, B. McCONKEY, R.J. GRANGER and P.G. LANDINE, 1990. Snow management and meltwater enhancement: final report. NHRI Contribution No.90021, National Hydrology Research Institute, Environment Canada, Saskatoon, Saskatchewan, 164 pp.

RATCLIFFE, D.A., 1981. The vegetation. In - The Cairngorms, their Natural History and Scenery, D. Nethersole-Thompson and A. Watson (Editors), The Melvern Press, Perth, Scotland, 42-76

SCHMIDT, R.A., Jr, 1972. Sublimation of wind-transported snow - a model. U.S. Forest Service Research Paper No.RM-90, Rocky Mountain Forest and Range Experiment Station, U.S. Department of Agriculture, Fort Collins, May, 24 pp.

SCHMIDT, R.A., 1982. Vertical profiles of wind speed, snow concentration and humidity in blowing snow. Boundary-Layer Meteorology, 23(2), 223-246

SNOEYINK, V.L. and D. JENKINS, 1980. Water chemistry. John Wiley and Sons, Toronto, Ontario, 463 pp.

TABLER, R.D., 1975. Estimating the transport and evaporation of blowing snow. In - Snow Management on the Great Plains, Great Plains Agricultural Council Publication No.73, University of Nebraska, Lincoln, 85-105

TABLER, R.D., J.W. POMEROY and B.W. SANTANA, 1990. Drifting snow. In - Cold Regions Hydrology and Hydraulics, W.L. Ryan and R.D. Crissman (Editors), Technical Council on Cold Regions Engineering Monograph, American Society of Civil Engineers, New York, N.Y., 95-145

TAKEUCHI, M., 1980. Vertical profiles and horizontal increase of drift-snow transport. Proceedings, Symposium on Snow in Motion, 12-17 August 1979, Fort Collins, Colorado, Journal of Glaciology, 26(94), 481-492

THORPE, A.D. and B.J. MASON, 1966. The evaporation of ice spheres and ice crystals. Journal of Applied Physics, 17(4), 541-548

TRANTER, M., T.D. DAVIES, P. BRIMBLECOMBE and C.E. VINCENT, 1987. The composition of acidic meltwaters during snowmelt in the Scottish Highlands. Water, Air, & Soil Pollution, 36(1-2), 75-90

TRANTER, M., P.W. ABRAHAMS, I.L. BLACKWOOD, P. BRIMBLECOMBE and T.D. DAVIES, 1988. The impact of a single black snowfall on streamwater chemistry in the Scottish Highlands. Nature, 332(6167), 826-829

PEATLANDS OF THE LAKE MELVILLE COASTAL PLAIN, LABRADOR

J.S. Price[1], D.A. Maioney, and F.G. Downey

Geography Department
Memorial University of Newfoundland
St. John's, Newfoundland
A1B 1Z6 CANADA

[1]Present address:
Department of Geography
Queen's University
Kingston, Ontario
K7L 3N6 CANADA

ABSTRACT

The peatlands formed on the coastal plain between Lake Melville and the Mealy Mountains represent the largest continuous expanse of wetland in Labrador. They have developed progressively as the coastal plain rose isostatically, with the oldest part of the peatland near the mountain being fen, and more juvenile ombrotrophic bog occurring toward the coast. The water balance of a 2.1 km^2 *basin, draining mostly fen and bog, is compared to that of a 3.2* km^2 *mountain basin and a 0.047* km^2 *section of string bog in the ombrotrophic zone. The mountain portion of the basin has a definite orographic effect, having increased and more frequent rainfall, but the channelized water from the mountain has little interaction with the wetland. Except in water tracks, the fen peatland does not readily transmit water along the regional gradient because of its broad expanse and low gradient. The string bog is very effective at storing water because of the storage characteristics of the pools. The peatland water balance indicates that only 10 to 15% of the inputs are lost as run-off, the remainder occurring as evaporation.*

INTRODUCTION

Wetlands comprise approximately one-fifth of Canada's land surface, and in northern Canada peatlands are the dominant wetland type. They form in response to climatic and hydrological processes which create a saturated environment where hydrophytic vegetation is produced faster than it decays. They present a technical problem in terms of building roads and pipelines, more so in the North because peatlands promote the occurrence of permafrost (Brown, 1974).

There are numerous hydrological environments which support peatlands, but in northern areas they are primarily ombrotrophic bogs (fed by meteoric water), and mineratrophic fens, which receive telluric water from surrounding mineral soils.

Bogs occur in poorly-drained areas where rainfall exceeds evaporation. Bay (1969) found bog run-off to be contingent on a high water-table following recharge by rainfall, and that run-off subsided quickly so that evaporation became the major water sink. Fens have a more stable water-table which is sustained by regional inflow (Bavina, 1975; Price and FitzGibbon, 1987), and therefore a more stable discharge regime. However, in the continuous permafrost zone, where fens occur in areas receiving summer inflow from overflowing streams and lakes and from late-lying snowbanks, the discharge regime may be strongly dependent on the position of the water-table (Roulet and Woo, 1986). In Labrador the subarctic and maritime influence has produced extensive patterned bogs and fens (Foster and King, 1984). The developmental sequence of patterned peatlands was inferred by Foster *et al.* (1983) to result from (1) paludification and general peat accumulation which smooths slope irregularities, thus converting channelized flow to surface flow, (2) slower peat accumulation in localized low, frequently-saturated areas, and (3) coalescence of these embryonic pools into arcuate pools along elevation contours. The role of hydrology in the developmental sequence is unclear. Foster and King (1984) suggest that patterned surfaces occur on relatively steep slopes with large inputs of water, whereas gentler slopes with little water movement are generally unpatterned. The hydrological behaviour of these environments is poorly documented. This study examines the effects of peatland morphology, the presence of peat, and the general topography on the summer yield from three basins.

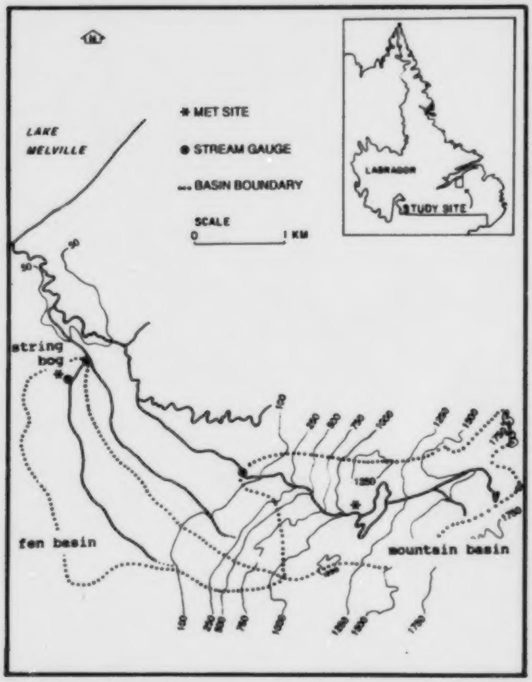

Figure 1. Study area, indicating boundaries of the main 2.1 km^2 peatland basin on the marine terrace, and the 3.2 km^2 mountain basin. The string bog subcatchment (0.047 km^2) is located at the meteorological station on the peatland.

STUDY AREA

The study area (53°33'N, 59°30'W) is located on the southern shore of Lake Melville, Labrador approximately 60-km east of Goose Bay (Figure 1). The area has been classified by Banfield (1981) as belonging to the interior Labrador climatic zone, which is a continental regime modified by the relatively warm lake to the north, and backed by the Mealy Mountains to the south. Mean January and July temperatures at Goose Bay are -16.4 and 15.8°C respectively (Canada, Environment Canada, 1982a). Mean annual precipitation is 946.1 mm, 56% of which is rainfall (Canada, Environment Canada, 1982b). Permafrost was not encountered.

The peatland study basin is situated on a gently-sloping marine terrace composed of fine sediments laid down in the Holocene (Tan and Vilks, 1987). The organic cover of peat is approximately 1.5-m thick, and is underlain by a thin layer of beach sands and lag deposits which mantle deep marine-clay deposits. This is responsible for the poor drainage in the area, and the development of the bog itself. The area is bounded to the south by the Mealy Mountain Plateau (450 to 750 m a.s.l.), which is an anorthosite bedrock criss crossed by gabbro dykes and sills. The area lies within the Lake Melville graben system.

Three basins were studied during the period June 26 to July 26, 1989. The main peatland basin (Figure 1) has a drainage area of 2.1 km^2. Forested sections of the basin include the riparian zone (*Picea mariana*) and mountain slope (*P. mariana* and *P. glauca*), which represent 13 and 14% of the basin area, respectively. The peatland portion of the basin is either horizontal fen or string bog (Canada, Environment Canada, 1987), which are 60 and 13% of the area, respectively. Within the main peatland basin, a string-bog sub-basin of a group of 40 bog pools was studied (Figure 2). It is linked to the channel of the larger peatland study basin by a soil pipe and channel which discharges from pool #30. Some non-channelized subsurface flow may be occurring along the southern margin of the sub-catchment. The pools are generally <1-m deep, and the strings (ridges) are typically 0.3 to 0.5-m high, consisting primarily of *sphagnum spp.* sometimes with *ericacea* and lichen cover. To contrast the run-off processes of the bog and mountain systems, a 3.2 km^2 mountain basin that drains onto the marine terrace (Figure 1) was also studied. This basin is 40% exposed bedrock, with white and black spruce in the valleys of the highly-jointed rock.

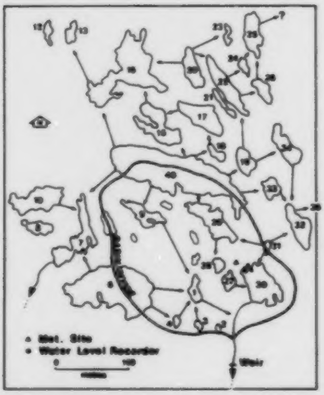

Figure 2. String bog study area. The arrows indicate the direction of water flow from the pools inferred from water surface elevation (Table 1), and the basin divide was plotted accordingly.

Table 1. Pond water surface elevation.

Pool #	Julian Day		
	178	182	203
1	19.348	19.384	19.397
2	19.701	19.712	19.72
3	19.522	19.575	19.59
4	19.424	19.487	19.502
6	19.762	19.783	19.765
7	19.597	19.622	19.607
8	19.533	19.579	--
9	19.408	19.445	19.434
10	19.832	19.855	19.837
12	19.431	19.461	19.451
13	19.42	19.447	19.457
15	19.44	19.475	19.445
16	19.433	19.463	19.452
17	19.563	19.59	19.569
18	20.012	20.045	20.02
19	20.012	20.064	20.027
20	19.758	19.796	19.787
21	19.752	19.79	19.773
22	19.75	19.784	19.771
23	19.468	19.52	19.505
24	19.559	19.598	19.585
25	19.382	19.421	19.405
26	19.595	19.624	19.613
27	19.582	19.63	19.629
28	19.629	19.667	19.656
29	19.686	19.719	19.705
30	19.34	19.382	19.393
31	19.993	20.058	20.058
32	19.819	19.863	19.854
33	19.926	19.973	19.956
34	18.911	18.962	18.95
35	19.174	19.213	19.206
36	19.346	19.364	19.374
37	19.363	19.365	--
38	19.279	19.307	19.29
39	19.247	19.285	19.27
40	--	20.207	20.195

METHODS

Rain was measured with tipping-bucket rain gauges at the main meteorological station located at the string-bog site, and in the mountains (Figure 1). Evaporation was determined at the meteorological site with the Priestley and Taylor (1972) combination model:

$$[1] \quad E = \alpha\,[s/(s + q)]\,(Q^{*} - Q_G)/L\rho$$

where E is the evaporation rate, s is the slope of the saturated vapour pressure - temperature curve, q is the psychrometric constant, Q^{*} is net radiation, Q_G is ground heat flux, L is the latent heat of vaporization, ρ is the density of water, and α is an empirical coefficient. To provide data for Equation 1, Q^{*} and Q_G were measured on a peat ridge at the meteorological site with a net radiometer and a soil heat-flux plate, and air temperature was measured at 1 cm with a thermistor. Hourly averages based on a sixty-second scanning interval were recorded by a data logger. Actual evaporation was estimated using weighing-type soil can lysimeters on a peat ridge, and at the edge of a pool. These values were recorded daily and used to determine α by rearranging Equation 1.

Streamflow was measured with V-notched weirs in the large peatland basin and from the sub-catchment. The weirs were calibrated against water elevation by collecting flow over a timed interval. Streamflow from the mountain watershed was measured with a current meter and related to stage so that a stage discharge relationship could be used to provide continuous data. In the string-bog sub-catchment staff gauges, were placed in 40 pools (Figure 2). The elevation of the water surface was measured on three occasions and expressed relative to a common arbitrary datum. The basin boundary was determined from the elevation of the bog pools, and enclosed an area of 4.7 ha.

RESULTS

The 350-m elevation difference between the mountain site and the peatland was sufficient to produce an orographic effect. Between July 6 and 25 the total rainfall in the mountain was 78 mm, compared to 54 mm in the peatland. Streamflow (per unit area) from the mountain basin was over 7 times higher than from the main peatland basin (Figure 3), far more than the difference between rainfall amounts. The high run-off ratio can be explained by 1) the poor water-storage characteristics of the mountain basin, which has a large proportion of bare rock, and thin soils in deep, narrow valleys, and 2) the lower evaporation rates from the mountain as implied by the lower air temperature, which averaged 13.9°C, compared to 15.7°C on the peatland.

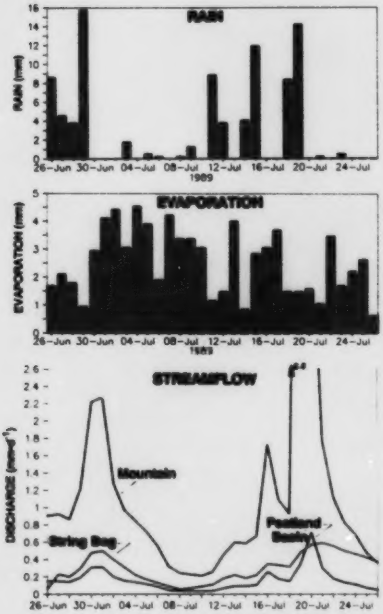

Figure 3. Rainfall (top), evaporation (middle) measured at the main meteorological site, and daily depth of run-off (bottom) from the mountain basin, the large peatland basin (Weir 1), and the string-bog sub-catchment (Weir 2).

The depth of run-off (discharge) from the 2.1 km^2 fen basin was generally slightly lower than from the string bog (Figure 3). The first major run-off event occurred in response to 32.4 mm of rainfall between June 26 and 29, and in the fen resulted in a peak discharge of 0.3 mm·d^{-1} on June 30 and July 1, compared to 0.5 mm from the bog. This period followed very hot dry conditions (up to 38.5°C on June 25) which created a storage deficit that had to be satisfied before significant run-off could occur. On July 20 a peak flow of 0.7 mm·d^{-1} issued from the fen, which exceeded that from the string bog (0.6 mm). This storm occurred following a week of rainy conditions (53.3 mm in total), which recharged the water-table to a higher position than for the previous run-off event. The relatively-large run-off peak demonstrates the fen's dependence on the water-table position. In a smaller valley-bottom fen, one would expect recharge from the larger hydrological system (i.e., surrounding mineral terrain) to sustain a higher water-table over dry periods, thereby reducing its dependency on antecedent conditions. In this large horizontal fen, the amount of recharge was inadequate to sustain the water-table during a dry spell, so its discharge was governed by antecedent conditions which affect the level of storage. The low gradient and large distances over the fen impart a long detention storage, which increases the opportunity for water to be lost by evaporation. However, the fen peatland basin has a shorter basin lag than the string bog (12 hours compared to 24 to 42 hours), which seems to contradict the evidence of high detention storage capacity. The shorter lag is due to direct precipitation onto source areas such as water tracks and channels within the fen.

Run-off from the bog did not exhibit so strong a dependency on the water-table as the fen because it was more effective at storing water under all conditions. The extremely long lag in the string bog reflects the non-channelized flow which must seep between pools toward pool #30 (Figure 2), which then drains through a soil pipe and emerges at the treed riparian zone of the main peatland channel. Furthermore, rain recharges the ground-water ridge of the peat strings separating the pools, and this ridge must subside completely before water transfer can occur between adjacent pools. Then, the seepage is retarded because of the low hydraulic conductivity of the lower layers of peat (5×10^{-6} $m \cdot s^{-1}$).

Evaporation measured with the lysimeters was used to determine the α value for Equation 1. The α parameter has been shown to be 1.26 for surfaces with no water limitation (Rouse *et al.*, 1977). Average α for the peat ridge was 1.1 (coefficient of variation = 0.34) suggesting some limitation to evaporation. This seems probable as the peat surface became very warm and dry. The average pool α value of 2.1 (coefficient of variation = 0.19) was greater than the calculated maximum value for the available radiant energy. This was due to the lateral advection of heated air over the adjacent ridges, which elevated the α value above 1.26. This compares favourably with a recent study of a small subarctic lake by Bello and Smith (1990), who found daily α values as high as 2.0 because of the local advection of heat energy over the lake surface. The seasonal α value found by Bello and Smith (1990) was 1.35. In the present study, the relatively small size of the ponds further enhanced the "oasis effect", thus boosting α. However, the high average value of 2.1 may be biased by (1) heating of the lysimeter, and (2) underestimation of Q^* over open water (the radiometer was over peat, which has a higher albedo). The areally weighted average α was 1.33 in the string bog, and 1.2 for the larger peatland. This resulted in a range of evaporation rates of 0.6 to 4.5 $mm \cdot d^{-1}$ for an average of 2.5 $mm \cdot d^{-1}$, which is an order of magnitude greater than run-off.

THE WATER BALANCE

A water balance was performed for the larger peatland basin and the string bog sub-catchment between June 26 and July 26 (Figure 4). The water balance can be written:

$$[2] \qquad \Delta S = P - E - Q$$

where P is precipitation, E is evaporation, Q is run-off and ΔS is the change in storage, which was taken to be the cumulative change in water level in pond #30. Over the short term, pond-water elevation may not adequately represent the daily storage changes in the peat because of evaporative enhancement in the pools.

However, over the period of the water balance this difference diminishes as the pool is recharged by subsurface inflow. Areally weighted rainfall in the main peatland basin was higher (94 mm) because of the orographic effect in the mountain portion, and it was 89 mm in the string bog. Evaporation was 75 and 79 mm, respectively. Run-off was extremely limited, totalling 5 and 9 mm for the large fen basin and string-bog basin respectively. The residual, x in Figure 4, was calculated using the right side of Equation 2, and thus should be comparable to ΔS. For the larger basin, the cumulative difference between x and ΔS was only 4 mm, whereas for the string bog it was 18 mm. The latter represents 20% of the input P, but is acceptable given the accuracy of the methods employed (Price and Woo, 1988). Some of the difference between x and ΔS can be attributed to the long lag in the water storage following rainfall events (see Figure 4) and the exaggerated rise in water level in pool #30 because of its position in the basin (Figure 2). Short-term storage changes in the peat ridges not accounted for by ΔS are important in delaying pool-to-pool water transfer, hence the discharge from the bog. The residual is not necessarily equal to the error in the water balance unless measurement errors cancel each other out, which cannot be ascertained. Precipitation is frequently underestimated in exposed locations (an open bog for example), and this may be partly responsible for the difference between ΔS and x. Error in measuring run-off comes from the measurement procedure and in the estimation of the basin area. However, even if the latter were misjudged by a factor of 2, the run-off depth would still be a small fraction of the evaporative losses.

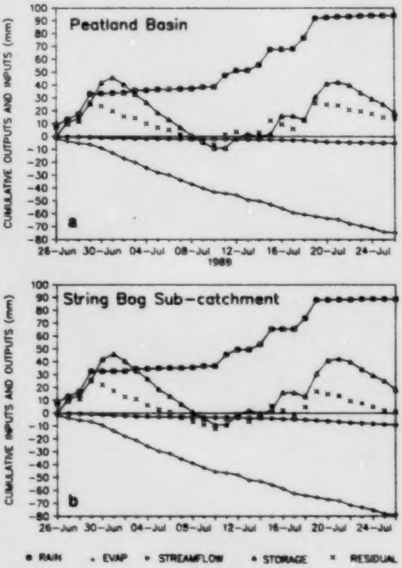

Figure 4. a) Cumulative water balance for the large peatland basin (top); and, b) for the string bog (bottom).

The streamflow losses were extremely small compared to other subarctic wetlands (Price and Woo, 1988; Roulet and Woo, 1986). The high storage capacity of the string bog within this peatland severely limits the rate of lateral water transfer, by retaining water in the pools, where evaporative loss rates are extremely high. The water-storage and flood-transmission properties of the string bog can be seen in Figure 4b, where the peak in ΔS comes 2 days after rainfall ceases. Furthermore, the ΔS in the pool (#30) is higher than the direct precipitation into the pool, because of the cumulative inflows from the more elevated pools.

CONCLUSIONS

The peatland is situated on a marine terrace which gently slopes away from the mountain towards Lake Melville. The distance across the terrace from mineratrophic mountain run-off has produced a trophic gradient, resulting in the development of fen for approximately 1 km, which gives way to bog as conditions become more and more ombrotrophic. The peatland forms which have developed therefore have a different hydrological behaviour. The limit of the fen is due to the eventual channelization of water from the mountain. In fact, most mountain run-off is constrained within incised channels that have eroded into the marine terrace, and has little opportunity to interact with the peatland. The bog appears to have become domed, thereby further limiting the inflow of mineralized water from the mountains.

The data indicate that the mountain basin exhibits very little storage capacity. Non-channelized mountain run-off and rainfall is detained on the fen because of its size and low gradient. The most remarkable storage characteristics are displayed by a string bog, where a very small (4.7 ha) sub-catchment detained flood peaks for up to 42 hours. This is due to slow water seepage rates from pool-to-pool, as water moves toward the main channel. Both peatland basins are effective at attenuating run-off, which in this study accounted for only 10 to 15% of the water losses there. The most important run-off events occur when the water-table is recharged by antecedent rainfall. Evaporation is the most important water sink, and this is enhanced in the string-bog pools by localized heat advection from peat ridges.

LIST OF SYMBOLS

E	evaporation
L	latent heat of vaporization
P	rainfall
Q	run-off
Q^*	net radiation
Q_G	ground heat flux
ΔS	change in water storage
ρ	water density
q	psychrometric constant
s	slope of the vapour pressure-temperature curve
x	residual from water balance calculations
α	co-efficient of evaporability

REFERENCES

BANFIELD, C.E., 1981. The climatic environment of Newfoundland. In - The Natural Environment of Newfoundland, Past and Present, A.G. Macpherson and J.B. Macpherson (Editors), Department of Geography, Memorial University of Newfoundland, St. John's, Newfoundland, 83-153

BAVINA, L.G., 1975. Water balance of swamps in the forest zone of the European part of the USSR. In - Hydrology of Marsh-Ridden Areas, Proceedings of the Minsk Symposium, June 1972, IAHS Publication No.105, International Association of Hydrological Sciences, UNESCO, Paris, 297-303

BAY, R.R., 1969. Runoff from small peatland watersheds. Journal of Hydrology, Vol.9, 90-102

BELLO, R. and J.D. SMITH, 1990. The effect of weather variability on the energy balance of a lake in the Hudson Bay Lowlands, Canada. Arctic and Alpine Research, 22(1), 98-107

BROWN, R.J.E., 1974. Distribution and environmental relationships of permafrost. In - Permafrost Hydrology, Proceedings of Workshop Seminar, 26-28 February 1974, Calgary, Alberta, Canadian National Committee of the International Hydrological Decade, 1-5

CANADA, ENVIRONMENT CANADA, 1982a. Canadian climate normals, 1951-1980. Vol.2 - Temperature. Canadian Climate Program, Atmospheric Environment Service, Environment Canada, Downsview, Ontario, 306 pp.

CANADA, ENVIRONMENT CANADA, 1982b. Canadian climate normals, 1951-1980. Vol.3 Precipitation. Canadian Climate Program, Atmospheric Environment Service, Environment Canada, Downsview, Ontario, 602 pp.

CANADA, ENVIRONMENT CANADA, 1987. The Canadian wetland classification system. Ecological Land Classification Series No.21, National Wetlands Working Group, Canada Committee on Ecological Land Classification, Land Conservation Branch, Canadian Wildlife Service, Environment Canada, Ottawa, Ontario, 18 pp.

FOSTER, D.R. and G.A. KING, 1984. Landscape features, vegetation and developmental history of a patterned fen in south-eastern Labrador, Canada. Journal of Ecology, 72(1), 115-143

FOSTER, D.R., G.A. KING, P.H. GLASSER and H.E. WRIGHT, Jr, 1983. Origin of string patterns in boreal peatlands. Nature, 306(5940), 256-258

PRICE, J.S., and J.E. FitzGIBBON, 1987. Groundwater storage - streamflow relations during winter in a subarctic wetland, Saskatchewan. Canadian Journal of Earth Sciences, 24(10), 2074-2081

PRICE, J.S., and M.-K. WOO, 1988. Studies of a subarctic coastal marsh. I. Hydrology. Journal of Hydrology, 103(3-4), 275-292

PRIESTLEY, C.H.B. and R.J. TAYLOR, 1972. On the assessment of surface heat flux and evaporation using large scale parameters. Monthly Weather Review, 100(2), 81-92

ROULET, N.T. and M.-K. WOO, 1986. Hydrology of a wetland in the continuous permafrost region. Journal of Hydrology, 89(1-2), 73-91

ROUSE, W.R., P.F. MILLS and R.B. STEWART, 1977. Evaporation in high latitudes. Water Resources Research, 13(6), 909-914

TAN, F.C. and G. VILKS, 1987. Organic carbon isotope ratios and paleoenvironmental implications for Holocene sediments in Lake Melville, southeastern Labrador. Canadian Journal of Earth Sciences, 24(10), 1994-2003

CONSTRAINTS ON THE ORIGIN OF ACIDITY IN COLOUR LAKE, AXEL HEIBERG ISLAND (79°25'N)

S. Schiff[1], M. English[2], M. Ecclestone[3], R. Elgood[2], M. Hinton[1] and L. Pezzutto[2]

[1]Waterloo Centre for Groundwater Research
University of Waterloo
Waterloo, Ontario
N2L 3G1 CANADA

[2]Department of Geography
Wilfrid Laurier University
Waterloo, Ontario
N2L 3C5 CANADA

[3]Department of Geography
Trent University
Peterborough, Ontario
K9J 7B8 CANADA

ABSTRACT

Colour Lake, a small pristine headwater lake in the High Arctic, has an exceptionally low natural pH of 3.7. Field research has been conducted on the Colour Lake watershed during springmelt, summer and early-fall periods over several years to ascertain the sources of acidity. Although all surface inflows to the lake are more alkaline than the lake, sulphur isotopes point to the presence of pyrite or another reduced Fe-S mineral within the basin. Oxidation of this mineral concomitant with the precipitation of iron hydroxides will generate acidity. Three areas of acidity generation have been identified. Seepage of ground water generated at the base of the frost-free layer into shallow littoral zones is extremely high in acidity and has a chemistry consistent with pyrite weathering but the seepage rate is too low to account for the steady-state pH of Colour Lake. Acidity is generated in all lake sediments but the flux has not yet been quantified. A small anoxic zone develops at depth in the lake containing elevated levels of Fe and SO_4^{2-} but little alkalinity. Upon lake ice-off and overturn, the oxidation of anoxic zone Fe^{2+} and subsequent precipitation of iron hydroxides is the major source of acidity to the lake identified to date. The existence of naturally occurring acid-generating mechanisms, especially those related to the depth of thawing of the permafrost, deserve further research in light of the projected effects of global climate warming on the High Arctic.

INTRODUCTION

Colour Lake is a small acidic lake located in the High Arctic (79°25'N, 90°45'W) on Axel Heiberg Island (Figure 1). Although the lake has a moderate salt content

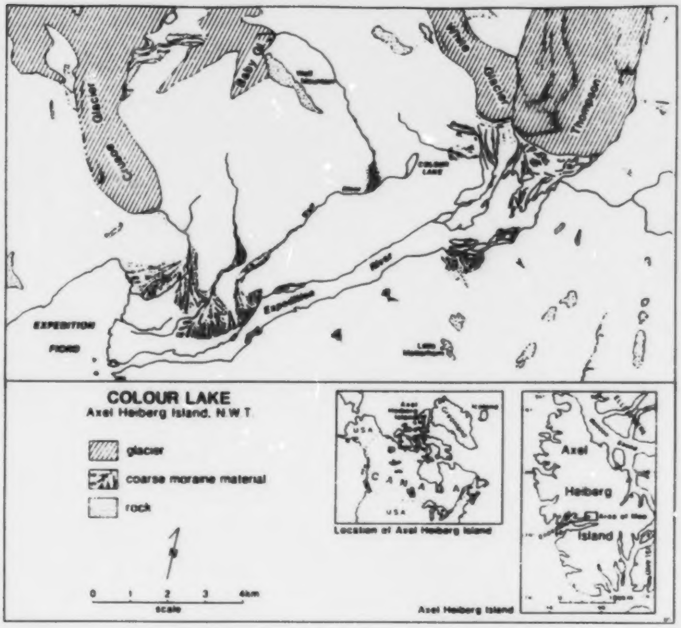
Glacier
Baby
Thompson
Glacier
EXPEDITION
FIORD
Expedition
River
Colour Lake
COLOUR LAKE
Axel Heiberg Island, N.W.T.
glacier
coarse moraine material
rock
0 1 2 3 4km
scale
U.S.A.
C A N A D A
U.S.A.
Location of Axel Heiberg Island
Axel
Heiberg
Island
Area of Map
Axel Heiberg Island

Figure 1. Location of Colour Lake catchment, Axel Heiberg Island (modified from Allan et al., 1987).

(Table 1), the ambient average water column pH (3.7) is extremely low. Because the watershed of this high-arctic lake is undisturbed except for occasional scientific expeditions, the origin of the exceptionally low natural pH of this pristine lake and the existence of natural acidifying processes in high-arctic systems are of scientific interest. The High Arctic is also a location where the maximum effects of global warming are likely to be realized (Manabe and Wetherald, 1980). Thus, understanding the natural acidifying processes is important in assessing the sensitivity of these systems to change due to global warming.

Research on the Colour Lake watershed has been the object of expeditions spanning five years and covering snowmelt, late-summer and early-fall periods (English *et al.*, 1991). Field pH measurements show that the lake is five times more acidic than any of the lake inflows during any of the sampling periods (Allan *et al.*, 1987; English *et al.*, 1991). Current hypotheses for the origin of the low pH of the lake water include: 1) a long lake-water residence time with acidity resulting from pyrite oxidized during the initial stages of lake formation following deglaciation,

2) the seepage into the nearshore lake littoral zones of acidic ground water originating at the base of the current frost-free layer in late-summer and acidic from the weathering of pyrite, 3) seepage into the lake of deeper, regional acidic ground water, and 4) in-lake acidification generated by weathering of lake sediments and by the seasonal reduction and oxidation of iron-rich sediments in the small anoxic zone at depth in the centre of the lake. Although the available data are somewhat limited due to the remoteness of the lake, an examination of the chemistry of Colour Lake and constraints on the hypotheses for the origin of the acidity are possible.

METHODS

Colour Lake is an oligotrophic lake with a maximum depth of 23.5 metres (Figure 2). Bedrock in the catchment consists of sandstones, shales and siltstones of late Mississippian and Tertiary age (Fricker, 1963). An ice cover of up to 2 m in thickness isolates the lake from atmospheric contact for 10 to 12 months per year (ice-off in August).

Field expeditions to Colour Lake watershed were facilitated by the Polar Continental Shelf Project and occurred yearly from 1959 (Ommanney, 1987). Data reported in this paper were collected during the snowmelt and early-summer period from May 14 to June 30, 1985, and during the late-summer and early-fall from August 14 to September 2, 1988 and August 20 to 28, 1989.

Colour Lake receives inflowing water from two major surface inflows

Table 1. Salient physical and chemical characteristics of Colour Lake, Axel Heiberg Island.

Area (10^4 m^2)	10.2
Mean Depth (m)	10.1
Maximum Depth (m)	24.0
[1]Water Renewal Time	25-50
[2,3]Water Column Chemistry	
Ca^{2+}	3170
Mg^{2+}	1400
Na^+	80
K^+	135
NH_4^+	0
H^+	200
SO_4^{2-}	5970
Cl^-	30
Mn	4.51
SiO_2	50
Al	6.7
Fe	1.24
DOC	0.4
conductivity	550
pH	3.74
TP	36
[4] $\Sigma+$	5879
$\Sigma-$	6000
$(\Sigma+ - \Sigma-)/\Sigma+$	2%

[1] *Based on an annual evapotranspiration of 5.8 cm·yr^{-1}, a mean depth of 10.1 m, a ratio of watershed (including lake): lake surface area of 7:1 and assuming evaporation from the lake surface is negligible and the water yield from the terrestrial basin is 50 to 100% of precipitation.*

[2] *Sampled June 15, 1985.*

[3] *All values in µeq·L^{-1} except SiO_2 (µM), Al (mg·L^{-1}), Fe (mg·L^{-1}), Mn (mg·L^{-1}), DOC (mgC·L^{-1}), conductivity (µS·cm^{-1} at 25°C) and total phosphorous (TP) (µg·L^{-1}).*

[4] *Including Al as Al^{3+}, Fe as Fe^{2+} and Mn as Mn^{2+}.*

(west, east), four minor surface inflows ("No-Name Creek", "Gordon Creek", and Streams A and B) and from subsurface seepage (Figure 3). Only the first three streams flow throughout the spring, summer and fall periods.

The lake hydrological budget was constructed from direct gauging of lake inflows and outflows, measurements of groundwater seepage and lake stage, and oxygen isotopes of water samples (English *et al.*, 1991). Mini-piezometers (Lee and Cherry, 1979) were installed to the base of the frost-free layer (approximately 30 to 40 cm) in near-shore lake areas. Hydraulic conductivities in the littoral sediments were obtained using the falling head test (Lee and Cherry, 1979).

Samples were collected for chemical and isotopic analysis from the lake, inflows, seeps and ground-water

Colour Lake

Geographical Location		79° 25'N, 90° 45'W
Height Above Sea Level		176m a.s.l.
Maximum Effective Length	L_m	650m
Maximum Effective Width	W_m	220m
Surface Area	A	102,070m^2
Volume	V	1,034,570m^3
Maximum Depth	Z_{max}	24.0m
Mean Depth	Z	10.1m
Drainage Basin Area (including lake)		0.8 km^2
Drainage Basin Area (excluding lake)		0.7 km^2
Mean Height of Drainage Basin		59m

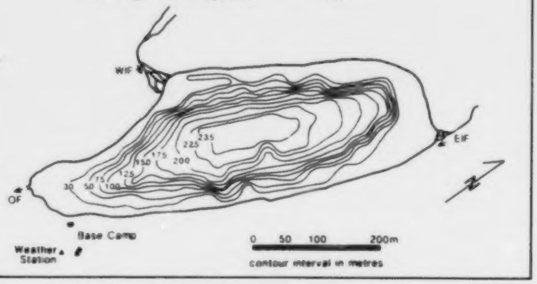
WIF
EIF
OF
30
50
75
100
125
150
175
200
225
235
Base Camp
Weather Station
0 50 100 200m
contour interval in metres

Figure 2. Morphometry of Colour Lake (modified from Allan et al., 1987).

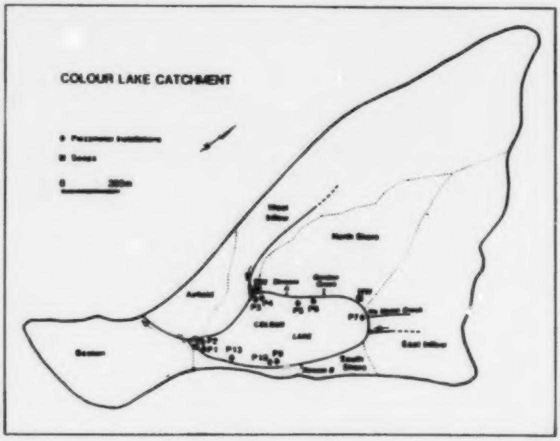
COLOUR LAKE CATCHMENT
COLOUR
LAKE

Figure 3. Sub-basins and streams of Colour Lake catchment (modified from Allan et al., 1987).

mini-piezometers. Conductivity and pH analyses were performed in the field. Major ion analyses were conducted at the Ontario Ministry of the Environment (cations 1985), Environment Canada (anions 1985) and the University of Waterloo Water Quality Laboratory (1988 and 1989).

Sulphur, oxygen and hydrogen isotope ratios were analysed at the Environmental Isotope Laboratory at the University of Waterloo. Stable isotope results are reported in ∂^{34}S‰ Cañon Diablo Troilite (CDT), ∂^{18}O‰ Vienna Standard Mean Oceanic Water (Vienna-SMOW) and ∂^{2}H‰ SMOW. Tritium results are reported in tritium units (T.U.) where 1 T.U. is 10^{-18} ^{3}H/^{1}H.

Porewater profiles were collected with an *in situ* dialysis membrane sampler (Hesslein, 1976). Details of sampling methods are given in Schiff and Anderson (1986).

RESULTS AND DISCUSSION

Origin and Magnitude of the Source of Acidity

Major ion chemistry of Colour Lake water is dominated by Ca^{2+}, Mg^{2+} and SO_4^{2-} (Table 1). All other ions are of very minor importance.

English *et al.* (1991) document the importance of the melting of the seasonal frost layer to the hydrological and chemical mass budgets of the lake basin. Although the major hydrological contribution occurs during springmelt, the major chemical contribution occurs during the summer and early-fall when the water percolates through and interacts with the thawed active layer. All the streams flowing into Colour Lake during springmelt when the soils are mostly frozen (Allan *et al.*, 1987) and in late August at the maximum extent of the thawed layer (Table 2) have a pH higher than the pH of Colour Lake.

Several of the streams have positive alkalinities and deliver acid-buffering capacity to the lake. The magnitude of the terrestrial alkalinity yield can be calculated from the hydrological mass balance, and stream and seepage chemistry obtained in the spring, summer and early-fall periods (English *et al.*, 1991). The yield of alkalinity ratioed to the lake surface area is, at maximum, approximately 90 $meq \cdot m^{-2} \cdot yr^{-1}$.

The H^+ concentration at steady state in Colour Lake will equal the total input (terrestrial yield plus precipitation) divided by the outflow volume (e.g., Schindler, 1986):

$$[1] \qquad [H^+] = \frac{\text{input}}{\text{outflow}} \qquad \frac{meq \cdot yr^{-1}}{m^3 \cdot yr^{-1}}$$

Table 2. Chemical data: August 1989 and springmelt 1985.

Sample	Date	Field pH	Ca mg·L^{-1}	Mg mg·L^{-1}	Na mg·L^{-1}	K mg·L^{-1}	Fe mg·L^{-1}	Alk mg·L^{-1}	SO$_4$ mg·L^{-1}	Cl mg·L^{-1}	NO$_3$ mg·L^{-1}	Charge Balance Error (%)
West Inflow	26.08.89	7.04	41.9	17.1	2.15	1.21	0.3	17	146	0.46	0.51	4
SW Seep	26.08.89	6.79	50.2	12.3	0.99	0.78	0	24	138	0.32	0	4
NW Seep	26.08.89	7.16	81.9	44.8	4.21	2.03	0	54	322	1.04	0.94	2
No-Name Creek	26.08.89	6.39	57.6	24.8	1.64	1.51	0	8	221	0.62	0	3
East Inflow	26.08.89	5.66	40.9	6.9	1.38	1.03	0	0	120	0.33	0	4
Precipitation	26.08.89	5.30	0.13	0.009	0.05	0.05	0	0	0.59	0.08	0.56	-18
Piezo 10	25.08.89	2.71	221	17	4.42	1.85	75.7	0	1290	2.6	0	-21
Piezo 5	25.08.89	4.41	127	79.3	4.4	4.34	3.42	0	608	1.19	0	3
Piezo 13	25.08.89	2.98	384	15	5.85	0.48	26.3	0	1530	2.46	0	-17
Piezo 4	25.08.89	5.58	--	--	--	--	--	--	--	--	--	--
Piezo 6	25.08.89	5.35	--	--	--	--	--	--	--	--	--	--
Piezo 7	25.08.89	5.08	--	--	--	--	--	--	--	--	--	--
West Inflow	06.06.85	6.22	3.1	0.7	0.15	0.35	--	--	4	0.27	0.03	--
East Inflow	06.06.85	5.41	15.7	1.5	1.26	0.63	--	--	44	1.1	0.13	--
Stream A	26.05.85	5.71	6.02	1.51	0.33	0.66	--	--	18	0.43	0.03	--
Stream B	06.06.85	5.29	18.2	0.21	0.23	0.2	--	--	40	0.5	0.25	--
Gordon Creek	29.05.85	4.04	32.2	2.6	0.46	0.54	--	--	--	0.5	0.25	--

In a steady-state water budget, the outflow must be less than the precipitation multiplied by the total watershed area (including the lake) due to evaporation. Using an annual precipitation of 5.8 $cm{\cdot}yr^{-1}$ measured at Eureka, N.W.T. (80°N, 85°W), assuming that evapotranspiration is zero and using a steady-state lake pH of 3.70 yields a maximum acidity source of 90 $meq{\cdot}m^{-2}{\cdot}yr^{-1}$. Thus the production of acid within the Colour Lake basin must exceed the terrestrial yield of alkalinity plus the acidity needed to maintain the H^+ steady-state concentration or an approximate total of 180 $meq{\cdot}m^{-2}{\cdot}yr^{-1}$.

Organic acids are not a potential source of acidity to Colour Lake. High-arctic systems are generally oligotrophic. Dissolved organic carbon (DOC) concentrations in Colour Lake are low: 0.4 $mg{\cdot}L^{-1}$. Using the ratio of Oliver *et al.* (1983) of 10 $\mu eq{\cdot}mgC^{-1}$, 0.4 $mg{\cdot}L^{-1}$ of DOC corresponds to only 4 $\mu eq{\cdot}L^{-1}$ of acidity. The only possible way organics could be important as an acidity source is if organic acids were to enter the lake and precipitate with Ca leaving the H^+ behind. However, this would require a large input of anionic DOC with unusually low pKa (high first acid dissociation constant) and thus a source of very acidic high-DOC water. DOC in the two major inflows are low, averaging 2.7 $mg{\cdot}L^{-1}$ throughout the flow period (Allan *et al.* 1985) and are not acidic. DOC in ground waters is typically lower than in surface waters. There is no evidence for a high DOC input to Colour Lake.

Pyrite has been reported to be present in the sedimentary rocks in the basin (Fricker, 1963). Oxidation of pyrite with oxygen generates acidity:

$$[2] \qquad FeS_2 + \frac{15}{4} O_2 + \frac{7}{2} H_2O \rightarrow Fe(OH)_3 + 4\ H^+ + 2\ SO_4^{2-}$$

and pyrite oxidation somewhere in the basin is a likely candidate for the source of acidity. The presence of pyrite and the processes affecting lake-water sulphate should be reflected in the sulphur isotopic signature of the sulphate. Sulphate from a nearby set of perennial springs (Sulphur Springs; Figure 1) has the typical isotopic signature of marine sulphates ($\partial^{34}S$ of 15 to 25‰; Figure 4) and is consistent with the observed presence of gypsum and anhydrite in the terrestrial basin. Sulphate from the western portion of the catchment (west inflow, southwest seep (SW)) is depleted by 35‰ relative to marine sulphate suggesting a sedimentary-pyrite or reduced-S source. The $\partial^{34}S$ of the sulphate in the northwest seep (NW), east inflow and in Colour Lake lies

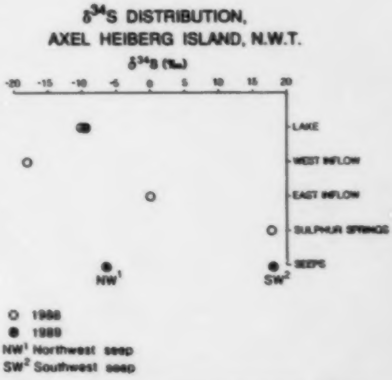

Figure 4. ***$\partial^{34}S$ in samples from Colour Lake catchment, Axel Heiberg Island. Error is ±0.2‰.***

between these two end members suggesting both an evaporite and a reduced-S source for the lake-water sulphate.

Oxidation of Pyrite during Initial Lake Formation

The acidity of Colour Lake could be a remnant feature of initial lake formation. Pyrite contained in the surficial soils would have been oxidized after the retreat of White Glacier, 9,000 to 10,000 years ago, and the initial surfical run-off in the catchment may have been very acidic. If the lake-water residence time is long, much longer than the 25 to 50 years calculated on the basis of hydrological input (Table 1), the lake may still contain a portion of the original acidity even though the pyrite has long since been completely weathered from these surficial soils. The hydrological water residence-time for the lake would have been underestimated if mixing of inflows within the lake is restricted. At least in some years, a substantial portion of the snowmelt water does not mix with the lake water but as a result of moat formation, proceeds directly out the lake outflow (Allan *et al.*, 1985; English *et al.*, 1991). Summer inflows may also not mix completely due to thermal stratification under the ice cover.

If the water residence-time is very long, the lake $\partial^{2}H$ and $\partial^{18}O$ values could be altered to lighter values by evaporation and sublimation of the lake ice cover (Hermichen *et al.*, 1985) or to heavier values by evaporation of lake water during ice-free months. Evaporation and sublimation result in kinetic isotopic fractionation and can cause isotope values to deviate from the meteoric water line. Colour Lake water, stream water and precipitation isotopic values all follow a linear trend and thus (Figure 5) provide no additional insight into the lake-water residence time.

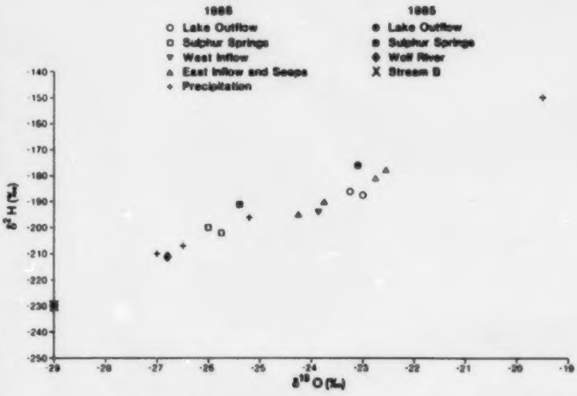

Figure 5. $\partial^{2}H$ versus $\partial^{18}O$ in samples from Colour Lake catchment, Axel Heiberg Island. Errors are ±0.2‰ in $\partial^{18}O$ and ±0.2‰ in $\partial^{2}H$.

Measurements of lake ^{3}H indicate that Colour Lake must have a short residence time. Lake water has a ^{3}H content of 96±8 T.U. compared to inflows of 55±12 T.U. A simple one-box model using the temporal ^{3}H inputs from Ottawa, Ontario corrected for latitude using the relationships of Weiss and Roether (1980), indicates that the water residence-time must be in the order of 20 to 25 years to result in the observed lake water ^{3}H activity.

Direct Seepage of Acidic Ground Water into Colour Lake

Although several well-defined surface streams exist, much of the catchment drains directly into the lake through subsurface seeps, especially during the fall (English *et al.*, 1991). Seepage waters from surface soils measured during the snowmelt period have a pH range of 4.23 to 7.03 (Allan *et al.*, 1987) and are not as acidic as lake water. However, during the late-summer field season in 1989, ground water with a pH as low as 2.71 (Table 2) has been observed seeping into the lake in a small restricted area of the catchment. Chemical analyses of waters from the piezometers on the southern shores of the lake (Piezometers 10 and 13, Figure 3; Table 2) show that these acidic seepage waters are elevated in calcium, sulphate and iron consistent with the combined weathering of gypsum and pyrite. Seepage waters from the northern shore are less acidic than lake water (e.g., Piezometer 5; Table 2).

The area of potential seepage was mapped based on the similarity in catchment geology, topography and on the amount of iron-staining in the nearshore sediments. Taking a hydraulic head of 3 to 5 mm measured in mini-piezometers in the littoral lake sediments (late-August 1989) over a flow period of three months and assuming a maximum hydraulic conductivity of 10^{-4} cm·s^{-1}, yields a seepage rate of 50 m^{3}·yr^{-1} and a source of acidity of only 1 meq·m^{-2}·yr^{-1}. A maximum limit to the acidity source can also be estimated by multiplying the area potentially contributing these extremely-acidic seepage waters by the run-off estimate (5.2 cm·yr^{-1}) calculated by Ohmura (1972) from climatological observations; an estimate which is in close agreement with the run-off value calculated by English *et al.* (1991) from hydrological measurements in the Colour Lake catchment. This upper limit using a basin-averaged run-off value corresponds to 26 meq·m^{-2}·yr^{-1}. Although the uncertainties in these 'back-of-the-envelope' calculations are undoubtedly substantial, the calculations yield information as to the potential contributions of some of the hypothesized sources of acidity. Based on our current data, acidity of shallow seepage waters is insufficient to account for the observed acidity of Colour Lake. Permeameter measurements on soil and sediment cores are currently underway to provide a better estimate of the hydraulic conductivity of the lake sediments.

Regional Acidic Ground-Water Inputs to Colour Lake

Colour Lake is located in an evaporite diapir but is confined by an underlying shale bed. If the shale bed is not continuous or watertight, deeper regional ground water may be slowly percolating in to and out of the lake. Since pyrite is located in the sedimentary strata in the Expedition Fiord area (Fricker, 1963), this ground water may be acidic. Water was collected for chemical analyses from the sulphur springs

(Figure 1) that are located approximately 125 metres below the lake level and separated from the lake by a dome of gypsum. The spring waters have a $\partial^{18}O$ of -25 to -26‰, considerably lighter than the lake water (-23‰; Figure 5) suggesting either recharge only by snowmelt waters when the ground is predominantly frozen or an origin under colder climatic conditions. High alkalinities were measured in the spring waters (1,040 to 1,160 $\mu eq \cdot L^{-1}$) and the waters contain NaCl (Cl 50,260 $mg \cdot L^{-1}$; Allan *et al.*, 1987) indicating the presence of halite below the gypsum dome. Colour Lake waters are depleted in NaCl (Table 1). Spring waters contain little ^{3}H, much lower than lake water or stream water (Table 3) indicating that the spring waters are older, receiving most of their recharge prior to the 1960s. ^{222}Rn activities were extremely high in the springs but undetectable (<10 $dpm \cdot L^{-1}$) in the lake throughout the water column under an ice cover (English and Schiff, unpublished data). Substantial inputs of regional ground water with high ^{222}Rn, high Cl or low ^{3}H are not evident in Colour Lake water. Either the ground-water system feeding Colour Lake is not continuous with the ground-water source for the springs or the deep regional ground-water input to Colour Lake is minimal.

Table 3. Tritium concentrations in samples from Colour Lake catchment, Axel Heiberg Island.

Sample	Date	^{3}H (T.U.)
Precipitation	26 Aug 89	39 ± 8
Precipitation	25 Aug 89	26 ± 8
West Inflow	25 Aug 89	51 ± 8
East Inflow	25 Aug 89	58 ± 8
Colour Lake Outflow	25 Aug 89	96 ± 8
Sulphur Springs	23 Aug 89	14 ± 8

In-Lake Processes

Weathering of the pyrite or other minerals contained in the lake sediments could also be a source of acidity to Colour Lake.

To examine the reactions occurring in the sediments and the flux of components from the sediments to the overlying water column, a porewater profile was collected at 4-m water depth. Sediment porewaters are acidic to a depth of at least 16 cm (Figure 6). Calcium, Mg^{2+}, Na^{+}, K^{+}, NH_4^{+} and Cl^{-} all exhibit modest increases in concentration with depth. A small increase in alkalinity and thus pH accompanies the increase in these major ions. Iron and sulphate increase dramatically with depth in the porewaters. Porewater SO_4^{2-} increases to twice the lake-water value by 16 cm and is balanced by the increase in porewater Fe. The lack of a porewater gradient in SO_4^{2-} in the upper 6 cm may be indicative of either a disturbance of the porewater profiles by convective mixing of porewaters or bioturbation, or a misidentification of the actual sediment-water interface (SWI) due to the presence of a macrophyte layer covering the sediments. This uncertainty in the location of the SWI prevents the calculation of the porewater fluxes. However precipitation of Fe^{2+} at the anoxic-oxic boundary must occur because of the much lower Fe concentrations in the

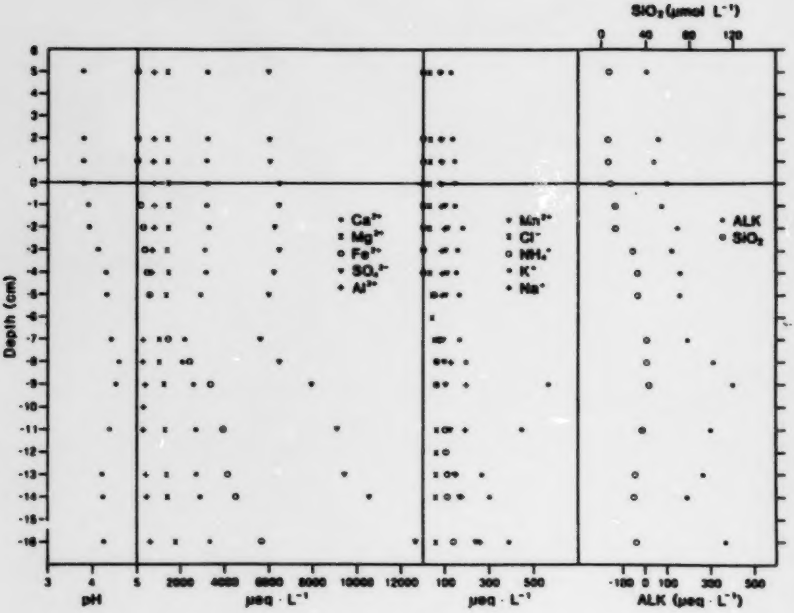

Figure 6. Sediment porewater profiles at 4 metres overlying water column depth in Colour Lake, Axel Heiberg Island in June 1985. Depth is positive above the sediment-water interface.

lake than in the porewaters and will generate acidity equal to the Fe^{2+} concentration in equivalents. Analyses of a sediment profile obtained in August 1989 with better control on the location of the sediment-water interface may permit a calculation of the acidity flux associated with shallow sediments.

A small portion of the hypolimnion (22 to 23.5 metres; <0.4% of the lake volume; Caflisch, 1972) becomes anoxic during the long under-ice stratification period. The anoxia results in water column alkalinities of 310 $\mu eq{\cdot}L^{-1}$ measured in May 1985 compared to -195 $\mu eq{\cdot}L^{-1}$ in the surface waters. Iron hydroxides precipitate readily upon oxygenation of these anoxic bottom waters. The alkalinity increase observed in May 1985 ($\Delta Alk = 505\ \mu eq{\cdot}L^{-1}$) is approximately balanced by the increases in Na^+ and K^+ which were recorded in 1984 (570 $\mu eq{\cdot}L^{-1}$; Allan *et al.*, 1987). Sulphate increases markedly in the anoxic zone ($\Delta SO_4^{2-} = 5{,}413\ \mu eq{\cdot}L^{-1}$; Allan *et al.*, 1987) and is not balanced by Mg^{2+} or Ca^{2+} but by Fe^{2+}. An increase in alkalinity is thus not associated with this release of ΔSO_4^{2-} and Fe^{2+} in the anoxic layer. Processes in the sediments at the maximum depth in the lake resulting in release of equimolar Fe^{2+} and SO_4^{2-} without Ca^{2+} and alkalinity are similar to processes occurring in sediments at shallower depths. Because the bottom waters are anoxic, the results of the weathering sequence in the sediments can be viewed in the water column of the small hypolimnetic anoxic zone.

The mineral weathering sequence responsible for the observed porewater and anoxic-zone chemistry is unknown. Oxygen is unlikely as an oxidant of pyrite in shallow sediments overlain by oxic waters. Although the kinetics of Fe^{2+} oxidation by O_2 are slow, diffusion of O_2 into the sediments is not fast enough to oxidize the pyrite below 16 cm depth to Fe^{2+} and ΔSO_4^{2-} without being consumed in the conversion of Fe^{2+} to Fe^{3+} at much shallower sediment depths. Pyrite is not stable in aqueous environments in the presence of iron hydroxides (abundant in the Colour Lake watershed; Fricker, 1963) and is oxidized rapidly by Fe^{3+} in the overall reaction (Stumm and Morgan, 1981):

[3] $$FeS_2 + 14\ Fe(OH)_3 + 26\ H^+ = 15\ Fe^{2+} + 2\ SO_4^{2-} + 34\ H_2O$$

Oxidation of FeS_2 by $Fe(OH)_3$ however generates a substantial quantity of alkalinity and produces a $\Delta Fe{:}\Delta SO_4$ ratio of 15:2 not a ratio of 1:1 as observed in the anoxic zone or in the porewaters (after correction of ΔSO_4 for small increases in Ca^{2+}, Mg^{2+}, K^+, Na^+ and NH_4^+ which are balanced by ΔSO_4^{2-} and not by alkalinity). Oxidation of FeS by $Fe(OH)_3$ also produces alkalinity and does not yield a 1:1 $Fe{:}SO_4$ ratio:

[4] $$FeS + 8\ Fe(OH)_3 + 16\ H^+ = 9\ Fe^{2+} + SO_4^{2-} + 20\ H_2O$$

Pyrite can also be oxidized by Fe^{3+} to Fe^{2+} and S° (e.g., Paciorek *et al.* 1981):

[5] $$FeS_2 + 2\ Fe^{3+} = 3\ Fe^{2+} + 2\ S^\circ$$

but this reaction does not produce ΔSO_4^{2-}.

The key to the mystery lies in the fact that Fe^{2+} and ΔSO_4^{2-} are observed simultaneously. The SO_4^{2-} cannot be misidentified S^{2-}. Even at a pH of 3.7, the observed total S concentration would result in a S^{2-} activity that combined with the observed Fe^{2+} greatly exceeds the Ksp for the quite insoluble FeS. The simplest explanation then suggests a $Fe\text{-}SO_4$ mineral. None of the principle $Fe\text{-}SO_4$ minerals such as jarosite ($KFe_3(SO_4)_2(OH)_6$), melanterite ($FeSO_4{\cdot}7H_2O$), copiapite (Fe, Mg, $Fe_4(SO_4)_6(OH)_2{\cdot}18H_2O$) or coquimbite ($Fe_2(SO_4)_3{\cdot}9H_2O$) (Teodorvich, 1961) yield weathering products compatible with the observed porewater chemistry (Schiff, 1986). It is thus likely that the weathering sequence is complex. Analyses of cores by X-ray diffraction, thin section and Mossbauer spectroscopy is currently underway to discover the minerals responsible for the observed weathering sequence in the lake sediments and also in the terrestrial catchment. Precipitation of $Fe(OH)_3$ following lake turnover (after ice-off) is a large source of acidity to Colour Lake, regenerating H_2SO_4:

$$[6] \qquad Fe^{2+} + \frac{1}{4} O_2 + \frac{5}{2} H_2O \rightarrow Fe(OH)_3 + 2\ H^+$$

Because the iron hydroxides are precipitating on sediments perennially overlain by oxic waters, this process is a net acid-generating mechanism for the lake. Iron hydroxides precipitated on sediments overlain by waters which experience seasonal anoxia will be reduced under anoxic conditions, recycled and thus not contribute to the acidity of the lake until precipitated in areas overlain by oxic waters. The lake is effectively mining a reduced iron sulphur mineral from the area overlain by anoxic waters.

Although the anoxic volume of the lake is small (<0.4%), this acidity is tremendously important in the lake acidity mass balance. A Fe^{2+} concentration equal to ΔSO_4^{2-} minus ΔALK (4,900 μeq·L^{-1}; Allan *et al.*, 1987) and an anoxic volume of 0.4% corresponds to an acidity source of approximately 200 meq·m^{-2}·yr^{-1}. This calculation is extremely sensitive to the volume of the anoxic zone; an anoxic hypolimnetic volume of 0.2% corresponds to an acidity flux of 100 meq·m^{-2}·yr^{-1}. Acidity generated from reactions in hypolimnetic sediments alone is the largest single source of acidity to Colour Lake, but is barely sufficient to account for the low water-column pH. The extent of the anoxic layer is dependent on the supply of organic carbon which drives the diagenetic reactions consuming O_2 in the sediments and the duration of the lake ice cover and thus is directly dependent on climatic factors.

CONCLUSIONS

Three sources of acidity to Colour Lake have been identified: nearshore seepage in summer, flux from lake sediments and the acidity produced upon reoxygenation of the anoxic hypolimnion with the concomitant precipitation of iron hydroxides. Of these sources, the largest, based on the limited data currently available, appears to be the acidity originating from sediment processes in the anoxic hypolimnion. The mineral sequence responsible for the generation of acidity appears to be a Fe-S mineral. Although pyrite is a likely candidate in both the terrestrial and aquatic portions of the catchment, sediment porewater profiles and the chemistry of the anoxic layer suggest that in the lake either another Fe-S mineral is present or secondary reactions are occurring which mask the identification of the primary weathering minerals.

The development of acidic seepage waters during the summer, and the higher alkalinity of surface inflows during springmelt compared to summer and fall, have important implications for the sensitivity of these systems to change due to global warming. The acid-generating minerals, possibly pyrite in the terrestrial catchment, have been weathered from the surficial soils resulting in surface inflows with relatively high pH values. At the base of the thawed layer, weathering has not completely exhausted the reservoir of Fe-S minerals and results in acidity production.

Thus deepening of the thawed layer due to an increase in the ambient summer temperatures or length of the thawing season would expose more acid-generating minerals and could significantly alter the geochemistry of surface waters in this area of the High Arctic. Our current research is directed at understanding and quantifying the importance of these terrestrial acid-generating reactions.

ACKNOWLEDGEMENTS

The Polar Continental Shelf Project supplied air transportation and field support. This project would not have been possible without their assistance. Dean Jeffries of Environment Canada provided anion analyses (1985) and Peter Dillon of the Ontario Ministry of Environment provided cation analyses (1985). Funding was provided by the National Sciences and Engineering Research Council (1985 to P. Adams, Trent University), Northern Scientific Training Program of the Department of Indian and Northern Affairs (1988 and 1989) and the Waterloo Centre for Groundwater Research. Pam Schaus of the Department of Geography at Wilfrid Laurier University drafted the figures.

REFERENCES

ALLAN, C., S. SCHIFF, D. PIERSON, M. ENGLISH, P. ADAMS and M. ECCLESTONE, 1985. Meltwater mixing processes in a naturally acidified high arctic lake. E@S, Transactions, American Geophysical Union, 66(46), abstract, 896

ALLAN, C., S. SCHIFF, D. PIERSON, M. ENGLISH, M. ECCLESTONE and W.P. ADAMS, 1987. Colour Lake, Axel Heiberg Island, N.W.T., a naturally acid, high arctic, lake - data report. In - Field Research on Axel Heiberg Island, N.W.T., Canada: Bibliographies and Data Reports with Appendices of Data from the McGill Subarctic Research Station, Schefferville, P.Q., P. Adams (Editor), McGill Subarctic Research Paper No.41, Axel Heiberg Island Research Report, Miscellaneous Papers No.2, Occasional Paper No.12, Department of Geography, Trent University, Peterborough, Ontario, Centre for Northern Studies and Research, McGill University, Montréal, Quebec, 67-189

CAFLISCH, T., 1972. Limnological investigations on Colour and Phantom lakes. Axel Heiberg Island Research Reports, McGill University, Montréal, Quebec, International Geographical Union, Field Tour Ea 2, Arctic Archipelago I, 22nd International Geographical Congress, Miscellaneous Papers by Fritz Müller and members of the Expedition, August, 49-56

ENGLISH, M., S. SCHIFF, M. ECCLESTONE, W.P. ADAMS, M. HINTON, L. PEZZUTTO, R. ELGOOD, C. ALLAN and D. PIERSON, 1991. Seasonal changes in the hydrochemistry of land drainage: Colour Lake catchment, Axel Heiberg Island, N.W.T. Northern Hydrology: Selected Perspectives, T.D. Prowse and C.S.L. Ommanney (Editors), Proceedings of the Northern Hydrology Symposium, NHRI Symposium No.6, National Hydrology Research Institute, Environment Canada, Saskatoon, Saskatchewan, 75-88

FRICKER, P.E., 1963. Geology of the Expedition area, western central Axel Heiberg Island, Canadian Arctic Archipelago. Jacobsen-McGill Arctic Research Expedition 1959-1962, Geology No.1, Axel Heiberg Island Research Reports, McGill University, Montréal, Quebec, December, 156 pp.

HERMICHEN, W.-D., P. KOWSKI and U. WAND, 1985. Lake Untersee, a first isotope study of the largest freshwater lake in the interior of East Antarctica. Nature, 315(6015), 131-133

HESSLEIN, R.H., 1976. An *in situ* sampler for close interval pore water studies. Limnology and Oceanography, 21(6), 912-914

LEE, D.R. and J.A. CHERRY, 1979. A field exercise on groundwater flow using seepage meters and mini-piezometers. Journal of Geological Education, 27(1), 6-10

MANABE, S. and R.T. WETHERALD, 1980. On the distribution of climatic change resulting from an increase in CO_2 content of the atmosphere. Journal of the Atmospheric Sciences, 37(1), 99-118

OHMURA, A., 1972. Some climatological notes on the Expedition area. Axel Heiberg Island Research Reports, McGill University, Montréal, Quebec, International Geographical Union, Field Tour Ea 2, Arctic Archipelago I, 22nd International Geographical Congress, Miscellaneous Papers by Fritz Müller and members of the Expedition, August, 5-13

OLIVER, B.G., E.M. THURMAN and R.L. MALCOLM, 1983. The contribution of humic substances to the acidity of colored natural waters. Geochimica et Cosmochimica Acta, 47(11), 2031-2035

OMMANNEY, C.S.L., 1987. Axel Heiberg Island visitations. In - Field Research on Axel Heiberg Island, N.W.T., Canada: Bibliographies and Data Reports with Appendices of Data from the McGill Subarctic Research Station, Schefferville, P.Q., P. Adams (Editor), McGill Subarctic Research Paper No.41, Axel Heiberg Island Research Report, Miscellaneous Papers No.2, Occasional Paper No.12, Department of Geography, Trent University, Peterborough, Ontario, Centre for Northern Studies and Research, McGill University, Montréal, Quebec, 56-66

PACIOREK, K.J.L., R.H. KRATZER, P.F. KIMBLE, W.A. TOBEN and A.L. VATASESCU, 1981. Degradation of massive pyrite: physical, chemical and bacterial effects. Geomicrobiology Journal, 2(4), 363-374

SCHIFF, S.L., 1986. Acid neutralization in sediments of freshwater lakes. Ph.D. thesis, Columbia University, New York, N.Y., 334 pp.

SCHIFF, S.L. and R.F. ANDERSON, 1986. Alkalinity production in epilimnetic sediments: acidic and non-acidic lakes. Water, Air, & Soil Pollution, 31(3-4), 941-948

SCHINDLER, D.W., 1986. The significance of in-lake production of alkalinity. Water, Air, & Soil Pollution, 30(3-4), 931-944

STUMM, W. and J.J. MORGAN, 1981. Aquatic chemistry: an introduction emphasizing chemical equilibria in natural waters. 2nd edition, John Wiley and Sons, New York, N.Y., 780 pp.

TEODOROVICH, G.I., 1961. Authigenic minerals in sedimentary rocks. Consultants Bureau, New York, N.Y., 120 pp.

WEISS, W. and W. ROETHER, 1980. The rates of tritium input to the world oceans. Earth and Planetary Science Letters, 49(2), 435-446

LONGITUDINAL DISPERSION IN THE ICE-COVERED ATHABASCA RIVER*

G. Van Der Vinne and D. Andres

Surface Water Engineering Group
Environmental Research and Engineering Department
Alberta Research Council
P.O. Box 8330, Postal Station F
Edmonton, Alberta
T6H 5X2 CANADA

ABSTRACT

Little is known about mixing processes in ice-covered rivers. To shed more light on these processes, five separate tracer dye tests were carried out under an ice cover at discharges between 30 $m^3 \cdot s^{-1}$ *and 75* $m^3 \cdot s^{-1}$ *on the Athabasca River between Hinton and Athabasca. The ice conditions varied significantly, depending on local ice-formation processes, with the thickness ranging between 0.5 m and 2.0 m. The mean velocities calculated from the travel times range between 0.26* $m \cdot s^{-1}$ *in reaches downstream of Fort Assiniboine where the river slope is as low as 0.00026, to 0.63* $m \cdot s^{-1}$ *for reaches with slopes of 0.00120 in the vicinity of Whitecourt. Transverse mixing was essentially complete for all the test reaches in the narrower upper parts of the river. Downstream of Vega Ferry, however, where the river widens, there were deviations in the peak concentrations across the sections of up to 30% from average. None of the study reaches was found to extend into the Fickian dispersion zone; all the data collected exhibited signs of non-Fickian or linear dispersion. Reach average values of the longitudinal dispersion parameter (*β*) were found to vary between 0.0064 and 0.0165. These are higher than those measured in most other rivers with similar hydraulic characteristics, but without ice covers. The dispersion model consistently overestimated the concentrations in the initial portion of the distributions and underestimated the concentrations in the tails.*

INTRODUCTION

The expansion of the pulp and paper industry in northern Alberta and the difficulties with the assessment of its impacts on the environment has underscored the lack of good quality design criteria to evaluate river-mixing characteristics in cold regions. Although there is considerable information in the literature on dispersion characteristics for open-water conditions, little is known about these processes under an ice-cover. Yet the most critical conditions occur during the winter period when the rivers are ice covered. During this time both the discharge and re-aeration are at a minimum, thus producing conditions in which the streams are the least capable of assimilating effluents. To address this lack of knowledge, five tracer dye studies were carried out on the Athabasca River during the winter period. These tests were performed at a variety of discharges and hydraulic conditions in five distinct reaches of the Athabasca River between Hinton and Athabasca, Alberta.

---

*Alberta Research Council Contribution Series Number 1910.

The purpose of this paper is to (1) describe the measurements carried out on the Athabasca River, (2) review briefly some of the theoretical background on longitudinal dispersion, and (3) report on the analysis carried out to evaluate the suitability of the existing theory to predict the spread of pollutants under an ice cover.

DISPERSION MEASUREMENTS

The dispersion measurements were carried out over a 555-km length of river between Hinton and Athabasca (Figure 1). The river was divided into five reaches which ranged in length from about 100 to 140 km, each of which reflected more or less consistant geomorphic and hydraulic characteristics. Dye was injected at the upstream end of each reach and concentrations were measured at three or four downstream locations at intervals of about 25 to 40 km in length depending on river access.

For each dye test, a predetermined volume of 20% Rhodamine WT dye was mixed with an equal volume of methyl alcohol to adjust the specific gravity of the dye mixture to that of water. The alcohol also served to prevent freezing during transport under the severe winter conditions. The injection apparatus consisted of a 1.5-m length of 8-cm diameter ABS (acrylonitrile butadienestyrene) pipe. The end of this pipe was configured with a 90° elbow which is orientated parallel to the flow in the downstream direction. Several small holes were drilled in the

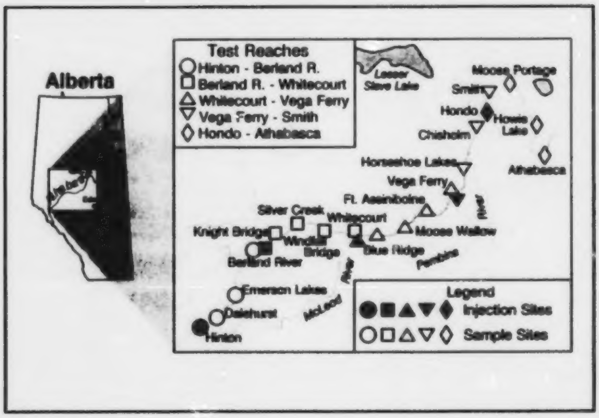
Alberta
Athabasca
Test Reaches
○ Hinton - Berland R.
□ Berland R. - Whitecourt
△ Whitecourt - Vega Ferry
▽ Vega Ferry - Smith
◇ Hondo - Athabasca
Lesser Slave Lake
Moose Portage
Smith
Hondo
Howie Lake
Chisholm
Athabasca
Horseshoe Lakes
Vega Ferry
Ft. Assiniboine
River
Silver Creek
Whitecourt
Knight Bridge
Windfall Bridge
Moose Wallow
Blue Ridge
Berland River
Pembina
Emerson Lakes
McLeod
Dalehurst
Hinton
Legend
●■▲▼◆ Injection Sites
○□△▽◇ Sample Sites

Figure 1. Study area.

long radius (upstream side) of the elbow to aid in the flushing of the pipe and to prevent dye from getting caught in the elbow. The pre-mixed dye was poured into the pipe via a funnel, followed immediately by 20 to 40 L of clean river water to ensure all the dye was removed from the ABS pipe and from the container holding the dye. By this method, all the dye was easily injected almost instantaneously into the flow.

Following injection at the upstream end of the river reach being characterized, two crews of two persons followed the dye cloud downstream, each of the crews sampling at alternating sites. At each site, a number of 20-cm diameter holes were augured through the ice to establish the flow distribution, the ice thickness, and the water level. The water level was referenced to temporary benchmarks established during a previous open-water survey so that the surveyed cross sections could be used to estimate the hydraulic characteristics under the ice cover.

The dye cloud was sampled over 3 holes across the channel. The primary sampling location was established in the main part of the flow and two secondary sampling holes were established midway between the primary sampling hole and both the left and right banks. Sufficient samples were taken at the primary sampling site to completely characterize the dye cloud. Two or more samples were taken to establish background fluorescent levels and at least 20 samples were taken over the duration of the dye cloud. Depending on the duration of the dye cloud, the interval between samples varied between 5 minutes and 2 hours. Sampling was usually continued until it was judged that the fluorescence was reduced to 20% of the peak and that the tail of the curve could be confidently extrapolated. In some cases, however, the tails of the dye cloud were cut short in order to give sufficient time to go to the next sampling site. The secondary sample sites were established to assess the extent of lateral mixing and to improve the estimates of the total volume of dye passing the sampling site. These were sampled at about one half of the frequency of the sampling at the primary site.

As soon as the samples were collected, they were transported to the mobile laboratory which each crew had at its disposal. The samples were maintained at temperatures of about 0° to 2°C (very nearly that of the river) and immediately run through the Turner Designs Model 10 fluorometer and the results recorded.

HYDRAULIC CHARACTERISTICS

In the entire stretch of river between Hinton and Athabasca the hydraulic characteristics vary considerably. However, on the scale of the sub-reaches, the hydraulic characteristics are much more homogeneous, albeit the variation at low flow is still considerable. The effects of an ice cover tend to increase the variability in any one of the sub-reaches, especially upstream of Vega Ferry where the slope is relatively high.

Ice-cover formation on the Athabasca River occurs by a combination of the juxtaposition of ice flows (which includes the redistribution of frazil) and by the consolidation of a juxtaposed cover in locations where the longitudinal forces on an advancing ice cover exceed the strength due to downward freezing of the juxtaposed cover. Downstream of Vega Ferry, where the slope is relatively mild, the predominant process is juxtaposition. This results in an ice cover of relatively uniform thickness in the order of 0.5 to 0.8 m. This uniform ice cover does not add to the hydraulic irregularities which, in these sub-reaches, is largely due to variation in the channel geometry.

Upstream of Vega Ferry, where the river slopes exceed 0.0010, variations in channel hydraulics arise from both irregular channel geometry and variable ice thickness. Because of the steep slopes, more of the cover tends to form by consolidation, resulting in frazil accumulations approaching 2 m in thickness. The high local velocities, even at the low flows during freeze-up, and the existence of numerous open leads result in the formation and subsequent deposition of significant amounts of frazil. This frazil tends to deposit in low-velocity areas hence concentrating the flow in the portion of the river cross section which offers the least resistance.

At least two discharge measurements were made in each reach for each of the dye tests. The first measurement was made as close as possible to the time and location of the injection. In addition to that, if a large number of tributaries were entering the study reach downstream, a second measurement was made at an appropriate location within the study reach. Finally, a discharge measurement was made at the reach exit, at a time as close as possible to the time when the dye peak passed by the most downstream sampling station.

Table 1 contains the relevant hydraulic characteristics for each sub-reach, taken from Andres *et al.* (1989). The average velocity (U) for each sub-reach was determined from the time of travel of the peak concentration (Beltaos, 1978). The average top width of the ice-water interface was determined by superimposing the average ice thickness on the open-water cross-sections obtained from Trevor *et al.* (1988). Slopes were taken from Kellerhals *et al.* (1972). The mean depth, hydraulic radius and composite Manning's roughness were calculated using the above parameters and the measured discharges.

ANALYSIS

The mixing process in rivers starts out as a three-dimensional process but because the depth is much smaller than the width, the pollutant concentration quickly becomes uniform over the depth. The mixing can then be treated as a two-dimensional problem. Further downstream, the pollutant concentration becomes essentially uniform over the width of the channel as well. Transverse mixing is then complete and further mixing is due to longitudinal dispersion, the process of increasing the spread of a pollutant along the channel length as the pollutant travels downstream.

Table 1. Sub-reach average hydraulic characteristics.

Sub-reach	Length (km)	Average Velocity $(m \cdot s^{-1})$	Discharge $(m^3 \cdot s^{-1})$	Width (m)	Depth (m)	Slope	Composite Roughness
Hinton - Dalehurst	19.93	0.48	31.3	112	0.58	0.00088	0.027
Dalehurst - Emerson Lake	27.83	0.45	32.0	109	0.64	0.00088	0.031
Emerson Lake - Berland River	54.41	0.49	33.5	93	0.73	0.00150	0.040
Berland River - Knight	26.78	0.60	39.5	99	0.67	0.00150	0.031
Knight - Silver Creek	22.08	0.63	39.5	112	0.55	0.00120	0.023
Silver Creek - Windfall	23.13	0.47	39.5	142	0.59	0.00120	0.032
Windfall - Whitecourt	32.78	0.51	39.5	110	0.71	0.00120	0.034
Whitecourt - Blue Ridge	25.94	0.60	40.0	104	0.64	0.00120	0.027
Blue Ridge - Moose Wallow	35.15	0.48	40.0	115	0.73	0.00084	0.031
Moose Wallow - Fort Assiniboine	34.85	0.31	40.0	119	1.09	0.00084	0.063
Fort Assiniboine - Vega Ferry	44.00	0.26	40.5	122	1.26	0.00064	0.071
Vega Ferry - Horseshoe Lake	27.67	0.26	41.4	170	0.95	0.00026	0.038
Horseshoe Lake - Chisholm	36.34	0.30	41.4	225	0.62	0.00017	0.020
Chisholm - Smith	34.52	0.28	49.8	208	0.85	0.00038	0.039
Hondo - Moose Portage	31.21	0.39	72.3	199	0.94	0.00038	0.031
Moose Portage - Howie Lake	56.24	0.37	73.8	175	1.13	0.00038	0.036
Howie Lake - Athabasca	31.59	0.37	75.3	239	0.86	0.00038	0.030

Because dispersion includes differential advection and turbulent diffusion as well as molecular diffusion, the process does not conform to Fick's law until some distance downstream from the point where the mixing becomes one-dimensional (Elhadi *et al.*, 1984).

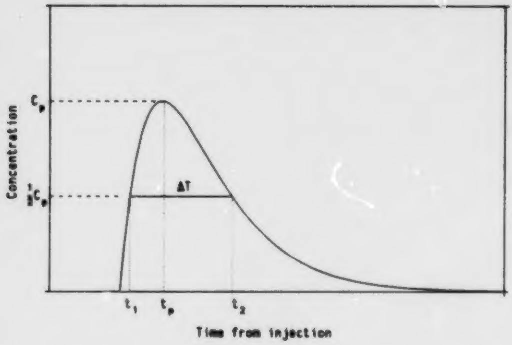

Figure 2. Definition sketch of time-concentration distribution variables.

Estimates of the transverse mixing length for each of the test reaches suggest that transverse mixing was not complete in the Vega Ferry-Smith and Hondo-Athabasca test reaches. As well, signs of incomplete transverse mixing were apparent at the first few sample sites in the other study reaches. This lack of complete transverse mixing resulted in the time-concentration curves measured across the width of the river at each site being perceptibly different from each other. However, the differences are very small in most cases, usually less than 5%. Only in two particular reaches are the differences large. The Hondo-Athabasca and Vega Ferry-Smith reaches produced peak concentrations which varied by as much as 30% from the mean peak concentration.

At most of the sample sites, one hole was sampled more extensively than the others. Since the deviation across the sections was not large in most cases, it was felt that the time-concentration curves obtained from these holes could be used, instead of the cross-section average, without introducing significant error. This will cause the velocities and peak concentrations to be slightly greater than they would be if the true average values were used in the analysis. The characteristics (see Figure 2 for definition sketch) of these representative curves are listed in Table 2.

Examination of the data in Table 2 suggests that the observed dispersion is in the linear range. That is, the standard deviation (σ_t) which can be related to the half-duration (ΔT) by:

$$\sigma_t = \alpha^{1/2} \Delta T \qquad [1]$$

when α is a constant equal to 5.55 (Beltaos, 1978), increases linearly with distance such that:

$$\sigma_t = \beta^{1/2} (x/U) \qquad [2]$$

In Equation 2, β is the longitudinal-dispersion parameter and x and U are the distance and mean velocity, respectively. If the ratio x/U is equivalent to the time to peak (t_p) then:

Table 2. Characteristics of representative time-concentration distributions.

Location	Distance from Injection (km)	Time to Peak (hrs)	Time to Beginning of Half-duration (hrs)	Half-duration (hrs)	Peak Concentration ($\mu g \cdot L^{-1}$)	Dosage ($hrs \cdot \mu g \cdot L^{-1}$)	Recovery Ratio
Hinton Injection							
Dalehurst	19.9	11.50	10.59	2.82	5.79	18.77	0.889
Emerson Lakes	47.8	28.50	26.03	6.92	2.12	17.96	0.869
Berland River	102.2	59.05	54.01	16.73	0.78	15.84	0.802
Berland Injection							
Knight Bridge	26.8	12.42	11.19	4.02	6.67	31.58	0.943
Silver Creek	48.9	22.10	20.03	7.92	3.58	31.71	0.947
Windfall Bridge	72.0	35.67	31.93	10.71	2.53	30.58	0.914
Whitecourt	104.8	53.70	47.64	15.71	1.83	32.00	0.956
Whitecourt Injection							
Blue Ridge	25.9	12.00	10.50	4.00	6.00	-	-
Moose Wallow	61.1	32.50	29.08	10.82	2.01	26.67	0.807
Fort Assiniboine	95.9	63.95	58.54	21.60	1.20	26.47	0.801
Vega Ferry	139.9	110.50	99.05	30.38	0.74	25.22	0.772
Vega Injection							
Horseshoe Lakes	27.7	30.00	28.09	4.58	4.25	27.92	0.874
Chisholm	64.0	64.03	61.71	8.66	2.47	25.98	0.813
Smith	98.5	98.00	91.97	21.01	1.06	23.94	0.902
Hondo Injection							
Moose Portage	31.2	22.50	21.55	4.40	5.70	32.02	1.001
Howie Lake	87.5	64.40	60.86	13.38	1.85	29.51	0.941
Athabasca	119.0	88.45	82.68	20.08	1.30	28.63	0.932

$$[3] \qquad \beta = 0.18\ (\Delta T/t_p)^2$$

Thus, β can be evaluated provided measurements of ΔT and t_p or x and U are available (Figure 3). Most of the existing literature (Elhadi *et al.*, 1984) suggests that β is a function of the ratio of the shear velocity to the mean velocity (U_*/U) for

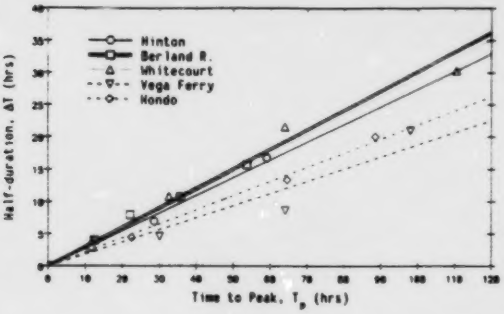

Figure 3. Variation of half-duration with time-to-peak from injection.

open-water conditions. Table 3 summarizes the calculated values of β along with the relevant reach-averaged hydraulic data.

Figure 4 illustrates a number of attempts to compare the open-water measurements in the linear range against the ice-covered measurements of β reported herein. It is interesting that when U_*/U is used as the independent variable both the open-water and the ice-cover measurements exhibit reasonable trends, albeit the ice-cover data plots higher than the open-water data. However, there is up to one order of magnitude scatter in the data over all ranges of U_*/U. No improvement results when β is correlated with U. In fact, the scatter becomes much worse. However, if β is correlated with U_* then some interesting trends develop. The open-water measurements exhibit no trend. However, the ice-cover points, including data from another investigator, plot within a very narrow,

Table 3. Reach-averaged hydraulic and mixing characteristics.

Injection Reach	Length (km)	Width (m)	Depth (m)	Slope	Velocity ($m \cdot s^{-1}$)	Shear Velocity ($m \cdot s^{-1}$)	Dispersion Parameter β
Hinton - Berland River	102	105	0.65	0.00126	0.48	0.063	0.0136
Berland River - Whitecourt	105	115	0.63	0.00131	0.54	0.064	0.0165
Whitecourt - Vega Ferry	140	128	0.94	0.00082	0.35	0.061	0.0155
Vega Ferry - Smith	99	211	0.81	0.00028	0.28	0.033	0.0064
Hondo - Athabasca	119	204	0.98	0.00038	0.37	0.043	0.0086

well-defined band. There is a distinct increase in the longitudinal-dispersion parameter with an increase in the shear velocity. This relationship can be written as:

$$[4] \qquad \beta = 0.725\, U_*^{1.4}$$

Since there is no theoretical basis for this relationship, it should not be applied to other ice-covered river reaches unless additional data demonstrate that it is appropriate.

As the temporal spread of the time-concentration curves increase, the peak concentrations must also decrease because the amount of dye remains constant (not including losses). Given β, the peak concentrations (C_p) can be predicted from:

$$[5] \quad C_p = (1/\sqrt{2\pi\beta})(M_oU/Qx)$$

where M_o is the mass of the injected tracer and Q is the discharge. Figure 5 shows a comparison between the measured and predicted value of C_p. Note that all measured values are equal to or less than the predicted values in both cases. The measured values may be less than the predicted values because the measured time-concentration curves may not contain all the dye that was injected. Some of the dye was lost through physical and chemical processes or was detained in

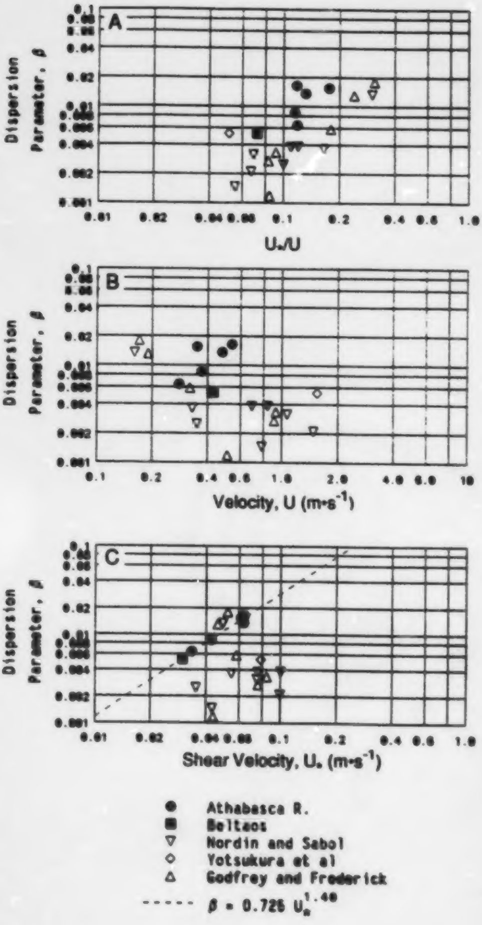

Figure 4. Variation of dispersion parameter (β) with: (a) dimensionless shear velocity, (b) velocity; and, (c) shear velocity.

areas of still water and a very small amount of dye was also lost to spillage during the injection process. The recovery ratios (M/M_0) shown in Figure 6 are the ratios of measured dye to injected dye. These varied between 0.8 and 1.0 with a tendency for the recovery ratio to decrease with distance from the injection point. However, errors introduced by estimating discharges and trailing edges of dye clouds are too large to define the trends accurately. Typical values of this ratio may be included in Equation 5 to provide a better prediction of the actual peak concentrations.

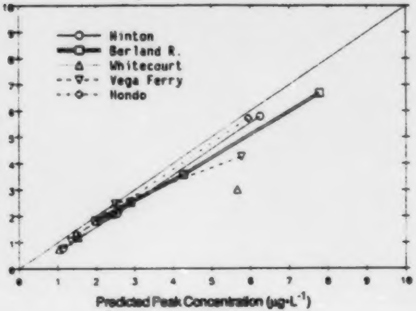

Figure 5. Comparison between calculated and measured peak concentrations.

Figure 7 shows the comparison between the measured concentration distributions and those calculated from:

$$[6] \qquad C = \frac{M_0 U}{\sqrt{2\pi \beta \; Qx}} \left[\frac{Ut}{x} \exp\left(1 - \frac{Ut}{x}\right) \right]^{1/\beta}$$

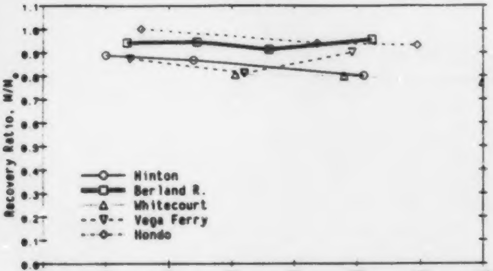

Figure 6. Variations of dye-recovery ratio with distance from injection.

The measured distributions exhibit a distinct skew about the peak whereas the computed curves are relatively symmetrical. Equation 6 tends to overestimate the duration of the rising limb of the distribution and underestimate the duration of the falling limb of the distribution. Also, since the velocity (U) is a reach-averaged value, the time of the peak is poorly estimated when the reach is not hydraulically homogeneous. This occurs in the Whitecourt-Vega Ferry reach where the predicted peaks lag behind the measured peaks at the first three sample sites but then precede the measured peak at the last sample site.

SUMMARY

Five separate tracer dye tests were carried out at discharges between 30 $m^3 \cdot s^{-1}$ and 75 $m^3 \cdot s^{-1}$ under an ice cover on the Athabasca River between Hinton and Athabasca. The ice conditions varied significantly, depending on local ice-formation processes, with the thickness ranging between 0.5 m and 2.0 m. The mean velocities calculated from the travel times ranged between 0.26 $m \cdot s^{-1}$ in reaches downstream of Fort Assiniboine where the river slope is low, to 0.63 $m \cdot s^{-1}$ for the steep reaches in the vicinity of Whitecourt.

Transverse mixing was essentially complete in the narrower upper reaches of the river but downstream of Vega Ferry, where the river widens, there were deviations from average of up to 30% in the peak concentrations across the sections. None of the study reaches was found to extend into the Fickian dispersion zone; all the data collected exhibited signs of non-Fickian or linear dispersion.

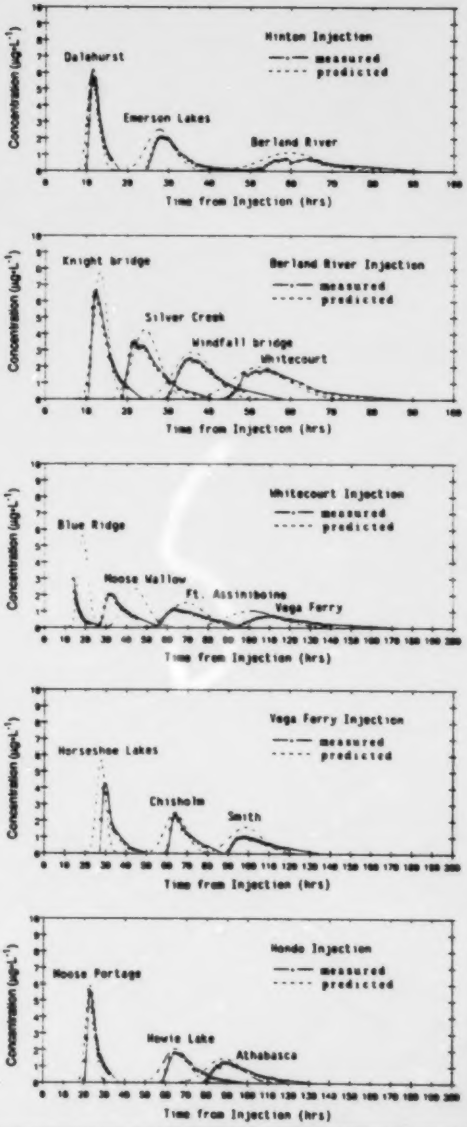

Figure 7. Comparison of measured and predicted time-concentration distributions.

Reach average values of the longitudinal-dispersion parameter (β) calculated from these experiments were found to vary between 0.0064 and 0.0165 and exhibited a good correlation with shear velocity. The existing data from open-water experiments exhibited a better correlation with dimensionless shear velocity. The data also suggest that the presence of an ice cover increases the rate of longitudinal dispersion, but measurements are needed for both open-water and ice-covered conditions on the same rivers to confirm this.

The measured time-concentration distributions showed a distinct skewness in the trailing edge of the dye clouds caused by dye being trapped in areas of still water and then slowly released back into the main flow. This effect may be more pronounced under ice conditions due to the greater variation in flow area caused by the ice cover. The dispersion model developed from open-water tests predicts virtually symmetrical time-concentration curves. It may be necessary to modify this model so it more accurately reflects the shape of the measured time-concentration distributions.

ACKNOWLEDGEMENTS

The work reported herein resulted from a joint venture undertaken by the Environmental Protection Service of Alberta Environment and the Surface Water Engineering Group of the Environmental Research and Engineering Department, Alberta Research Council. Numerous individuals contributed to and provided support for this project. J. Thompson, B. Trevor, P. Mostert, R. Bilyk, and C. Ray of the Alberta Research Council assisted with the field work. B. Trevor also reduced and plotted all of the data. G. Coles and the staff of the Water Survey Section of the Alberta Environment provided discharge measurements.

LIST OF SYMBOLS

C	concentration of dye ($\mu g \cdot L^{-1}$)
C_p	peak concentration of dye ($\mu g \cdot L^{-1}$)
M	mass of dye measured at a sample site (kg)
M_o	mass of dye injected (kg)
Q	river discharge ($m^3 \cdot s^{-1}$)
t	time from injection (hrs)
t_p	time of peak concentration (hrs)
ΔT	time that concentration is greater than one-half of the peak concentration (hrs)
U	average flow velocity ($m \cdot s^{-1}$)
U_*	shear velocity ($m \cdot s^{-1}$)
x	distance from injection (km)
α	shape parameter of concentration distribution
β	dispersion parameter
σ_t	standard deviation of concentration distribution (hrs)

REFERENCES

ANDRES, D., G. Van Der VINNE and B. TREVOR, 1989. Low flow winter travel time characteristics of the Athabasca River, Hinton to Athabasca. Surface Water Engineering Report No. SWE-89/06, Resource Technologies Department, Alberta Research Council, Edmonton, Alberta, 31 pp.

BELTAOS, S., 1978. An interpretation of longitudinal dispersion data in rivers. Transportation and Surface Water Engineering Report No. SWE-78/03, Alberta Research Council, Edmonton, Alberta, 36 pp.

BELTAOS, S., 1979. Mixing characteristics of the Athabasca River below Fort McMurray - winter conditions. AOSERP Report No.40, prepared for the Alberta Oil Sands Environmental Research Program by the Transportation and Surface Water Engineering Report, Alberta Research Council, Edmonton, Alberta, April, 110 pp.

ELHADI, N., A. HARRINGTON, I. HILL, Y.L. LAU and B.G. KRISHNAPPAN, 1984. River mixing - a state-of-the-art report. Canadian Journal of Civil Engineering, 11(3), 585-609

GODFREY, R.G. and B.J. FREDERICK, 1970. Stream dispersion at selected sites. U.S.G.S. Prof. Paper 433-K., U.S. Geological Survey, Washington, D.C., 38 pp.

KELLERHALS, R., C.R. NEILL and D.I. BRAY, 1972. Hydraulic and geomorphic characteristics of rivers in Alberta. River Engineering and Surface Hydrology Report No.72-1, Alberta Research Council, Edmonton, Alberta, 52 pp.

NORDIN, C.F. and G.V. SABOL, 1974. Empirical data on longitudinal dispersion in rivers. U.S.G.S. Water Resources Investigations, 20-74, U.S. Geological Survey, Denver, Colorado, August, 332 pp.

TREVOR, B., J. THOMPSON and D. ANDRES, 1988. Low flow hydraulic characteristics of the Athabasca River, Hinton to Athabasca. Surface Water Engineering Report No. SWE-88/13, Resource Technologies Department, Alberta Research Council, Edmonton, Alberta, 15 pp.

YOTSUKURA, N., H.B. FISCHER and W.W. SAYRE, 1970. Measurement of mixing characteristics of the Missouri River between Sioux City, Iowa, and Plattsmouth, Nebraska. U.S.G.S. Water Supply Paper, 1899-G, U.S. Geological Survey, Washington, D.C., 29 pp.

ECONOMIC IMPACT OF RIVER ICE JAMS IN CANADA*

G. Van Der Vinne[1], T.D. Prowse[2] and D. Andres[1]

[1]Surface Water Engineering Group
Environmental Research and Engineering Department
Alberta Research Council
P.O. Box 8330, Postal Station F
Edmonton, Alberta
T6H 5X2 CANADA

[2]Northern Environment Project
National Hydrology Research Institute
11 Innovation Boulevard
Saskatoon, Saskatchewan
S7N 3H5 CANADA

ABSTRACT

This paper summarizes a survey to evaluate the economic impact of damage caused by river ice jams across Canada. Information on most of the costs were collected by a mail survey conducted in early 1989 although some were obtained from newspapers, journals and reports. Most of the documented damage occurred in three provinces: Ontario, New Brunswick and Quebec; only 6% was in the western provinces and the territories. Out-of-channel or floodplain damage costs were much greater than river-structure damage costs. Commercial and residential sectors of the economy were most affected by ice-related floods while bridge damage accounted for 82% of that to river structures. The total surveyed cost of ice jam damage was at least $766 million, and possibly as great as $1.3 billion, while the average annual cost over the last ten years was $22 million. These figures may, however, still be underestimates, given the length and availability of records, and the lack of information on such items as environmental impacts.

INTRODUCTION

River ice jams and related ice runs are responsible for economic damage ranging from the flooding of communities to the destruction of bridges. Although many individual events have been reported, only one attempt has been made in the past to compile the relevant information on economic impacts from across the entire country. Atkinson (1973) estimated flood-damage costs from 27 different sites across Canada from 1900 to 1970. Since then, some work has been done to compile damage costs on a provincial scale, notably Kindervater's (1985) study of New Brunswick ice-related damages, but none from across Canada. Thus it is difficult to judge the overall economic significance of ice-jam damage.

---

*Alberta Research Council Contribution Series Number 1809; National Hydrology Research Institute Contribution Series Number CS-90012.

To generalize about the economic significance of past ice-jam events or predict potential future damage, the existing and often disparate data concerning ice-jam costs must be collected and categorized. To this end, a survey of various private and public agencies was conducted to compile information on river ice-jam damage costs across Canada. This survey was proposed by the Working Group on River Ice Jams as part of its mandate from the National Research Council of Canada, Subcommittee on Hydraulics of Ice Covered Rivers. This paper describes the data collection procedure, summarizes the information collected in the survey, and estimates the annual costs of ice-jam related damage.

DATA COLLECTION

No central agency is responsible for keeping records of damage caused by river ice jams, therefore it was necessary to collect the damage costs from a wide variety of sources. Some of the information was readily available in publications, but much of the data was unpublished and was obtained from the original sources by means of a mail survey conducted in early 1989 (see sample questionnaire: Appendix I). Due to the time-frame of the study, it was not possible to complete an exhaustive search, therefore the damage costs presented herein should be taken as possible underestimates.

In any mail survey, errors can distort the results. These fall into two categories: completeness and accuracy. Completeness errors are caused by noncoverage or nonresponse. Noncoverage errors occur when certain sources of information are ignored. These can be minimized by careful design of the mailing list. Nonresponse, however, is more difficult to control because there are always some people who will not respond to a survey (Cochran, 1977).

Table 1. Survey response according to type of agency.

Type of Agency	Total Contacts	Response	
		Total	%
Railways	14	2	14
Hydro-electric Companies	10	4	40
Emergency Measures Organizations	12	4	33
Transportation Departments	13	6	46
Environment Departments	23	15	65
Conservation Authorities	36	11	31
Other	31	15	48
Total	139	57	41

The agency responses are shown in Table 1. A full list of these agencies is available in Van Der Vinne, 1989. Although the overall response rate was 41%, both the highest and lowest response rates deviate significantly from the mean. The best (65%) was from federal and provincial departments of environment while the worst (14%) was from railway companies. This is somewhat misleading because follow-up telephone calls concentrated on the former rather than private companies. This was done because the government agencies were likely to have damage totals which included those affecting private corporations such as railways.

The dollar values placed on damage varied considerably depending on their source. Actual or paid-out costs were used if available but, in many cases, only estimates were given. Paid-out damages tend to be lower than actual damages because not all are eligible for compensation. Conversely, estimates, such as those found in newspaper articles, are generally inflated to increase the apparent magnitude of a disaster (Kindervater, 1985). Methods of assessing actual damage may differ as well. Some structural damages are reported as the full cost of replacing the structure whereas other costs are reported as the depreciated value of the structure at the time the damage occurred (Kindervater, 1985).

To properly compare damage costs from ice-jam events occurring in different years, inflation must be considered. Kindervater (1985) used the Building Construction Index to standardize flood costs in New Brunswick. Although this index is particularly well suited to account for inflation in structural damage, it is not applicable to other costs arising from flood damage or to indirect costs such as rental of alternate facilities. Therefore, the more general Cost of Living Index was used to convert all damage costs to 1988 dollars.

DAMAGE COSTS AND CLASSIFICATION

The number of ice-jam damage events reported in each province varied because of the size of the province, its population, the length of record and the propensity for ice jams to form. The complete list of damage events reported for this study is shown in Table 2. The costs are split into direct damage costs, which cover the cost of repair or replacement, and indirect costs which cover costs such as the loss of use of facilities. For example, if an ice jam causes flooding in a residential area, the direct damage cost would be the cost of repairing or replacing the residences, while indirect costs would cover temporary lodging for displaced residents.

Unfortunately, damage costs were not available for a number of reported events. These are indicated with a dollar sign ($) in Table 2. The exclusion of these from the damage totals is one reason why the totals reported in this study should be considered underestimates.

The most costly single ice-jam damage event reported was that on the Sydenham River at Wallaceburg, Ontario in 1968. The damage was estimated at $23 million or almost $87 million in 1988 dollars. Ontario also reported the most events. This is not surprising considering that it is one of the largest and most populous provinces. Its good historical record, dating back to 1853, also contributes to the hig number of

Table 2. Ice-jam damage events across Canada (1988$).

BRITISH COLUMBIA (Location)	Year	Month	River Structure		Flooding		Total Damage		Lives Lost
			Direct	Indirect	Direct	Indirect	Direct	Indirect	
Similkameen River, Princeton	1986	February	--	--	$10,816	$1,082	$10,816	$1,082	--
Illecillewaet River, Revelstoke	1985	December	$13,509	--	$	--	$13,509	--	--
Nicola, Similkameen, Tulameen and Lillooet Rivers	1984	January	$917,979	$11,709	$76,108	--	$994,087	$11,709	--
Bulkley River, Quick	1984	December	--	--	$	--	--	--	--
Nicola River, Merritt	1980	December	$8,054	--	$12,886	--	$20,940	--	--
Nicola River, Merritt	1979	December	$5,323	--	$5,323	--	$10,647	--	--
Nechako River, Prince George	1970	January	--	--	$	--	--	--	--
Kitsumkalum River, Dutch Valley	1968	--	--	--	$	--	--	--	--
Nechako River, Prince George	1968	December	--	--	$	--	--	--	--
Nechako River, Prince George	1943	--	--	--	$150,800	$188,500	$150,800	$188,500	--

ALBERTA (Location)	Year	Month	River Structure		Flooding		Total Damage		Lives Lost
			Direct	Indirect	Direct	Indirect	Direct	Indirect	
Peace River, Peace River	1982	January	--	--	$47,571	--	$47,571	--	--
Athabasca River, Fort McMurray	1977	--	--	--	$5,483,358	--	$5,483,358	--	--
Athabasca River, Whitecourt	1963	--	--	--	$150,800	$188,500	$150,800	$188,500	--
Bow River, Calgary, Canmore	1950	--	--	--	$377,000	$942,500	$377,000	$942,500	--
Red Deer River, Red Deer River	1947	March	--	--	$377,000	$754,000	$377,000	$754,000	--
Red Deer River, Red Deer	1943	April	--	--	$904,800	$1,357,200	$904,800	$1,357,200	--
Athabasca River, Fort McMurray	1936	April	--	--	$	--	--	--	--
Red Deer River, Red Deer River	1901	March	$	--	$	--	--	--	--
Athabasca River, Fort McMurray	1881	April	--	--	$	--	--	--	--
Athabasca River, Fort McMurray	1875	April	--	--	$	--	--	--	--
Bow River, Siksika Resort	--	Spring-Fall	--	--	$	--	--	--	--

SASKATCHEWAN (Location)	Year	Month	River Structure		Flooding		Total Damage		Lives Lost
			Direct	Indirect	Direct	Indirect	Direct	Indirect	
Souris River Basin, Weyburn	1979	Spring	--	--	$17,745	--	$17,745	--	--
S. Saskatchewan River, Saskatoon	1975	January	--	--	--	$198,718	--	$198,718	--
N. Saskatchewan River, Prince Albert	1974	Spring	$	$	$	$	--	--	--
S. Saskatchewan River, Sask. Landing	1952	April	$2,009,825	--	--	--	$2,009,825	--	--

Table 2. Continued.

MANITOBA (Location)	Year	Month	River Structure		Flooding		Total Damage		Lives Lost
			Direct	Indirect	Direct	Indirect	Direct	Indirect	
Icelandic River	1986	April	$216,314	--	$108,157	--	$324,471	--	--
Netley Creek	1986	April	$324,471	--	$75,710	--	$400,181	--	--
Red River, Breezy Point	1986	Spring	$	--	--	--	--	--	--
Assiniboine River, Portage la Prairie	1983	April	--	--	$70,867	--	$70,867	--	--
Valley River, Grand Plains	1983	April	$9,164	--	$12,218	--	$21,382	--	--
Woody River	1983	Spring	$	--	$	--	--	--	--
Assiniboine River	1983	Spring	$	--	--	--	--	--	--
Valley River, Gilbert Plains	1981	April	$5,728	--	$5,728	--	$11,456	--	--
Valley River, Gilbert Plains	1979	April	$90,498	--	$47,911	--	$138,409	--	--
Boyne River, Carman	1979	--	--	--	$763,024	--	$763,024	--	--
Woody River	1976	Spring	$	--	$	--	--	--	--
Netley Creek	1974	April	$189,848	--	$81,364	--	$271,212	--	--
Icelandic River	1974	April	$1,627,273	--	$1,084,848	--	$2,712,121	--	--
Fisher River	1974	April	$271,212	--	$271,212	--	$542,424	--	--
Wavey Creek	1974	April	$189,848	--	$216,970	--	$406,818	--	--
Lake Winnipeg	1974	May	$1,627,273	--	--	--	$1,627,273	--	--
Assiniboine River	1969	Spring	$	--	--	--	$	--	--
Assiniboine River, Winnipeg	1904	Spring	$	--	$1,885,000	$942,500	$1,885,000	$942,500	--

ONTARIO (Location)	Year	Month	River Structure		Flooding		Total Damage		Lives Lost
			Direct	Indirect	Direct	Indirect	Direct	Indirect	
Goulais River, Kirby's Corner	1988	April	--	--	$120,000	--	$120,000	--	--
Credit River, Churchville	1987	March	--	--	$21,839	--	$21,839	--	--
Winisk River, Winisk	1986	May	--	--	$12,978,852	$5,407,855	$12,978,852	$5,407,855	2
Thames River, Dover & Raleigh Twp.	1985	February	--	--	$4,982,730	$1,531,069	$4,982,730	$1,531,069	--
Thames River, Kent County	1985	February	--	--	$104,698	--	$104,698	--	--
Credit River, Mississauga area	1985	February	--	--	$175,431	$17,450	$175,431	$17,450	--
Sydenham River, Dresden	1985	March	--	--	$2,026,415	--	$2,026,415	--	--
Don River, Toronto	1984	--	--	--	$468,357	--	$468,357	--	2
Credit River, Mississauga	1984	--	--	--	$50,348	--	$50,348	--	--
Catfish Creek, Pt. Bruce	1984	February	--	--	$620,572	--	$620,572	--	--
Rideau Valley (Hydro-generation)	1982	Spring	--	--	--	--	--	--	--
Humber River and Woodridge	1981	February	--	--	$42,960	--	$42,960	--	--
Rideau Valley, Ottawa	1981	Spring	--	--	$214,800	--	$214,800	--	--
Humber River, Toronto	1981	February	$78,760	--	$17,184	--	$95,944	--	--

Table 2. Continued.

ONTARIO (Continued) (Location)	Year	Month	River Structure		Flooding		Total Damage		Lives Lost
			Direct	Indirect	Direct	Indirect	Direct	Indirect	
Humber River, Bolton	1981	March	$1,432	--	$4,296	--	$5,728	--	--
Dufferin Creek, Pickering/Ajax	1981	February	--	--	$18,616	--	$18,616	--	--
Thames River, Tilbury N. Twp.	1981	February	--	--	$2,962,808	$547,883	$2,962,808	$547,883	--
Ganaraska River, Port Hope	1980	March	--	--	$	--	--	--	--
Thames River, Dover Twp.	1979	March	--	--	$2,840,932	$528,083	$2,840,932	$528,083	--
South Nation River, Plantagenet	1978	--	--	--	$368,173	--	$368,173	--	--
Grand River	1974	May	--	--	$355,855	--	$355,855	--	--
Niagara River, Hamilton	1969	January	$	--	$	$	--	--	--
Sydenham River, Dresden	1968	February	--	--	$1,362,796	--	$1,362,796	--	--
Bighead River, Meaford	1968	February	--	--	$	--	--	--	--
Sydenham River, Wallaceburg	1968	February	--	--	$86,673,684	--	$86,673,684	--	--
Moira River, Belleville	1968	January	--	--	$	$	--	--	1
Saugeen River, Durham	1967	--	--	--	$131,950	$207,350	$131,950	$207,350	--
Big Otter River, Vienna	1967	--	--	--	$196,040	$320,450	$196,040	$320,450	--
Credit River, Glen Williams	1965	--	--	--	$271,440	$339,300	$271,440	$339,300	--
Lower Thames River, Chatham	1965	January	--	--	$	--	--	--	--
Nottawasaga River, Barrie	1965	February	--	--	$	$	--	--	--
Otonabee River, Peterborough	1960	April	--	--	$	$	--	--	--
Niagara River, Niagara	1955	March	--	--	$	$	--	--	--
Highland Creek, Toronto	1955	March	--	--	$	$	--	--	--
Lower Thames River, Chatham	1951	January	--	--	$	$	--	--	--
Rideau River, Ottawa	1948	March	--	--	$3,693,651	--	$3,693,651	--	--
Saugeen River, Walkerton	1948	March	--	--	$	$	--	--	1
Ganaraska River, Port Hope	1948	March	--	--	$85,238	--	$85,238	--	--
Etobicoke Creek, Etobicoke	1948	February	--	--	$	$	--	--	--
Sydenham River, Wallaceburg	1947	April	--	--	$2,262,000	$3,393,000	$2,262,000	$3,393,000	--
Grand River, Brantford/Guelph/Gault	1947	April	$12,723	--	$2,827,500	$4,147,000	$2,840,223	$4,147,000	--
Thames River, St. Marys/Tavistock	1947	--	--	--	$452,400	$603,200	$452,400	$603,200	--
Etobicoke Creek, Brampton	1946	January	--	--	$155,652	--	$155,652	--	--
Bayfield River, Bayfield	1943	March	--	--	$0	--	--	--	--
Beaver River, Clarksburg	1938	--	--	--	$60,320	$75,400	$60,320	$75,400	--
Thames River, Chatham/Thamesville	1937	--	--	--	$4,524,000	$6,786,000	$4,524,000	$6,786,000	--
Moira River, Belleville	1936	March	--	--	$974,150	--	$974,150	--	--
Detroit River, Lake St. Clair	1933	--	--	--	$754,000	$1,790,750	$754,000	$1,790,750	--
Kettle Creek, St. Thomas	1930	February	--	--	$389,130	--	$389,130	--	--
Maitland River, Stratford	1929	March	--	--	$	$	--	--	1
Otter Creek, Tillsonburg	1929	January	--	--	$2,334,783	--	$2,334,783	--	--
Grand River	1929	March	$166,739	--	$933,913	--	$1,050,652	--	--
Moira River, Belleville	1928	March	--	--	$194,565	--	$194,565	--	--
Don River, Toronto	1927	March	--	--	$	$	--	--	1

Table 2. Continued.

ONTARIO (Continued) (Location)	Year	Month	River Structure		Flooding		Total Damage		Lives Lost
			Direct	Indirect	Direct	Indirect	Direct	Indirect	
Ausable River, Port Frank	1923	--	--	--	$150,800	$207,350	$150,800	$207,350	--
Credit River, Mississauga	1911	March	--	--	$57,742	$	$57,742	--	4
Moira River, Belleville	1910	March	--	--	$115,484	--	$115,484	--	--
Lower Thames River, Chatham	1910	March	--	--	$461,935	--	$461,935	--	--
Grand River, Dunnville	1904	--	--	--	$94,250	$131,950	$94,250	$131,950	--
Grand River, Galt	1898	March	--	--	$173,226	--	$173,226	--	--
Etobicoke Creek, Etobicoke	1893	December	--	--	$577,419	--	$577,419	--	--
Moira River, Belleville	1890	February	--	--	$57,742	--	$57,742	--	--
Moira River, Belleville	1890	January	--	--	$230,968	--	$230,968	--	--
Moira River, Belleville	1888	April	--	--	$34,645	--	$34,645	--	--
Moira River, Belleville	1887	April	--	--	$23,097	--	$23,097	--	--
Thames River, London	1887	April	--	--	$	$	--	--	4
Grand River, Fergus	1883	April	--	--	$17,323	--	$17,323	--	--
Grand River, Brantford	1868	March	--	--	$	$	--	--	--
Moira River, Belleville	1865	March	--	--	$199,210	--	$199,210	--	--
Moira River, Belleville	1864	March	--	--	$184,774	--	$184,774	--	--
Ganaraska, Port Hope	1857	February	$	$	$	$	--	--	1
Ganaraska, Port Hope	1853	March	--	--	$	$	--	--	--
Millhaven Creek, Odessa	annual	March-April	--	--	$30,000	--	$30,000	--	--
Northern Ontario Railways	annual	--	$5,000	$10,000	--	--	$5,000	$10,000	--

NEWFOUNDLAND (Location)	Year	Month	River Structure		Flooding		Total Damage		Lives Lost
			Direct	Indirect	Direct	Indirect	Direct	Indirect	
Harry's River, Stephenville	1984	February	--	--	$117,089	--	$117,089	--	--
Terra Nova River, Glovertown	1984	February	--	--	$11,709	--	$11,709	--	--
Exploits, Gander and Connie Rivers	1983	--	--	--	$41,542,662	--	$41,542,662	--	--
Exploits River, Badger	1983	February/March	--	--	$44,320	$10,992	$44,320	$10,992	--
Rushoon River, Rushoon	1983	March	--	--	$3,849	$367	$3,849	$367	--
Codroy River, Grand Bay	1978	January	$	--	--	--	--	--	--
Exploits River, Badger	1977	January	--	--	$33,744	$8,436	$33,744	$8,436	--
Rushoon River, Rushoon	1973	February	--	--	$15,042	--	$15,042	--	--
Harry's River, Black Duck, Sidney	1971	February	$	--	--	--	--	--	--

Table 2. Continued.

QUEBEC (Location)	Year	Month	River Structure		Flooding		Total Damage		Lives Lost
			Direct	Indirect	Direct	Indirect	Direct	Indirect	
Ste-Anne River, Ste. Anne-de-la-Pérade	1987	April	$7,799,564	--	--	--	$7,799,564	--	--
Ste-Marie-Beauce	1987	April	--	--	$10,399,419	--	$10,399,419	--	--
Chaudière River, Ste-Marie	1987	April	--	--	$10,000,000	--	$10,000,000	--	--
Yamachiche River Area, Louiseville	1983	--	--	--	$1,832,765	--	$1,832,765	--	--
Chaudière and Saint-François	1982	April	--	--	$529,892	--	$529,892	--	--
Rivières des Milles Îles	1981	February	--	--	$	--	--	--	--
Eastern Townships, Richmond	1981	February	--	--	$4,296,000	--	$4,296,000	--	--
St. Lawrence Seaway	1981	January	--	--	--	$859,200	--	$859,200	--
Beauharnois Canal	1978	December	--	$500,000	--	$500,000	--	$1,000,000	--
Ottawa & St. Lawrence, Montréal	1976	March-April	--	--	$45,532,591	--	$45,532,591	--	--
Chaudière & Saint-François Basins	1970	Spring	--	--	$3,329,564	--	$3,329,564	--	--
Chaudière & Saint-François Basins	1969	Spring	--	--	$2,033,371	--	$2,033,371	--	--
Chaudière & Saint-François Basins	1968	Spring	--	--	$427,527	--	$427,527	--	--
Chaudière & Saint-François Basins	1967	Spring	--	--	$2,573,677	--	$2,573,677	--	--
Beauceville	1957	December	--	--	$9,610,738	--	$9,610,738	--	--
Châteauguay River, Châteauguay	1943	--	--	--	$245,050	$377,000	$245,050	$377,000	--
Chaudière River, St-Joseph-de-Beauce	1937	--	--	--	$904,800	$1,583,400	$904,800	$1,583,400	--
St. Lawrence River, Montréal	1936	--	--	--	$942,500	$1,508,000	$942,500	$1,508,000	--

NORTHWEST TERRITORIES* (Location)	Year	Month	River Structure		Flooding		Total Damage		Lives Lost
			Direct	Indirect	Direct	Indirect	Direct	Indirect	
Hay River, Hay River	1985	--	--	--	$695,736	--	$695,736	--	--
Hay River, Hay River	1963	--	--	--	$3,953,374	--	$3,953,374	--	--
Liard River, Fort Simpson	1963	May	--	--	$3,294,479	--	$3,294,479	--	--

**Other known sites include: Aklavik, Arctic Red, Fort Good Hope, Fort Liard, Fort McPherson, Fort Norman and Nahanni Butte but no damage costs were provided. Similarly, more recent ice-jam floods have occurred at Fort Simpson and Hay River.*

Table 2. Continued.

NOVA SCOTIA (Location)	Year	Month	River Structure		Flooding		Total Damage		Lives Lost
			Direct	Indirect	Direct	Indirect	Direct	Indirect	
North River, Colchester County	1988	October	$26,300	$5,700	--	--	$26,300	$5,700	--
North River, Colchester County	1981	February	--	--	$91,148	--	$91,148	--	--
LaHave, Sackville Rivers	1981	February	--	--	$44,925	--	$44,925	--	--
Salmon River	1978	January	$3,876	--	$422,430	--	$426,306	--	--
Salmon River, Antigonish	1973	February	--	--	$9,025	--	$9,025	--	--
Smaller Streams, Truro	1972	March	--	--	$3,240	--	$3,240	--	--
Province Wide	1971	February	--	--	$1,612,527	--	$1,612,527	--	--
Province Wide	1962	April	$	--	--	--	--	--	2
Province Wide	1958	January	--	--	$935,948	--	$935,948	--	--
Province Wide	1956	January	$9,910,035	--	$18,829,066	--	$28,739,100	--	--
Province Wide	1952	January	--	--	$678,673	--	$678,673	--	--
LaHave, Truro, Antigonish	1952	January	$	--	$	--	--	--	--
Province Wide	1936	March	--	$16,366	$	--	--	$16,366	--
Province Wide	1935	January	$	--	$	--	--	--	--
East River, Halifax, Truro	1920	March	$	--	$247,004	--	$247,004	--	--
Salmon River	1906	December	--	--	$	--	--	--	--
Bridgetown	1904	April	--	$	$	--	--	--	--
Cumberland County	1902	March	$	--	$	--	--	--	--
Province Wide	1895	April	$	--	--	--	--	--	--
Province Wide	1883	March	$	--	--	$	--	--	--

YUKON (Location)	Year	Month	River Structure		Flooding		Total Damage		Lives Lost
			Direct	Indirect	Direct	Indirect	Direct	Indirect	
Yukon River, Dawson City	1979	--	--	--	$2,910,136	--	$2,910,136	--	--
Stewart River, Mayo	1973	--	--	--	$23,041	--	$23,041	--	--
Ross River, Ross River	1973	--	--	--	$45,824	--	$45,824	--	--
Stewart River, Mayo	1972	--	--	--	$14,890	--	$14,890	--	--
Yukon River, Dawson City	1967	--	--	--	$182,912	--	$182,912	--	--
Stewart River, Mayo	1965	--	--	--	$103,833	--	$103,833	--	--
Yukon River, Dawson City	1965	--	--	--	$158,573	--	$158,573	--	--
Yukon River, Dawson City	1963	--	--	--	$27,994	--	$27,994	--	--

Table. 2 Continued.

NEW BRUNSWICK (Location)	Year	Month	River Structure		Flooding		Total Damage		Lives Lost
			Direct	Indirect	Direct	Indirect	Direct	Indirect	
Saint John River, Perth/Andover	1987	--	$2,294,242	--	$11,000,000	$19,000,000	$13,294,242	$19,000,000	--
Saint John River, Perth/Andover	1986	--	--	--	$7,676,721	$10,816	$7,676,721	$10,816	--
Restigouche River, Matapédia	1984	April	--	--	$58,545	--	$58,545	--	--
Saint John River, Florenceville	1981	February	--	--	$14,320	--	$14,320	--	--
Saint John Basin, Basin Wide	1979	April	--	--	$3,750,044	--	$3,750,044	--	--
Saint John Basin, Basin Wide	1976	April	$1,593,641	--	$9,106,518	--	$10,700,159	--	2
Upper Saint John, Madawaska	1974	April-May	$787,600	--	$896,627	--	$1,684,227	--	--
Nashwaak River, Nashwaak Valley	1970	--	$2,474,552	$1,656,583	$362,865	--	$2,837,417	$1,656,583	--
Saint John Basin, Basin Wide	1970	February	$1,257,366	--	$27,337,393	--	$28,594,759	--	3
Saint John Basin, Fredericton	1968	April	--	--	$376,842	--	$376,842	--	--
Nashwaak River, Durham	1953	--	$57,918	--	--	--	$57,918	--	--
Saint John River, Cormors	1951	April	--	--	$461,935	--	$461,935	--	--
Oromocto River, Basin Wide	1950	April	$852,381	--	$4,830,159	--	$5,682,540	--	--
Wards Creek, Kings County	1947	February	$	--	$	--	--	--	2
Province Wide	1936	March	$14,231.056	--	$17,788,820	--	$32,019,876	--	--
Saint John River, Fredericton	1935	April	$	--	$	--	--	--	--
Saint John River, York County	1934	April	$219,486	--	$3,861,344	--	$4,080,830	--	--
Saint John River, Hartland etc.	1933	May	--	--	$	--	--	--	3
Saint John River, Fredericton	1932	April	$	--	$	--	--	--	--
Saint John River, Basin Wide	1923	April-May	--	--	$38,913,043	--	$38,913,043	--	2
Saint John River, Hartland	1920	April	--	--	$	--	--	--	--
Keswick River, North Forks	1913	April	$346,452	--	--	--	$346,452	--	--
Nashwaak River, Stanley	1902	--	$30,026	--	--	--	$30,026	--	1
Saint John River, Hartland	1902	March	$577,419	--	$17,323	--	$594,742	--	1
Saint John River, Grand Falls	1901	April	--	--	$461,935	--	$461,935	--	--
Green River	1896	April-May	$	--	$	--	--	--	--
Saint John River, Fredericton	1887	April-May	$57,742	--	$3,464,516	--	$3,522,258	--	--
Saint John River, Fredericton	1857	April	--	--	$	--	--	--	--
Saint John River, Kinsclear	1831	April	--	--	$	--	--	--	--
Saint John River, Fredericton	1789	April	--	--	$	--	--	--	--

high number of reported events. New Brunswick also has good historical records dating back to 1887. On the other hand, Prince Edward Island reported no costs related to ice-jam damage but this was likely due to the fact that no significant ice jams have occurred there. Overall, events were reported more frequently in recent years. This may be due to increased awareness and documentation, but actual damage may also be becoming more frequent due to greater population and increased river-valley development.

Flood Damage

A breakdown of flood damage into various economic sectors is shown in Table 3. The total aggregate cost of ice-jam related flood damage reported in Canada is over $505 million. A large portion of this total, $322 million, is unspecified, i.e., not identified as belonging to a particular economic sector. The total of specified flood damage is $183 million, of which 39% occurs in the commercial sector, 32% in the residential sector, 15% to roads and railways and the remainder is divided among municipal, agricultural and other sectors of the economy.

River-Structure Damage

River-structure damage classified by type of river structure is given in Table 4. The total cost is over $52 million, $34 million of which is identified as damage to particular type of river structures. Damage to bridges accounts for 82% of the total while road and railway embankment damage accounts for an additional 7%.

Navigation Cost

Very few economic losses to navigation were reported (Table 5). The most costly event occurred in 1984 on the St. Clair River in the western district of the St. Lawrence Seaway. Over $13 million in indirect damage was incurred by shippers because their path was blocked by an ice jam. All the other reported events involved direct damage to ships by ice. Together these events caused over $10 million in direct damage, although more than $8 million of this cost was incurred during one event in the St. Lawrence Seaway in Quebec. The total reported cost to navigation, both direct and indirect was almost $24 million.

Total Damage

The total reported historical cost of river ice-jam damage, including the cost to navigation, is approximately $581 million (refer to Tables 5 and 6). Direct damage amounts to $511 million while indirect damage is only $70 million. Indirect damage is expected to approach 50% of the direct (Kindervater, 1985) but the reported indirect damage amounts to less than 14% of the direct. It is very likely, then, that

Table 3. Annual costs to various economic sectors caused by ice-jam flooding (1988$).

Canada	Commercial	Municipal	Residential	Agricultural	Roads/Railway	Other	Unspecified	Total
1988	$0	$0	$120,000	$0	$0	$0	$0	$120,000
1987	$0	$568,536	$2,788,084	$0	$0	$0	$47,064,637	$50,421,257
1986	$1,185,402	$5,729,947	$5,529,813	$1,285,988	$4,157,602	$0	$8,381,257	$26,270,009
1985	$602,577	$2,342	$1,026,154	$3,580,000	$859,538	$0	$3,462,918	$9,533,529
1984	$309,115	$0	$830,162	$128,798	$74,937	$59,715	$0	$1,402,728
1983	$610,922	$620,588	$660,782	$0	$0	$12,218	$41,613,529	$43,518,039
1982	$109,856	$47,571	$258,484	$161,552	$0	$0	$0	$577,463
1981	$4,892,683	$13,151	$983,976	$1,831,528	$511,224	$28,106	$859,200	$9,119,868
1980	$0	$0	$12,886	$0	$0	$0	$0	$12,886
1979	$258,186	$254,096	$336,263	$2,323,850	$3,912,950	$97,596	$9,163,616	$16,346,556
1978	$189,900	$0	$232,530	$368,173	$0	$0	$500,000	$1,290,604
1977	$0	$6,327	$35,853	$0	$0	$0	$0	$42,180
1976	$1,935,135	$2,265,656	$8,753,641	$455,326	$5,966,363	$11,383	$35,251,605	$54,639,109
1975	$0	$0	$0	$198,718	$0	$0	$0	$198,718
1974	$0	$1,238,921	$13,561	$0	$0	$352,576	$1,301,818	$2,906,876
1973	$0	$0	$24,067	$0	$0	$0	$68,865	$92,932
1972	$3,240	$0	$0	$0	$0	$0	$14,890	$18,130
1971	$0	$706,499	$0	$0	$0	$906,028	$0	$1,612,527
1970	$0	$668,800	$1,681,870	$555,997	$7,330,195	$0	$20,792,960	$31,029,822
1969	$0	$0	$0	$0	$0	$0	$2,033,371	$2,033,371
1968	$56,790,105	$67,832	$30,147,368	$0	$0	$0	$1,835,544	$88,840,849
1967	$0	$0	$0	$0	$0	$0	$3,612,379	$3,612,379
1965	$0	$0	$0	$0	$0	$0	$873,146	$873,146
1963	$0	$0	$0	$0	$0	$0	$7,615,147	$7,615,147
1958	$0	$0	$0	$0	$0	$0	$935,948	$935,948
1957	$0	$0	$0	$0	$0	$0	$9,610,738	$9,610,738
1956	$1,486,505	$0	$0	$0	$0	$0	$17,342,561	$18,829,066
1952	$0	$0	$0	$0	$0	$0	$678,673	$678,673
1951	$205,305	$0	$128,315	$0	$128,315	$0	$0	$461,935
1950	$0	$0	$0	$0	$0	$0	$6,149,659	$6,149,659
1948	$0	$0	$0	$0	$0	$0	$3,778,889	$3,778,889
1947	$0	$10,552	$113,651	$0	$0	$0	$14,691,897	$14,816,101
1946	$0	$0	$0	$0	$0	$0	$155,652	$155,652
1943	$0	$0	$0	$0	$0	$0	$3,223,350	$3,223,350
1938	$0	$0	$0	$0	$0	$0	$135,720	$135,720
1937	$0	$0	$0	$0	$0	$0	$13,798,200	$13,798,200
1936	$0	$0	$0	$0	$444,720	$0	$20,768,750	$21,213,470
1934	$974,150	$0	$22,454,857	$19,483	$412,854	$0	$0	$3,861,344
1933	$0	$0	$0	$0	$0	$0	$2,544,750	$2,544,750
1930	$0	$0	$0	$0	$0	$0	$389,130	$389,130
1929	$0	$0	$933,913	$0	$0	$0	$2,334,783	$3,268,696
1928	$0	$0	$0	$0	$0	$0	$194,565	$194,565
1923	#1,751,087	$0	$11,556,522	$0	$3,502,174	$0	$32,461,410	$39,271,193
1920	$247,004	$0	$0	$0	$0	$0	$0	$247,004
1911	$0	$0	$0	$0	$0	$0	$57,742	$57,742
1910	$0	$0	$0	$0	$0	$0	$577,419	$577,419
1904	$0	$0	$0	$0	$0	$0	$3,053,700	$3,053,700
1902	$0	$0	$0	$0	$0	$17,323	$0	$17,323
1901	$461,935	$0	$0	$0	$0	$0	$0	$461,935
1898	$0	$0	$0	$0	$0	$0	$173,226	$173,226
1893	$0	$0	$0	$0	$0	$0	$577,419	$577,419
1890	$0	$0	$0	$0	$0	$0	$288,710	$288,710
1888	$0	$0	$0	$0	$0	$0	$34,645	$34,645
1887	$0	$0	$0	$0	$577,419	$0	$2,910,194	$3,487,613
1883	$0	$0	$0	$0	$0	$0	$17,323	$17,323
1865	$0	$0	$0	$0	$0	$0	$199,210	$199,210
1864	$0	$0	$0	$0	$0	$0	$184,774	$184,774
Total	$72,013,106	$12,200,818	$58,622,753	$10,909,413	$27,878,292	$1,484,946	$321,713,919	$504,823,246

indirect damages are under-reported. If the direct damages are multiplied by a factor of 1.5 to account for indirect damage, the total would then become $766 million. Atkinson (1973) estimated aggregate damage costs between 1900 and 1970 to be $234 million (1988$) using an average multiplier of 2.5 to account for indirect damage. Direct-damage costs reported by Atkinson were only one-third of those

Table 4. Annual costs of ice-jam damage to various types of river structures (1988$).

Year	Bridges	Control Structures	Intakes Outfalls	Docks & Piers	Road/Railway Embankments	Other	Unspecified	Total
1988	$0	$0	$0	$0	$0	$0	$32,000	$32,000
1987	$2,079,884	$0	$0	$0	$22,507	$191,851	$7,799,564	$10,093,806
1986	$0	$0	$0	$0	$0	$0	$540,785	$540,785
1985	$0	$0	$0	$0	$0	$13,509	$0	$13,509
1984	$351,267	$11,709	$175,634	$0	$70,253	$320,824	$0	$929,688
1983	$0	$9,164	$0	$0	$0	$0	$0	$9,164
1982	–	–	–	–	–	--	--	$0
1981	$37,232	$0	$12,888	$28,640	$0	$7,160	$0	$85,920
1980	$0	$8,054	$0	$0	$0	$0	$0	$8,054
1979	$0	$69,204	$0	$0	$0	$0	$26,617	$95,821
1978	$0	$0	$0	$0	$3,876	$500,000	$0	$503,876
1976	$1,593,641	$0	$0	$0	$0	$0	$0	$1,593,641
1974	$1,747,962	$135,606	$0	$867,879	$721,153	$949,242	$271,212	$4,693,055
1970	$3,392,251	$353,550	$0	$0	$1,642,700	$0	$0	$5,388,501
1956	$0	$0	$0	$0	$0	$0	$9,910,035	$9,910,035
1953	$57,918	$0	$0	$0	$0	$0	$0	$57,918
1952	$2,009,825	$0	$0	$0	$0	$0	$0	$2,009,825
1950	$852,381	$0	$0	$0	$0	$0	$0	$852,381
1947	$0	$0	$0	$0	$0	$12,723	$0	$12,723
1936	$14,231,056	$0	$0	$0	$16,366	$0	$0	$14,247,422
1934	$219,486	$0	$0	$0	$0	$0	$0	$219,486
1929	$0	$0	$0	$0	$0	$116,739	$0	$116,739
1913	$346,452	$0	$0	$0	$0	$0	$0	$346,452
1902	$607,445	$0	$0	$0	$0	$0	$0	$607,445
1887	$57,742	$0	$0	$0	$0	$0	$0	$57,742
Total	$27,584,540	$587,288	$188,522	$896,519	$2,476,855	$2,112,049	$18,580,213	$52,425,985

Table 5. Navigation costs due to ice jams (1988$).

Year	Location	Direct Damage	Indirect Damage	Total Cost
1984	St. Clair River, Windsor, Ontario	–	$13,582,339	$13,582,339
1981	St. Lawrence Seaway, Quebec	$8,592,000		$8,592,000
1978	St. Lawrence, Beauharnois Canal	$968,877		$968,877
1981	North River, Nova Scotia	$1,232		$1,232
1947	Grand River, Brantford, Ontario	$579,619		$579,619
	Total	$10,141,727	$13,582,339	$23,724,066

Table 6. Total direct and indirect damage costs (excluding navigation) reported across Canada (1988$).

Province	River Structure		Flooding		Total Damage		Lives Lost
	Direct	Indirect	Direct	Indirect	Direct	Indirect	
British Columbia	$944,866	$11,709	$255,933	$189,582	$1,200,799	$201,290	0
Alberta	$0	$0	$7,340,529	$3,340,529	$7,340,529	$3,242,200	0
Saskatchewan	$2,009,825	$0	$17,745	$198,718	$2,027,569	$198,718	0
Manitoba	$4,551,630	$0	$4,623,009	$942,500	$9,174,639	$942,500	0
Ontario	$209,654	$0	$139,030,692	$26,034,090	$139,240,346	$26,034,090	17
Quebec	$7,799,564	$500,000	$92,657,895	$4,827,600	$100,457,459	$5,327,600	0
New Brunswick	$24,779,879	$1,656,583	$130,378,951	$19,010,815	$155,158,831	$20,667,399	14
Nova Scotia	$9,940,210	$22,066	$22,873,986	$00	$32,814,196	$22,066	2
Newfoundland	$0	$0	$41,768,415	$19,794	$41,768,415	$19,794	0
Yukon	$0	$0	$3,467,203	$00	$3,467,203	$00	0
Northwest Territories	$0	$0	$7,943,589	$00	$7,943,589	$00	0
Canada	$50,235,628	$2,190,358	$450,357,947	$54,465,299	$500,593,574	$56,665,657	33

reported during the same period for the present study. Total damage costs in Canada could be therefore as high as $1.3 billion if Atkinson's multiplier to account for indirect damage costs is correct.

Three provinces recorded the bulk of damage. 31% of the total damage occurred in Ontario. 30% in New Brunswick. and 20% in Quebec. Damage costs are not as great in other provinces. Newfoundland experienced 7% of the total damage while Nova Scotia sustained 6% of the total. Only 6% of the total occurred in the western provinces and the territories. This is likely because these areas have less population. less development and a shorter history than the other provinces. Flood damage accounts for 86% of the total reported damage. river structure damage. 10% and navigation costs. 4%. The relatively low cost of damage to these is likely because river structures have been increasingly better designed to withstand most ice-jam events. A total of 33 lives were also reported lost during ice-jam events. either in Ontario. New Brunswick or Nova Scotia.

The average annual cost of damage reported over the last ten years is just under $17 million. similar to the $15 million annual cost reported by Atkinson (1973). However. when the reported annual costs are adjusted to include unreported indirect costs. the average annual cost of ice-jam related damage becomes approximately $22 million. The annual cost of damage has been rising significantly approximately following the growth in population as can be seen in Figure 1. Some of the increase in damage costs. however. may also be due to increased awareness and more diligent reporting of events.

DISCUSSION

Despite attempts to canvas as wide a reporting audience as possible. the potential for underestimation of total-damage costs is relatively high. for a number of reasons. Firstly. although not all agencies contacted would be expected to be sources of relevant data. the relatively-low return rate (i.e.. 41%) creates a definite possibility of some underestimation. Similarly. there

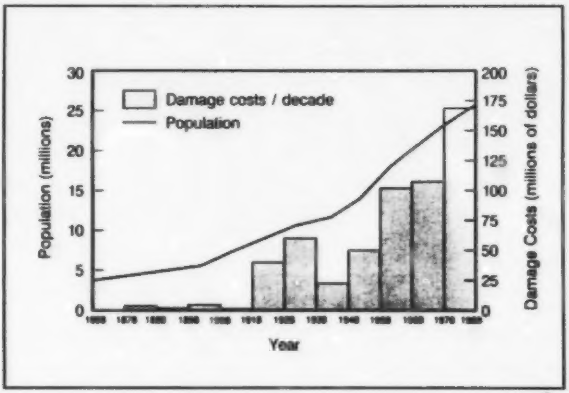

Figure 1. Growth of ice-jam damage costs per decade compared with growth of population (1988$).

was even a dearth of cost figures for many reported events, as evident in Table 2. Second, given the myriad of private and multi-level public agencies that could possibly archive such data, it is highly probable that some sources were overlooked. Third, despite canvassing a lengthy period, completeness of the record is unknown. As mentioned, ice-jam events appear to have been more frequently recorded in recent years. Although this could reflect an increased frequency of ice-jam episodes, it is more likely due to an increased awareness of the problem and/or enhanced development of flood-prone areas. In view of the better quality of the more recent records, the last 10 years were used as the basis for an average damage total. Importantly, however, such a short record may statistically have a wide margin of error and may under- or over-estimate the true long-term annual damage cost. Significant underestimation would occur if the 10-year period does not contain a statistically-valid proportion of large-magnitude, high-recurrence interval events. The importance of this point can be placed into perspective by considering, for example, the $1.5 billion damage costs that are projected to accrue from a one in a hundred year ice-jam flood on the Athabasca River at Fort McMurray (ECOS, 1982). Damage from this one infrequent, large-order event translates into an annual cost of $5 million or approximately one quarter of the $22 million-average derived from the 10-year record employed in this survey. Unfortunately, such long-term damage analyses have not been conducted for many ice-jam prone areas in Canada. This one example does, however, suggest that the national average may be considerably larger than the $22 million derived from the 10-year record made available to this study.

It should also be pointed out that there are many "costs" associated with ice jams that are virtually impossible to obtain simply because their physical and economic significance is only now being recognized. For example, modification of the flow and the related ice regime can produce significant environmental effects such as bed and bank scour on riverine biota/habitats and the impact of flooding on tributary water systems. The importance of this issue is reflected in the fact that there are presently two groups in Canada trying to address the scale of the problem: a) the National Research Council of Canada, Subcommittee on Hydraulics of Ice Covered Rivers, Task Force on Environmental Effects of River Ice, and b) the New Brunswick Subcommittee on River Ice. Given the potential scope of environmental impacts associated with flow regulation, it will be some time before "damage costs" can even be approximated. Merely the recognition of such additional sources of damage, however, reinforces the supposition that total damage is significantly underestimated when based on conventional sources of data.

Despite some of the above potential short-comings in achieving a truly comprehensive record of ice-jam damage, the figures derived from this survey do demonstrate that damage costs and their scale of impact are significant. More accurate figures can only be achieved through: identification and quanitification of all damage types, and improved documentation and archiving of relevant costs by the responsible agencies.

CONCLUSIONS

This study of the economic impact of river ice jams has provided a number of important facts. The total reported historical cost of river ice-jam damage including estimated indirect damages is at least $766 million and could be as great as $1.3 billion. Total direct damage was found to be three times greater than reported in a previous study. Also, a total of 33 lives have been reported lost in ice-jam flood events. The average annual cost of river ice-jam damage in Canada over the last ten years is $22 million and has increased with population. Even such figures, however, may considerably underestimate the total damage because of the difficulty in canvassing all possible data sources, uncertainties in the coverage of large-magnitude, low-frequency events, and the lack of information about all sources of damage, including those related to negative environmental effects.

The majority of reported damage occurred in three provinces: Ontario, New Brunswick and Quebec. Only 6% of reported damage occurred in the western provinces and the territories.

Flood-damage costs are much greater than river-structure damage costs. Commercial and residential sectors of the economy are most affected by flood damage, while damage to bridges accounts for 82% of river-structure damage. The total cost to navigation is only $24 million, however, only five events were reported.

The survey results indicate that the costs associated with river ice-jam damage are considerable. Conventional damage costs may be reduced if more effort is applied to damage prevention. Because flooding causes most of the damage, the most effective means of damage reduction would be to place restrictions on future floodplain development. In some areas of Canada, extensive damage still occurred to bridges even though they were designed to withstand ice forces. Increasing the bridge-design standards in these areas may reduce damage costs considerably. Further research into more effective prediction and control of ice jams may also help reduce damage costs in the future. Without these efforts, the cost of damage will undoubtedly increase as more development of floodplain land occurs.

NOTE: For a number of cited reasons, the total damage figures presented in this report are probably underestimates. The compiled cases, however, provide an excellent cornerstone to develop a more comprehensive and updated record. Readers are encouraged to forward any additional damage information regarding cited or other ice-jam cases to the authors.

ACKNOWLEDGEMENTS

This report was made possible with funds provided by the National Hydrology Research Institute and the Alberta Research Council. A special acknowledgement is owed to all the people who took time out from their busy schedule to respond to the survey. Also, thanks to B. McCarthy of the National Hydrology Research Institute who tabulated the data and conducted part of the literature search.

REFERENCES

ATKINSON, C.H., 1973. Problems and economic importance of ice jams in Canada. Seminar on Ice Jams in Canada, Snow and Ice Subcommittee, Technical Memorandum No.107, Associate Committee on Geotechnical Research, National Research Council of Canada, Ottawa, Ontario, July, 1-16

COCHRAN, W.G., 1977. Sampling techniques. 3rd edition, John Wiley and Sons Inc., New York, N.Y., 428 pp.

ECOS, 1982. Fort McMurray, flood damage reduction program, Phase II-B, flood damage estimates. Technical Report by ECOS Engineering Services Limited for Alberta Environment and the City of Fort McMurray

KINDERVATER, A.D., 1985. Flooding events in New Brunswick - an historical perspective. Report No.84-65, Water Planning and Management Branch, Atlantic Region, Inland Waters Directorate, Environmment Canada, Dartmouth, Nova Scotia, March, 247 pp.

Van der VINNE, 1989. Evaluation of the economic impact of river ice jams in Canada. Resource Technologies Department Report No.SWE-89/05, Alberta Research Council, Edmonton, Alberta

APPENDIX I: ECONOMIC IMPACT OF RIVER ICE JAMS - COST OF DAMAGE SURVEY

National Hydrology Research Institute - Alberta Research Council

Economic Impact of River Ice Jams
Cost of Damage Survey

Province or Territory: ____________________

Agency: ____________________

Event Location:
River: ____________________

City/Town: ____________________

Year: _____ Month: __________

Number of Lives Lost _____

Damage Type	Direct Damage Costs ($)	Code a-actual e-estimate p-paid out	Indirect Costs (loss of use) ($)	Code a-actual e-estimate p-paid out
River Structures				
• bridges				
• control structures (dams, dikes, weirs)				
• intakes/outfalls				
• docks, piers, etc.				
• road/railway embankments				
• other: __________				
Total costs				
Flooding				
• commercial				
• municipal				
• residential				
• agricultural				
• roads/railways				
• other: __________				
Total costs				
Navigation				
Total cost of damage				

Average annual cost of damage prevention at this location:

technique: ______________________________________

cost: __________

Average annual loss of revenue from hydro-electric projects to avoid damage at this location: __________

Name, address, and phone number of individual filling out this form:

____

____

____

____

Other sources of information:

ESTIMATION OF MASS-BALANCE AND RUN-OFF COMPONENT OF URUMQI GLACIER NO.1 FROM WATER-BALANCE ANALYSIS

Z. Yang

Lanzhou Institute of Glaciology and Geocryology
Chinese Academy of Sciences
Lanzhou, CHINA

ABSTRACT

Tianshan Glacier Station is the only comprehensive experimental basin with complete and long-term observations in the cold region of western China. The area above the hydrological site of Glacier No.1 is 3.34 km², and 58.4% of it is glacier-covered. The elevation range is 3,693 to 4,486 m. Meteorological and hydrological measurements from 1959 to 1987 have been used in this paper. Mass-balance data are very difficult to obtain from stake observations, so the water balance is one of the important methods used to estimate glacier mass balance. Water-balance analysis shows that the mean annual glacier mass balance of Glacier No.1 is about -88 mm, and that the run-off components from ice melt, summer snowmelt, winter snowmelt and firn meltwater are 43.6%, 38.5%, 11.2% and 6.7%, respectively.

INTRODUCTION

Hydrological methods are successfully applied to estimate the mass balance, and the run-off components of Urumqi Glacier No.1, based on the hydrological and meteorological data measured at Tianshan Station. The results are in basic agreement with measurements of glacier mass balance.

STUDY AREA

The Urumqi stream basin lies at the mid-section of the eastern Tianshan Mountains, covering a 924 km^2 area (above Heroical Bridge Hydrological Station), of which 4.2% is glacier covered (Figure 1). The basin lies between 1,830 m and 4,500

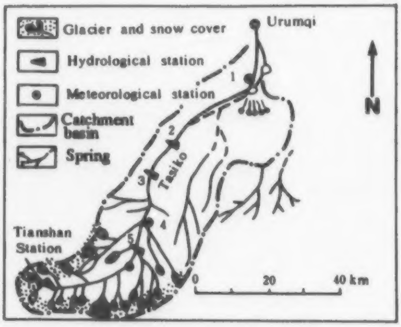

Figure 1. Locations of hydro-meteorological stations in Urumqi stream basin.

1. Wulabo 2. Youth Channel 3. Heroical Bridge 4. Hosia 5. Yue jin Bridge

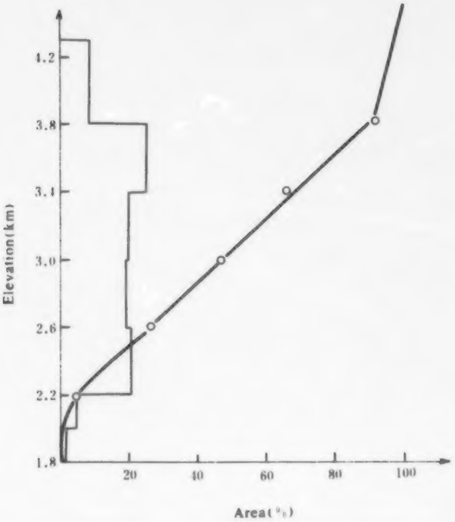

Figure 2. Area-elevation curve for Urumqi stream basin above Heroical Bridge.

m a.s.l., with 53% of the whole basin above 3,000 m a.s.l. (Figure 2). Urumqi Glacier No.1 is composed of the eastern and western branch glaciers, both located at the source of Urumqi stream which is in a glacier cirque with a length of 2.41 km and an area of 1.84 km^2. The highest elevation of the glacier, the glacier terminus and snow line are 4,486 m, 3,734 m and 4,050 m a.s.l., respectively (Xie and Zhang, 1988).

According to the data from the Tianshan meteorological station (3539 m a.s.l.), the long-term average air temperature (1959 to 1987) is -5.4°C, the average air temperatures of spring (March to May), summer (June to August), autumn (September to November) and winter (December to February) are -5.3°C, 4.0°C, -5.1°C and -14.9°C, respectively. Air temperatures remain continuously below 0°C for 7 to 8 months. May to September is the period of glacier ablation, with an average air temperature of 2.3°C. Long-term average precipitation is 530.8 mm.

DISTRIBUTION OF PRECIPITATION WITH ALTITUDE IN THE URUMQI BASIN

A study of the distribution of precipitation with altitude in an alpine region is important for accurate estimation of average precipitation. There are seven hydrological stations and two meteorological stations along the Urumqi stream, and some rain gauges in the glacierized area.

Based on long-term, synchronous precipitation measurements from Urumqi, Wulabo, Youth Channel, Heroical Bridge and Tianshan meteorological stations, the annual average precipitation decreases with altitude in the low-altitude zone, increases in the mid-altitude zone, and decreases towards higher elevations. In spring, autumn and winter, the precipitation distribution with elevation is similar to the annual precipitation distribution, but summer precipitation increases with altitude (Figure 3).

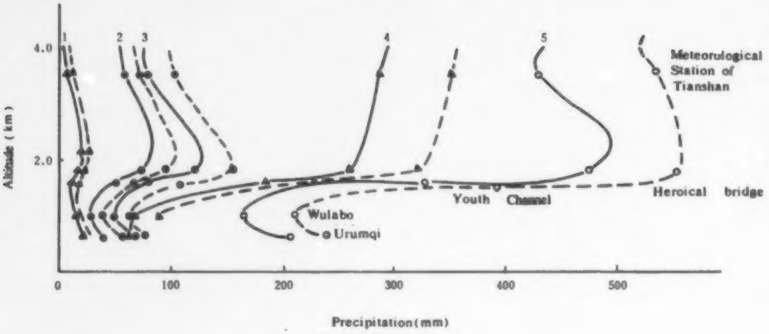

Figure 3. Distribution of precipitation with altitude in the Urumqi basin (Yang et al., 1987).

1. Winter 2. Autumn 3. Spring 4. Summer 5. Year
Solid line = measured precipitation;
Dashed line = corrected precipitation

Precipitation measurements show that the measured precipitation is less than the actual. The observation errors of precipitation are mainly affected by wind speed (13.9% reduction), wetting losses (8.4%) and evaporation losses (3.7%). The effect of wind speed is related to the type of precipitation. For example, the underestimates of precipitation for snow, rain and snow, and rainfall are 15.8%, 14.3% and 6.7%, respectively (Yang *et al.*, 1988). Total precipitation figures must also be increased by 25%, 18.8%, 26.4% and 27.9% for the summer, autumn, spring and winter periods, respectively.

MASS-BALANCE ANALYSIS OF URUMQI GLACIER NO.1

Changes of Glacier Mass Balance

The glacierized area includes both the glacier-covered and ice-free areas of the glacier basin. The glacierized area (above hydrological site) of glacier No.1 is 3.34 km^2, 58.4% of which is covered by the glacier (1959 to 1965 and 1980 to the present). The hydrological site covers an ice-free area of 1.68 km^2 for calculation of measured discharge (1982 to present) (Figure 4). Therefore, discharge measurements from glacier-covered and ice-free areas may be compared. The water balance equation of the glacier-covered area is:

$$P_i - R_i - E_i = \Delta B_n \qquad [1]$$

while that of the ice-free area is:

[2] $$P_b - R_b - E_b = \Delta V$$

where P, R and E are precipitation, run-off and evaporation, respectively; the subscripts refer to ice-covered (i) and ice-free (b) areas; ΔB_n is the glacier mass balance and ΔV is the change in water storage in the ice-free area, which approaches zero over many years.

The water-balance equation for the whole glacierized area becomes:

[3] $$P - R - E = \Delta W$$

where:

$$P = P_i + P_b$$
$$R = R_i + R_b$$
$$E = E_i + E_b$$
$$\Delta W = \Delta B_n + \Delta V$$

Knowing precipitation in the glacierized area (P) and assuming it is relatively uniform for the glacier-covered and ice-free areas, glacier meltwater run-off (R_i) and ice-free area run-off (R_b) can be obtained by the run-off coefficient method:

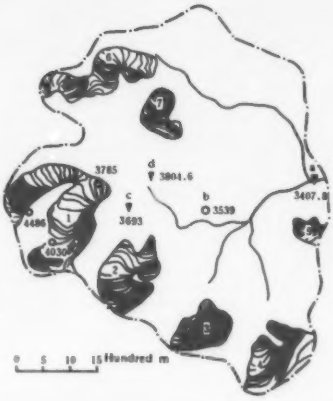

Figure 4. Location of hydro-meteorological station of Urumqi upstream basin.

o. Rain gauge.
a. Haisa hydrological site.
b. Tianshan meteorological station.
c. Glacier No.1 hydrological site.
d. Hydrological site of ice-free area.

[4] $$R_i = \alpha_i \cdot P \cdot F_i$$

[5] $$R_b = \alpha_b \cdot P \cdot F_b$$

where F_i is the glacier-covered area (km^2), F_b is the ice-free area (km^2), α_i is the coefficient of run-off on the glacier surface, and α_b is run-off coefficient for the ice-free area.

An estimate of α_i was made by first calculating run-off from:

[6] $$P - E_i = R_i$$

Mean annual precipitation in the glacierized area of Glacier No.1 was used in Equation 6 for P. To obtain an estimate of this, a spatial study of precipitation data was conducted. Based on synchronous measurements of precipitation from five gauges in the glacierized area (i.e., at the Tianshan meteorological station, hydrological site of Glacier No.1, glacier terminus, and in the firn and ice-free areas) during 1982 to 83, the lowest precipitation was noted to occur in the ice-free area and the largest in the firn area. Precipitation values for the Tianshan meteorological station and at the hydrological site of Glacier No.1 (Table 1) fell in-between these extremes. Precipitation from Tianshan Station (longest available record in the area) is therefore assumed to represent the mean precipitation of the glacierized area of Glacier No.1 to within ±5%.

An estimate of the mean annual evaporation for the glacier area (E_i) was made from the results of a 1962 to 1963 study by Xie and Cao (1965) who found the seasonal evaporation over ice to be approximately 70 mm. This value is considered to be a good approximation of the long-term summer evaporation rate since the mean summer temperature in 1962 to 1963 was close to the long-term average summer temperature. Furthermore, it agrees with other work (Golubev *et al.*, 1980; Krenke *et al.*, 1980). Inserting $E_i = 70$ and an average value for P into Equation 6 gives R_i which then permits calulation of α_i from:

$$[7] \qquad \alpha_i = \frac{R_i}{P}$$

resulting in $\alpha_i = 0.85$.

The run-off coefficient for the ice-free area (α_b) was derived directly from a similar form of Equation 7 using discharge and precipitation data from 1981 to the present measured at a study area near Glacier No.1 (Figure 4d). Use of the resultant value of $\alpha_b = 0.70$ assumes that the hydrological response of this study area is representative of the entire ice-free area.

Using Equations 4 and 5, R_b and R_i have been obtained for Urumqi Glacier No.1 during the 1959 to 1987 period, then compared with values of measured run-off from the total glacierized area (R). When $R>R_b+R_i$, the glacier is in a condition of negative balance. Conversely, $R<R_b+R_i$ indicates that the glacier is in a condition of positive balance, and $R=R_b+R_i$ is the case of zero mass balance. The differences between measured (R) and estimated run-off (R_i+R_b) are the values of pure glacier mass balance ΔB_n (Table 1).

The effect of correcting the precipitation figures is shown in Table 2. Based on the results of stake measurement data, Urumqi Glacier No.1 has lost 3.25 m of ice in 28 years (Xie and Zhang, 1988). Compared with the water balance results using measured and corrected precipitation (Table 2), the differences from 3.25 m are about +34% and -21% respectively. All estimates agree that Urumqi Glacier No.1 has retreated over the past 28 years.

Table 1. Water balance estimates for Urumqi Glacier No.1.

Year	Measured Precipitation P(mm)	Corrected Precipitation P'(mm)	Run-off (10^4 m^3) R	Run-off (10^4 m^3) R_b	Run-off (10^4 m^3) R_i	Evaporation (10^4 m^3) E	Mass Balance (10^4·m^3) ΔB_n	Glacier Run-off (10^4·m^3)
	(1)	(2)=(1)+[(1)×0.25]	(3)	(4)	(5)	(6)	(7)=(4)+(5)-(3)	(8)=(5)-(7)
1958-1959	472.8	591.0	120.5	57.5	97.9	42.0	+ 34.9	63.0
1959-1960	423.5	529.4	113.2	51.5	87.7	37.6	+ 26.0	61.7
1960-1961	434.5	543.1	165.3	52.9	90.0	38.5	- 22.4	112.4
1961-1962	444.2	555.3	219.5	54.0	92.1	39.4	- 73.4	165.5
1962-1963	495.5	619.4	199.0	60.3	102.7	43.9	- 36.0	138.7
1963-1964	444.2	555.3	155.8	54.0	92.1	39.4	- 9.7	101.8
1964-1965	502.3	627.9	152.3	61.1	104.0	44.6	+ 12.8	91.2
1965-1966	373.8	467.3	162.4	45.5	77.4	33.2	- 39.5	116.9
1966-1967	428.0	535.0	109.4	52.1	88.7	37.9	+ 31.4	57.3
1967-1968	377.6	472.0	120.8	45.9	78.3	33.5	+ 3.4	74.9
1968-1969	471.0	588.8	119.2	57.3	97.5	41.9	+ 35.6	61.9
1969-1970	380.5	475.6	142.2	46.3	78.9	33.7	- 17.0	95.9
1970-1971	465.5	581.9	120.2	56.6	96.5	41.3	+ 32.9	63.6
1971-1972	489.4	611.8	103.3	59.5	101.4	43.4	+ 57.6	43.8
1972-1973	354.0	442.5	189.6	43.1	73.4	31.3	- 73.1	146.5
1973-1974	418.4	523.0	222.0	50.9	86.7	37.1	- 84.4	171.1
1974-1975	446.2	557.8	139.7	57.4	88.7	40.2	+ 6.4	82.3
1975-1976	462.5	578.1	82.3	59.5	91.9	41.7	+ 69.1	22.8
1976-1977	382.9	478.6	209.1	49.6	75.7	34.6	- 83.8	159.5
1977-1978	436.1	545.1	164.9	56.5	86.2	39.4	- 22.2	108.4
1978-1979	418.7	523.4	135.0	54.6	82.3	37.9	+ 1.9	80.4
1979-1980	366.8	458.5	124.9	48.2	71.7	33.2	- 5.0	76.7
1980-1981	448.5	560.6	183.2	58.9	87.7	40.6	- 36.6	124.3
1981-1982	486.0	607.5	141.9	63.8	95.0	44.1	+ 16.9	78.1
1982-1983	408.2	510.3	132.1	53.6	79.7	37.1	+ 1.2	78.5
1983-1984	368.2	460.3	120.8	48.4	71.9	33.4	- 0.5	72.4
1984-1985	340.1	425.1	214.2	44.7	66.5	30.8	- 103.0	169.5
1985-1986	353.8	442.3	318.7	46.5	69.1	32.1	- 203.1	272.2
1986-1987	420.3	525.3	137.2	55.2	82.2	38.1	+ 0.2	82.0
Mean Value	424.6	530.8	155.8	53.3	86.1	38.0	- 16.5	102.5

Table 2. Water Balance Results For Urumqi Glacier No.1.

Precipitation P	Run-off R	Evaporation E	Mean Value of Glacier Mass Balance ΔB_n		Glacier Ice Loss	Years
(mm)	(mm)	(mm)	$(10^4 \cdot m^3)$	(mm)	(m)	
424.6	155.8	74.0	-29.2	-150	4.35	1959-1987
530.8*	155.8	114.0	-16.5	- 88	2.56	1959-1987

**Corrected precipitation increased (25%) over measured values.*

Run-off Components

The run-off component of Urumqi Glacier No.1 can be obtained from water-balance analysis (Table 3). The mean annual amount of ice and snow meltwater supplied to Urumqi stream from Urumqi Glacier No.1 has been found to be 102.5 x 10^4 m^3, of which glacier ice-melt run-off, summer snowmelt and winter snowmelt in the glacier ablation area, and snow meltwater from the firn area account for 43.6%, 38.5% and 11.2%, and 6.7%, respectively.

In dry years (1963, 1977 and 1986), characterized by low precipitation and high air temperatures, a large amount of glacier meltwater is released. In such years, over 70% of run-off from Glacier No.1 is supplied by glacier meltwater, and about 20% by summer snowmelt water. Therefore, a big loss of glacier storage occurs in dry years (see balance years 1962 to 1963, 1976 to 1977, and 1985 to 1986 in Table 3).

The results of run-off component analysis for the mountain outlet of Urumqi stream and the glacierized area of Glacier No.1 are summarized in Table 4. The findings shows the contribution of glacier and snow meltwater to total mountain stream run-off increases with elevation.

SUMMARY

The above analysis shows that not only can the changes of glacier mass balance be obtained, but also the various roles of each element of the water balance in space and time, and run-off components can be estimated from water-balance analysis. The water-balance method, therefore, offers an important scientific basis for studying mountain water resources, and the advance and retreat of glaciers. The accuracy of this method depends primarily upon the accuracy of precipitation estimates, especially mountain precipitation, and discharge measurement.

Table 3. Run-off components from Urumqi Glacier No.1.

Year	Glacier Ablation Area						Firn Area		Total Meltwater
	Summer Snowmelt		Winter Snowmelt		Glacier Ice Melt		Snowmelt		
	$10^4 m^3$	%	$10^4 m^3$	%	$10^4 m^3$	%	$10^4 m^3$	%	$10^4 m^3$
1958-1959	30.2	47.9	9.0	14.3	19.8	31.4	4.0	6.4	63.0
1959-1960	35.8	58.0	13.3	21.6	8.6	14.0	4.0	6.4	61.7
1960-1961	32.5	28.9	15.2	13.5	57.5	51.2	7.2	6.4	112.4
1961-1962	40.2	24.3	11.3	6.8	103.4	62.5	10.6	6.4	165.5
1962-1963	26.2	18.9	5.7	4.1	97.4	70.6	9.4	6.4	138.7
1963-1964	37.4	36.7	10.5	10.3	47.4	46.6	6.5	6.4	101.8
1964-1965	18.1	19.8	4.8	5.3	62.5	68.5	5.8	6.4	91.2
1965-1966	40.1	34.0	8.8	7.5	60.5	52.1	7.5	6.4	116.9
1966-1967	35.5	62.0	12.4	21.6	5.7	10.0	3.7	6.4	57.3
1967-1968	44.7	59.7	6.1	8.1	19.3	25.8	4.8	6.4	74.9
1968-1969	35.2	56.9	4.8	7.8	17.9	28.9	4.0	6.4	61.9
1969-1970	37.7	39.3	11.9	12.4	40.2	41.9	6.1	6.4	95.9
1970-1971	32.0	50.2	9.5	14.9	18.0	28.5	4.1	6.4	63.6
1971-1972	23.3	53.3	9.1	20.8	8.6	19.5	2.8	6.4	43.8
1972-1973	35.4	24.2	15.2	10.4	86.5	59.0	9.4	6.4	146.5
1973-1974	37.5	21.9	11.9	7.0	110.7	64.7	11.0	6.4	171.1
1974-1975	23.3	28.3	5.1	6.2	48.1	58.4	5.8	7.1	82.3
1975-1976	13.7	60.1	2.6	11.5	4.9	21.3	1.6	7.1	22.8
1976-1977	18.8	11.8	7.7	4.8	121.7	76.3	11.3	7.1	159.5
1977-1978	48.4	44.6	13.6	12.6	38.7	35.7	7.7	7.1	108.4
1978-1979	46.8	58.2	8.3	10.3	19.6	24.4	5.7	7.1	80.4
1979-1980	23.9	31.2	13.4	17.5	33.9	44.2	5.5	7.1	76.7
1980-1981	46.7	37.6	15.6	12.6	53.2	42.7	8.8	7.1	124.3
1981-1982	39.0	49.9	10.4	13.3	23.1	29.7	5.6	7.1	78.1
1982-1983	36.1	46.0	10.2	13.0	26.6	33.9	5.6	7.1	78.5
1983-1984	28.4	39.2	9.0	12.4	29.9	41.3	5.1	7.1	72.4
1984-1985	27.0	15.9	11.6	6.8	118.9	70.2	12.0	7.1	169.5
1985-1986	40.0	14.7	7.7	2.8	205.2	75.4	19.3	7.1	272.2
1986-1987	36.3	44.3	9.9	12.2	27.8	36.4	5.8	7.1	82.0
Mean Value	33.4	38.5	10.1	11.2	52.2	43.6	6.8	6.7	102.5

Table 4. Run-off Component of Urumqi Stream Basin.

Basin	Rainfall Water (%)	Snow Meltwater (%)	Ice Meltwater (%)	Ground Water (%)	Amount of Run-off ($10^8 \cdot m^3$)
Urumqi Stream	48.0	20.5	8.6	22.9	2.32
Glacierized Area of Glacier No.1	--	34.2	65.8	--	155.8

REFERENCES

GOLUBEV, G.N., M.B. DYURGEROV, M.B. ZASLAVSKAYA, B.B. BARKE, V.V. POPOVNIN, I.V. PILOV, E.K. CHEKANSKAY and V.M. SHALAGINOY, 1980. Dynamics and regime of water-ice balance components of the Djankuat Glacier and its basin, in the central Caucasus. Materialy Clyatsiologicheskiy Issledovanii N°.38, Mezhduvedomstvenni Geoficheskii Komitet, Akademii Nauk SSSR, Moskva, (in Russian) 147-152, (in English) 220-225

KRENKE, A.N. and A.M. TAREEVA, 1980. Estimation of glacial run-off in the Caucasus by the field of air temperature at the equilibrium line of glaciers. Materialy Glyatsiologicheskiy Issledovanii N°.63, Mezhduvedomstvenni Geoficheskii Komitet, Akademii Nauk SSSR, Moskva, (in Russian) 31-37, (in English) 112-117

XIE, W.R. and M.S. CAO, 1965. (Results of preliminary evaporation measurements on the snow surface of Glacier No.1, source of the Urumqi River, Tianshan Mountain). Research on the Glaciology and Hydrology of the Tianshan Urumqi River, (in Chinese) 70-73

XIE, Z.C. and J.H. ZHANG, 1988. (Glacier mass balance of China). In - An Introduction to the Glaciology of China, Science Press, Beijing, (in Chinese) 69-74

YANG, Z.N., S.S. ZHU, N.J. LI and Y.L. LI, 1987. (Preliminary analysis of the mountain water balance of the Urumqi River). Proceedings, 2nd National Conference on Glaciology, Geographical Society of China, (in Chinese) 248-258

YANG, D.J., T. JIANG, Y.S. ZHANG and E.S. KANG, 1988. (Analysis and correction of errors in precipitation measurement at the head of the Urumqi River, Tianshan). Journal of Glaciology and Geocryology, 10(4), (in Chinese) 384-399

SECTION 2

MODELLING

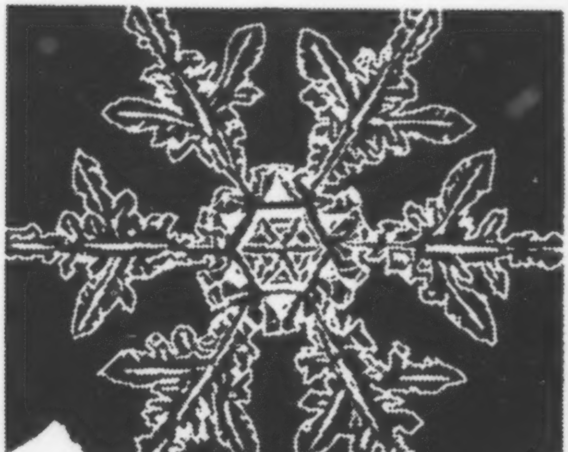

INTERACTIVE MODELLING OF COLD REGIONS WATERSHEDS WITH SSARR

E.A. Cassell[1] and T. Pangburn[2]

[1]University of Vermont
School of Natural Resources
George D. Aiken Center
Burlington, Vermont 05405-0088
U.S.A.

[2]U.S. Army Cold Regions Research and Engineering Laboratory
72 Lyme Road
Hanover, New Hampshire 03755-1290
U.S.A.

ABSTRACT

Until recently, capabilities of hydrological models to account for the effect of cold regions processes on run-off forecasting have been limited by the difficulty of data acquisition and the absence of modelling environments which have convenient process-level based interactive features. The work reviewed here describes results from research on modifications that have enhanced the Streamflow Synthesis and Reservoir Regulation (SSARR) model's ability to account for cold regions effects. These investigations have led to the development of a systems dynamic model version of SSARR. This new model, SSARR-DS, provides an extremely user-friendly environment that offers convenient data input and constructive interactive features.

INTRODUCTION

The Streamflow Synthesis and Reservoir Regulation (SSARR) model is a generalized watershed model for computing run-off from rainfall and/or snowmelt events. SSARR was developed by the North Pacific Division of the U.S. Army Corps of Engineers to allow the simulation of watershed systems for the "planning, design, and operation of water control works" (U.S. Army, 1972). The SSARR model tries to achieve "a balance between hydrologic theory and practical considerations related to daily operational use" (U.S. Army, 1972). SSARR synthesizes run-off from snowmelt, rain, or their combination, within hydrological units that are considered to be relatively homogeneous. The run-off may then be routed from upstream to downstream through channels and reservoirs that define a complex watershed or river system. The run-off also can be analyzed in conjunction with reservoir outflows so that impacts of reservoir regulation operational strategies can be simulated. SSARR has been, and is, widely used for such modelling in the U.S.A. and abroad.

This paper focuses on two phases of research that have been conducted concerning the SSARR model. The first phase, reported in the background section, deals with the modification of SSARR for improved accounting of the effect of cold regions processes on run-off forecasting. The second phase deals with work in which the watershed portion of SSARR was programmed into the STELLA language, an object-oriented programming environment that uses finite-difference methods for simulation, calibration and sensitivity analyses. The resulting model, SSARR-DS, provides many of the capabilities of SSARR to be used in cold regions hydrology within an extremely user-friendly environment that offers convenient data input, superior output capabilities and constructive interactive features.

BACKGROUND

Study Area

All modelling discussed in this paper was conducted on data from the W-3 sub-watershed within the Sleepers River Research Watershed (SRRW) that is located in northeastern Vermont near the town of Danville (See Figure 1). The 8.42 km^2 W-3 subwatershed (Figure 1) is located at latitude 44.5°N and longitude 72.2°W. W-3 is about 60% forested with hardwoods, softwoods and mixed stands with the remainder of the area being in pastureland and cropland. Elevations range from 346 m at the stream gauging site to 695 m at the head of the drainage. The straight line distance from the lowest to highest point is approximately 4.44 km. The soils range from coarse-textured sandy loams and loamy sands to fine-textured silt loams. The year around infiltrative and permeability characteristics of the watershed soils are high enough so as to largely preclude surface run-off in the higher elevations (Anderson *et al.*, 1977).

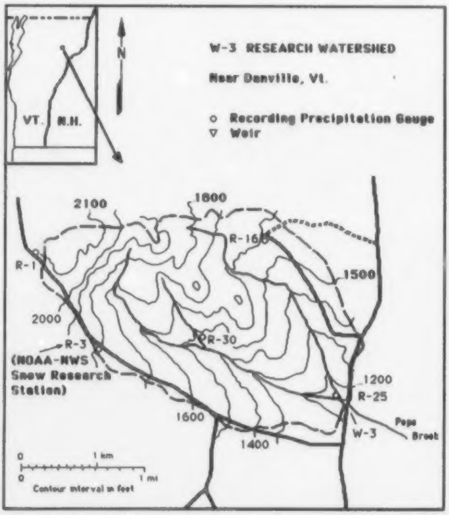

Figure 1. W-3 sub-watershed, Sleepers River Research Watershed, North Danville, Vermont.

W-3 has moist summers and long cold winters and is subject to rapid weather changes. The mean annual average temperature is about 4°C, with a January mean of -8°C. Between 40 to 60 days per year have a minimum temperature below -18°C. The mean annual potential evapotranspiration is about 533 mm and the mean annual precipitation is about 1,219 mm. Total snowfall averages about 3,048 mm per year with the maximum water equivalency of the snow being about 280 mm in March or early-April. The main snowmelt period is in March and April.

SSARR Model Calibration for Warm Periods in Temperate Regions

The initial hydrological model of the W-3 sub-watershed is based on work by Stokely (1980), who designed and implemented a DYNAMO watershed model based on the generalized watershed portion of the SSARR model (U.S. Army, 1972). Stokely (1980) used the basic equations taken directly from SSARR model documentation. As precipitation falls on the watershed, it is initially divided between run-off and soil moisture based on a table of percent run-off (ROP) versus the soil-moisture index (SMI) (Figure 2). Water that does not run off is stored as soil moisture. Soil moisture is depleted by potential evapotranspiration, using daily observed pan evaporation, which is reduced as the soil-moisture volume becomes less. The total run-off is then apportioned between baseflow, subsurface flow, and surface flow. The amount of water that percolates to baseflow is defined by an empirically-derived relationship. This relationship relates the percent of total run-off that becomes baseflow (BFP) to the baseflow infiltration index (BII) (Figure 2). The BII value is a model state that is updated as a function of time. The rate of change of BII with time is governed by a time constant.

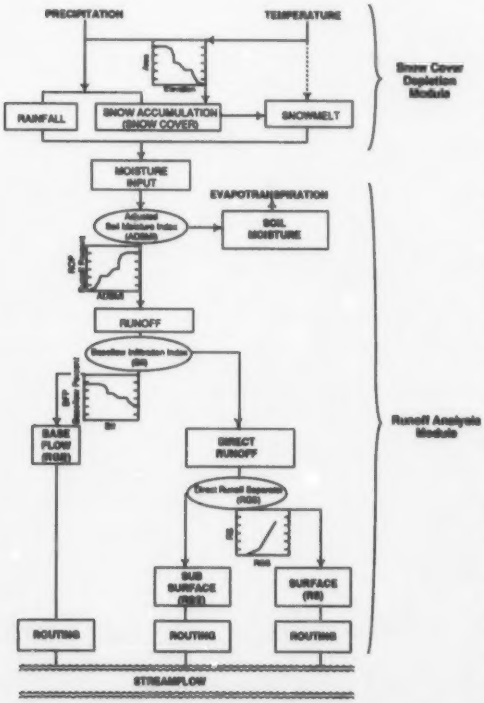
PRECIPITATION
TEMPERATURE
Snow Cover Depletion Module
RAINFALL
SNOW ACCUMULATION (SNOW COVER)
SNOWMELT
MOISTURE INPUT
EVAPOTRANSPIRATION
Adjusted Soil Moisture Index (ASMI)
SOIL MOISTURE
ROP
ASMI
RUNOFF
Baseflow Infiltration Index (BII)
BFP
BII
BASE FLOW (RGB)
DIRECT RUNOFF
Runoff Analysis Module
Direct Runoff Separation (RGS)
RS
RGS
SUB SURFACE (RGS)
SURFACE (RS)
ROUTING
ROUTING
ROUTING
STREAMFLOW

Figure 2. Schematic of SSARR model (after U.S. Army, 1972).

After baseflow has been subtracted from run-off, the remaining volume, direct run-off, is the sum of subsurface generation and surface flow generation. In the original SSARR model (U.S. Army, 1972), surface flow is determined as a surface-subsurface separation function of the direct run-off. This function is generally some minimum percent of the direct run-off, plus an additional percent if the direct run-off exceeds the maximum subsurface input rate. Stokely (1980) adjusted the surface-subsurface separation function based on the fact that there is seldom an observation of surface flow at the SRRW (Dunne and Black, 1970). He made surface flow (RS, Figure 2) a function of the precipitation rate (PRE) with surface flow only occurring when PRE exceeded published values of the average infiltration capacity of SRRW soils (Pionke *et al.*, 1986). Once base, subsurface, and surface flows are generated, SSARR uses a routing method to delay and smooth quantities of flow to the stream. In general, linear storage routing is used, based on the continuity equation for any number of phases for each of the three flow types. By varying the number of phases and the storage coefficients (routing constants) for each flow type, considerable freedom exists in shaping a flow hydrograph predicted for the model. Stokely (1980) calibrated the model for summer periods and found that a single reservoir or phase sufficed for each flow type for the W-3 sub-watershed. The time constants for surface flow, subsurface flow, and baseflow were found to be 2.5, 5, and 243 hours, respectively. Using these time constants to determine the outflow from each reservoir, streamflow is defined as the sum of the three outflows.

With the empirically-derived relationships and parameters available, the calibrated SSARR model must be supplied with the necessary input data. Initial values must be specified for baseflow infiltration (BII) and soil-moisture indices (SMI) as well as initial values in the baseflow and subsurface and surface flow reservoirs. SMI is specified using actual point volumetric soil-moisture data averaged over the sub-watershed using a Theisson polygon analysis. The initial value of SMI is obtained by multiplying the average thickness of the A-horizons of soils in the sub-watershed (Pionke *et al.*, 1986) by the actual volumetric moisture content. When periods of simulation are chosen such that they are preceded by periods of dryness, the initial volumes of the surface flow and subsurface reservoirs as well as the BII are initialized as zero. The initial volume of the baseflow reservoir may be calculated using the observed initial flow and the baseflow routing constant (243 hrs). The input data required are the hourly weighted basin precipitation and the daily pan evaporation measurements. In the absence of daily pan evaporation, mean values of seasonal evapotranspiration may be used.

Modifications to SSARR for Cold Regions

With a calibrated model for W-3 summer storms, methods are required for making modifications to reflect cold regions effects. Discrepancies between predicted and actual flows due to cold regions effects are associated with the dynamic behaviour of the hydrological effect of various cold regions phenomena. The phenomena include the temperature dependence of the kinematic viscosity of water and soil moisture retention, seasonal interception changes, snow accumulation and ablation, frozen ground, and ice formation in stream channels. All of these phenomena affect the timing and volume of discharge from the watershed. Algorithms are developed to account for the hydrological effects of these phenomena, and modifications are made to improve the capabilities of SSARR model forecasting in cold regions.

Cold Temperature Effects

Stokely (1980) first tested cold snowless periods to separate out the effects of temperature on the timing of flood peaks and on soil-moisture retention. In general, the model underpredicts the amount of run-off during this time period and the predicted early recession reveals a low-rapid fall in discharge values compared to actual values. These discrepancies suggested variations in run-off production, which are controlled by the SMI/ROP relation and run-off component timing coefficients.

Stokely (1980) attributed the discrepancies of discharge timing to the temperature dependence of the kinematic viscosity of water. The flow of water through porous media depends directly on the hydraulic conductivity of the particular medium. This, in turn, varies inversely with the kinematic viscosity of water. As temperature falls from 17°C to 0°C, the viscosity increases by about 60%. Therefore, to modify SSARR for colder periods, the time constraints for the surface flow and subsurface reservoirs (Figure 2) were multiplied by a factor that contained this kinematic viscosity relationship. The baseflow time constant was not changed because groundwater temperatures remain relatively constant throughout the year (Davis and Dewiest, 1966). Mean daily air temperatures were used in this study to determine the kinematic viscosity adjustment factor.

Stokely (1980) also modified the model to account for interception changes due to autumnal foliage drop and the temperature dependence of soil-moisture retention. Nearly 80% of the autumnal foliage drop in central Vermont and New Hampshire occurs during a single week, usually starting the first windy or rainy day after October 5 (Ryan, 1979). When simulations are made after this date there is an increase in the amount of precipitation that reaches the ground. An increase of 9.33% was made to the total percent run-off (ROP, Figure 2) to incorporate this effect into the SSARR model. This percentage was derived by consideration of the various cover types within W-3.

In addition, Stokely (1980) performed a numerical analysis to determine the temperature dependence of soil-moisture retention. He found that as temperature falls, field capacity increases. Field capacity is the amount of water held in soil after excess water has drained away and the rate of downward movement has materially decreased (Ward, 1975). This relationship is embodied in the SMI term of SSARR (Figure 2). As temperature decreases, the storage capability of the SMI volume increases and an increased ROP occurs. As was done with the viscosity-related modification, mean daily air temperature is used as an input parameter for soil-moisture retention modifications.

Snow Accumulation and Ablation

To simulate watershed dynamics for snow-covered periods, a DYNAMO version of the National Weather Service River Forecasting System (NWSRFS) snowmelt model was coupled with the temperature-modified watershed component of SSARR (Stokely, 1980). Two approaches are generally used for simulating snowmelt. One is the energy-balance approach, which depicts most of the detail of the physical system but requires extensive data sets that are not generally available in an operational environment. The second approach is the temperature-index method, which uses air temperature as a lumped indicator of basin snowmelt. Temperature index is the basis for the NWSRFS model. The NWSRFS model was chosen by Stokely (1980) because as "a 'state-of-the-art' model which is simultaneously operational, it does not require the extensive data necessary to implement an energy-balance model. It is associated with a federal agency directly responsible for accurate flood forecasting, the National Weather Service". The DYNAMO version of the NWSRFS, based upon Anderson (1973), consists of two general sectors, a meltwater production unit and a meltwater storage and transmission component.

Frozen Ground

Stokely (1980) and Peaco (1981) both analyzed the effect of frozen ground on SSARR model prediction. Bullard (1954) notes that frozen ground is particularly important in connection with snowmelt floods in the eastern United States. Storey (1955) states that frozen soil influences run-off production, in that "its structure determines how fast rain or melting snow can enter the soil. The depth of penetration of soil frost determines how fast the frost leaves the soil during thaws ... The extent of frozen soil indicates how much of a watershed might be affected."

Stokely (1980) used the theory of Bloomsburg and Wang (1969) to calculate when soils become impermeable. Each soil type is analyzed in this fashion and a percent frozen area is determined. As particular soil types become impermeable, more water is routed to the surface flow reservoir and to the stream channel in the SSARR model. The remainder of the watershed, which is not frozen or impermeable, is modelled in the normal SSARR snowmelt mode. Stokely (1980) could only locate three potential frozen-ground run-off events in the data of Anderson *et al.* (1977). These events showed great predictive improvement, but Stokely (1980) concluded that additional frozen-ground events would be necessary to expand and substantiate his findings.

Peaco (1981) related areal extent of frost to an index of the soil heat deficit. He concluded that additional data and research are needed to develop the appropriate index. The surface-energy transfer data, such as that collected at R-3 (Figure 1), and concurrent soil heat-deficit measurements could be used to develop such an index.

Ice Cover on Rivers

There has been considerable research on in-channel effects of flow under ice covers on rivers, but extensive research on the effect of ice covers on watershed flood forecasting has not yet been accomplished. The 1981 to 1982 winter season was analyzed (Pangburn and McKim, 1984) to determine the effect of an ice cover on SSARR model run-off prediction at W-3. No frozen ground was measured during the 1981 to 1982 winter season, so the temperature-modified SSARR model with the NWSRFS snowmelt model was used. Thirteen storm periods were analyzed with six periods having observed ice cover on Pope Brook, the W-3 main channel. When the model simulated the ice-cover storms, two areas of discrepancy were observed: first, an underprediction of the total volume of run-off; and secondly, what appeared to be a cyclic over/underprediction during the simulated event. It is hypothesized that the underprediction of the total run-off is caused by storage of water due to the presence of an ice cover in the channel. The cyclic behavior is attributed to the change in the travel paths of water to the stream channel due to the resistence of the ice cover as well as limiting the surface input from near-channel source areas. With observations of ice, SSARR is again modified by an additional storage reservoir in the stream channel and a term that diverts water from surface flows to the subsurface reservoir.

Watershed Thermal Budget Modelling

Pangburn (1987) described early results on using water temperature data to conduct streamflow separation and to quantify the volume and timing of snowmelt run-off. In recent studies, the effect of differing spatial and temporal scales on thermal budget of watersheds have been analysed.

DEVELOPMENT OF SSARR-DS

There is an increased emphasis on process-related research and studies which are concerned with the interrelation of all phases of water, energy and biogeochemical budgets. Such research benefits from a modelling approach which maintains modular components of 'known' physical processes and offers a combinational structure to account for the complete system's dynamic behaviour. With this in mind SSARR-DS, a systems-dynamics model, was created within the structure of the STELLA software package (Richmond *et al.*, 1987) and operates on the Macintosh Plus, SE and II computers. SSARR was originally coded into the DYNAMO language by Stokely (1980) and later converted into the STELLA language at CRREL.

Basis of SSARR-DS

SSARR-DS, like SSARR, is based on hydrological theory, watershed-specific rainfall-run-off relationships, flow-component separation relationships and a number of parameters that define a homogeneous hydrological unit. Calibration of

SSARR-DS (like the original SSARR) requires input of appropriate numerical values to describe these relationships, initial conditions, various hydrological factors as well as measured climatological and run-off values. SSARR-DS includes two major modules: the Snow Cover Depletion Module and the Run-off Analysis Module (U.S. Army, 1972).

SSARR-DS - An Object-Oriented Program

SSARR-DS is developed in the object-oriented programming (OOP) environment of STELLA. STELLA allows highly non-linear complex dynamic systems to be simulated by 'object oriented programs' created by placing defined 'objects' on the screen then connecting these objects so that flows, feedback loops and control structures operate as an interconnected whole system. A watershed is but one example of a complex dynamic system that can be modeled in STELLA. Once a STELLA model is completed, convenient data outputs include a choice of graphical displays and tabular presentations. Model diagrams and listings of the code (and comments) are easily outputted. Operation is highly interactive.

The STELLA diagram for the Run-off Analysis Module of SSARR-DS, simply the STELLA representation of the SSARR model, is given in Figure 3. The 'objects' used within STELLA are shown and include:

a. *rectangles* - are referred to as 'stocks' or 'bathtubs'; function to accumulate or decrement flows; reflect conditions in the system at a point in time.

b. *arrowed pipelines from/to 'clouds' with connected circles* - are referred to as 'flows'; functions to allow flow into or out of stocks; attached circles are the flow regulators (valves) that contain logic controlling flow through the pipeline.

c. *circles* - are referred to as 'converters'; converts inputs into outputs; inputs may be equations/logical statements, etc. (open circles) or numerical relationships (circles containing tildes). Converters do not accumulate but change instantaneously over the simulation run.

d. *single-lined arrows* - are referred to as 'connectors'; depict the causal linkages among the objects (variables) in the model. Connectors have no numerical value.

Inputs to SSARR-DS

Like SSARR, SSARR-DS can provide useful forecasts of run-off only when the model is calibrated. Calibration and operational simulations require input of a number of parameters and relationships including (i.e., initial values for the stocks, converter constants and equations, times-series data and other graphical relationships)

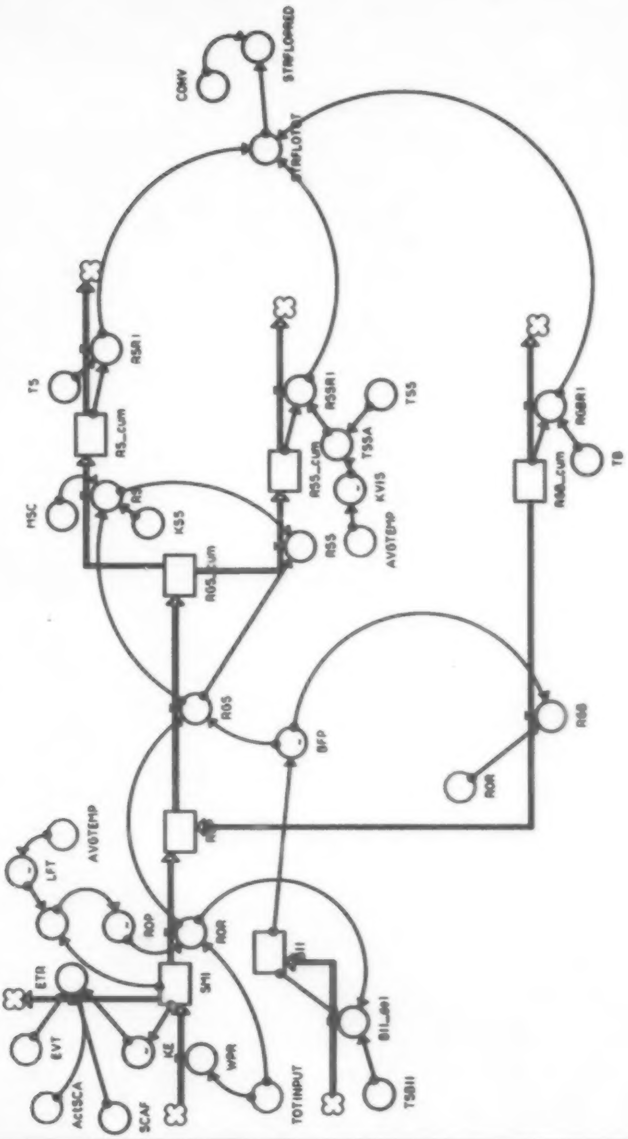
STRFLOWPRED
CONV
STRFLOTOT
TS
RSR1
RS_cum
RSC
RS
KSS
RSSR1
TSS
RSS_cum
TSSA
KVIS
RSS
AVGTEMP
ROS_cum
ROS
BFP
RGBR1
TB
RGB_cum
RGB
ROR
AVGTEMP
LFT
RDP
ROR
ETR
SMI
EVT
KE
WPR
BII
BII_del
ActSCA
SCAF
TOTINPUT
TSBII

Figure 3. STELLA diagram of run-off analysis module of SSARR-DS (see Cassell and Pangburn [1991] for model description).

associated with the specific watershed and particular event being modelled. Some inputs are required by the run-off analysis module and others by the snowcover depletion module.

There are four categories of parameters and relationships that must be input to SSARR-DS.

1. Time-Series Information - time-series information was input as hourly values for the events modelled in this paper, however, SSARR-DS allows entry as multi-hour or daily averages values.

2. Initial Conditions - a SSARR-DS (like a SSARR) simulation is initiated prior to the rising limb of the flow event being modelled when the observed watershed run-off is solely (or nearly so) the result of stable base flow. Values for all 'stocks' (the rectangles) are entered to reflect the "initial conditions" associated with this base flow period or that exist at time = 0.

3. Watershed-Specific Relationships - these relationships define run-off characteristics and other basic relationships such as temperature effects and watershed area-elevation relationships.

4. Watershed-Specific Constants - numerical values for a variety of watershed-specific constants.

CALIBRATION OF SSARR-DS

A hydrological model is considered calibrated when predicted flows agree (within some acceptable limit) with observed flows in timing, quantity and under a variety of climatological conditions. Calibration of SSARR-DS requires considerable flow and climatological data and other information about the watershed. The model is then fine-tuned by trial and error adjustment of watershed run-off characteristics until adequate fit is achieved of historical run-off data. Some input is general and applicable to many watersheds, other is specific to the watershed and/or specific run-off event being modelled. Cundy and Brooks (1981) classified model parameters and relationships as those that primarily determine streamflow volumes or shape of the hydrograph. Calibration of SSARR is discussed in U.S. Army (1972). Stokely (1980) presents the calibration of the DYNAMO version of SSARR.

Once values for all constants, initial conditions, and relationships are input, the model is run and simulated values for run-off are generated. When using a Macintosh SE and IIci each SSARR-DS simulation run takes about 45 and 15 seconds, respectively. Figure 4 shows typical graphical output from example SSARR-DS forecasted events. A full description of SSARR-DS and its calibration is given in Cassell and Pangburn (1991).

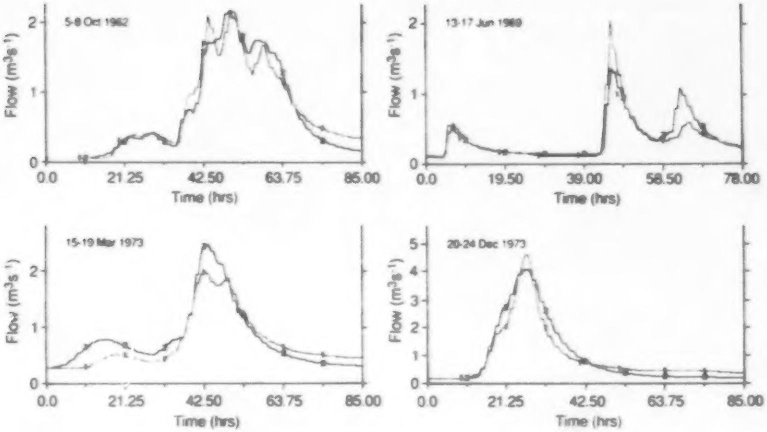

Figure 4. Example SSARR-DS forecasted events. Actual Flow = 1, Simulated Flow = 2.

HOW SSARR-DS WORKS

Neither SSARR-DS or other watershed models ever perfectly describe watershed behavior. Different models may be extremely sensitive to different parameters. Since data must be collected consistent with model needs and not necessarily to describe actual watershed behaviour, it is important to understand how the model functions as a simulation device. Because SSARR-DS is coded in STELLA, the model can be conveniently and rapidly dissected to examine the internal workings of the model and to assess the sensitivity of the model to various parameters.

To outline an example of the logic of SSARR-DS and internal model workings the temperature-index snowmelt routine is shown in Figure 5. Air temperature, base temperature, and melt factor are the components on which temperature-index snowmelt is based. To determine snowmelt the difference between air temperature and base temperature if greater than zero, is multiplied by a melt factor. This routine is built in STELLA by graphical construction of the structural diagram that represents the theory. Once the structural diagram is constructed, the relational logic is added, and an initial value of the snowpack water equivalent (SnowWE-'stock') is specified, the model can be run. To view the dynamic behaviour of this routine (or the full SSARR-DS) you can animate the diagram and plot and tabulate the variables of interest over time. To illustrate the animation of the temperature-index snowmelt module diagram, Figure 5 also shows the status of the animated diagram at three different times in the simulation. As the simulation proceeds the SnowWE stock is

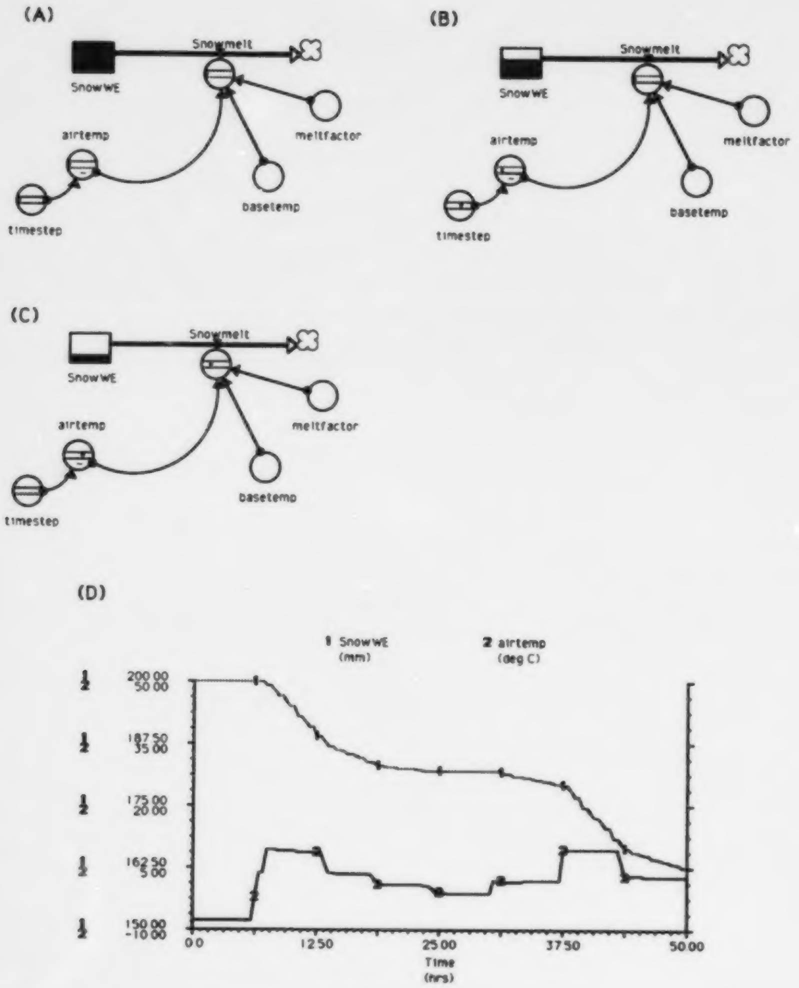
(A)
Snowmelt
SnowWE
airtemp
meltfactor
basetemp
timestep
(B)
Snowmelt
SnowWE
airtemp
meltfactor
basetemp
timestep
(C)
Snowmelt
SnowWE
airtemp
meltfactor
basetemp
timestep
(D)
1 SnowWE (mm)
2 airtemp (deg C)
200.00
50.00
187.50
35.00
175.00
20.00
162.50
5.00
150.00
-10.00
0.0
12.50
25.00
37.50
50.00
Time (hrs)

Figure 5. STELLA temperature-index snowmelt routine.

(A) At simulation time 0 hours.
(B) At simulation time 25 hours.
(C) At simulation time 50 hours.
(D) Graphical STELLA output.

emptying, i.e., decreasing water equivalent and the rates or 'converters' are changing as indicated by the movement of their 'needle gauge' (from left to right). This animation along with the tabular and graphical capabilities of SSARR-DS gives the modeller the ability to visualize the dynamic behaviour of physical systems. It cannot be overemphasized how convenient the interactive nature of SSARR-DS makes the examination of large systems models to determine if certain parameters cause numerical errors or exert too large an effect on other model parameters.

Parameter Sensitivity Analyses

Understanding model sensitivity, in a general sense, greatly assists in the interpretation of divergence of simulated and observed run-off values and provides a basis for recommending appropriate data-gathering strategies for use in the SSARR-DS model. Kang (1977) carried out systematic evaluations of the sensitivity of SSARR output to several model parameters and concluded that SSARR model parameters have sufficient flexibility to control model output and to rapidly reconstruct hydrographs. Accurate simulation by SSARR-DS requires careful definition of initial conditions including the representative watershed-wide initial soil moisture index (SMI) and the percentage of the watershed covered by snow at the beginning of the simulation. The simulation is sensitive to the watershed melt temperature, to the snowmelt rate coefficient, to lower ranges of soil moisture, and to the initial percentage of the watershed area under snowcover.

Time Sensitivity Analysis

STELLA interpolates between user-defined time steps with either Euler's, or 2nd or 4th order Runge-Kutta simulation algorithms (Richmond *et al.*, 1987). In such interpolations, as the time step approaches zero, estimated solutions approach exact solution. In the world of hydrology, data are usually not available for every instant in time, but rather as average values over some time period (such as average daily, average six hour, average hourly, average annual, etc.). Sub-watershed W-3 is a small watershed. To understand its behaviour it was necessary to consider changes in run-off on an hourly basis. Therefore, all SSARR-DS simulations used a hourly time increment and the input data either were either hourly average or a six-hour average values. Model simulation results are extremely sensitive to the average time period represented by each input data value. The user must exercise caution in choice of the simulation time step needed to adequately describe the run-off and to provide consistency with the frequency of the input data.

SUMMARY AND CONCLUSIONS

Using data from the Sleepers River Research Watershed, in northern Vermont, USA, modifications have been made to the U.S. Army SSARR model. These modifications have improved the forecasting accuracy of SSARR under varying cold regions conditions. In addition to these modifications, a systems-dynamics model version of SSARR has been developed. This new model, SSARR-DS, provides an extremely user-friendly environment that offers convenient data input, superior output capabilities and constructive interactive features.

The results from these studies are being used for further work in two areas. Firstly, further development work in creating STELLA routines and models is proceeding. Secondly, additional research on physical-based process models is being conducted to characterize the watershed thermal distribution as it relates to snowmelt forecasting. By using a modular systems approach similar to SSARR-DS, decision rules will be developed for selecting the appropriate model based on the spatial attributes of the study watershed.

REFERENCES

ANDERSON, E.A., H.J. GREENAN, R.Z. WHIPKEY and C.T. MACHELL, 1977. NOAA-ARS cooperative snow research project - watershed hydro-climatology and data for water years 1960-1974. Joint Publication, U.S. Department of Commerce, NOAA/NWS and U.S. Department of Agriculture, ARS, NOAA Publication No.S/T 77-2854, June, 312 pp.

BLOOMSBURG, G.L. and S.J. WANG, 1969. Hydrology of frozen ground floods. NTIS PB-187, U.S. Department of Commerce, 269 pp.

BULLARD, W.E., 1954. A review of soil freezing as affected by snow cover, plant cover and soil conditions in northwestern United States. AIHS Publication No.39, Comptes-rendus et Rapports de la Commission des Neiges et des Glaces, Tome IV, Assemblée Générale de Rome, Association Internationale d'Hydrologie Scientifique, 132-136

CASSELL, E.A. and T. PANGBURN, 1991. A systems dynamics model for computing watershed runoff. CRREL Special Report No.615, Cold Regions Research and Engineering Laboratory, U.S. Army Corps of Engineers, Hanover, New Hampshire, in press

CUNDY, T.W. and K.N. BROOKS, 1981. Calibrating and verifying the SSARR model - Missouri River watersheds study. Water Resources Bulletin, 17(5), 775-782

DAVIS, S.N. and R.J.M. DEWIEST, 1996. Hydrogeology. John Wiley and Sons, Inc., New York, N.Y., 463 pp.

DUNNE, T. and R.D. BLACK, 1970. An experimental investigation of runoff prediction in permeable soils. Water Resources Research, 6(2), 478-490

KANG, N., 1977. Sensitivity of parameters of SSARR model reconstruction of streamflows and regulation of reservoirs. Water Department, Hydro-Québec, Montréal, Quebec, 10 October, CRREL Draft Translation, Cold Regions Research and Engineering Laboratory, 1981, U.S. Army Corps of Engineers, Hanover, New Hampshire, 41 pp.

PANGBURN, T., 1987. Forecasting of snowmelt runoff using water temperature data. Proceedings, 44th Annual Eastern Snow Conference, 3-4 June 1987, Fredericton, New Brunswick, 108-113

PANGBURN, T. and H.L. McKIM, 1984. USACRREL's snow, ice, and frozen ground research at the Sleepers River Research Watershed. Proceedings, 41st Annual Eastern Snow Conference, 7-8 June 1984, Washington, D.C., 229-240

PEACO, D., 1981. Frozen ground hydrology in watershed simulation: model development and analysis of the 1979-80 winter in the Sleepers River Research Watershed in northeastern Vermont. Resource Policy Center Report DSD No.332, M.Sc thesis, Thayer School of Engineering, Dartmouth College, Hanover, New Hampshire, 180 pp.

PIONKE, H.B., B.J. CHAMBERLAIN, P.L. McCLURE, K. BAHLEDA and J.C. KEPES, 1986. Data directory, data and data collection site characteristics for the Sleepers River Research Watershed, N. Danville, Vermont. Northeast Watershed Research Center, University Park, Pennsylvania, 93 pp.

RICHMOND, B., S. PETERSON and P. VESCUSO, 1987. An academic user's guide to STELLA. High Performance Systems, Lyme, New Hampshire, 392 pp.

RYAN, D., 1979. Ecosystem research at the Sleepers River Research Watershed. Resource Policy Center Report No.162, Thayer School of Engineering, Dartmouth College, Hanover, New Hampshire, 15 pp.

STOKELY, J.L., 1980. Watershed modeling in cold regions: an application to the Sleepers River research watershed in northern Vermont. M.Sc. thesis, Thayer School of Engineering, Dartmouth College, Hanover, New Hampshire, June, 241 pp.

STOREY, H.C., 1955. Frozen soil and spring and winter floods. In - Water: The Yearbook of Agriculture, U.S. Department of Agriculture, Washington, D.C., 179-184

U.S. ARMY CORPS OF ENGINEERS, 1972. Program description and user manual for SSARR model. North Pacific Division, U.S. Army Corps of Engineers, Portland, Oregon, September, 188 pp.

WARD, R.C., 1975. Principles of hydrology. McGraw-Hill, London, 403 pp.

ESTIMATES OF EVAPORATION IN THE YUKON AND NORTHWEST TERRITORIES

J. Haas

39 Hobart Crescent
Nepean, Ontario
K2H 5S3 CANADA

ABSTRACT

This paper examines the water-balance equation for fourteen selected river basins in the Yukon and Northwest Territories as well as the impact of climate change on its components. Evaporation/evapotranspiration is studied in more detail using the complementary relationship evapotranspiration model. Alternative evaporation/evapotranspiration results are used for the calculation of water balance. The results show decreasing trends in water storage. The water balance is then modified for alternative 'after-the-climate-change' values of evaporation/evapotranspiration and precipitation; the results indicate the possibility of changes in water storage and run-off.

INTRODUCTION

Present-day scientific and technical knowledge indicates that precipitation in the northern regions of the country is underestimated (Woo and Marsh, 1978; Marsh and Woo, 1977). This complicates the calculation of the water balance. A further difficulty for northern water resources might be the possibility of human-induced climate change; some predictions indicate that global climatic change will become significant before the middle of the next century. The warming effect is likely to cause changes in precipitation and evaporation, two principal elements of the hydrological cycle. The time scale of the expected climate change is quite similar to that required for planning medium- to large-scale water-management activities. The planning, management and evaluation of water-resource systems have traditionally assumed an unchanging climate, which may no longer be true. Therefore, there exist two important tasks in assessing northern water resources: 1) to evaluate (or to re-evaluate) the water-balance equation for river basins of interest; and, 2) to assess the effect of the climate-change factor on water-management systems.

The assessment of the impact of climate change on physical systems in general and on water-resource systems in particular is currently at a very rudimentary level. Considerable basic developmental effort is required to establish appropriate research methods and to amass basic relevant information. Accordingly, the objectives of this paper were: 1) to design a methodology for the calculation of the water balance with special regard to the possible underestimation of precipitation measurements; 2) to develop an appropriate data base; and, 3) to modify the water-balance equation applying the results of the assessment of the possible impact of climate change scenarios on evaporation/evapotranspiration and precipitation. To test the methodology and the results, fourteen river basins throughout the Yukon Territory (Y.T.) and the Northwest Territories (N.W.T.) were selected.

Sufficient results on evaporation/evapotranspiration and on the water balance from high altitudes do not exist. This paper is simply a trial of one evaporation/evapotranspiration model and the importance of the results is in indicating that there are discrepancies in the water balance.

METHODOLOGY

The paper deals with two principal subjects: 1) the calculation of the water balance using historical data as well as post-climate-change simulated data, and 2) climate change and its impact on water resources. While 1) is a standard water-resource excercise (even though often neglected), 2) represents a new area of work and deserves some introduction.

The methodology used in this paper has mostly been developed in Haas and Marta (1988); the paper summarizes results obtained by applying this methodology to fourteen selected river basins in the Y.T. and the N.W.T.

The subject of climate change and its impact on water resources can be evaluated at two levels:

- through a general description of climate change, and
- by an examination of specific water-resource implications at a regional scale.

The general description level consists of: 1) observations and evidence of climate change and a review of this evidence; 2) an explanation of the causes of climate change, natural and man-made, including an evaluation of their significance; and, 3) modelling of climate change. The specific water-resource level includes: a) quantitative inputs from the general level (i.e., estimates of changes in major climatic variables); b) simulations of the hydrological-regime change corresponding to the expected change in climatic variables; and c) a performance evaluation of water-resource systems for the simulated post-climate-change regime (Klemeš, 1985).

Topic a) necessarily includes all major climatic characteristics such as air temperature, precipitation, evaporation and evapotranspiration, humidity and others. Since these parameters interact and their variation in nature involves complicated interrelated physical processes, it is extremely difficult to study them together in all their complexity. The approach adopted here is to investigate one climatic variable in depth and to include others only in simplified form or, if necessary, to the degree needed to assess their impact on that one selected variable. The variable selected for special study should satisfy two basic conditions. First, it should be one of the primary climatological parameters which causes a direct and measurable impact on water resources. Second, a modelling tool which enables adequate description of this variable should be available. This tool should be sufficiently tested and geographically transferable. It should at least show promise of climatological transferability. A model is geographically transferable when, after being developed and tested for one geographical area, it yields good results in a different location, and requires changes only in spatially-specific parameters such as longitude, latitude and altitude. Similarly, a model is climatologically transferable when, after being developed for present-day climate situations and proven to be geographically transferable, it functions satisfactorily with new data and thus requires minimal to no adjustments for new situations, such as climate-change scenarios. Finally, data preparation and use of the model should preferably be simple.

The climatic variable selected as the main focus of this study is evaporation/evapotranspiration. (Hereafter, the term evapotranspiration will also mean evaporation, unless otherwise specified.) The importance of the ability to calculate evapotranspiration without locally 'adjusted' parameters for a realistic calculation of the water balance as well as the possibility of describing changes in evapotranspiration caused by eventual climate change is self-evident. From among the several modelling tools that are readily available, the models developed at the National Hydrology Research Institute by Fred Morton were selected. (For a detailed description see Morton, 1983a, 1983b and 1985).

From the early 1970s the Morton models have been tested over a widening range of environments. The models were applied on more than 150 river basins in Canada, Ireland, Australia, New Zealand, Japan, the southern United States, Brazil and a number of countries in Africa. In many of these applications the models' estimates of the areal evaporation were tested by comparing model results with estimates of areal evaporation derived from river-basin water balances for the same time periods (Morton, 1983a). Such work, however, has not been conducted in the cold northern regions of Canada.

While the calculation of evapotranspiration and of the water balance are fairly well tested and are limited mostly by availability of data, existing models describing the greenhouse warming effect on primary climatological variables such as precipitation and temperature are still rather new and problematic, even though significant progress was achieved in the last two years or so (American Meteorological Society, 1990). The main problem with these climatological models, which are usually called General Circulation Models (GCMs), remains the same as before - the spatial resolution of the results is still rather coarse. GCM data points of the so-called grid-point networks are defined geographically by longitude and latitude with no regard to functional and spatial characteristics of hydrological, agricultural or other specific systems. The above considerations are not meant to suggest that the results of GCMs are substandard, but to simply clarify that they are not tested or assessed in this paper and are handled merely as one possible type of simulated data.

Table 1. Fourteen study areas.

River Basin	Precipitation Station	Longitude	Latitude	Drainage area (km^2)	[1]Annual Precipitation (mm)	Elevation (m)
Yukon Territory						
Tom Creek	Watson Lake	60.12	128.82	435	425	689
M'Clintock	Whitehorse	60.72	135.07	1700	261	703
Firth River	Komakuk Beach	69.58	140.18	5710	136	14
Babbage River	Shingle Point	68.95	137.22	1510	214	55
Mackenzie River Basin						
Lake Buffalo	Fort Smith	60.00	111.85	3330	323	203
Martin River	Fort Simpson	61.75	121.23	2050	305	169
Cameron River	Yellowknife	62.45	114.48	3630	225	205
Carcajou River	Norman Wells	65.28	126.85	7400	290	73
Caribou Creek	Inuvik	68.27	133.67	625	245	68
North-Eastern Arctic						
Prince River	Baker Lake	64.30	96.00	2100	225	12
Tree River	Coppermine	67.83	113.08	5810	198	9
Freshwater	Cambridge Bay	69.10	105.12	1490	135	27
Big River	Sachs Harbour	71.98	125.28	36.40	113	86
n/a	Resolute	74.72	94.94	n/a	124	67

[1] *Sources of data: Canada, Environment Canada, 1989 and Acres Consulting Services, 1982.*

The methodology developed in this paper was applied to the fourteen study areas (river basins) throughout the Yukon and N.W.T. (Table 1). The selection criteria for the study areas were as follows: 1) they should cover a wide range of climatological, geographical and environmental conditions; 2) the study should include representative areas of the Yukon Coastal Plain, the Mackenzie River basin, the Arctic Islands as well as examples from the eastern Arctic; 3) the study areas should cover regions of existing or planned economic activity; and last, but not least, 4) their selection was heavily affected by the availability of data.

The selection of study areas in the Yukon Territory was 'simplified' by the serious lack of necessary data. To calculate evapotranspiration using Morton's model, temperature, humidity and solar-radiation data are needed, but to the best of the author's knowledge suitable solar-radiation data are available only for Whitehorse and Watson Lake. To have at least something in the Yukon Coastal Plain, solar-radiation data from Inuvik (i.e., from the N.W.T., but still reasonably close) were used for

Shingle Point and Komakuk Beach. For the Mackenzie River basin, five study areas were selected, representing different sections of the river between Fort Smith and Inuvik. Finally, five locations in the northeastern Arctic were selected as well. Table 1 shows the drainage area, total annual precipitation and approximate elevation of the selected areas.

DATA BASE

For calculation of evapotranspiration and water balance and for the subsequent evaluation of changes in evapotranspiration and precipitation the following monthly and annual data were used: 1) the General Circulation Models (GCM) data for the northern parts of the country; 2) climatological data required by Morton's models for the evapotranspiration calculation, i.e., temperature, humidity and sunshine radiation data; 3) precipitation and run-off data used for the water-balance calculation; 4) normals of climatological and precipitation data; and, 5) GCM-based calculated shifts in temperature and precipitation used for calculation of simulated data.

This paper utilized results obtained by the GCM developed at the Goddard Institute for Space Studies (GISS model) and adjusted by the Canadian Climate Centre (Hengeveld and Street, 1986). These GISS outputs served simply as one possible type of numerical input for this study and are not discussed or evaluated in detail. These data sets, however, are currently widely used in climate-change impact-assessment studies across Canada.

The GISS model provides simulated data for temperature, precipitation and several other types of meteorological and climatological data for latitude-longitude grid points. Two methods of 'regionalization' of GISS-grid data were applied to obtain simulated data for individual study areas (Haas and Marta, 1988).

The GISS model results were selected because of their superior consistency. Cohen (1988) concluded that the results from the GISS grid points provide better results than other models. He compared GISS results with those of other models and conducted an extensive evaluation of GISS and the Geophysical Fluid Dynamics Laboratory (GFDL) model. In Haas and Marta (1988), these two models (i.e., GISS and GFDL) were also compared (an identical set of data from the Lake Diefenbaker area was used for both applications) and the GISS model seemed to provide more consistent results.

The GISS model provides simulated mean monthly and annual temperature and precipitation data for: 1) the time period 1951 to 1980 (this is the same time period used for calculating current climate "normals" and it is called the 1 x CO_2 situation); and 2) the situation with a 100% increase of CO_2 in the atmosphere, the so-called 2 x CO_2 situation or scenario.

EVAPORATION AND EVAPOTRANSPIRATION

The models selected for use in this paper are those developed by Morton: the complementary relationship areal evapotranspiration (CRAE) model and the associated complementary relationship wet-surface (CRWE) model.

There are several publications available, some of which are listed in the references, on the concept of complementary relationship and the associated models, therefore the principles and processes that are the conceptual basis of CRAE and CRWE models are not repeated here.

The models are considered quite conservative. Obtained evapotranspiration estimates for temperate regions are usually 10 to 20% lower than those of other models. (For comparison of the Meyer formula and CRAE model see Feng *et al.* (1989) and Haas and Marta (1988)). However, the applications of CRAE and CRWE models presented in this paper are among the first ones for northern Canada and extensive testing of the Morton models for this region is necessary. Any error associated with the actual evapotranspiration results would have, of course, an impact on the water-balance components. Specifically, the overestimation of areal evapotranspiration would cause the overestimation of the error in the precipitation measurements, i.e., underestimation of precipitation would not be so serious. All this should be the subject of further work together with comparison of the results of the CRAE model with those obtained by other studies and with an evaluation of other components of the water-balance equation. The CRAE and CRWE models were applied for all fourteen study areas. Table 2 presents results for average annual potential and areal evapotranspiration. Table 3

Table 2. Average annual potential and areal evapotranspiration.

Study Area	Potential Evapotranspiration (mm·yr^{-1})	Areal Evapotranspiration (mm·yr^{-1})
Yukon Territory		
Watson Lake	671.9	227.2
Whitehorse	687.7	184.6
Komakuk Beach	197.3	188.4
Shingle Point	254.1	211.0
Mackenzie River Basin		
Fort Smith	655.0	281.1
Fort Simpson	658.7	229.8
Yellowknife	695.8	228.0
Norman Wells	559.8	199.3
Inuvik	405.3	180.9
North-Eastern Arctic		
Baker Lake	320.4	201.2
Coppermine	254.3	194.2
Cambridge Bay	183.3	150.3
Sachs Harbour	168.4	156.0
Resolute	121.4	116.9

shows (for eleven study areas) results for wet-surface evaporation.

WATER BALANCE

As noted earlier in this paper, climate-change induced impacts on water resources will occur at the watershed level and, therefore, sensitivity assessments must be conducted at the regional scale. The recommended approach (see Beran, 1986; Gleick, 1986; and Klemeš, 1985) is to couple appropriate GCM results with modified water-balance models. The following version of the basic water-balance equation was chosen for this study:

[1] $$R \quad P \quad E \quad \Delta S$$

where R is run-off, P is precipitation, E is evaporation and ΔS is storage change. Consequently, the types of information required to adequately estimate flows under a 2 x CO_2 climate change situation are as follows:

Table 3. Average annual wet-surface evapotranspiration (mm·yr^{-1}).

Study Area	Wet-Surface Evaporation	
	Pan-Size mm·yr^{-1}	Lake-Size mm·yr^{-1}
Yukon Territory		
Watson Lake	681.1	475.8
Whitehorse	711.4	480.5
Shingle Point	269.2	248.8
Mackenzie River Basin		
Fort Smith	670.9	496.9
Fort Simpson	671.4	471.9
Yellowknife	735.1	526.0
Norman Wells	569.3	402.8
Inuvik	416.2	313.9
North-Eastern Arctic		
Baker Lake	339.3	281.8
Coppermine	268.4	237.8
Resolute	127.4	125.3

1) present time flows,
2) changes in precipitation,
3) changes in actual evapotranspiration,
4) changes in water storage of the basin; and,
5) representativeness of point data, particularly precipitation measurements, for the basin.

Monthly total precipitation data used in this study are listed in Table 1. Flow data used in this study are the monthly and annual natural flows (or so-called 'naturalized' (i.e., measured) flows adjusted for human influences) as provided by the Water Survey of Canada (WSC). A recent study by Ozga (1989) provides necessary adjustments to streamflow data for several streamflow-measurement stations. The relevant changes were incorporated into the hydrological data section of the data base of this study. Also, the WSC data base shows streamflow data in cubic metres per second. To input these data into the water-balance equation, they have to be converted into monthly or annual run-off in mm per month or mm per year, respectively. The evapotranspiration data used in calculation of the water balance are the results of the CRAE model described above.

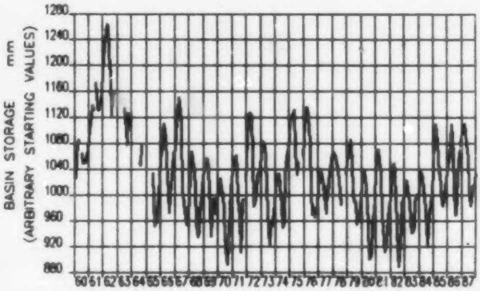

Figure 1. Example of the water-storage curve for the whole period of available data. McClintock River near Whitehorse (1,700 km² basin).

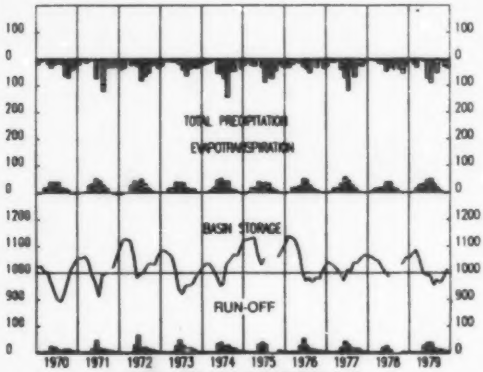

Figure 2. Example of the graphical analysis of all components of the balance equation. McClintock River near Whitehorse.

Specific water-storage information for the study area was not available, and also considered non-essential. Alternatively, it is assumed that short-term changes in water storage "average themselves out" over the long term.

As mentioned before, present-day knowledge indicates that the primary source of error in calculating water balance is usually a problem with precipitation measurement. Therefore, initially unmodified data were used for the water-balance calculation. This first step showed the (usually declining) trend in water storage. This trend was then iteratively reduced or eliminated by making precipitation adjustments. Figure 1 shows the example of the water-storage curve obtained for M'Clintock River near Whitehorse for the whole period of available data (1960 to 1987) after the precipitation data were adjusted by 40 percent. Figure 2 presents an example of the graphical analysis of all components of the water-balance equation for the same area for 1970 to 1979. In both cases graphical possibilities of the BSTOR (Basin STORage calculation) program were utilized (provided by Water Resources Branch, Environment Canada).

The summary results of the water-balance calculations are presented in Table 4 (for eleven study areas); it shows that if, for now, we accept the simplified theory that the precipitation is the only source of errors it has to be increased by 14 to 100 percent to obtain the water-storage curve with no trend. Usually, the further north the study area is located, the bigger the correction. However, two limitations apply: 1) As it is now, there is only one precipitation measurement station in every study area. Problems are possibly caused not only by a systematic underestimation in precipitation measurement, but also by the fact that some of the stations are not representative of their respective river basins. 2) It is quite probable that there are also problems with streamflow and evapotranspiration. A quick and simple rectification of the trend of water-storage curves indicates that underestimation of total precipitation is the most likely source of error.

Table 4. Water balance calculation - annual totals (mm·yr^{-1}).

Study Area	Precipitation (mm·yr^{-1})	Evapotranspiration (mm·yr^{-1})	Run-off (mm·yr^{-1})	Precipitation Adjustment (+%)
Yukon Territory				
Watson Lake	447.5	230.2	205.0	14
Whitehorse	371.7	184.6	179.0	40
Komakuk Beach	346.5	190.9	220.1	100
Shingle Point	425.8	211.8	221.6	50
Mackenzie River Basin				
Fort Smith	414.7	272.8	29.5	14
Norman Wells	434.9	192.8	303.2	54
Inuvik	293.1	186.1	81.3	30
North-Eastern Arctic				
Baker Lake	476.4	197.4	193.1	70
Coppermine	388.9	191.9	201.5	45
Cambridge Bay	261.5	151.5	77.6	100
Sachs Harbour	238.9	160.1	54.4	75

CHANGES IN PRECIPITATION AND EVAPOTRANSPIRATION

The GISS General Circulation Model results were used to calculate the precipitation and temperature shift due to climate change. (For a description of the methodology see Haas and Marta, 1988). Simulated temperature data were used together with modified relative-humidity and global solar-radiation normals for simulated runs of the CRAE and CRWE models. (Relative humidity can be calculated from the dry-bulb and dew-point temperature data - see Morton (1983a) and program HELHUMID in Haas and Marta (1988)). Again, the lack of data was an obstacle - complete sets of the necessary data were available for only five study areas out of fourteen. Simulated areal evapotranspiration results are summarized in Table 5. Simulated wet-surface evaporation results are listed in Table 6.

Simulated, 'post-climate-change' evapotranspiration data were used together with simulated average monthly precipitation data and average monthly historical run-off data for the initial, very preliminary calculations of the change in annual water storage. This, in turn, can be used for the approximate estimates of changes in run-off.

Table 5. Simulated 'post-climate-change' areal evapotranspiration.

Study Area	Potential Evapotranspiration ($\mathrm{mm \cdot yr^{-1}}$)	Areal Evapotranspiration ($\mathrm{mm \cdot yr^{-1}}$)
Whitehorse	689.9	288.0 (+56%)
Fort Smith	683.3	412.6 (+47%)
Norman Wells	595.3	346.4 (+74%)
Inuvik	437.9	303.5 (+68%)
Baker Lake	320.2	293.9 (+46%)

Table 6. Simulated 'post-climate-change' wet-surface evapotranspiration.

Study Area	Wet-Surface Evaporation	
	Pan-Size ($\mathrm{mm \cdot yr^{-1}}$)	Lake-Size ($\mathrm{mm \cdot yr^{-1}}$)
Whitehorse	728.6	543.6 (+13%)
Fort Smith	696.7	579.0 (+17%)
Norman Wells	607.4	498.3 (+24%)
Inuvik	464.2	401.8 (+28%)
Baker Lake	341.1	328.8 (+17%)

CONCLUSIONS

The overall goal of this paper has been to investigate the availability of data needed for the water-balance calculation, to calculate the water balance for selected areas of the Yukon and N.W.T., and to assess the possible impacts of several selected climate-change scenarios on precipitation and evapotranspitation and, as a consequence, on water balance and run-off.

The data base was designed to: 1) store climatological data needed for the evapotranspiration calculation; 2) store and organize hydrological (streamflow), meteorological (precipitation) and climatological (evapotranspiration) data; 3) include water-storage change data resulting from the water-balance calculation; 4) add the simulated post-climate-change data of temperature, relative humidity, evapotranspiration and precipitation based on the General Circulation Models' results; and finally, 5) to illustrate changes in run-off.

The data-base preparation has shown insufficient coverage of solar-radiation measurement (in particular for the Yukon) as well as a rather meagre precipitation measurement network. The scarcity of precipitation data was the reason why the water-balance calculation for the selected study areas was usually based on results from only one precipitation station (only one was available).

The water-balance calculations for the thirteen study areas (the area around Resolute, N.W.T., has an incomplete data base and the water balance cannot be calculated) represent the major contribution of this paper. They reveal discrepancies between precipitation and hydrometric data and add weight to the long existing suspicion that measurements of snowfall lead to an underestimation of its water content.

Estimates of evapotranspiration and wet-surface evaporation (which is of particular importance for industrial development applications) under 2 x CO_2 climate-change conditions used a combination of relevant GCM-based temperature forecasts and hypothesized alterations of historical values of humidity. (For detailed description of humidity alteration methods see Haas and Marta (1988), Section 6.2 Sensitivity of evaporation to change in relative humidity and insolation). In all study areas the simulated annual evapotranspiration and wet-surface evaporation exceeded historical data. If this proves true in the future, the economic and sociological consequences would be immense.

Two recommendations are directly related to the limitations of the paper:

The climatological data-measurement network in the Yukon and N.W.T. is insufficient. This is particularly true in the case of solar-radiation data. The precipitation-measurement network is very sparse as well and enables only approximate estimates. For improved measurements, an expansion of the measurement network is essential.

Post-climate-change testing scenarios are so far almost completely dependent on results obtained from general-circulation models. Alternative approaches should be tested as well - for example using inputs from different areas as the 'proxy' or 'simulated' data. At the present time, only a very preliminary assessment of the effect of climate change on water-management systems is possible.

Further recommendations are based on the results of this paper. The major recommendation is that:

It is imperative to clarify the current discrepancies, to separate the systematic errors in measurement from real trends in water storage, which might represent the "early warning", indicating changes in the water balance due to natural or man-made changes in climate. Every river basin evaluated in this study shows discrepancies in its water balance. The water storage seems to be declining and, to adjust for that, the precipitation component (most likely to be in error) has to be adjusted by 14 to 100%.

Last, but not least:

The scope of the study covered only fourteen areas (only eleven areas for the simulated data) and only several post-climate-change scenarios have been tested so far. Both of these shortcomings should be rectified. Also, the post-climate-change analysis of run-off has only begun; much more work has to be done.

ACKNOWLEDGEMENTS

The author would like to thank Fred Morton and Vlado Schilder for their advice. For calculating water balance the author used the BSTOR program, kindly made available by Shin-Young Shiau, Water Resources Branch, Environment Canada. The study was supported by the Northern Affairs Program of the Department of the Indian Affairs and Northern Development under contract number 89-0089. The views expressed in this paper are those of the author and are not necessarily endorsed by DIAND.

REFERENCES

ACRES CONSULTING SERVICES, 1982. Northwest Territories water resources study. Report No. PG465.00, Acres Consulting Services for Water Resources Division, Department of Indian Affairs and Northern Development, Ottawa, Ontario, 116 pp.

AMERICAN METEOROLOGICAL SOCIETY, 1990. Symposium on global change systems. Special sessions on climate variations and hydrology. Preprints, 5-9 February 1990, Annaheim, California, American Meteorological Society, 192 pp.

BERAN, M., 1986. The water resource impact of the future climatic change and variability. Summary of Working Paper 10, Institute of Hydrology, Wallingford, England, 30 pp.

CANADA, ENVIRONMENT CANADA, 1989. Climatological station cataloque: the North - Y.T. / N.W.T. Atmospheric Environment Service, Downsview, Ontario, 21 pp.

COHEN, S.J., 1988. Application of climate model output to impact studies: water resources. Symposium/Workshop Proceedings, The Impact of Climate Variability and Change on the Canadian Prairies, B.L. Magill and F. Geddes (Editors), 9-11 September 1987, Edmonton, Alberta, Alberta Climate Advisory Committee, Alberta Environment, Edmonton, Alberta, 63-89

FENG, G.Z., G.S. STRONG and W. NICHOLAICHUK, 1989. Comparison of Meyer and Morton evaporation techniques from open water surfaces. NHRI Contribution No.89010, Hydrology Division, National Hydrology Research Institute, Environment Canada, Saskatoon, Saskatchewan, February, 48 pp.

GLEICK, P.H., 1986. Methods of evaluating the regional hydrologic impacts of global climatic changes. Journal of Hydrology, 88(1-2), 97-116

HAAS, J. and T.J. MARTA, 1988. Assessing the effect of climate change on the operation of a water-supply reservoir. Water Planning and Management Branch, Inland Waters Directorate Environment Canada, Ottawa, Ontario, December, Vol.I - Report, 108 pp.; Vol.II - Appendices, 133 pp.

HENGEVELD, H.G. and R.B. STREET, 1986. Development of CO_2 climate change scenarios for Canadian regions. Unpublished report, Canadian Climate Centre, Atmospheric Environment Service, Downsview, Ontario, 10 pp.

KLEMEŠ, V., 1985. Sensitivity of water resource systems to climate variations. WMO Report No.WCP-98, World Meteorological Organization, Geneva, 17 pp. + 5 annexes

MARSH, P. and M.-K. WOO, 1977. The water balance of a small pond in the High Arctic. Arctic, 30(2), 109-117

MORTON, F.I., 1983a. Operational estimates of areal evapotranspiration and their significance to the science and practice of hydrology. Journal of Hydrology, 66(1-4), 1-76

MORTON, F.I., 1983b. Operational estimates of lake evaporation. Journal of Hydrology, 66(1-4), 77-100

MORTON, F.I., 1985. The complementary relationship areal evapotranspiration model: how it works. Proceedings, National Conference on Advances in Evapotranspiration, American Society of Agricultural Engineers, 377-384

OZGA, W.J., 1989. 1988-89 summary report for review of hydrometric survey data for selected gauging stations in the Northwest Territories. Report No.NWT-IWD-WRD-89-001, Ozga Engineering Services for Inland Waters Directorate, Western and Northern Region, Environment Canada, Yellowknife, N.W.T., 65 pp.

WOO, M.-K. and P. MARSH, 1978. Analysis of error in the determination of snow storage for small high arctic basins. Journal of Applied Meteorology, 17(10), 1537-1541

A BASIN WATER-STORAGE MODEL TO FORECAST COLUMBIA RIVER DISCHARGE

W. Tangborn

HyMet Company
2366 Eastlake Avenue East
Suite 435
Seattle, Washington 98102
U.S.A.

ABSTRACT

A new streamflow forecasting method is proposed using a simulation/forecasting model that requires only standard observations of precipitation and temperature. Forecasts are based solely on the water stored in the basin on the day of the forecast. Water storage is defined as the sum of the snowpack water content, soil moisture and ground water, and is simulated in 6-hour time increments on the basis of observed precipitation and temperature at selected weather stations in or near the Columbia basin. Using a split-sample test of error evaluation, the model was first calibrated for the 1940 to 1969 period to produce continuous daily water-storage values that gave the most accurate forecasts. Retrospective forecasts for a verification period (1970 to 1988) were then generated for each year and each season beginning on January 1 and ending June 1, for seasons ending on July 31, and compared with historic forecasts made by the Northwest River Forecast Center. The basin water-storage model showed a significant reduction in forecast error for all seasons, with an average decrease in the mean error of the six main forecast seasons of 12.3 to 7.9 percent. The April 1 to July 31 mean forecast error was reduced from 10.2 to 4.8 percent. In addition to a decreased error in seasonal forecasts, the proposed model provides unlimited forecast frequency, a negligible delay between a weather event and forecast, and extremely low-cost data collection and model application.

SETTING

The drainage area of the Columbia River above The Dalles, Oregon (237,000 square miles or 613,830 km^2) includes large parts of the states of Washington, Idaho and Oregon, and smaller fractions of Montana, British Columbia, Wyoming and Nevada (Figure 1). Mean annual run-off at The Dalles is 193,100 cfs (5,470 m^3·s^{-1}), which is 11.5 inches (292 mm) per year averaged over the drainage basin. Precipitation into the basin varies from 6 inches to 150 inches (150 to 3,800 mm); the annual average is 22.4 inches (569 mm). Total evaporation is approximately 12.9 inches (328 mm) per year.

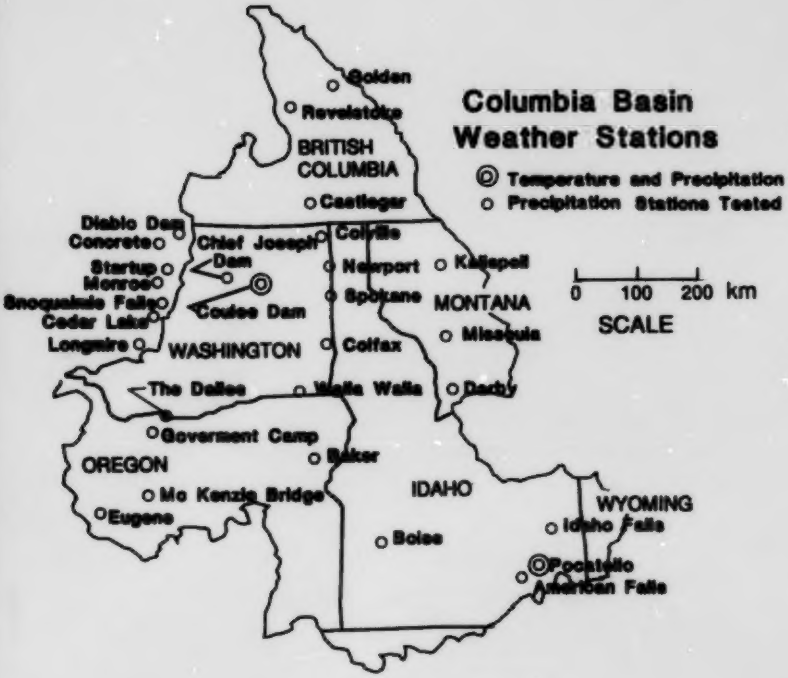
Columbia Basin
Weather Stations
Temperature and Precipitation
Precipitation Stations Tested
0 100 200 km
SCALE
Golden
Revelstoke
BRITISH COLUMBIA
Castlegar
Diablo Dam
Concrete
Chief Joseph Dam
Colville
Startup
Monroe
Snoqualmie Falls
Cedar Lake
Longmire
Coulee Dam
Newport
Kalispell
Spokane
MONTANA
Missoula
WASHINGTON
Colfax
The Dalles
Walla Walla
Darby
Goverment Camp
OREGON
Baker
Mc Kenzie Bridge
Eugene
IDAHO
Boise
WYOMING
Idaho Falls
Pocatello
American Falls

Figure 1. Columbia River Basin with weather stations tested for use in forecasting streamflow at The Dalles, Oregon.

MODEL DESIGN

There are three primary steps to adapting this model to a specific basin for real-time forecasts:

1. Selection of precipitation and temperature stations.

2. Calibration by simulating basin water-storage variables and forecasting seasonal streamflow for a long-term period (20 to 30 years).

3. Organizing the necessary files for updating the data base during the forecasting season.

Seasonal forecasts are based on the total water stored in the basin on the day the forecast is made. Basin storage includes the sum of the snowpack water content, soil moisture and ground-water storage. These and other hydrological variables are continuously calculated by the model in 6-hour time increments and stored as daily values in a temporary work file. Evaporation from the soil mantle and sublimation from snow are calculated on the basis of potential evapotranspiration (ET) (determined from a temperature algorithm), the amount of soil moisture available, and the snowcover area. Snowmelt caused by various energy sources, including rain-on-snow, is also continuously calculated by a temperature-driven algorithm. The basic design of this model has been given in earlier reports (Tangborn, 1980, 1987, 1988).

The catchment is divided into two elevation zones of equal area, separated by the Columbia basin's mean elevation of 5,080 feet (1,549 m). The lower zone has a mean elevation of 4,060 feet (1,238 m) and the upper zone a mean of 6,030 feet (1,838 m). All storage components and other variables are calculated separately for both zones, then combined to produce the seasonal run-off forecast.

SPLIT-SAMPLE TESTS

The reliability of a forecasting model depends entirely on the error that can be expected in future forecasting applications. One of the primary sources of forecast error is the meteorological data used to develop the snowpack and other water-storage variables. Approximately 30 precipitation stations were first tested to determine those most representative for this catchment. A split-sample procedure was used to identify those that were optimum for application in the forecasting model. Initially the 1950 to 1969 period was used for calibration to determine the regression coefficients, and the 1970 to 1986 period for verification. (The 1950 to 1969 regression coefficients are then used to calculate 1970 to 1986 run-off, Figure 2). After the optimum stations were found from the 1950 to 1969 sample, the records were extended to 1940 wherever possible and the calibration period revised to 1940 to 1963 and the verification period to 1964 to 1989.

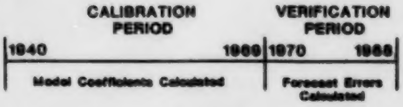

Figure 2. Split-sample periods used for calibration and verification of the HyMet model.

It is important to note that a split-sample test will produce substantially different results than a full-period test. Reliability in a real-time situation is greatly improved by a split-sample testing procedure. Because the error determination is completely independent of data used in calibrating the model, a precipitation station with poor quality data is readily detected and can be eliminated.

CAPABILITIES OF THE HYMET FORECASTING MODEL

As applied to Columbia River forecasting, the most significant capabilities of this model are:

1. Beginning on about December 1, forecasts can be made at any time and for any season of up to ten months in length. Short-term (1 to 30 days) forecasts are particularly accurate during the snowmelt period.

2. The only input data required are daily precipitation observations at six stations, maximum and minimum temperature at two stations and the unregulated daily discharge of the Columbia River at The Dalles.

3. Forecasts are based on the calculated volume of stored water in the catchment on the day the forecast is made. Total storage consists of the snowpack, soil moisture and ground-water storage. Daily information on the current status of these and other variables can be obtained throughout the year.

4. Forecast accuracy is improved by the automatic application of a pre-forecast "test-season" that estimates the error of the main forecast.

5. Based on retrospective, split-sample forecasts for the 1970 to 1989 period, forecast errors are significantly less than the current operational forecasting method. The average reduction is about 4.4 percent in the mean error for the six main forecast seasons.

BASIN PRECIPITATION

Knowing the amount of moisture that enters the basin as precipitation is one of the most important aspects of forecasting. The input of precipitation to this catchment is estimated by daily observations at six stations in or near the basin. The assumption is made that the weighted daily precipitation observed at these gauges is a simple index of the total basin's daily precipitation:

(basin precipitation = coefficient x gauge precipitation).

The precipitation station that produced the lowest forecast error in the initial set of stations was Longmire, Washington, located near Mount Rainier and just outside the catchment's western boundary. Precipitation recorded at Longmire was then weighted in 1 percent increments with each of the others in the 30-station sample to determine the optimum mixture to produce the minimum error. A simulated precipitation record was then constructed from the weighted Longmire and the optimum station's observations (which turned out to be Eugene, Oregon). The simulated station was then tested with each of the remaining stations to determine the one next most optimum. This procedure was repeated until the reduction in forecast error became insignificant (the Root Mean Square Error [RMSE] changed less than 0.01 percent). Only six stations were found to be of value in reducing forecast error when weighted with Longmire. However, it should be noted that many other possible precipitation stations in or near the Columbia basin have not been tested and it is likely others will be found that will reduce the forecast error even further. Results of the weighting procedure for the highest four stations are shown in Figures 3 to 5. All six stations and the relative weight given to each are listed in Table 1 (see Figure 6 for locations).

It may seem remarkable that precipitation stations such as Longmire or Eugene predict Columbia basin precipitation more accurately than most of the stations located within the catchment above The Dalles. That this is the case probably reflects more on the quality of the observational record of these stations than on their locations. It should be noted that Longmire precipitation has also been found to be optimum for use in the HyMet model to forecast seasonal run-off for both the Cowlitz and Nisqually Rivers for Tacoma City Light (Tangborn and Brookshier, 1985).

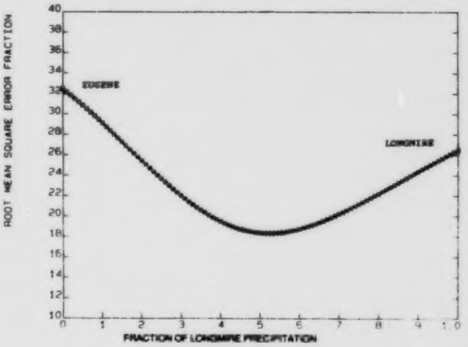

Figure 3. Weighting of Longmire, Washington versus Eugene, Oregon precipitation to determine the optimum mix of daily observations to forecast Columbia River streamflow. The root-mean-square-error fraction is calculated from the forecast error for seven forecast seasons beginning on January 1. Weighting is in 0.01 increments. The split-sample calibration period is 1940 to 1968 and the verification period is 1970 to 1988.

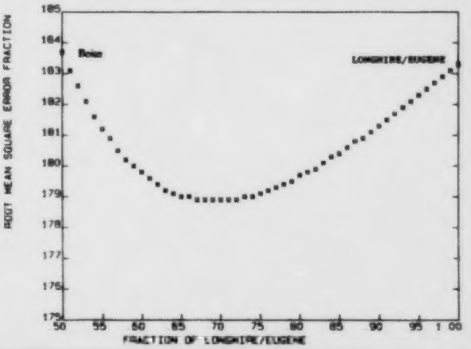

Figure 4. Weighting of combined Longmire/Eugene versus Boise, Idaho precipitation to determine the optimum mix of daily observations to forecast Columbia River streamflow. Note the change in scale of the root-mean-square-error.

The most significant reduction in error occurs from a nearly even mix of Longmire and Eugene precipitation. There is a reduction in the RMSE of 0.258 to 0.184, or a decrease of about 29 percent. The question needs to be asked as to why the combination of just these two stations provides such an extraordinarily accurate representation of precipitation over the entire Columbia River basin, while either one individually does not. Obviously both stations must accurately sample precipitation rates and intensity of Pacific winter storms that deposit moisture into much of the Columbia basin.

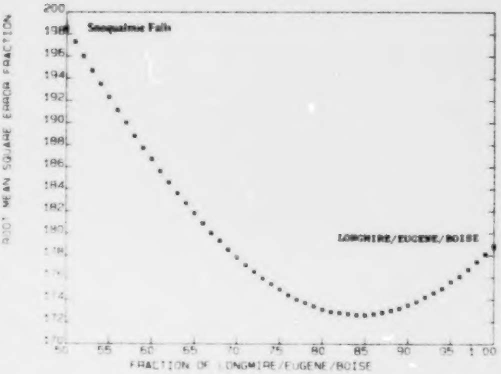

Figure 5. Weighting of combined Longmire/Eugene/Boise versus Snoqualmie Falls precipitation to determine the optimum mix of daily observations to forecast Columbia River streamflow. Note the change in scale of the root-mean-square-error.

Table 1. Precipitation stations used in final model.

Station	Province or State	Index No.	Weight %	Annual Precipitation *(inches)* *(mm)*	Elevation *(feet)* *(m)*	RMSE (1)	RMSE (2)
Longmire	WA	6894	27	84.4 2144	2762 842	0.258	--
Eugene	OR	2709	25	47.5 1207	364 111	0.307	0.1839
Boise	ID	1022	24	12.2 310	2838 865	0.358	0.1789
Snoqualmie Falls	WA	7773	14	60.8 1544	440 134	0.263	0.1741
Revelstoke	BC	6750	7	37.5 953	1494 455	0.419	0.1726
Pocatello	ID	7211	4	11.7 297	4454 1358	0.496	0.1725

(1) Root mean square error average for seven forecasts (January 1 to July 1, for seasons ending July 31), made with each individual precipitation station.

(2) Root mean square error average for seven forecasts made with weighted precipitation (this station plus station(s) above).

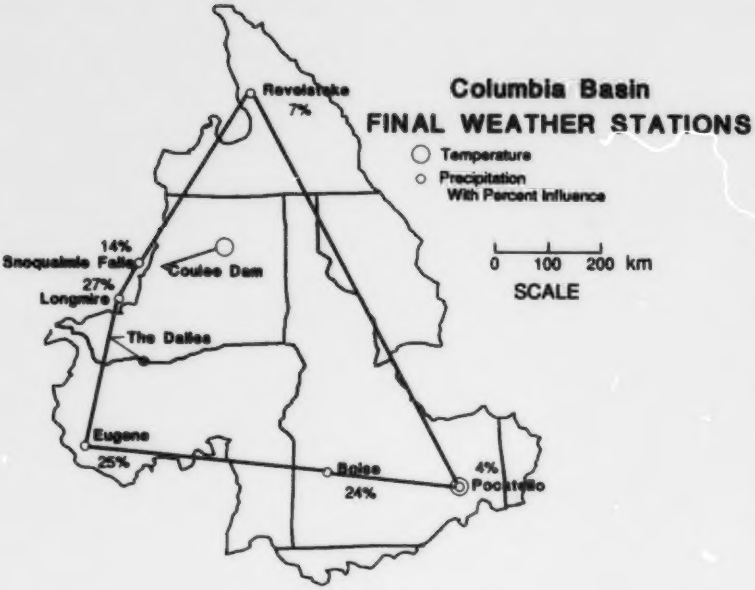
Columbia Basin
FINAL WEATHER STATIONS
Temperature
Precipitation With Percent Influence
0 100 200 km
SCALE
Revelstoke
7%
14%
Snoqualmie Falls
Coulee Dam
27%
Longmire
The Dalles
Eugene
25%
Boise
24%
4%
Pocatello

Figure 6. Final precipitation selection to represent Columbia Basin total precipitation. Relative weights for each station are shown adjacent to station as percentages. The two temperature stations used to determine the basin temperature distribution are Grand Coulee Dam (elevation = 518 m) and Pocatello (1,358 m).

Observing the path of the major storms over the Pacific Northwest as demonstrated by a time-lapse display of daily streamflow reveals a consistent pattern in their movement (Tangborn, 1989). The larger, more intense storms in particular tend to enter the Columbia basin around the southern end of the Olympic Mountains, crossing a Longmire-Eugene line, then moving in a SW-NE direction into British Columbia. It seems probable that an accurate sampling of the precipitation intensity in the early stages of the more intense storms (after they strike land) would predict precipitation rates throughout the Columbia Basin.

These findings are even more perplexing because over half the run-off at The Dalles is derived from the drainage area that is within British Columbia, but a precipitation weight of only 7 percent is assigned to one station in Canada (Revelstoke).

BASIN TEMPERATURE

Air temperature is also a critical variable in hydrological simulation. Combined with precipitation, temperatures are initially applied to determine snow accumulation at the two elevation zones within the catchment. In addition, temperature is applied to calculate snowmelt, evaporation, and sublimation. As temperature is strongly dependent on elevation, it is necessary to determine the 6-hour mean temperature as a function of elevation.

Daily maximum and minimum temperatures at two stations are used to estimate 6-hour temperature means throughout the basin by applying an assumed sinusoidal daily temperature pattern. The lapse rate is calculated on the basis of the 6-hour temperature determinations made at each station and used to calculate temperatures in each elevation zone.

Out of the six stations that were tested two were selected (Table 2):

Table 2. Temperature Stations.

Station	State	ID	Elevation	Temperature °F/°C		
				Annual	Oct - Mar	Apr - Sep
Pocatello	ID	7211	4454	°F 46.7 °C 8.2	33.4 0.8	60.0 15.5
Coulee Dam	WA	1767	1700	°F 50.0 °C 10.0	36.6 2.6	63.4 17.4

These two stations are separated by a horizontal distance of 465 miles (748 km) and vertically by 2,754 feet (839 m). Although Pocatello's elevation is considerably greater there is only a 3°F (1.7°C) decrease in the mean annual temperature at this higher station (in part likely due to the latitude difference). Figure 7 shows the mean daily temperature for these two stations.

BASIN WATER STORAGE

The total amount of transient water stored in the basin on a particular day is often the most important factor in determining subsequent run-off. The more accurately storage is known, the more accurate is the forecast. The other influential factor is the weather (mainly precipitation and temperature) that occurs during the forecast season. However, except for periods of 3 to 5 days or less, these meteorological variables cannot be forecast, leaving basin water storage as the most critical factor that can be calculated. Transient water is defined as any stored moisture that varies from day-to-day and is influential in control-ling streamflow within the basin.

The three natural reservoirs found to be the most significant in the Columbia Basin water balance are the snowpack, soil moisture and ground water. It should be noted that soil moisture does not contribute to streamflow (except for a negligible amount of seepage to the ground-water system), but still is influential because soil-moisture requirements must be satisfied before run-off can occur. Each forecast is based on the sum of these three equally weighted components. Daily variations in total storage for two divergent years (1974 and 1977) plus the 1960 to 1989 mean as calculated by the calibrated model are shown in Figure 8, and the separate components (snowpack, soil moisture and ground water) for one year (1989) in Figure 9. Figure 10 demonstrates the average relative contribution of each component to the total storage.

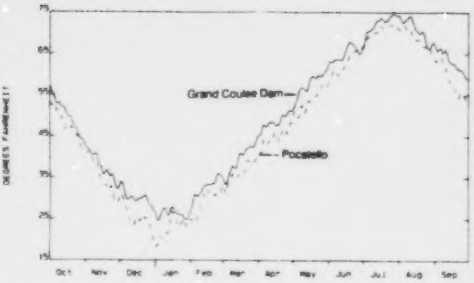

Figure 7. Mean daily temperature throughout the water year (1940 to 1988 average) for Grand Coulee Dam and Pocatello.

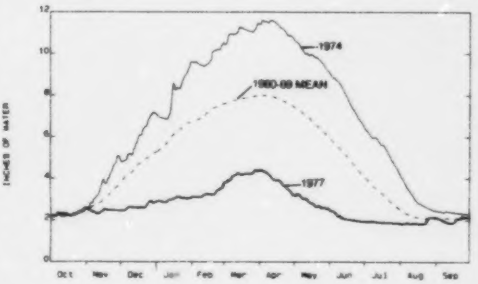

Figure 8. Total Columbia Basin water storage as calculated daily by the model for two diverse years and the 1960 to 1989 mean.

Forecasts are based on the total water stored as snow water content, soil moisture and ground water in the catchment on the day the forecast is made.

$$[1] \qquad R(s) = A(St) + B$$

Where R is the forecast run-off for the season (s), e.g., April 1 to July 31; St is the total water storage on the forecast day, e.g., April 1; and, A,B are linear regression coefficients determined by fitting observed run-off with calculated storage for a period of 20 to 30 years.

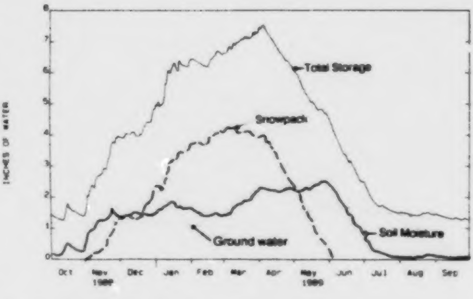

Figure 9. Average (1940 to 1989) daily water storage in the snowpack, soil moisture and ground water averaged over the Columbia River drainage basin.

APPLICATION OF A TEST SEASON

The error of the main season forecast can be reduced by more than 50 percent through the application of a pre-forecast test season, which is a short-term season just prior to the main forecast season. A test-season forecast is made automatically within the model and the forecast error determined before the main season forecast is generated. The test-season error is often an indicator of the error of the main season forecast (likely due to an inaccurate water-storage determination), therefore it can be used to reduce the main season error. In operational forecasting, the length of the test-season is determined by trying from 1 to 20 day seasons for the calibration period. The length that is found to produce the greatest error reduction is then used in the current-year forecast. A detailed explanation for the test-season is given in an earlier report (Tangborn, 1977). A test-season provides the greatest error reduction for short-term forecasts and for seasonal forecasts after about March 1.

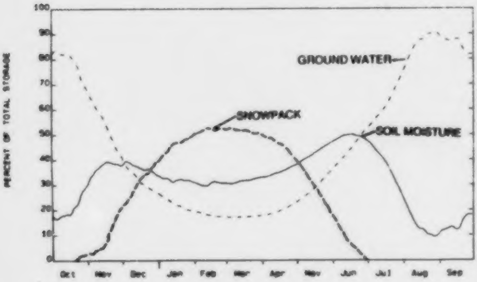

Figure 10. The relative daily mean contribution of each of the three main storage components to total Columbia Basin water storage.

CALIBRATION

An automatic calibration program was used to determine the optimum model coefficients to simulate the three water-storage components. There are 26 calibration parameters for each elevation zone that are optimized individually in the automated program by a trial and error process. Each iteration was repeated until reduction in the RMSE reached a preset minimum, then the next parameter was optimized. The process was repeated continuously in a predetermined pattern of parameter sequences.

Forecast seasons tested were from January 1 to July 1 (January 1 to July 31, January 2 to July 31 ... July 1 to July 31, or 182 seasons per year). Therefore, 5,460 seasonal forecasts varying in length from 212 to 31 days (for a 30-year calibration period (1940 to 1969)), were made for each iteration. The RMSE used for optimization is the average mean error of these 5,460 forecasts. Although the 182 seasons are not completely independent from each other, it is felt that the sample is sufficiently large and enough independence exists between seasons to provide a statistically valid method of calibration. Also, as a separate period of years is used for calibration from that for verification, the meteorological data used to simulate water storage are completely different than the data used to calculate forecast errors.

Approximately 2,000 hours of computer time have been used thus far in calibrating this model. At 15 minutes per run (one full set of forecasts), this translates to about 8,000 iterations and 45 million individual forecasts.

RESULTS

Comparisons of forecasts made with the Northwest River Forecast Center model for the 1970 to 1988 period are given in Figure 11 and Table 3. The HyMet forecasts are based on a split-sample (the model was first calibrated for the 1950 to 1969 period), thus the results are a fair appraisal of how well the HyMet model will perform in the future for forecasting at The Dalles site. Table 3 shows the mean percent error and the explained variance fraction for each of the main seasons for a 19-year period (1970 to 1988).

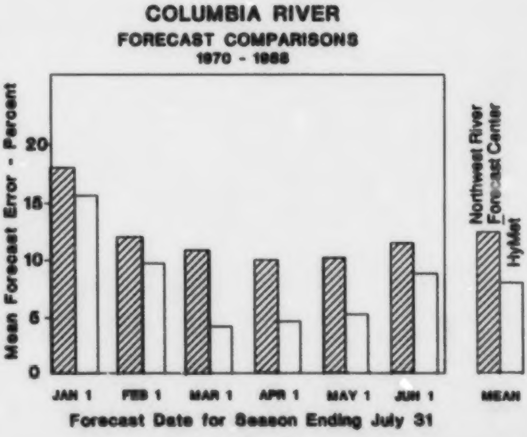

Figure 11. Comparison of forecast accuracy for the 1970 to 1988 period between the Northwest River Forecast Center forecasts (hatched) and the HyMet model.

Table 3. Summary of error comparison.

Season	NWRFC		HyMet	
	Error %	R-Squared	Error %	R-Squared
January - July	18.6	0.45	15.5	0.64
February - July	12.3	0.76	9.8	0.86
March - July	11.1	0.80	4.0	0.98
April - July	10.2	0.83	4.8	0.96
May - July	10.4	0.83	5.1	0.96
June - July	11.0	0.84	8.3	0.92

NWRFC is the Northwest River Forecast Center, located in Portland, Oregon (Columbia Basin Water Management Report, 1988).

HyMet forecasts are retrospective and based on a split-sample with a calibration period of 1940 to 1969.

REFERENCES

COLUMBIA WATER MANAGEMENT GROUP, 1988. Columbia River water management report, 1988. Columbia Water Management Group, Portland, Oregon, 29 pp.

TANGBORN, W.V., 1977. Application of a new hydrometeorological streamflow prediction model. Proceedings, 45th Annual Meeting, Western Snow Conference, 18-21 April 1977, Albuquerque, New Mexico, 35-43

TANGBORN, W.V., 1980. A model to forecast short-term snowmelt runoff using synoptic observations of streamflow, temperature, and precipitation. Water Resources Research, 16(4), 778-786

TANGBORN, W.V., 1987. Forecasting seasonal runoff of the Baker River, North Cascades, Washington. Proceedings, Workshop on Hydropower in Cold Climates, T. Carstens (Editor), 30 June - 2 July 1987, Trondheim, Norway, various pagings

TANGBORN, W.V., 1988. Calculation of snowpack water content and snowcover area. Proceedings, Workshop on Snow Hydrology, 23-26 November 1988, Manali, H.P., India, Central Water Commission and Himal Pradesh State Electricity Board, 1-19

TANGBORN, W., 1989. A time-lapse analysis of drought in North America, 1930-88. Oceans '89: an International Conference Addressing Methods for Understanding the Global Ocean, 18-22 September 1989, Seattle, Washington, Vol.1, IEEE Publication No.89CH2780-5, 236-241

TANGBORN, W.V. and N. BROOKSHIER, 1985. Forecasting seasonal runoff for hydroelectric operations using simulated water storage. In - A Critical Assessment of Forecasting in Water Quality Goals in Western Water Resources Management, 11-13 June 1984, Seattle, Washington, American Water Resources Association, 127-132

PRELIMINARY FINDINGS FROM EXPERIMENTS ON FRAZIL AND ANCHOR ICE IN A CIRCULAR FLUME*

G. Tsang[1] and B. Trapp[2]

[1]National Hydrology Research Institute
11 Innovation Boulevard
Saskatoon, Saskatchewan
S7K 3H5 CANADA

[2]National Water Research Institute
P.O. Box 5050
Burlington, Ontario
L7R 4A6 CANADA

ABSTRACT

Mathematical and physical reasoning show that frazil and anchor ice can be best studied in the laboratory from a Lagrangian frame of reference. This can be realized by conducting experiments in a circular flume with a rotating bottom. Promising quasi-quantitative data on the growth, evolution and distribution of anchor and frazil ice were obtained from preliminary experiments conducted in such an apparatus. Centrifugal force was found to be a distorting factor in frazil distribution and should be quantified in the future.

INTRODUCTION

Frazil and anchor ice form in turbulent waters. Conceptually, the cooling of water and the formation of frazil and anchor ice are shown in Figure 1 and the distribution of frazil and anchor ice in the downstream direction are shown in Figure 2. Laboratory and field measurements on the formation, evolution and distribution of frazil and anchor ice, however, are meagre.

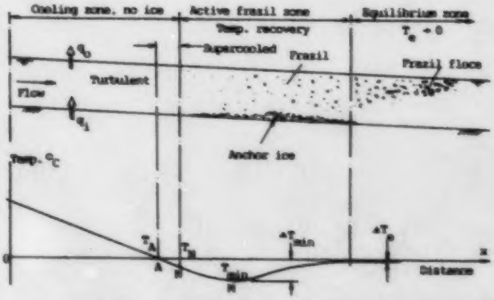
Cooling zone, no ice
Active frazil zone
Equilibrium zone
Temp. recovery
$T_e = 0$
Supercooled
Frazil
Frazil floes
q_b
Turbulent
Flow
q_i
Anchor ice
Temp. °C
T_A
T_N
ΔT_{min}
ΔT_e
x
0
A
N
T_{min}
M
Distance

Figure 1. Cooling of water and forming of ice in river (see List of Symbols for definitions).

---

*National Hydrology Research Institute Contribution Series Number CS-90011.

Tsang (1988) is probably the only field measurement of frazil distribution in the literature. Laboratory investigation of these two forms of ice was the main objective of this study. For further background information on frazil and anchor ice, readers may refer to Osterkamp (1978), Martin (1981), Tsang (1982) and Forest *et al* (1990). It should be mentioned that the distribution curves shown in Figures 2 and 3 are time-averaged curves. Because of flocculation of frazil, the concentration of frazil at a point in space is not constant, but a function of the thickness of the floc passing it.

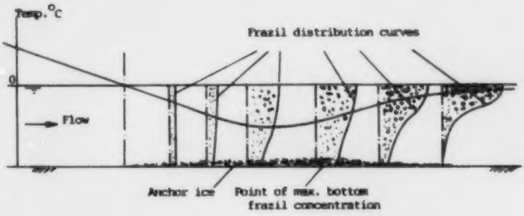
Temp.°c
Frazil distribution curves
0
Flow
Anchor ice
Point of max. bottom frazil concentration

Figure 2. Distribution of frazil at different locations.

OBJECTIVES

The general physical processes of frazil and anchor-ice formation, evolution and distribution are conceptually known and are generally supported by observations. However, to place the understanding on a rigorous basis, quantitative relationships governing these processes have to be established. In the laboratory investigation reported here, and still in progress, the following were studied:

1. Photographs of the evolution and flocculation of frazil under different hydrothermal conditions.

2. Distribution of frazil as a function of space and time under different hydrothermal conditions.

3. Photographs of the formation and growth of anchor ice.

4. Effect of frazil and anchor ice on flow resistance.

These investigations were conducted under controlled conditions including:

1. the heat-loss flux at the water surface;

2. the depth and velocity of the flow; and,

3. the roughness of the bottom.

It was hoped that from the data obtained, the desired quantitative relationships could be established and further studies be developed.

METHODOLOGY

The evolution, properties, behaviour and effects of frazil and anchor ice can be studied in either an Eulerian or a Lagrangian frame of reference. With the Eulerian approach, the reference coordinate is fixed in space and the time derivative of a parameter (p) is given by:

[1] $$Dp/Dt = u(\partial p/\partial x) + \partial p/\partial t$$

for a one-dimensional flow, where u is the flow velocity in the x direction. According to Equation 1, to study p, observations must be made at many points along the stream to evaluate $\partial p/\partial x$ and at each, time-series observations must be made for evaluating $\partial p/\partial t$. In addition, the flow velocity, which generally is a function of both location and time, must also be measured. This means that an investigation would be expensive and demanding. Even for the special case shown in Figures 1 and 2, in which the environmental and hydraulic parameters remain constant so that all the thermal and ice parameters at a point, except the thickness of anchor ice, become time invariants, Equation 1 will still retain the following form:

[2] $$Dp/Dt = u(\partial p/\partial x)$$

To evaluate Dp/Dt, multi-point measurements of p and u are needed. Such an undertaking would be laborious and costly. Furthermore, a constant environment and constant flow conditions are difficult to maintain, even in a laboratory. The overall conclusion was that the Eulerian approach is not appropriate for the present investigation.

With the Lagrangian approach, the coordinate is fixed to the observer. If the observer moves with the same parcel of water downstream, then the time derivative of p for the parcel of water will be given by:

[3] $$Dp/Dt = \partial p/\partial t$$

Equation 3 shows that only the time-series measurement of p from a floating station is needed to evaluate Dp/Dt. This, of course, is a much easier task. With the Lagrangian approach, the maintenance of a constant environment and hydraulic conditions is not required. To evaluate the hydrothermal effects, one only needs to record the hydrothermal parameters.

This can be realized by making frazil and anchor-ice observations from a drift boat or raft. Such an approach has been used by Ontario Hydro (Arden and Wigle, 1972) in studying the formation of frazil floes in the upper Niagara River. In the laboratory, however, a parallel methodology is difficult to realize because it requires a long flume and a large cold room. Both are expensive to build and operate. A better way is required so that the study can be done in a commonly available cold room.

Although it is preferable to study frazil and anchor ice in a straight channel, the inclusion of bends in the channel may be acceptable if the centrifugal effect in the bends can be tolerated or quantified. Furthermore, if the long channel is laid out in a helical form, then the water will be flowing perpetually in a bend and the space requirement will be substantially reduced. In this channel, water will flow under the action of gravity. If the flow in the helical channel can be sustained without the action of gravity, then the helical channel can be compressed into a ring. This means that the investigation of frazil and anchor ice can be conducted in a circular flume. The thermal and ice conditions of the water in the flume will be equivalent to those of a parcel of water travelling down the long helical flume.

Flow in a circular flume can be induced by moving the bottom (see Figure 3-a). When the drag on the moving bed is counter-balanced by the drag on the two side walls, an equilibrium flow state will be established. The vertical and horizontal velocity distributions of the equilibrium flow relative to a coordinate fixed to the ground are shown in Figures 3-a and 3-b. Relative to a coordinate fixed to the rotating bottom, the vertical and horizontal velocity distributions are shown in Figures 3-c and 3-d. They are obtained by subtracting the absolute velocity of the flow (Figures 3-a and 3-b) from the linear velocity of the rotating bed. It is the velocity relative to the flume bed that was used in this investigation. It can be seen from Figure 3-d that unwanted boundary layers are introduced at the two side walls. The simulated flow, therefore, is confined to the region beyond them. The presence of these two boundary layers and the centrifugal effects are taken into consideration when interpreting the experimental results.

Hence, it was decided to study the frazil and anchor-ice problems

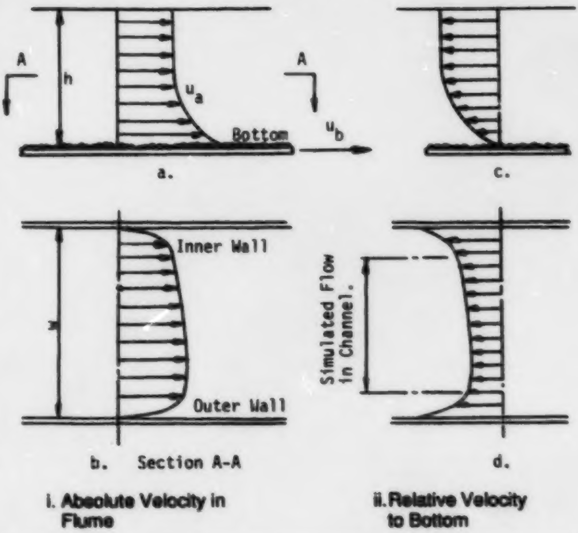

i. Absolute Velocity in Flume

ii. Relative Velocity to Bottom

Figure 3. Velocity distribution in flume with rotating bed.

using the Lagrangian approach in a circular flume with a rotating bed.

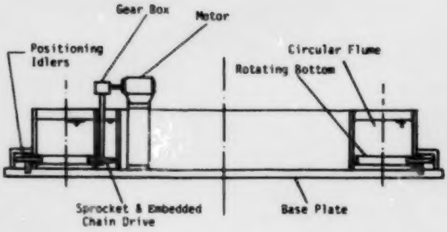

Figure 4. Configuration of flume with rotating bottom.

EXPERIMENTAL SET-UP

Figure 4 shows the general form of the circular flume. It was constructed on a base plate. The inside diameter of the outer wall was 115.00 cm (45¼") and the outside diameter of the inner wall was 84.38 cm (33¼"), giving a flume width of 15.31 cm (6"). The above dimensions were derived to make better use of materials rather than for any particular scientific reason. The base plate and the side walls were made of acrylic sheets. A 1.59 cm (5/8") thick annular ring of WHMW plastic (trade name, similar, but cheaper and inferior to Teflon) was placed inside the flume to serve as the rotating bottom. To drive the bottom, a chain was embedded in a groove cut to the inside rim of the annular ring. A sprocket driven by a variable-speed motor engaged the chain and caused the ring to rotate. The position of the ring was confined by four idler wheels housed in water-tight casings. The drive shaft of the sprocket and the sprocket itself were housed in a water-tight well. The water film between the ring and the base plate served as a lubricant. Provisions were made for securing a lining to the top of the ring. The linings were made of 0.64 cm (¼") PVC (poly-vinyl chloride) sheets in a shallow trough form. The height of the trough sides was 0.64 cm (¼"). Sedi-ment particles of chosen sizes could be glued to the bottom of the lining to provide the desired bottom roughnesses. Figure 5 shows the flume after its fabrication. The cubic steel frame at the back is the stand to which the flume was bolted. The flume and the stand were placed in a heated box in the cold room so only the water surface was exposed to the cold air and ice would not form on the side walls.

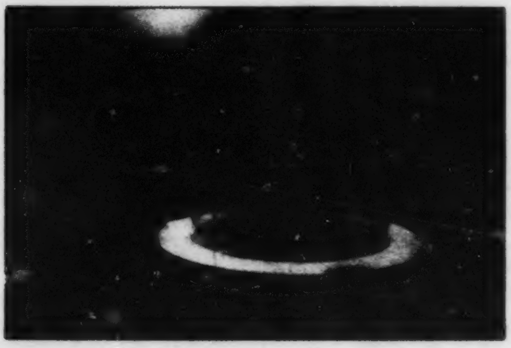

Figure 5. Photograph of flume after completion.

A frazil instrument based on Tsang's (1985) patented design was constructed to measure the concentration of frazil. The instrument consists of three sensor probes and a reference probe (Tsang, 1989). Because ice is practically non-conductive, a comparison of the electrical resistance of a sample of frazil-laden water with an ice-free water sample permits evaluation of the frazil content. Although the instrument works, it has yet to be calibrated.

Cross-polarized lighting was used when photographing the formation and evolution of frazil and anchor ice in the flume. The light source was placed in the centre of the flume. The first polarizing sheet was attached to the outside of the inner wall and the second polarizing sheet to the lens of the camera. By adjusting the orientation of the latter sheet, the best camera image could be obtained. For the preliminary study reported here, a video camera was used and photographs were made from still images on a television monitor.

The power input to the motor driving the bottom ring was to be measured to show the effect of frazil and anchor ice on flow resistance. The power to the motor was controlled by a regulator which converted the AC power input into DC output of constant current but variable voltage. Attempts were made to measure the DC voltage and current independently; the product giving the power input to the system. Using the power input difference to the system for the same flow, but under ice-free and ice-present conditions, it was hoped that the resistance effect of frazil and anchor ice on the flow could be isolated. Although such an approach appeared plausible, the preliminary findings showed that the crude nature of the power supply and mechanical design would not permit such refined measurements. The experimental result would likely lead to qualitative conclusions at best.

PRELIMINARY FINDINGS

During the first year and a half of the study major efforts were concentrated on the design and construction of the equipment and instrument, setting up the apparatus, and mechanical and electronic trouble-shooting. However, some preliminary experiments were conducted to test the feasibility of the general approach, to obtain baseline information under ice-free conditions, and to establish procedures for later experiments. The findings are necessarily quasi-quantitative. They serve to guide the next stage of the study rather than to provide a data set for analysis.

Ice-Free Velocity Distribution

The velocity distribution in the flume under ice-free conditions measured with a Nova current meter is given in Figure 6; the velocity was relative to the rotating flume bed. Four-mm pebbles were used for the bottom roughness of the bed. The equivalent Nikuradse's sand grain roughness was determined hydraulically in a long flume to be 16.8 mm. From the velocity distribution it can be seen that if the boundary layers at the two side walls are excluded, a pseudo one-dimensional longitudinal flow might be assumed. The different velocities across the flume were caused by different rotating speeds of the flume bottom ring due to different radial distances from the centre of rotation.

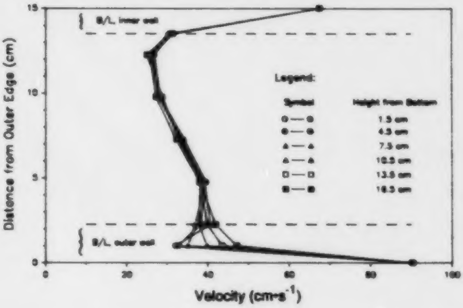

Figure 6. Relative velocity distribution in flume.

Formation of Frazil and Anchor Ice

Figure 7 shows time-series photographs of the flume. Frame "a" shows the flume before the formation of ice when the bottom was not moving (at 2 min 0.5 s); the rough pebble bottom can be seen. The dark line at the bottom serves as the reference datum. For this particular experiment, the flume was left overnight to be cooled under stationary conditions. There was a temperature gradient in the flume and the temperature of -1.471°C, sensed by the thermometer, was colder than the mean temperature of the water. When the bottom began to rotate, the temperature of the mixed water was -1.389°C, as shown in "b". At this time, the water was seeded with ice particles scraped from a slab of ice to produce frazil. Because of wobbling of the rotating bottom, the thickness of the light bottom in "b" appears to be thinner than that in "a". In "c", the formation of anchor ice by frazil crystals adhering to the bottom can be seen. The ice crystals adhere to the bottom by their edges and not their broad sides. This confirms that the "activeness" of frazil crystals occurs at the growing edges (Tsang, 1982). Some frazil crystals can be seen in the flow, but they are out of focus. In this experiment, the bottom rotated from left-to-right so that the flow of water relative to the bottom was from right-to-left, although in Figure 7, the water flowed from left-to-right, though at a slower velocity than that of the bottom. The formation of anchor ice on the bottom was not uniform, photographs "d" and "e" show a lump of anchor ice coming into view. Further adhesion of frazil crystals to the top of the anchor-ice lump can also be seen in "e". More frazil is seen in photographs "d" and "e". During this early stage of frazil production, the frazil was largely in the form of individual crystals and small clusters. The growth of anchor ice, however, was remarkable. The formation of anchor ice, largely during the early period of frazil production, as depicted in Figure 2, was confirmed. The flocculation of frazil can be seen in "f", as the supercooling of the water was quickly reduced to - 0.912°C. Comparing "f", "c" and "b", the thickening of the bottom layer is unmistakable and can be quantified. More frazil-crystal adhesion at the top of the anchor ice in "f" than in "c" can also be seen. Photograph "g" shows the end of the experiment. The flume bottom is now covered by a thick layer of anchor ice. The suspended frazil has turned into thick slush floating at the top. Comparing "g" and "a", one sees the differences in bed

Figure 7. Sequential photographs showing formation of anchor ice and flocculation of frazil.

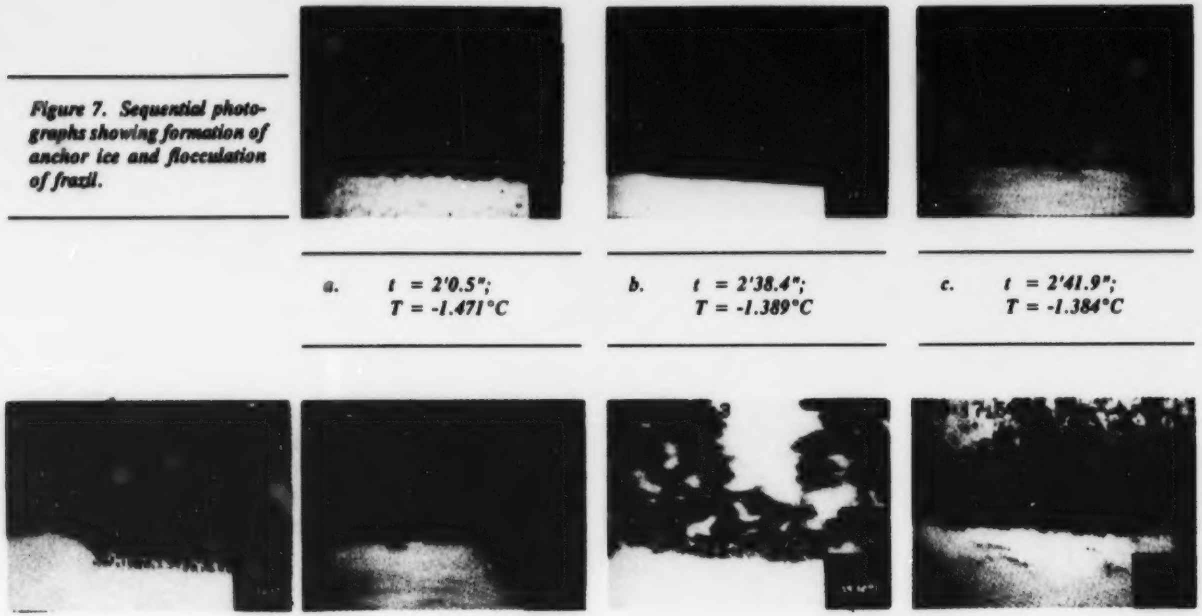

a. $t = 2'0.5''$; $T = -1.471°C$

b. $t = 2'38.4''$; $T = -1.389°C$

c. $t = 2'41.9''$; $T = -1.384°C$

d. $t = 2'44.2''$; $T = -1.365°C$

e. $t = 2'44.3''$; $T = -1.363°C$

f. $t = 2'48.3''$; $T = -0.912°C$

g. $t = 17'54.5''$; $T = 0.00°C$; End.

conditions caused by frazil- and anchor-ice formation. In actual situations, the initial supercooling would likely be the order of only a few hundredths of a degree and it would take much longer to produce the conditions shown in Figure 7. To improve the quality of the photographs in Figure 7 polarized flash light will be used in future experiments.

Concentration of Frazil

Figure 8 shows the three sensor probes of the frazil instrument immersed in the circular flume; the reference probe immersed in a stilling well is also visible at the back. The stilling well prevents intrusion of frazil into the reference probe. In the flume, the water flows counter-clockwise; the probes were numbered 1, 2 and 3 in streamwise order. For this experiment, the three probes were placed along the centre-line of the flume. The depth of immersion, however, was increased by 2.5 cm in the 2, 1, 3 order with Probe 2 just below the water surface. Pebble bottom roughness was used and the bottom was rotated at 15 rpm. In the sensor probes, cylindrical water samples of 2.22 cm diameter by 1.9 cm height (⅞" dia. x ¾" height) were measured. The water was first cooled to about -1°C without moving the bottom. Then the bottom was moved and the supercooled water seeded with ice particles.

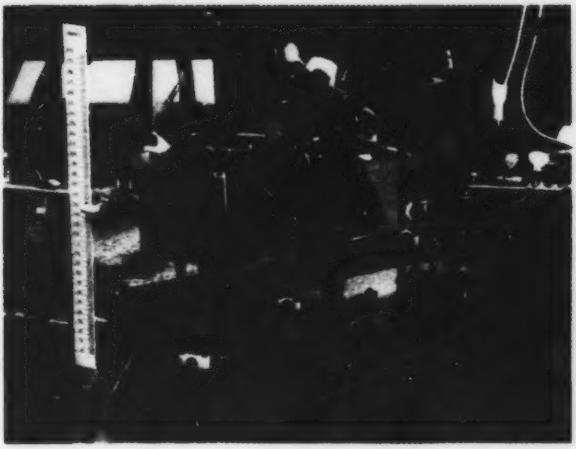

Figure 8. Frazil measuring probes in flume.

Figure 9 shows the concentration (uncalibrated) recordings measured by the three probes for the initial period immediately after seeding. From these, one sees that the concentration of frazil decreased with depth. The highest concentration was at Probe 2 and the least at Probe 3. From such signatures, the average concentration at given depths, and the size and frequency distribution of the frazil flocs can be obtained easily. Towards the end of the period, frazil

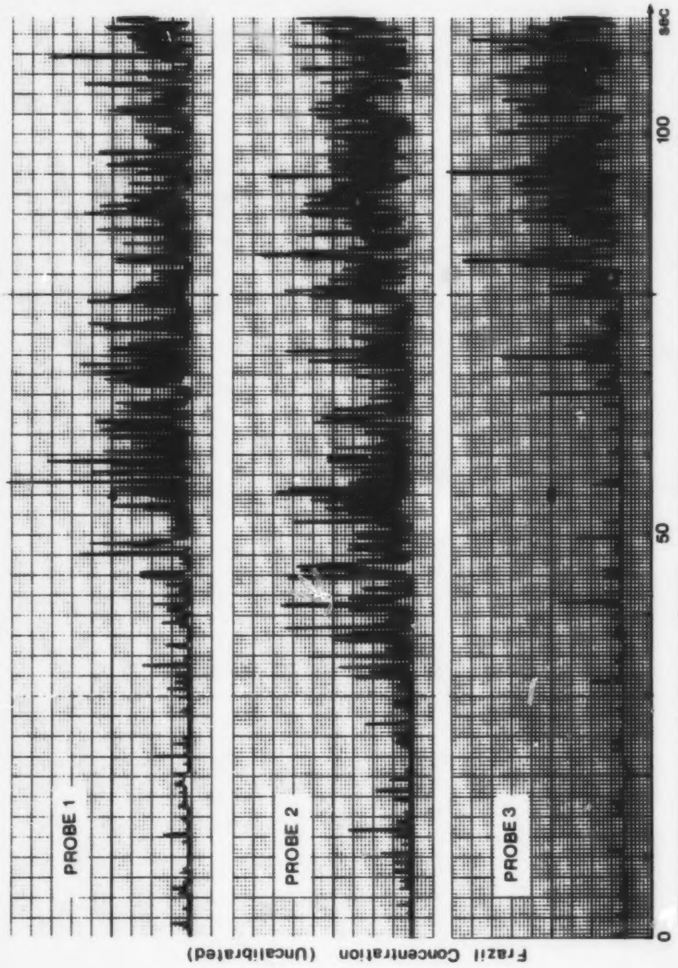

Figure 9. Frazil concentration at three points of equal radial positions but at slightly different depths during initial forming period.

concentration signals for Probes 2 and 3 did not return to the zero baseline, indicating possible frazil adhesion to them. This problem is being remedied by controlled heating of the probes. Because they were not calibrated, the concentrations shown can only be considered as quasi-quantitative.

Figure 10 shows the concentration of frazil at the same points during the later melting period of the experiment. The chart speed was reduced from 2 mm·s^{-1} (Figure 9) to 0.5 mm·s^{-1} to encompass a longer period. From Figure 10 it can be

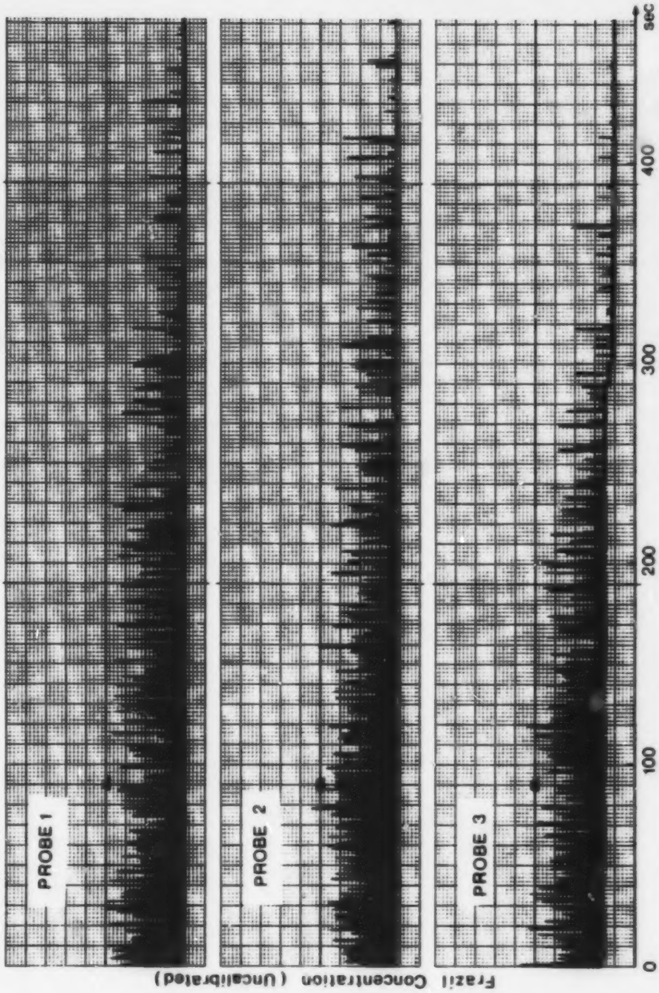

Figure 10. Frazil concentration at three points of equal radial positions but at slightly different depths during later melting period.

seen that the concentration of frazil still decreased with depth during the melting period. In spite of the slower chart speed and the more spiky recordings, the flocs were better defined, indicating greater consolidation of the flocs. For the signature measured with Probe 3, there was a sharp lowering of the baseline at t = 300 seconds. It was likely that some ice had frozen onto the electrodes of the probe and caused a higher zero reading. When this adhering ice was washed away by the warming water, the lower designed baseline was re-established.

To test the centrifugal effect on frazil distribution, another experiment was conducted for which the initial supercooling was limited to about 0.1°C and the rotating speed of the bottom was 20 rpm. The sensor probes were placed at the same depth close to the surface but at different radial positions - Probe 1 near the inner wall, Probe 2 at the centre-line and Probe 3 near the outer wall. Under the centrifugal force produced by the circular motion, the heavier substance in the ice/water mixture, namely water, piled up on the outside of the flume and the lighter substance, namely frazil, was pushed to the inside. Figure 11 shows the difference in frazil concentration at the three points. The large radial gradient of frazil concentration caused by the centrifugal force was unmistakable. While the concentration of frazil at the inner wall was high, the presence of frazil at the outer wall was almost zero. However, Figure 11 was from the late stage of the experiment during which the periodic presence of frazil agglomerations could be detected. For the early stages, the centrifugal effect was less pronounced. The centrifugal effects should be quantified in the future.

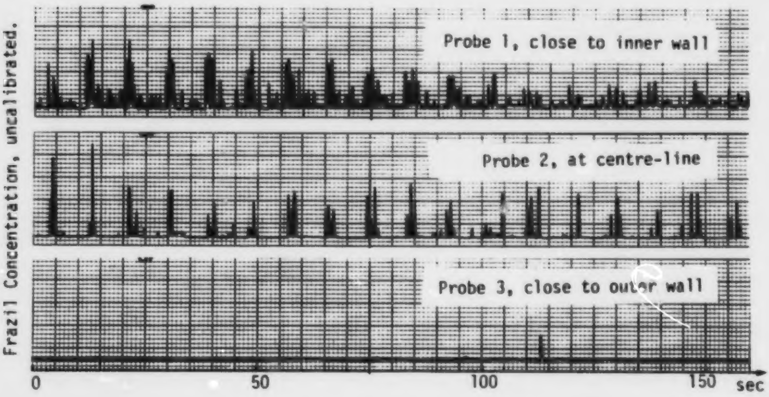

Figure 11. Frazil concentration at different radial positions.

CONCLUSIONS AND FUTURE WORK

The preliminary experiments show that frazil and anchor ice can be studied in a circular flume with a rotating bottom. Such a study could lead to expanded understanding of the basic physical processes and the parameters influencing them. The centrifugal effect was strong and this requires careful consideration in interpreting the experimental findings. Conducting similar experiments in flumes of different diameters may be a way to quantify the centrifugal effect and extrapolate the experimental findings to straight channels.

For the next stage of the investigation, efforts will concentrate on quantifying the measured parameters, computerizing the data-acquisition process, and data analysis. Better photographic techniques will also be given attention.

ACKNOWLEDGEMENTS

The authors wish to thank Manitoba Hydro, New York Power Authority, Ontario Hydro and Hydro-Quebéc for partial financial support of the study, and their colleague, Hemming Chew, for reading the manuscript.

LIST OF SYMBOLS

B/L	Boundary layer
h	Depth
p	Parameter
q_i	Heat flux at river bed
q_o	Heat flux at water surface
t	Time
T	Temperature of water
T_A	Freezing temperature
T_e	Equilibrium temperature
T_{min}	Minimum temperature
T_N	Nucleation temperature
u	Flow velocity in x direction
u_a	Absolute velocity
u_b	Bottom velocity
W	Width
x	Direction of flow
Δ	Increment or difference

REFERENCES

ARDEN, R.S. and T.E. WIGLE, 1972. Dynamics of ice formation in the upper Niagara River. Proceedings of the Banff Symposia, the Role of Snow and Ice in Hydrology, Vol.2, September 1972, IAHS Publication No.107, International Association of Hydrological Sciences, I.U.G.G., UNESCO-WMO-IAHS, 1296-1313

FOREST, T., A. OMSTEDT, S. DALY and K. AXELSON, 1990. Report on frazil ice. Draft report, IAHR Working Group on Thermal Regimes, International Association for Hydraulic Research, August, 105 pp.

MARTIN, S., 1981. Frazil ice in rivers and oceans. Annual Review of Fluid Mechanics, Vol.13, 379-397

OSTERKAMP, T.E., 1978. Frazil ice formation: a review. Journal of the Hydraulics Division, American Society of Civil Engineers, 104(HY9), 1239-1255

TSANG, G., 1982. Frazil and anchor ice: a monograph. Report, Subcommittee on Hydraulics of Ice Covered Rivers, Associate Committee on Hydrology, National Research Council of Canada, Ottawa, Ontario, February, 93 pp.

TSANG, G., 1985. An instrument for measuring frazil concentration. Cold Regions Science and Technology, 10(3), 235-249

TSANG, G., 1988. A theory for frazil distribution in turbulent flow. Proceedings, 9th International Symposium on Ice, IAHR, H. Saeki and K. Hirayama (Editors), 23-27 August 1988, Sapporo, Japan, Committee on Ice Problems, International Association for Hydraulic Research, Vol.2, 152-169; Discussion and reply, Vol.3, 264-265

TSANG, G., 1989. Laboratory investigation of frazil evolution, flocculation and the formation of anchor ice: Progress Report No.1 to Ontario Hydro, Manitoba Hydro and the New York Power Authority. NHRI Contribution No.89070, National Hydrology Research Institute, Environment Canada, Saskatoon, Saskatchewan, 130 pp.

ON COMPUTER SIMULATION OF ICE MOTION IN RIVERS

O.G. Vinogradov, A. Springer and P. Wierzba

Department of Mechanical Engineering
University of Calgary
Calgary, Alberta
T2N 1N4 CANADA

ABSTRACT

This paper deals with the phenomenon of ice run and ice jam in rivers. A new approach based on a computer-simulation technique which allows a quantitative rather than a qualitative description of the problem is considered. The paper is based on some fundamental results in the area of simulation of multibody dynamics carried out at the University of Calgary over the last few years, and is intended to show the potential application of the simulation methodology to river-ice mechanics. A numerical example of the surface motion of ice disks in a section of the Liard River is given as an illustration.

INTRODUCTION

There are two instances during the yearly cycle of river regimes in northern areas when the flow of isolated ice bodies is taking place: 1) in the fall, when the freezing process is accompanied by the flow of small ice formations (ice pans) leading to their accumulation and eventual freeze-up; and, 2) in the spring, when a dynamic ice break-up and run may occur (Gerard, 1989). The present paper deals with the flow of isolated ice bodies and is intended to study the formation of clusters, the rate of ice accumulation near obstructions, and the possibility of forming bridges.

The process of flow of isolated ice bodies interacting with each other and various natural and man-made obstructions is very complicated and, to the best of the authors' knowledge, no quantitative assessment of it is available at the present time. The complexity of the phenomenon is due to the variety of factors affecting its outcome, such as: river obstructions, and ice-flow geometry; ice-water interaction; mechanical properties of ice; and friction and adhesive properties of ice.

The existing practice of assessing the possibility of an ice jam is based on multiyear observations in any specific location of interest (e.g., Prowse, 1986). Although the associated experience is in many respects extremely valuable it is impossible, however, to extend it to other geographical locations considering the variety of factors governing its outcome. Besides, field observations taken alone do not allow an assessment of the sensitivity of the outcome to the various factors which may be important in the problem of ice management.

The alternative is to conduct physical simulation tests in a laboratory. However, aside from being very time- and cost-consuming, such tests are limited in terms of the factors which can be taken into account simultaneously. In addition, given the above constraints, it is practically impossible to investigate the statistical characteristics of the process. At best, such tests allow the investigation of a specific set of conditions which may not be the critical ones.

Another alternative is an investigation of the ice-flow phenomenon in rivers by numerical simulation. The outcome of such a numerical experiment should not be different from the real-life event provided that the laws governing the phenomenon are known and can be presented in a mathematical form, and also that the input data are correct. If the above conditions are met, it is clear that computer simulation allows one to take into account not only the various parameters but also this random distribution. By running the simulation program a sufficient number of times, the statistical data characterizing, for example, the probability of an ice jam in a specific setting can be assessed.

Another advantage of the computer-simulation approach in investigating river-ice flow is the potential for upgrading the program and the governing equations if more information becomes available, or a better understanding of the phenomenon develops. The authors are convinced that this approach should be taken as a long-term strategy with respect to the problem under construction.

In this paper a brief outline of the application of the concepts of multibody dynamics to motion of broken ice on the surface of a river is given. In the example that follows, some results of simulation for a section of the Liard River are presented. The paper concludes with a brief discussion of the validity of computer simulation in river-ice research.

BACKGROUND

Fundamental research in the simulation of the dynamics of multibody systems (MBS) moving on a surface has been ongoing at the University of Calgary over the past few years (Vinogradov, 1986, 1987; Vinogradov and Wierzba, 1986; Vinogradov and Springer, 1988). A MBS is a system comprised of isolated bodies and clusters of bodies moving together as an object. The specific feature of a MBS is its topological variability, which means a change in either the geometrical arrangement of bodies in a cluster or in the number of bodies in a cluster or in the total number of bodies in a system. The topological variability of a MBS is caused by interactions between the bodies and between the bodies and the system boundaries. Note that the bodies are considered to be interacting only if there is a positive reaction between them. When solid bodies represent a solid phase in a liquid medium, the interaction between the two phases also becomes important. In the following, a solid body is assumed to be circular disk with constant thickness. It should be noted, however, that this restriction is not critical since solid bodies made out of disks can also be used within the framework of the developed methodology.

The difficulty of analyzing a MBS is due to the following specific mathematical features associated with:

1) the system of governing equations cannot be written in advance since the topology of a MBS varies in time;

2) the moments in time, when the system topology changes are taking place, are unknown; and,

3) the existence of a positive reaction between any two interacting disks means that these two disks remain in contact over some time interval.

The latter requirement constitutes a geometrical constraint and is expressed in the form of an algebraic equation stating that the distance between two disks does not change during this time; such algebraic equations must be solved together with the differential equations of motion; the resulting system of differential-algebraic equations (DAE) is highly nonlinear.

The computational difficulties of the problem under consideration are caused by the number of disks and by the problem of solving a highly nonlinear system of DAEs. The former is associated with computer time and data management, whereas the latter is associated with the accumulated error and thus the validity of the results. A new concept of quasi-rigid bodies (QRB) introduced by two of the authors earlier (Vinogradov and Springer, 1988) reduces the number of degrees-of-freedom in a MBS thereby positively affecting both of the above concerns.

In general, in a cluster of disks each one may move with respect to the surrounding disks. However, if a few disks do not change their relative positions during some time interval then this subcluster may be treated as a QRB during this time interval. This fact may allow a reduction in the total number of degrees-of-freedom (DOF) associated with a cluster. Indeed, a cluster comprising N disks has N DOF if the relative rotational DOF for each disk is excluded and disks do not form QRBs. However, if M disks form a QRB then the number of DOF of the cluster equals N - M + 3, where 3 takes into account the fact that a QRB has three DOF. The minimum number of disks forming a QRB is three which was called a primitive QRB by Vinogradov and Springer (1990). It is clear that if only primitive QRBs exist then no gain in the number of DOF is attained.

The idea of a QRB and the reasoning behind its identification is explained here by way of an example. Figure 1a shows a simple six-disk system and Figure 1b the corresponding graph, indicating the connectivity between the disks. The graph can be interpreted as a truss system in which a node is actually a joint. It is clear that if the geometrical integrity of two truss elements (123 and 456) is not violated then each of these elements behaves as a QRB, whereas the connection between the two truss elements allows for one degree of freedom. However, connections 12, 13, etc. are one-sided, which means that they may exist only if there is a positive reaction between the two interacting bodies. This requirement can be verified by considering the internal forces in a given truss system subjected to given external forces. For example, the sub-cluster 123 behaves as a QRB only if the forces in truss elements 12, 23, and 13 are compressive. An algorithm generalizing this example has been developed for an arbitrary MBS (Vinogradov and Springer, 1990).

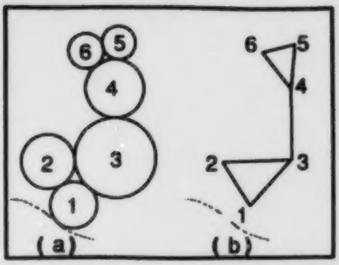

Figure 1. Six-disk system (a) and corresponding graph (b).

Thus at any moment in time a MBS can be broken down into the isolated disks, isolated QRBs, single disks belonging to a cluster, and QRBs belonging to a cluster. The simulation procedure involves the following qualitatively different steps: 1) identification of the system topology at any moment in time; 2) generation of the system of DAE; 3) solution of the system of DAE; and, 4) identification of a moment in time when the system topology changes. In the following, a brief outline of results in the above-mentioned areas is given for the motion of disks on a surface.

The topological analysis is based on the information contained in the incidence matrix characterizing the connectivity between the elements of the system. For example, if two disks i and j have a common interface then the matrix element equals 1; otherwise it equals 0. This type of information is sufficient to identify relative positions of isolated disks, clusters of disks and QRBs in a MBS. The details of the topological analysis can be found in Vinogradov and Springer (1990) and Springer (1989). As long as the topology of the system is known the equations of motion can be automatically generated by computer (Vinogradov and Springer, 1988; Springer, 1989). The system of nonlinear DAEs is solved using the fourth order Runge-Kutta method in conjunction with the concept of index reduction developed by Gear *et al.* (1970). The details of the numerical procedure can be found in (Springer, 1989).

The solution of DAEs is valid only over the time interval when the topology of the MBS remains the same. A change in topology may be due to two events: 1) when the compressive force at an interface of any two disks becomes equal or less than zero, which means that these two disks should not be considered in contact at this interface any longer; and, 2) when a collision within an MBS takes place resulting in an instantaneous change in the disks' velocities. When, in a time-stepping procedure, the first event is encountered then, at this moment, a new topological situation is analyzed, new DAEs are generated and the time-stepping process continues. If the second event, however, is encountered then the new velocities for all bodies in the system are assigned as new initial conditions for the next time step while retaining the same system of DAEs.

The following computer algorithms implementing the above ideas were developed: 1) to analyze the topology of an arbitrary multibody system, including identification of QRBs; 2) to generate differential equations of motion and algebraic constraint equations; and, 3) to solve the highly nonlinear system of equations of motion for an arbitrary force function and boundary conditions. A computer code utilizing the above algorithms was written and it allowed the simulation to be performed for an arbitrary geometry of the boundary and obstructions, random distribution of disks on the surface, and random disk sizes. A computer-simulation run allows the determination of the rate of disk accumulation near the obstructions and boundaries, and also the associated forces acting on these obstructions from the disks.

APPLICATION TO RIVER-ICE MOTION

The fundamental research carried out at the University of Calgary in the area of simulation of multibody dynamics creates a foundation for the application of computer-simulation methods to river-ice mechanics. However, to simulate an ice run and ice accumulation leading to a bridging, the interaction of broken ice with water should be taken into account. Such an interaction has two aspects: 1) the broken ice-water mixture is in fact a two-phase medium; and, 2) any interaction with respect to the ice-floe water-flow creates a drag force. At this stage the first factor is partially taken into account by considering a flow along a channel with variable geometry and against various obstacles according to the potential flow theory. As far as the second factor is concerned, only the resistance due to skin friction is taken into account at the present. Although the drag force for a single disk moving slowly in its plane can be found elsewhere, the drag force for a cluster of disks is, to the best of authors' knowledge, not known.

Another factor which plays an important role in the dynamics of broken-ice motion is the ice-ice friction coefficient. Energy dissipation caused by the friction is responsible for the ice floes' accumulation which may result in the jamming of a channel. This follows from Liouville's well-known classical-mechanics theorem in which the density of particles increases with time in any dynamical system with the dissipation of energy.

In the case of ice, if two floes remain in contact sufficiently long they may refreeze. This effect of adhesion can, in principle, be incorporated into the computer code if relevant experimental data become available.

NUMERICAL EXAMPLE

As a numerical example, part of the Liard River geometry is considered (Prowse, 1986) (Figure 2). The distribution of ice floes on the river surface is assumed to be random. Accordingly, the computer generates an ice floe which is random in its size and in its location at the entry into the control area. A normal distribution is assumed for the floe sizes; the location across the river at which a floe enters the control area is assumed to be uniformly distributed; and the time increment between the generation of two sequential floes is assumed to follow the Poisson distribution. Note that the parameters of the Poisson distribution control the density of floes on the water surface.

The simulation was conducted for the following input conditions. The x- and y-components (Figure 2) of the free stream velocity (V) were $V_x = 2\ \mathrm{m \cdot s^{-1}}$ and $V_y = 0.4\ \mathrm{m \cdot s^{-1}}$. The average rate of disk generation was 1 disk per 10 seconds. The medium disk radius was taken as 50 m, while the distribution of the disk radii was between 30 m and 80 m. The disk thickness was taken as being the same for all disks and equal to 2 m. The coefficient of friction was assumed to be 0.5 in order to accommodate the effect of surface roughness. The coefficient of restitution was taken to be 0.01. The time step was 10 s, however, if any event took place within this time step, the program would go back and search for the timing of this event.

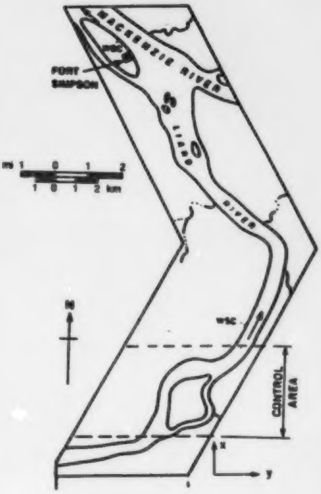

Figure 2. Control area of the section of Liard River.

Briefly, the simulation scenario develops as follows. The simulation clock starts at time T = 0, at which time the first floe generated at the entrance into the control area starts moving downstream according to the potential theory of the water flow. Figure 3 shows several snapshots of the simulation process at various times: at T = 10 s two floes have been generated, at T = 1,200 s one of the floes has touched the island, later a flow around the island takes place and an accumulation of floes (increase in density) is clearly seen, at T = 1,350 s the simulation is stopped.

DISCUSSION

The intent of this paper was to show the potential of computer simulation with respect to the problems of river-ice mechanics. The only example of simulation presented serves as an illustration of what kind of a system (river and obstacle geometry, distribution of ice disks) can be investigated and, accordingly, should not be viewed as an attempt to simulate a "real" ice run. In this respect an important question arises whether a real ice run can be simulated using the above-described approach. The latter comes down to the question of validity of the methodology.

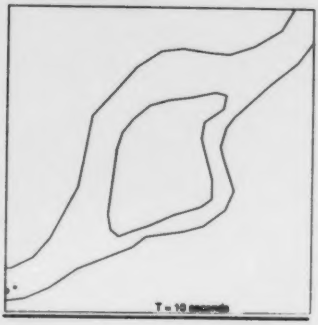

Figure 3a. Simulation output after 10 s of ice run.

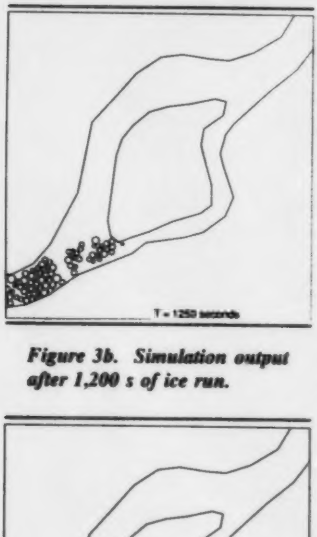

Figure 3b. Simulation output after 1,200 s of ice run.

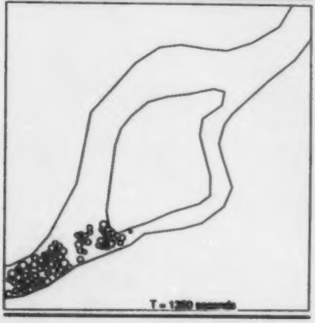

Figure 3c. Simulation output after 1,350 s of ice run.

This, in general, is associated with two factors: 1) the validity of the mathematical model; and, 2) the complexity of the model. The second factor leads to computational errors which, in time-stepping calculations, may result in significant distortion of the outcome of the simulation. Although this factor is extremely important, its discussion is beyond the scope of this paper. The first factor, however, merits some elaboration.

The validity of a mathematical model should be judged by the number and type of assumptions on which the model is based. The mathematical model in this paper is restricted to describing the flow on the water surface. The implication of this is that only the initiation of the ice jam can be simulated since after an ice bridge is formed the ice system becomes three-dimensional.

The shape of ice floes may play a significant role in the processes of interaction and accumulation. The circular shape of a floe adopted in this paper may look like a serious drawback to the methodology. However, this assumption can be easily removed. Indeed, within the framework of this methodology, a disk with a random shape made out of circular disks can be generated. The geometrical constraints for the circular disks making up the irregular one can be formulated such that the latter will retain its geometrical shape.

The mathematical model of the cluster of floes does not have limitations imposed by simplifying assumptions. Nor are there any limitations caused by the shape of the boundaries and obstructions. Thus the DAE system is quite general.

Notwithstanding the above considerations, a comparison of simulation runs with a proper laboratory experiment would significantly benefit the validation of the methodology.

ACKNOWLEDGEMENTS

The financial assistance provided by the Natural Sciences and Engineering Research Council of Canada in the form of an operating grant is gratefully acknowledged.

REFERENCES

GEAR, G.W., B. LEIMKUHLER and G.K. GUPTA, 1970. Automatic integration of Euler-Lagrange equations with constraints. Proceedings, International Conference on Computational and Applied Mathematics, 24-27 July 1984, Leuven, Belgium, Journal of Computational and Applied Mathematics, Vols 12-13, 77-90

GERARD, R., 1989. Hydroelectric power development and the ice regime of inland waters: a northern community perspective. NHRI Contract Report No.89001, Contract No.KW504-8-1248, Department of Civil Engineering, University of Alberta, Edmonton, Alberta for Hydrology Division, National Hydrology Research Institute, Environment Canada, Saskatoon, Saskatchewan, March, 122 pp.

PROWSE, T.D., 1986. Ice jam characteristics, Liard-Mackenzie Rivers confluence. Canadian Journal of Civil Engineering, 13(6), 653-665

SPRINGER, W.A.J., 1989. Simulation of the motion of clusters of rigid bodies around obstructions. M.Sc. thesis, Department of Mechanical Engineering, University of Calgary, Calgary, Alberta, 118 pp.

VINOGRADOV, O.G., 1986. Simulation methodology of vessel-ice floes interaction problem. Proceedings, 5th International Offshore Mechanics and Arctic Engineering (OMAE) Symposium, V.J. Lunardini, Y.S. Wang, O.A. Ayorinde and D.V. Sodhi (Editors), Vol.4, 13-18 April 1986, Toyko, Japan, American Society of Mechanical Engineers, New York, 601-606

VINOGRADOV, O.G., 1987. Simulation methodology for a flow of interactive flows *[sic]* around an obstacle. International Journal of Modelling & Simulation, 7(1), 28-31

VINOGRADOV, O.G. and A. SPRINGER, 1988. Algorithm for simulating flow of interacting rigid bodies. Proceedings, IASTED International Symposium on Applied Simulation and Modelling, 18-20 May 1988, Galveston, Texas, 134-138

VINOGRADOV, O.G. and A. SPRINGER, 1990. Simulation of motion of multi-body system with interactions. Proceedings, 1990 Summer Computer Simulation Conference, B. Svreck and J. McRae (Editors), 16-18 July 1990, Calgary, Alberta, 51-55

VINOGRADOV, O.G. and P. WIERZBA, 1986. Simulation of motion of cluster of ice floes. Proceedings, IASTED International Symposium on Applied Simulation and Modelling, 4-6 June 1986, Vancouver, B.C., 408-411

SECTION 3

OTHER CONTRIBUTIONS

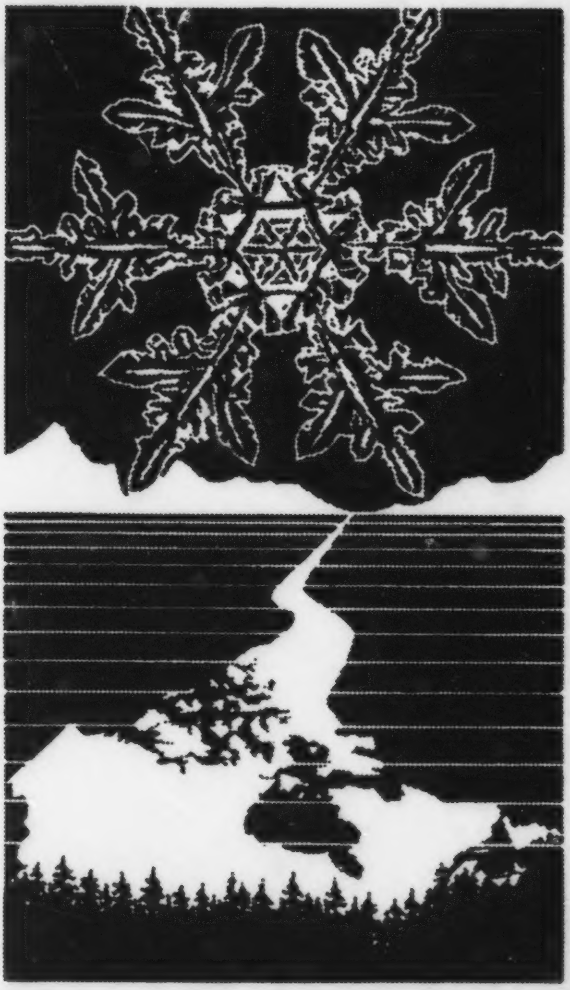

TRANSFORMATION OF HEAVY METALS UNDER TIDAL FLOWS IN THE SEVERNAYA DVINA ESTUARY

V.F. Brekhovskikh, A.N. Malutin and M.A. Mordasov

Water Problems Institute of the U.S.S.R.
Academy of Sciences
13/3 Sadovo-Chernogriazskaya
Moscow, U.S.S.R.

ABSTRACT

Formation of a geochemical barrier at the mouth of the Svernaya Dvina estuary, northwestern U.S.S.R., has been studied through changes in the occurrence of heavy metals in the tidal mixing zone. The main river channel was sampled at ten sites and the concentrations of humic and fulvic acids determined. Heavy metals were either dissolved or suspended. Three different zones were identified -- river, delta and frontal. Stability of the HA and FA sedimentation boundary is related to electrical conductivity and to lack of mixing between fresh and saline waters. The most significant changes take place at conductivities between 0.42 and 2.71 $S{\cdot}m^{-1}$.

The use of river estuaries for waste disposal from population and industry concentrations in coastal regions leads to a sharp fall in their productivity. Recent investigations show that most of the terrigenous organic and inorganic substances settle in the mixing zone of river- and sea-water resulting in their accumulation in estuarine bottom sediments (Anikeev, 1987; Artemiev *et al.*, 1982). Heavy metals (HM) occupy an outstanding place among pollutants since they are not subject to chemical or biological degradation and their increased concentration is detrimental to aquatic ecosystems. The main hydrochemical processes affecting HM behaviour and migration in the mixing zones of river- and sea-water are:

- sedimentation resulting from settling on suspensions;
- coagulation of colloids;
- flocculation of high-molecular humic organic substances;
- desorption of metals from the surface of suspended and bottom sediment particles; and,
- dissociation of complex compounds of heavy metals with organic ligands, (Mur and Kamamurti, 1987).

The river- and sea-water mixing zone functions as a complex geochemical barrier, where quick changes in water temperature, salinity, pH, redox potential, etc., occur, leading to modification of substance transformation and accumulation. The present work is aimed at studying the geochemical barrier formation in the Severnaya Dvina

*Paper presented, review process not complete.

estuary and changes in the forms of HM occurrence in the mixing zone subject to tidal flows. The estuary of the Severnaya Dvina River occupies vast area in the lower reaches of the river from the mouth of the Pinega to the sea boundary of the delta, as well the south-eastern part of Dvinskaya Bay in the White Sea. The sea boundary follows the 8-m isobath. The delta, with three main branches and numerous islands, is 37-km long and 45-km wide. Its area is 896 km^2, 54% of which is occupied by islands. Tides in the Severnaya Dvina estuary are of a semi-diurnal, abnormal, shallow-water type. Water fluctuations at the sea side of the delta (5% probability) reach 150 cm.

Two flows of Severnaya Dvina water can be traced in Dvinskaya Bay: one moving along the Zimni Bereg coast of the White Sea, formed by waters from the Maimak, Karabel and Murmanst branches; the second one, less intensive, flows from the Letniy Bereg. General cyclonic circulation of Dvinskaya Bay waters counteracts the movement of the second flow. These two flows determine the salinity distribution in the estuary.

Field work was carried out in the estuary during the summer low-flow period of 1988 to 1989. The stations were located in the main channel as follows:

No. 1	16-km upsteam of Arkhangelsk;
Nos. 2-7	along the navigable Maimak branch;
No. 8	abeam the central part of the Mudjng Island; and,
Nos. 9-10	along the main channel to the outlet buoy.

Diurnal dynamics of water temperature, salinity, pH and forms of HM occurrence were studied at station No. 10 located near the outlet buoy (Figure 1). Samples were taken with the help of bathometers, made of organic glass, at the surface, 0.5 m below, and 0.5 m from the bottom. Immediately after sampling water temperature, pH and salinity were measured. Concentrations of humic acids (HA) and fulvic acids (FA) were determined using spectrophotometry with preliminary concentration on DEAF-cellulose (Lapin *et al.*, 1987; Krasukov and Lapin, 1988).

To study HM occurrence in riverine and estuarine waters, complex analysis based on membrane filtration, ion-exchange chromotography and atom-emission spectrometry with inductively coupled plasma (ICP) were used (Kimstatch *et al.*, 1986; Kocharian *et al.*, 1989). This analysis obtained information on the following dissolved and suspended forms:

I. Ionic inorganic and neutral organic forms.
II. Complex compounds of heavy metals with organic bases (proteins, polypeptides, hidroxanic acids[1], amino-acids etc.).
III. Complex compounds HM+FA, HM+HA, organic-mineral humic compounds.

---

[1] The editors were unable to confirm this term with the author; it is believed to be a part of the hydroxyl acid group.

IV. Hydrophile components of suspended organic forms, inorganic components of suspensions.

The total HM content in water samples and the above fractions were determined using a plasmic spectroanalyser JI-32P (Jobin Ivon, France) with dynamic correction of background. The excellent analytical characteristics of ICP atom-emission spectrometry, such as low limits of element detection (up to 10^{-7} $g \cdot L^{-1}$), and high reproducibility (Sr = 0.001 to 0.03), ensured the direct determination of HM and organic substances in Fractions II to IV without any preliminary concentration. Preliminary concentration of HM with 8'-mercaptoxinolyn was used in analyzing water samples in Fraction I.

Table 1 presents some hydrodynamic characteristics of water samples taken at ten stations. The analysis allows us to single out three different zones in the Severnaya Dvina Estuary - the Dvinskaya Bay of the White Sea.

The first zone is a river one, characterized by small variations in electrical conductivity (0.28 to 0.34 $S \cdot m^{-1}$) and a sharp fall of total HM content in the dissolved phase (from 342.0 to 195.0 $mg \cdot L^{-1}$).

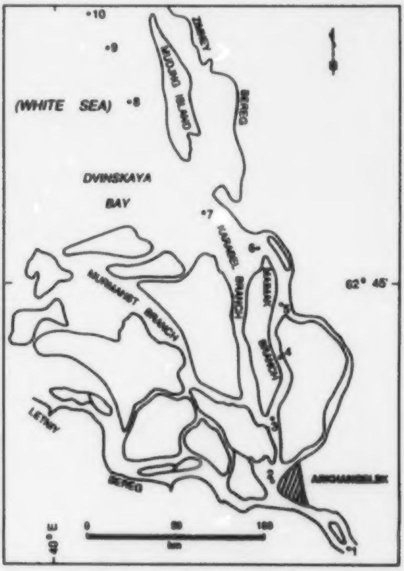

Figure 1. Location of the stations in the Severnaya Dvina Estuary.

The second zone is the river delta. Its development or degradation depends on the river run-off, water level in the estuary, hydrodynamic and other factors, determining short-term and seasonal fluctuations in the hydrological, hydrochemical and hydrobiological regime of the estuary. About 50% of the sediment is accumulated here, promoting the accumulation of pollutants, brought in by river waters. Thus, at Stations 5 to 7 electrical conductivity increases to 0.56 $S \cdot m^{-1}$. The HA content 0.90 to 1.06 $mgC \cdot L^{-1}$ (milligrams of carbon per litre) and FA is 3.04 to 5.92. The total HM content falls to 82.0 $mg \cdot L^{-1}$.

The third zone is the frontal zone. It is characterized by a sharp increase in electrical conductivity (from

Table 1. Measured characteristics of the water in the Severnaya Dvina Estuary, Dvina Bay, White Sea.

Station No.	T°C	pH	$S \cdot m^{-1}$	Ca^{2+} $mg \cdot L^{-1}$	Mg^{2+} $mg \cdot L^{-1}$	HA $mgC \cdot L^{-1}$	FA $mgC \cdot L^{-1}$	HM $mg \cdot L^{-1}$
1	18.1	7.3	0.30	24.5	4.9	1.22	5.97	395.9
2	18.2	7.3	0.28	24.4	4.9	1.26	5.64	275.8
3	17.9	7.4	0.36	25.8	5.3	1.10	5.84	199.2
4	17.6	7.5	0.34	26.4	8.4	1.18	5.92	209.8
5	17.4	7.5	0.42	30.7	28.4	1.06	3.78	108.0
6	16.6	7.5	0.46	39.5	52.9	1.00	3.55	84.4
7	16.8	7.5	0.56	--	--	0.90	3.04	31.3
8	14.0	7.7	0.84	80.4	128.9	0.56	1.39	28.3
9	12.6	7.8	1.60	118.9	313.9	0.13	0.58	27.4
10	12.4	7.8	2.71	162.7	447.6	0.10	0.20	26.9

0.84 to 3·84 $S \cdot m^{-1}$) and considerable changes in HA and FA concentrations (up to 0.1 and 0.2 $mgC \cdot L^{-1}$, respectively). The total content of dissolved HM forms falls to 30.0 $mg \cdot L^{-1}$).

The dynamics of the decrease in the concentration of organic components allows us to evaluate the direction and intensity of transformation and sedimentation of dissolved organic matter and to determine the location of the geochemical barrier from its components. The tendency of HA and FA to decrease in estuarine waters (stations Nos. 4 to 10) testifies to the intensive sedimentation of high-molecular organic substances as a result of their flocculation against the background of increased salinity (Lapin *et al.*, 1990).

Analysis of the experimental data allows us to determine the boundaries of the zones of HA and FA sedimentation. These are waters with an electrical conductivity of 3.52 $S \cdot m^{-1}$. Changes in HA and FA concentrations, observed at the increase in the electric conductivity of estuarine waters, can be described as:

$$C_{HA} = 0.33\ x^{-1.22}$$
$$C_{FA} = 1.06\ x^{-1.51}$$

Where C_{HA} is the concentration of humic acids, C_{FA} the concentration of fulvic acids, and x the electrical conductivity.

The stable character of the C_{HA} and C_{FA} dependence on electrical conductivity allow us to conclude that this dependence is caused by organic matter sedimentation and not by dilution of river water by sea water. Besides, sedimentation of organic matter occurs as a result of "entrainment" of dissolved metal fractions in a process of organic-mineral flocs. The average values of self-purification of the Severnaya Dvina River water from dissolved forms of different metals are shown in Table 2.

Table 2. Dissolved metals, Severnaya Dvina River.

Fe	74.4 to 83.2%
Mn	35.2 to 40.7%
Cu	76.8 to 85.8%
Zn	76.2 to 88.0%
Ni	68.1 to 80.0%
Pb	43.6 to 54.2%
Cd	53.2 to 59.6%
Co	43.1 to 52.7%

The ratios of the dissolved and suspended forms of the metals in Table 2 were determined in order to study qualitative and quantitative changes in HM distribution and migration in the Severnaya Dvina estuary.

With a steady increase in the total HM content in the water, the most appreciable changes in the dissolved fraction should be observed when comparing metal distribution with the form of their occurrence in typically riverine waters (station Nos. 1 to 4) and in the zone of river-water and sea-water mixing (stations Nos. 5 to 10). Analysis of the distribution of HM concentrations according to their forms of occurrence in the geochemical barrier zone (Figures 2A and B) leads to the following conclusions:

1. An increase in water salinity results in an increase in the relative content of Fraction I in dissolved form for all the metals under review.
2. A decrease in the relative content of Fraction II in the solution is typical for all the metals, with the exception of Mn and Fe.

The behaviour of Mn and Fe can be explained by the fact that the greater part of these elements is found in suspension only due to sorption onto surface particles or phytoplankton. The increase in the salinity promotes the desorption of Mn and Fe from the suspensoid and transformation of the plankton fraction of elements into the lipid form which increases the content of these elements in the solution under the increased background salinity (Anikeev, 1987).

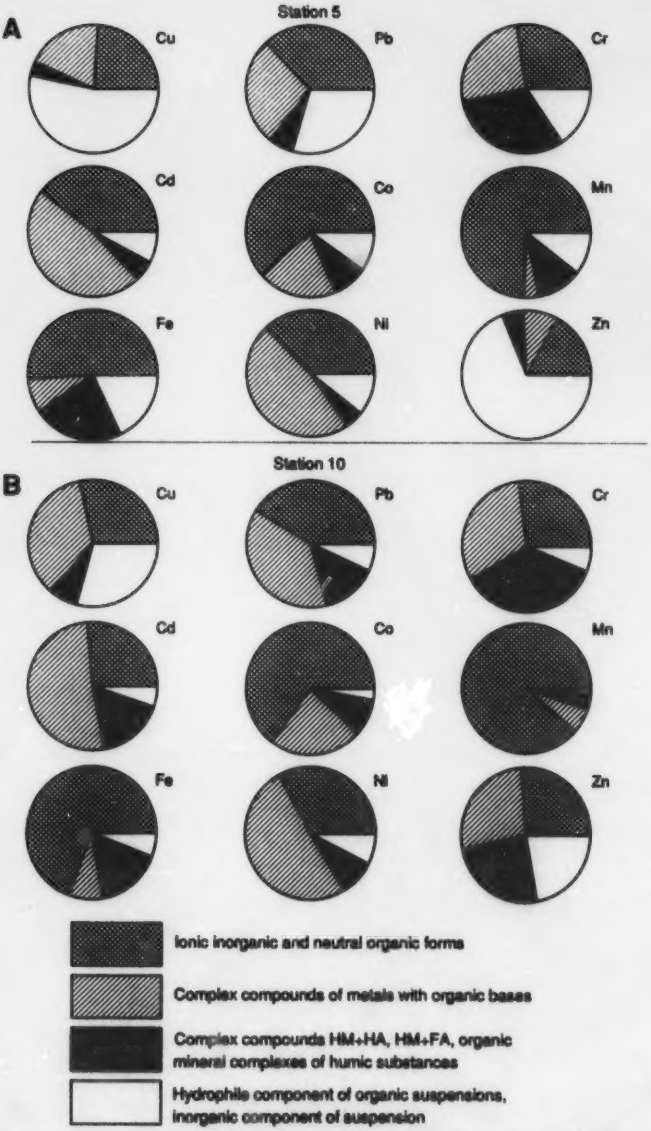

Figure 2. HM occurrence in the geochemical barrier zone. (A) Station No. 5. (B) Station No. 10.

At the river side of the geochemical barrier (station No. 5) the greater part of Zn, Cu, Pb, Cr and Ni migrate in compounds with humic substances (27.8, 35.2, 38.5, 31.8, 51.2 and 52.2%, respectively). Their relative content in Fraction III rises from 3 to 15% with the increase in salinity.

The increase in the relative content of ionic and inorganic forms of HM with the rise in estuary water salinity is evidently caused by the intensification of dissociation of organic-metal complexes, mainly Zn, Cu and Pb (to a lesser extent Cr, Cd, Fe and Ni) as well as by the desorption of their labile forms from suspended particles under the impact of the mineral components of sea water (Lapin *et al.*, 1990). This is most clearly manifested in the sharp fall of Zn, Fe and Mn content in suspension (Fraction IV) accompanied by the considerable increase in the relative content of these metals in Fraction I. Increased water salinity in the zone of the geochemical barrier leads to coagulation of colloid metal forms, causing their sedimentation (Anikeev, 1987). However, the role of hydrodynamic processes should not be neglected either: stirring up the upper layer of bottom sediment increases the concentration of suspended particles in the water, which is an important factor in HM transformation.

A diurnal experiment, accompanied by sampling in near-surface and near-bottom layers during different tidal phases, was carried out to study the dynamics of the solid and dissolved metal fraction ratios under the impact of the semi-diurnal tidal phenomena at the sea boundary of the geochemical barrier (station No. 10).

In accordance with the range of changes in the ratio between suspended and dissolved fractions, the metals can be divided into two groups:

I. Cu, Zn, Pb, Cr, Ni, Cd
II. Fe, Co, Mn

The first group is characterized by the prevalence of dissolved fractions over the suspended ones; the opposite situation is typical of the second group. The plots in Figure 3 show changes in the ratio between dissolved and suspended forms during different tidal phases in the near-surface (0.5 m from the surface) and near-bottom (0.5 m from the bottom) water layers. The figure shows that when the water is rising, an appreciable increase in the suspended Co, Mn, Ni and Cd fractions in the near-surface layer is observed, whereas the proportion of Cu, Zn, Pb, and Fe in suspension falls during this tidal phase. The electrical conductivity case is 1.98 to 2.71 $S{\cdot}m^{-1}$. In the near-bottom layer the ratio between suspended and dissolved forms of metals changes, which is evidently caused by intensified HM desorption from suspended particles.

Data presented in Table 3 illustrate changes in the metal content in ionic inorganic and neutral organic forms (Fraction I) during different tidal phases. The range of these changes is rather broad. Thus, for Co, Cd, Cr and Ni, the concentration content of metals in Fraction I varies from 0.02 to 0.21, for Pb, Mn and Fe from 0.09 to 0.55 for Cu and Zn from 0.33 to 0.82. This is caused by both the different content of the investigated metals in a sample and the different desorption capacity

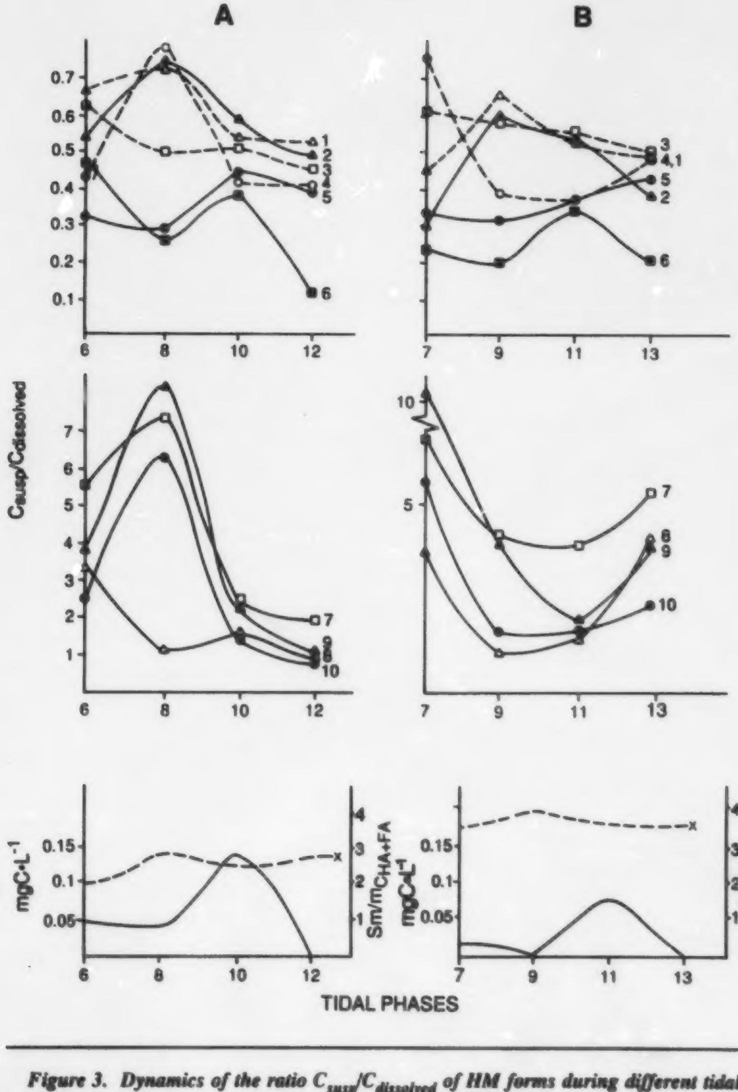

Figure 3. Dynamics of the ratio $C_{susp}/C_{dissolved}$ of HM forms during different tidal phases. (A) Near-surface layer. (B) Near-bottom layer.
1 - Cd, 2 - Ni, 3 - Pb, 4 - Cr, 5 - Cu, 6 - Zn, 7 - Mn, 8 - Fe, 9 - Al and 10 - Co.

Table 3. Content of HM in Fraction I (C_{frI}), as compared to the total HM content in dissolved fractions (C_{dis}) during different tidal phases in the Severnaya Dvina Estuary.

Tidal Phase	Sample No.	Electric Conductivity $S \cdot m^{-1}$	Microelements, C_{frI}/C_{dis}								
			Cu	Pb	Cr	Cd	Co	Mn	Fe	Ni	Zn
Ebb	65	1.98	0.52	0.27	0.16	0.05	0.07	0.17	0.32	0.06	0.31
	78	3.54	0.40	0.30	0.10	0.02	0.09	0.09	0.26	0.12	0.74
Tide	85	2.26	0.53	0.55	0.18	0.05	0.12	0.13	0.35	0.16	0.67
	98	3.84	0.71	0.47	0.21	0.12	0.15	0.26	0.38	0.17	0.82
Ebb	10^s	2.26	0.49	0.40	0.12	0.11	0.08	0.27	0.34	0.19	0.54
	11^b	3.68	0.45	0.30	0.11	0.07	0.08	[illegible]	0.16	0.12	0.58
Tide	12^s	2.71	0.38	0.29	0.10	0.03	0.04	0.12	0.21	0.06	0.74
	13^b	3.52	0.33	0.36	0.17	0.07	0.10	0.21	0.31	0.09	0.39

Note: s-sample, taken in the near-surface layer; and, b-sample, taken in the near-bottom layer.

of these metals. Another reason for this may be dissociation of complex compounds of heavy metals and organic substances (e.g. HM +FA or HM+ HA) (Lapin *et al.*, 1990; Linnik and Nabivanets, 1986).

Thus the study of metal occurrence in the estuarine waters of the Severnaya Dvina (Cu, Pb, Cr, Cd, Co, Mn, Fe, Zn and Ni) shows that the most significant changes in the concentration and composition of the dissolved metals occurs at the electrical conductivity of 0.42 to 2.71 $S \cdot m^{-1}$.

These changes are caused mainly by the effect of high-molecular component of the dissolved organic substances - humic and fulvic acids. The HA content in the estuarine waters of the Severnaya Dvina is 1.06 to 1.22 $mgC \cdot L^{-1}$, FA is 3.78 to 5.97 $mgC \cdot L^{-1}$. These acids are subject to intensive settling as a result of flocculation under the effect of mineral components of the sea water.

A stable trend to the increase in the content of inorganic and ionic forms of HM is revealed. This trend is observed against the background of reduced total content of dissolved metal forms. The increase in the concentration of the above-mentioned metal forms under increased salinity of estuarine waters is caused by the transition of inorganic and ionic metal forms from bottom sediment and suspension into the solution as a result of desorption caused by the increased salinity and hydrodynamic phenomena, as well as by the dissociation of complex metal compounds with dissolved organic substances. This process occurs in estuarine water and bottom sediments due to the competing effect of calcium and magnesium cations in the sea water.

REFERENCES

ANIKEEV, V.V., 1987. Korotkoperiodicheskie geokhimicheskie protessy i zagriaznenie okeana (Short-period geochemical processes and ocean pollution). Nauka, Moscow, (in Russian) 193 pp.

ARTEMIEV, V.E., L.L. DEMINA and M.B. VAINSHTEIN, 1982. Organicheskoe veschestvo i mikroelementy v vodakh estuariya reki Kubani i Yugo-Vostochnoi chasty Azovskago moria (Organic matter and trace elements in the estuarine water of the Kuban River and southeastern part of the Sea of Azov). Okeanologia, 22(5), (in Russian) 764-769

KIMSTATCH, V.A., I.A. LAPIN, E.G. TCHUDINA and G.V. VARVANINA, 1986. Application of physico-chemical methods to study forms of heavy metal occurrence in natural waters. Abstracts, International Symposium on New Sensors and Methods for Environmental Characterization (SMEC), 10-12 November 1986, Kyoto, Japan, 3-10

KOCHARIAN, A.G., A.N. MALUTIN, I.A. LAPIN, E.G. TCHUDINA and G.V. VARVANINA, 1989. Study of humic organic substances and heavy metals in the Ivankovo Reservoir waters. Toxicological and Environmental Chemistry, 24(1-2), 83-93

KRASYUKOV, V.N. and I.A. LAPIN, 1988. Sposob opredelnenia gumusovykh veschestv v prirodnykh vodakh (Way of determining humic substances in natural waters). Author Certificate N°1385041, USSR B1, N°12, (in Russian) 175 pp.

LAPIN, I.A., V.V. ANIKEEV and V.I. ILITCHEV, 1987. Mekhanizm sedimentatsii rasatvorennogo organichskogo veschestva v estuariyakh (Mechanism of dissolved organic matter sedimentation in estuaries). Doklady Akademii Nauk SSSR, 301(6), (in Russian) 1475-1478

LAPIN, I.A., A.N. MALYUTIN, G.V. VARVANINA, É.G. CHUDINOV, A.G. KOCHARYAN, I.A. EDIGAROVA, V.F. GEKOV, A.B MAGAK'YAN and K.I. SAFRONOVA, 1990. Study of the distribution and migration of heavy metals in Volga delta water. Water Resources, a translation of Vodnye Resursy, 17(1), 67-74

LINNIK, P.N. and B.I. NABIVANETS, 1986. Formy migratsii metallov v prestnykh poverkhnostnykh vodakh (Forms of metal migration in natural fresh waters). Gidrometeoizdat, Leningrad, (in Russian) 272 pp.

MUR, J.V. and KAMAMURTI, 1987. Tjakhelye metally v prirodnykh vodakh (Heavy metals in natural waters). Moscow Mir, (in Russian) 286 pp.

NORTHERN RIVER: BOD-DO MODEL

V.F. Brekhovskikh and G.V. Volpian

Water Problems Institute of the U.S.S.R.
Academy of Sciences
13/3 Sadovo-Chernogriazskaya 103064
Moscow, U.S.S.R.

ABSTRACT

A simple model for predicting the oxygen regime in northern rivers is reviewed. The variables and parameters to be determined include the initial values of BOD and DOD, depth and flow velocity distribution along the river, the deoxygenation coefficient, and the re-aeration coefficient at different reaches, oxygen consumption by bottom sediments and the capacity of additional sources of organic substances in the river. Model calculations of dissolved oxygen concentration in the Sukhona River, the left tributary of the Severnaya Dvina River, U.S.S.R., are presented. This river has a high dissolved oxygen deficit in its lower reaches, particularly when under ice cover, because of industrial, municipal and pulp-and-paper effluents. The model was found to be very sensitive to variations in the coefficients of deoxygenation and re-aeration. Determination of the BOD decay rate is very important for the upper reaches of the Sukhona, whereas determination of the re-aeration coefficient is essential for the lower reach.

Transformation of organic substances both of natural and anthropogenic origin in northern rivers depends on two factors: 1) low intensity of photosynthesis, from which water is enriched in oxygen; and, 2) long-term ice formation and low temperatures, which decrease the rate of biochemical oxidation of organic substances (Kozlova and Topnikiv, 1989). As a result, large amounts of effluent discharged into rivers create an extensive zone of dissolved oxygen deficit and, when the river is covered with ice, anoxia is observed (Brekhovskikh, 1988). For example, such a situation was observed in the 1950s in the North Saskatchewan River which was polluted by the effluent from the City of Edmonton (Bouthillier, 1987). In winter months, dissolved oxygen levels were as low as 1.0 ppm (or even less) at a distance of 100 to 320 km downstream from the city. Therefore, simple and reliable models, predicting the consequences of economic activity in northern regions, may be of great importance in ecological monitoring.

This paper presents the results of calculations of dissolved oxygen concentration in the Sukhona River, the left tributary of the Severnaya Dvina River. A modified Streeter-Phelps model is used, which presents two ordinary differential equations:

*Paper presented, review process not complete.

[1a] $$V(x)\,\frac{dL}{dx} = -[K_1(x) + K_3(x)] \cdot L + R_a$$

[1b] $$V(x)\,\frac{dD}{dx} = K_1(x) \cdot L - K_2(x) \cdot D + R_s$$

where x is the distance from the river source, V(x) flow velocity, L(x) organic substances concentration or carbonaceous BOD, $D(x)=(C_s - C)$ dissolved oxygen deficit, C_s the saturation concentration of dissolved oxygen, C(x) the real oxygen concentration, R_a additional organic matter inflow along the river course, R_s rate of oxygen consumption by bottom sediment, $K_1(x)$ the carbonaceous BOD decay rate (or deoxygenation) coefficient, $K_2(x)$ the re-aeration coefficient and $K_3(x)$ the sedimentation and adsorption coefficient.

The model is universal enough as it accounts for all the main features of processes in the water body, additional input of organic substances along the river course and includes oxygen consumption by bottom sediments (the photosynthesis and the nitric phase of BOD were negligible in our case). The discharge of the ground water with low oxygen content may greatly influence the oxygen regime of northern rivers. This must be taken into account for a point or distributed oxygen sink, an additional term being introduced in Equation 1.

The model is based on the following approximations:

- the flow is supposed to be steady along the whole river course;
- longitudinal dispersion is neglected (the ratio $V^2/2K_1E > 100$ is true for every reach of the river, where E is the coefficient of longitudinal dispersion; Dobbins, 1964);
- biochemical oxidation of easily degradable substances is described by the reaction of the first order; and,
- basic oxygen input is due to re-aeration (photosynthesis is absent); the re-aeration rate being proportional to the dissolved oxygen deficit, and the rate of oxygen saturation is supposed to depend only on water temperature, which is assumed to remain constant.

The hydraulic characteristics of the Sukhona River vary considerably along its course, so it must influence model coefficient values. In our case these coefficients are determined according to the varying flow velocity and to the depth at different reaches of the river:

[2] $$K_1(x) = K^\circ_1 + nV/H$$

where K°_1 is the coefficient determined by standard procedure in laboratory experiments with unstirred water samples, H the river depth and n the dimensionless coefficient ($n = 3.0 \times 10^{-6}$) (Krenkel and Novotny, 1979).

The coefficient of re-aeration was determined as a function of flow velocity (V) and depth (H) (Bouthillier, 1987):

[3a] $K_2(x) = 3.74\ V^{0.5}/H^{1.5}$ at $V = (0.1 \text{ to } 0.5)\ m{\cdot}s^{-1}$, H can be any value.

[3b] $K_2(x) = 5.01\ V/H^{1.67}$ at $V = (0.5 \text{ to } 2.0\ m{\cdot}s^{-1})$, $H > 1$ m

Corrections for water temperature (T) were introduced in Equations 2 and 3 in accordance with:

[4a] $K_1^{T_2} = K_1^{T_1} \cdot \Theta_1^{T_2 - T_1}$

[4b] $K_2^{T_2} = K_2^{T_1} \cdot \Theta_2^{T_2 - T_1}$

where $\Theta_1=1.075$, $\Theta_2=1.024$.

The data, obtained from 1967 to 1982 by the Northern Division of Hydrometeorological Observations and Environmental Monitoring Committee, show that the Sukhona River is considerably polluted by industrial (30,000 $m^3{\cdot}d^{-1}$) and municipal effluents from the town of Sokol. The BOD_5 index of these wastewaters is up to 523 ppm. Besides, untreated effluent from the Sokol pulp-and-paper mill (137,000 $m^3{\cdot}d^{-1}$) are disposed into the Pel'shma River, which flows into the Sukhona 20-km downstream from Sokol. All this increases the dissolved oxygen deficit (DOD) in the lower reaches of the river, especially when the river is covered with ice.

Since hydraulic characteristics vary considerably, the integration step in numerical application of the model was 20 km. A four-step Runge-Kutta method was used on an IBM PC-AT. Initial values of BOD and DOD concentrations were based on the data obtained at different gauges of the Northern Division of Hydrometeorological Observations and Environment Monitoring Committee in 1967 to 1983 (July and March). Figure 1 (a,b) presents the model curves and average values of dissolved oxygen deficit in corresponding gauges, as well as standard deviations.

Figure 1a shows that the summer maximum deficit of dissolved oxygen equal 5.0 ppm. This curve is in good agreement with long-term (15 years) field observations, especially if we take into account the fact that the standard deviations from the average long-term values are rather high.

The dissolved oxygen deficit increases in the upper reaches of the river in winter, when there is no re-aeration (K_2=0), whereas in downstream reaches its variations are negligible (Figure 1b). The model curve shows the situation in the upper river reach is a little bit worse than in the lower one. It may be explained by additional oxygen losses from oxidation of wood debris (wastes of the pulp-and-paper mill).

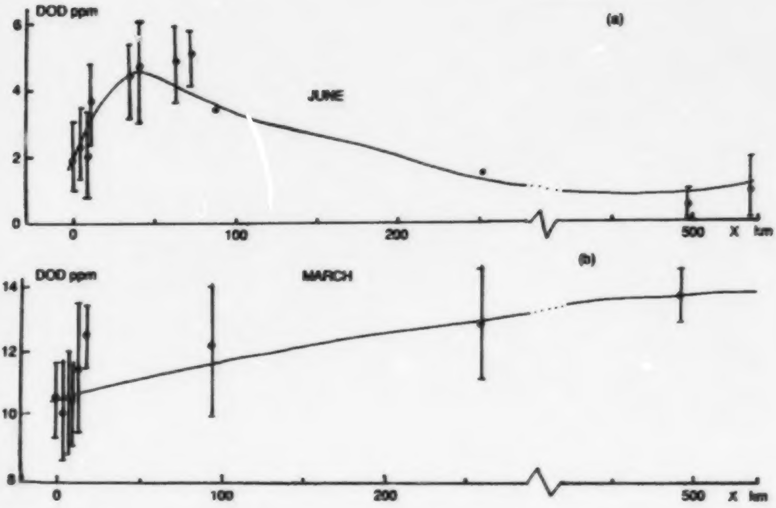

Figure 1. Distribution of dissolved oxygen deficit all over the Sukhona in (a) summer and (b) winter low-flow periods.

I = *range in field measurement data,* — = *model curves.*

It is interesting to note that the model is rather sensitive to changes of the coefficients of BOD decay rate and re-aeration. Equations 2 and 3 for these coefficients are based on experimental data. At the same time, all the basic flow characteristics may undergo considerable change. Therefore, the relations which are traditionally used in the model limit the area of its application, since these relations deal with real river flow values (e.g., values for the low-flow period).

Let us consider variations in the coefficients within a certain range of actual values. In this case, modelling ensures a more exact assessment of the meaning of every parameter in the distribution of dissolved oxygen deficit over different reaches of the streamflow. According to (Harrison, 1980), the values of the coefficients of re-aeration and BOD decay rate (base e) are:

$0.11\ d^{-1} \le K_1 \le 0.59\ d^{-1}$, the average $\bar{K}_1 = 0.35\ d^{-1}$; and,

$0.31\ d^{-1} \le K_2 \le 1.19\ d^{-1}$, the average $\bar{K}_2 = 0.75\ d^{-1}$;

within the 95% confidence interval.

Let us consider now the model sensitivity to variations of the BOD decay rate K_1. Assuming that initial conditions are: $L_{x=0} = 15.0$ ppm, $D_{x=0} = 2.0$ ppm, $R_a = R_s = 0.3$ ppm·d^{-1} by fixed $K_2 = \bar{K}_2 = 0.75$ d^{-1}, we may derive a set of DOD curves. Three of them are shown in Figure 2a - for $K_1 = 0.11$, 0.35 and 0.59 d^{-1}. All the curves have a characteristic maximum of dissolved oxygen deficit in the upper reach of the river. At K_1=0.59 d^{-1}, the maximum value of dissolved oxygen deficit (5.5 ppm) is observed, whereas at K_1=0.11 d^{-1} the maximum is not clearly expressed (2.2 ppm). Thus, a five-fold change in K_1 results in a two-fold change in the deficit value at the extreme point. The increase in K_1 is accompanied by an earlier appearance of a critical deficit.

The model may also be influenced by variations in the re-aeration coefficient K_2. Figure 2b presents three DOD curves (K_2=0.31, 0.75 and 1.19 d^{-1}) for the same initial conditions and fixed value of $\bar{K}_1$=0.35 d^{-1}. The figure shows that the decrease in the re-aeration rate from 1.19 to 0.31 d^{-1} (4 times) results in a 2.5-fold increase in the dissolved oxygen deficit at the extreme point. If K_2 decreases, the extreme point of the curve shifts to larger x values; the critical oxygen deficit appears in this case in the lower reaches of the river, being equal to 7.0 ppm at K_2=0.31 d^{-1}.

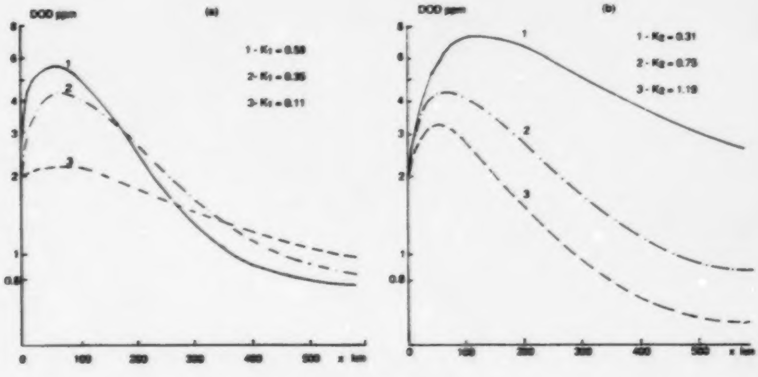

Figure 2. Distribution of the dissolved oxygen deficit at fixed values of K_1(a) and K_2(b).

CONCLUSIONS

1. A rather simple model can be used to predict the oxygen regime in northern rivers. The variables and the parameters to be determined are as follows: the initial values of BOD and DOD; depth and flow velocity distribution along

the river; the deoxygenation coefficient and the re-aeration coefficient at different reaches; oxygen consumption by bottom sediments; and, the capacity of additional sources of organic substances in the river.

2. The model is very sensitive to the variations in the coefficients of deoxygenation and re-aeration. Determination of the BOD decay rate is very important for the upper river reaches, whereas for the lower reaches determination of the re-aeration coefficient is essential.

LIST OF SYMBOLS

C	oxygen concentration (ppm)
C_s	saturation oxygen concentration (ppm)
D	dissolved oxygen deficit (ppm)
E	longitudinal dispersion ($m^2 \cdot d^{-1}$)
H	river depth (m)
K^0_1	deoxygenation coeff. in lab. experiments (d^{-1})
K_1	deoxygenation coeff. (d^{-1})
K_2	re-aeration coeff. (d^{-1})
K_3	sedimentation and adsorption coeff. (d^{-1})
L	organic substance concentration (ppm)
n	dimensionless coefficient
R_a	additional organic matter inflow ($ppm \cdot d^{-1}$)
R_s	oxygen consumption by bottom sediment ($ppm \cdot d^{-1}$)
V	flow velocity ($m \cdot s^{-1}$)
Θ_1, Θ_2	temperature correction factors

REFERENCES

BOUTHILLIER, P.H., 1987. A review of water pollution control in Alberta. Proceedings, 1987 CSCE Centennial Conference 1987, 19-22 May 1987, Montréal (Quebec), Vol.2, Canadian Society of Civil Engineering, 271-282

BREKHOVSKIKH, V.F., 1988. (Hydrophysical factors of oxygen regime formation in the water bodies). Nauka, Moscow, (in Russian) 167 pp.

DOBBINS, W.E., 1964. BOD and oxygen relationships in streams. Journal of the Sanitary Engineering Division, 90(SA3), American Society of Civil Engineers, 53-78

HARRISON, G.W., 1980. A stream pollution model with the intervals for the rate coefficients. Mathematical Biosciences, 49(1-2), 111-120

KOZLOVA, E.I. and V.E. TOPNIKOV, 1990. Microbiological and hydrochemical investigations of the Sukhona River and some of its tributaries. Water Resources, a translation of Vodnye Resursy, 16(6) [1989], 604-610

KRENKEL, P.A. and V. NOVOTNY, 1979. River quality model construction. In - Modeling of Rivers, H.W. Shen (Editor), Wiley-Interscience Publication, New York, N.Y., 1-22

WATER STORAGE IN ALPINE GLACIERS**

M.M. Brugman

National Hydrology Research Institute
11 Innovation Boulevard
Saskatoon, Saskatchewan
S7N 3H5 CANADA

ABSTRACT

Liquid water is temporarily stored within an alpine glacier and modifies the pattern of terminus stream discharge (Tangborn, Krimmel and Meier, 1975). The release of glacially-derived water can maintain river discharge from glacierized areas during critical periods such as late-summer, and years that are unusually warm and dry (Young, 1977, 1980). The goal of this study is to increase the accuracy of run-off models from glacierized northern regions. In this paper, the issue of water storage within a glacier is examined using a simple model derived from direct observations. These include measurements of snow accumulation and meltwater production, tracer advection and dispersion, stream discharge and conductivity, and ice volume change. Evidence of long-term (seasonal) glacier water storage is contrasted to that of short-term (daily) meltwater production and run-off.

Glaciers examined include four non-surge type glaciers, a glacier showing some degree of flow instability and a surge-type glacier. The glaciers compared in this study are located in western North America and in the European Alps. Surface-ablation and stream-discharge data are used to analyze the relative importance between the release of glacially-stored water versus the enhanced melting of surface snow and ice. Dye tracing, turbidity and conductivity data are used to examine the relative importance between water storage at the surface, within the glacier and at the bed of the glacier. The problem of characterizing englacial as compared to basal water storage is discussed and data evaluated. Water storage is modelled for stagnant zones located along the length of an arborescent subglacial water channel, and is evaluated with dye dispersion data obtained by the author and others. Glacier mass-balance and ice-volume changes are contrasted for several basins in order to evaluate the accuracy of water-storage predictions and run-off models.

Water storage within a glacier is at a maximum when the glacier is covered with a deep wet snowpack and the glacier flow velocities are very high. For the first case, if the snowpack is thick, then a great amount of surface melt may be stored within the intergranular void space. The total amount of water that may be stored within this surface "sponge" zone is further increased when a deep firn-pack exists,

***Paper presented, review process not complete.**
****National Hydrology Research Institute Contribution Series Number CS-90005.**

---

as measured by the integrated glacier mass balance over several decades. When glacier sliding velocities are high (such as during early summer or a glacier surge), basal cavities may enlarge and store great volumes of water at (or near) the glacier bed. The rate of water flow through a glacier is reduced at time of high ice flow rates, because the higher glacier shear-strain rates accelerate closure of subglacial and englacial water channels. The stored basal water is released either when the cavities collapse or a mature arborescent drainage system eventually develops.

Results indicate glacier water-storage and release behaviour, as well as ice-accumulation and meltwater-production rates, are determined by snow and firn depths, near-surface porosity and permeability, glacier albedo and roughness, extent and depth of crevassing; water storage is further determined by maturity of glacier water drainage systems, subglacial bed permeability, basal rheology and glacier flow behaviour. Recent ice-volume change surveys suggest that more meltwater is produced within a glacier that is measured using standard glacier mass-balance techniques (as described by Østrem and Stanley, 1966). Hydrological models of long-term water storage in glaciers must be re-examined using more complete measurements of glacier ice-volume change, mass balance and meltwater production within a glacier.

REFERENCES

ØSTREM, G. and A.D. STANLEY, 1966. Glacier mass balance measurements, a manual for field work. Glaciology Section, Department of Energy, Mines and Resources, Ottawa, 81 pp.

TANGBORN, W.V., R.M. KRIMMEL and M.F. MEIER, 1975. A comparison of glacier mass balance by glaciological, hydrological and mapping methods, South Cascade Glacier, Washington. Proceedings of the Moscow Symposium, Snow and Ice in Mountainous Areas, August 1971, IASH Publication No.104, International Association of Scientific Hydrology, IUGG, 185-196

YOUNG, G.J., 1977. Relations between mass balance and meteorological variables on Peyto Glacier, Alberta, 1967-1974. Proceedings of the Symposium on the Dynamics of Temperate Glaciers, 6-9 September 1977, Munich, Germany, 4th European Geophysical Society Meeting, Zeitschrift für Gletscherkunde und Glacialgeologie, 13(1/2), 111-125

YOUNG, G.J., 1980. Formirovanie pechnogo stoka v lednikovom basseine v Skalistykh gorakh Kanady/Streamflow formation in a glacierized watershed in the Rocky Mountains, Canada. Materialy Gliatsiologicheskikh Issledovanii, Khronika, Obsuzhdeniia, Mezhduvedomstvennyi Geofizicheskii Komitet, Sektsiia Gliatsiologii, Institut Geografii, Academy Nauk SSSR/Data of Glaciological Studies, Chronicle, Discussion, Section of Glaciology of the Soviet Geophysical Committee and Institute of Geography, Academy of Sciences of the U.S.S.R., No.39, Moskva/Moscow, Iiuni/July, in Russian 55-62, in English 134-139

SNOWMELT INFILTRATION INTO FROZEN SOIL AT SITES IN THE DISCONTINUOUS PERMAFROST ZONE NEAR MAYO, YUKON TERRITORY

C.R. Burn

Department of Geography
University of British Columbia
Vancouver, British Columbia
V6T 1Z2 CANADA

ABSTRACT

The near-surface ground thermal and hydrological regimes of four sites near Mayo, central Yukon, were monitored during spring 1985 and 1988 to determine: the snowmelt infiltration into frozen ground, in absolute terms and as a fraction of snowpack water equivalent; the extent of soil warming associated with infiltration; and, the frost heave associated with infiltration. Three of the sites are underlain by permafrost up to 30-m thick; at the other, the soil is only frozen seasonally. Infiltration was monitored via neutron probe, soil temperatures were determined with thermistors, and frost heave was measured with magnetic heavemeters. Between 10 and 70 percent of the snowpack water infiltrated the frozen soil at the sites. Maximum infiltration was recorded in coarsest-grained soils which were unsaturated during the preceding fall. At these sites most infiltration was driven by gravity rather than by soil temperature gradient, but at sites which were saturated during fall, temperature-induced infiltration was observed. Relatively little of the infiltration caused soil frost heave: most of the water filled soil pore spaces. Ground temperatures to 3-m depth increased during snowmelt. The increase in soil temperature was due to conduction and sensible-heat transfer by the infiltrating water rather than refreezing.

INTRODUCTION

The infiltration of snowmelt into frozen soil is of significance to both the thermal and the hydrological regimes of permafrost terrain. Infiltration may retard the rate of snowmelt run-off, and the transfer of sensible and latent heat via infiltrating water may warm the soil in preparation for thawing (Marsh and Woo, 1984). Snowmelt infiltration is an important source of soil moisture in the Prairies (Granger *et al.*, 1984; Gray *et al.*, 1985); in the discontinuous permafrost zone of Alaska most ground-water recharge occurs during snowmelt (Kane and Stein, 1983a).

Snowmelt infiltration has been associated with percolation down macropores and cracks, and with absorption and gravity-driven steady-state infiltration into the

*Paper not presented, review process complete.

---

unsaturated soil (Kane and Stein, 1983b). Infiltration rates are generally related inversely to soil water (ice) content (Kane, 1980). However, at sites underlain by thick frozen ground, near-surface soil temperatures during snowmelt are below 0°C and decrease with depth: such conditions are optimal for downward temperature-induced water migration (Mackay, 1983).

The field research reported here comprises an examination of snowmelt infiltration into frozen soil at four sites in the boreal forest near Mayo, central Yukon Territory. Field measurements were made in 1985 and 1988. The purposes were to determine: (1) the magnitude of snowmelt infiltration into frozen soil at the various sites; (2) the effect of infiltration on the ground thermal regime; and, (3) the amount of frost heave that may occur during snowmelt.

BACKGROUND

In the boreal forest, snowmelt occurs as the snowpack is warmed by advected air masses or by radiative heating from exposed ground and tree surfaces. Percolation and refreezing of meltwater may bring the snowpack to an isothermal state close to 0°C, and may lead to the development of basal ice layers (Marsh and Woo, 1984). Release of latent heat during formation of basal ice may raise the ground surface temperature close to 0°C.

Snowmelt may infiltrate the ground by gravity flow down cracks and soil macropores, but such infiltration is limited by water freezing rapidly in these spaces. Kane and Stein (1983b) report field results from infiltration tests in frozen, dry soil, which indicated a rapid infiltration rate at the start of tests (10^{-5} $m \cdot s^{-1}$), declining over the first 100 minutes of measurement by approximately one order-of-magnitude. Infiltration then continued at a constant rate for several days. Rouse (1984) has also documented steady infiltration into the active layer before thawing at sites near Churchill, Manitoba.

Water Movement in Saturated Frozen Soil

At temperatures below 0°C, a considerable proportion of the water in some soils is in the liquid phase (see Figure 1; Williams, 1982). The amount of unfrozen water (θ_u) depends on the specific surface area of the soil (Anderson and Tice, 1972). The hydraulic conductivity of frozen soils is associated with θ_u: it varies with soil type and declines appreciably with temperature (Burt and Williams, 1976).

Like liquid water in dry soil, the unfrozen moisture in freezing soil is held at high tension (Koopmans and Miller, 1966). The pressure difference between the ice and water in equilibrium is approximately proportional to the temperature depression below 0°C, and is described by the Clausius-Clapeyron equation. By assuming that the ice pressure remains constant (at atmospheric pressure), the Clausius-Clapeyron equation may be arranged in finite form to give, close to 0°C:

$$[1] \qquad \Delta P_w = 1.2\ \text{MPa} \cdot \text{K}^{-1} \times \Delta T$$

where P_w is the water pressure and T temperature (Williams, 1982). Note that P_w declines if T declines with depth, since $\Delta T < 0$.

Therefore, even with gentle ground-temperature gradients, on the order of 0.5°C m^{-1}, pressure-head gradients on the order of 60 $m \cdot m^{-1}$ may occur. These tension gradients may draw water along the interconnected water films on the surface of soil particles, and lead to transfer across ice masses by regelation (Miller *et al.*, 1975). Clearly such pressure gradients may influence the movement of water downward into frozen soil during snowmelt. The change of infiltration rate with time observed by Kane and Stein (1983b) may have been due to transition from bulk-water movement into empty macropores to steady flow along the interfacial films of soil particles (Burn and Smith, 1985).

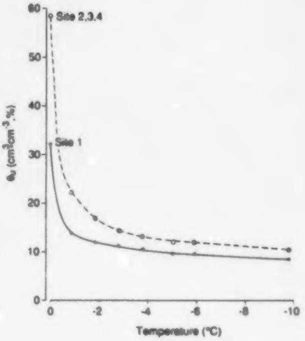

Figure 1. Unfrozen water-content (Θ_u) characteristic curves for the soils at the study sites determined by Time Domain Reflectometry (from Smith and Burn, 1987).

Soil Thermal Regime During Snowmelt

When snowmelt begins, percolation and refreezing of meltwater within the snowpack bring the snow rapidly to an isothermal state near 0°C (Marsh and Woo, 1984; Marsh, 1988). In some cases, latent heat released during meltwater refreezing is conducted into the ground and warms the soil. At other sites, particularly if there is a significant period of diurnal darkness, considerable radiative cooling of the snowpack may occur at night. A result is that some of the heat released by meltwater refreezing may flow to the atmosphere rather than into the soil (Bengtsson, 1982). At the sites discussed in this paper, there are over 8 hours of diurnal darkness during snowmelt.

Some authors have suggested that snowmelt infiltration and refreezing in the soil also contributes to soil warming (e.g., Wright, 1981; Marsh and Woo, 1984). This must occur principally at low temperatures in moist soils, for within the temperature range where the unfrozen water content changes, between -3°C and 0°C (see Figure 1), a substantial amount of ice must be thawed as the soil warms. The latent heat released by freezing infiltrate will only raise the soil temperature slightly. In dry soil some of the infiltration may not freeze, but instead fulfill the soil's unfrozen water content.

SITE CONDITIONS

Mayo (63°35'N, 135°35'W) has a mean annual air temperature of -4°C and is in the widespread permafrost zone (Figure 2a). The study area is 3 km south-southeast of Mayo in a body of glacio-lacustrine sediments, which contains several thermokarst lakes (Figure 2b). Ice-rich permafrost in the study area is up to 30-m thick.

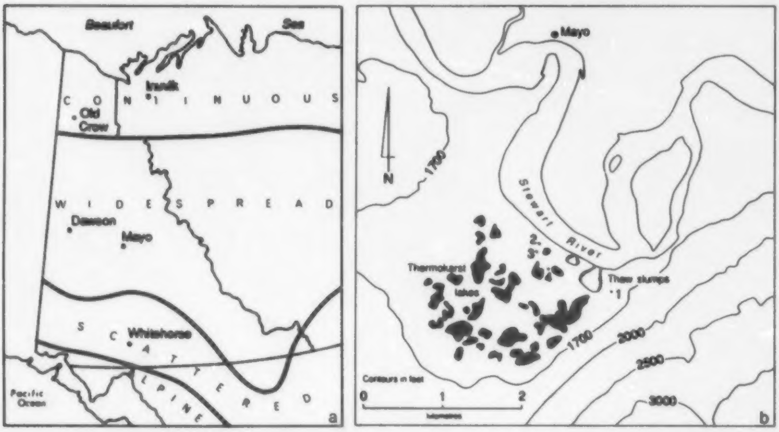
Beaufort
Sea
Inuvik
CONTINUOUS
Old Crow
WIDESPREAD
Dawson
Mayo
SCATTERED
Whitehorse
ALPINE
Pacific Ocean
a
Mayo
N
1700
Stewart River
2
3
4
Thermokarst lakes
Thaw slumps
1
1700
2000
2500
3000
Contours in feet
0
1
2
kilometres
b

Figure 2. (a) Permafrost distribution in the Yukon Territory. (b) Location of study sites near Mayo.

Measurements of snowmelt infiltration were made at four sites. Site 1 is located in colluvial silt loam in a drained lake between the valley side and a thaw slump (see Figure 2b). Sites 2, 3 and 4 are in the glacio-lacustrine silty clay which underlies most of the study area. Permafrost is present at the sites in the silty-clay sediments, but is not found below the drained lake. The unfrozen hydraulic conductivity of the silty clays, determined by constant-head permeameter tests, is on the order of 10^{-8} to 10^{-9} $m \cdot s^{-1}$; that of the colluvial material is 10^{-7} to 10^{-8} $m \cdot s^{-1}$.

Surficial materials and conditions at each site are indicated in Table 1. The microtopography at each site is undulating, with an amplitude of a few centimetres, but the 100 m^2 surrounding the sites is flat. At a larger scale, Site 3 is in a hollow. Soil composition and moisture contents are presented from soils collected during drilling in July, 1985. During fall 1984 and 1987 the water-table at Site 4 was at the soil surface. The greatest snow depths measured at the sites during winter 1987/88, and the average snow density on March 21, 1988 are also reported in Table 1.

Table 1. Ground conditions at study sites.

Site	Mean Annual Ground Temperature at 5 m (°C)	Active-Layer Depth, 23/9/87 (cm)	Organic Thickness (cm)	Snow Depth/Density 21/3/88 (cm)	($g \cdot cm^{-3}$)
1	0.8	--	10	45	0.20
2	-1.7	120	10	46	0.21
3	-0.8	80	10	30	0.24
4	0.1*	90	4	48	0.20

				Average Moisture Content, July 1985 (% Dry Weight)	
Site	% Sand	% Silt	% Clay	Active Layer	Permafrost Upper Metre
1	55	33	12	24	--
2	5	57	38	29	160
3	20	55	25	28	130
4	6	68	26	31	105

** Permafrost is approximately 1.5 m thick at site 4.*

FIELD ACTIVITIES

The purpose of field work during snowmelt was to monitor the infiltration into the soil and to determine the effect of refreezing on the ground thermal regime. Near-surface ground temperatures were monitored with thermistors (YSI 44033), calibrated at the ice point, spaced at 15-cm intervals to depths of 115 cm. Measurements of deeper ground temperatures were made on cables with sensors placed at 50-cm intervals to a 5-m depth.

Changes in soil moisture content were measured over intervals of 15 cm with a neutron probe (CPN 503DR). The probe was calibrated in the laboratory, but not at the field sites. Sequential, repeated measurements (10 times) of the same soil interval, conducted during summer 1985 with an identical instrument, suggested that measurement precision was ±0.07 cm water over the 15-cm measurement interval. Quantitative measurements of *changes* in soil water content during snowmelt could be made. These may be regarded as reliable at depths below 15 cm, when the probe was surrounded by at least 15 cm of soil, but in the surficial 15 cm, the readings may be complicated by changes in snow density at the base of the snowpack. In the following discussion of results, the reader's attention is directed to measurements of snowmelt infiltration below the surficial 15 cm of the soil.

Measurements of frost heave associated with snowmelt infiltration were made with a magnetic heavemeter (Mackay and Leslie, 1987). The precision of the heavemeter is ±0.5 mm. The water equivalent of the snowpack was determined before snowmelt began with a Mt. Rose sampler.

During 1985, measurements were made twice weekly between April 1 and May 3. Snowmelt was not complete at the end of the period. In 1988, measurements were made twice weekly from mid-March to April 25, with more frequent measurements during the latter part of the period. No snow remained at the sites on April 25, 1988.

CHANGES IN SOIL MOISTURE DURING THE WINTER

Throughout winter 1984/85 soil moisture changes were measured by neutron probe, and vapour traps, comprising inverted cans with a Gortex-covered opening, were placed at Sites 1 and 3 to collect vapour that emerged from the soil. The results have been reported by Smith and Burn (1987). The uppermost 90 cm of the soil at Site 1 and the uppermost 30 cm at Site 3 were enriched with water during the winter, due to upward temperature-induced moisture migration. In addition, 4.07 mm and 2.15 mm of water left the soil and were caught in the vapour traps at Sites 1 and 3, respectively. Therefore, although the soil as a whole lost water, the surface layers were replenished from below.

During 1987/88, soil moisture changes were not measured over the winter, but vapour traps were placed at Site 3. Between October 15, 1987 and March 13, 1988, 1.6 mm were caught in the vapour traps. The evidence from 1984/85 suggests that a vapour loss of this magnitude can be replenished from below, and that the surface layer of the soil does not necessarily dry over the winter.

Table 2. Mean and mean maximum monthly air temperatures (°C) during snowmelt at Mayo, 1985 and 1988.

Mean			
	March	April	May
1985	-9.5	-1.5	7.2
1988	-5.5	3.0	9.9
Normal	-11.7	-0.4	7.5
Mean Maximum			
	March	April	May
1985	-2.1	3.9	13.5
1988	0.4	8.5	15.4
Normal	-4.1	5.9	14.2

RESULTS

Table 2 indicates the mean monthly temperatures for the snowmelt periods in 1985 and 1988. Snowmelt was completed earlier in 1988 due to warm air temperatures. During 1988 daily maximum temperatures were above 0°C after April 4, and above 10°C after April 15.

Some infiltration was measured at all sites in 1985, but by May 3 over 20 cm of snow still remained at each site. In 1988 continuous infiltration was observed by neutron probe from early April until the end of snowmelt.

Infiltration

1985 Snowmelt. Snowmelt infiltration was monitored closely at the study sites between mid-April and May 3, 1985. Infiltration at Sites 1 to 4 during this period is presented in Figure 3; total infiltration is indicated in Table 3. Snowmelt had infiltrated into the upper 45 cm of soil at Site 2 by May 2. The moisture-content increase at depth at Sites 1 and 2 indicates the ability of frozen soil to conduct water. The soil recharge recorded up to May 3 was on the order of centimetres, accounting for between 10 (Site 4) and almost 70 percent (Site 1) of the snowpack water equivalent.

Table 3. Snowmelt infiltration from mid-April to May 3, 1985 and during snowmelt in 1988, Mayo study sites.

Site	1985 (cm)	1988 (cm)
1	7.3	4.2
2	2.3	3.4
3	0.3	1.1
4	0.9	0.9

As discussed earlier, temperature-induced potential gradients may be important for snowmelt uptake by frozen soil. The data from Site 4 support this suggestion, since the soil at the site was saturated during the fall, and frost heave due to ice segregation was observed during snowmelt.

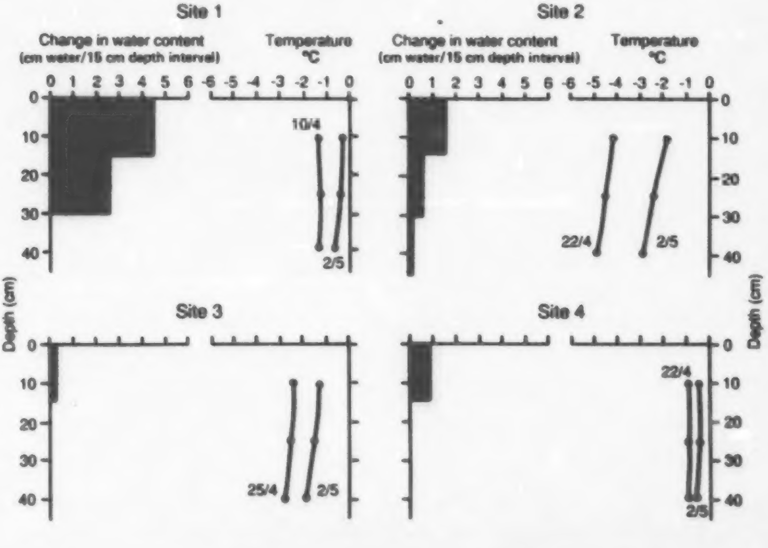

Figure 3. Infiltration and accompanying soil warming during snowmelt 1985. Infiltration is displayed as the cm increase in soil moisture content over each 15-cm interval measured by the neutron probe.

1988 Snowmelt. Figure 4 indicates the temporal change in moisture content with depth during snowmelt at Sites 1 to 4. Infiltration was restricted to the uppermost 45 cm of the soil at Sites 1, 2 and 4. The increase in water content due to infiltration appears to have occurred in a conventional manner at Sites 2 and 4.

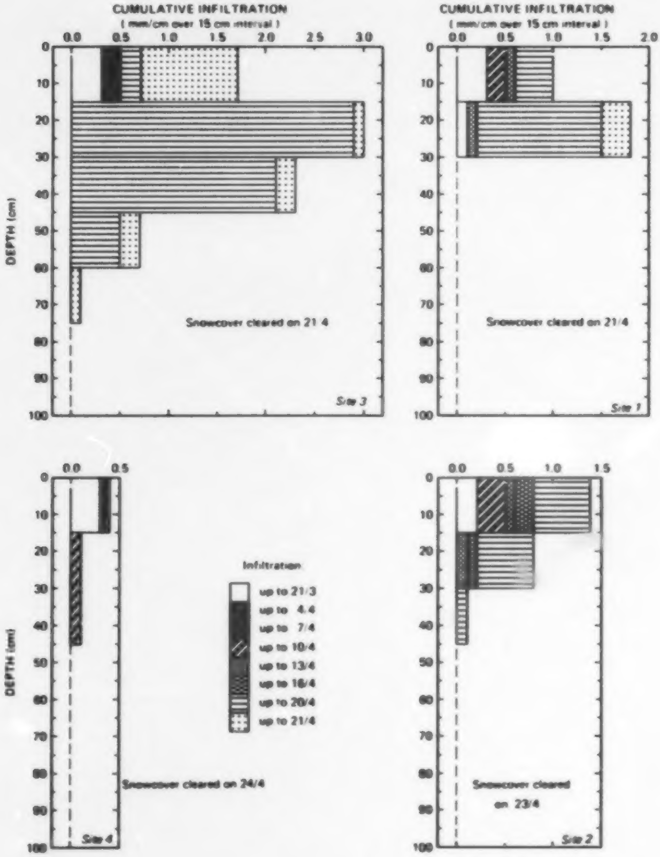

Figure 4. *Cumulative infiltration at the study sites during snowmelt 1988. Infiltration is displayed as the average mm increase in moisture content per cm over 15-cm intervals in the soil profile. Values may be multiplied by 1.5 to provide the cm increase in moisture content for each interval. The shading indicates the various dates when increases in soil-moisture content were observed. Increases in moisture content were measured relative to the soil-moisture content on March 13, 1988.*

At Sites 1 and 3, a large increase in soil moisture content was observed within the active layer during the last two days of snowmelt. However, the apparent increase in soil moisture content was not greatest in the surficial 15 cm. This may partly be due to reduced influence of snow at the ground surface on the neutron-probe signal, as indicated above. However, because soil wetting continued at Site 3 for two days after the snowcover had cleared, these results also suggest interflow from areas adjacent to the site. Therefore, only soil moisture changes observed before April 20 are unequivocally due to infiltration. The subsequent observations may be of lateral water movement within frozen soil as recorded by Parmuzina (1979).

A comparison of the snowpack water content in mid-March 1988 with the total change in moisture content of the soil at Sites 1 to 4 during snowmelt is presented in Table 4. The least infiltration was measured at Site 4, where the water-table was within 1 cm of the surface during fall 1987, indicating that the active layer was saturated. Maximum infiltration occurred at Site 1. The large amount of infiltration at Site 1 is similar to observations at dry sites in the Mackenzie Delta (Marsh, 1988). Total infiltration at the Mayo sites accounted for between 10 and 50 percent of the snowpack water equivalent, although at Site 3 interflow may have obscured observations. Since run-off was not observed at any site, and ponding was only observed at Site 4, the remainder of the snowpack at the other sites is assumed to have sublimated or evaporated.

Table 4. Water equivalent of the snowpack in mid-March 1988, and total increase in soil moisture content during snowmelt 1988.

Site	Snowpack Water Equivalent (cm)	Soil-moisture Increment (cm over the 120 cm of measured soil column)	%
1	8.7	4.2	48
2	9.6	3.4	35
3	7.2	1.1	15
4	9.8	0.9	10

NOTE: Snowpack water equivalent determined as the mean of 10 samples collected at each site on March 13 with Mt. Rose snow sampler.

NOTE: Percentage indicates proportion of the snowpack that infiltrated the soil during snowmelt.

In order to compare the relative efficiency of temperature-induced infiltration with gravity-controlled moisture flow, the total infiltration at Sites 1 and 4 may be considered. Some temperature-induced infiltration may have occurred at Site 4, where the soil was close to, or at, saturation. Throughout snowmelt, near-surface ground-temperature gradients at Site 4 were greater (Figure 5), but total infiltration at Site 4 was lower by a factor of five. Similar results were obtained in 1985. Since the hydraulic conductivity, when frozen, of the coarser soil at Site 1, with its lower θ_u, will be lower than that of Site 4, these data suggest that temperature-induced infiltration accounts for, at most, 20 percent of the total infiltration at Site 1. This is consistent with the frost-heave measurements at Site 1 (see Table 5), where less than 10 percent of measured infiltration contributed to heave. The bulk of snowmelt infiltration at unsaturated sites is therefore driven by gravity.

Measurements of frost heave are compatible with gravity-driven infiltration. Segregational frost heave is caused by the movement of water under temperature-induced potential gradients within freezing soil (Williams, 1982). The limited heave observed at most sites (Table 5) indicates that most infiltration occupied soil pore space rather than creating ice lenses.

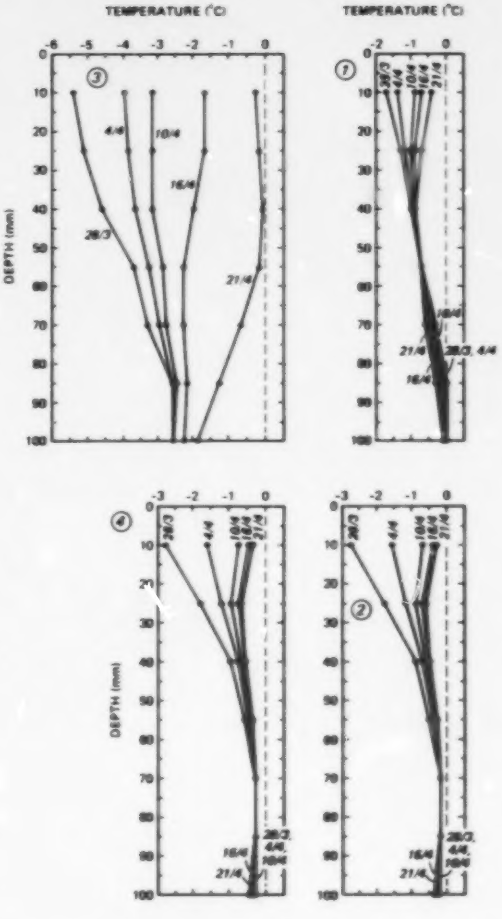

Figure 5. Soil warming at Sites 1 to 4 during late-March and April, 1988.

Influence of Snowmelt Infiltration on Ground Temperatures

The direct influence of snowmelt infiltration on the ground thermal regime is restricted to the active layer and near-surface permafrost. At none of the sites monitored in 1988 did warming below 3 m accompany snowmelt. At Sites 1, 2 and

4, the impact was restricted to the uppermost metre (Figure 5). However, it is important to note that soil temperatures at all sites began to rise before infiltration, and before daily maximum air temperatures rose above 0°C. Soil warming occurred after March 28, at Sites 1, 2 and 4, although infiltration was not noticed until April 7. At Site 3, warming began after March 25, although infiltration was not observed until April 4. Therefore, initial soil warming between March 28 and April 4 cannot have been due to infiltration, and was a response to sensible-heat flux into the ground and not latent heat.

Table 5. Snowmelt infiltration and accompanying soil heave, mid-April to May 3, 1985 and March 13 to April 25, 1988.

1985		
Site	Snowmelt Infiltration (cm)	Heave of Magnets (cm)
1	7.3	0.75
2	2.3	0.20
3	0.3	-- *
4	0.9	0.20
1988		
Site	Snowmelt Infiltration (cm)	Heave of Magnets (cm)
1	4.2	0.60
2	3.4	0.00
3	1.1	0.30
4	0.9	0.00

** Magnets were installed at site 3 during 1987.*

By the time infiltration began, soil temperatures were warm enough to require thawing of pore ice as further warming occurred (see Figures 1 and 5). Consider, for instance, Site 4 in 1988, where 0.45 cm of infiltration were recorded between April 4 and 10. Between April 4 and 21, soil temperatures increased as indicated on Figure 5. For the purposes of illustration, the soil profile may be divided into five intervals, each 15-cm thick. The mean temperature change in the uppermost horizon, 0 to 15 cm, was 1.3°C, from -1.6 to -0.3°C. This corresponds to a decrease in ice content of 0.12 $cm^3 \cdot cm^{-3}$ over the 15-cm interval, or 1.80 cm^3. In the interval below, 15 to 30 cm, the temperature rose from -1.3 to -0.5°C, leading to a decline in ice content of 0.05 $cm^3 \cdot cm^{-3}$ over the interval, or 0.75 cm^3. Overall, the change in temperature involved thawing 3.30 cm^3 of ice (Table 6), in addition to servicing the heat capacities of other soil materials. Freezing of 0.45 cm^3 of infiltration was clearly inadequate to raise soil temperatures. Freezing of infiltrating water could only have effected the observed soil warming at Site 1 because of the gentler slope of the unfrozen water-content characteristic curve (see Table 7). Note that freezing of infiltration must have been in macropores or ice lenses in order to be consistent with the unfrozen water-content characteristic during soil warming. As soil temperature rose, ice in micropores would thaw and remain as water unless the temperature dropped. Observations (Figure 5) indicate that soil warming was continuous once it began. The small amount of frost heave at the sites indicates that if infiltrating water froze most remained in macropores.

Table 6. Change in soil temperature and accompanying change in soil ice/water content, April 4 to 21, 1988.

Depth Interval	Temperature °C		Θ_u %		Change (Θ_u)	
	4/4	21/4	4/4	21/4	%	cm
0 - 15	-1.6	-0.3	0.18	0.30	0.12	1.80
15 - 30	-1.3	-0.5	0.19	0.26	0.07	1.05
30 - 45	-0.8	-0.5	0.23	0.26	0.03	0.45
45 - 60	-0.6	-0.5	0.25	0.26	0.01	0.15
60 - 75	-0.5	-0.4	0.26	0.27	0.01	0.15
0 - 75						3.30
Total Infiltration (12/3 to 21/4)						0.90

At Site 3 considerable soil warming occurred after April 16 (Figure 5). If ground-water movement at this site did begin during this period and continued after snowmelt, it is likely that the soil water remained in the liquid phase. Therefore the temperature increment would be due to transfer of sensible heat by conduction or meltwater rather than to release of latent heat.

CONCLUSIONS

The results presented in this paper may be summarized as follows:

Infiltration: The total infiltration of snowmelt into frozen soil depends primarily on soil moisture content during the preceding fall. For the most part, snowmelt infiltrates the soil due to gravity; temperature-induced potential gradients are of secondary influence. Frost heave during snowmelt is limited under the conditions experienced at Mayo, and comprises only a small fraction of the infiltration.

Ground temperatures: Soil warming accompanied snowmelt. Ground temperatures increased to depths of 3 m during the melt. However at the sites with silty-clay soil, freezing of the infiltration does not account for the thawing of pore ice and the increase in ground temperatures.

Table 7. Changes in soil temperature and accompanying changes in soil ice/water content at Sites 1, 2 and 3; April 4 to 21, 1988.

Depth Interval	Temperature °C		Θ_u %		Change Θ_u	
	4/4	21/4	4/4	21/4	%	cm
Site 1						
0 - 15	-1.5	-0.4	0.13	0.17	0.04	0.60
15 - 30	-1.3	-0.6	0.13	0.16	0.03	0.45
30 - 45	-1.0	-0.7	0.14	0.16	0.02	0.30
0 - 45						1.35
Total Infiltration (12/3 to 21/4)						4.20
Site 2						
0 - 15	-1.6	-0.3	0.18	0.30	0.12	1.80
15 - 30	-1.3	-0.5	0.19	0.26	0.07	1.05
30 - 45	-1.0	-0.5	0.21	0.26	0.05	0.75
45 - 60	-0.8	-0.4	0.23	0.28	0.05	0.75
0 - 60						4.35
Total Infiltration (12/3 to 21/4)						4.40
Site 3						
0 - 15	-4.0	-1.7	0.13	0.18	0.05	0.75
15 - 30	-3.9	-1.7	0.13	0.18	0.05	0.75
30 - 45	-3.6	-1.9	0.13	0.17	0.04	0.60
45 - 60	-3.5	-2.3	0.14	0.15	0.01	0.15
60 - 75	-3.2	-2.4	0.14	0.15	0.01	0.15
75 - 90	-2.8	-2.2	0.14	0.15	0.01	0.15
0 - 90						2.55
Total Infiltration (12/3 to 21/4)						1.10

ACKNOWLEDGEMENTS

The field work was supported by the National Hydrology Research Institute, Environment Canada. Support at the University of British Columbia was provided by the Killam Committee. The field assistance of Peter Beattie and the hospitality of Jim and Shann Carmichael are gratefully acknowledged. J.R. Mackay and H.O.

Slaymaker have given valuable advice and discussion throughout the project. Extremely helpful comments on the manuscript were also made by P.J. Jordan and the reviewers.

LIST OF SYMBOLS

P_w	Soil water pressure (Pa)
T	Soil temperature (K)
θ_u	Volumetric unfrozen water content (%, $cm^3 \cdot cm^{-3}$)

REFERENCES

ANDERSON, D.M. and A.R. TICE, 1972. Predicting unfrozen water contents in frozen soils from surface area measurements. Highway Research Record, No.393, 12-18

BENGTSSON, L., 1982. Percolation of meltwater through a snowpack. Cold Regions Science and Technology, 6(1), 73-81

BURN, C.R. and M.W. SMITH, 1985. Comment on "Water movement into seasonally frozen soils" by Douglas L. Kane and Jean Stein. Water Resources Research, 21(7), 1051-1052

BURT, T.P. and P.J. WILLIAMS, 1976. Hydraulic conductivity in frozen soils. Earth Surface Processes, a Journal of Geomorphology, 1(4), 349-360

GRANGER, R.J., D.M. GRAY and G.E. DYCK, 1984. Snowmelt infiltration to frozen Prairie soils. Canadian Journal of Earth Sciences, 21(6), 669-677

GRAY, D.M., P.G. LANDINE and R.J. GRANGER, 1985. Simulating infiltration into frozen Pacific soils in streamflow models. Canadian Journal of Earth Sciences, 22(3), 464-472

KANE, D.L., 1980. Snowmelt infiltration into seasonally frozen soils. Cold Regions Science and Technology, 3(2-3), 153-161

KANE, D.L. and J. STEIN, 1983a. Field evidence of groundwater recharge in interior Alaska. Permafrost, Fourth International Conference, Proceedings, 17-22 July 1983, Fairbanks, Alaska, National Academy Press, Washington, D.C., 572-577

KANE, D.L. and J. STEIN, 1983b. Water movement into seasonally frozen soils. Water Resources Research, 19(6), 1547-1557

KOOPMANS, R.W.R. and R.D. MILLER, 1966. Soil freezing and soil water characteristic curves. Soil Science Society of America Proceedings, 30(6), 680-685

MACKAY, J.R., 1983. Downward water movement into frozen ground, western arctic coast, Canada. Canadian Journal of Earth Sciences, 20(1), 120-134

MACKAY, J.R. and R.V. LESLIE, 1987. A simple probe for the measurement of frost heave within frozen ground in a permafrost environment. In - Current Research, Part A, Geological Survey of Canada Paper No.87-1A, Ottawa, Ontario, 37-41

MARSH, P., 1988. Soil infiltration and snow-melt run-off in the Mackenzie Delta, N.W.T. Proceedings, 5th International Conference on Permafrost, K. Senneset (Editor), 2-5 August 1988, Trondheim, Norway, Tapir Publishers, Vol.1, 618-621

MARSH, P. and M.-K. WOO, 1984. Wetting front advance and freezing of meltwater within a snow cover. 1. Observations in the Canadian Arctic. Water Resources Research, 20(12), 1853-1864

MILLER, R.D., J.P.G. LOCH and E. BRESSLER, 1975. Transport of water and heat in a frozen permeameter. Soil Science Society of America Proceedings, 39(6), 1029-1036

PARMUZINA, O.Yu., 1979. K voprosu o pereraspredelenii vlagi v merzlykh gruntakh (po naturnym nabliudeniiam) [Moisture redistribution in frozen soils (based on field observations)]. Problemy Kriolitologii (Problems of Cryolithology), Vol.8, (in Russian) 194-197

ROUSE, W.R., 1984. Microclimate at arctic tree line. 2. Soil microclimate of tundra and forest. Water Resources Research, 20(1), 67-73

SMITH, M.W. and C.R. BURN, 1987. Outward flux of vapour from frozen soils at Mayo, Yukon, Canada: results and interpretation. Cold Regions Science and Technology, 13(2), 143-152

WILLIAMS, P.J., 1982. The surface of the earth: an introduction to geotechnical science. Academic Press Canada, Don Mills, Ontario, 223 pp.

WRIGHT, R.K., 1981. The water balance of a lichen tundra underlain by permafrost. McGill Subarctic Research Paper No.33, Climatological Research Series No.11, Centre for Northern Studies, McGill University, Montréal, Quebec, 110 pp.

USE OF PERIPHYTON INDICES AS A BIOLOGICAL MEASURE OF WATER QUALITY IN SMALL RIVERS

E.A. Goncharevich

Water Problems Institute of the U.S.S.R.
Academy of Sciences
13/3 Sadovo-Chernogriazskaya 103064
Moscow, U.S.S.R.

ABSTRACT

The paper is devoted to the study of periphyton in the Moskva River tributaries. Data on the qualitative composition of periphyton allow for an indication of water quality using saprobility indices and the desirability function method.

Gradual deterioration of the environment from progressive urbanization is becoming a matter of increasing concern, both for scientists and for the public. Ecological problems are among the most acute.

Water-quality monitoring, using a series of chemical and biological indices, will be an essential component of environmental monitoring as a whole. No matter how thoroughly the chemical composition of water is studied, we cannot answer the question of the biological value of water. For this, it is necessary to study its biological component - the response of the biota to the character and degree of pollution. Periphyton is one of the most sensitive biocenoses for bioindication. It is a complex biocenosis, comprising organisms "overgrowers", both animals and plants. The main groups of periphyton include algae, protozoa and rotifers, characterized by considerable species variety and a quick response to changes in the external environment. These characteristics make them the best bioindicators of condition of a water body. However, periphyton remains the poorest studied unit in an aquatic system due to its complex taxonomic composition.

Work on bioindication according to periphyton indices was carried out for the Moskva River tributaries - the Ruza, Istra, Yauza, Pakhra and Nerskaya. They are small rivers of the Moskva Basin. Their flow is almost totally regulated or subject to considerable man-induced changes. Conditions affecting water-quality in these rivers differ, so they can be regarded as "model" streamflows.

The flows of the Ruza and Istra are regulated by numerous reservoirs and polluted by agricultural effluents. The Yausa flows across the city of Moscow, collecting both run-off and industrial effluents. The hydrological regime of the Nerskaya River is least disturbed, but even here the absence of a water preservation zone has had a negative effect on the environment.

---

*Paper not presented, review process not complete.

Sampling stations were located in the deltas of these rivers, thus ensuring the best determination of resultant water quality. Samples were taken on a monthly basis during the two vegetation seasons of 1985 to 1986. Periphyton samples were taken from neutral substrata, mainly from stones, since organic substrata considerably affect the periphyton species composition, thus distorting the results of water-quality analyses. The number of organisms in the samples was determined according to a sight scale, recommended by the International CMEA Commission. Species, whose amount was estimated at 5 to 9 points according to the sight scale, were considered as dominant; those estimated at 3 points as subdominant; at 1 to 2 points as rare.

In order to estimate water quality in the Moskva River tributaries according to the periphyton communities, we used a traditional method suggested by Pantle and Buck (1955) and modified by Slàdoček (1973). While calculating the saprobility index (S) we took into account the frequency of occurrence of certain species (h) (determined according to the sight scale) and the indicative value (s). The saprobility index is calculated as:

$$[1] \qquad S = \frac{\sum sh}{\sum h}$$

In spite of seasonal fluctuations, the dynamics are rather stable for every sampling station, regardless of the season of the year. This testifies to the stable character of pollution. The lowest index value (1.92, 1.91), showing that the water is clean, was found in the Ruza and Istra, the upper tributaries of the Moskva River. The species composition of the dominant forms is characterized by the prevalence of beta- and oligomesosaprobic organisms. They are:

algae - *Cladophora glomerata*, *Diatoma vulgare*, *Synedra ulna*, etc.;
protozoa - *Frontonia acuminata*, *Stentor polymorphus*, *Euplotes patella*; and,
rotifers - *Cephalodella auriculata*, *C.ventripes*, *Euchlanis dilatata*.

Alfamesosaprobic organisms (alga *Ulothrix zonata*; cyanobacterium *Oscillatoria tenuis*; protozoa *Chilodonella cucullus*, *Vorticella convallaria* and *Carchesium polypium*) appear in the Yauza periphyton. Among rotifers the alfamesosaprobic species *Rotaria rotatoria* is frequently observed.

The Pakhra river seems to be subject to appreciable pollution: its saprobility index is close to that of the Yauza River. The "leading" organisms in this river are *Cladophora glomerata* and *Oscillatoria tenuis*.

The Nerskaya River is peculiar from the viewpoint of the conditions of its water-quality formation. The river flow is not regulated, though its hydrological regime is considerably modified by water withdrawal for irrigation. Endemic macrophyte scutiform *Nimphoidus pellata* (Gmel.) (Ktze.) is preserved here. The content of humic acids is rather high. The dominant complex includes algae (*Cladophora glomerata, Navicula gracilis, N. cryptocephala*) and rotifer Euchlanis dilatata. The Nerskaya River is not heavily polluted: its saprobility index is 1.94, which corresponds to the betamesosaprobic zone.

Table 1 presents the number of different species and some water quality indices for the Moskva River tributaries.

Table 1. Species and water quality indices.

River Index	Ruza	Istra	Yauza	Pakhra	Nerskaya
Number of Species					
Algae	88	66	38	41	43
Protozoa	12	14	14	9	6
Rotatoria	6	8	10	11	4
Total	106	88	62	61	53
S	1.92	1.91	2.36	2.24	1.94
D	0.46	0.42	0.25	0.35	0.54

Thus, the evaluation of water quality in the Moskva River tributaries according to saprobic indicators allows us to refer them to one and the same zone - to the betamesosaprobic zone. However, differences in the species composition of periphyton communities in the analyzed rivers testify to appreciable differences in their water quality, as compared to those revealed by the saprobility index. This system was developed as a result of studying water bodies in Western Europe. Therefore, use of saprobic indicators, compiled there, can be used in other regions with great care.

The determination of indicative forms for specific water bodies is just an attempt to apply biological methods to water-quality estimation. For this purpose the desirability function method (Maksimov, 1980) was used to determine organism-indicators by comparing scatter diagrams for a standard clean river reach with a heavily polluted one. In order to evaluate the degree of pollution, we used a generalized index of water quality, based on the desirability function. The value of this index varies from 0 to 1: the smaller the index, the worse the water quality. In our work we used a list of 25 species-indicators (Goridchenko and Maksimov, 1985), including 25 species: 13 - algae, 8 - protozoa and 4 - rotifers. A generalized index (D) was calculated for every tributary on the basis of observed and indicative types:

$$D = \sqrt[n]{d_1 \cdot d_2 \cdot \ldots d_n} \qquad [2]$$

Table 1 shows the considerable advantage of the desirability function method when applied to water-quality evaluation. It reveals appreciable differences in the water quality of the analysed rivers. Thus, the generalized desirability index for the Ruza, Istra and Nerskaya Rivers is almost twice as high as that for the Yauza River, i.e., considerable deterioration of water quality in a small river is evident, if the latter flows through a city.

REFERENCES

GORDICHENKO, T.P. and V.N. MAKSIMOV, 1985. On the improvement of the Moskva River periphyton). Biological Sciences, VINITI Publ., (in Russian) 25 pp.

MAKSIMOV, V.N., 1980. (On one way of estimating the quality of natural waters). In - Self-Purification and Bioindication of Polluted Waters, Nauka Publ., Moscow (in Russian), 212-218

PANTLE, R. and H. BUCK, 1955. Die biologische Überwaschung der Gewasse und die Darstellung der Ergebnisse. Gas und Wasserfach, 96(18), 5-604

SLÀDEČEK, V., 1973. System of water quality from biological points of view. Ergebnisse Limnologie (Arch. Hydrobiologie), Vol.7, 1-28

YUKON AND NORTHWEST TERRITORIES GROUND-WATER DATA BASE

P. Hardisty[1], V. Schilder[2], T. Dabrowski[1] and J. Wells[3]

[1]Piteau Engineering Ltd.
Calgary, Alberta
T3B 0M6 CANADA

[2]Indian and Northern Affairs Canada
Ottawa, Ontario
K1A 0H4 CANADA

[3]Integrated Environments Ltd.
Calgary, Alberta
T2N 3P9 CANADA

ABSTRACT

Recognizing the importance of ground water to the Canadian North, and the need to foster and protect this valuable resource for the future, the Department of Indian and Northern Affairs (INAC) has sponsored development of a ground-water data base for the Yukon and N.W.T. No such system for collecting and archiving hydrogeological data from the territories existed before initiation of this project.

The data base is designed for IBM-compatible PCs, and is based on dBase-IV software. Data from each well, piezometer or spring are divided into sections on general information (location, name), aquifer characteristics (pump test data, water levels), well completion (depth, screen location), geology (drilling log, permafrost data), and water quality (main ions, metals, organics, trace organics, and bacteriological parameters). The data base has specific fields for over 280 hydrogeological parameters, and large comment fields for additional information.

As part of the project, approximately 35,000 pieces of hydrogeological data for the Yukon and N.W.T., representing about 1,200 wells, boreholes and springs, were collected from various sources throughout Canada. Most of these data have now been screened, rated for quality, and input into the data base. New data are being collected as they became available. Data files on diskette are available from INAC upon request, however INAC maintains control over data-file modification and input. Data files can be accessed and reports generated by other users with Relational Report Writer software.

*Paper presented, review process complete.

It is anticipated that the data base will prove to be a useful tool in such areas as regulatory control, ground-water exploration, protection and contamination investigations, and regional and local hydrogeological studies.

INTRODUCTION

Over the past five decades, ground water has come to be considered as a valuable resource which must be fostered and protected for the future. Recognizing this, and the importance of ground water as a source of domestic and industrial supply in Yukon and Northwest Territories (N.W.T.), Indian and Northern Affairs Canada (INAC) has moved to establish a computerized ground-water data-base system for the northern territories. This data base is the first step towards the compilation of a detailed resource inventory for the territories, which will eventually include all available data on water-supply wells, monitoring wells, springs and seeps, and other information of hydrogeological interest.

This paper provides a brief introduction to ground-water resources in the region north of sixty degrees latitude, explains the need for and benefits of the data base, and provides details of data-base design and contents. As a summary, the potential applications of the data base in such fields as ground-water exploration and protection, scientific study, and resource management and policy making are discussed.

GROUND WATER IN YUKON AND N.W.T.

Ground-Water Use

Approximately one in every four Canadians rely on ground water for their main source of domestic water supply, and only in Prince Edward Island is ground water of greater importance for domestic supply than in Yukon (Hess, 1986). Over 15,000 people in Yukon depend on ground water for day-to-day domestic use, representing approximately 63 percent of the population. In 1981, the last time a comprehensive study of ground-water use in Canada was conducted, ground water supplied 13,700 municipal users in Yukon with over 3,400,000 m^3 of water. These figures stand in sharp contrast to those of N.W.T., where only about one percent of the population depends on ground water for domestic supply. In 1981, ground water supplied about 19,000 m^3 to 2,020 users in N.W.T. (Hess, 1986). However, ground water is of significant importance for industrial use in N.W.T.; in 1981 the mining sector pumped over 9,100,000 m^3 of ground water, accounting for about 62 percent of total industrial water use in the territory. Since that time, however, several large mines in N.W.T. have closed down, significantly reducing the volumes of ground water pumped. In comparison, industrial ground-water use in Yukon was negligible (Hess, 1986).

Figure 1 shows a map of ground-water use in Yukon and N.W.T. (after Hess, 1986). This map shows that over two-thirds of Yukon is covered with aquifers that

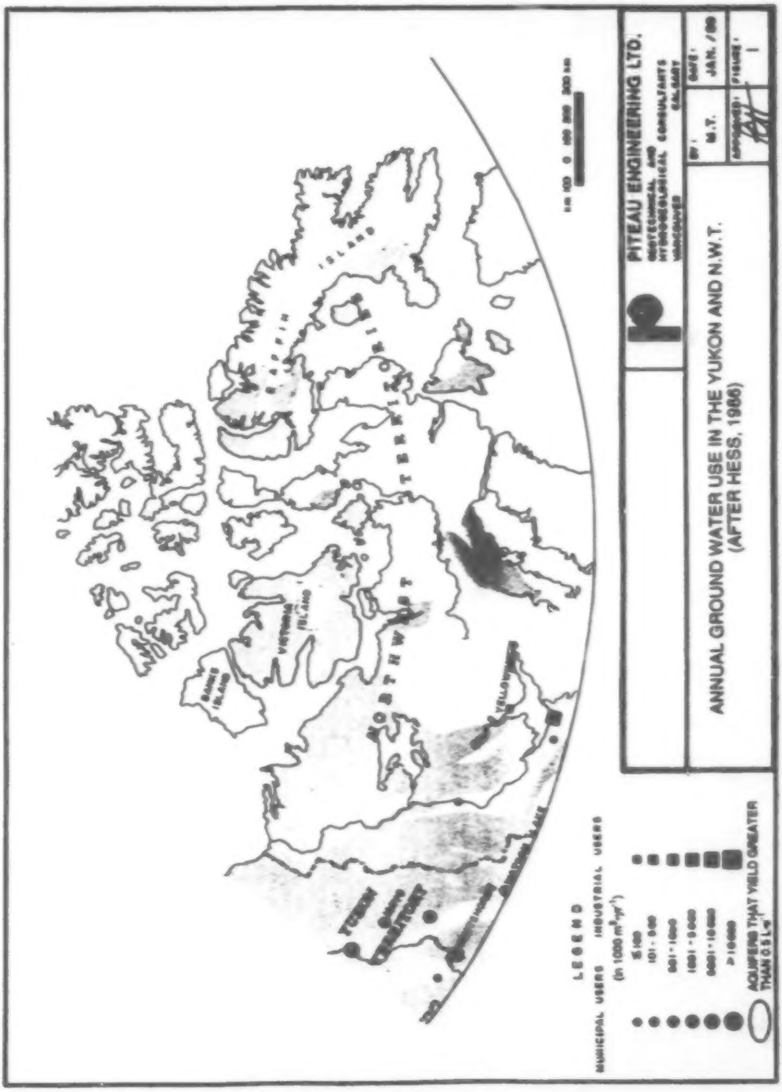

PITEAU ENGINEERING LTD.
GEOTECHNICAL AND HYDROGEOLOGICAL CONSULTANTS
VANCOUVER CALGARY
ANNUAL GROUND WATER USE IN THE YUKON AND N.W.T.
(AFTER HESS, 1986)
BY: M.T.
DATE: JAN. /88
APPROVED:
FIGURE: 1
km 100 0 100 200 300 km
LEGEND
MUNICIPAL USERS
INDUSTRIAL USERS
(in 1000 m³yr⁻¹)
≤100
101 - 500
501 - 1000
1001 - 5000
5001 - 10000
>10000
AQUIFERS THAT YIELD GREATER THAN 0.5 L s⁻¹
YUKON TERRITORY
NORTHWEST TERRITORIES
BAFFIN ISLAND
VICTORIA ISLAND
BANKS ISLAND
YELLOWKNIFE

Figure 1. Annual ground-water use in the Yukon and N.W.T. (after Hess, 1986).

have potential yields of over 0.5 $L \cdot s^{-1}$. N.W.T., in comparison, has fewer areas hydrogeologically suited to ground-water abstraction; here, ground water has special significance to large industrial operations such as mines.

Ground-water Protection

Another area of increasing concern to the public, government and industry is the protection of ground-water supplies from contamination. Throughout Canada, the U.S.A. and Europe, the incidence and severity of aquifer contamination associated with all manner of industrial, municipal and agricultural wastes is increasing. Contamination can render water supplies unfit for use, requiring development of expensive alternate supplies; the presence of toxic or carcinogenic substances in drinking water may pose a danger to public health; and environmental damage to streams and lakes may occur. In response to such problems, many jurisdictions have introduced regulations requiring ground-water monitoring and aquifer restoration.

To date, concerns over ground-water contamination in Yukon and N.W.T. have not been significant, but with increased water use, industrial development and rapid population growth, this is sure to change.

Legislation

Legislation governing water use and protection in Yukon and N.W.T. comes under the Northern Inland Waters Act (NIWA) and its Regulations. The purpose of the Act is to ensure the conservation, development and proper utilization of the water resources of Yukon and the N.W.T. The Yukon Territory Water Board and Northwest Territories Water Board have licensing powers under this Act.

All water-use applications to the Water Boards undergo a formal review process which includes determining if a licence is required, posting of notices inviting interested parties to a public hearing, technical review, and ministerial approval should a licence be required. All applications, be they for ground-water or surface-water licences, are dealt with by the Boards. Licences are also required for discharge of wastes into inland waters.

Any proposed use of inland waters in N.W.T. and Yukon by a municipality, company, agency or private individual must either be licensed by the appropriate territorial Water Board or authorized by the Regulations. The licence sets out conditions governing the large-scale use of surface water and ground water. Individual landowners using water adjacent to their property for domestic use are exempt from these conditions. This includes abstractions from private wells. In Yukon and N.W.T., licences are not required for abstractions of less than 50,000 imperial gallons (225 m^3) per day .

At present, no legislation pertaining specifically to ground water in Yukon and N.W.T. exists. Some aspects of ground-water protection are dealt with in various guidelines published by INAC on topics such as reclamation, pits and quarries, land use, tailings ponds, and environmental operation of hydrocarbon well sites.

However, no legislation, guidelines or voluntary system at present exist for the submission of well drilling records in the territories. Nor are there any detailed regulations regarding monitoring requirements and minimum aquifer protection standards at industrial plants and waste-disposal sites.

DATA-BASE RATIONALE

The statistics presented in the previous section underline the importance of ground water to the people of the Canadian North. Yet until now, there has existed no single repository of hydrogeological data for Yukon and N.W.T. All Canadian provinces have established ground-water data-management schemes and regulatory bodies to control the use, development and protection of ground water.

Hydrogeological data exist for Yukon and N.W.T., but are scattered amongst various federal and territorial government departments, private consultants, drilling contractors, and archives across the country. This data base is the first step towards bringing together all existing data in an organized fashion. This will allow gradual establishment of a ground-water resource inventory in the territories, consisting of a complete and wide-ranging set of hydrogeological information accessible to members of government, industry, and the public.

Such an inventory will allow the resource to be put into perspective in terms of its distribution, use, value, and susceptibility to long-and short-term damage. It will also provide the necessary data with which regulatory bodies may make informed decisions regarding the management and protection of ground water in the future.

Applications for the data base are foreseen in such areas as resource management, aquifer protection and monitoring, legislation and policy formulation, and hydrological studies. Computer filing, sorting and retrieval of information also make this a powerful tool for ground-water exploration and development by industry, consultants, and drilling companies, and the popular and accessible personal computer format of the data base allows the information to be accessed and manipulated by a large number of individuals and organizations.

DATA-BASE DESIGN

Software

The data base is based on the popular dBase-IV software, the improved version of the well known dBase-III and III-Plus packages developed by Ashton-Tate

Corporation. The advantages of user familiarity, compatibility with most PCs and ease of operation make the dBase line of programs a popular choice. Many other data-base management systems emulate dBase and files can be used interchangeably. The choice of software for the data base was made following a detailed assessment of users' needs, preferences and hardware constraints. The data base is a fully interactive user-friendly system.

Hardware

The data base is designed to run on IBM-compatible AT and 386 machines. Minimum requirements include 640K RAM, 3 Mb of hard disk space, and DOS 3.1 or newer. Speed of operation will vary depending on processor power and speed. Colour or monochrome monitors are supported. Program discs can be supplied in either 5¼ inch or 3½ inch formats.

Design and Contents

The data base is divided into five main information categories. Data from a given well or spring are grouped into these categories:

1. **General Information**: Includes well or spring location, owner information, references, types of data available, and comments.
2. **Well-Construction Data**: Includes well depth, diameters, casing and screen information, completion details, depth of ground-water-bearing zones, and pump data.
3. **Geology**: Provides a complete lithological/drilling log for the well, including depth and geological descriptions, geophysical logging and permafrost information.
4. **Aquifer Characteristics:** Multiple aquifer test data can be accommodated and are indexed by test date. For each record, such things as test type and duration, test yield, drawdown, transmissivity, storativity, hydraulic conductivity and static water-level can be recorded.
5. **Water Quality:** Includes main ion chemistry, metals, organics, a full suite of trace organic compounds including hydrocarbons, EPA-volatile and extractable-priority pollutants, and bacteriological parameters. Multiple analyses are indexed by sampling date, allowing water-quality data from several years to be stored for a given well or spring.

All told, the data base has specific fields for over 280 hydrogeological parameters, and large comment fields at the end of each of the five data fields for written notes and observations. Figures 2 through 6 show reproductions of the nine data-base screens, showing each parameter field and screen layouts. Figure 7 shows a schematic diagram of the data-base structure, illustrating the five information categories.

SCREEN 1

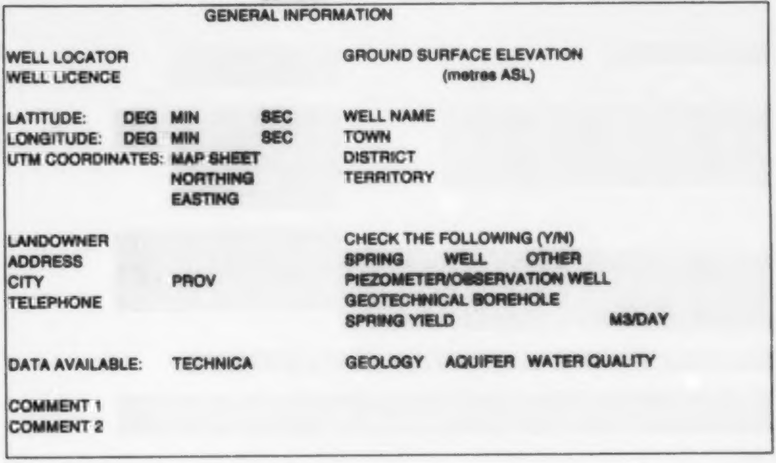

GENERAL INFORMATION

WELL LOCATOR   GROUND SURFACE ELEVATION
WELL LICENCE   (metres ASL)

LATITUDE: DEG MIN SEC   WELL NAME
LONGITUDE: DEG MIN SEC   TOWN
UTM COORDINATES: MAP SHEET   DISTRICT
NORTHING   TERRITORY
EASTING

LANDOWNER   CHECK THE FOLLOWING (Y/N)
ADDRESS   SPRING WELL OTHER
CITY PROV   PIEZOMETER/OBSERVATION WELL
TELEPHONE   GEOTECHNICAL BOREHOLE
SPRING YIELD M3/DAY

DATA AVAILABLE: TECHNICA   GEOLOGY AQUIFER WATER QUALITY

COMMENT 1
COMMENT 2

SCREEN 2

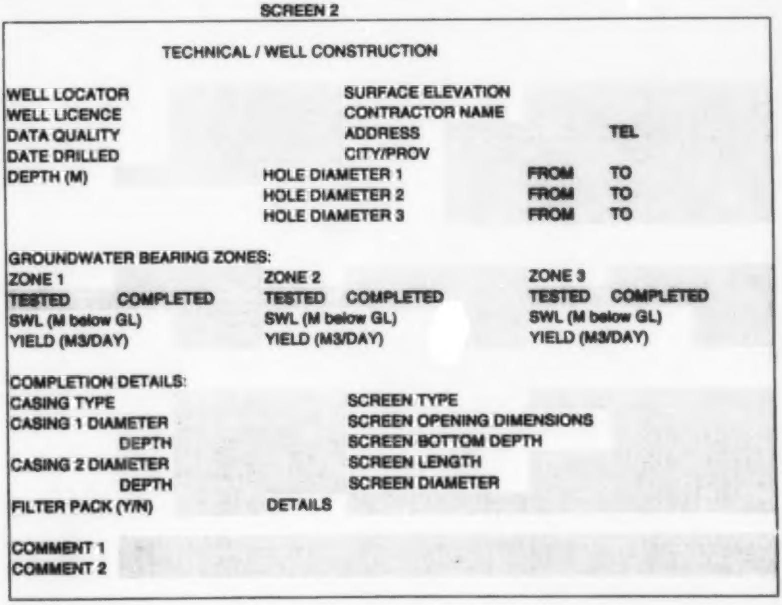

TECHNICAL / WELL CONSTRUCTION

WELL LOCATOR   SURFACE ELEVATION
WELL LICENCE   CONTRACTOR NAME
DATA QUALITY   ADDRESS TEL
DATE DRILLED   CITY/PROV
DEPTH (M)   HOLE DIAMETER 1 FROM TO
HOLE DIAMETER 2 FROM TO
HOLE DIAMETER 3 FROM TO

GROUNDWATER BEARING ZONES:

ZONE 1	ZONE 2	ZONE 3
TESTED COMPLETED	TESTED COMPLETED	TESTED COMPLETED
SWL (M below GL)	SWL (M below GL)	SWL (M below GL)
YIELD (M3/DAY)	YIELD (M3/DAY)	YIELD (M3/DAY)

COMPLETION DETAILS:
CASING TYPE   SCREEN TYPE
CASING 1 DIAMETER   SCREEN OPENING DIMENSIONS
DEPTH   SCREEN BOTTOM DEPTH
CASING 2 DIAMETER   SCREEN LENGTH
DEPTH   SCREEN DIAMETER
FILTER PACK (Y/N) DETAILS

COMMENT 1
COMMENT 2

Figure 2. Data-base display screens 1 and 2.

SCREEN 3

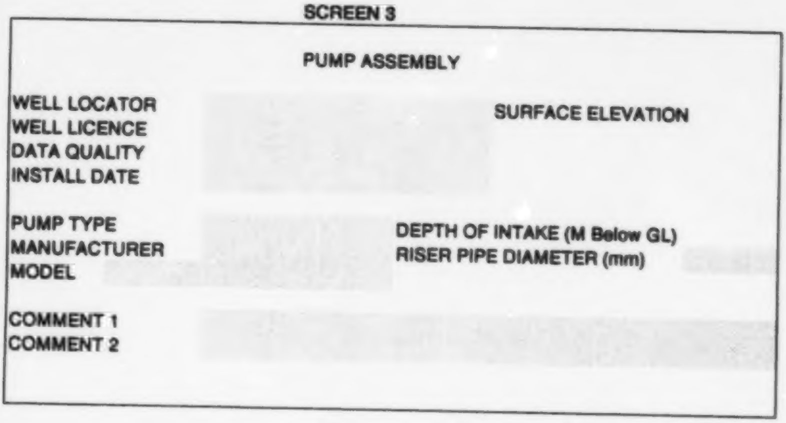

PUMP ASSEMBLY

WELL LOCATOR
WELL LICENCE
DATA QUALITY
INSTALL DATE

SURFACE ELEVATION

PUMP TYPE
MANUFACTURER
MODEL

DEPTH OF INTAKE (M Below GL)
RISER PIPE DIAMETER (mm)

COMMENT 1
COMMENT 2

SCREEN 4

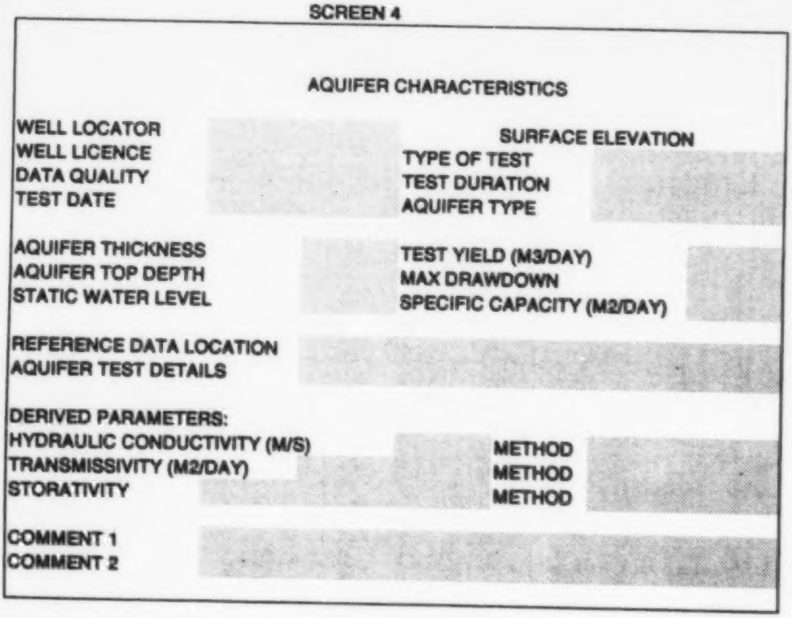

AQUIFER CHARACTERISTICS

WELL LOCATOR
WELL LICENCE
DATA QUALITY
TEST DATE

SURFACE ELEVATION
TYPE OF TEST
TEST DURATION
AQUIFER TYPE

AQUIFER THICKNESS
AQUIFER TOP DEPTH
STATIC WATER LEVEL

TEST YIELD (M3/DAY)
MAX DRAWDOWN
SPECIFIC CAPACITY (M2/DAY)

REFERENCE DATA LOCATION
AQUIFER TEST DETAILS

DERIVED PARAMETERS:
HYDRAULIC CONDUCTIVITY (M/S) METHOD
TRANSMISSIVITY (M2/DAY) METHOD
STORATIVITY METHOD

COMMENT 1
COMMENT 2

Figure 3. Data-base display screens 3 and 4.

SCREEN 5

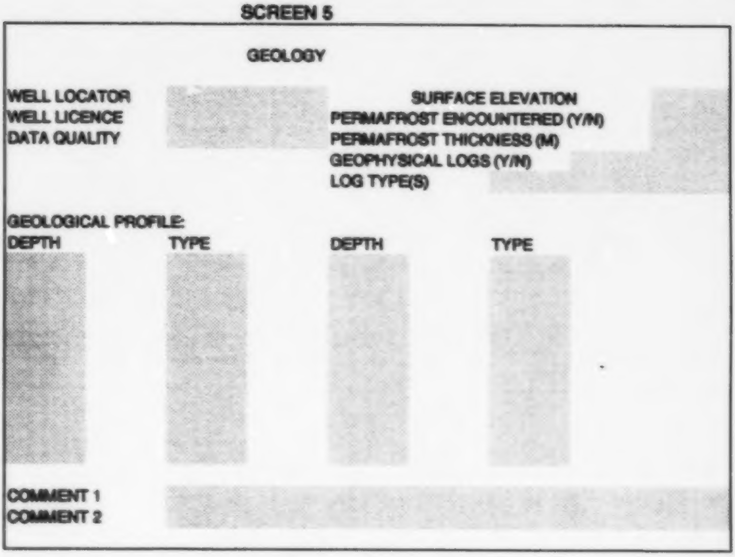

GEOLOGY

WELL LOCATOR
WELL LICENCE
DATA QUALITY

SURFACE ELEVATION
PERMAFROST ENCOUNTERED (Y/N)
PERMAFROST THICKNESS (M)
GEOPHYSICAL LOGS (Y/N)
LOG TYPE(S)

GEOLOGICAL PROFILE:

DEPTH	TYPE	DEPTH	TYPE

COMMENT 1
COMMENT 2

SCREEN 6

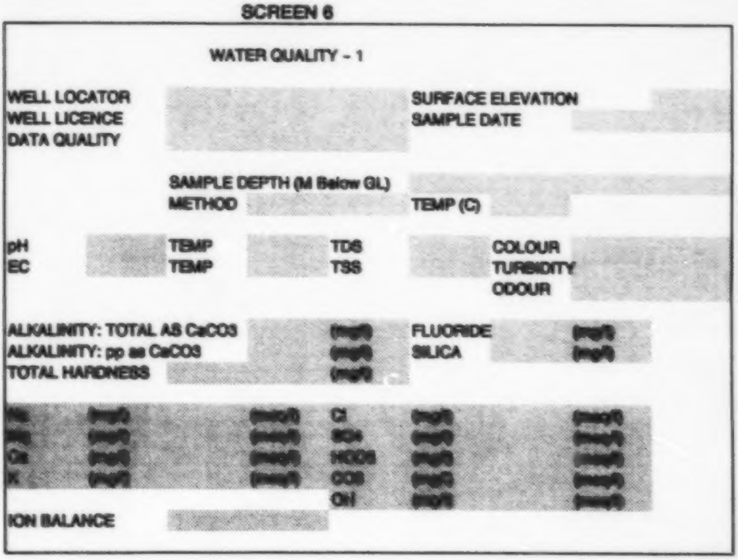

WATER QUALITY - 1

WELL LOCATOR
WELL LICENCE
DATA QUALITY

SURFACE ELEVATION
SAMPLE DATE

SAMPLE DEPTH (M Below GL)
METHOD
TEMP (C)

pH
EC
TEMP
TEMP
TDS
TSS
COLOUR
TURBIDITY
ODOUR

ALKALINITY: TOTAL AS CaCO3 (mg/l)
ALKALINITY: pp as CaCO3 (mg/l)
TOTAL HARDNESS (mg/l)
FLUORIDE (mg/l)
SILICA (mg/l)

Na	(mg/l)	(meq/l)	Cl	(mg/l)	(meq/l)
Mg	(mg/l)	(meq/l)	SO4	(mg/l)	(meq/l)
Ca	(mg/l)	(meq/l)	HCO3	(mg/l)	(meq/l)
K	(mg/l)	(meq/l)	CO3	(mg/l)	(meq/l)
			OH	(mg/l)	(meq/l)

ION BALANCE

Figure 4. Data-base display screens 5 and 6.

SCREEN 7

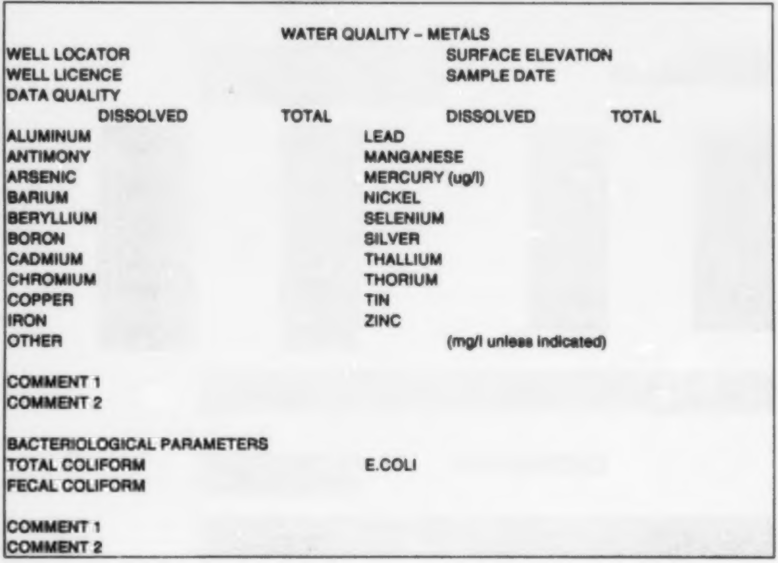

WATER QUALITY – METALS

WELL LOCATOR			SURFACE ELEVATION		
WELL LICENCE			SAMPLE DATE		
DATA QUALITY					
	DISSOLVED	TOTAL		DISSOLVED	TOTAL
ALUMINUM			LEAD		
ANTIMONY			MANGANESE		
ARSENIC			MERCURY (ug/l)		
BARIUM			NICKEL		
BERYLLIUM			SELENIUM		
BORON			SILVER		
CADMIUM			THALLIUM		
CHROMIUM			THORIUM		
COPPER			TIN		
IRON			ZINC		
OTHER				(mg/l unless indicated)	

COMMENT 1
COMMENT 2

BACTERIOLOGICAL PARAMETERS

TOTAL COLIFORM	E.COLI
FECAL COLIFORM	

COMMENT 1
COMMENT 2

SCREEN 8

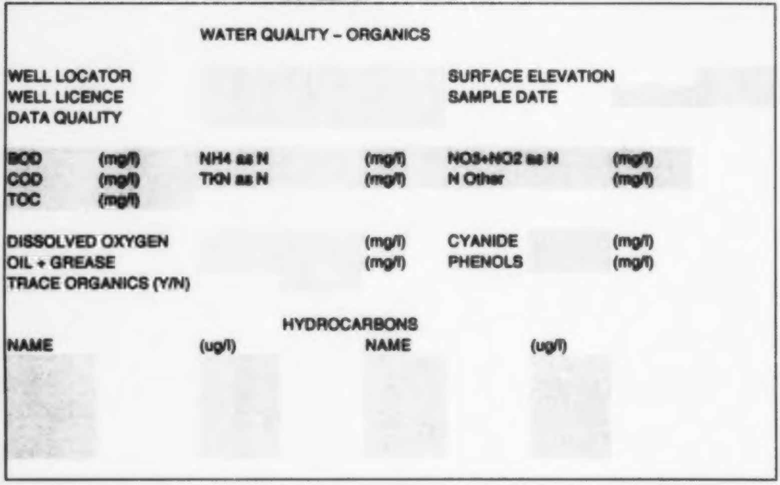

WATER QUALITY – ORGANICS

WELL LOCATOR	SURFACE ELEVATION
WELL LICENCE	SAMPLE DATE
DATA QUALITY	

BOD	(mg/l)	NH4 as N	(mg/l)	NO3+NO2 as N	(mg/l)
COD	(mg/l)	TKN as N	(mg/l)	N Other	(mg/l)
TOC	(mg/l)				

DISSOLVED OXYGEN	(mg/l)	CYANIDE	(mg/l)
OIL + GREASE	(mg/l)	PHENOLS	(mg/l)
TRACE ORGANICS (Y/N)			

HYDROCARBONS

NAME	(ug/l)	NAME	(ug/l)

Figure 5. Data-base display screens 7 and 8.

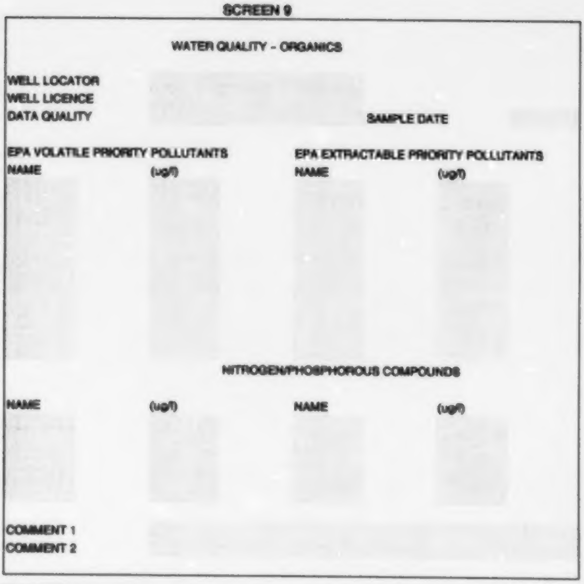

SCREEN 9

WATER QUALITY - ORGANICS

WELL LOCATOR
WELL LICENCE
DATA QUALITY
SAMPLE DATE

EPA VOLATILE PRIORITY POLLUTANTS

NAME	(ug/l)

EPA EXTRACTABLE PRIORITY POLLUTANTS

NAME	(ug/l)

NITROGEN/PHOSPHOROUS COMPOUNDS

NAME	(ug/l)	NAME	(ug/l)

COMMENT 1
COMMENT 2

Figure 6. Data-base screen 9.

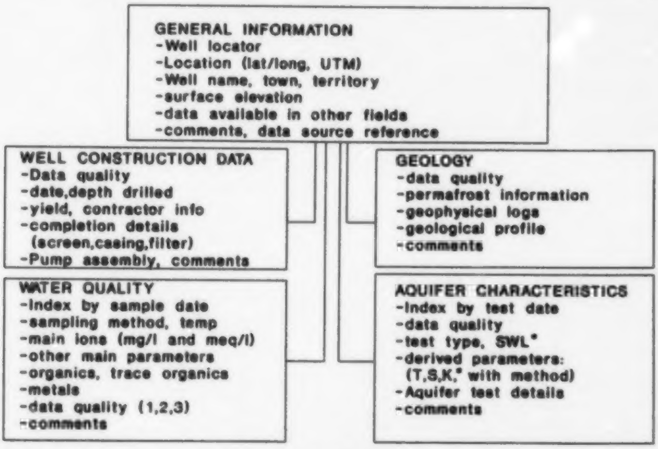
GENERAL INFORMATION
-Well locator
-Location (lat/long, UTM)
-Well name, town, territory
-surface elevation
-data available in other fields
-comments, data source reference
WELL CONSTRUCTION DATA
-Data quality
-date,depth drilled
-yield, contractor info
-completion details
(screen,casing,filter)
-Pump assembly, comments
GEOLOGY
-data quality
-permafrost information
-geophysical logs
-geological profile
-comments
WATER QUALITY
-Index by sample date
-sampling method, temp
-main ions (mg/l and meq/l)
-other main parameters
-organics, trace organics
-metals
-data quality (1,2,3)
-comments
AQUIFER CHARACTERISTICS
-Index by test date
-data quality
-test type, SWL*
-derived parameters:
(T,S,K,* with method)
-Aquifer test details
-comments

SWL = Static water level; T = Transmissivity; S = Storativity; K = Hydraulic Conductivity

Figure 7. Ground-water data-base schematic of data fields.

DATA

Data Collection

In conjunction with design and development of the data base, a data-collection programme was instituted to locate and gather all available hydrogeological data from Yukon and N.W.T. Sources of data included the National Hydrology Research Institute in Saskatoon, the Arctic Institute of North America, the Public Works Departments of Yukon and N.W.T., agencies of Territorial Governments, INAC and other federal government departments. Data from private sources were also collected. In total, this initial phase of data collection resulted in over 35,000 pieces of hydrogeological information, including geological/drilling logs, consultants' reports, water-quality analyses, and published papers. At present, the data base contains approximately 800 well and spring records, with the majority of the data coming from Yukon.

Future Data Collection

New data will be added to the data base as they become available. It is hoped that the data base will provide an incentive for concerned groups, agencies and companies to submit, on a voluntary basis, hydrogeological information which they may have available.

Data Quality Control

All data contained in the data base have been screened, checked, and rated for quality by a qualified hydrogeologist. This ensures users that data retrieved from the data base accurately reflect measurements recorded in the field or laboratory, and that erroneous data have been eliminated. All data are rated on a three-tiered scale, consisting of the categories "good", "fair", and "inferior". Each rating is assigned following specific guidelines based on such factors as sources and author of data, field techniques used, type and applicability of analyses, etc. Users can specify data quality as a search parameter, or use it as an indicator of data reliability.

Data Base Output

Data can be retrieved from the data base in the form of printed standard or custom reports, by modem link between computers, or as data files on floppy disc. The data base comes equipped with three standard reports, giving well-owner/location information, a basic water-quality report, and well-depth/yield data. Users also have the option of producing custom-made reports using add-on software provided with each master copy of the data base, which provides complete flexibility in data retrieval and sorting.

In the example shown in Table 1, the data base has been searched for all springs in the area of latitude 63°N and longitude 125°W in N.W.T. From these records, the spring yield, temperature, pH and chloride concentration of spring water have been printed. Table 2 presents the output of a data-base search for all wells or test holes in the Fort Smith region of the N.W.T. From these records, well depth, screen depth and length, static water level and a geological log are printed.

FUTURE OF THE DATA BASE

The design of the data base, using the dBase-IV system, allows for flexibility. Various peripheral data bases can be built to work with the existing one. Examples could include adding data bases for aquifer test data, literature references, ground-water use licences and applications, and ground-water monitoring/hazardous-waste site information. Hardware upgrading, say to the newer 386 or 486 machines, would greatly increase the speed of data-base processing and the number of data files easily accommodated within the data base. Upgrading to more powerful PCs can be accomplished without program modification. Data-base files are also designed for full compatibility with Geographic Information Systems (GIS).

APPLICATIONS

The data base and data-collection efforts described in this paper represent the first step towards creation of a comprehensive ground-water resource inventory for Yukon and N.W.T. As the importance of ground water as a source of domestic and industrial supply increases, and as concerns over ground-water conservation, protection from contamination, and aquifer remediation grow, this information will become steadily more valuable and of interest to more groups. Applications for the data base are seen in a wide variety of fields including permafrost hydrology, water-quality and water-balance studies, northern hydrogeology, resource management, environmental-impact assessment, and water supply.

Resource Management

If a ground-water regulatory body (such as those existing in each of the provinces of Canada and many states of the U.S.A.) is ever considered for either Yukon or N.W.T., the ground-water data base may form an integral part of such a group. In most other North American government bodies responsible for ground water, the maintenance of a ground-water data base is a key function.

The availability of a comprehensive hydrogeological data bank will provide regulators and policy makers with the necessary information on which to base more informed decisions on issues such as licensing of wells, regulation of ground-water use and aquifer protection.

Table 1. Results of data-base search produced in table format.

TABLE 1

SEARCH CRITERIA: All springs in area encompassed by Lat 63 and Long 125

LIST: Spring location, name, yield, temperature, pH and chloride content.

LOCATOR	NAME	LAT		LONG		YIELD m3/DAY	TEMP C	pH	Cl mg/l
		DEG	MIN	DEG	MIN				
NMR-1-S	SOUTH REDSTONE SPRING	63	24	125	52	1300.00	54	7.43	74.4
NMR-2-S	REDSTONE JCT SPRING #1	63	32	125	0	0.00			

Table 2. Results of data-base search produced in table format.

SEARCH CRITERIA: All wells in Ft. Smith region, NWT

LIST: Well depth, screen position, geological log

LOCATOR	NAME	LOCATION	WELL DEPTH (m)	SCREEN LENGTH (m)	SCREEN BOTTOM DEPTH (m)	GEOLOGICAL LOG	
						DEPTH (m)	SOIL TYPE
NFL-1	Ft. LIARD 1984 WELL	Ft. LAIRD	18.24	1.50	18.20	0.00	SILT
						4.90	GRAVEL
						10.00	SILT
						11.00	SAND AND GRAVEL
						18.20	SAND
						0.00	
						0.00	
						0.00	
						0.00	
						0.00	
NJMR-1	JEAN MARIE R. EXP WELL	JEAN MARIE RIVER	85.00	0.00	0.00	0.00	SAND AND SILT
						1.00	SILT AND SAND, PEBBLE
						3.60	GRANITE BOULDERS
						4.30	CLAY AND SILT, DRY
						5.80	DIABASE BOULDERS
						6.10	SAND AND SILT, MOIST
						6.80	SAND, SILT, CLAY
						12.20	SHALE, DRY
						0.00	
						0.00	
NLLM-1	LAC LA MATRE 1984 WELL	LAC LA MATRE	0.00	1.80	11.80	0.00	SILTY SAND
						6.70	TILL
						10.60	FRACTURED DOLOMITE
						0.00	
						0.00	
						0.00	
						0.00	
						0.00	
						0.00	
						0.00	

Ground-Water Exploration

The primary steps in any ground-water exploration program are independent of climate and location. Exploration efforts usually begin with a thorough review of all available information from the area in which drilling is proposed. This includes collection and review of all well records for the area (where this service is available), examination of maps, air photos, and any relevant publications or papers. These sources provide the hydrogeologist with an initial idea of where and at what depth ground water is most likely to be encountered, what flow rates and pressures can be expected, and what the quality of ground water is likely to be. Potential test-hole drilling sites can then be chosen and a field reconnaissance conducted to determine site access and geological suitability. The ground-water data base will provide explorers with quick access to available hydrogeological data.

General Hydrogeological Studies

Despite large strides over the past several years, large gaps in our understanding of northern hydrogeology remain. Van Everdingen (1990) identified several areas where research is required, including regional hydrochemical studies, the influence of ground-water chemistry on surface-water quality, and investigations of the role of permafrost barriers and seasonal freezing and thawing of aquifers on ground-water chemistry and flow. Although similar lists were made over fifteen years ago, these and other fundamental questions still require further study.

Many local and regional hydrogeological field surveys and general reconnaissance studies are available, including Brandon (1965) and Brook (1977, 1983). However, many areas of Yukon and N.W.T. remain unstudied.

Permafrost Hydrogeology

Permafrost has several unique properties which can affect such things as the way wells are drilled and completed, where and how ground water may be explored for and how ground water and solutes move through the subsurface. As ground freezes, a number of its physical properties change. One of the most important effects of freezing from a hydrogeological perspective is a marked decrease in hydraulic conductivity. As temperature declines, more interstitial water freezes, and effective porosity and permeability of the material are reduced.

A relatively-large body of literature exists on the nature of permafrost and the design and construction of engineering works in permafrost areas. Topics such as pipeline construction, slope stability, design of excavations, permafrost degradation and other geotechnical subjects have received a good deal of attention. However, the effects of permafrost on ground-water flow, water chemistry, and solute transport are still not fully understood.

The ground-water data base will provide an excellent means of quickly and efficiently accessing data on ground-water/permafrost systems. This facility may aid and stimulate further study in areas such as the effects of permafrost and partially frozen rock-soil media on ground-water chemistry, and the chemical behaviour of ground-water contaminants in frozen ground, among others.

Ground-water Contamination, Protection and Environmental Concerns

Ground-water contamination can occur as a result of many different activities. The concentration of large numbers of people and industrial operations in small areas often produces vast quantities of waste, from sewage effluent to household garbage to industrial by-products.

Deterioration of water quality is often the first impact felt as a result of improper waste disposal. Landfills, dumps, storage tanks and collection areas located on or near permeable geological formations, such as unconsolidated sediments or fractured and jointed bedrock, have the potential to contaminate ground water. Precipitation, snowmelt and run-off can percolate through uncovered material, leaching out and carrying away contaminants. Leaking containers and tanks can introduce liquids directly into the ground. Potentially dangerous substances stored in unlined pits or underground storage tanks, spread or spilled onto the ground may eventually make their way to the water-table and underlying aquifers.

Ground-water quality may also be impacted through agricultural operations, road construction and right-of-way maintenance. Chemical fertilizers, pesticides, herbicides, farm waste, and other chemicals can contaminate aquifers. Streams and lakes polluted by sewage or industrial effluents can affect aquifers with which they are in hydraulic connection.

The subject of contaminant hydrogeology has to date received little attention in Yukon and N.W.T. The large area and low population density of the territories seem to have buffered to some extent the impacts of ground-water pollution on the environment and ground-water users. This situation, as experience in many other parts of the world has shown, cannot be expected to continue indefinitely. Several instances of ground-water contamination in Yukon and N.W.T. have been identified recently, and it is expected that new cases will come to light with increasing frequency as the level of development in the North increases, and perhaps as contaminants buried or stockpiled over the last few decades begin to show up in ground-water seeps, springs and wells.

Examples of potential ground-water pollution which are coming to light include concern over waste-oil and industrial-liquids disposal, leaking gasoline service-station storage tanks, abandoned waste-disposal pits from the war and post-war years which may contain oils and pesticides such as DDT, herbicides and other chemicals; PCB-contaminated sites similar to those now causing concern in other parts of Canada; municipal landfills; and other sites.

Establishment of the data base is a necessary step in the development of effective ground-water protection strategies. With the help of the data base, problem areas can be defined and targeted for investigation, long-term trends in water quality can be examined, and records of all future investigation/remediation programmes can be compiled and compared. Two major ground-water contamination assessments at sites in Yukon have already made use of the data base. In each case consultants used available data to get an idea of local geology and background ground-water quality prior to designing site investigation programs.

Needs for Future Study

The following is a summary of hydrogeological topics identified as requiring additional study in Yukon and N.W.T.

- Regional and basin hydrogeological studies. Mapping of hydrogeological units, variation in water chemistry, expected yields, locations of springs and seeps, and water-balance calculations.
- Ground-water recharge processes, focusing on the role of permafrost and the behaviour of the active layer.
- Examination of the effects of permafrost on ground-water flow and quality.
- Review of current drilling and well-completion practices. Formulation of guidelines to promote sound practice and protection of aquifers.
- Examination of the use and effectiveness of various geophysical techniques in ground-water exploration in permafrost zones.
- Monitoring of key aquifers to determine long-term water-level and hydrochemical trends. This monitoring could determine if certain aquifers are being over pumped or contaminated, and if protection or prevention measures are required. Possible effects of climatic change on northern aquifers could also be assessed.
- Forecasting of long-term trends in ground-water use in Yukon and N.W.T. Estimation of expected changes in ground-water use over the next few decades, and recommendation of changes or precautions which will be required to provide for anticipated demands.
- Assessment of the implications of climatic change for ground-water resource management and protection in Yukon and N.W.T.
- Study of ground-water contamination and related subjects in Yukon and N.W.T. Of particular concern is the protection of current and future ground-water users from the adverse effects of aquifer pollution.
- Processes of contaminant advection and dispersion in frozen or partially-frozen ground.
- Behaviour of various common contaminants/solutes (such as chlorides, metals, organics) in frozen or partially-frozen ground.
- Effects of various contaminants on the arctic and subarctic environments.
- Aquifer remediation methods best suited to the arctic and subarctic environments.

SUMMARY

A computerized ground-water data-base system has been developed for Yukon and Northwest Territories. The data base has been designed for operation on a personal computer, and is available through the Department of Indian and Northern Affairs, Canada. The system accommodates a wide range of hydrogeological data, including well-construction information, aquifer-test data, geological logs, and water-quality data. Initial data collection and screening efforts have provided the data base with a foundation of approximately 800 well and spring records, representing a major portion of the currently available data. Efforts towards ensuring regular additions of new data are underway.

This data base represents the first comprehensive gathering of hydrogeological data for the Canadian North. Potential applications for the data base are seen in the areas of ground-water exploration and development, resource management and policy making, environmental impact studies, ground-water contamination studies, and aquifer protection. It is hoped that compilation of this data bank will promote interest in ground-water issues in the Canadian North.

REFERENCES

BRANDON, L.V., 1965. Groundwater hydrology and water supply in the District of Mackenzie, Yukon Territory, and adjoining parts of British Columbia. GSC Paper No.64-39, Geological Survey of Canada, Ottawa, Ontario, 102 pp. + 2 maps

BROOK, G.A., 1977. Surface and groundwater hydrology of a highly karsted sub-arctic carbonate terrain in northern Canada. In - Karst Hydrogeology, J.S. Tolson and F.L. Doyle (Editors), Proceedings, 12th International Congres, International Association of Hydrogeologists, UAH Press, Huntsville, Alabama, 99-108

BROOK, G.A., 1983. Hydrology of the Nahanni, a highly karsted carbonate terrain with discontinuous permafrost. Permafrost, Fourth International Conference, Proceedings, 17-22 July 1983, Fairbanks, Alaska, National Academy Press, Washington, D.C., 86-90

HESS, P.J., 1986. Ground-water use in Canada, 1981. NHRI Paper No.28, National Hydrology Research Institute, IWD Technical Bulletin No.140, Inland Waters Directorate, Environment Canada, Ottawa, Ontario, 43 pp. + maps

van EVERDINGEN, R.O., 1990. Ground-water hydrology. In - Northern Hydrology: Canadian Perspectives, T.D. Prowse and C.S.L. Ommanney (Editors), NHRI Science Report No.1, National Hydrology Research Institute, Environment Canada, Saskatoon, Saskatchewan, 77-101

SOME ASPECTS OF GLACIER HYDROLOGY IN CHINA*

Hu Xiaogang[1] and Yang Zhenniang[2]

[2]Lanzhou Institute of Glaciology and Geocryology
Chinese Academy of Sciences
Lanzhou, CHINA

[1,2]This paper was written while the author was a visiting scholar at the:
Department of Geography
McMaster University
Hamilton, Ontario
L8S 4K1 CANADA

ABSTRACT

The characteristics of continental- and maritime-type glaciers in China are reviewed. The former have lower accumulation and move slower than the latter. Energy-balance studies confirm that radiation, which increases with decreasing latitude and increasing altitude, is the most important component, followed by sensible heat. Maximum heat inputs were measured in the eastern Himalaya and Karakorum. Local factors affecting the regime are the glacier surface, albedo, topography, and the meso-climate.

The paper discusses the various indices developed to relate ablation to temperature, and to predict run-off. Run-off characteristics are partitioned within the basin according to ice-covered and ice-free areas, and values calculated. The total amount of glacier meltwater for western China is estimated at 563 x 10^8 m^3 from a glacierized area of more than 58,500 km^2.

INTRODUCTION

Outside of the polar regions, glaciers cover 22.4 x 10^4 km^2 of the earth's surface. About 12% of them are located in China (Wang, 1989). These thousands of glaciers occur over an extensive area that spans about 2,700 km (72° to 104°E) from east to west and about 2,400 km (27° to 49°N) from south to north. Generally, there are three characteristics of glacier distribution: (1) all of them are found in high mountains and plateaus in western China, (2) there are as many as 45,000 glaciers, most of which are valley glaciers, (3) they cluster in several mountain areas, including the Tian Shan, Kunlun Shan, Karakorum, Himalaya, Tanggula Shan, Nianqintanggura Shan, and Qilian Shan (Figure 1).

---

*This paper was presented by Dr. Yang Zhenniang as a theme paper on cold regions in China. Other theme papers from the circumpolar countries which were presented will appear in a companion volume entitled "Northern Hydrology: International Perspectives".

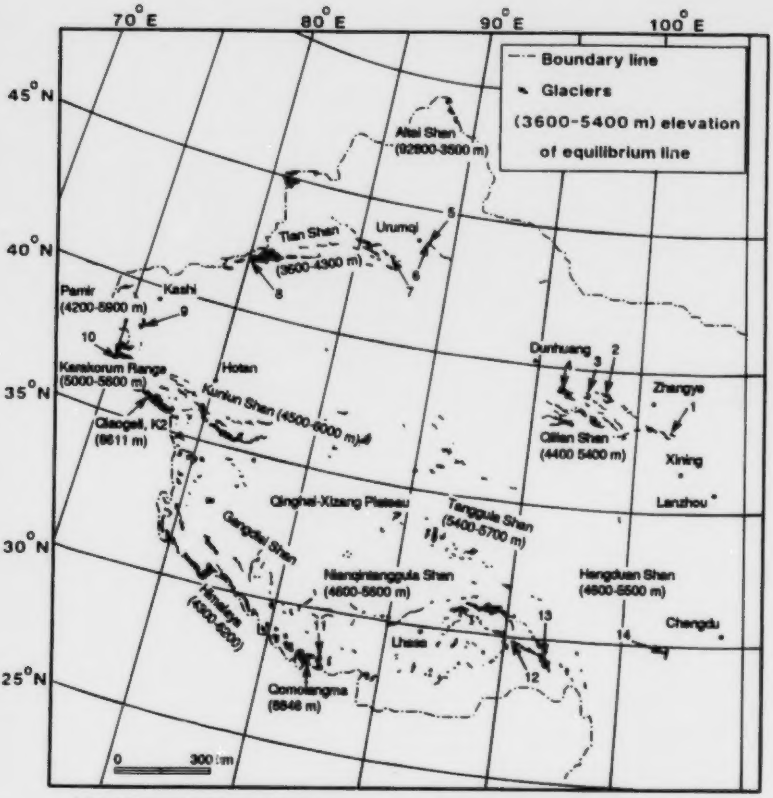
70° E
80° E
90° E
100° E
45° N
40° N
35° N
30° N
25° N
Boundary line
Glaciers
(3600-5400 m) elevation
of equilibrium line
Altai Shan
(92800-3500 m)
Tian Shan
(3600-4300 m)
Urumqi
Pamir
(4200-5900 m)
Kashi
Karakorum Range
(5000-5800 m)
Hotan
Kunlun Shan (4500-6000 m)
Qiaogeli, K2
(8611 m)
Dunhuang
Zhangye
Qilian Shan
(4400 5400 m)
Xining
Lanzhou
Qinghai-Xizang Plateau
Tanggula Shan
(5400-5700 m)
Gangdisi Shan
Nianqintanggula Shan
(4600-5600 m)
Hengduan Shan
(4600-5500 m)
Chengdu
Himalaya
(4300-6200)
Lhasa
Qomolangma
(8846 m)
1
2
3
4
5
6
7
8
9
10
11
12
13
14
0
300 km

1. No.4 Shuguanhe Glacier, Qilian Shan.
2. No.1 Yanglonghe Glacier, Qilian Shan.
3. Qiyi Glacier, Qilian Shan.
4. No.12 Laohugou Glacier, Qilian Shan.
5. Bogda North slope, Tian Shan.
6. Heigou Glacier, Tian Shan.
7. No.1 Tianshan Glacier, Tianshan
8. Qiongtailan Glacier, Tian Shan.
9. Qierbulake Glacier, Pamir.
10. Batura, Karakorum Range.
11. Rongbu Glacier, Qomolangma (Mt. Everest).
12. Guxiang Glacier, Nianqintanggula Shan.
13. Zhuxigou Glacier, Nianqintanggula Shan.
14. Gongga Glacier, Henduan Shan.

Figure 1. Distribution of glaciers in China.

Glaciers are classified in China into two types, depending on their thermal and physical characteristics. Most belong to the continental type, while the maritime-type glaciers occupy only a small area. The continental glaciers experience lower temperatures and receive less precipitation than the maritime ones which require abundant precipitation for their nourishment (Table 1). The flow velocity of continental glaciers in general is much lower than that of the maritime type (Li and Zhen, 1982; Huang *et al.*, 1988; Ren, 1989; Shi and Xie, 1964; Shi and Li, 1981; Yuan *et al.*, 1982; Xie *et al.*, 1982).

Table 1. Some hydrological and climatic difference between maritime-type and continental-type glaciers.

	MARITIME	CONTINENTAL
Temperature at EL	>-6.0°C	<-6.0°C
Precipitation at EL	1,200 to 3,000 mm	<1,000 mm
Englacial Temperature (10 m)	0.0°C	<0.0°C
Temperature Gradient	0.50 to 0.54°C/100 m	0.60°C/100 m
Precipitation Gradient	60 to 70 mm/100 m	<30 mm/100 m
Ablation Season	April to October	May to September
Glacier Terminum Elevation	about 3,000 m; minimum 2,400 m	about 4,000 to 5,000 m
Ablation Rate	3,500 to 10,000 mm·yr^{-1}	1,000 to 3,500 mm·yr^{-1}

EL = equilibrium line.

GLACIER MELT HEAT SOURCES

The surface energy balance of a melting glacier can be written as:

$$[1] \qquad Q_m + Q_n + Q_p + Q_l + Q_s = 0$$

where Q_m is the heat used to melt snow or ice, Q_n is the net radiation, Q_p is the heat convected by rain, Q_l is the latent heat flux, Q_s is the sensible heat flux. Q_n can be measured directly. Q_s and Q_l can be calculated by transfer equations assuming logarithmic profiles of air temperature, vapour pressure and wind speed (Kondo and Inoue, 1988). Q_m can be calculated from ablation-stake measurements. Q_p is usually considered to be small and has often been ignored in China.

Heat-exchange studies on mountain glaciers show the following general results.

1) The most important source of glacier melting is radiation, accounting for 59.0 to 92.1% of the total heat budget. This is followed by sensible heat which can contribute 6.6 to 35.4% of the total melt energy.

2) The composition of heat budgets has an obvious regional regularity. In regions with continental glaciers, such as the Qinghai-Xizang Plateau and its western flank, the radiative heat flux increases with decreasing latitude and increasing altitude. In the maritime glacier regions, the influence of moist air from southeastern and southwestern monsoons becomes more important and the percentage contribution of sensible heat increases. On Glacier No.4 Shuguanhe, in the Qilian Shan (continental-type), sensible-heat input is 2.92 $MJ \cdot m^{-2} \cdot d^{-1}$, but it is 5.39 $MJ \cdot m^{-2} \cdot d^{-1}$ on glacier No.3 Guxiang in the Nianqintanggula Shan (maritime-type). These represent 14.3% and 26.4% of their respective total energy inputs (Wang *et al.*, 1982). The minimum value of sensible heat of 0.95 $MJ \cdot m^{-2} \cdot d^{-1}$ (or 7.9%) occurs on Qieerganbulake Glacier in the Pamirs, an arid continental mountainous region. The latent heat of condensation is important mostly on maritime glaciers, due to the warm moist air, with the maximum value reported on Giuxiang Glacier (2.16 $MJ \cdot m^{-2} \cdot d^{-1}$ or 10.6%). The minimum value of 0.12 $MJ \cdot m^{-2} \cdot d^{-1}$ (or 0.9%) occurs on No.1 Yanglonghe Glacier in the middle part of the Qilian Shan (continental). Evaporation increases with aridity and elevation. Strong evaporation happens often in firn basins. On Qieerganbulake Glacier, evaporation accounts for about 4.97 $MJ \cdot m^{-2} \cdot d^{-1}$ or 41.5% of the total heat output.

3) A high value of incoming heat occurs in the regions of Nianqingtanggula, the eastern part of the Himalaya and the Karakorum. Here, total incoming energy reaches 20.52 to 25.96 $MJ \cdot m^{-2} \cdot d^{-1}$, of which 80 to 98% is used for glacier melting. The average ablation is 6.0 $cm \cdot d^{-1}$, representing the highest value in the middle latitude region (Bai, 1989; Bai and Yu, 1985) (Table 2).

Table 2a. Location and dates of studies.

#	GLACIER	MOUNTAINS	LOCATION		ELEVATION (m)	DATE
1	Qiongtailan	Tian Shan	41°45'N	80°17'E	4,000	July 1978
2	Qiongtailan	Tian Shan	41°45'N	80°17'E	4,000	July 1978
3	No.1 Tianshan	Tian Shan	43°06'N	86°49'E	4,830	Jun-Aug 1962
4	No.1 Tianshan	Tian Shan	43°06'N	86°49'E	3,810	July 1983
5	No.1 Yanglonghe	Qilian Shan	39°14'N	98°35'E	4,457	Aug 1977
6	No.4 Shuguanhe	Qilian Shan	37°30'N	101°40'E	4,200	Aug 1963
7	Qieerganbulake	Pamir	38°15'N	75°06'E	4,750	Jun-Jul 1960
8	Rongbu	Himalaya	28°12'N	86°51'E	5,440	May 1960
9	Rongbu	Himalaya	28°02'N	86°57'E	6,325	Apr-May 1966
10	No.3 Guxiang	Nianqintanggula Shan	29°55'N	95°30'E	4,400	Jul-Aug 1965
11	Batura	Karakorum	36°34'N	74°40'E	3,368	July 1974
12	Batura	Karakorum	36°35'N	74°24'E	4,475	Jul-Aug 1974

Table 2b. Surface type and heat inputs (numbers refer to same glaciers as in Table 2a).

#	SURFACE	NET RADIATION		SENSIBLE HEAT		CONDENSATION	
		MJ·m^{-2}·d^{-1}	%	MJ·m^{-2}·d^{-1}	%	MJ·m^{-2}·d^{-1}	%
1	Bare Ice	16.08	60.5	9.34	35.4	1.08	4.1
2	Debris-Covered	12.67	72.5	4.19	24.0	0.61	3.5
3	Firn	12.27	84.4	1.49	10.3	0.77	5.3
4	Dirty Ice	13.07	82.6	1.05	6.6	0.17	1.1
5	Ice Crust Snow	12.03	91.0	1.07	8.1	0.12	0.9
6	Bare Ice	16.85	82.7	2.92	14.3	0.61	3.0
7	Firn	11.05	92.1	0.95	7.9	--	--
8	Debris-Covered	23.05	94.6	0.72	2.9	0.59	2.5
9	Firn	3.94	--	0.80	--	--	--
10	Ice-Snow, Debris-Covered	12.84	63.0	5.39	26.4	2.16	10.6
11	Debris-Covered	24.46	96.6	0.66	2.6	0.20	0.8
12	Clear Ice, Dirty Ice	20.54	85.5	2.85	11.9	0.63	2.6

Table 2c. Ablation and heat output (numbers refer to same glaciers as in Table 2a).

#	ABLATION		SENSIBLE HEAT		EVAPORATION		OTHERS		BULK TRANSFER COEFFICIENT
	MJ·m^{-2}·d^{-1}	%	MJ·m^{-2}·d^{-1}	%	MJ·m^{-2}·d^{-1}	%	MJ·m^{-2}·d^{-1}	%	
1	21.69	81.6	--	--	4.90	18.4	--	--	1.068-2.587
2	6.64	38.0	5.51	31.5	5.32	30.5	--	--	--
3	12.80	88.1	--	--	1.73	11.9	--	--	0.222-0.473
4	14.78	93.4	--	--	1.05	6.6	-1.54	-9.7	0.318(mean)
5	10.84	82.0	--	--	1.82	13.7	0.56	4.3	0.695(mean)
6	17.35	85.1	--	--	1.94	9.5	1.09	5.4	0.167-0.716
7	6.77	56.4	--	--	4.97	41.5	0.26	2.1	0.134-0.230
8	8.45	34.7	6.08	24.9	7.75	31.8	2.08	8.6	--
9	--	--	--	--	--	--	--	--	--
10	19.76	97.0	--	--	0.63	3.0	2.32	9.1	1.080(mean)
11	19.77	78.1	0.71	2.8	2.52	10.0	0.4	1.7	--
12	20.92	87.1	0.07	0.3	2.63	10.9	-0.93	-4.3	0.511-0.800

4) The main factors affecting heat exchange on mountain glaciers are albedo, glacier surface regime, topography and local climate. The albedo varies greatly, between 0.81 and 0.12, depending on the glacier surface conditions (Table 3).

As the snow becomes ice, the albedo gradually decreases. Albedo is small in the ablation area, because of the dirty surface, the debris cover, and the uneven ablation (Zen and Cao, 1984). But when the debris cover exceeds some critical thickness, its insulation effect weakens the ablation. For example on Rongbu Glacier at Qomolangma, melt is enhanced when the debris-cover thickness is less than 2.0 cm, but melt is retarded when the thickness exceeds 3.0 cm (Xie, 1975). Another example is that a debris-cover thickness exceeding 10.0 cm causes the melt to be about 20 to 30% lower than a bare glacier surface, as shown at West Qiongtailan glacier in the Tian Shan (Su and Zhang, 1985).

In China, the following empirical relationship between glacier melt and run-off and energy balance is frequently used.

[2] $$Q = aQ_m^b$$

where Q is discharge from an experimental plot ($m^3 \cdot s^{-1}$), Q_n is an energy balance value ($MJ \cdot m^{-2} \cdot d^{-1}$) and, a and b are empirical coefficients.

Table 3. Albedo of different glacier surfaces in China.

	WESTERN QILIAN SHAN	TIAN SHAN	KARAKORUM
Elevation	4200 - 4700 m	3760 - 4220 m	2,660 - 5,000 m
Observation Time	1958-1977 (Apr - Aug)	1983 (July)	1974 (June - Aug)
Snow	0.806 - 0.941	0.806 - 0.957	0.730 - 0.810
Old Snow	0.498 - 0.785	0.511 - 0.790	0.456 - 0.714
Clean Firn	0.440 - 0.536	0.457 - 0.715	0.485 - 0.680
Clean Ice	0.309 - 0.461	0.336 - 0.529	0.323 - 0.388
Slight Dirty Ice	0.328 - 0.345	--	0.232 - 0.274
Dirty Ice	0.225 - 0.302	0.211 - 0.267	--
Strong Dirty Ice	0.122 - 0.185	0.146 - 0.221	0.109 - 0.168
Debris-Covered Ice	0.100 - 0.157	0.154 - 0.192	0.191 - 0.243

RELATIONSHIP BETWEEN ABLATION DEPTH AND TEMPERATURE

Although Equation 2 provides a useful relationship for run-off prediction, the value of Q_m is difficult to obtain. In China, temperature is often used as an index of the energy balance to obtain ablation rates (A; $mm \cdot d^{-1}$).

Rongbu Glacier (Himalaya):

[3] $A = 0.225\ (T + 4)^{2.7}$

No.4 Shuguanhe Glacier (Qilian Shan):

[4] $A = 0.281\ (T + 4)^{2.6}$

No.1 Tianshan Glacier (Tian Shan):

[5] $A = 0.242\ (T + 4)^{2.8}$

West Qiongtailan Glacier (Tian Shan):

[6] $A = 0.268\ (T + 4)^{2.6}$

The synthetic expression can be approximated as:

[7] $A = q\ (T + 4)^{2.7}$

where T is the temperature of the glacier surface (°C) and q is a coefficient reflecting the influence of climate conditions in different regions (Yang, 1982):

[8] $q = 0.382\ b^2$

where $b = Q_n/Q_t$, Q_n being the radiation-balance value and Q_t the total heat received during the melt season. When there is no direct measurement of temperature on the glacier, an approximate method is given by Khodakov (1975):

[9] $T_m = HdT/dH + T_o - J_t$

and:

[10] $\log J_t = 0.28 \log L - 0.07$

where H is the altitude difference between the meteorological station and the median elevation of the glacier (m), dT/dH the temperature gradient (°C/100 m), T_o the temperature at the station (°C), J_t the temperature jump, L the glacier length (km), and T_m the temperature at the median elevation of the glacier (°C).

GLACIER RUN-OFF PREDICTION

The snow on glacier surfaces begins to melt in late-April or early-May on continental-type glaciers, and in early-April on maritime-type glaciers. The melt is weak, and the meltwater is absorbed into the snow layers, and any run-off on the surface is arrested during the cold nights. As the season advances, the melt increases to sustain continuous run-off on the glacier surface; thus forming a network of channels. In smaller glaciers, the meltwater moves along the major channels which directly enter the streams. However, in larger glaciers, much of the water disappears into the glaciers through cracks and moulins, to emerge from under the terminus in one or more large streams. This outflow is sometimes maintained even during the winter (Yang, 1988), such as on the Qiongtailan Glacier (continental) and Gongga Glacier (maritime).

A glacierized basin can be divided into a glacier-covered and an ice-free area, so that the annual total run-off (R) is composed of:

[11] $R = R_i + R_b$

where

[12] $R_b = R_s + R_p$

and

[13] $R_i = R_{ss} + R_{sp} + R_{si}$

where R_i is run-off from the glacier, R_b is run-off from the bare slopes, R_s and R_p are snow-melt and rainfall run-off on bare slopes, R_{ss} is the snow and firn melt run-off on the glacier surface, R_{sp} is rainfall run-off on the glacier surface and R_{si} is glacier ice-melt run-off.

Daily melt run-off has a marked diurnal cycle, with the peak discharge arriving several hours after peak melt; and the time lag depends on the physical characteristics of the glacier and the distance of the glacier to the hydrological station. On small glaciers run-off drains quickly (Figure 2) but the regulating action of large glaciers is more pronounced and the daily fluctuation of discharge is much reduced (Figure 3).

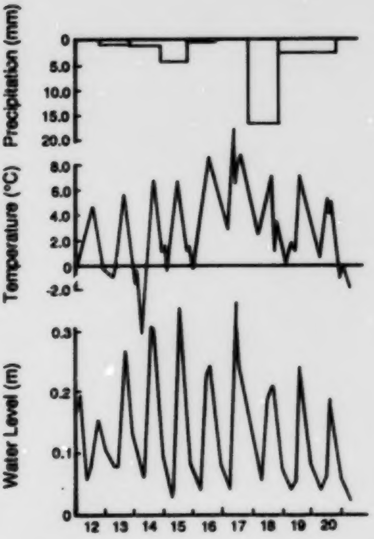

Figure 2. Daily variation in precipitation, temperature and water level at a gauging station below a continental glacier (No.1 Glacier, Tian Shan, June 1981).

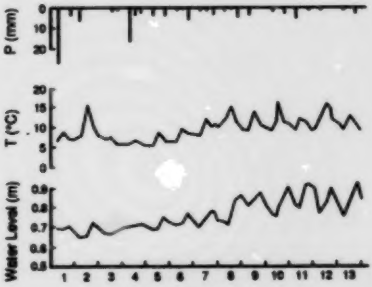

Figure 3. Daily variation in precipitation, temperature and water level at a gauging station below a maritime glacier (Gongga Glacier, Hengduan Shan, July 1982).

The synchronous variation between temperature and melting run-off discharge is more significant in continental(C)- than in maritime(M)- type glaciers (Figures 4 and 5), and the seasonal distribution of their discharge is shown in Table 4. To accommodate such differences, two kinds of relationship have been proposed:

$$Q = \alpha \exp(\beta \bar{\bar{T}}) \qquad [14]$$

$$Q = \gamma + \kappa \bar{\bar{T}} + \eta \bar{\bar{T}}^2 \qquad [15]$$

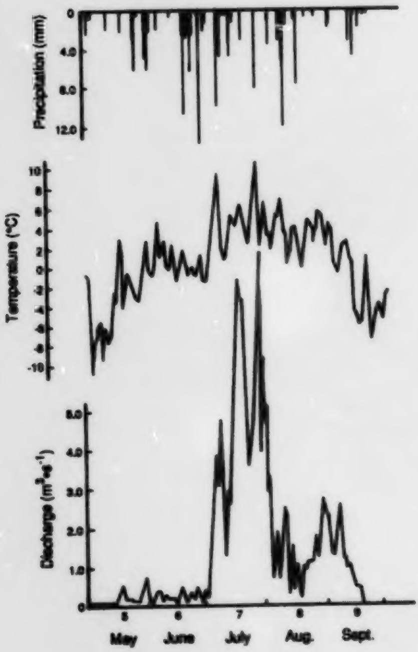

Figure 4. Daily variation in precipitation, temperature and discharge from a large continental glacier (Laohugou Glacier, Qilian Shan, 1982).

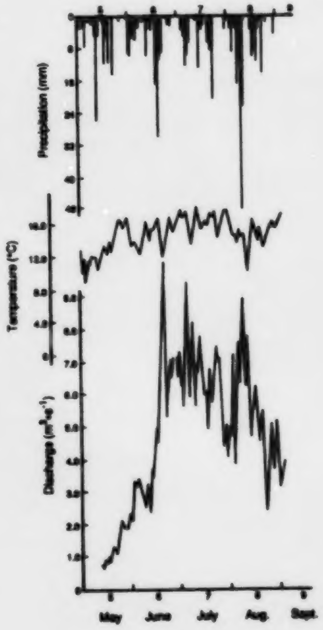

Figure 5. Daily variation in precipitation, temperature and discharge from a large maritime glacier (Guxiang Glacier, Nianqintanggula Shan, 1982).

where Q is the discharge ($m^3 \cdot s^{-1}$), $\bar{T}$ is the mean temperature on the glacier surface during a period (°C), and α, β, γ, κ, η are empirical coefficients (Kang, 1983; Hu, 1988; Yang, 1988; Li, 1985).

Table 4. Typical run-off distribution in melt season.

GLACIERS	MAY	JUNE	JULY	AUG	SEPT	JUNE-AUG	TYPE
	(%)	(%)	(%)	(%)	(%)	(%)	
No.12 in Qilian Shan	4.5	10.0	46.4	29.4	9.7	85.8	C
No.1 in Tian Shan	3.6	17.0	38.7	35.6	5.1	91.3	C
Quntailan in Tian Shan	7.6	19.5	31.3	29.8	11.8	80.6	sub-C
Rongbu in Himalaya	3.9	17.8	33.2	29.7	15.4	80.7	C
Gongga in Henduan Shan	17.0	16.8	24.9	23.8	17.5	65.5	M

These empirical relationships cannot be used to predict daily discharge if there is a strong time lag between daily temperature and discharge. An analysis of the data from Heigou Glacier (Tian Shan) showed that in early-summer, the lag is 3 to 4 days on average, but is reduced to one day after late-July or early-August (Hu, 1988).

The discharge can be treated as a stochastic process, so that the glacier-melt run-off process Q(t) can be separated using a linear model:

$$[16] \qquad Q(t) = \tau(t) + \rho(t) + D(t) + \xi(t)$$

where $\tau(t)$ is the trend component, $\rho(t)$ is the cyclical component, D(t) is the dependence component composition, and $\xi(t)$ is the random component. Both $\tau(t)$ and $\rho(t)$ are defined by solar radiation and can be eliminated. D(t) can be analysed by autoregression (Box and Jenkins, 1976). The following approach has been used:

$$[17a] \qquad Q(t) = \alpha_1 T(t-a) + \alpha_2 T(t-b) + \ldots + \xi(t)$$
$$\Phi_i(B^i)\, \xi(t) = \Theta_j(B^j)\, \varepsilon(t)$$

or

$$[17b] \qquad Q(t) = \alpha_1 T(t-a) + \alpha_2 T(t-b) + \ldots + \xi(t)$$
$$\Phi_i(B^i)\, \xi(t) = \Theta_j(B^j)\, \nabla \varepsilon(t)$$

where a,b,... are time lag (days), $\xi(t)$ is the error term, B is the transfer operator, $i = 1,2,\ldots p$, $j = 1,2,\ldots q$, $B\,\xi(t) = \xi(t-1)$, $B^j\,\xi(t) = \xi(t-j)$, ∇ the differential operator, $\nabla\,\xi(t) = \xi(t) - \xi(t-1)$, $\varepsilon(t)$ is the final residual error which is serially independent. Figure 6 shows a result of daily-discharge simulation using this method, applied to

Heigou Glacier. This example illustrates that the combination of a deterministic and a stochastic element can be used to forecast daily-melt discharge from a glacier (Hu, 1989).

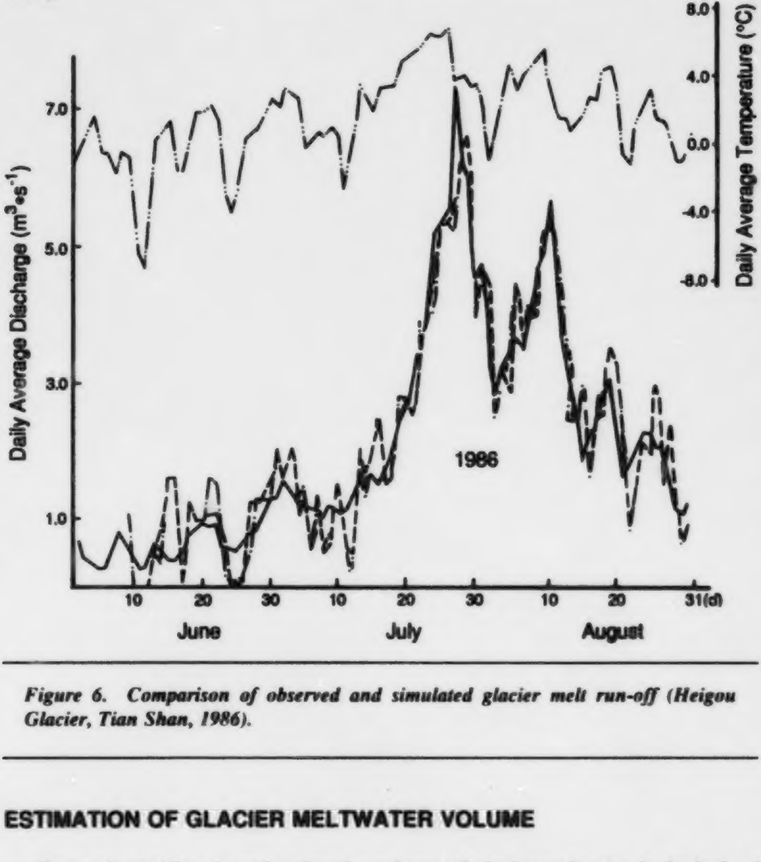

Figure 6. Comparison of observed and simulated glacier melt run-off (Heigou Glacier, Tian Shan, 1986).

ESTIMATION OF GLACIER MELTWATER VOLUME

One main problem in estimating the volume of glacier meltwater is the lack of hydrometeorological data. The glacier melt run-off (M_g in $m^3 \cdot s^{-1} \cdot km^{-2}$) can be defined as:

$$[18] \qquad M_g = W_g/(S\ T_a) = (W - W_b)/(S\ T_a)$$

where W_g is the glacier-meltwater amount (m^3), W is the total volume of water from the glacierized region (m^3), W_b is the run-off volume from the bare slope (m^3), S is the glacier area (km^2), T_a is the melt period (day). Typical run-off values (M_g) have been obtained from several glaciers in China (Table 5). M_g can be estimated from basins without direct measurement as follows:

$$[19] \qquad M_g = K[M_g' + [dH'(dT/dH) + dT'] dM_g/dT]$$

where K is the modification coefficient of the ablation area. $K = F_g/F_g'$. F_g are the percentage of ablation area for the glaciers where M_g is to be determined, and F_g' is that for the glacier where M_g' has been measured. dH' is the difference in the elevation of the equilibrium lines between the two glaciers. dT' is the temperature-modification value due to the climatic difference between the two glaciers (i.e., the temperature difference between two glaciers at the same elevation). dT/dH is the temperature lapse rate, usually equal to $-0.0065\ ^{\circ}C \cdot m^{-1}$. dM_g/dT is the increment of M_g with temperature, empirically found to be $5.0\ m^3 \cdot s^{-1} \cdot km^{-2} \cdot {}^{\circ}C^{-1}$. If two glaciers are located in the same climatic region, dT' = 0, and Equation 19 becomes:

$$[20] \qquad M_g = K [M_g' + dH'(dT/dH) (dM_g/dT)]$$

Table 5. The measured glacier meltwater from major mountainous regions in China.

#	MOUNTAIN	GLACIER	H (m)	F (km^2)	S (km^2)	H' (m)	F_g (%)	M_g ($m^3 \cdot s^{-1} km^{-2}$)
1	Qilian	No.4 Shuguanhe	3,760	2.88	1.36	4,500	28.0	53.0
2	Qilian	Qiyi	4,100	3.06	3.04	4,650	24.4	53.7
3	Qilian	Laohugou East	4,440	36.0	24.55	4,820	19.7	43.0
4	Qilian	Laohugou West	4,050	26.4	14.48	4,600	19.7	37.0
5	Tian Shan	Bogda North	--	--	24.44	3,809	45.0	56.1
6	Tian Shan	Urumqi No.1	3,690	3.34	1.95	3,780	22.0	39.9
7	Tian Shan	Qiongtailan	2,981	344.3	182.5	4,300	37.0	95.6
8	Pamir	Qieerganbulake	4,330	16.0	9.88	4,665	--	40.0
9	Himalaya	Rongbu	5,150	326.0	152.0	--	--	33.2
10	Nianqing	Guxiang	2,670	19.84	4.34	--	--	186.7
11	Tanggula	Zhuxigou	3,000	80.0	20.0	4,200	--	191.8
12	Hengduan	Gongga	3,620	78.04	41.89	5,100	0.27	110.1

For two glaciers located not only in the same climatic region but with similar elevation for their equilibrium lines the equation is therefore reduced to:

$$[21] \qquad M_g = KM_g'$$

The difference in M_g is caused only by the difference in the percentage of the ablation area.

Using Equations 18 and 19, the total volume of glacier meltwater is:

$$[22] \qquad W_g = 86.4\ M_g\ T_a\ S$$

The total amount of glacier meltwater for western China is estimated to be about 563 x 10^8 m^3. Table 6 summarizes the meltwater production for various mountainous regions.

Table 6. Distribution of glacier areas and the amounts of meltwater in different mountainous regions of western China.

#	MOUNTAINS	AREA OF GLACIERS		AMOUNT OF MELTWATER	
		km^2	%	(10^8 m^3)	%
1	Altai	293.20	0.5	3.85	0.7
2	Tian	9,195.98	15.7	95.92	17.0
3	Qilian	1,972.50	3.4	11.56	2.0
4	Kunlun	12,482.20	21.3	62.98	11.2
5	Pamir	2,992.85	5.1	17.05	3.0
6	Karakorum	4,647.17	7.9	28.71	5.1
7	Qiangtang Plateau	3,108.81	5.3	16.03	2.8
8	Tanggula	2,082.00	3.5	16.33	2.9
9	Gangdisi	1,667.75	2.8	8.88	1.6
10	Nianqintanggula	7,536.00	12.9	150.24	26.7
11	Hengduan	1,617.62	2.8	51.16	9.1
12	Himalaya	11,055.00	18.8	100.71	17.9
TOTAL		58,651.08	100.00	563.42	100.00

CONCLUSION

Glacier-hydrological research in China is mainly applied. The amount of glacier meltwater, the temporal and spatial variation of melt run-off, and the contribution to streamflow were, and still remain, the emphases of research. Basic glacier-melt characteristics, the major features of glacier-melt run-off, as well as indexing methods for melt and run-off estimation, have been established. Several problems remain to be addressed, however, including a better understanding of the dynamics of glacier melt, the movement of meltwater on, in and at the bed of glaciers, and how glacier hydrology will respond to global change. Models encompassing detailed energy and water balance will become increasingly important, and hence, future research should focus on the physical processes of glacier melt and meltwater run-off.

ACKNOWLEDGEMENTS

We are grateful to Dr. M.- K. Woo of McMaster University for his friendship, encouragement, advice and comments on this manuscript.

REFERENCES

BAI, Z. and X. YU, 1985. Energy exchange and its influence factors on mountain glaciers in west China. Annals of Glaciology, Vol.6, 154-157

BAI, Z., 1989. Radiation and heat balance on alpine glaciers in China. In - An Introduction to the Glaciers in China, Science Press, Beijing, 29-54

BOX, G.E.P. and G.M. JENKINS, 1976. Time series analysis: forecasting and control. Holden-Day, Toronto, 575 pp.

CAO, Z., 1988. The hydrologic characteristics of the Gongga glacier in Mt. Gongga area. Journal of Glaciology and Geocryology, 10(1), 57-65

HU, X. and N. LI, 1989. A stochastic meltwater run-off model of Heigou Glacier No.8 in the southern slope of Mt. Bogda. Journal of Glaciology and Geocryology, 11(3), 279-286

HU, X., 1989. Simulation of the stochastic processes of melt run-off from Heigou Glacier on Mt. Bogda, China. In - Snow Cover and Glacier Variations, S.C. Colbeck (Editor), Proceedings of Baltimore Symposium, 10-19 May 1989, IAHS Publication No.183. International Association of Hydrological Sciences, 61-70.

HU, X. and N. LI, 1988. The glacier melting run-off on south flank of Mt. Bogda. Journal of Glaciology and Geocryology, in press

HUANG, M., 1982. Some flow characteristics of continental-type glaciers in China. Journal of Glaciology and Geocryology, 4(2), 35-45

KANG, E., 1983. The glacier meltwater run-off on North flank of Mt. Bogda in Tianshan and its contribution to river flow. Journal of Glaciology and Geocryology, 5(3), 113-122

KHODOKOV, V.G., 1975. Glaciers as water resource indicators of the glacial areas of the USSR. In - Snow and Ice in Mountainous Areas, Proceedings of the Moscow Symposium, August 1971, IAHS Publication No.104. International Association of Hydrological Sciences, 22-29

KONDO, H. and J. INOUE, 1988. Heat balance on the icefield of San Rafael Glacier, the Northern Patagonia Icefield. Bulletin of Glacier Research (Japanese Society of Snow and Ice), No.6, 1-8

LI, J. and B. ZHEN, 1982. The characteristics of modern glaciers in Qinghai-Xizang Plateau. Bulletin of Glaciology and Geocryology (Glaciology), Science Press, Beijing, 14-17

LI, N., 1985. Characteristics run-off in the Glacier No.1 region at headwater of Urumqi river, Tianshan. Journal of Glaciology and Geocryology, 7(2), 163-170

REN, B., 1989. Present variation of modern glaciers in China. In - An Introduction to the Glaciers in China, Science Press, Beijing, 171-186

SHI, Y. and Z. XIE, 1964. The basic characteristics of modern glaciers in China. Journal of Geography, 30(3), 183-208

SHI, Y. and J. LI, 1981. Glaciological research of Qinghai-Xizang Plateau in China. Proceedings of Symposium on Qinghai-Xizang Plateau, Vol.2, Science Press, Beijing, 1589-1598

SU, Z. and W. ZHANG, 1985. The condition of glacier forming, amounts, distribution and form. In - Glaciers and Climate of Tuomuer Peak in Mt. Tianshan, XingJiang Press, Urumqi, 33-43

WANG, Z., Y. DENG *et al.*, 1982. The water-heat condition of the development of maritime glacier in Guxiang. Memoirs of Lanzhou Institute of Glaciology and Geocryology, Academia Sinica, No.3, 82-91

WANG, Z., 1989. Recent variation of glaciers and the influence of climate and glacier fluctuations in run-off in China. In - Snow Cover and Glacier Variations, S.C. Colbeck (Editor), Proceedings of Baltimore symposium, 10-19 May 1989, IAHS Publication No.183, International Association of Hydrological Sciences, 45-52

XIE, Z., 1975. The characteristics of glacier ablation on Rongbu Glacier. In - Glaciers and Landforms, Science Press, Beijing, 67-70

XIE, Z., B. ZHEN *et al.*, 1982. The distribution, features and variations of glaciers in China. Bulletin of Glaciology and Geocryology (Glaciology), Science Press, Beijing, 1-13

YANG, Z., 1988. Glacier water resources of Qilian Mountain. Journal of Glaciology and Geocryology, 10(1), 36-46

YANG, Z., 1982. Basic characteristics of run-off in glacierized area in China. In - Hydrological Aspects of Alpine and High Mountain Areas, J.W. Glen (Editor), Proceedings of the Exera Symposium, 19-30 July 1982, IAHS Publication No.138, International Association of Hydrological Sciences, 295-307

YANG, Z., 1989. Run-off from glacier melting water in China and its nourishment to rivers. In - An Introduction to the Glaciers in China, Science Press, Beijing, 187-204

YUAN, J., Z. WAN, Y. DENG and Z. KANG, 1982. Basic characteristics of maritime glaciers in Guxiang, Xizang. Bulletin of Glaciology and Geocryology (Glaciology), Science Press, Beijing, 21-22

MODELLED ESTIMATES OF CHANGES IN THE WATER BALANCE OF FORESTED NORTHERN RIVER BASINS

Yu.G. Motovilov and N.A. Nazarov

Water Problems Institute of the U.S.S.R.
Academy of Sciences
13/3 Sadovo-Chernogriazskaya, 103064
Moscow, U.S.S.R.

ABSTRACT

A forest-basin hydrological model, methods of analysis and verification of the model are considered. The water balance and river run-off component changes are estimated on the basis of numerical experiments for different areas of forest and spatial analysis in northern regions (case study of the Vologda River basin, area 1,270 km^2), northern European part of U.S.S.R. Conclusions are derived about the water-protection function of forests during a year by considering the possible influence of the forest on precipitation. As shown by numerical experiments, snowmelt and annual run-off are slightly sensitive to the major changes in forest area and their location in the watershed.

INTRODUCTION

Intensified human activity leads to changes in hydrological processes and water balances in northern river basins of the forest zone. Difficulties in investigating these hydrological systems are caused by the active human impact on natural processes and by specific conditions created by forest vegetation, which modifies the thermal and hydrological regime of the territories. Besides, the field-data and network observations are insufficient and cause problems when using traditional water-balance methods.

In this situation, forest-basin hydrological models, as a supplement to traditional methods, can be effective in solving many hydrological problems. (Kuchment *et al*, 1986.) Such a model is considered in the present paper. It was applied to estimating water-balance component changes relative to changes in forest area and their location in watersheds of the northern forest zone of the U.S.S.R. (Nazarov, 1988; Nazarov and Sirin, 1988).

*Paper not presented, review process not complete.

DESCRIPTION OF THE MATHEMATICAL MODEL

The model is based on a schematic simulation of the forest-basin system and hydrological processes taking place within its boundaries (Figure 1).

Interception

The rate of change in the depth of precipitation on the canopy (C) can be described by the equation:

$$\frac{dC}{dt} = \eta(R - E_\eta - \tilde{R}_p)$$

$$[1] \qquad E_\eta = \begin{cases} E_o, & C > C_{max} \\ E_o\,C/C_{max}, & C \leq C_{max} \end{cases}$$

$$\tilde{R}_p = \begin{cases} (C - C_{max})/\tau_o, & C > C_{max} \\ 0, & C \leq C_{max} \end{cases}$$

$$R_p = R(1 - \eta) + \tilde{R}_p$$

where C_{max} is canopy storage capacity; t = time variable; E_η = actual evaporation rate; E_o = free water or snow-evaporation rate; $\tilde{R}_p$ = net precipitation rate under the vegetation cover; R_p = total net precipitation rate; η = free through-fall coefficient; and, τ_o = characteristic time from the onset of precipitation (R) on the vegetation cover until its input to the watershed.

Snowpack Accumulation and Snowmelt

It is assumed that precipitation (R_p) contributes to snow accumulation if the air temperature T < 0°C. Otherwise, it is assumed that the precipitation is liquid and, together with snowmelt water, forms rain and snowmelt-water input (R_y) to the watershed. The snowmelt rate is calculated from the variable degree-day factor and air temperature (T). Computations of snow-water equivalent, snowcover depth (h), and its net-supply rate, are made separately for forest lands and fields, taking into account the changes in the snow-covered area, snow compaction, and changes in its water-holding capacity (Nazarov, 1988; Nazarov and Sirin, 1988).

Thermal Snow and Soil Regime

It is assumed that the vertical temperature profiles of the snow, frozen and thawed ground differ only slightly from linear, and the migration of the moisture to the

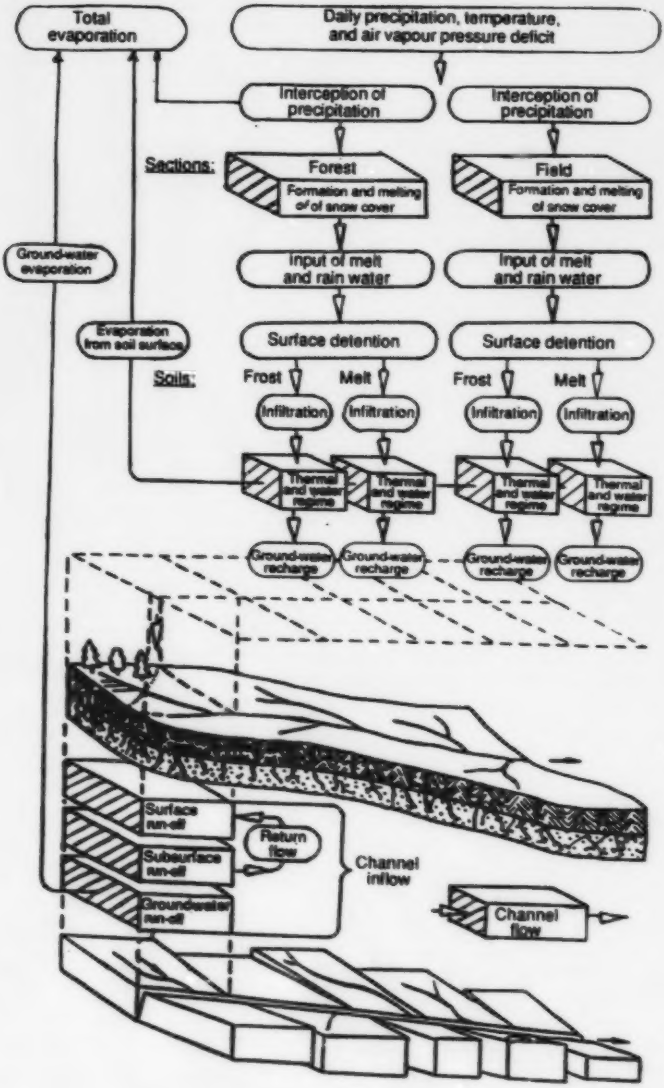
Total evaporation
Daily precipitation, temperature, and air vapour pressure deficit
Interception of precipitation
Interception of precipitation
Sections:
Forest
Formation and melting of of snow cover
Field
Formation and melting of snow cover
Ground-water evaporation
Input of melt and rain water
Input of melt and rain water
Evaporation from soil surface
Surface detention
Surface detention
Soils:
Frost
Melt
Frost
Melt
Infiltration
Infiltration
Infiltration
Infiltration
Thermal and water regime
Thermal and water regime
Thermal and water regime
Thermal and water regime
Ground-water recharge
Ground-water recharge
Ground-water recharge
Ground-water recharge
Surface run-off
Return flow
Subsurface run-off
Groundwater run-off
Channel inflow
Channel flow

Figure 1. Schematic of hydrological cycle of the northern basin in a forest zone.

freezing front is negligible. Under these conditions the soil-frost depth dynamics (H) can be described by the following equations (Nazarov and Sirin, 1988):

$$[2] \qquad \lambda_s \frac{T_s - T}{h} = \lambda_f \frac{T_f - T_s}{H}$$

$$[3] \qquad \rho_w \; L_i \, (\Theta - \Theta_u) \frac{dH}{dt} = \lambda_f \frac{T_f - T_s}{H} - \lambda_t \frac{T_g - T_f}{H_g - H}$$

and the soil thaw depth (H_t) can be described by the expression:

$$[4] \qquad \rho_w \; L_i \; \dot{I} \frac{dH_t}{dt} = -\lambda_t \frac{T_f - T_s}{H_s}$$

where λ_s, λ_f and λ_t are thermal conductivity in the snow, frozen and thawed soils, respectively; T_s = temperature at the "snow-soil" interface; T_f = soil temperature at the frozen front ($T_f = 0°C$); ρ_w, ρ_i are the density of water and ice respectively; L_i = latent heat of ice fusion; Θ = volumetric moisture content in a specified near-surface soil layer Z; Θ_u= unfrozen soil water content at 0°C; H_g = depth of ground-water level with a temperature T_g; and, $\dot{I}$ = volumetric ice content of soil, $\dot{I} = \rho_w \, (\Theta - \Theta_u)/\rho_i$.

Water Regime of Thawed and Frozen Soils

The rate of infiltration (J), soil water evaporation (E) and percolation (G) of gravitational moisture out of the lower soil-layer boundary (Z) is calculated using flow relationships and the water-balance equation:

$$[5] \qquad Z \frac{d\Theta}{dt} = J - E - G$$

$$J = \begin{cases} J_{max} & R_y > J_{max} \\ R_y, & R_y \leq J_{max} \end{cases}$$

$$E = \begin{cases} K_e \, d \, B \, (\Theta - \Theta_r)/(P - \Theta_r), & h = 0 \\ O, \; h > 0 \end{cases}$$

$$G = \begin{cases} J, & \Theta > \Theta_f \\ O, & \Theta \leq \Theta_f \end{cases}$$

where J_{max} = infiltration capacity of the soil; P, Θ_f, and Θ_r are porosity, field capacity and residual soil moisture, respectively; d = air vapour-pressure deficit; K_e = evaporation parameter; and B = weighting function of the forest species and age composition (Krestovskii, 1986).

The soil infiltration capacity (J_{max}) can be determined as:

$$[6] \qquad J_{max} = \begin{cases} \dfrac{K_o}{(1 + 8\bar{I})^2} \left(\dfrac{P - \bar{I} - \Theta_r}{P - \Theta_r} \right)^4, & \bar{I} > 0 \\[2ex] K_o^{\cdot} + \dfrac{K_s}{2(t - t')^{0.5}}, & \bar{I} = 0 \end{cases}$$

where $\bar{I} = \beta I$; β = frozen part of the soil layer Z; K_o = saturated hydraulic conductivity; and, t' = shift time, calculated similarly to the infiltration sorptivity (K_s) according to Eagleson (1978).

Transformation of Flow

The watershed area is divided into a number of large cells (LC), in which "ℓ" zones of rain- and snow-melt run-off formation are singled out: slope surface (ℓ = 1); subsurface soil layer with a developed root system (ℓ = 2) and a groundwater aquifer with waters drained by the stream network (ℓ = 3). Besides, the different order streams are distinguished in which transformation of channel flow occurs. Number and size of distinguished areas are defined by the LC area (F) structure and drainage-network density.

Transformation of the effective rain and snowmelt input (Y_ℓ) to the channel inflow (q_ℓ) on LC is computed using a system of equations:

$$[7] \qquad \frac{dS_\ell}{dt} = Y_\ell - q_\ell$$

$$[8] \qquad S_\ell = \tau_\ell \, q_\ell$$

where:

$$[9] \qquad \tau_\ell = \begin{cases} \dfrac{m}{(m + 1)} \left(\dfrac{n_s L_\ell}{i_\ell^{0.5}} \right)^m q^{m-1}, & \ell = 1 \\[2ex] \dfrac{(\bar{P} - \bar{\Theta}_f) L_\ell}{2 K_\ell \, i_\ell^{0.5}}, & \ell = 2 \\[2ex] \dfrac{\mu L_\ell}{2 K_\ell \, i_\ell}, & \ell = 3 \end{cases}$$

where S_j = detention storage; n_s = equivalent (for LC) Manning roughness coefficient for the slope surface; $m = 0.6$ for turbulent flow, μ = specific yield coefficient; K_j, $j = 2, 3$ = factor, characterizing the filtration properties of soils in the direction of relatively confining layer; i_j and L_j ($j = 1, 2, 3$) are the slope and characteristic channel-free slope length; $\bar{P}$ and $\bar{\Theta}_f$ are derived as the average parameters P and Θ_f over the LC area.

The effective water-input rate Y_j, $j = 1, 2, 3$ is evaluated for each of LC values as the average weighted value over the heterogenous area of flow formation:

$$[10] \qquad Y_j = \sum_{k=1}^{2} \sum_{i=1}^{2} f_k \, \varphi_{k,i} \, D_{k,i,j} \, \tilde{R}_{k,i,j}$$

where f_k is the fraction of the area occupied by forests or fields; D is the parameter roughly taking into account the surface detention and draining effects on the flow; φ = fraction of the area with frozen or thawed soils; and, $\tilde{R}$ = rate of water input into a homogeneous area:

$$[11] \qquad \tilde{R} = \begin{cases} R_y - J + R_R, & j = 1 \\ G_j, & j = 2,3 \end{cases}$$

where R_R = rate of return flow, which is formed due to the excess of the subsurface flow rate over the infiltration capacity of the specified soil layer (Z), averaged over LC area.

Equations 7 to 9 are the basis for the computation of the lateral inflow into the LC channel network and for the description of flow transformation in the channel streams. For modelling of unsteady water flow in the main river channel, the kinematic wave equations are used.

The differential equations with their respective initial and boundary conditions that are taken into account in the described model can be realized using numerical integration methods, or by finding preliminary analytical solutions in the form of recurrence formulae. A detailed description of the model and of logical relations between its blocks are given by Nazarov (1988) and Nazarov and Sirin (1988). They use a time step $\Delta t = 1$ day (0.2 day for numerical integration of kinematic-wave equations).

DETERMINATION OF THE PARAMETERS

Most of the model parameters are determined from maps. These are the morphometric characteristics of the slopes and channel network, characteristics of the vegetation cover and landuse. The stream length of partial watersheds of higher order is specified from maps and for the partial watersheds of lower order (1 to 3) from available drainage-network structure models (Strahler, 1957).

The channel-free slope length L_i, i = 1, 2, 3 in Equation 9 is determined as:

$$[12] \qquad L_i = F \Big/ \left(2 \sum_{n=NL}^{SL} A_n N_n\right)$$

where SL = network order; NL = smallest stream order taken into account for a given i, NL = 1, 2, ... , SL; and, A_n and N_n are the stream length and stream number of n-th order.

Hydrological constants of snow, ice, soils and thermal conductivities for different media, and the Manning roughness coefficient for the slopes and channels are determined from corresponding tables and diagrams. Filtration parameters and certain coefficients (e.g., in the formulae for computations of snow melting and evaporation) are derived from experimental estimates with subsequent refining of the estimates upon calibration of the model.

The spatial inhomogeneities and dynamics of a number of the drainage characteristics are described by distribution functions, for which statistical parameters are known. For instance, the gamma-distribution is used for spatial variability of the snow cover and for the area of frozen and thawed ground, whereas the exponential distribution is used for the active area at the expense of surface detention dynamics.

VERIFICATION OF THE MODEL

As a typical example of a northern plains river, we considered the Myagrino section of the Vologda River basin, in the forest zone of the European U.S.S.R. (Figure 2). The main characteristics of this basin are: area 1,270 km^2 with 65% forests, 1% lakes, 1% bogs, river length of 90 km and slope of 0.060%. Ground-water lies at a depth of 3 to 5 m, it rises to the surface in spring, as a rule. The spring flood provides about 60 to 70% of the annual run-off yield. The Vologda River and its tributaries are unregulated. The basin, with a river

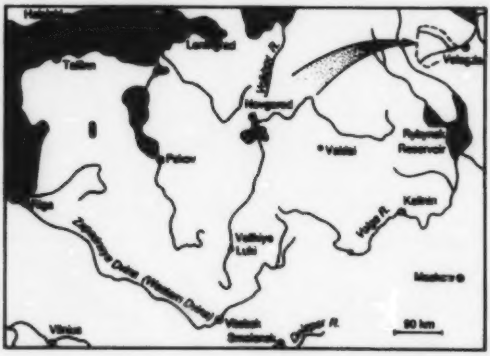
Helsinki
Leningrad
Tallinn
Volkhov R.
Vologda
Novgorod
Pskov
Valdai
Rybinsk Reservoir
Riga
Kalinin
Volga R.
Velikiye Luki
Zapadnaya Dvina (Western Dvina)
Moscow
Vilnius
Vitebsk
Smolensk
Dnieper R.
90 km

Figure 2. Location of the Vologda River basin.

network of 8-th order, was divided into 14 LC, mainly coinciding subwatersheds with tributaries, each being defined by their own topography, hydrographic network, soil and vegetation cover and land use. The thickness of the soil layer was taken as 0.60 m for the forest and 0.50 m for the field. The calculation period was one year beginning on October 1. The following field data were required: daily precipitation, air temperature and air vapour-pressure deficit. The possible influence of forest aerodynamics on the precipitation was taken into account by the introduction of a correction factor of 1.15 to the field rain-gauge data.

Examination of control results were performed using data on run-off, snow water equivalent, snow-cover depth and frozen-soil depth for forest lands and fields.

The model was calibrated against the hydrographs of rain and snowmelt run-off for years with different precipitation 1972 to 1974, and 1974 to 1984 - for test and numerical runs of the model. The calibration was performed using independent observational data. The computation results for the spring flood hydrograph of the Vologda River were considered in order to estimate more precisely some parameters (Nazarov 1988). The hydrograph calculations showed that after the transition from the calibration to the testing years the correlation coefficient decreased from 0.92 to 0.81, and the mean square deviation of calculation from the natural variability of discharge increased from 0.40 to 0.67. The error in calculations of snow water equivalent and snowcover depth differ only slightly from that of the hydrograph. The frozen soil depth simulation error was slightly higher.

An example of the simulation tests of hydrological processes are presented in Figures 3 and 4. In addition to the hydrographs (the ground-water component of the river run-off was taken into account), the observed snowcover and frozen-soil characteristics are compared with the calculated ones. The figures show results from modelling soil-moisture evaporation (against background of the observed air temperature), rain- and snowmelt water input and soil-moisture storage in the subsurface soil layer.

NUMERICAL EXPERIMENTS

Numerical experiments were carried out to estimate the forest-water protection and water-regulation function using the model for the Vologda River basin. In the first experimental series, the following scenarios were considered: field watershed (no forest, $f_2 = 0\%$); uniform forest area of the watershed (FAW) with $f_2 = 50\%$, natural FAW ($f_2 = 65\%$); and, the total forest cover on the watershed ($f_2 = 100\%$). It was considered that coniferous, deciduous and mixed vegetation occupied 20, 30 and 50% of forest area, respectively. The age of the forest is 30 to 40 years. Initial and boundary conditions were taken without changes.

The estimates of water and river run-off components for the Vologda River basin are given in Table 1. They show that the increase in FAW leads to:

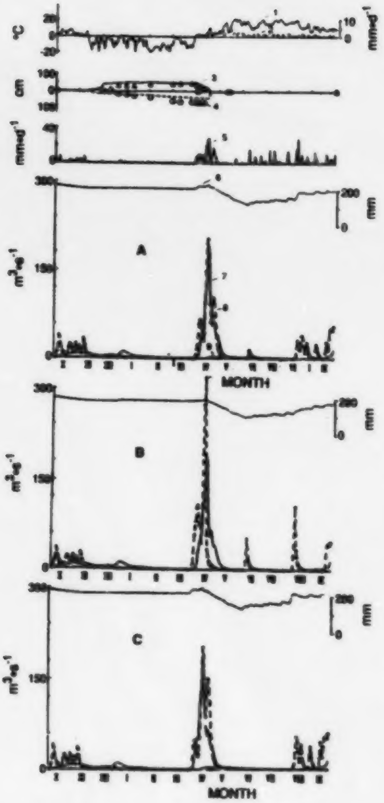

Figure 3. Characteristics of hydrometeorological processes, the Vologda basin, 1980 to 1981.

1 = air temperature, 2 = evapotranspiration, 3 = snow depth, 4 = frozen soil depth, 5 = input of rain- and meltwater onto the surface basin, 6 = soil moisture, 7 & 8 = observed and calculated hydrographs, 9 = ground-water flow. A = natural FAW, B = FAW is 0%, C = FAW is 100%.

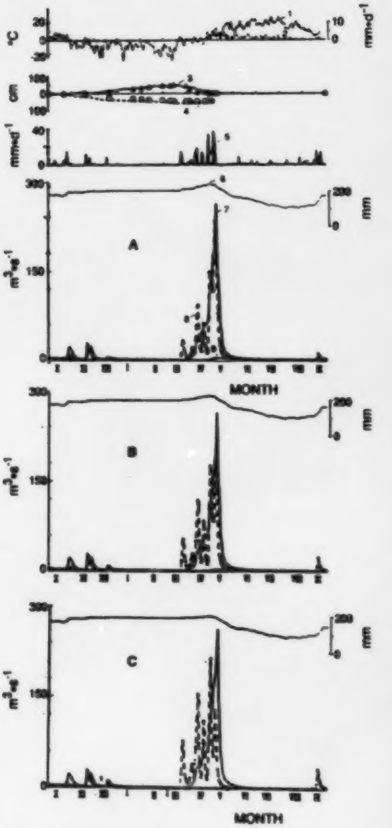

Figure 4. Characteristics of hydrometeorological processes, the Vologda basin, 1983 to 1984.

1 to 9 = same as Figure 3. A = natural FAW, B = forest is in the upper part of the basin (f_2 = 45%), C = forest is in the lower part of the basin (f_2 = 20%).

Table 1. The influence of forest area on water-balance and river-run-off components (case study of the Vologda River basin). First experimental series.

	f_2	R^*	E^*	ΔW	y	y_s	y_{ss}	y_g	y_m	y_{ll}	y_{lg}	Q_{max}
	%	mm										$m^3 \cdot s^{-1}$
1980	0	480	296	-47	268	206	14	48	182	7.4	7.0	241
	50	516	314	-32	272	123	92	57	202	11	10	203
	65	528	321	-27	$\frac{271}{315}$	109	102	60	$\frac{223}{248}$	$\frac{12}{12}$	11	$\frac{235}{264}$
	100	552	333	-17	272	65	142	65	211	15	14	307
1981	0	596	349	-11	266	168	68	30	198	6.2	5.4	235
	50	641	365	8	280	91	149	40	214	13	8.2	154
	65	656	370	14	$\frac{280}{280}$	75	162	43	$\frac{214}{198}$	$\frac{15}{22}$	9.5	$\frac{179}{143}$
	100	686	382	27	286	30	207	49	198	19	11	225
1984	0	622	378	-34	267	181	70	16	157	15	2.1	319
	50	669	399	-31	292	96	171	25	165	11	4.1	226
	65	684	406	-30	$\frac{296}{220}$	76	191	29	$\frac{165}{149}$	$\frac{10}{25}$	5.0	$\frac{202}{188}$
	100	716	420	-27	310	25	251	34	169	7.4	6.6	201

Denominator denotes measured characteristics.

- a growth of total annual evaporation (E^*) caused by an increase in soil moisture with a possible increase in precipitation depth (R^*) above the forest canopy. In this case the water which is intercepted by forest and herbaceous vegetation varies from 9 to 13%;
- an increase in the annual soil-water storage increment (ΔW) due to the increase in precipitation as compared to the evaporation in the forest (the forest promotes the moistening of the basin);
- a tendency to an increase in annual run-off (y) for 1980, 1981 and 1984 by 2, 8 and 10%, respectively (water-protection function of the forest);
- a sensitivity of river run-off components to changes in FAW: the increase in FAW results in a 2 to 6-fold decrease in the surface run-off component (y_s), while the subsurface (y_{ss}) and ground-water (y_g) components increase 1.5 to 10 times. Thus, experiments confirm that the forest on the watershed transfers fast surface flow into the slower underground one (water-regulation function of the forest);
- a slight increase in the snowmelt run-off (y_m), (not more than 12%), but for high FAW ($f_2 \rightarrow 100\%$) it can decrease (e.g., hydrometeorological conditions

of 1980 and 1981). We explain this by a possible increase in precipitation and maximum snow-water equivalent in the forest. The decrease in (y_m) at $(f_2 \rightarrow 100\%)$ can be explained by transfer of a significant part of snowmelt water into underground water through the relatively slightly frozen forest soils;

- a 1.5-fold decrease in maximum water discharges of snowmelt run-off in 1984. It is caused mainly by less intensive snowmelt and the input of snowmelt water to the surface of the basin in the forest as well as by the water-regulation function of forest soils. For snowmelt run-off in 1980 and 1981, Q_{max} tended to decreases with the increase in FAW. This is caused by the differences in snowmelt duration in the forest versus field parts of basin. It promotes the formation of an extended multipeak snowmelt run-off hydrograph on the partly forested watershed. The increase in Q_{max} at $(f_2 \rightarrow 100\%)$ can be explained by simultaneous snowmelt over the watershed. It is interesting that the single peak hydrographs are usually formed at $(f_2 \rightarrow 100\%)$; and,
- a decrease in the low flow depth in June to July $(y_{l,f})$ of 1980 and 1981. It is caused by the transfer of a considerable part of the snowmelt water to underground storage and its subsequent decrease. The ground-water component $(y_{l,g})$ prevails in the low flow and $y_{l,g}$ has a pronounced tendency to increase (up to 1.5 to 3 times) with the increase in FAW. Considerable precipitation fell during the period of low flow in 1984, so the calculated ground-water component of run-off was not high.

It is known (Nazarov and Sirin, 1988) that some specialists question the increase in precipitation above the forest canopy. For that reason, a second experimental series was made. It differed from the first without the precipitation correction factor, which was taken as 1.0, i.e., precipitation above the forest equalled that measured in the field. The analysis showed that the main tendencies in the water-balance component changes in the forest watershed are the same for both series, but there are still some differences. If the correction factor is 1.0, the calculated annual river run-off decreases (approximately by 10%) with the increase (from 0 to 100%) in FAW. This is caused mainly by an increase in evapotranspiration in the forest. The snowmelt run-off changes slightly. So if, in the first experimental series, minimal values of y_m were fixed at $f_2 = 50\%$ for snowmelt of 1980 and 1981, in the second series they were fixed at the natural FAW level $(f_2 = 65\%)$.

The water-balance and river run-off components were also studied in a third experimental series for the following forest locations: 1) forest in the upper part of watershed; and, 2) forest in the lower part of watershed (equal to the upper one). It was assumed that FAW on the areas of "non-felled" forest corresponded to the natural FAW. As a result, the average FAW for whole catchment area was 45% in the first case and 20% in the second (Table 2). The correction factor, which takes into account the effect of forest on precipitation, was equal to 1.15. Calculations show (Figure 4) that the impact of forest disposition and FAW (f_2) corresponds to the modelling results discussed above and modern ideas. With the increase in FAW in the second test, the changes in water-balance structure slightly influences the

Table 2. The influence of forest area and its location on change in water-balance and river-run-off components. Third experimental series.

	Forest in the upper part of basin			Forest in the lower part of basin		
	1980	1981	1983	1980	1981	1983
R^*, mm	513	639	665	494	615	641
E^*, mm	313	364	398	306	356	387
ΔW, mm	-33	7	-31	-40	-4	-33
y, mm	268	274	286	270	273	277
y_s, mm	140	103	108	163	140	149
y_{ss}, mm	72	132	153	55	99	108
y_g, mm	56	39	25	52	34	20
y_l, mm	11	12	11	9	8.7	14
y_{lg}, mm	10	8.3	4.1	8.7	6.6	2.9
y_m, mm	194	206	161	190	206	157
Q_{max}, $m^3 \cdot s^{-1}$	184	161	228	215	210	284

growth of the mean watershed precipitation (by 3 to 4%), evapotranspiration (by 2 to 3%) and soil moisture (by 12 to 18%). Total annual river run-off yield (y) does not actually change with the simultaneous decrease in the overland component y_s (by 14 to 26%) and increase in subsurface and ground-water flow (y_{ss} + y_g). A similar trend is pointed out for the low (y_{lf}) and snowmelt (y_m) flow. "De-forestation" of the lower part of the watershed has a considerable effect on the decline of the snowmelt run-off peak (Q_{max}) (by 15 to 23% for different hydrometeorological situations). Calculations show that the decrease in Q_{max} is caused, first, by the increase in the mean FAW and, second, by the forest distribution in the upper part of the watershed (as was shown by the modelling examples for watersheds in the north-west of the U.S.S.R. (Nazarov and Sirin, 1988). When the forest is far from the gauge, the lag time between melt-water and rain-water inflow to the drainage system increases. The additional transformation of the run-off wave occurs in the river network.

SUMMARY

The numerical experiments carried out with this model do not contradict the field experiments and observations of the forest-water protection function in the north of the European U.S.S.R. In accordance with modelling results, an expansion of the forest and area promotes:

- an increase in maximum snow water equivalent and a decrease in frost depth in forest soils characterized by high permeability;
- transfer of a considerable part of the rain- and melt-water into underground storage and additional moistening of the soil;
- an increase in evapotranspiration and interception; and,
- an increase in the underground-flow component with a simultaneous decrease in the surface-run-off component on the watershed slopes.

Further investigation of man-induced changes to the water balance in northern forest watersheds should be aimed at increasing the accuracy of the calculation methods of annual and snowmelt run-off. As was shown by our investigations for middle-area watersheds, these hydrological characteristics are slightly sensitive to considerable changes in the forest area and its distribution in the watershed. Whether the changes in these characteristics are within the range of calculation errors can only be better assessed following careful natural experiments.

LIST OF SYMBOLS

A_n	stream length of n-th order (m, km)
B	weighting function of the forest species and age composition
C	depth of water on the canopy (m, mm)
C_{max}	canopy storage capacity (m, mm)
D_k, D_i, D_l	detention parameter
d	air vapour pressure deficit (mb)
E	rate of evaporation from the soil (m·s^{-1}, mm·d^{-1})
E_o	potential evaporation rate (m·s^{-1}, mm·d^{-1})
E_η	rate of evaporation of interception water (m·s^{-1}, mm·d^{-1})
E^*	total annual evaporation (m, mm)
F	fraction of watershed area (m^2, km^2)
f_k	fraction of the area with fields (or forests)
G	percolation rate (m·s^{-1}, mm·d^{-1})
H	soil frost depth (m, cm)
H_g	ground-water depth (m, cm)
H_t	soil thaw depth (m, cm)
h	snow depth (m, cm)
$\dot{I}$	volumetric ice content in the frozen soil
i	slope
J	infiltration rate (m·s^{-1}, mm·d^{-1})
J_{max}	infiltration capacity (m·s^{-1}, mm·d^{-1})
K_e	parameter of evaporation (m·s^{-1} mb, mm·d^{-1} mb)
K_l	parameter of filtration (m·s^{-1}, mm·d^{-1})
K_o	saturated hydraulic conductivity (m·s$^{-0.5}$, mm·d$^{-0.5}$)
K_s	infiltration sorptivity (m·s^{-1}, mm·d^{-1})

L_i	latent heat of ice fusion ($J \cdot kg^{-1}$)
L_i	channel - free slope length (m)
m	flow-regime factor
N_n	stream number of n-th order
NL	smallest stream order
n_s	Manning roughness coefficient ($s \cdot m^{-0.33}$)
P	porosity
$\bar{P}$	average P over the area
Q_{max}	maximal discharge ($m^3 \cdot s^{-1}$)
q_i	lateral inflow to the channel ($m \cdot s^{-1}$, $mm \cdot d^{-1}$)
R	rate of precipitation measured on the field area ($m \cdot s^{-1}$, $mm \cdot d^{-1}$)
R_R	return flow rate ($m \cdot s^{-1}$, $mm \cdot d^{-1}$)
R_p	total net precipitation rate ($m \cdot s^{-1}$, $mm \cdot d^{-1}$)
R_y	rate of water input (rain + snowmelt) into watershed ($m \cdot s^{-1}$, $mm \cdot d^{-1}$)
R^*	total annual precipitation (m, mm)
$\bar{R}$	rate of water input into homogeneous area ($m \cdot s^{-1}$, $mm \cdot d^{-1}$)
$\bar{R}_p$	rate of net precipitation under vegetation cover ($m \cdot s^{-1}$, $mm \cdot d^{-1}$)
S_i	detention storage (m, mm)
SL	network order
T	air temperature
T_f	temperature at the bottom of frozen soil layer (T_f = 0°C)
T_g	groundwater temperature (°C)
T_s	soil surface temperature (°C)
t	time (s, d)
t'	shift time (s, d)
Y_i	effective water-input rate ($m \cdot s^{-1}$, $mm \cdot d^{-1}$)
y	total annual run-off (m, mm)
y_g	annual ground-water run-off component (m, mm)
y_{if}	low flow (m, mm)
y_{ig}	ground-water component of the low flow (m, mm)
y_s	annual surface run-off component (m, mm)
y_{ss}	annual subsurface run-off component (m, mm)
Z	depth of the active soil layer (m)
β	frozen part of soil layer
ΔW	change in the soil moisture for the year (m, mm)
η	free through-fall coefficient
Θ	volumetric soil moisture
Θ_f	volumetric field capacity of the soil
Θ_r	volumetric residual soil moisture
Θ_u	volumetric liquid (unfrozen) content in the frozen soil at 0°C
$\bar{\Theta}_f$	average Θ_f over the area
λ_f	thermal conductivity of the frozen soil ($W \cdot m^{-1} \cdot s$)
λ_s	thermal conductivity of the snow ($W \cdot m^{-1} \cdot s$)
λ_t	thermal conductivity of the unfrozen soil
μ	specific yield coefficient
ρ_i	density of ice ($kg \cdot m^{-3}$)
ρ_w	density of water ($kg \cdot m^{-3}$)

τ_l	lag time (s, d)
τ_o	drainage parameter of interception equation (s, d)
φ_k, φ_i	fraction of the area with frozen (thawed) soil

Indexes denote:

k=1 field area
k=2 forest area
i=1 thawed soil
i=2 frozen soil
$\ell=1$ surface slope
$\ell=2$ active soil layer
$\ell=3$ ground-water aquifer

REFERENCES

EAGLESON, P.S., 1978. Climate, soil, and vegetation. 5. A derived distribution of storm surface runoff. Water Resources Research, 14(5), 741-748

KRESTOVSKII, O.I., 1986. Vliyanie virubok i vosstanovleniya lesov na vodnost rek (Influence of woodcutting and restoration of forest on the river runoff). Gidrometeoizdat, Leningrad, (in Russian) 118 pp.

KUCHMENT, L.S., V.N. DEMIDOV and Yu.G. MOTOVILOV, 1986. A physically-based model of the formation of snowmelt and rainfall-runoff. IAHS Publication No.155, International Association of Hydrological Sciences, 27-36

NAZAROV, N.A., 1988. Model of formation of the flood hydrograph of northern plains rivers. Water Resources, a translation of Vodnye Resursy, 15(4), 305-315

NAZAROV, N.A. and A.A. SIRIN, 1988. Models i algoritmy rascheta formirovanifiga rechnogo stoka na lesnom vodosbore (Models and computation algorithm of the runoff formation in a forest catchment). Mezhduvedomstvennyni Geofizicheskini kom't pri Prezidiume Akademii Nauk SSSR, Moskva, (in Russian) 107 pp.

STRAHLER, A.N., 1957. Quantitative analysis of watershed geomorphology. Transactions, American Geophysical Union, 38(6), 913-920

STUDY OF SURFACE WATER QUALITY IN THE NORTHERN REGION SUBJECT TO POLLUTION

A.N. Shammasov

Water Problems Institute of the U.S.S.R.
Academy of Sciences
13/3 Sadovo-Chernogriazskaya 103064
Moscow, U.S.S.R.

ABSTRACT

This paper discusses the results of investigations to protect northern waters from the effects of water pollution produced by phosphate ore extraction. Specifically, the research focused on water-treatment methods relying on the use of treated effluent instead of freshwater. The physical and chemical properties of dissolved and suspended pollutants in the water, and the seasonal dynamics of its chemical composition are reported. Results of laboratory experiments aimed at decreasing pollutant concentrations are also discussed.

In the northern regions, pollution from open-pit mining has specific features:

- clear dependence of the surface-water flow on the season of the year;
- appreciable impact of pollutants on river water of low salinity; and,
- influence of nutrients on eutrophication.

The work reported herein was aimed at investigating surface-water quality related to phosphate-ore extraction with special reference to protection against water pollution; specifically, selection of water-treatment methods to permit the use of treated effluent instead of freshwater. The physical and chemical properties of dissolved and suspended pollutants in the water, and the seasonal dynamics of its chemical composition, were studied, and laboratory experiments were carried out aimed at decreasing the concentration of pollutants.

During phosphate mining in the Leningrad region, surface water flows through the Luga River, into the Gulf of Finland. Hydrographically, the system is part of the Baltic Sea watershed. The average amount of precipitation in the region is 643 $mm \cdot yr^{-1}$ and snowcover depth is about 10 to 15 cm (in some years up to 20 to 30 cm). The ground-water quality is defined by hydrocarbonates.

The main part of the Tallinn-Volkhov catchment consists of the Rivers Luga and Narva. Their flows contain hydrocarbonates; mostly calcium and magnesium, rarely sodium and calcium, and are moderately hard, neutral or weakly alkaline.

---

*Paper not presented, review process not complete.

Wastewater from the quarry is formed by ground-water inflow from the aquifer, precipitation and snowmelt run-off. Long-term investigations estimate water inflow at about 8 $L \cdot h^{-1} \cdot m^{-2}$. The total stripped area is about 400 m^2.

Surface run-off during the observation period totalled 28,000 to 47,200 $m^3 \cdot d^{-1}$, the average value being 31,200 $m^3 \cdot d^{-1}$. Stricter new environmental standards need new methods of waste-water treatment, as well as the use of treated wastewater instead of freshwater in industrial water-supply systems. The latter requires the decrease in water hardness to 1.8 $meq \cdot L^{-1}$. In this case the characteristics of re-used treated wastewater should be as follows: phosphates - up to 0.13 $mg \cdot L^{-1}$; fluorides - 1.5 $mg \cdot L^{-1}$; oil products - 0.1 $mg \cdot L^{-1}$; and, suspended solids - up to 10 $mg \cdot L^{-1}$. Wastewater characteristics (see Table 1) show that special attention should be paid to reducing the hardness (prior to using treated wastewater in industrial recycling systems) and to reducing the content of suspended solids, fluoride, phosphates and oil products.

Figure 1 shows the average water-quality variations in spring (March to April) as the concentration of hardness salts and phosphates grows, so most of the experimental studies were based on these characteristics.

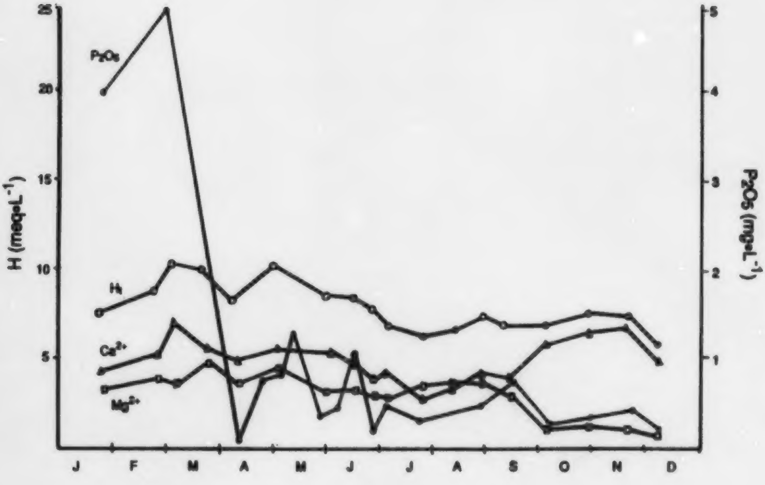

Figure 1. Intra-annual changes in the phosphates and hardness salts concentration in quarrier effluents (averaged data).

Table 2 presents the chemical characteristics of suspended solids. Table 3 gives their physical characteristics. Table 2 shows that suspended solids consist mainly of silicates (up to 10.1%), phosphates (9.01%) and magnesium salts (1.0%), as well as sodium (up to 18.7%), iron (1.0%) and calcium (0.9%). High phosphate content results from the occurrence of phosphate ore.

Table 1. Physico-chemical characteristics of disposed wastewater.

N°	Parameters	Value
1.	pH	8.10-8.35
2.	Temperature, °C	2.0-20.0
3.	Hardness (total), meq·L^{-1} (H_t)	6.5-9.7
4.	Mineralization (total), mg·L^{-1}	372.0-607.0
5.	Alkalinity, meq·L^{-1}	7.6-7.0
6.	Calcium, meq·L^{-1}	2.9-4.6
7.	Magnesium, meq·L^{-1}	3.6-5.1
8.	Phosphates (as P_2O_5), mg·L^{-1}	0.2-5.0
9.	Potassium, mg·L^{-1}	17.5-30.0
10.	Sodium, mg·L^{-1}	30.0-36.9
11.	Iron (total), mg·L^{-1}	traces
12.	Chlorides, mg·L^{-1}	25.0-54.0
13.	Fluorides, mg·L^{-1}	0.3-2.4
14.	Nitrites, mg·L^{-1}	0.01-0.12
15.	Nitrates, mg·L^{-1}	0.6-1.4
16.	Silicates, mg·L^{-1}	6.2-31.5
17.	COD, mg·L^{-1}	14.4-36.9
18.	Oil products, mg·L^{-1}	0.4-10.1
19.	Suspended solids, mg·L^{-1}	32.0-140.0
20.	Sulphates, mg·L^{-1}	61.0-102.0

Table 2. Suspended solids in wastewater.

Contaminant	Weight Concentration %
Si	10.1
Al	0.1
Ca	0.9
Mg	1.0
Fe	1.0
Mn	0.1
Ni	0.1
Ti	0.1
V	0.1
Cr	0.1
Cu	0.01
Pb	0.001
Ba	0.1
P	9.01
B	0.1
K	0.32
Na	1.87

Table 3. Physical properties of suspended solids.

Density g·cm^{-3}	Electric charge of the particle surface mV	Amount of the particle surface per unit weight of the particle m^2·g^{-1}	Particle size µm
1.9 - 2.4	-9.8 - 13.1	351	5 - 126

The greater part of the particles were 30 to 100 µm (84%). The electro-kinetic potential of the particles is -19.4 mV.

Laboratory data on the chemical treatment of wastewater show that many reagents are unsuitable due to:

- the need for high doses with expensive chemicals (such as NaOH);
- the high concentration of phosphates and nitrates in treated effluent when using reagent $(NH_4)_3PO_4$;
- the increase in total salinity and non-carbonate hardness when using NaF or $Ca(OH)_2$; and,
- the low efficiency of some chemicals (e.g., $(NH_4)_3PO_4$) when treated water is at a low temperature.

The laboratory experiments show that the optimum waste-water treatment implies the combined use of $Ca(OH)_2$ and NaOH. This is because there are many bicarbonate complexes in the quarry waters, ensuring the formation of carbonates. These carbonates are necessary for binding hardness ions and phosphates into hardly soluble complexes (e.g. $CaCO_3$ and $Ca_5OH(PO_4)_3$).

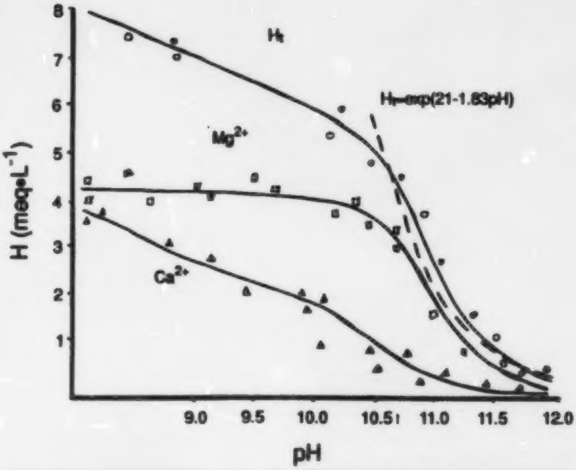

Figure 2. Dependence of the decrease in hardness on the pH of treated effluents.

Figure 2 displays the inverse relationships between hardness (salts) and water alkalinity. For pH ranging from 10.5 to 12, the salt concentration in the water is approximated by the following equation:

$$[1] \qquad H_t = \exp(21 - 1.83\,pH)$$

Experiments for real quarry effluents revealed the following dependence for the determination of the dose of lime required for phosphate removal (Figure 3):

$$[2] \qquad C_{P_2O_5} = 73.1\ D^{-1.39}\ CaO$$

Here $C_{P_2O_5}$ is the residual phosphate concentration in the form of $C_{P_2O_5}$ in the quarry water (mg·L^{-1}); D_{CaO} is the lime dose (as its active part) in mg·L^{-1}.

The analysis of Equation 2 shows that the lime dose required for phosphate removal (0.127 mg·L^{-1}) is considerably lower than the dose of lime required for hardness decrease. That is why the concentration of hardness salts should be used as a basic criterion under the selected reagent method of quarry effluent treatment. In this case, to simplify the control process, Equation 1 can be used, allowing for its normalizing with the alkalinity meter.

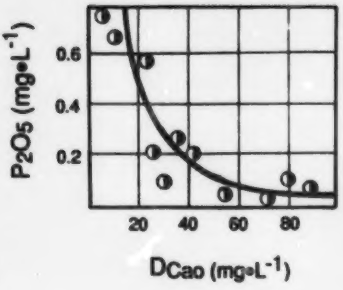

Figure 3. Dependence of the residual phosphate concentration on the dose of lime (as CaO).

Analysis of the experimental results shows that the increase in the lime dose, the temperature of treated water, and the duration of settling, affect phosphate removal, the decrease in hardness, and total mineralization. Phosphates and salts, contained in the quarry effluents, exercise a negative impact on water treatment. The following conditions should be regarded as optimum for hardness decrease and phosphate removal from quarry effluents: 1) lime dose = 340 mg·L^{-1} (as CaO); and, 2) NaOH dose = 50 mg·L^{-1}. Such conditions ensure the required standards for phosphate and hardness salts concentration in the quarry effluent will be reached.

Thus, the proposed scheme and method of surface effluent treatment allows us to protect the fishing waters against pollution and to decrease the consumption of fresh water by industry.

ACKNOWLEDGEMENTS

The author wishes to express his thanks to Dr. V.K. Golyshev and chemical engineer L.G. Tsvetkova of the Leningrad Institute for Civil Engineers for their assistance during the investigations, and to I.M. Semina, interpreter from the Water Problems Institute of the U.S.S.R. Academy of Sciences, for her help in preparing the paper.

SELECTED OTHER READING

GOLYSHEV, V.K., A.N. SHAMMASOV and N.G. TSVETKOVA, 1985. (Treatment of chemical wastewaters and mining quarry effluents for use in a system of recycling water supply). In - Wastewater Treatment in the System of Water Withdrawal and Recycling

Water Supply Systems. Collection of the Arcticles of the Leningrad Institute for Civil Engineers. (in Russian)

SHAMMASOV, A.N., 1985. (Treatment of quarry effluents for use as industrial water supply). Proceedings of Workshop on Increasing the Reliability of Municipal and Industrial Water Supply in Leningrad and the Leningrad Regions. Leningrad Agency for Scientific Information. Leningrad. (in Russian) 33-41

RESPONSE OF RIVERINE AND LACUSTRINE BIOCENOSES TO HUMAN IMPACT

N.S. Zolotareva and M.A. Mordasov

Water Problems Institute of the U.S.S.R.
Academy of Sciences
13/3 Sadovo-Chernogriazskaya 103064
Moscow, U.S.S.R.

ABSTRACT

The paper deals with the role played by the various dimensions of dominating algae types in ensuring permanent hydrobiocenotic composition under increased anthropogenic loading, (using the phytocenosis of the Severnaya Dvina River, its tributaries and lakes of the Solovetsk Islands as a case study).

Increased anthropogenic loading, caused by economic activity, leads to both a quantitative and qualitative deterioration of aquatic biocenosis. However, a relative stability of the dominating algae types - diatomic and green - as well as the subdominant ones - euglenes and cyanes - was observed during a 10-year study of phytoplankton of the Severnaya Dvina River, its tributaries, and some lakes of the Solovetsk Islands. The above-mentioned evrybionts types, inhabiting different biotypes under a wide range of ambient conditions (illumination, water temperature and salinity), include the following algae:

diatomic - *Asterionella formosa* Hass., *Navicula radiosa* Kütz., *Melosira granulata* (Ehrb.), *Synedra ulna* (Kütz.) Grun., *Cyclotella compta* Kütz., *Fragilaria capucina* Derm., *Nitzschia closterium* W.Sm.;
green - *Ankistrodesmus falcatus* (Corda) Ralfs., *Scenedesmus quadricauda* (Turp.) Kütz., *Scenedesmus bijuga* (Turp.) Breb., *Scenedesmus obliquus* (Turp.) Kütz., *Tetrastrum staurogeniaeforme* (Schröder.) Lemm., *Chlamydomonas angulosa* Dill., *Chlorella vulgaris* Benjerinck, *Ulothrix zonata* (Weber and Mohr.) Kütz., *Cladophora fracta* (Vahl.) Kütz.;
cyanes - *Oscillatoria chlorina* (Kütz.) Gom., *Anabaena flos-aquae* (Lyng.) Breb., *Microcystis aeruginosa* Kütz. emend Elenk; and,
euglenes - *Euglena viridis* Ehrb., *Euglena deses* Ehrb.

*Paper not presented, review process not complete.

Most of them are found not only in the plankton, but also in periphyton, neiston and benthos. They are capable of vertical migration, possess buoyancy, photo- and hemotaxis. All this allows them to survive in a water column, in spite of unfavourable abiotic conditions. They gather in frontier layers: in the surface microlayer, near the thermocline and at the water-sediment interface. From time-to-time they change their biotype.

Increased anthropogenic loading does not lead to changes in the dominant phytoplankton types, but does result in a decrease in species variety. The latter was estimated by the Shannon-Weaver (1963) index. On the whole, this value fell from 4.3 in mesosaprobic zones of the Severnaya Dvina, its tributaries and the lakes of the Solovetsk Islands to 2.5 under polysaprobic conditions.

The quantitative and qualitative deterioration was accompanied either by a decrease in the algal biomass and quantity, or a sharp decrease in one part of the dominant phytoplankton type. In the first case phytoplankton development was suppressed: its quantity fell by 39% and biomass by 53%. In the second case "blooming" of diatomic, green, or blue-green algae was observed with simultaneous enlargement of their colonies and an increase in the number of small cells contained in them. The "blooming" was accompanied by a 2 to 3-fold growth of phytoplankton biomass. Further on, the intensive growth of algae was followed by a sharp fall in the number of cells that had decreased in size.

The degree of pollution of the river reaches and lake areas investigated varied from meso- to polysaprobic zones with the preservation of the same dominant types. Comparison of the results of previous hydrobiological investigations, carried out in this region (Chuksina, 1981; Velichkovskii, 1927) and our data (Brekhovskikh *et al.*, 1989; Zolotareva 1988) showed that the qualitative composition has remained practically unchanged for the whole 20th century.

The transition from meso- to polysaprobic conditions is accompanied by a decrease in the biomass, caused by diminution of the cells' dimensions, and the growth of heterotrophic organisms. On the whole, in the mesosaprobic zone, the small-size cellular forms accounted for 54%, medium-size 38%, large 8%; and in the polysaprobic zones 94, 4 and 2%, respectively. At the same time the autotrophic organisms declined from 83% to 69% and the heterotrophic ones increased from 17 to 31%. According to our results, the main changes in phytoplankton, occurring under intensified human impact, manifest themselves in biomass variations under a modified complex of dominant types. An attempt was made to evaluate them using the generalized function of desirability (D), which is an average desirability of separate (partial) parameters (Maksimov *et al.*, 1983; Sakharov and Ilijash, 1982). In our studies these parameters were the biomasses of the dominant types of phytoplankton. The values of particular desirabilities (d) were combined into a single index of generalized desirability (D) as follows:

$$[1] \qquad D = \sqrt[n]{d_1 \cdot d_2 \cdot d_3 \cdot \ldots d_n}$$

The standard scale of desirabilities was used according to which D served as a criterion for evaluating the systems' conditions (phytoplankton was evaluated on the basis of its biomass). We found that D = 1.00 to 0.80 indicated excellent conditions; D = 0.80 to 0.63 - good; D = 0.63 to 0.37 - satisfactory; D = 0.37- to 0.20 - bad; and, D = 0.20 to 0.00 - very bad conditions (Maksimov *et al.*, 1983; Sakharov and Ilijash, 1982).

The above method revealed good phytoplankton conditions in the mesosaprobic zones (D = 0.75 to 0.84) and satisfactory conditions in the polysaprobic zones (D = 0.44 to 0.64).

Changes in the biomass, within the range of satisfactory phytoplankton conditions, are shown (Brekhovskikh *et al.*, 1989; Zolotareva, 1988) to be connected with a variety of sizes of the dominating algae types. This variety is an important factor, maintaining the permanent composition of the hydrobiocenoses. For cells of one type, but different sizes, the ability to exist under various surface-to-volume ratios is ensured; i.e., different exchange conditions with the environment are created.

Different size forms of dominant phytoplankton types were accounted for by using the same index (Shannon and Weaver, 1963). We calculated the portion of every dimensional form of a certain type, related to its quantity or biomass. On the basis of long-term investigations of phytoplankton in the Severnaya Dvina River, in its tributaries and in some lakes of the Solovetsk Islands, we found that changes in the dimensions of dominant organisms' cells started long before the quantitative and qualitative deterioration in the biocenosis could be observed. Intensified pollution under mesosaprobic conditions is accompanied by an increase in the variety of the dimensions of algae cells, whereas under polysaprobic conditions its decrease was observed. In the first case, the number of dimensional forms of investigated algae types increased from 3-16 to 6-23, and in the second case it fell from 9-13 to 2-5. Accordingly, the indices of the variety of dimensional forms of dominant algal types grew from 1.8 to 3.7 and fell from 2.5 to 1.7.

In spite of the fact that the complex of dominant phytoplankton types remained practically unchanged, the 2 to 4-fold decrease in the biomass, explained by degeneration of cells in transition from mesosaprobic to polysaprobic conditions, was observed. This decrease is evident in evaluating the phytoplankton biomass decrease using the desirability function (D) scale. Under polysaprobic conditions D = 0.44-0.64, under mesosaprobic conditions D = 0.75 to 0.84.

Thus, the existence of dominant forms in several dimensions allows phytoplankton to survive under intensified human impact due to a decrease in the cell size. This decrease in phytoplankton biomass does not lead to a violation of normal cenosis conditions and dominant type complexes.

If the quality of phytoplankton in rivers and lakes is subject to a considerable anthropogenic load, it is necessary first to evaluate changes in the variety of the dimensions of its dominant types and the related dynamics of its biomass. This will allow us to reveal the impact on both separate hydrobionts and the hydrobiocenosis as a whole.

REFERENCES

BREKHOVSKIKH. V.F.. N.S. ZOLOTAREVA and M.A. MORDASOV. 1989. (Phytoplankton of the Svernaya Dvina River basin). In - Abstracts. Scientific Conference on Complex Problems of Protection and Rational Use of Small Rivers' Water Resources in the Svernaya Dvina River Basin. Arkhangelsk. (in Russian) 48-50

CHUKSINA. N.A.. 1981. (Hydrobiological study of the Svernaya Dvina and Pechora Rivers and of the sea areas desalted by these rivers). In - Ocherki po Istorii Gidrobiologicheskikh Issledovanii v SSSR (History of Hydrobiological Studies in the USSR). Nauka. Moscow. (in Russian) 89-96

MAKSIMOV. V.N.. L.A. GAN'SHINA and V.A. ABAKUMOV. 1983. (Evaluation of river water quality on the basis of phytoplankton species composition). Seriia Biologicheskaya. N°5. Izvestiia Akademii Nauk SSSR. (in Russian) 731-736

SAKHAROV. V.B. and L.V. ILIYASH. 1982. Metod funktsii zhelatel'nosti pri analize sezonnoy suktsessii planktona (Method of desirability function in the analysis of phytoplankton seasonal succession). Biologicheskie Nauki. N°1. (in Russian) 59-66

SHANNON. C.E. and W. WEAVER. 1963. The mathematical theory of communication. University of Illinois Press. Urbana. Illinois. 117 pp.

VELICHKOVSKII. V.A.. 1927. (Phyto- and zooplankton of the Svernaya Dvina River near Archangelsk). Transactions of the Polar Chemical - Bacteriological Institute. Vol.1. Archangelsk. (in Russian) 152-156

ZOLOTAREVA. N.S.. 1988. (Variety of dimensional forms of plankton algae in the Svernaya Dvina estuary). In - Abstracts. All-Union Conference on Complex Problems of Protection and Rational Use of the Water Resources in the northern part of the European USSR (Case Study of the Svernaya Dvina Basin Rivers). Arkhangelsk. (in Russian) 141-142

APPENDIX A

LIST OF PARTICIPANTS

Mr. Victor BARTNICK
502-1001 W. Pender Street
Vancouver, British Columbia
V6E 2M9 CANADA
Phone: (604) 666-0404
Fax: (604) 666-3325

Dr. Spyros BELTAOS
National Water Research Institute
Environment Canada
P.O. Box 5050
Burlington, Ontario
L7R 4A6 CANADA
Phone: (416) 336-4898
Fax: (416) 336-4989

Dr. Lars BENGTSSON
Department of Water Resources
Engineering
Lund Technical University, Box 118
22100 Lund SWEDEN
Phone: +46-46-108980
Fax: +46-46-104435

Dr. V.F BREKOVSKIKH
Water Problems Institute of Academy of
Science U.S.S.R.
13/3 Sadovo-Chernogriazskaya
103064 Moscow U.S.S.R.
Phone: 208-45-64
Telex: Vodojem 114494

Dr. Melinda BRUGMAN
National Hydrology Research Institute
Environment Canada
11 Innovation Boulevard
Saskatoon, Saskatchewan
S7N 3H5 CANADA
Phone: (306) 975-5966
Fax: (306) 975-5143

Mr. Chuck BRUMWELL
Water Survey of Canada
#8 - 184 South Industrial Drive
Prince Albert, Saskatchewan
S6V 7L8 CANADA
Phone: (306) 953-8541

Mr. G. Glenn BURSEY
Fracflow Consultants Inc.
Hydrogeological and Geological
Engineering Consultants
36 Pearson Street
St. John's, Newfoundland
A1A 3R1 CANADA
Phone: (709) 739-7270
Fax: (709) 753-5101

Dr. Edward F. CHACHO
USA CRREL, Building 4070
Fort Wainwright, Alaska
99703-7860 USA
Phone: (907) 353-5149
Fax: (907) 353-5142

Dr. Stewart COHEN
Canadian Climate Centre/CCAI
4905 Dufferin Street
Downsview, Ontario
M3H 5T4 CANADA
Phone: (416) 739-4389
Fax: (416) 739-4521

Mr. Doug CRAIG
National Hydrology Research Institute
Environment Canada
11 Innovation Boulevard
Saskatoon, Saskatchewan
S7N 3H5 CANADA
Phone: (306) 975-5753
Fax: (306) 975-5143

Mr. Paul CUTLER
Department of Geography
University of Toronto
100 St. George Street
Toronto, Ontario
M5S 1A1 CANADA
Phone: (416) 828-3929
Fax: (416) 828-5328

Dr. Kersi DAVAR
475 Glengarry Place
Fredericton, New Brunswick
E3B 5Z8 CANADA
Phone: Home-(506) 455-5252
Office-(506) 453-4521
Fax: (506) 453-3568

Mr. Mike Demuth
National Hydrology Research Institute
Environment Canada
11 Innovation Boulevard
Saskatoon, Saskatchewan
S7N 3H5 CANADA
Phone: (306) 975-5754
Fax: (306) 975-5143

Dr. Tom Edwards
Department of Earth Sciences
University of Waterloo
Waterloo, Ontario
N2L 3G1 CANADA
Phone: (519) 885-1211 Ext. 3231
Fax: (519) 888-4521

Dr. Mike English
Department of Geography
Wilfrid Laurier University
Waterloo, Ontario
N2L 3C5 CANADA
Fax: (519) 886-9351

Mr. Glenn Ford
Water Resources Division
Indian and Northern Affairs Canada
200 Range Road
Whitehorse, Yukon
Y1A 3V1 CANADA
Phone: (403) 667-3104
Fax: (403) 668-4070

Dr. Andrew Fountain
U.S. Geological Survey
P.O. Box 25046 MS-412
Denver, Colorado
80225-0046 USA
Phone: (303) 236-5025
Fax: (303) 236-5025

Dr. Robert Gerard
Department of Civil Engineering
University of Alberta
Edmonton, Alberta
T6G 2G7 CANADA
Phone: (403) 492-2066
Fax: (403) 492-0249

Mr. Robert E. Gieck
Water Research Centre
Institute of Northern Engineering
University of Alaska
460 Duckering Building
Fairbanks, Alaska
99775-1760 USA
Phone: (907) 474-7331
Fax: (907) 474-6087

Mr. Peter Glenday
Cold Regions Research Centre
Department of Geography
Wilfrid Laurier University
Waterloo, Ontario
N2L 3C5 CANADA
Phone: (519) 884-1970
Fax: (519) 886-9351

Mr. Don Goller
Water Survey of Canada
#8 - 184 South Industrial Drive
Prince Albert, Saskatchewan
S6V 7L8 CANADA
Phone: (306) 953-8574

Dr. Barry Goodison
Canadian Climate Centre
4905 Dufferin Street
Downsview, Ontario
M3H 5T4 CANADA
Phone: (416) 739-4345
Fax: (416) 739-4521

Dr. Don Gray
Department of Agr/Civil Engineering
University of Saskatchewan
Saskatoon, Saskatchewan
S7N 0W0 CANADA
Phone: (306) 966-7828
Fax: (306) 966-8710

Dr. Dennis Gregor
National Water Research Institute
Environment Canada
867 Lakeshore Road, P.O. Box 5050
Burlington, Ontario
L7R 4A6 CANADA
Phone: (416) 336-4611
Fax: (416) 336-4989

Dr. Jiri (George) HAAS
39 Hobart Crescent
Nepean, Ontario
K2H 5J3 CANADA
Phone: (613) 829-3590

Mr. John HAEMMERLI
Environnement Canada
1141 Route de L'Église
5e étage, CP 10100
Ste-Foy, Québec
G1V 4H5 CANADA
Phone: (418) 648-4881
Fax: (418) 649-6213

Mr. Stewart HAMILTON
Department of Earth Sciences
Carleton University
1 Colonel By Drive
Ottawa, Ontario
K1S 5B6 CANADA
Phone: (613) 788-4416
Fax: (613) 788-4490

Mr. Paul E. HARDISTY
Piteau Engineering Ltd.
Suite 100, 4500 Sixteen Avenue N.W.
Calgary, Alberta
T3B OM6 CANADA
Phone: (403) 286-2522
Fax: (403) 247-4811

Mr. Chris HILL
Canatec Consultants Limited
#110 - 3553 Thirty-first Street N.W.
Calgary, Alberta
T2L 2K7 CANADA
Phone: (403) 282-5321
Fax: (403) 289-0465

Dr. Larry HINZMAN
Water Research Center
Institute of Northern Engineering
University of Alaska
460 Duckering Building
Fairbanks, Alaska
99775-1760 USA
Phone: (907) 474-7331
Fax: (907) 474-6087

Mr. Wayne HYDE
210 - 1102 Eighth Avenue
Regina, Saskatchewan
S4R 1C9 CANADA
Phone: (306) 780-5344

Mr. Richard JANOWICZ
Water Resources Division
Indian and Northern Affairs Canada
200 Range Road
Whitehorse, Yukon
Y1A 3V1 CANADA
Phone: (403) 667-3145
Fax: (403) 668-4070

Mr. Jesse JASPER
Environment Canada
P.O. Box 2970
Yellowknife, Northwest Territories
X1A 2R2 CANADA
Phone: (403) 920-8503
Fax: (403) 873-6776

Dr. Peter JOHNSON
Department of Geography
University of Ottawa
Ottawa, Ontario
K1N 6N5 CANADA
Phone: (613) 564-2471
Fax: (613) 564-6529

Mr. Murray JONES
Environment Canada
P.O. Box 43
Fort Smith, Northwest Territories
X0E 0P0 CANADA
Phone: (403) 872-2158
Fax: (403) 872-2028

Dr. Doug L. KANE
Water Research Center
Institute of Northern Engineering
University of Alaska
460 Duckering Building
Fairbanks, Alaska
99775-1760 USA
Phone: (907) 474-7808
Fax: (907) 474-6087

Dr. Ånund KILLINGTVEIT
Norwegian Hydrotechnical Laboratory
Trondheim, NORWAY N-7034
Phone: +47-7-59-23-00
Fax: +47-7-59-23-76

Mr. Don KRAWCHUK
Water Survey of Canada
#8 - 184 South Industrial Drive
Prince Albert, Saskatchewan
S6V 7L8 CANADA
Phone: (306) 953-8534

Dr. Esko KUUSISTO
Hydrological Office
Water Research Institute
National Board of Waters
P.O. Box 436
SF-00101 Helskinki 10, FINLAND
Fax: 358-0-192 95 77
Phone: 358-0-192 91

Dr. John KWONG
National Hydrology Research Institute
Environment Canada
11 Innovation Boulevard
Saskatoon, Saskatchewan
S7N 3H5 CANADA
Phone: (306) 975-4719
Fax: (306) 975-5143

Mr. Charles LABATIUK
276 Fir Street
Sherwood Park, Alberta
T8A 2B1 CANADA
Phone: (403) 675-5386
Fax: (403) 492-0249

Mr. Robert LAPORTE
Travaux publics
Services d'architecture et génie
Environnement Canada
Les Terrasses de la Chaudière
Ottawa, Ontario
K1A 0H3 CANADA
Phone: (819) 997-6102
Fax: (819) 997-9113

Mr. Brian LATHAM
Water Resources Division
Indian and Northern Affairs Canada
P.O. Box 1500
Yellowknife, Northwest Territories
X1A 2R3 CANADA
Phone: (403) 920-8251
Fax: (403) 873-5763

Mr. Dennis LAWSON
Environmental Protection
Environment Canada
Room 300, 2365 Albert Street
Regina, Saskatchewan
S4P 4K1 CANADA
Phone: (306) 780-6462
Fax: (306) 780-6466

Mr. Rory LEITH
Environmental Surveys Branch
Environment Canada
224 West Esplanade
North Vancouver, British Columbia
V7M 3H7 CANADA
Phone: (604) 666-3843
Fax: (604) 666-3325

Dr. Antoni LEWKOWICZ
Erindale College
Department of Geography
University of Toronto
Mississauga, Ontario
L5L 1C6 CANADA
Phone: (416) 828-3930
Fax: (416) 828-5328

Mr. Herbert LOUIE
970 Burrard Street
Vancouver, British Columbia
V6Z 1Y3 CANADA
Phone: (604) 663-2215
Fax: (604) 663-3597

Mr. Donald LUM
800 Kipling Avenue
Toronto, Ontario
M8Z 5S4 CANADA
Phone: (416) 231-4111 Ext. 7176
Fax: (416) 239-0616

Mr. Neill LYONS
Integrated Program Branch
Environment Canada
224 West Esplanade
North Vancouver, British Columbia
V7M 3H7 CANADA
Phone: (604) 666-3527
Fax: (604) 666-6713

Mr. Arbind MAINALI
T. Blench Hydraulics Lab
University of Alberta
Edmonton, Alberta
T6G 2N4 CANADA
Phone: (403) 492-3587
Fax: (403) 492-0249

Dr. Philip MARSH
National Hydrology Research Institute
Environment Canada
11 Innovation Boulevard
Saskatoon, Saskatchewan
S7N 3H5 CANADA
Phone: (306) 975-5752
Fax: (306) 975-5143

Mr. Tim J. MARTA
Inland Waters Directorate
Environment Canada
Place Vincent Massey
Seventh Floor, 351 St. Joseph Blvd.
Hull, Quebec
K1A 0H3 CANADA
Phone: (819) 997-3821
Fax: (819) 997-8701

Mr. Richard MUELLER
New York Power Authority
P.O. Box 191
Marcy, New York
13403-0191 USA
Phone: (315) 792-8206
Fax: (315) 792-8401

Dr. D. Scott MUNRO
Erindale Campus
Department of Geography
University of Toronto
Mississauga, Ontario
L5L 1C6 CANADA
Phone: (416) 828-3929
Fax: (416) 828-5328

Mr. Simon OMMANNEY
National Hydrology Research Institute
Environment Canada
11 Innovation Boulevard
Saskatoon, Saskatchewan
S7N 3H5 CANADA
Phone: (306) 975-5751
Fax: (306) 975-5143

Professor Gunnar ØSTREM
Norway Water Resources and Energy
Administration, P.O. Box 5091-Mj
Oslo-3, NORWAY 0310
Phone: +47-2-959300
Fax: +47-2-959000
Telex: 79397 mueo

Mr. Tim PANGBURN
U.S. Army CRREL
72 Lyme Road
Hanover, New Hampshire
03755-1290 USA
Phone: (603) 646-4296
Fax: (603) 646-4644

Dr. Wayne POLLARD
Department of Geography
McGill University
805 Sherbrooke Street W.
Montréal, Quebec
H3A 2K6 CANADA
Phone: (514) 398-4454
Fax: (514) 398-7437

Dr. John POMEROY
National Hydrology Research Institute
Environment Canada
11 Innovation Boulevard
Saskatoon, Saskatchewan
S7N 3H5 CANADA
Phone: (306) 975-5511
Fax: (306) 975-5143

Dr. Jonathan PRICE
Department of Geography
Queen's University
Kingston, Ontario
K7L 3N6 CANADA
Phone: (613) 546-6033
Fax: (613) 545-6122

Dr. Terry D. PROWSE
National Hydrology Research Institute
Environment Canada
11 Innovation Boulevard
Saskatoon, Saskatchewan
S7N 3H5 CANADA
Phone: (306) 975-5737
Fax: (306) 975-5143

Mr. Richard (Rick) RADDATZ
Atmospheric Environment Service
Ninth Floor, 266 Graham Avenue
Winnipeg, Manitoba
R3C 3V4 CANADA
Phone: (204) 983-6223

Mr. Arthur REDSHAW
Inland Waters Directorate
Environment Canada
P.O. Box 2970
Yellowknife, Northwest Territories
X1A 2R2 CANADA
Phone: (403) 920-8500
Fax: (403) 873-6776

Ms. Vicki REMENDA
Waterloo Centre for Groundwater Research
University of Waterloo
Waterloo, Ontario
N2L 3G1 CANADA
Phone: (519) 885-1211 Ext. 2793
Fax: (519) 888-4521

Dr. Fred ROOTS
Office of the Science Advisor
Environment Canada
Fourth Floor, 10 Wellington
Les Terraces de la Chaudière
Ottawa, Ontario
K1A 0H3 CANADA
Phone: (819) 997-2393
Fax: (819) 953-1626

Mr. Dale ROSS
Environment Canada
P.O. Box 2970
Yellowknife, Northwest Territories
X1A 2R2 CANADA
Phone: (403) 920-8504
Fax: (403) 873-6776

Dr. Wayne ROUSE
Department of Geography
McMaster University
Hamilton, Ontario
L8S 4K1 CANADA
Phone: (416) 525-9140 Ext. 4538
Fax: (416) 546-0463

Dr. Knut SAND
Norwegian Hydrotechnical Laboratory
N-7034 Trondheim, NORWAY
Phone: +47-7-59-23-00
Fax: +47-7-59-23-76

Dr. Sherry SCHIFF
Department of Earth Sciences
University of Waterloo
Waterloo, Ontario
N2L 3G1 CANADA
Phone: (519) 885-1211 Ext. 2473
Fax: (519) 888-4521

Mr. David SHERSTONE
Science Institute of the Northwest Territories
Box 1617
Yellowknife, Northwest Territories
X1A 2P2 CANADA
Phone: (403) 873-7592
Fax: (403) 873-0227

Dr. A. SMALL
Department of Geography
Wilfrid Laurier University
Waterloo, Ontario
N2L 3C5 CANADA
Phone: (519) 884-1970
Fax: (519) 886-9351

Dr. Alan STANLEY
48 Robert Street
Ottawa, Ontario
K2P 1G2 CANADA

Mr. Wayne STARLING
Box 658
Fort Smith, Northwest Territories
X0E 0P0 CANADA
Phone: (403) 872-2558
Fax: (403) 872-3472

Professor William STOLTE
Department of Civil Engineering
University of Saskatchewan
Saskatoon, Saskatchewan
S7N 0W0 CANADA
Phone: (306) 966-5341
Fax: (306) 966-8710

Dr. Wendell TANGBORN
2366 Eastlake Avenue East, #435
Seattle, Washington
98102 USA
Phone: (206) 323-1970
Fax: (206) 324-3705

Mr. Thorkild THOMSEN
Greenland Power Supply
20, Hauser Plads
DK 1127 Copenhagen K, DENMARK
Phone: +45-33-13-84-72
Fax: +45-33-32-05-61

Mr. Garry THORNE
Whiteshell Research
Atomic Energy of Canada Ltd.
Pinawa, Manitoba
R0E 1L0 CANADA
Phone: (204) 753-2311
Fax: (204) 753-2455

Mr. Robert TIMLIN
Department of Earth Sciences
Carleton University
1 Colonel By Drive
Ottawa, Ontario
K1A 5B6 CANADA
Phone: (613) 788-4416
Fax: (613) 788-4490

Dr. Dennis TRABANT
Water Resources Branch
US Geological Survey
800 Yukon Drive
Fairbanks, Alaska
99775-5170 USA
Phone: (907) 479-5645
Fax: (907) 456-0356

Mr. Thomas-Louis TREMBLAY
1246 Haro #902
Vancouver, British Columbia
V6E 1E7 CANADA
Phone: Home-(604) 683-5172
Office-(604) 666-8008
Fax: Office-(604) 666-3325

Dr. Gee TSANG
National Hydrology Research Institute
Environment Canada
11 Innovation Boulevard
Saskatoon, Saskatchewan
S7N 3H5 CANADA
Phone: (306) 975-5760
Fax: (306) 975-5143

Mr. Gary VAN DER VINNE
Environmental Research & Eng. Dept.
Alberta Research Council
P.O. Box 8330, Postal Station F
Edmonton, Alberta
T6H 5X2 CANADA
Phone: (403) 450-5276
Fax: (403) 461-2651

Dr. Robert VAN EVERDINGEN
2712 Chalice Road N.W.
Calgary, Alberta
T2L 1C8 CANADA
Phone: (403) 289-6823
Fax: (403) 282-7298

Dr. Oleg VINOGRADOV
Department of Mechanical Engineering
University of Calgary
Calgary, Alberta
T2N 1N4 CANADA
Phone: (403) 220-5771
Fax: (403) 282-8406

Mr. Jack WEDEL
6 Cranbrook Way
Winnipeg, Manitoba
R2C 0N9 CANADA
Phone: (204) 222-1855

Dr. Ming-Ko WOO
Department of Geography
McMaster University
Hamilton, Ontario
L8S 4K1 CANADA
Phone: (416) 525-9140 Ext. 3526
Fax: (416) 546-0463

Mr. Herb WOOD
Water Resources Branch
Environment Canada
P.O. Box 1693
Inuvik, Northwest Territories
X0E 0T0 CANADA
Phone: (403) 979-2621
Fax: (403) 979-2154

Mr. Whitlow WYATT
1020 Henry Street
Regina, Saskatchewan
S6H 3H4 CANADA
Phone: Home-(306) 693-6231
Office-(306) 780-5344

Dr. YANG Zhenniang
Lanzhou Institute of Glaciology and Geocryology
Chinese Academy of Sciences
Lanzhou, CHINA

Dr. Gordon J. YOUNG
Cold Regions Research Centre
Department of Geography
Wilfrid Laurier University
Waterloo, Ontario
N2L 3C5 CANADA
Phone: (519) 884-1970
Fax: (519) 886-9351

Environment Canada Environnement Canada

Indian and Northern Affairs Canada Affaires indiennes et du Nord Canada

Canada